Overdeepenings under the Greenland Ice Sheet and their control on ice dynamics

PhD Thesis

Submitted in accordance with the requirements for the degree of Doctor of Philosophy

A H Jones

2024

Overdeepenings under the Greenland Ice Sheet and their control on ice dynamics

PhD Thesis

Submitted in accordance with the requirements for the degree of Doctor of Philosophy

Department of Geography

Andrew Hughes Jones

June 2024

Declaration

I, the author, confirm that the Thesis is my own work. I am aware of the University's Guidance on the use of Unfair Means. This work has not previously been presented for an award at this, or any other university

Abstract

Ice loss from the Greenland Ice Sheet (GrIS) is currently the most significant single global contributor to barystatic sea level rise. The discharge of ice directly into the ocean from marine terminating glaciers is the cause of approximately 40% of this sea level rise. Understanding the processes that control how ice slides over the bed is fundamental to improving predictions of future GrIS mass loss. This thesis aims to investigate the possible significance of bed topography for sliding rates and mechanisms by: first, improving understanding of the location and morphology of overdeepenings under the GrIS, which are key landscape features that dictate the locations of riegels and adverse slopes; and second, investigating the dynamics of ice flow through the major outlet glaciers that dominate discharge of ice to the ocean, which involves flow through complexly overdeepened glacially eroded troughs. The thesis begins by compiling the first high resolution, GrIS-wide dataset of overdeepenings for Greenland, and analysing velocity patterns of ice flowing through these overdeepenings: overdeepenings are found to be ubiquitous features under the GrIS, and a small but statistically significant increase in ice velocity is observed on the adverse slopes of overdeepenings. Next, the control exerted on ice dynamics by overdeepenings is explored in detail for two separate glaciers with overdeepened beds near the terminus (Helheim and Upernavik Isstrøm II, where high-quality bed topography was available) were observed to exert a 'marine-isolating' effect on the flow of inland ice, with ice dynamics dominated by marine processes downstream of the riegel and by melt processes inland of the riegel. Further, intriguing patterns of seasonal velocity variation were observed within the overdeepening under high melt conditions at Upernavik Isstrøm II that supported the possibility that adverse slopes of overdeepenings suppress the development of efficient channelised subglacial drainage, which is a key mediator of rates of sliding. A machine learning based automated method utilising k-means clustering for identifying distinct seasonal velocity typologies characteristic of those at Upernavik Isstrøm II was then developed and used to classify all areas of fast-flowing ice of the GrIS. This enabled an ice sheet-wide statistical analysis of whether such the patterns, presumed caused by overdeepenings, are widespread. Limited evidence was found to support systematic and consistent differences in seasonal velocity typology as a result of the presence of overdeepenings; however, examples of modulation of ice dynamics by overdeepenings in

single and adjacent groups of catchments were easily identified and these examples were widespread across the GrIS, suggesting more work on this topic is needed. Finally, a wider analysis of seasonal ice dynamics using the typology dataset for the whole of the GrIS makes three key findings: 1) a statistically significant relationship between melt availability and seasonal velocity typology is demonstrated for the first time; 2) seasonal velocity typologies driven by marine process are found to be relatively rare suggesting that marine processes are not a dominant control on seasonal ice dynamics for the GrIS; 3) the spatial patterns of seasonal velocity typologies generated by automated classification that were interpreted to be representative of channelised subglacial hydrology aligned very closely with published field and modelling data estimating the inland channelisation limit. The study therefore shows a possible importance of overdeepenings in controlling ice dynamics by modulating subglacial hydrology and demonstrates the value of investigating flow typology beyond the immediate vicinity of outlet glacier termini.

Acknowledgements

This PhD has taken a while. Consequently, there are a large number of people who have helped along the way and are deserving of my thanks.

I feel incredibly fortunate to have had the best supervision team a student could hope for, Dr Darrel Swift and Prof Stephen Livingstone. Your passion for the discipline never fails to inspire. You have been unwaveringly supportive and incredibly patient and understanding of the personal and professional challenges that are inevitably faced when studying part time (and working more than full time!) over a period of 10 years. Thanks for sticking with it, I really couldn't have done it without you. Perhaps the most valuable thing I will take from the time studying for my PhD is the personal and professional relationships we have built. I look forward to socialising and collaborating with you both for many years to come.

Thanks also to everyone, staff and students, in the Department of Geography at the University of Sheffield. A brilliant bunch of people and a fantastic research culture to be a part of. So many people have been warm, supportive, and encouraging throughout my studies. There are too many to mention by name, but if you have ever sat at a picnic table with me in the University Arms beer garden, this is probably you!

This PhD would not have been possible without the support I have received from Sheffield Hallam University. They have sponsored me through the PhD, but more importantly they have freed up time for me to undertake my studies. In particular, the sabbatical I have had this semester to allow me to finish writing up has been critical. I owe a debt of gratitude to Tony Goodier as Head of Department for approving this, and to Beth Meeds for supporting it. Beth – thank you so much your support, I would never have been able to finish this if you hadn't picked up so many of my responsibilities this year. I really appreciate everything that you have done for me. Thanks also to all my other colleagues in the Department of the Natural and Built Environment for all your help and support, especially those in the Dynamic Earth Research Group for constant encouragement and belief in me. Particular thanks are warranted to Remy Veness and Niall Gandy who have picked up a lot of my teaching and marking during my sabbatical. Things haven't been easy at SHU over the last 6 months, but Rob Storrar and Natasha Dowey have offered me incredible support through the restructuring process – thank you.

The greatest regret I have of not getting this thesis finished a couple of months sooner is that my dear friend Dr Stephen Rippington never got to read it. I remember being incredibly touched when I was mentioned in the acknowledgments for his thesis when he completed in 2007, and I was very much looking forward to returning the favour, putting him in mine and sending it to him. Whenever we chatted about my project he always had valuable insight to give, and enthusiastic thoughts to share. Musing on the challenges of a PhD he had this advice on life to offer in the acknowledgements to his thesis, which I will reproduce here so that those who don't read beyond this section have something of value they can take from my thesis. "*I've always thought the key to sticking at anything is to laugh when things aren't going so well and to have as much fun as possible when they are*". Sage advice. The world has lost a great geoscientist and a top bloke too early.

Finally, to my family. Thanks to my Mum and Dad, Marta Makowska and Colin Jones, for always supporting me, and encouraging me to go where my passions take me. Thanks to my brothers Alex and Duncan, and my sister Helena for all being legends. My in-laws Gordon Pates and Pam Pates have been incredibly supportive over the 20+ years I have known them, but especially since the kids came along at almost the exact time I started this PhD. They are always there to pick up the slack and jump into childcare mode when required – thank you. My kids, George and Bea, are awesome. Always there with a cuddle when needed and an excellent distraction from work stuff. They can also be quite motivating at times. The point at which I knew I would get this finished was a couple of months ago when Bea asked me "Daddy, could you give up on your PhD?". When I told her that yes, I could give up if I wanted to, she replied "I'm really proud of you for not giving up". I guess you kind of have to see it through when a seven year old tells you that. Lastly, to my wife, Beck. You have been incredible throughout, always supportive and encouraging. You have picked up so much stuff to free up the time and headspace I needed to get finished and I appreciate you more than you will ever know. I really couldn't have done it without you. I guess I owe you that holiday I promised.

Andrew Jones

26 June 2024

Contents

List of Figures

List of Tables

Chapter 1 Introduction

1.1 Rationale

The Greenland Ice Sheet (GrIS) has undergone sustained and dramatic change since the mid 1990s losing over 4 trillion tonnes of ice causing over 10 mm of global mean sea level rise (IMBIE Team, 2020). This represents approximately 20% of the total global mean sea level rise over this period (Frederikse et al., 2020). The GrIS is currently the most significant single global contributor to barystatic sea level rise, and continued mass loss in Greenland may contribute up to a further 0.18 m sea level rise by 2100 (Fox-Kemper et al., 2021). Developing an understanding of the processes driving GrIS changes is critical to our ability to model and predict the magnitude of future ice loss and resulting sea level change, and what can be done to mitigate and manage these changes.

GrIS contributions to sea level rise are made up of two components: surface mass balance losses (from melting) and dynamic ice losses (from ice flux). The relative proportion of loss attributable to these two components has varied over time. Prior to the onset of sustained negative mass balance of the ice sheet in the mid-1990s, dynamic losses were dominant, making up approximately two thirds of total net mass loss (Rignot et al., 2008). As surface air temperatures increased, contributions from melting increased in line (Van den Broeke et al., 2016). There is some uncertainty as to the precise contributions of melt and flux based losses, but evidence suggests that melt losses now account for approximately 60% of net mass loss, with flux losses making up approximately 40% (IMBIE Team, 2020). Within these ice sheet wide headline attributions of loss to melt and ice flux there appears to be significant spatial variation over the GrIS. The proportion of losses due to ice flux is much greater than 40% in some areas, and much less in others (Khan et al., 2015; Mouginot et al., 2019) (Figure 1.1). Indeed, to further the complexity of the study of these systems, surface mass balance and ice dynamics are not independent of one another. There is evidence to suggest that increased ice flux is correlated with increased surface mass balance losses because greater surface melt lubricates the bed and causes ice sliding velocity, and thus total ice flux, to increase (Zwally et al., 2002; Rignot et al., 2008). Hypsometric adjustment to the ice sheet due to SMB changes will also modify the dynamics of the ice sheet (Bartholomew et al., 2011). Other studies have suggested that the relationship between melt and ice velocity may be inverse at times, with the potential for high melt to promote

efficient channelised subglacial drainage during the later melt season and thus seasonally reduce sliding velocity (Sole et al., 2013; Tedstone et al., 2013; Davison et al., 2020). The exact nature of the balance between the potential for higher melt to increase or decrease net ice flux in Greenland is currently uncertain (Nienow et al., 2017), in part because much of the work from which extrapolations have been made is focused in the land terminating sector in the south west of the GrIS (Davison et al., 2019). This area only makes up a small proportion of the GrIS and is also atypical of the majority of the ice sheet which is made up of faster flowing marine terminating outlet glaciers (Mouginot et al., 2019). As such, there is considerable uncertainty regarding the net contribution of dynamic GrIS processes to future sea level rise (Shannon et al., 2013).

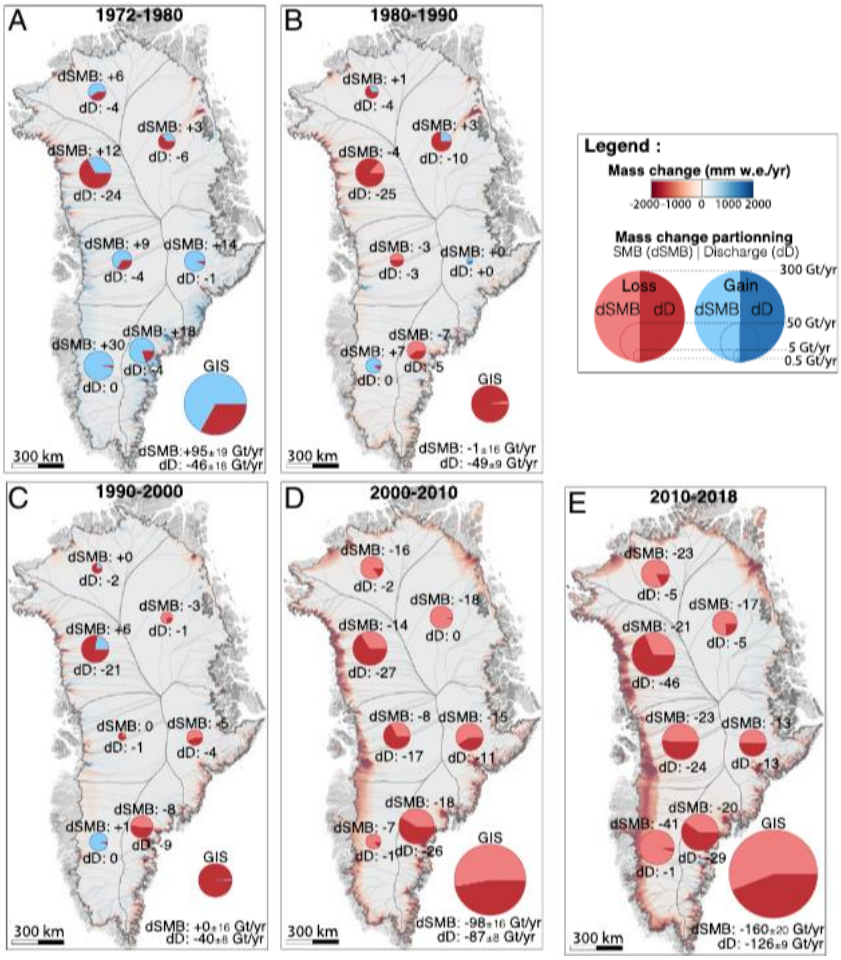

Figure 1.1 Partitioning of the mass loss between anomalies in SMB, dSMB, and ice discharge, dD, by regions for the time period 1972–2018 in gigatons, or 1012kg; (A) 1972–1980, (B) 1980–1990, (C) 1990–2000, (D) 2000–2010, and (E) 2010–2018. Shown are SMB in light tone (red for loss, blue for gain), and D in dark tone (red for loss, blue for gain). The size of the circle is proportional to the absolute magnitude of the change in SMB or D. Reproduced from Mouginot et al. (2019)

Overdeepenings are closed topographic basins in the bed of ice masses due to differential

rates of erosion (Cook and Swift, 2012). They are thought to be ubiquitous features under fast moving outlet glaciers (Cook and Swift, 2012; Patton et al., 2015, 2016) but there has been limited work undertaken to accurately map them for the GrIS sheet, and a mapping exercise has never been conducted using the most recent high resolution bed models such as BedMachine (Morlighem et al., 2017). Subglacial topography exerts control on patterns of ice flow through both physically resisting flow, and through modulating subglacial hydrology. Adverse bedslopes force ice flowing through overdeepenings to flow uphill at the downstream end of the overdeepening causing backstress which may impede ice flow, slowing velocity, and imparting a stabilising effect (Van der Veen 1997; Motyka et al., 2003). Adverse bedslopes are also anticipated to modulate basal sliding rates and mechanisms through their control on subglacial drainage system morphology and efficiency (Hooke et al., 1989; Jansson, 1995). As water at the bed of an overdeepening is forced uphill to exit the depression, basal water pressures are consistently high causing lower effective pressure, and potentially increased ice velocity. The action of these processes suggests that ice flow through overdeepenings may vary, and be more complex, than flow through non-overdeepened areas (Cook and Swift, 2012).

Despite the likely ubiquity of overdeepenings near the margin of the GrIS, and their potential to exert controls on ice dynamics (with the associated sea level rise implications), investigation of these processes has been limited to a relatively small number of mountain glaciers (Hooke et al., 1988; Hooke and Pohjola, 1994; Jansson, 1995; Iken et al., 1996; Fountain and Walder, 1998; Hock et al., 1999). In the context of the GrIS, investigation of the role of overdeepenings in ice dynamics processes has primarily focused on the backstress exerted by adverse slopes and the stabilising effect this may have on outlet glaciers (e.g. Carr et al., 2015; O'Regan et al., 2021). There has been no study of the potential for adverse slopes to modify subglacial hydrological configuration of the GrIS which may increase ice velocity.

As a result of the challenges in determining the impact of complex feedbacks in ice dynamics, they have often been omitted from models and estimates of future change (Goelzer et al., 2020). Indeed, The first four Intergovernmental Panel on Climate Change (IPCC) Assessment Reviews (AR) did not include a contribution for dynamic ice sheet changes in the predictions for future sea level rise from the GrIS. AR5 did include sea level rise

predictions based on dynamic ice sheet change, but these were limited to calving and marine melt, and hypsometric SMB ice flow interactions, and did not take account of seasonal subglacial hydrological processes (Church et al., 2013). Seasonal subglacial hydrological processes have been incorporated in some of the models (Calov et al., 2018) used for IPCC projections of sea level in the most recent AR6 report (Fox-Kemper et al., 2021) representing substantial advances in the understanding of this area of study. However, despite these steps forward in knowledge, there is still large uncertainty in future projections, a position summarised effectively by the AR6 statement that "…*although there is* ***high confidence*** *that the dynamic response of Greenland outlet glaciers is controlled by bedrock topography, there is* ***low confidence*** *in quantification of future mass loss from Greenland triggered by warming ocean conditions, due to limitations in the current understanding of ice–ocean interactions, its implementation in ice-sheet models, and knowledge of bedrock topography*." (Fox-Kemper et al., 2021, pg. 1258). There is clearly much more work to be done to develop process understanding of ice sheet dynamics to a position that will enable accurate predictions of future changes to be confidently made and understanding topographic controls and seasonal processes will be key to this. Indeed, more recent modelling work by Felikson (2022) suggests that ignoring seasonal processes can bias decadal modelling mass projections by up to a 39% underestimate or 25% overestimate depending on other glacier parameters. It is the furthering of the currently quite limited understanding of seasonal ice dynamics processes of the GrIS that forms the primary rationale for this thesis.

1.2 Research aims and objectives

The overall aim of this thesis is to determine the location and morphology of overdeepenings under the Greenland Ice Sheet, and to examine their impact on hydrology and ice dynamics.

In order to achieve this aim a number of research questions (RQs) have been developed, each with associated objectives.

RQ1: How common are overdeepenings under Greenland outlet glaciers and how variable is their geometry?

Objective a) Develop a semi-automated workflow for mapping all overdeepenings under fast flowing ice on the Greenland Ice Sheet and extracting morphometric parameters, and implement this to derive a high resolution dataset of all overdeepenings.

Objective b) Investigate patterns and potential process relationships in overdeepening morphometry.

RQ2: Does bed topography modulate ice velocity in overdeepenings?

Objective a) Explore at an ice sheet scale whether annual mean ice velocity is modulated when flowing through an overdeepening.

Objective b) Determine whether seasonal ice velocity (e.g. timing and magnitude of speedup and slowdown) varies along glacier length, and the extent to which these variations may be linked to bed topography.

RQ3: Are there any broad scale patterns that link seasonal velocity signature to bed topography or other GrIS-wide factors?

Objective a) Develop an automated workflow for identifying distinct seasonal velocity variation typologies and classify velocity time series data points into these typologies at an ice sheet scale.

Objective b) Explore the extent to which there is evidence at the ice sheet scale for patterns in ice dynamics modulated by overdeepenings identified for individual glaciers in **RQ2**

Objective c) Quantify the spatial and temporal patterns (and potential process relationships) between seasonal ice velocity typology and other relevant factors.

1.3 Thesis structure

The thesis will be composed of eight chapters including this introduction. Details of the individual chapters will be given below. Chapter 2 expands on the introduction and rationale given in Chapter 1 and presents the scientific background and context from the relevant

literature related to the themes of study of the thesis. Chapters 3-6 present the substantive results of the research conducted. Chapter 7 is an overarching discussion of the findings of the thesis as a unified body of work, drawing the results from the chapters together and revisiting and specifically addressing the research questions and objectives. Chapter 8 summarises the principal conclusions of the thesis.

Chapter 2. Scientific context and background

This chapter provide a review of the literature relevant to the aim of the study and the research questions. Key concepts and principles are introduced and explained, areas where existing scientific understanding is good are identified, areas where knowledge is contested are highlighted and discussed, and important themes that have received little scientific attention to date are put forward. The chapter is broadly split into three sections covering: overdeepening origin, evolution, and mapping; glacier and ice sheet dynamics; and the role of overdeepenings in ice sheet dynamics.

Chapter 3. Overdeepening location and character under the Greenland Ice Sheet

This first part of this chapter is focused around answering **RQ1, how common are overdeepenings under Greenland outlet glaciers and how variable is their geometry?** It develops a semi-automated method for mapping overdeepenings under the Greenland ice sheet and implements this to produce a new dataset of overdeepenings using the high resolution BedMachine dataset (Morlighem et al., 2017). This is the first time that overdeepenings have been mapped at this resolution at an ice sheet scale, representing an order of magnitude improvement in mapping resolution compared to previous studies. A full morphometric analysis is then conducted for the overdeepenings mapped, including consideration of the impact of the glacial setting (e.g. proximity to confluence, diverging / converging flow, underlying lithology) on overdeepening occurrence and form. The second part of the chapter starts to answer **RQ2, does bed topography modulate ice velocity in overdeepenings?** A comparison of the difference in velocity between ice in overdeepenings compared to the wider ice sheet is made, and the potential control of overdeepenings on mean annual ice velocity are examined.

Chapter 4. **Seasonal velocity patterns along GrIS marine terminating glacier centre lines**

This chapter is focused on answering **RQ2, does bed topography modulate ice velocity in overdeepenings?** The approach taken is to investigate Helheim and Upernavik Isstrøm II as case studies to explore a) whether seasonal velocity patterns vary at different points along a glacier centre line, and b) whether there is evidence of subglacial topography modulating seasonal velocity patterns. Both case studies areas have prominent overdeepenings and the morphology of these overdeepenings (from the analysis conducted in Chapter 3) is analysed alongside seasonal patterns of ice velocity derived from high temporal and spatial resolution ice velocity data to investigate potential process relationships. A conceptual model is presented which explains observed variation in seasonal velocity typologies on normal and adverse slopes. The work presented in this chapter is based on posters presented at EGU Vienna in 2016 and 2018 (Jones et al., 2016; Jones et al., 2018).

Chapter 5. Identification and classification of seasonal ice velocity typologies using machine learning.

This chapter is specifically focused **on RQ3 objective A**. A methodology is developed which facilitates the automatic identification and classification of ice velocity modes at high spatial resolution at an ice sheet scale. The approach uses a K means clustering algorithm to determine a set of distinct seasonal velocity typologies and classifies approximately 750,000 individual time series points to a typology. Two separate analyses are conducted to determine the seasonal velocity topologies for points spaced along the central flowlines for all Greenland outlet glaciers (generated in Chapter 3), and for the adverse and normal slopes of all overdeepenings mapped in the dataset created in Chapter 3. This allows detailed analysis of the variations in seasonal velocity typologies within overdeepenings, and a broad analysis of seasonal velocity typologies across all fast flowing areas of the GrIS. The analysis conducted covers four years (2016-2019). Process significance of the typologies identified is discussed and a comparison with key previous studies is given.

Chapter 6. Season ice velocity typologies in Greenland: an ice sheet wide analysis of patterns and control.

This chapter is focused on answering **RQ3**, **are there any broad scale patterns that link seasonal velocity signature to bed topography or other GrIS-wide factors?** A full analysis of the data generated in Chapter 5 is conducted to investigate whether there is evidence for widespread control of seasonal velocity typology by bed topography at the ice sheet scale. Specifically, are the patterns of seasonal velocity observed at Upernavik Isstrøm II in Chapter 4 evident elsewhere on the ice sheet, and if so, how ubiquitous are these patterns? Wider patterns and processes relating to seasonal velocity typology (beyond the potential controls of bed topography and overdeepenings) are then considered. These include the relationship between surface melt and seasonal velocity typology, marine processes as a control on seasonal velocity typology, and the potential for estimating the inland limit of subglacial channelisation using the mapping of seasonal velocity typology.

Chapter 7. Discussion

This chapter provides an overarching discussion drawing together and summarising the key findings of Chapters 3-6 in relation to the research questions set out in section 1.2. The chapter goes on to consider the implications for future GrIS change that can be drawn from the findings of the thesis. Finally, limitations of the research conducted, and possibilities for future research are discussed.

Chapter 8. Conclusion

Key conclusions for the research questions are summarised.

1.4 A note on the duration of study

It is worthy of note that this PhD thesis has been completed part time over the course of 10 years. One impact that this has inevitably had, is that things have changed and advanced during the period of study. As much of the research conducted has been quite technical the relatively frequent release of ever improved datasets has been an issue to deal with. As a

result of this, different velocity datasets have been used for different elements of the research for example. In other cases (such of the use of BedMachine v3 throughout the thesis), the dataset originally used has been used in research that follows for consistency, even when newer versions have been released in the interim. These issues are discussed in full in Chapter 7 (discussion).

Chapter 2 Scientific context and background

2.1 Introduction

This chapter will be comprised of three key sections. First (section 2.2), the origin and evolution of overdeepenings will be discussed, including key controls hypothesised for their formation, and a review of existing mapping of overdeepenings will be given. Secondly (section 2.3), there will be a substantial section on glacier and ice sheet dynamics. Whilst the primary aim of this thesis is to investigate the control that overdeepenings may exert on ice dynamics, this section will cover key glaciological background and theory in a context not specific to overdeepenings. Finally (section 2.4), focus will return to overdeepenings and introduce some of the existing theory and observations of their control on ice dynamics, and how general theory on glacial dynamics might apply specifically in overdeepenings.

2.2 Overdeepenings

2.2.1 Origin and evolution

Overdeepenings are "closed topographic depressions in the beds of present and former ice masses" produced by glacial erosion (Cook and Swift, 2012, p333). Understanding the origin and evolution of overdeepenings, and the impact they have on ice dynamics is complex, with significant circularity between processes. Overdeepenings are formed by erosional processes controlled by the dynamics of overlying ice. Once they have formed, they then exert control on the ice dynamics (Marshall et al., 1996; Jamieson et al., 2010) and so potentially self-regulate their own future evolution (Alley et al., 2003). However, it is this complexity that renders the study of overdeepenings of value. Furthering our understanding of overdeepenings can simultaneous expand our understanding of the patterns of palaeo ice flow and sediment movement over the timescale of overdeepening formation (Alley et al., 1997). It also enables better conceptualisation and modelling of future ice sheet behaviour (Weertman, 1974; Thomas, 1979; Schoof, 2007; Creyts and Clarke, 2010; Jamieson et al., 2012) in areas of fast flowing ice close to the margin of the Greenland Ice Sheet (GrIS), where overdeepenings are thought to be ubiquitous features (Holtedahl, 1967; Shepherd and Wingham, 2008; Swift et al., 2008; Jordan, 2010; Patton et al., 2015, 2016).

There is a comprehensive body of literature relating to glacial landscape evolution and many of the associated erosive processes are well understood (Glasser and Bennett, 2004). However, overdeepenings have been less well studied than many other features and the specific mechanisms of their origin and evolution are uncertain (Cook and Swift, 2012).

The overdeepening of glacier beds is caused by varying erosion rates at different locations on a glacier. There are two principal factors which can control the differential erosion of the glacier bed; the erosive power of the glacier, and the resistance of the bedrock to erosion. These will be considered in turn below.

2.2.1.1 Erosion, melt availability, and glacier geometry

Many glacial erosion models make the assumption that the rate of erosion of the bed is proportional to the speed at which ice is sliding over the bed (Hallet, 1979; Oerlemans, 1984; Anderson et al., 2006; Egholm et al., 2011). For a steady state glacier, ice flux will commonly be at a maximum at the equilibrium line altitude (ELA), and it is therefore hypothesised that erosion (Anderson et al., 2006; Egholm et al., 2009), and by extrapolation overdeepenings, may often be located close to the long term average ELA (Boulton, 1996; Anderson et al., 2006). Areas of convergent flow on a glacier will also cause ice to thicken and / or accelerate, increasing the erosive potential (Alley et al., 2003; Amundson and Iverson, 2006; MacGregor et al., 2009), and overdeepenings are commonly observed at glacier confluences e.g. (Iken et al., 1996; Hock et al., 1999). Whilst maximum flux at the ELA may be the case in mountain glacier or land terminating ice sheet contexts, the vast majority of Greenland outlet glaciers terminate in a marine environment (Mouginot et al., 2019).When terminating in a marine environment, an ice stream or outlet glacier will often maintain accelerating flow all the way to the calving front (Alley et al., 1989; Rosenau et al., 2015). In these situations, it is therefore likely that high ice flux may also occur close to the calving front, and that maximum flux may not be at the ELA. It is perhaps unsurprising then that overdeepenings appear to be extremely common close to the termini of fast flowing Greenland outlet glaciers (Patton et al., 2016). However, in many cases the timing of formation of overdeepenings is not well constrained, and so it is plausible that overdeepenings currently near the margin of the GrIS may have formed when ice was more extensive and their current position was actually further inland (Cook and Swift, 2012).

The availability of water at the bed of a glacier is also fundamental to the erosive power.

Basal thermal regime is a vital control on erosive power and therefore should be highest where basal melting is highest (e.g. convergent flow and where overdeepenings thicken ice (Glasser, 1995)). Water at the bed has a lubricating effect which causes increases in ice velocity (and therefore erosive power) by ice slipping over the bed (Hallet, 1979; Iverson, 1991; Glasser, 1995). The presence of water at the bed can also facilitate the formation of efficient subglacial channels and the flushing out of eroded sediment through these channels (Röthlisberger, 1972; Alley et al., 1997). Whilst basal melting will be high at areas of maximum ice thickness (e.g. the ELA) and this will provide sufficient melt to enable sliding, the level of melt may not be high enough to force evolution of efficient subglacial channels and flush out sediment (Röthlisberger, 1972; Alley et al., 1997) and the level of surface runoff generated at the ELA is low (Fountain and Walder, 1998). As such, a layer of sediment can accumulate at the bed causing a self-regulating process where the bed is protected from further erosion which slows or prevents further overdeepening of the base (Alley et al., 1997; Alley et al., 2003). As a result of this, multiple overdeepenings might occur with adverse bedslopes being protected by suppression of efficient drainage. Thus, rather than expecting the profile to evolve into one long overdeepening, as envisaged by Patton et al. (2016), a glacier system could contain numerous smaller stable overdeepenings. Further down glacier at lower elevations, air temperatures will be higher, and the level of surface runoff generated will be substantially increased (Fountain and Walder, 1998; Herman et al., 2011). This melt will access the bed via crevasses and moulins, lubricate the bed and enable ice velocity to speedup and increase erosion, and enable efficient channels to form which can flush eroded sediment from the system (Röthlisberger, 1972; Alley et al., 1997). It is likely that these melt water driven processes are made possible due to high surface runoff at areas close to the margin, and that this may explain the high prevalence of overdeepenings at glacier termini (where ice is thinner and flow likely more diffluent than at the ELA) both in alpine (Fountain, 1994; Lawson et al., 1998) and ice sheet (Patton et al., 2016) contexts.

2.2.1.2 Geological control

Geological context controls both where overdeepenings form, and their morphometric properties, in a number of ways. Differential resistance of bedrock to erosion by non-glacial means (such as fluvial processes) will shape the preglacial landscape and determine initial

valley geometry (Stange et al., 2013) and therefore have a control on where overdeepenings are initiated when an area becomes glaciated (Glasser, 1995; Preusser et al., 2010). Any preexisting topography that will locally cause ice to speedup or thicken, or for melt transfer to the bed to increase, is likely to increase erosive potential and therefore initiate the overdeepening of the underlying bed. Mechanisms by which this may occur include: topographic steering causing convergent flow into non-glacial closed topographic basins (Kessler et al., 2008), valleys narrowing and causing convergent flow or junctions in valleys causing tributaries to join (Lloyd, 2015), and valley floor perturbations causing crevassing aiding transit of supraglacial runoff to the bed (Hooke, 1991).These may all have an impact on where overdeepenings initially form.

The resistance of bedrock to glacial erosion has also been shown to influence where overdeepenings form (Preusser et al., 2010), and the shape an overdeepening evolves to, with more resistant bedrock tending towards narrower deeper valleys (Hirano and Aniya, 1988; Augustinus, 1992; Brook et al., 2004; Swift et al., 2008).

2.2.2 Mapping of overdeepenings

Despite the importance of overdeepenings in relation to ice dynamics (Hooke and Pohjola, 1994; Egholm et al., 2011, 2012; Cook and Swift, 2012) and other applied issues such as glacial lake outburst flood (GLOF) risk assessment (Magnin et al., 2020), engineering projects (Taylor and Wilson, 1997), and safe disposal of nuclear waste (Talbot, 1999; Fischer et al., 2021), there has been relatively limited large scale mapping of overdeepenings, with much investigation focused on individual features or over small areas e.g. (Haeberli et al., 2016; Pomper et al., 2017; Magrani et al., 2020).

Comprehensive mapping of overdeepenings has been conducted in some areas including Labrador, Canada (Lloyd, 2015; Lloyd et al., 2023), the Himalaya-Karakoram (Preusser et al., 2010; Linsbauer et al., 2016), the Swiss Alps (Preusser et al., 2010; Magrani et al., 2020), and Peru (Preusser et al., 2010; Colonia et al., 2017). To date, the only study to attempt to comprehensively map overdeepenings under contemporary ice sheets is that of Patton et al. (2016) which developed an automated method of mapping overdeepenings in Greenland and Antarctica. This resulted in the mapping of a total land area of nearly 20 million km^2 and a dataset of approximately 14,000 overdeepenings (c. 10,000 for Antarctica and 4,000 for Greenland). However, this study used relatively coarse resolution bed data (5 km for

Antarctica and 1 km for Greenland). As a result, once quality assurance procedures were run on the dataset, only 1,099 overdeepenings (764 for Antarctica and 335 for Greenland) were deemed of high enough quality to be including in the morphometric analysis.

2.2.2.1 Improvements in bed data

A likely explanation for the relative paucity of work mapping overdeepenings under extant ice sheets conducted to date is that spatially comprehensive high resolution data on bed geometry has only become available relatively recently, since the early 2010s. Sparce point measurements and individual radar lines available prior to this enabled investigation of individual glaciers but it was only once a critical mass of denser arrays of measurements had been compiled through programmes like CReSIS (Gogineni et al., 2001) for Greenland in the 1990s and 2000s, that interpolated surfaces of this data were able to be produced (e.g. Bamber et al., 2013). Similar work was conducted, and data products became available for Antarctica (e.g. Fretwell et al., 2013)). These interpolated bed topography datasets were generated by applying kriging to interpolate data from radar surveys and yielded a spatial resolution of between 1-5 km, and it was these datasets that were used by Patton et al. (2016) to map overdeepening in Greenland and Antarctica.

Methods of generating bed topography datasets that have been developed more recently refined basic kriging approaches by incorporating mass conservation modelling from velocity data to generate much higher accuracy estimations of ice thickness between observed thickness along radar lines (Morlighem et al., 2017). Combined with further collections of measured bed data through NASA's Operation Ice Bridge (Rodriguez-Morales et al., 2013), the resulting BedMachine product provides bed data for Greenland at a grid resolution of 150 m, over an order of magnitude higher than the best data previously available (Morlighem et al., 2017). To date, ice sheet wide mapping of overdeepenings in Greenland has not been conducted using this much improved data, and the dataset generated by Patton et al. (2016) remains the only comprehensive study of overdeepenings in Greenland (Figure 2.1).

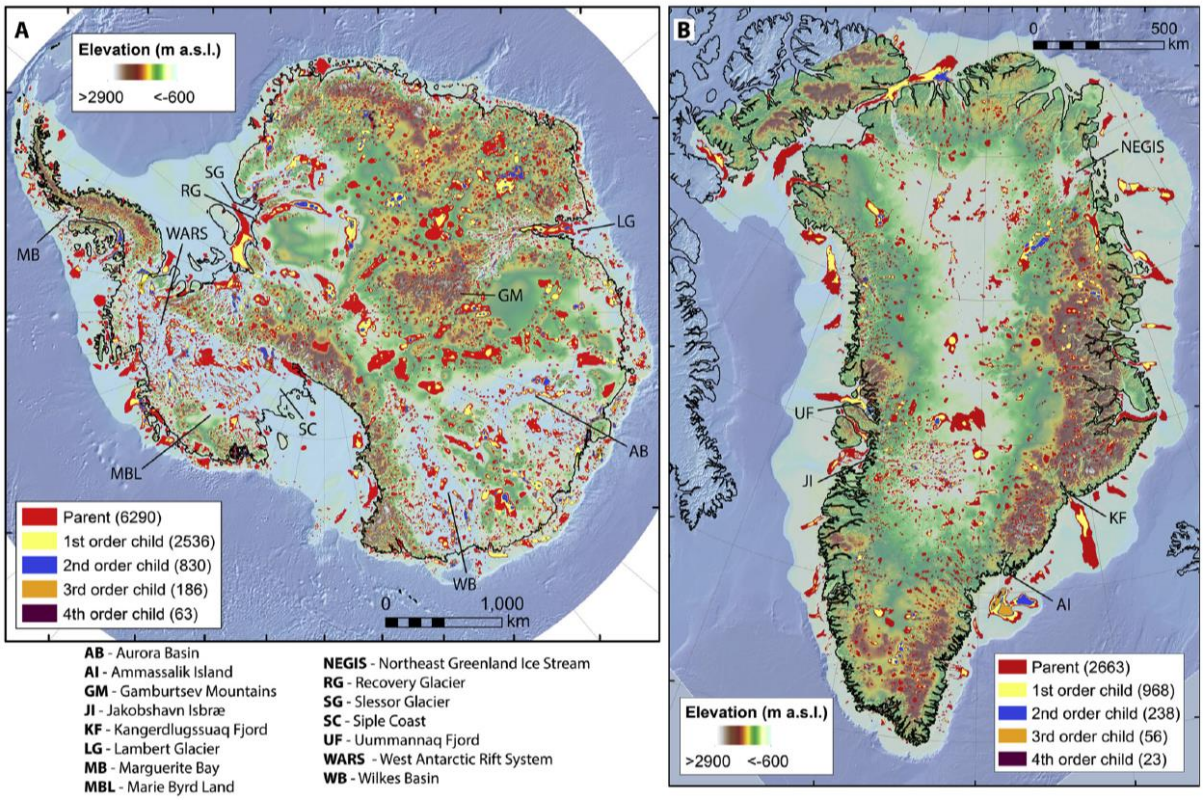

Figure 2.1 Ice sheet scale mapping of overdeepenings. A) Antarctica. B) Greenland. Reproduced from Patton et al. (2016).

2.3 Ice sheet dynamics

2.3.1 Subglacial hydrological processes

2.3.1.1 The importance of melt

Sliding of a glacier over its bed has been recognized as a fundamental process in how the dynamics of a glacier operate since the earliest studies of glaciers in the European Alps by glaciologists such as Horace De Saussure, Louis Agassiz, James Forbes, Willam Hopkins, and John Tyndall in the 1840s. Field observations in this period comparing ice velocity at the surface and near the bed at the Glacier de Bois and the Mer de Glace showed that the majority of ice motion down a valley was most likely explained by sliding rather than ice deformation (Hopkins, 1862). Early lab experiments by Hopkins also demonstrated the importance of the presence of liquid water at the ice / bed interface to enable efficient sliding. Hopkins hypothesised that delivery of melt water into the glacial system was likely a critical driver in enabling sliding, both as a means of supplying water to the bed, and more generally increasing the interior temperature of the glacier and contributing to raising the temperature at the bed above the melting point (Hopkins, 1862).

From the very first recorded measurements of glaciers, it was established that the motion of ice down a valley was variable in space and time (Forbes, 1842), and that temporal variations in motion were observable at both seasonal and shorter timescales. Intuitive links between rates of ice motion, and the presence of water and variations in air temperature, were made by Forbes, who stated "(flow) is more rapid in summer than in winter, in hot than in cold weather, and especially more rapid after rain, and less rapid in sudden frosts" (Forbes (1843) in Clarke, (1987), pg. 8). However, specific theories explaining the precise role that subglacial water plays in glacial sliding were not developed until over a hundred years after these initial observations (Clarke, 1987).

Work by Weertman in the late 1950s and early 1960s was the first to establish a complete theory of glacial sliding (Weertman, 1957), and to identify mechanisms by which cavities that formed behind obstacles at the bed could grow and coalesce to form a continuous film of water at the bed, and that even a very thin layer (e.g. less than 1 mm, or less than an order of magnitude of the obstacles at the bed) could cause substantial increases in ice velocity (Weertman and others, 1962; Weertman, 1964). These two arrangements of the flow of water under a glacier (linked cavities and films) have come to be referred to as 'inefficient' or 'distributed' forms of subglacial drainage (these concepts will be returned to and expanded further in section 2.3.1.2, below). These concepts were developed further by Lliboutry (1968) who proposed that water in subglacial cavities could be pressurised, reducing the effective pressure of the ice at the bed, and therefore reducing friction and increasing sliding velocity. It was not until the 1980s that the precise role of water at the bed, and in particular the importance of water pressure, became better understood. Early use of finite element analysis modelling (Iken, 1981) combined with detailed field observations in the Swiss Alps (Iken et al., 1983) in the groundbreaking work of Almut Iken established the dominant control of water pressure on glacier sliding velocity. Specifically, Iken et al. (1983) showed that maximum horizontal velocity was coincident with maximum vertical velocity, *not* maximum vertical displacement of the glacier (Figure 2.2). This indicated that it is the initial transition phase of the development and pressurisation of cavities that causes ice speedup, and that further increases in the absolute magnitude of water available will not necessarily drive further increases in ice velocity.

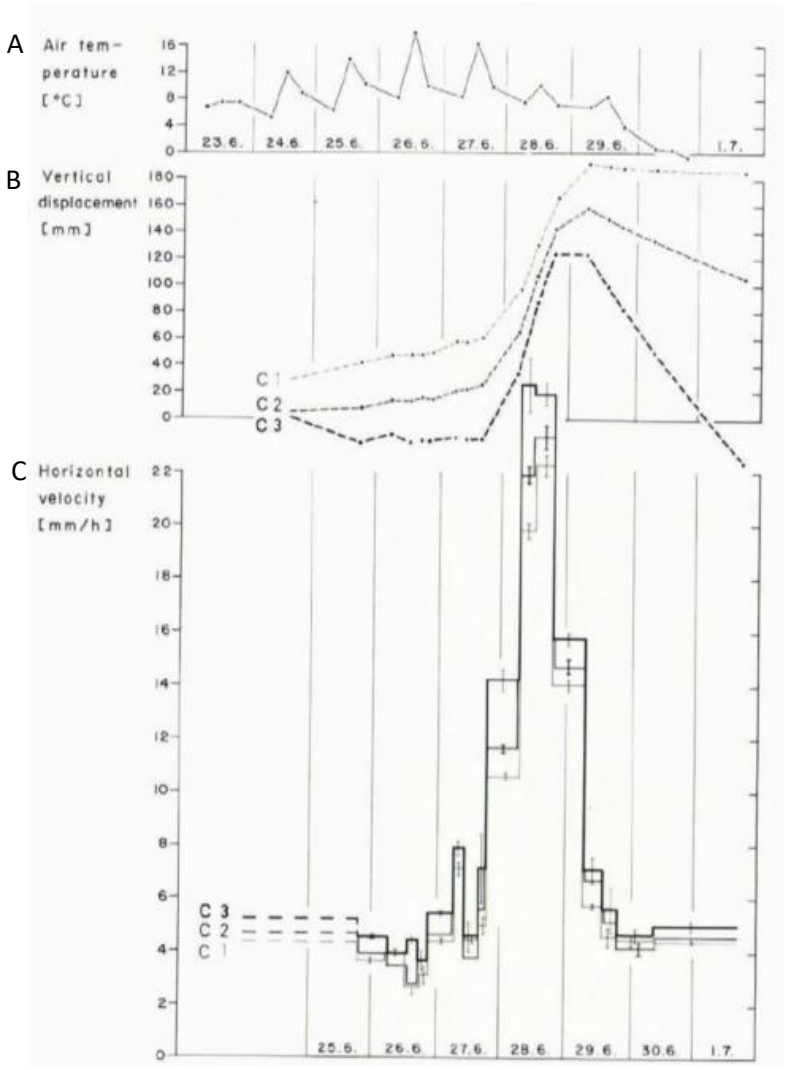

Figure 2.2Theoldolite measurements of glacier movement at Unteraargletscher, Switzerland, 1975. A) air temperature. B) Vertical displacement of three survey poles, C) horizontal velocity. C1 is near the glacier margin, C3 is on the medial moraine. C3 is the horizontal velocity of the same poles. Reproduced from Iken et al. (1983).

A wide range of subsequent studies replicated the observations of Iken (1981), (Copland et al., 2003; Mair et al., 2003; Bingham et al., 2006) but these patterns are not universal. Other studies found a relationship between water input and velocity but at low effective pressures (Harper et al., 2007), whilst others observed greater correlation between velocity and total water storage (Vieli et al., 2004).

2.3.1.2 Distributed and channelised subglacial drainage

It was established in section 2.3.1.1 that water flowing under a glacier can do so in a very thin film, or through a series of linked cavities, and that in these configurations the restricted nature of the flow leads to pressurisation of the system above atmospheric pressure (Röthlisberger, 1972; Shreve, 1972). A range of overlapping and interchangeable

terms have been established to describe these configurations, including “inefficient”, “slow”, “un-channelised”, “non-arborescent”, and “anatomising” (Davison, 2019). For consistency, they will be referred to throughout this thesis as “**distributed**”.

The alternate configuration of the flow of water in a subglacial system is through a network of channels. Channels can either be melted into the base of the ice (Rothlisberger, 1972; Hooke et al, 1990), or incised into the bed (Nye, 1976). Due to the consistently higher cross sectional area and interconnectedness of channels, water flow will be faster, and at lower pressure when compared with flow through distributed systems (Rothlisberger, 1972). The range of terms established for these systems are reflective of this and include “fast”, “arborescent”, and “efficient” (Davison, 2019). For consistency, they will be referred to throughout this thesis as “**channelised**”.

All subglacial drainage forms discussed to this point have been in hard bedded glacier contexts, but channelised (e.g. canals (Kyrke-Smith and Folwer, 2014) and distributed (e.g. porous flow (Boulton et al., 2001)) drainage configurations have also been identified in sediment rich soft bedded contexts.

Figure 2.3 illustrates in cross section a range of different configurations of distributed and channelised subglacial drainage in both hard and soft bedded contexts, as discussed above. Figure 2.4 illustrates schematics of idealised channelised and distributed flow in cross section, along ice motion longitudinal section, and planform view.

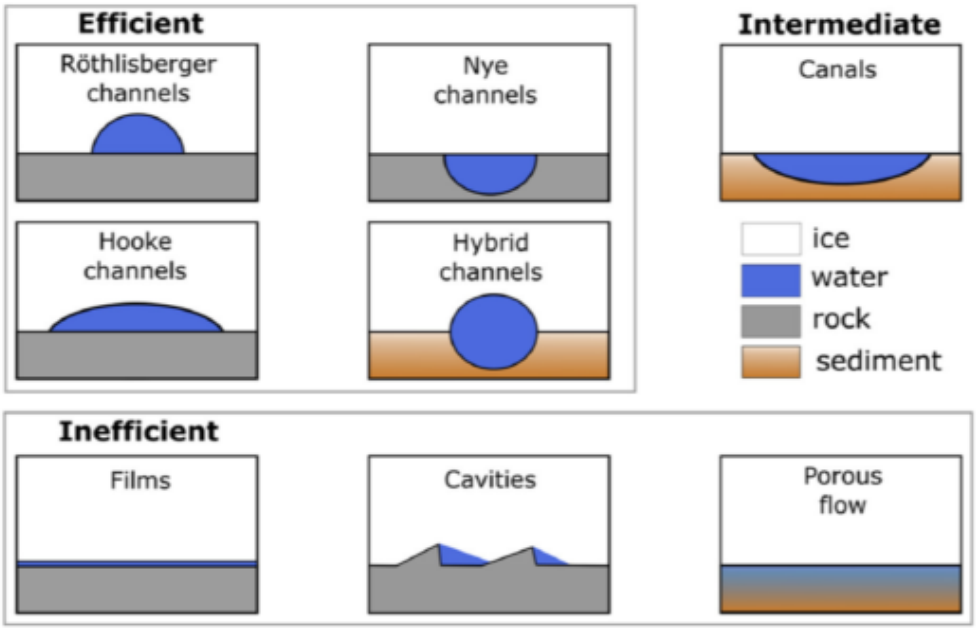

Figure 2.3 Conceptualised channelised (efficient), and distributed (inefficient), and example intermediary subglacial drainage forms. Channels and cavities are depicted as filled with water, but this will not always be the case. Ice flow is into the page, except for inefficient cavities, where ice flow is left to right (reproduced from Davison et al. (2019)).

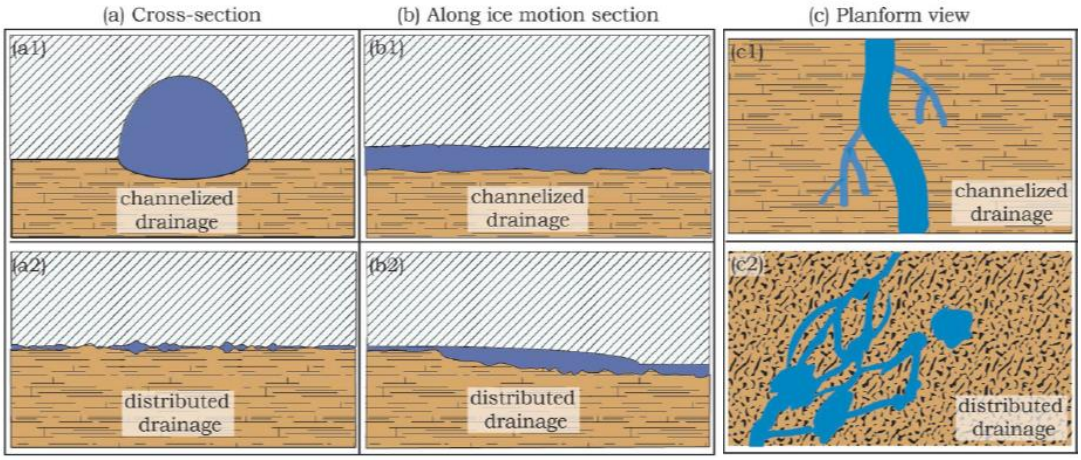

Figure 2.4 Schematic views of channelised and distributed subglacial drainage systems in A) cross section, B) along ice motion longitudinal section, C) planform view. Reproduced from Grau Galofre et al. (2022).

2.3.1.3 Seasonal evolution of subglacial drainage configuration

So far in this section channelised and distributed drainage configurations have been introduced separately for clarity. However, it is now well established that channelised and distributed configurations are end-members on a continuum, and that configurations will shift and evolve through space and time (Hubbard and Nienow, 1997; Schoof, 2010; Greenwood et al., 2016; Davison et al., 2019). A commonly proposed model of seasonal

evolution of subglacial hydrological configuration is shown in the schematics in Figure 2.5. The initial condition before the melt season is a distributed system. At melt onset this becomes pressurised and ice velocity increases. As meltwater input to the system is sustained, linked cavities expand and form a channel. Flow becomes efficient and depressurises, slowing ice velocity. Creep closure due to low basal water pressure causes the channel to reduce in diameter and late season melt events can potentially repressurise the system causing ice velocity to increase. Post melt season, the channel closes completely and the system reverts to a distributed system. This conceptual model explains the patterns in seasonal ice dynamics seen by Iken et al. (1983), discussed in section 2.3.1.1, which have also been widely observed on many other alpine glaciers (Nienow et al., 1998; Mair et al., 2003; Vincent and Moreau, 2016).

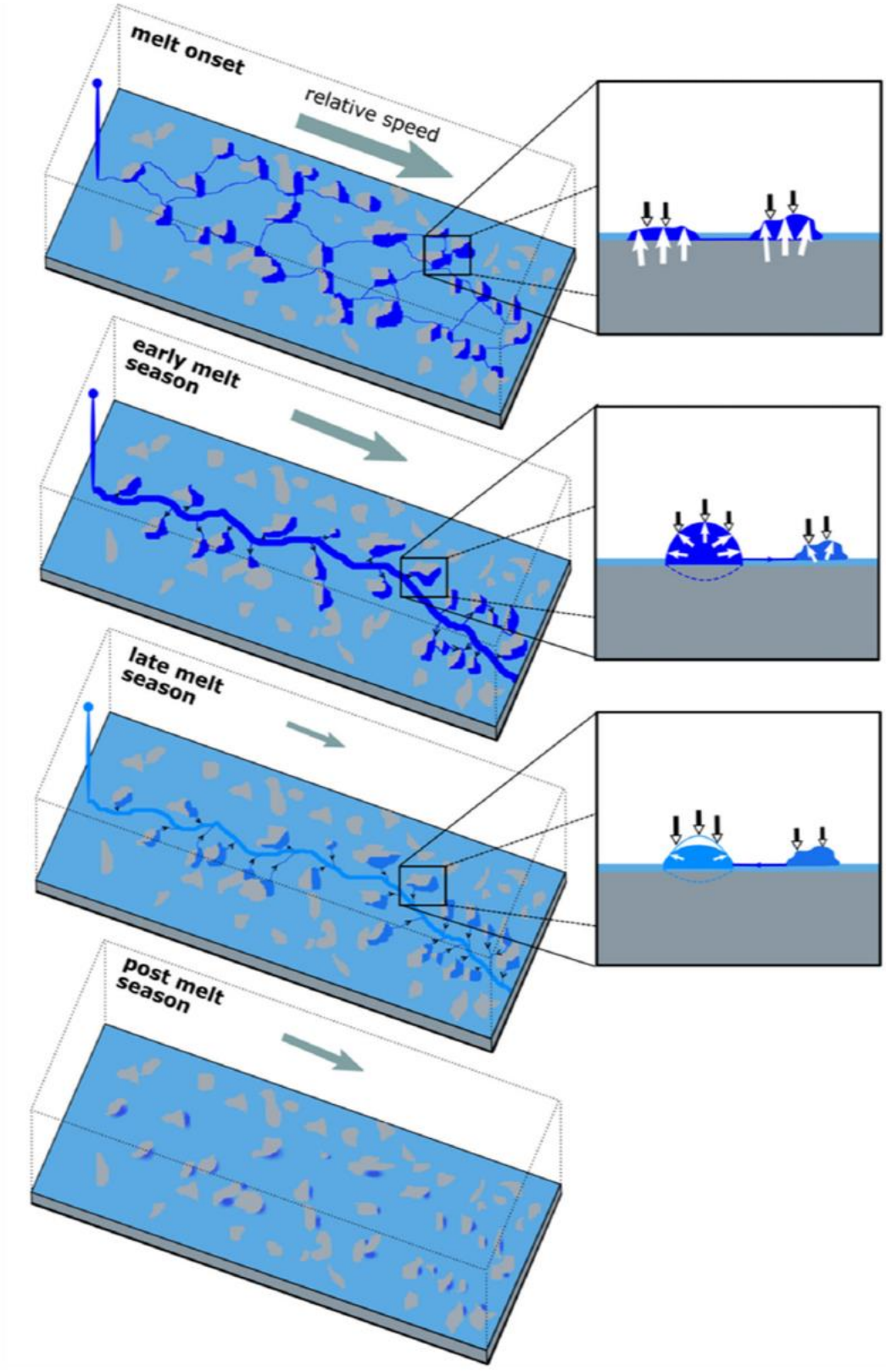

Figure 2.5 Schematic of active drainage system hydro-dynamic interactions. (Left) Black arrows indicate water flow direction. (Right) Cavity cross-sections – black and white arrows indicate closing and opening mechanisms , respectively. Size of grey arrows in left panels indicate velocity change from preceding period. Blue shading indicates basal water pressure (darker equals higher pressure). Figure and caption reproduced from Davison et al. (2019).

The conceptual model of seasonal evolution of subglacial drainage configuration presented above means that the impact of melt being delivered into the glacial system may not be limited to an immediate change in velocity. For example, there have been observations of water stored subglacially in upglacier areas over winter due to late drainage of firn in the accumulation area that then encounters a subglacial system with low transmissivity due to early conduit closure in these areas. These upglacier areas then effectively have a 'head start' at the onset of the melt season next spring and so can speedup very quickly, but then also transition to efficient drainage much more quickly with an associated summer low in velocity (Hodge, 1974; Holmlund and Hooke, 1983; Iken and Bindschadler, 1986; Kamb and Engelhardt, 1987; Krimmel and Vaughn, 1987). Similar processes have been hypothesised to explain recent observations of autumn velocity accelerations. Such seasonal velocity signals are considered quite rare and are not frequently reported within the literature (Nanni et al., 2023). In the few studies which do present autumn accelerations, the explanatory mechanism suggested is late season reduced subglacial drainage efficiency (due to onset of subglacial channel closure through creep closure as melt decreases) being particularly susceptible to a sudden influx of water which could be from rainfall events, drainage of supraglacial lakes, or release of stored water such as firn aquifers (Hodge, 1974; Sugiyama and Gudmundsson, 2003; Harper et al., 2005; Hart et al., 2019; Nanni et al., 2023).

Nanni et al.'s (2023) comprehensive study of 48 glaciers in the western Pamirs is particularly insightful in providing evidence to support this hypothesis. They found that whilst the spring speedup events observed showed an up glacier migration (e.g. speedup happened closest to the terminus first) due to melt onset occurring earlier at lower elevation, the pattern for the autumn speedup events was reversed with initiation at higher elevations *first* which then migrated further downglacier over time (Figure 2.6). This is as would be expected if the cause of the speedup was a switch back from channelised to distributed drainage configuration. Melt onset occurring later (and total melt being lower) at higher elevations should result in channelised drainage systems further upglacier in the system becoming less well developed initially, and the earlier decrease of melt at these higher elevations means creep closure processes in subglacial channels will start earlier than at lower elevations down glacier.

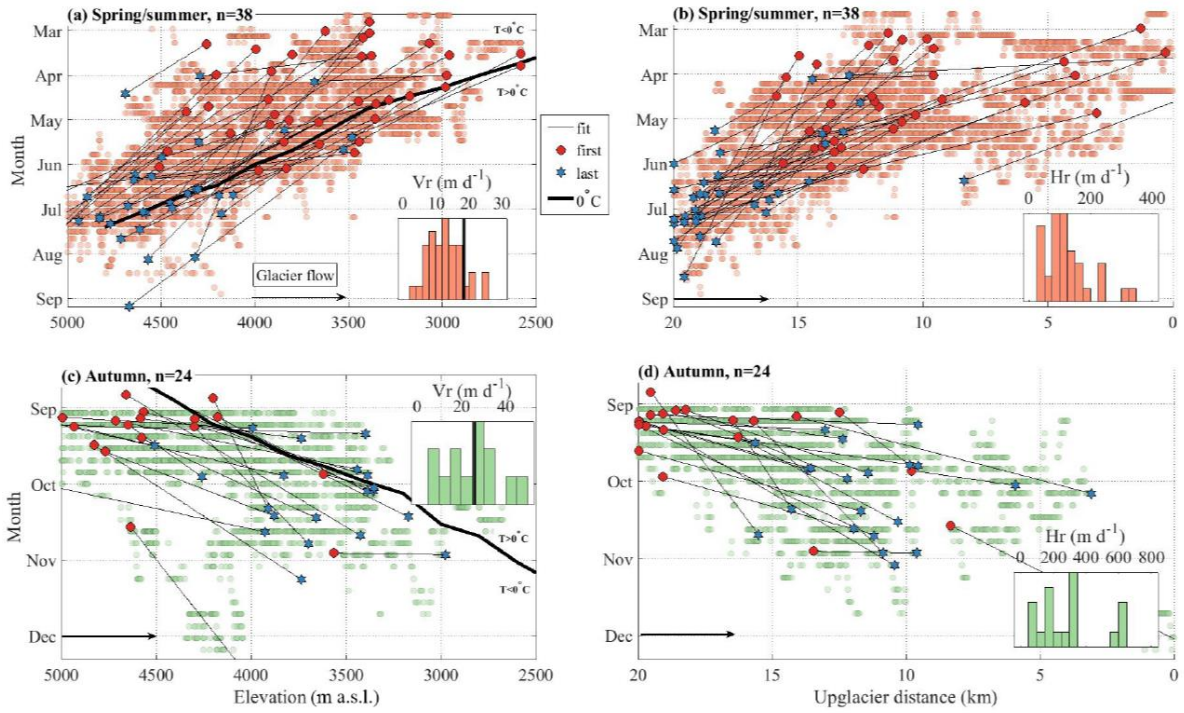

Figure 2.6 Example of downglacier migration of autumn speedup events. Points mark the elevation and upglacier distance of first and last observed locations of speedup in spring and autumn for each glacier in the study. Reproduced from Nanni et al. (2023)

It is also worthy of note that in their data Nanni et al. (2023) found examples both where locations on a glacier demonstrated spring / summer accelerations and autumn accelerations, and examples where only autumn accelerations occurred. The examples of the autumn only accelerations in the Pamirs were all located at higher elevations in the upper reaches of the study area (Figure 2.7). This suggests that in these regions insufficient melt was getting to the ice bed interface in spring and summer to cause a speedup, and that the autumn accelerations were likely due to a subglacial drainage configuration that had remained distributed all year being overwhelmed by the release of stored runoff at a period sometime after the melt initially occurred.

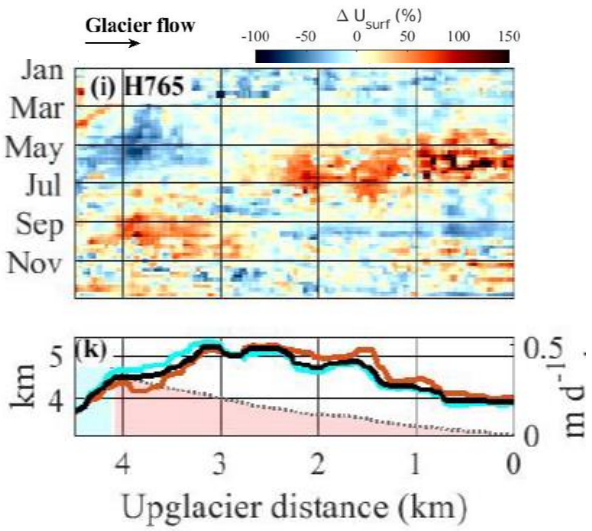

Figure 2.7 An example of Hadyrsha 756 Glacier in the western Pamirs which demonstrates seasonal ice velocity speedup only in the autumn in the region between 3-4 km upglacier. Note that in the region 0-2.5 km from the terminus there are clear velocity peaks in both spring / summer and autumn, but at the upglacier end c. 3.5 km from the terminus there is only an autumn peak. Figure and caption reproduced from Nanni et al. (2023)

2.3.1.4 Subglacial hydrology in ice sheet contexts

It is important to acknowledge that until relatively recently, our understanding of the importance of subglacial hydrology on the dynamics of the GrIS (and subsequently the role it plays in mass loss) was extremely limited. The previous studies discussed so far in this chapter (sections 2.3.1.1 - 2.3.1.2) almost exclusively relate to work undertaken at alpine glaciers, and it is in these contexts where development of fundamental theory occurred. Until the early 2000s it was estimated that, in terms of ice velocity, the ice sheet as a whole would likely respond slowly to increased air temperatures resulting from climate change due to the period of time required to conduct heat from the surface through many thousands of meters of ice to the bed (Alley and Whillans, 1984; Reeh, 1985; Zwally et al., 2002). Speedup in ice velocity concurrent with summer surface melt had been observed at some Greenland outlet glaciers (Reeh and Olesen, 1986; Joughin et al., 1996; Mohr et al., 1998), but this was assumed to be limited to very fast flowing ice near the margin. No evidence of seasonal ice velocity speedup in other areas (e.g. slower moving ice, and areas further inland towards the ELA) had been observed, and even on some very fast moving outlet glaciers such as Jakobshavn Isbræ, field studies had not observed patterns of summer speedup even far below the ELA within c. 30 km of the calving front (Echelmeyer and

Harrison, 1990; Zwally et al., 2002).

The landmark study of Zwally et al. (2002) was the first to observe a summer speedup event linked to surface melt much further inland on the GrIS (near the ELA) than previous studies. This opened up the possibility that some of the theory relating to subglacial hydrology developed in alpine contexts over the previous 50 years might be applicable in ice sheet contexts, and that as a result, the dynamic response of the ice sheet to climate change might be much quicker than previously thought (Nienow et al., 2017). A further study by Das et al. (2008) directly linked the drainage of supraglacial lakes to summer speedup events and demonstrated that delivery of surface melt water to the bed via hydrofracture was possible even through ice nearly 1,000 m thick as long as melt volume was sustained to keep fractures full, as is the case when a crevasse is under an overlying lake. Such hydrofracture also requires an existing fracture or weakness to be exploited. The establishment of the fact that the surface and the bed of the GrIS are hydrodynamically linked (even in areas of thick ice, far from the margin, near the ELA), prompted a profusion of studies into this previously largely ignored area. There are a number of full and detailed reviews on the subglacial hydrology of the GrIS and the reader is referred to these for a comprehensive coverage of the last 20 years of scientific progress (see Chu, 2014; Greenwood et al., 2016; Nienow et al., 2017; Davison et al., 2019). What follows here is a more selected review of the key issues which are directly related to the aims of this thesis.

2.3.1.5 Ice flow self-regulation: limits and thresholds

It is now universally accepted that it is possible for surface melt water to access the bed of the GrIS, and that this will exert some control on the dynamics of ice flow (see section 2.3.1.4). The exact nature of these controls, and crucially, whether the impact of increasing surface melt rates under warming future climate scenarios will result in net increases or decreases in total ice flux is still uncertain. Some studies have suggested that increased surface melt runoff in a warming climate will initiate positive feedbacks by increased lubrication of the bed leading to increased ice velocity causing dynamic thinning, possibly also reducing the stability of soft beds, and therefore hastening the retreat of the ice sheet (Zwally et al., 2002; Parizek and Alley, 2004; Palmer et al., 2011; Shannon et al., 2013; Bougamont et al., 2014). The counter view is that as has been observed in alpine valley glaciers (see sections 2.3.1.1 - 2.3.1.2), high melt will cause efficient channelised subglacial

drainage configurations to occur causing late season slowdowns, and increasing melt may result in this occurring earlier in the melt season, and at areas increasingly further inland, and that this negative feedback could be sufficient for increasing melt rates to decrease net ice flux (Nienow et al., 2017). Late season slowdowns have been recorded since the hydrodynamic links in Greenland were first observed; indeed Zwally et al. (2002) noted this in their study. The key question is whether the increased velocities driven by the initial melt will be offset by the subsequent slowdown once subglacial drainage has become channelised. The complexity of this question is increased further as it has been demonstrated by both observation (Sundal et al., 2011) and modelling (Schoof, 2010) that evolution to channelised subglacial drainage only occurs when threshold levels of melt are exceeded. As such, a given position on a glacier or ice sheet may see a velocity slowdown resulting from channelisation in some years but not others, depending on the melt levels in that year (Figure 2.8). It follows therefore, that an inland limit of channelisation should exist on the GrIS, and that this may migrate from year to year based on melt variability (De Fleurian et al., 2016; Koziol and Arnold, 2018).

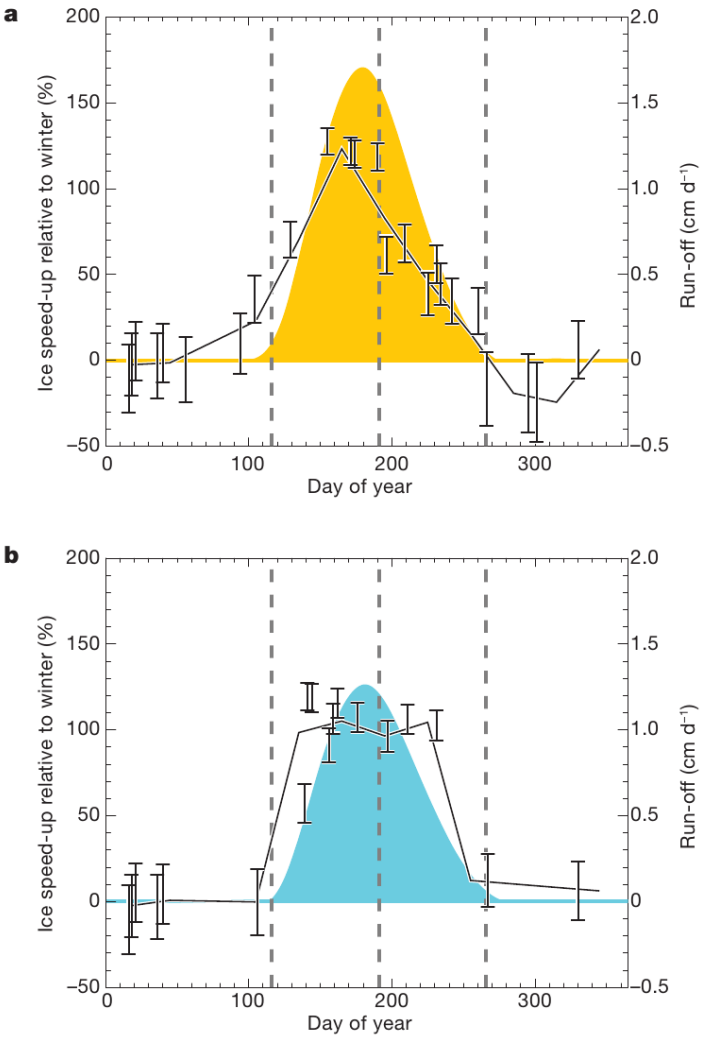

Figure 2.8 Graphs showing the seasonal velocity patterns for 5 major glaciers in the land terminating sector in the SW of the Greenland ice sheet. Velocities are derived from satellite observations and are 35 day averages relative to winter means, taken within the 500-600 m surface elevation band. Individual velocity measurements are shown as points with one -sigma uncertainty. Solid lines show monthly average velocity. Shaded coloured areas are modelled estimates of daily surface run-off rates. A) Speed-up in years of high melting (1995 and 1998). B) Speed-up in years of low melting (1993, 1996, and 1997). Figure and caption reproduced from Sundal et al. (2011).

A number of studies have attempted to determine the net effect of increased melt on dynamic ice flux, and there appears to be some consensus from studies covering the period of warming between the late 1990s and 2012 that slowdown due to enhanced channelisation later in the season did offset increased velocity earlier in the season under higher melt scenarios (van de Wal et al., 2008; Sole et al., 2013; Tedstone et al., 2013, 2015; Van De Wal et al., 2015; Stevens et al., 2016). Put simply, these studies found that at annual timescales ice motion did not scale with melt, and higher melt scenarios apparently led to reduced overall net ice flux.

There are some caveats that need to be applied to these findings (i.e. those that suggest net reduction of ice flux under increased melt conditions). Most studies conducted to date have been quite limited spatially, focused almost entirely in the ablation zone of the land terminating sector of the GrIS, with the majority of studies only considering individual glaciers or small selections of glaciers. Figure 2.9 gives a fairly comprehensive review of the relevant body of work on channelisation patterns and limits, and illustrates graphically how constrained the area covered by existing research is. In part, the limited spatial coverage is due to the logistical complexity and cost of field observation techniques. The only method to truly directly measure the conditions at the bed is to drill boreholes to measure basal water pressure (Meierbachtol et al., 2013). The challenges this presents are obvious, and increase as study sites move inland, further from support infrastructure, and into areas of thicker ice.

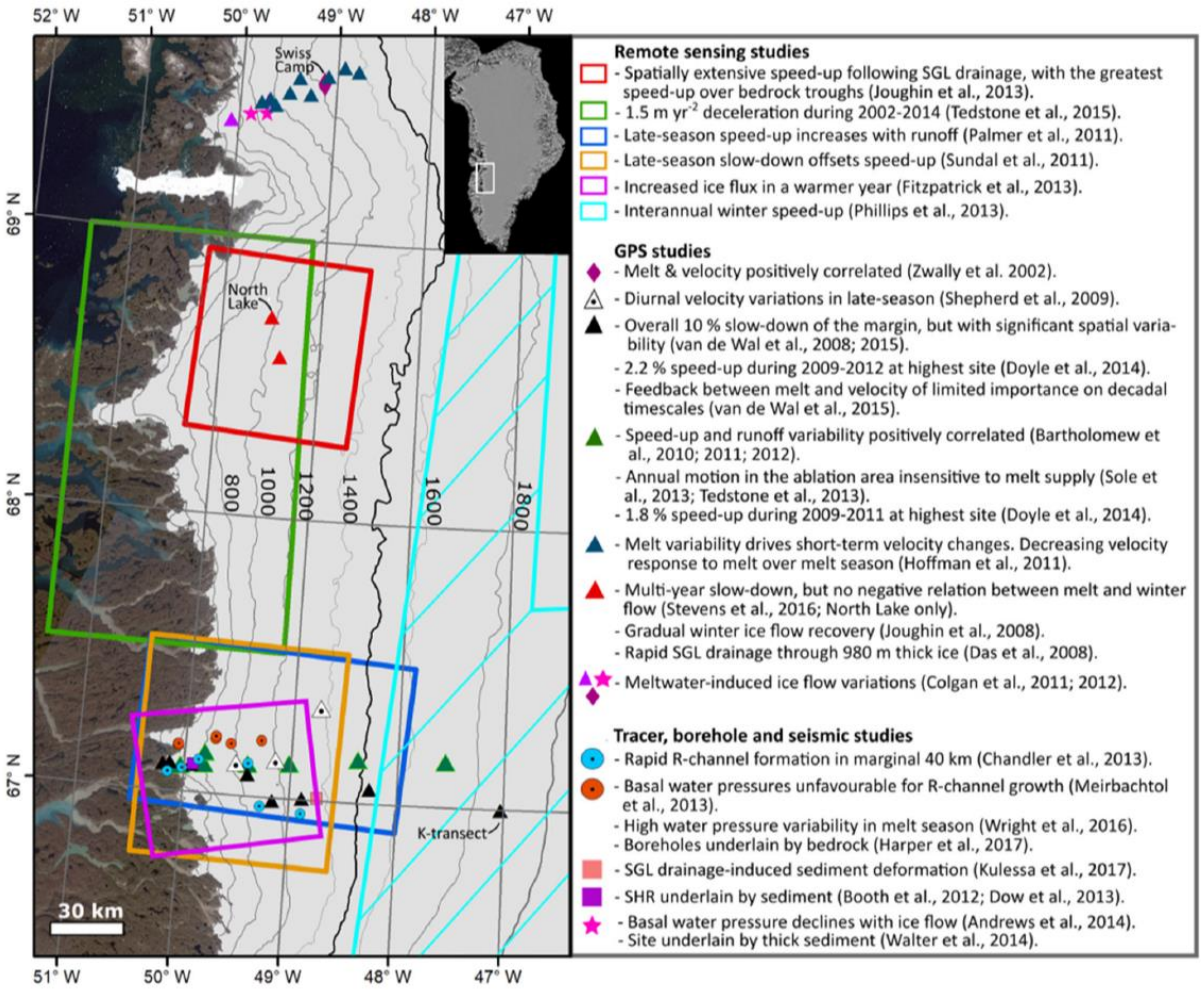

Figure 2.9 Overview of key observations on studies investigating hydrology and ice dynamics in Greenland, reproduced from Davison et al. (2019). The bold contour (1,500m) represents the approximate elevation of the equilibrium line during 1991–2011.

Recent advances in the development of remote probes (such as 'Cryoeggs' (Prior-Jones et al., 2021)) that can allow the monitoring of basal water pressure by positioning probes via moulins (rather than requiring boreholes to be drilled), could offer the possibility of greatly increasing the amount of direct measurement, but even such approaches are far from straight forward (Prior-Jones et al., 2021). Tracer studies have also been used to infer basal conditions from the transit time of dye through the glacial system (Chandler et al., 2013). Despite the value of such measurements, the logistical complexity means that the total body of data collected using these approaches in ice sheet contexts is quite limited (Davison et al., 2019). Whilst still being challenging to deploy (and maintain), installation of Global Navigation Satellite Systems (GNSS) equipment to measure changes in ice elevation and velocity (from which subglacial hydrological configuration can be inferred based on expected dynamic response), offers the benefit of being left in situ to collect longitudinal datasets with relatively limited intervention. GNSS data has led to major developments in our understanding of how subglacial systems operate (Zwally et al., 2002; Hoffman et al., 2011; Sole et al., 2013; Tedstone et al., 2013; Doyle et al., 2014), but as with tracer studies, the amount and coverage of this point data is sparse (Davison et al., 2019). Studies covering larger areas rely on velocity data derived from satellite imagery (Joughin et al., 2013; Tedstone et al., 2015; Williams et al., 2020). Satellite imagery derived velocity approaches have historically been limited by the interval of repeat imagery acquisition and the high computational demands of processing (Rosenau et al., 2015), but advances in computing power and the launch of new satellite constellations such as the European Space Agency (ESA) Sentinels 1 and 2 has made ice sheet wide 6 day average velocity data available in recent years (Vijay et al., 2019; Solgaard et al., 2022). All studies investigating ice dynamics at an ice sheet scale in Greenland have used remote sensing derived data. This is covered in more detail in section 2.3.1.8.

Whilst there has been a heavy focus in the existing body of literature on channelisation limits in the ablation zone, some studies have started to investigate seasonal ice dynamics driven by melt above the ELA, and this work indicates that the future response of the ice sheet may not be as simple as extrapolating out the patterns established in the ablation zone of higher melt equalling increased channelisation leading to a slowdown and a net annual decrease in ice flux. Both modelling (De Fleurian et al., 2016) and observational

(Doyle et al., 2014) studies have identified that above the current ELA, increased melt is likely to cause increased ice velocity without late season slowdown to below the winter average (Figure 2.10).

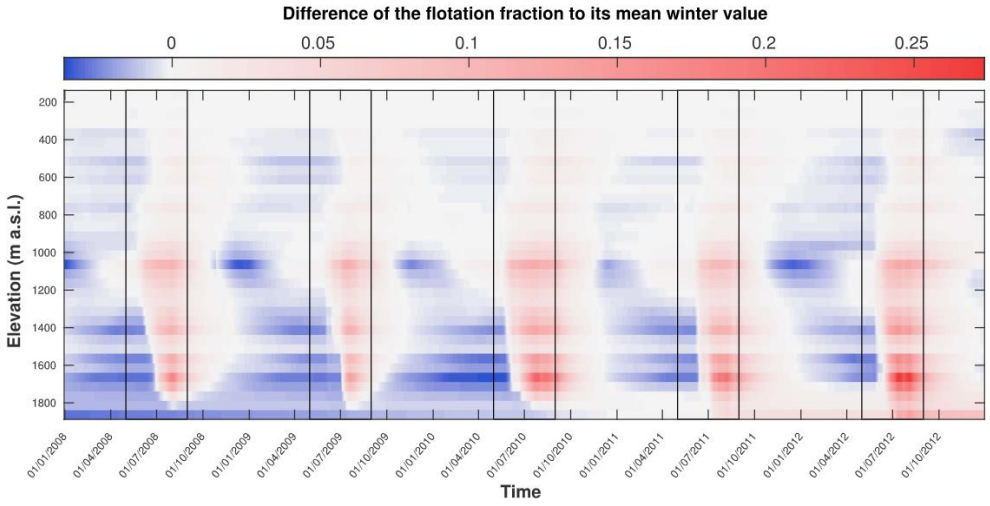

Figure 2.10 Seasonal evolution of the subglacial hydrology above the ELA for part of the land terminating sector of the ice sheet in SW Greenland. Black lines represent the start and end of summer. Reproduced from de Fleurian (2016).

The variation in the response of the ice sheet to increased melt around and above the ELA (compared to at lower elevations in the ablation zone) is hypothesised to be due to thicker ice and lower surface slopes restricting the development and sustained operation of efficient channels (Meierbachtol et al., 2013; Dow et al., 2014). Thus, increased melt would be associated with increased net ice flux in this zone of the ice sheet. Specific modelling of potential future melt scenarios in the land terminating sector of the south west GrIS has also found support for this hypothesis. Koziol and Arnold (2018) found that under a predicted 2100 melt regime of 4 x 2011 melt, despite channelisation encroaching 20 km further inland than modelled for 2012, enhanced creep closure rates due to thicker ice resulted in a substantive summer velocity increase, with no associated winter velocity decrease, leading to an overall net annual increase in ice velocity of 25%. As such, there is considerable uncertainty on the limits of future channelisation and the impact it may have on the future dynamics of the ice sheet, and this is commonly recommended as an area for future research.

2.3.1.6 Current established limits of channelisation

Limits of the current inland extent of channelisation are also uncertain. Table 2.1 summarises studies that have specifically identified whether subglacial drainage was channelised or distributed at a given location. It is important to note that for most studies the distance inland specified is not a limit, rather just the point at which the measurements were taken. The study by Chandler et al. (2013) conducted tracer measurements at multiple points on a longitudinal transect and therefore positioned the channelisation limit for Russell / Leverett (~ 67°N) glaciers at between ~ 41-57 km inland, under an ice thickness of between ~ 1,000-1,200 m. Modelling studies for Russell glacier also identified a specific limit of between ~ 35-50 km and an ice thickness of between ~ 800-1,100 m which corroborates field observations (De Fleurian et al., 2016; Koziol and Arnold, 2018). Studies which determined channelised / distributed configurations for a single point within this area around 67°N (but did not specify a specific limit) are in line with the ~ 35-57 km limit. It is interesting to note that the two of the three studies located further north (~ 70°N) than those around ~ 67°N identified distributed drainage much closer to the margin (~ 20-30 km inland) suggesting a parameter linked to latitude or climate was modulating the channelisation limit. Recent modelling studies have started to produce estimates of the likely limit of channelisation over more extensive areas of the ice sheet (Maier et al., 2022), and this work indicates that the controls on channelisation are likely multifaceted, complex, and spatially variable (Figure 2.11).

Table 2.1 Studies that have specifically attempted to define the limits of channelisation in subglacial drainage for the GRIS.

Authors	Finding	Distance inland	Ice thickness	Type of study	Location
Chandler et al. (2013)	Channelised drainage	~ 41 km	~1,000 m	Tracer	Russell / Leverett, SW Greenland (~ 67°N)
	Distributed drainage	~ 57 km	~ 1,200 m		
Chandler et al. (2021)	Channelised	~ 41 km	~900-1,000	Tracer	Leverett, SW Greenland (~

	drainage		m		67°N)
Van De Wal et al. (2015)	Channelised drainage	~ 13 km	~ 600 m	Borehole water pressure	Kangerlussuag, SW Greenland (~ 67°N)
Andrews et al. (2014)	Channelised drainage under moulins, but distributed in boreholes within 1.6 km	~ 20 km	~ 600 m	Borehole and moulin water pressure	FOXX, Sermeq Avannarleq, W Greenland (~ 69°N)
Meierbachtol et al. (2013)	Distributed drainage, minimal pressure variations	34 km	~ 830 m	Borehole water pressure	Isunnguata Sermia, SW Greenland (~ 67°N)
De Fleurian et al. (2016)	Channelised drainage	~ 50 km	~ 1,000-1,100m	Modelling	Russell, SW Greenland (~ 67°N)
Koziol and Arnold (2018)	2012 (high melt year), channelised drainage	~ 50 km	~ 1,000-1,100m	Modelling	Russell, SW Greenland (~ 67°N)
	2009 (low melt year), channelised drainage	~ 35 km	~ 800–900 m		
Dow et al. (2014)	Distributed drainage	~ 70 km	~ 1,200 m	Modelling	Russell, SW Greenland (~ 67°N)
Banwell et al. (2016)	Channelised drainage	~ 30 km	~ 1,000 m	Modelling	Paakitsoq, W Greenland (~ 69°N)
Doyle et al. (2018)	Distributed drainage	~ 30km	~ 600 m	Borehole water	Store, W Greenland (~

				pressure	70°N)
Maier et al. (2022)	Channelised drainage	Variable	Variable	Modelling	All W coast

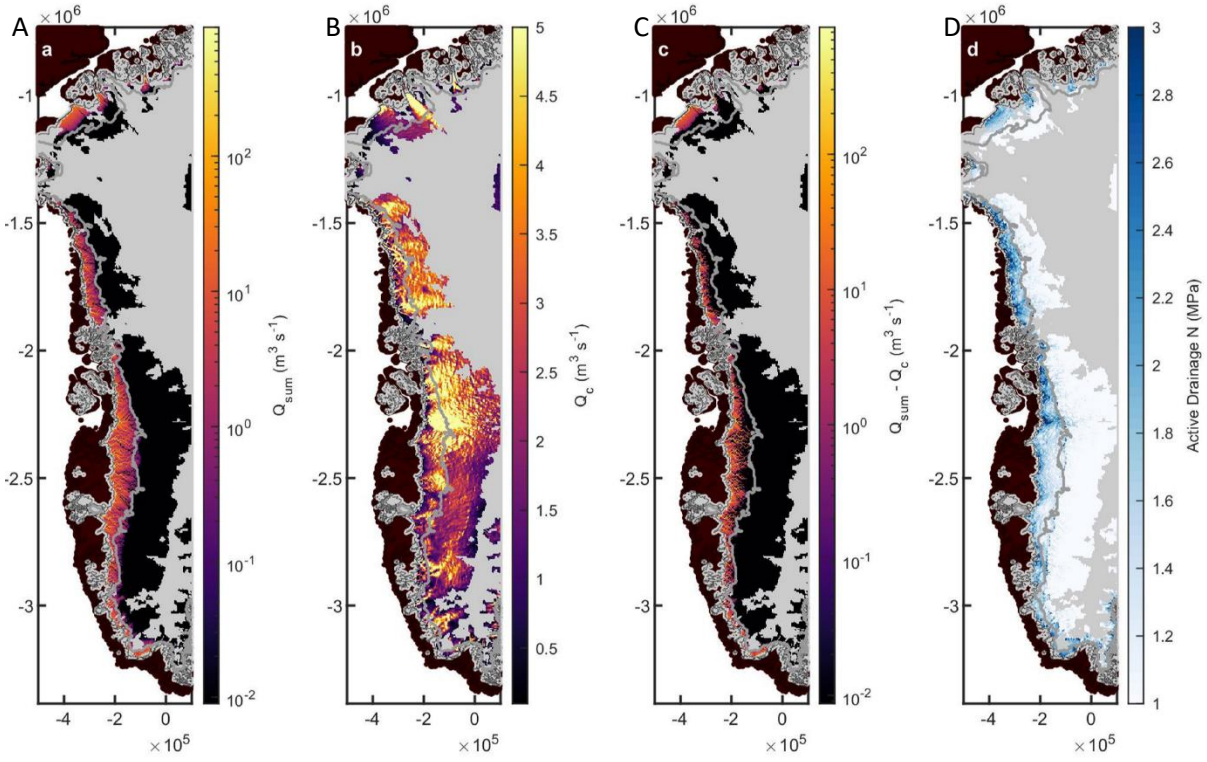

Figure 2.11 Drainage analysis of the Greenland Ice Sheet, figure and caption reproduced from Maier et al. (2022). A) Summer mean accumulated discharge (Qsum). B) Critical discharge (Qc) required for channel formation. C) Regions where the accumulated discharge exceeds the critical discharge indicating channel formation is likely. D) Modelled effective pressure within active drainage pathways. Figure and caption reproduced from Maier et al. (2022).

2.3.1.7 Multi year trends in ice velocity: land terminating sector in the SW of the GrIS

As was discussed at the beginning of section 2.3.1.5, processes have been identified in Greenland whereby melt reaching the bed caused lubrication and pressurisation of the ice / bed interface, reduced effective pressure and friction, and therefore caused ice velocity to increase, and this has the potential to cause year on year increases in ice velocity with increasing melt under warming climate scenarios (Zwally et al., 2002; Parizek and Alley, 2004; Palmer, 2011;Shannon et al., 2013; Bougamont et al., 2014). Alternatively, increased melt may increase channelisation which could offset any increases in ice velocity earlier in the melt season, or even cause a net decrease in annual ice velocity scenarios (van de Wal

et al., 2008; Sole et al., 2013; Tedstone et al., 2013, 2015; Van De Wal et al., 2015; Stevens et al., 2016). A number of studies have been conducted to explore how these processes may be controlling the longer term velocity trends of the GrIS and these will be considered in more detail here.

Multiple studies have suggested that during the sustained period of warming in the early 2000s net ice velocity decrease in the land terminating sector in the south west of the GrIS was widespread (Tedstone et al., 2015; Williams et al., 2020) (Figure 2.12a and b), and this was taken as evidence of the self-regulating effect of increased channelisation in scenarios of atmospheric warming. However, these signals of slowdown are not universally observed. A study by Joughin et al. (2018) found much more limited evidence of ice velocity slowdown than that reported by Tedstone et al. (2015) and Williams et al. (2020), and, in the area extending approximately 350 km further south of those studies, found almost no significant slowdown over the period 2000-2016 (Figure 2.12c). However, there is some difficulty in directly comparing these studies due to the differing methods adopted. Questions have been raised as to whether the methods adopted by Tedstone et al. (2015) and Williams et al. (2020) accurately reflected the true annual velocity changes (Joughin et al., 2018; Halas et al., 2023). This is as a result of decisions taken as to when satellite image pairs were selected (due to the limitations of feature tracking in optical imagery adopted as the method for velocity generation in these studies), how these are averaged, and that there is the potential for over representation of the summer signal when channelisation effects were at a maximum. The level of interannual velocity decrease observed in these studies is also relatively small (-1.5 m a^{-1} over 2002-2014 in Tedstone et al. (2015)) compared to the increase in velocity observed over each summer period (~100 m a^{-1}) meaning the possibility for bias in methods impacting on the result needs to be carefully considered. Joughin et al. (2018) adopted a different methodology in their study, using SAR imagery to generate winter velocities for comparison between years. As such, the concerns over timing and the relative weightings of summer signals are allayed, but if summer processes (such as enhanced channelisation) were causing a decrease in summer velocity, but not influencing winter velocities, then this will not be identified by this approach.

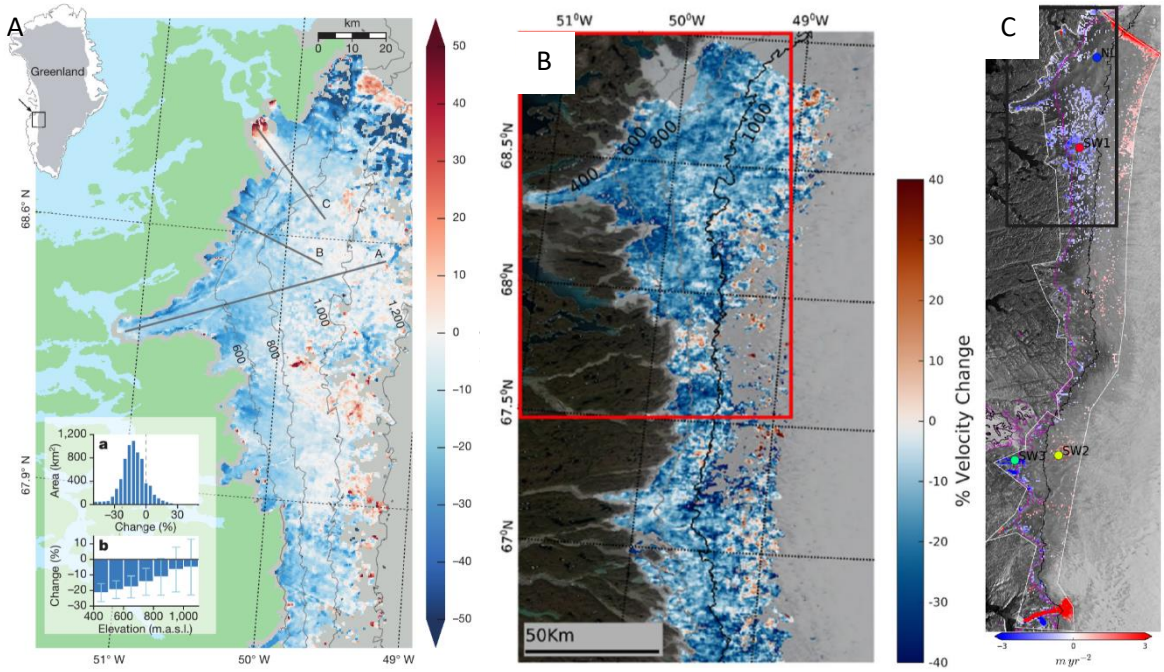

Figure 2.12 Ice velocity decrease in the SW of the GrIS. A) percentage change in ice velocities during the period 2007–14 compared with the period 1985–94, reproduced from Tedstone et al. (2015). B) percentage change in ice velocities during the period 2003-2012 compared with the period 1992-2003. The red rectangle shows the approximate area covered in pane a. Reproduced from Williams et al. (2020). C) significant ($p < 0.05$) trends (colour) for the period from winter 2000-2001 to 2016-2017 calculated for the area enclosed by the white outline. The black rectangle shows the approximate area covered in pane a. Reproduced from Joughin et al. (2018).

In addition to a slowdown between 2003-12, Williams et al. (2020) also observed a period of speedup between 2010-12 and 2017-19 (Figure 2.13a). This was hypothesised to be due to a reduction of ~15% in mean surface melt production coincident with a period of atmospheric cooling over this interval, and the associated decrease in channelisation that may be associated with such a reduction in melt. However, other studies have failed to reproduce this observation exactly. Halas et al. (2023) found agreement with the 2003-2012 slowdown identified by Williams et al. (2020), but observed a much more complex and spatially heterogeneous pattern of speedup and slowdown between 2012-2019 (Figure 2.13b).

In summary, there is some evidence to suggest a net slowdown of ice velocity in the south west of the GrIS concurrent with atmospheric warming in the period ~2000-2012, but the magnitude of this change, and the spatial extent over which a significant change in velocity was observed is uncertain. Due to different methodological approaches adopted by different studies, results may not be directly comparable, and further development of methods may be required to generate truly conclusive observations. However, there does not appear to be any evidence to suggest long term ice velocity speedup caused by atmospheric warming during the period 2000-2012. It seems likely that there was

subsequent acceleration in ice velocity in some areas of the land terminating sector in the south west of the GrIS coincident with the period of atmospheric cooling between 2013-2019 (Williams et al., 2020), but these trends appear complex and highly spatially variable, with some areas that experienced acceleration whilst neighbouring areas experienced further slowdown. As such, it must be concluded that there is not a simple linear response between atmospheric temperature and ice dynamics in this region of the ice sheet, and the processes operating are complex and multifaceted.

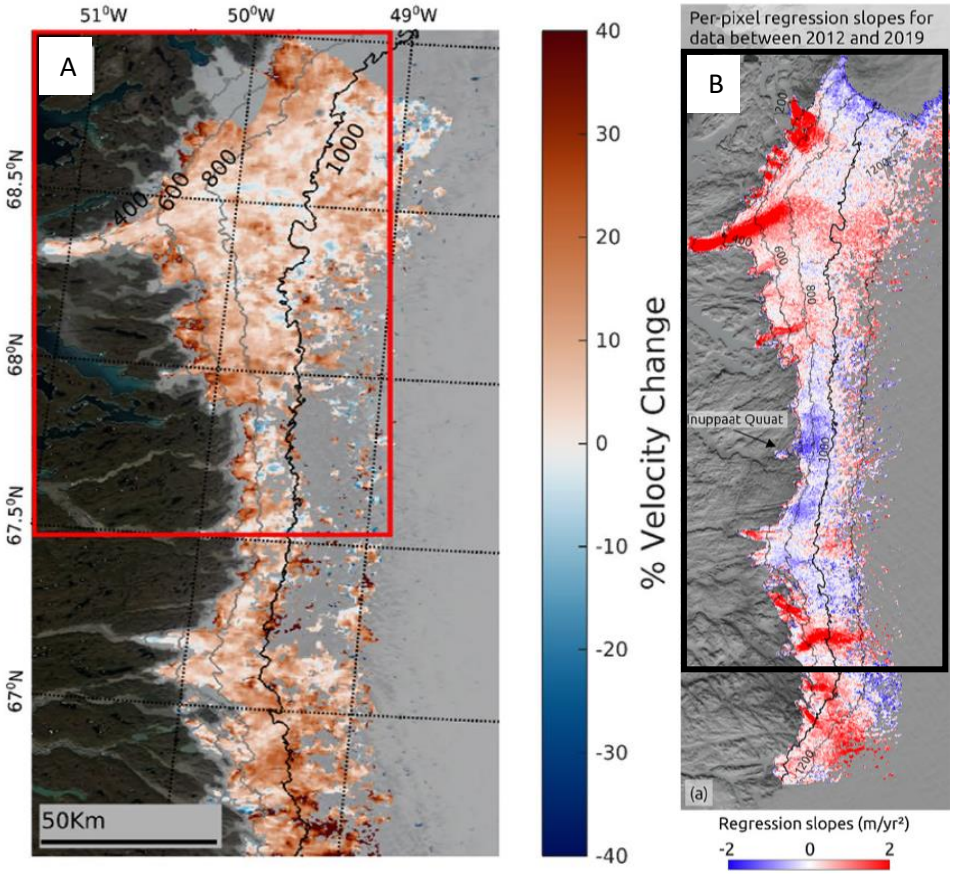

Figure 2.13 A) percentage change in ice velocities during the period 2010-2012 compared with the period 2017-2019. The red rectangle shows the approximate area covered in pane a in Figure 2.12. Reproduced from Williams et al. (2020). B) Map displaying the linear regression slopes computed on a per pixel basis from 2012-2019. Black rectangle shows the approximate area covered by pane a. Reproduced from Halas et al. (2023).

2.3.1.8 Multi year trends in ice velocity: beyond the south west

Much of the research conducted into multi year ice velocity trends in Greenland at the regional scale and above (e.g. covering more than c. 5-10 glaciers) has been focused in the land terminating sector in the south west of the ice sheet. There are likely two reasons for this. In the land terminating sector, the ice sheet is not subject to marine processes at the

margin, and so this acts as a real world laboratory for studying the control of subglacial hydrological process on ice dynamics without the confounding factors of marine influence (discussed further in section 2.3.2). There has also been a high density of field study in this sector which is inevitably self perpetuating over time, and therefore also draws focus from remote sensing based studies. In addition, many studies beyond the south west region have often focused on frontal retreat (Howat and Eddy, 2011) or total ice discharge (Enderlin et al., 2014) rather than specifically on changes in ice velocity. For example, Enderlin et al's. (2014) study '*An improved mass budget for the Greenland ice sheet*' determined annual ice velocity change for 178 Greenland outlet glaciers between 2000-2012 to allow mass budgets to be calculated, but there was no specific reporting or discussion of these velocity results within the paper. Overall, there is quite a limited body of literature exploring changes in ice velocity for the whole ice sheet scale at decadal timescales. The two major studies of note are those of Moon et al. (2012) and Rosenau et al. (2015), who both conducted ice sheet wide studies of over 200 glaciers between 2000-2012. Following a comprehensive review of the literature, it appears that there are no follow up studies of a similar nature investigating changes between 2012 and present (analogous to those studies by Williams et al. (2020) and Halas et al. (2023) for SW Greenland). The study by King et al. (2018) did extend analysis to 2016, but the analysis presented was highly spatially aggregated. This appears to be a major gap in our understanding of the macro scale long term dynamics of the GrIS and would warrant further study.

The study by Rosenau et al. (2015) calculated velocity for approximately 300 Greenland outlet glaciers between 1999-2012 with repeat velocity measurements every four years. Overarching findings of this study were that, over the study period as a whole, the patterns were highly spatially heterogenous in their distribution, but the majority of large outlet glaciers in NW, CW, and SE accelerated. N, NE, and CE showed no or very small changes (Figure 2.14). The most spatially coherent results were the consistent acceleration along a 1000 km stretch of the SE coast between 2003-2005, followed by an abrupt slowdown until 2008 (Rosenau et al., 2015). This trend in the SE was also observed by Murray et al. (2010). Moon et al. (2012) conducted a similar style of study to Rosenau et al. (2015) generating a decade long velocity inventory for over 200 Greenland outlet glaciers. Broad patterns were in agreement with Rosenau et al. (2015), but with some additional nuance in the analysis,

especially around the lack of a uniform pattern of synchronous regional velocity trends. For example, Moon et al. (2012) highlighted that in the NW region between 2000 – 2005 there was an average 8% speedup in ice velocity, followed by a further increase of 18% between 2005—2010. Despite this overall regional trend of acceleration, there was significant variation between the response of individual glaciers. A third of glaciers in the region accelerated steadily over the 10 year period, ~15% decelerated between 2000 – 2005 and then accelerated more rapidly between 2005 – 2010, a third of the glaciers showed no change, and ~25% slowed over the decade.

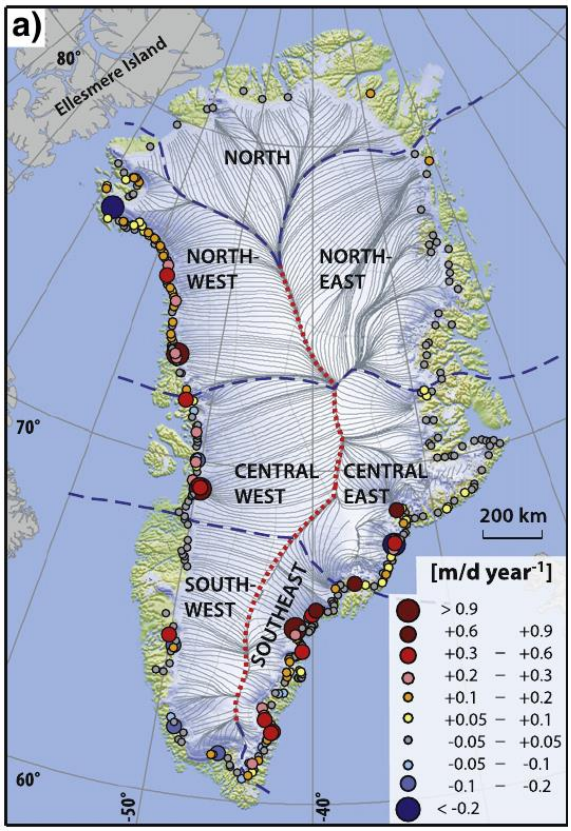

Figure 2.14 Linear velocity changes (1999–2012) for over 300 observed outlet glaciers. Reproduced from Rosenau et al. (2015).

Studies have been conducted considering ice velocity at the ice sheet scale, but over shorter, sub-decadal periods of ~5 years, or with a regional focus but for longer periods. For example, Joughin et al. (2010) covered all of Greenland but only between 2000/01 - 2005/06. Some heterogenous patterns were observed, but the overall conclusions were of much more widespread acceleration across the ice sheet than was found in other studies (Moon et al., 2012; Rosenau et al., 2015) over the same period. Again, the comparability of

results between studies with varying methodological approaches was raised here; due to data availability Joughin et al. (2010) calculated average velocity between Dec-Apr 2000/01, but used a later period of Sept-Jan for the 2005/06 average. This inconsistency may in part explain the more widespread pattern of acceleration observed. Hill et al. (2018) is an example of a study at a multi decadal timescale, but conducted regionally. The study focused on the northern sector of the GrIS over a 20 year period. Patterns of ice velocity showed substantial variability between outlet glaciers in close proximity to one another, with no consistent trend linked solely to patterns of atmospheric warming. Acceleration of ice velocity was found to be high where ice is grounded, but little or no change to ice velocity was observed where outlet glaciers terminate in a floating ice tongue.

2.3.2 Calving and marine processes

Marine processes and ice interactions at the margin have the capacity to influence ice velocity in a number of ways, including: force balances at the lateral margins, force balance at the bed (including both bed slope and flotation factors), sea temperature changes, subglacial melt discharge, and sea ice / mélange changes. For detailed discussion on these processes, including how our understanding has developed over the last 30 years, readers are referred to the excellent review paper by Catania et al. (2020). Key issues specifically pertinent to this thesis will be summarised in turn below.

2.3.2.1 Calving

Calving is a key mechanism of mass exchange through a glacier, and an extremely efficient means by which a glacier or ice sheet can lose mass very rapidly when not in equilibrium (Van der Veen, 2002). Where the rate of mass loss due to calving is higher than the rate of ice flux through the glacier, the ice front will retreat. Increased subsurface sea temperatures have the capacity to enhance subsurface melt rates at the terminus directly causing thinning and increased floatation (Motyka et al., 2003; Nick et al., 2009) which may increase ice velocity (Pfeffer, 2007). Increased calving rates will increase ice discharge, potentially leading to retreat of the calving front of a marine terminating glacier (Benn, Cowton, et al., 2017). Increased subsurface ocean temperatures also increases calving rates due to undercutting reducing terminus stability and therefore potentially increasing velocity (Motyka et al., 2003; Nick et al., 2009). Increased sea temperatures may also impact calving

rates by causing enhanced (or earlier seasonal onset of) sea ice and rigid mélange break up. The presence of sea ice and rigid mélange has been shown to supress calving rates and so a seasonal switch to open water conditions (or a longer term trend towards more open water conditions) may be linked to retreat of the calving front and associated velocity increase as discussed above (Sohn et al., 1998; Joughin, Das, et al., 2008; Amundson et al., 2010; Howat et al., 2010; Moon et al., 2015). As such, there are a variety of mechanisms whereby increased calving might be expected in warming climate scenarios where sea temperatures rise, potentially leading to frontal retreat of marine terminating glaciers.

Velocity increases linked to reduced stability as a result of retreat and enhanced calving have been observed to occur at a variety of spatial and temporal scales. Intra-annual (seasonal) patterns will be discussed in section 2.3.3, longer term inter-annual and multi-annual trends are discussed here.

One of the most prominent and well-studied examples given as an illustration of frontal retreat driven by enhanced calving is that observed on Jakobshavn Isbræ in the late 90s / early 2000s. Jakobshavn is the largest outlet glacier in Greenland and drains over 6% of the total ice sheet (Echelmeyer and Harrison, 1990). As a result of its importance to the overall mass balance of the GrIS, regularly repeated thickness and velocity measurements have been taken since 1991. The calving front at Jakobshavn had retreated ~26 km from the Little Ice Age (LIA) maximum by 1953 but stabilised in this position until the 1990s (Sohn et al., 1998). In 2000 a progressive retreat of the ice shelf was initiated leading to the almost complete disintegration by 2003. Coincident with this dramatic retreat of the calving front, ice velocity was observed to almost double from 5,700 m a^{-1} in 1992 to 9,400 m a^{-1} in 2000, and then further to 12,600 m a^{-1} by 2003 (Joughin et al., 2004).

A number of other studies have observed similar patterns of interannual ice velocity increase coincident with retreat of the calving front both on individual glaciers (Howat et al., 2005; Luckman et al., 2006; Nettles et al., 2008) and over multiple glaciers (Howat et al., 2008; Joughin et al., 2010; Murray et al., 2010; Bevan et al., 2012). As a result, by the late 2000s and into the early 2010s, it was widely hypothesised that there was a causal relationship between retreat and acceleration as reflected by the conclusions of Joughin et al. (2010 pg. 425) who stated that *"Our results for the whole ice sheet expand upon the conclusions of previous regional studies (Howat et al., 2005, 2008; Joughin et al., 2010) to*

indicate that where speed-up and retreat coincide, the speed-up is largely the result of the loss of resistive stress as the terminus recedes". Some modelling studies have also supported calving linked speedup and suggested that the ice dynamics of major outlet glaciers such as Helheim are not sensitive to melt (Nick et al., 2009). However, there was broad acknowledgement within these studies linking frontal retreat to ice velocity increase that this was not based on a full process understanding, and there are significant uncertainties about whether this is actually a cause and effect relationship (Andersen et al., 2010; Vieli and Nick, 2011). It is also clear that there is substantial variation in how different outlet glaciers respond to retreat of the calving front, and that retreat does not always result in velocity speedup. For example, Petermann Glacier, on the north coast of Greenland, experienced a substantial calving event in 2010 as a result of which over 25% (~20 km) of its floating ice shelf was lost. No subsequent increase in ice velocity was observed following this retreat (Nick et al., 2012).

A significant limitation to determining cause and effect of velocity speedups has been the spatial resolution of the velocity data used. Many studies cited in the paragraph above (e.g. (Joughin et al., 2010; Murray et al., 2010; Bevan et al., 2012)) rely on velocity measurements at a single point near the calving front to determine the speedup and slowdown of a glacier. Considering ice velocity in a one dimensional way like this means it is not possible to consider potential variable response in ice dynamics at different points on the glacier, or to investigate the timing and lag of velocity response at different distances upglacier from the calving front. More recent research which utilises a much greater range of velocity data to encompass spatial variation beyond a single point near the terminus, and of higher temporal resolution (e.g. weekly) than has previously been possible, has started to identify process relationships suggesting that at certain timescales (including inter-annual) surface melt may exert a much stronger control on variation in ice dynamics than has previously been considered likely. In particular, a novel study by Ultee et al. (2022) conducted normalised cross correlation analysis between runoff, terminus position, and ice velocity variability using a variety of lag periods. They found that in all years of their study, Helheim's ice velocity was at least as well correlated with runoff as with terminus position, and that the strongest correlations between ice velocity and terminus position were actually for negative lag periods indicating that terminus position may be *responding* to velocity variation rather

than *causing* the variation. They conclude that runoff is likely the dominant control on velocity variation at Helheim for seasonal and inter-annual timescales, but that terminus position is the dominant control over multi-annual timescales (2009-2017 in this case) (Ultee et al., 2022). Recent work by Larsen et al. (2023) has also demonstrated the varying control of runoff and terminus position on ice velocity at different points in the glacial system. They observed that at Upernavik Isstrøm II terminus position was the dominant control on velocity variation close to the terminus, but that this calving induced acceleration was only observable up to 6 km inland, and beyond this runoff controlled velocity variation became dominant.

Investigation of changes in ice dynamics at the ice sheet scale using data not limited to velocity measured at single points near the calving front of glaciers is extremely limited. Perhaps one of the only studies to do so is that of Williams et al. (2021) which compared multi-decadal ice velocity variation at the margin of 45 outlet glaciers (encompassing all regions of Greenland) to the velocity variations 50-100 km inland on these glaciers. They found a stark difference between the west and east coasts in terms of how far inland calving related acceleration could propagate. Propagation of acceleration was found to be almost ubiquitous on the west coast (even up to distances of >100 km inland), but not observed at all on the east coast (with the exception of Kangerlussuaq), affirming the complexity of these systems and suggesting that bed topography may be playing an important role in controlling ice dynamics (Williams, Gourmelen, and Nienow, 2021). These studies clearly highlight the limitation in restricting analysis to individual point locations close to the margin, both in terms of how representative the signals here are of the wider ice sheet, and in terms of being able to confidently ascertain cause and effect rather than basic correlation.

2.3.2.2 Forces at the lateral margins

Frontal retreat may influence ice velocity due to reduction in resistive stress between ice and both the fjord walls and the bed (Paterson, 1994; Howatt, 2005; Luckman, 2006; Howatt, 2008; Pfeffer, 2007; Carr, 2014). However, this will depend on the specific topographic conditions (both laterally and of the bed) at the point of retreat (Joughin 2004). Retreat into a laterally widening fjord will decrease the resistance provided by the fjord walls on ice flow, potentially increasing ice velocity and accelerating retreat further.

Conversely, retreat into a constricting fjord geometry may have a bottle necking effect, increasing resistive stress, stabilising retreat and decreasing velocity (O'Neel et al., 2005; Kochtitzky and Copland, 2022). A classic example which demonstrates both these processes is the pattern of ice dynamics as Columbia Glacier (Alaska, USA) retreated through Columbia Bay (see Figure 2.15, (McNabb and Hock, 2014)). Between 1989-1994 the section of the bay the glacier was retreating through is parallel sided and retreat was accelerating. Beyond this point the bay narrows to a pronounced bottle neck which forms a lateral topographic pinning point, and despite atmospheric warming over this period, retreat decelerated between 1994-2006. North of the bottle neck, the bay widens out substantially and between 2006-2012 retreat accelerated rapidly (McNabb and Hock, 2014).

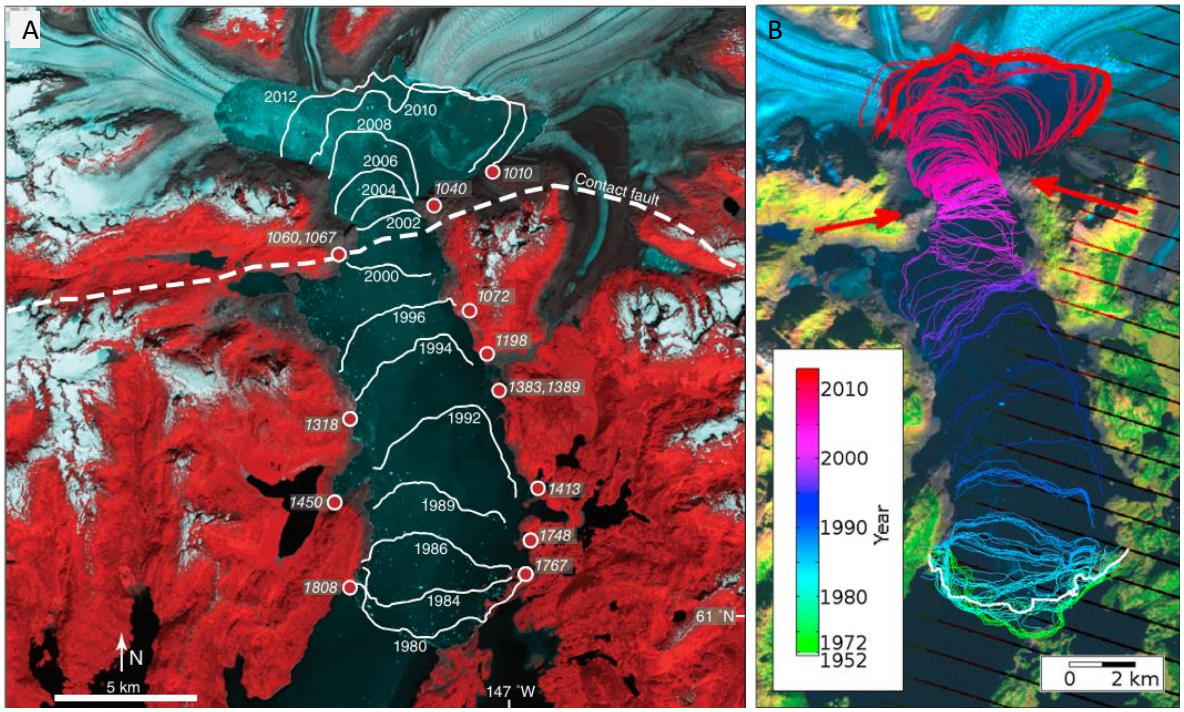

Figure 2.15 A) False-colour image of Columbia Glacier on 2 July 2014. Solid white lines indicate the retreating Columbia Glacier ice margin since 1980 (McNabb and Hock, 2014); Reproduced from (Carlson et al., 2017). B) Terminus positions over time for Columbia Glacier. Colour of terminus outline indicates the year from which the scene was acquired. Red arrows indicate location of topographic pinning points, where the glacier's retreat slowed dramatically during the period 2000–2004. Reproduced from McNabb and Hock (2014)

2.3.2.3 Force balance at the ice / bed interface

In the same way that a narrowing embayment may cause a lateral topographic pinning point, high points in the bed can act as vertical topographic pinning points and stabilise the retreat of outlet glaciers (Jamieson et al., 2012; Carr et al., 2015; Clason et al., 2016; Åkesson et al., 2018; O'Regan et al., 2021). The retreat of Humbolt Glacier (north

Greenland) provides an excellent case study for a number of mechanisms by which retreat can vary based on topographic conditions. At ~90 km, Humbolt Glacier is the widest marine terminating outlet glacier in Greenland (Carr et al., 2015). As such, despite being forced by broadly identical atmospheric and ocean conditions, its large width affords substantial variation in bed topography, and any variation in ice dynamics can be attributed to these (and other resulting physical properties of the glacier) rather than climate forcing. Figure 2.16 shows the retreat of Humbolt Glacier since 1975 which was extremely variable across the width of the glacier. In the southern section there has been almost no retreat. In the northern section, retreat increased with distance north from the boundary with the southern section as ocean depth increases reaching a maximum at the head of the deep trough at T1 (Figure 2.16a). North of the trough, the higher bed elevation acts as a pinning point greatly reducing the rate of retreat.

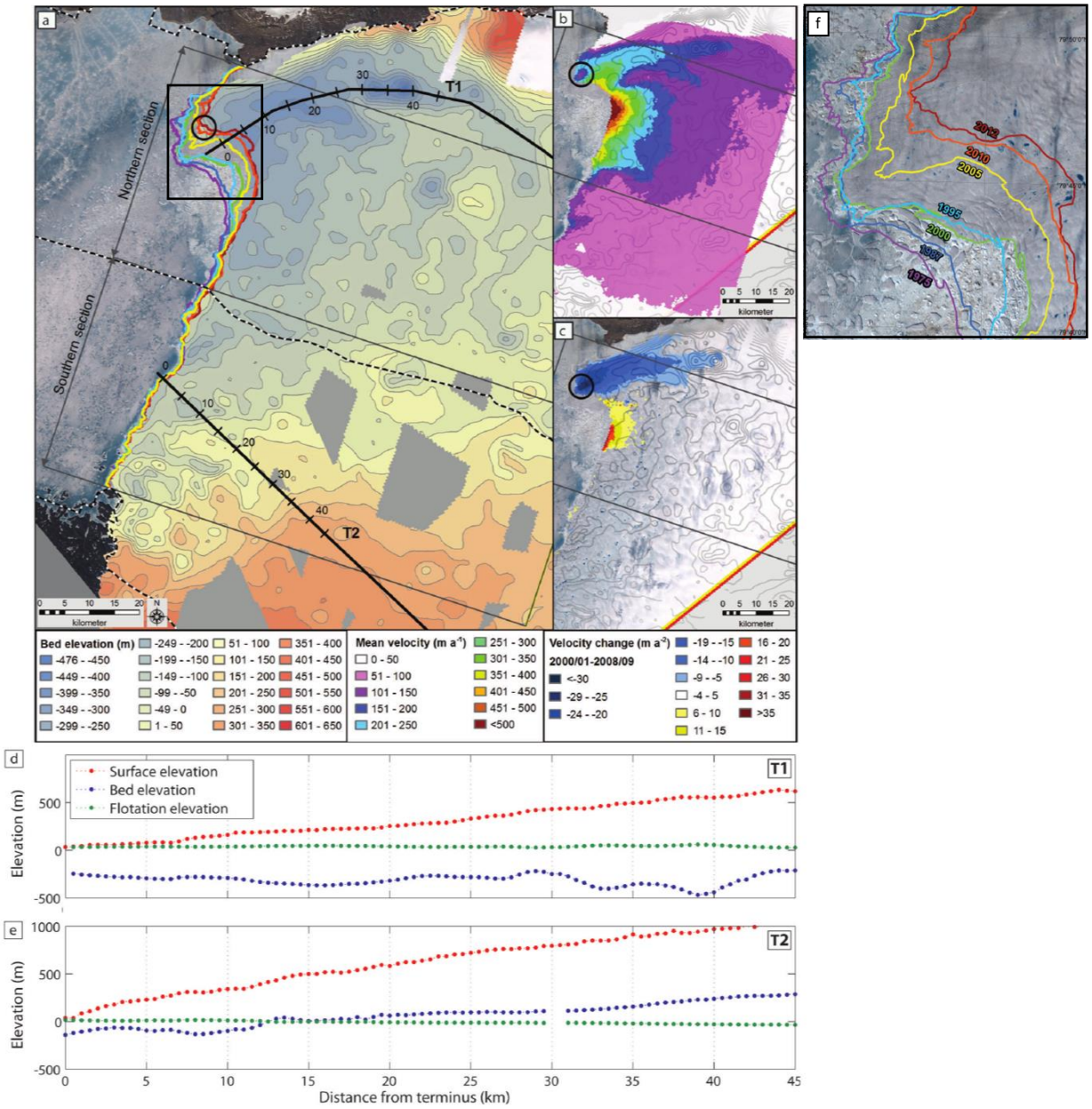

Figure 2.16 Basal topography and surface elevation profiles for Humbolt Glacier HG. A) Basal topography of HG, with frontal positions (colour-coded as in F), transects T1 and T2 (thick black lines) as shown in D and E, and potential basal pinning point (circled in black). B) Mean ice velocity field for HG (colour scale), overlain on basal topography (grey contours), and potential basal pinning point (circled in black). C) Change in ice velocity for HG between winter 2000/01 and 2008/09 (red-yellow: acceleration; blue: deceleration), overlain on basal topography (grey contours), and potential basal pinning point (circled in black). D, E) Surface elevation, basal topography and flotation elevation for transects along D) transect 1 and transect 2. F) Inset area marked by black rectangle in a showing years for retreat mapped. Figure and caption reproduced from Carr et al. (2015).

As retreat onto a pinning point of high ground in the bed will increase basal drag, reduce floatation, and inhibit retreat, retreat down an adverse bed slope into deeper water will increase floatation and reduce the resistive drag between the ice and the bed with resultant increases in ice velocity (Weertman, 1974; Schoof, 2007). Such accelerated ice velocity as a

calving front retreats down an adverse slope has been observed at numerous Greenland outlet glaciers. Kangerlussuaq Glacier on the east coast of Greenland experienced two periods of retreat, between 2004 – 2006 and between 2016 – 2019 where ice velocity and retreat rate both accelerated as the ice front moved down an adverse slope before stabilising on localised bedrock highs (Kehrl et al., 2017; Brough et al., 2019). The study by Catania et al. (2018) is perhaps the most comprehensive investigation of these processes. They studied 15 marine terminating glaciers on the west coast of Greenland and found widespread evidence that glacier retreat accelerates through wide overdeepened sections of the bed where bedslopes are adverse in gradient, and that the length of overdeepening upstream of the terminus at the time of retreat onset is a strong predictor (R^2 0.8) of total observed retreat (Figure 2.17).

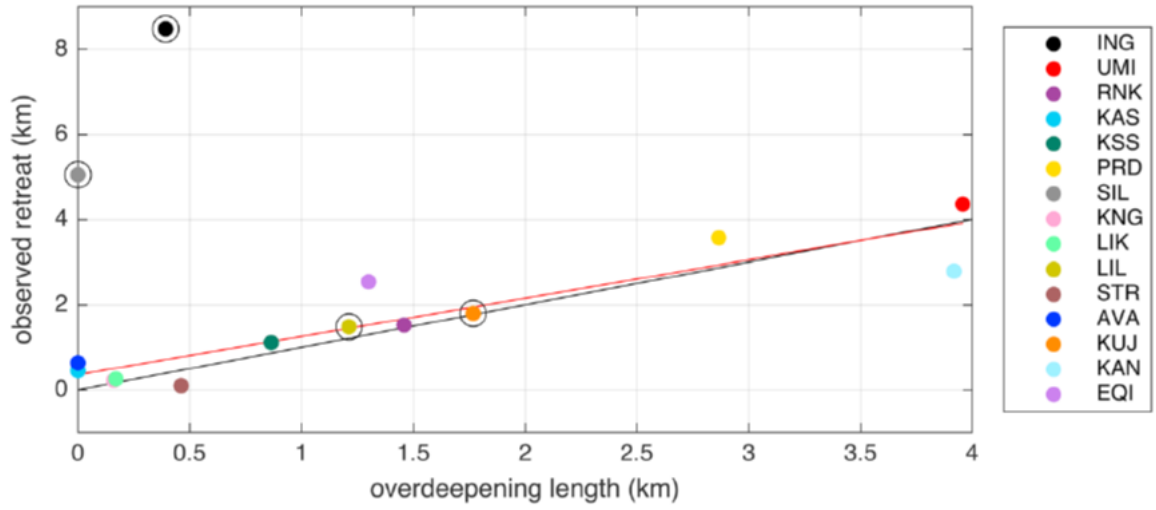

Figure 2.17 Overdeepening length upstream of the terminus at the time of progressive retreat onset plotted against total retreat observed since progressive retreat onset for 15 marine terminating glaciers on the West coast of Greenland. Points outlined with black circles have poorly constrained bed data at progressive retreat onset locations. The black line gives the 1:1 relationship. The red line shows a linear regression using only glaciers well constrained with MCBed. The R^2value of the linear regression is 0.8. Reproduced from Catania et al. (2018).

2.3.3 Intra annual / seasonal velocity variations

In sections 2.3.1.7 and 2.3.1.8 significant consideration was given to the longer term trends in ice velocity, and how external forcings may modulate velocity over the period of years to decades. Study on these timescales is important as it develops a picture of how glaciers respond to sustained forcings. However, many of the processes controlling the dynamics of outlet glaciers operate at much shorter timescales (of days, weeks and months), and so to

gain a full understanding of the processes controlling a glacier's motion, observations and analysis must also be undertaken at a timescale congruent to these processes (Greene et al., 2020). For clarity, throughout this thesis the term "seasonal" will be used to refer to processes and patterns at a sub annual timescale, associated with increases in temperature through spring and summer, followed by decreases in temperature through autumn and winter.

2.3.3.1 Early observations

Seasonal variations in ice velocity have been observed on a large number of glaciers in Greenland since the early 2000s, made possible by the ever expanding availability of high temporal and spatial resolution satellite imagery (Howat et al., 2010; Moon et al., 2014, 2015; King et al., 2018; Davison et al., 2020; Greene et al., 2020; Cheng et al., 2022). It is unclear whether such seasonal variations are a new phenomena resulting from climate warming over the last 25 years, or if they were previously simply undetected due to satellite imagery being less ubiquitous. It is established from field based survey using GNSS that Jakobshavn Isbræ is known to have been in a stable position with no seasonal variation in velocity in the mid 1980s (Echelmeyer and Harrison, 1990), but that significant seasonal variability has been observed since the early 2000s, coincident with increased atmospheric and ocean warming (Luckman et al., 2006). What does seem clear is that seasonal variations of ice velocity in Greenland are currently extremely widespread, and observed across all regions (King et al., 2018).

Early observations of seasonal variations in the dynamics of outlet glaciers in Greenland largely either focused on individual glaciers in some detail (such as for Jakobshavn in 1995, (Luckman and Murray, 2005), see Figure 2.18)) or multiple glaciers in less detail (e.g. Howat et al. (2008) which considered nine glaciers in west Greenland for 2001 and 2006, but only in terms of coarse differences in summer and winter average velocities).

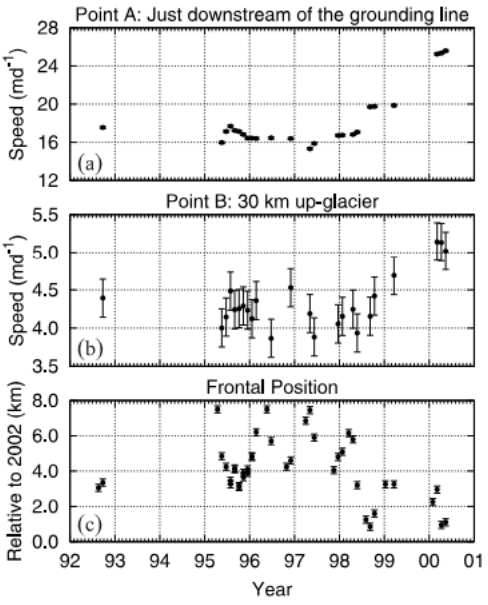

Figure 2.18 The evolution through the 1990s A) and B) of surface speeds at two points on Jakobshavn Isbræ. C) The frontal position relative to the approximate September 2002. Reproduced from Luckman and Murray (2005)

One of the first studies to consider seasonal velocity variation for multiple glaciers at relatively high temporal resolution in Greenland was that of Howat et al. (2010), which covered six glaciers in Uummannaq district on the west coast. This allowed the development of meaningful insight into the seasonal patterns of velocity variation, including the differing responses between glaciers, and for process interpretations to be hypothesised to explain these differences. For example, Figure 2.19a and Figure 2.19b show the seasonal velocity variations for Rink Glacier and Inngia Isbræ respectively. The two glaciers are within 50 km of one another and terminate in the same embayment so are both subject to almost identical atmospheric and ocean forcing. However, their seasonal velocity responses are very different. Ice velocity speedup at Rink Glacier appeared to coincide with sea ice clearing and the ice front position starting to retreat. Speedup continued throughout the summer as the ice front position continued to retreat, even once temperatures had started to decrease in June and July (Figure 2.19a). In contrast, at Ingria Isbræ ice velocity speedup started as temperature started to increase in mid-March almost a month before sea ice cleared and the ice front position started to retreat. Velocity started to slow as temperature started to decrease in June even whilst ice front position was still substantially retreating (Figure 2.19b). The interpretation of these differences is that at Rink Glacier, seasonal velocity variation was being driven predominantly by reduced back stress as a result of sea ice break

up and seasonal retreat of the ice front position (as discussed conceptually in sections 2.3.2.2 and 2.3.2.3, above), whereas at Inngia Isbræ seasonal velocity variation was being driven by melt accessing the bed causing lubrication and pressurisation of the subglacial hydrological system, reducing effective pressure and causing velocity to increase (as discussed conceptually in section 2.3.1) (Howat et al., 2010).

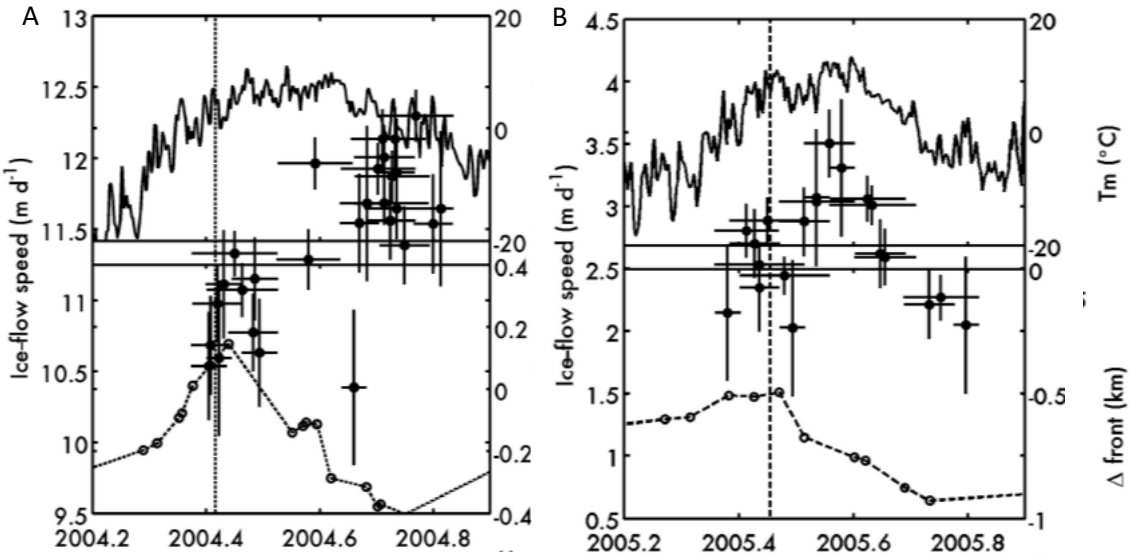

Figure 2.19 A) Ice-flow speed of Rink Glacier. The horizontal spans of the error bars denote the time separation of the images. Vertical hatches mark the day on which ice-free conditions are first observed at the glacier front in MODIS imagery. Circles with hatches are change in the ice-front position (negative values are retreat). The solid curve is mean daily air temperature B) The same data but for Inngia Isbræ. Figure and caption reproduced from Howat et al. (2010).

2.3.3.2 Typologies of seasonal velocity variation

Whilst early observations of seasonal velocity variations made in the 2000s identified that different glaciers may behave in different ways, the low number of glaciers studied (and the low number of years covered by studies), did not facilitate generalisations to be made from these results. In a landmark paper, Moon et al. (2014) leveraged the much more expansive satellite imagery data and ice velocity processing techniques that had become available to conduct a study of seasonal velocity variation covering 55 marine terminating glaciers distributed across the west and south east coasts of Greenland over five annual cycles between 2009-2013. Gaps in velocity data were minimal due to the utilisation of interferometric synthetic aperture radar speckle tracking techniques rather than optical satellite imagery (which can be highly occluded by cloud cover) used in earlier studies (Howat et al., 2008, 2010). In total the data coverage was sufficient for the analysis of

seasonal velocity patterns in 91% of cases giving a dataset of 249 individual glacier seasonal velocity patterns. Analysis of this dataset revealed three clearly distinct typologies of seasonal velocity variation, with 211 of 249 (88.8%) seasonal velocity patterns able to be confidently manually classified as one of these typologies. Moon et al. (2014) termed these typologies Type 1, Type 2, and Type 3 and these have been widely adopted in the subsequent literature (Vijay et al., 2019, 2021; Davison et al., 2020; Solgaard et al., 2022). The Moon typologies (Figure 2.20) are fundamental to much of the work presented in this thesis, and frequent reference will be made to them, especially in Chapters 4, 5, and 6.

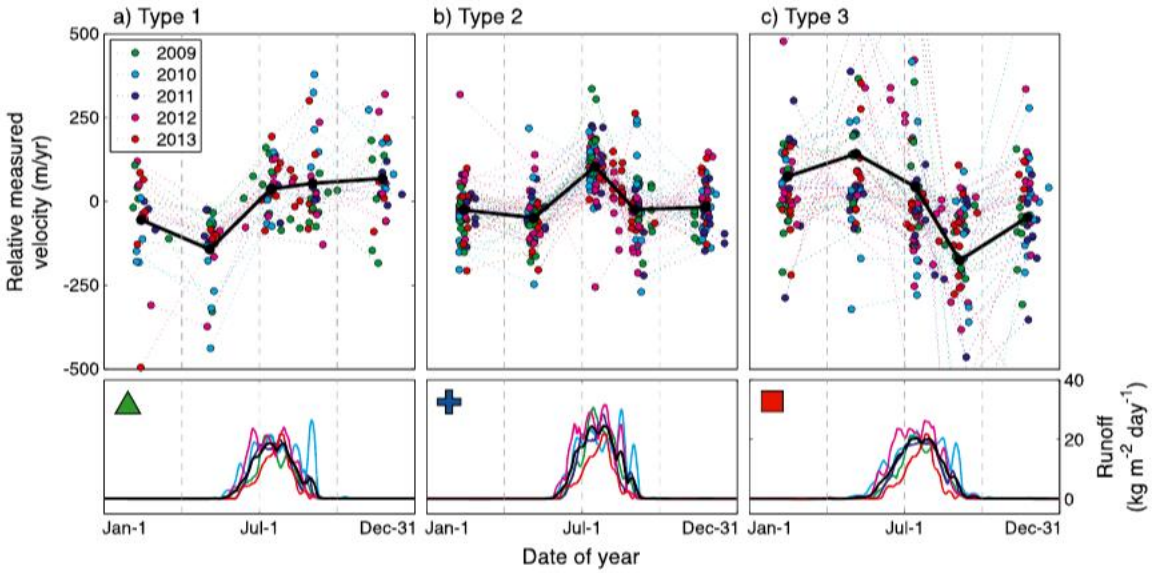

Figure 2.20 Marine-terminating Greenland outlet glaciers with distinct seasonal velocity modes and associated ice sheet runoff. Top row: Plots include all glaciers with dominant seasonal velocity modes for A) type 1, B) type 2, and C) type 3 behaviour. Mean velocity pattern is indicated (thick black line). Bottom row: Smoothed daily runoff (kg/m2d) from RACMO2.3 for 2009–2013 for glaciers with the designated dominant seasonal velocity mode. Mean runoff is included for each year (coloured lines) as well as the 4 year mean runoff (black line). Figure and caption reproduced from Moon et al. (2014).

2.3.3.3 Moon typologies

A short review of the descriptive characterisation of each typology, and the process interpretation for each typology (as illustrated in Figure 2.20) is given below. All description and interpretation is that of Moon et al. (2014).

2.3.3.3.1 Type 1

Type 1 is characterised by speedup between late spring and early summer which then remains high until winter or the following spring. Type 1 shows strong correspondence between variations in speed and terminus position throughout the season, with retreat

coincident with speedup and advance coincident with slowdown. Melt may play a role in Type 1 behaviour during spring / summer speedup, but what makes Type 1 distinct from Types 2 and 3 is the sustained speedup occurring after cessation of melt and runoff.

2.3.3.3.2 Type 2

Type 2 is characterised by a strong early summer speedup followed by midsummer slowdown with velocity then relatively stable between late summer and spring the following year. Winter velocity may be higher than spring and autumn, but remains lower than the summer peak. Type 2 shows a strong correspondence between speed and runoff with summer speedup initiating with melt onset, and further acceleration and subsequent deceleration trending with melt increase and decrease through the season respectively. As runoff and velocity changes trend closely with one another and no mid or late season velocity low is observed, this suggests that channelised subglacial drainage is not developed (or is limited), for Type 2 glaciers. There is no obvious relationship between seasonal speed and ice front position.

2.3.3.3.3 Type 3

Type 3 is characterised by a pronounced mid-summer slowdown leading to a distinct late summer minimum velocity which then recovers over the winter. Type 3 contrasts with Type 2 as there is substantial decrease in velocity during mid summer whilst runoff is still high. This pattern is consistent with the expected signal of an evolution from distributed to channelised subglacial drainage (as discussed in section 2.3.1.2). There is no obvious relationship between seasonal speed and ice front position.

2.3.3.4 Subsequent ice sheet wide studies of seasonal velocity variation

Three further studies have been conducted following on from the work of Moon et al. (2014). Vijay et al. (2019) essentially repeated the general approach of Moon et al. (2014) but utilising much higher temporal resolution velocity data derived from Sentinel 1 SAR data. The 12 day repeat cycle of this satellite gave ~30 velocity measurements per year, compared with ~5 measurements per year (approximately one 12 day average per season) in the original Moon et al. (2014) paper. There was also more robust measurement and analysis of frontal seasonal retreat conducted for each glacier, and some information on melt was inferred from SAR backscatter intensity (Figure 2.21). Despite the richer data, Vijay

et al. (2019) broadly confirmed the findings of Moon et al. (2014). As in Moon et al. (2014), classification of individual glaciers to a typology for each year was performed manually by visual assessment.

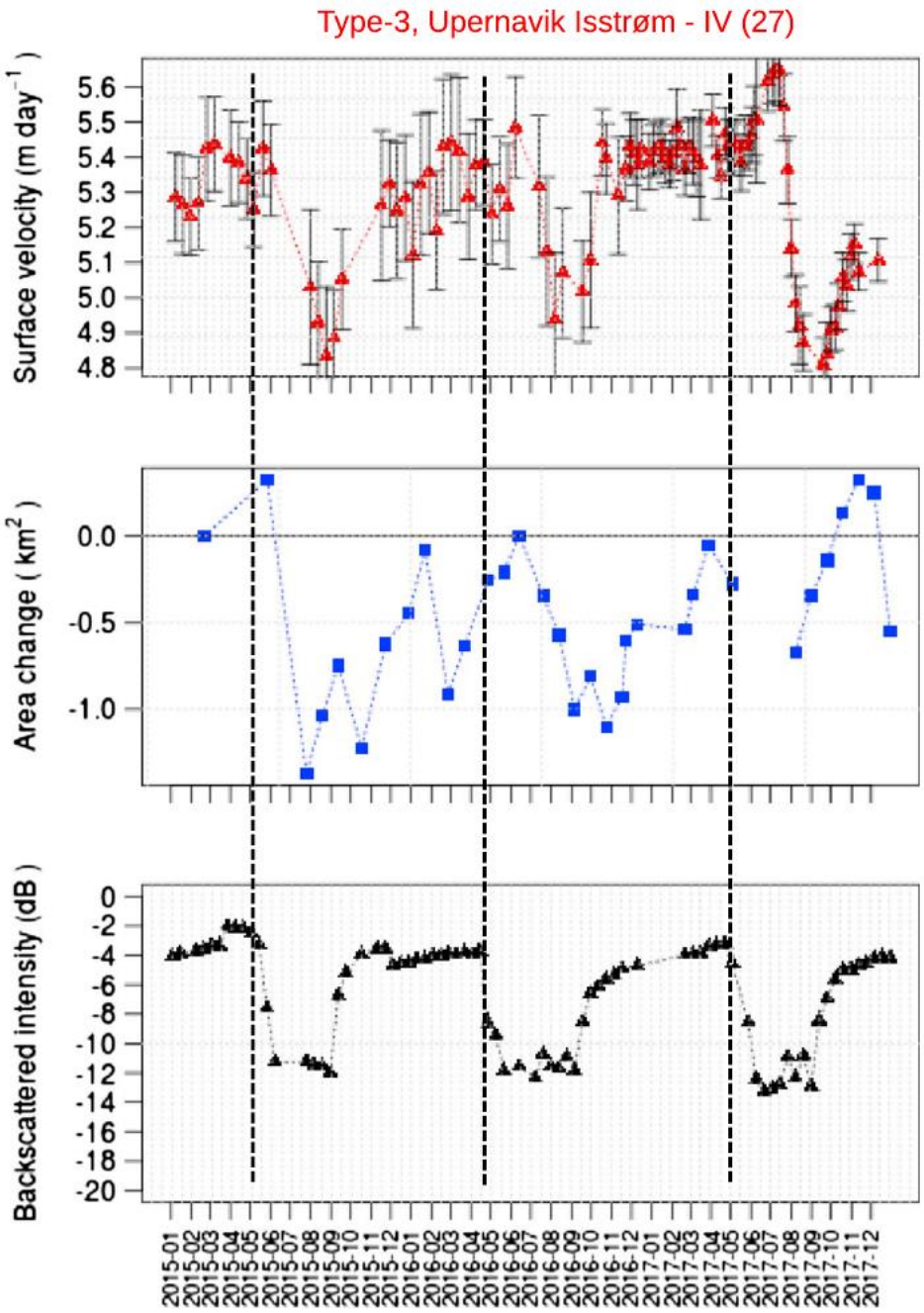

Figure 2.21 Example showing the Type 3 pattern surface velocity together with area change and backscattered intensity during 2015–2017. The vertical dashed line indicates the onset of surface melt as depicted from the seasonal trend of backscattered intensity. Reproduced from Vijay et al. (2019)

Vijay et al. (2021) progressed the study of seasonal velocity typologies by implementing a semi-automated method for classifying typology for the first time. The classification was

performed by selecting exemplar glaciers for each typology and then measuring the cumulative residuals of each individual glacier to the exemplars and classifying them if they were within a prescribed residual limit. The study only classified glaciers as Type 2 or Type 3. Type 1 was excluded from the study, the reasons for this are not made completely clear. The semi-automated approach did allow the inclusion of a much larger number of glaciers (221) than in previous studies, and gave a complete coverage around the margin of the ice sheet for the first time (Figure 2.22). It is important to note that all three studies discussed so far (Moon et al., 2014; Vijay et al., 2019, 2021) only measured velocity for each glacier at a single location close to the calving front. As such, these results were only representative of the ice dynamics at the margin and showed nothing of what was happening further inland.

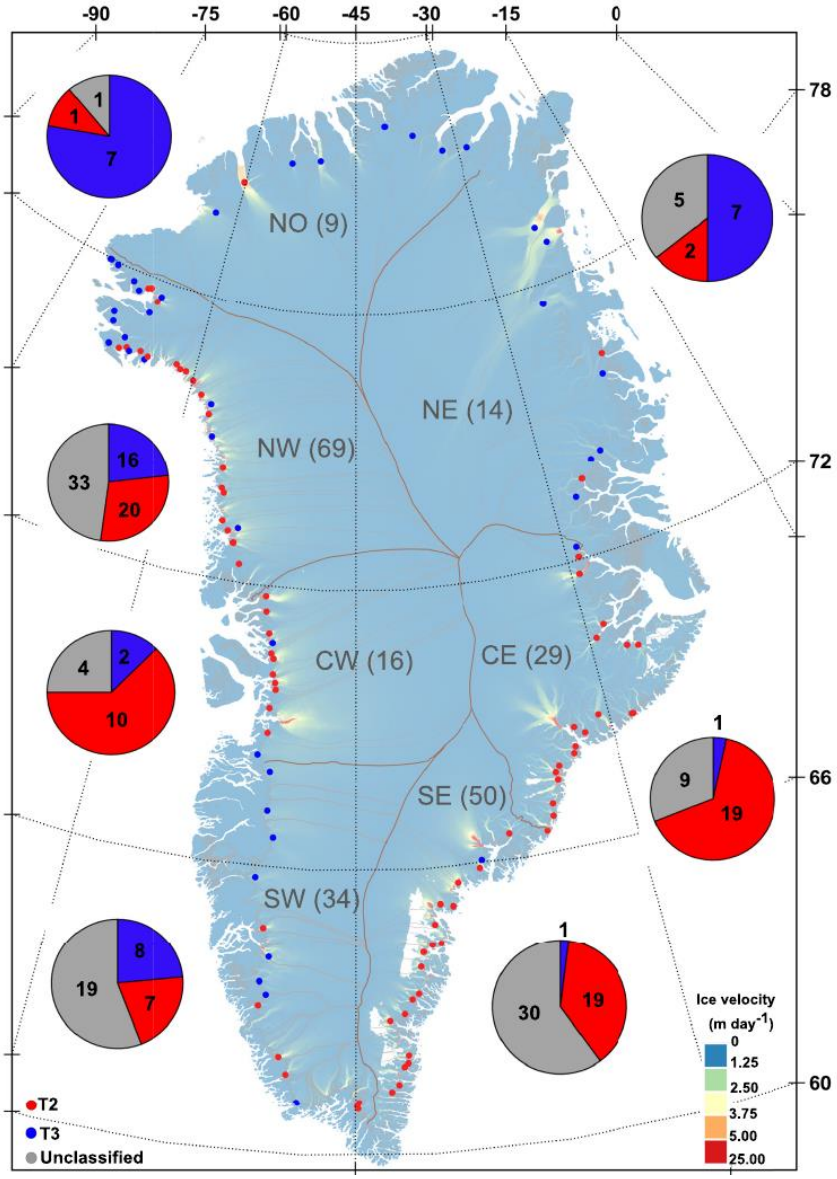

Figure 2.22 Seasonal ice velocity classification map of Greenland showing the location of type-2 (blue dots) and type-3 (red dots) glaciers in different. Pie charts display number of type-2 (blue), type-3 (red) and unclassified (grey) glaciers in each basin. Reproduced from Vijay et al. (2021). NOTE: the legend for the points on the map contained an error when published and the colours are the wrong way around. Blue = T2 and red = T3.

The most recent comparable study is by Solgaard et al. (2022). This study was substantially different for a number of reasons. This was the first study not to limit measurements to individual points close to the calving margin for each glacier. Velocity data was used in its raw raster format, and patterns of seasonal velocity variability were analysed for each cell in the raster. This vastly increased the number of observation points from <250 in previous studies to over 100,000. In order to analyse such a large dataset a machine learning approach was implemented and individual velocity time series data points were classified using a K means cluster analysis. Four clusters were used, but these were interpreted as being representative of more and less pronounced versions of both Type 2 and Type 3, so as in Vijay et al. (2021), Type 1 was not considered (Figure 2.23).

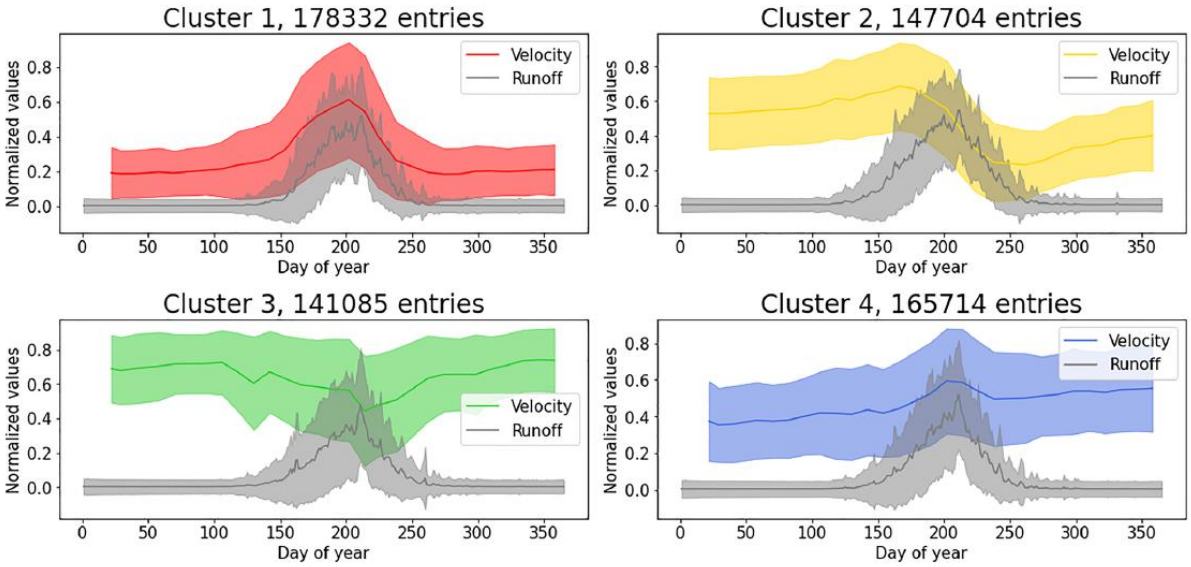

Figure 2.23 Cluster outputs for Greenland velocity 2017-2021. The mean and standard deviation of the clusters shown together with the mean of the normalized runoff. Clusters 1 and 4 are representative of Type 2 seasonal variation, clusters2 and 3 are representative of Type 3 seasonal variation. Reproduced from Solgaard et al. (2022).

This raster based approach opened up the possibility of investigation of along glacier variation in seasonal velocity typology at an ice sheet wide scale for the first time (Figure 2.24). A full analysis of these variations was not given, but a handful of example glaciers were highlighted where there was variation in seasonal velocity typology along the centre

line of the glacier.

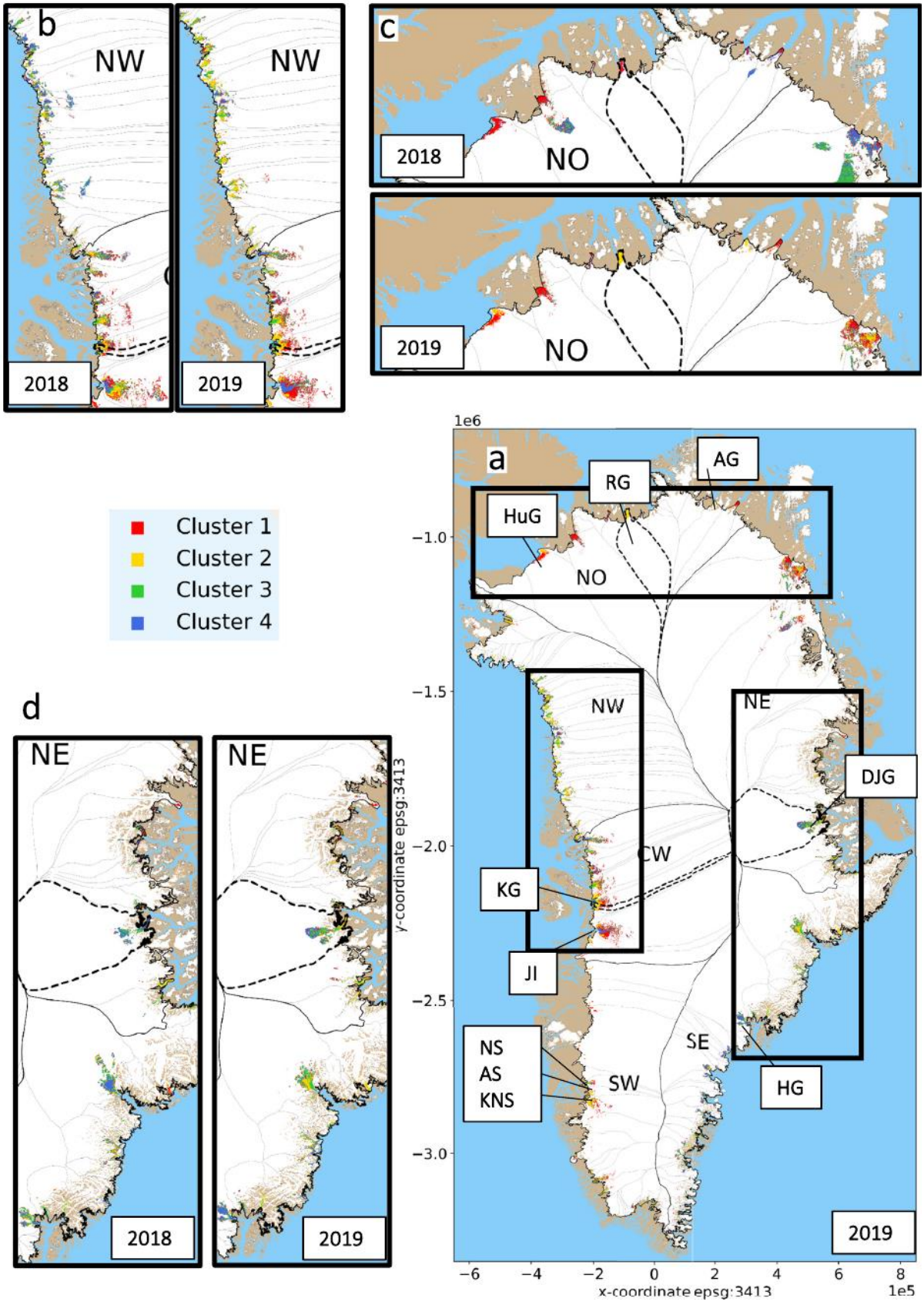

Figure 2.24 A) Overview of the Greenland Ice Sheet and a view of the spatial distribution of the clusters in 2019. Sectors of the ice sheet is indicated in full black lines, glacier catchments in thin grey. Specific glacier catchments: HuG: Humboldt Glacier, AG: Academy Glacier, RG: Ryder Glacier, DJG: Daugaard-Jensen Glacier, HG: Helheim Glacier, KNS: Kangiata Nunaata Sermia, AS: Akullersuup Sermia, NS: Narsap Sermia, JI: Jakobshavn Isbræ and KG: Kangilernata Sermia. B–D) are zoom-ins on the three areas marked in A) and show the cluster distribution in 2018 and 2019. The legend applies to all subfigures. Figure and captions reproduced from Solgaard et al. (2022).

2.3.3.5 Ice sheet scale interpretation of patterns of seasonal dynamics

The four papers discussed in sections 2.3.3.3 and 2.3.3.4 were all in agreement in terms of the broad spatial patterns of seasonal velocity variation, and the likely process interpretations for these patterns. Both Moon et al. (2014) and Vijay et al. (2019) linked Type 1 variation to seasonal retreat of the calving front. However, the analysis of this relationship was limited to subjective visual comparison rather than a robust statistical analysis. There were many exceptions within the data and the significance of the proposed relationship was not tested. Both studies also only measured velocity at single points close to the margin for each glacier, so there was no investigation of how far inland these effects may propagate.

All four studies (Moon et al., 2014; Vijay et al., 2019, 2021; Solgaard et al., 2022) strongly suggested that seasonal typology is linked to subglacial drainage configuration and therefore to melt. Melt data was presented for all studies, but analysis was largely limited to subjective visual interpretation of patterns in the graph figures. There was good evidence of late season slowdown occurring for Type 3 glaciers whilst melt was still high in the data presented by all four studies, and Vijay et al. (2021) established that in aggregate the melt season for Type 2 glaciers was shorter than for Type 3 glaciers. Spatial patterns of Type 2 and Type 3 variation did also appear to support the links to melt with higher Type 2 prevalence in higher latitude areas which experience lower melt, and higher Type 3 prevalence in lower latitude areas which experience higher melt (Vijay et al., 2021; Solgaard et al., 2022). Speculative links between melt rates in a given year and changes in relative Type 2 / Type 3 prevalence were also made (Vijay et al., 2019; Solgaard et al., 2022). Overall, despite the apparently strong relationship between melt and seasonal typology, no studies provided a robust statistical analysis in this regard, and the statistical significance of this relationship was not tested.

Both Moon et al. (2014) and Solgaard et al. (2022) presented the notion of a Type 2 and

Type 3 not as independent typologies, but rather as end members on a continuum. Switches between different typologies of some individual glaciers between years (e.g. Solgaard et al. (2022) demonstrated that Academy Glacier and Humbolt glacier both switched from Type 2 in 2017 and 2018 (low melt years) to Type 3 in 2019 (a high melt year)) which offers some support but the hypothesis was not robustly and systematically tested. The data generated by Solgaard et al. (2022) was the first of its kind to facilitate the possibility of investigating how seasonal velocity typology varies along the centreline of a glacier, and how this might link to the concept of seasonal typologies as a continuum. However, this did not form a substantive element of their analysis. One figure in the supplementary material did demonstrate that for Kangilernata Sermia Type 3 dominated in the downstream region of the glacier, where as Type 2 dominated in the upstream region. Despite the limited discussion given to this in the paper, this is perhaps the strongest evidence in support of the concept of Type 2 and Type 3 as end members of a continuum.

2.4 The role of overdeepenings in ice sheet dynamics

Subglacial topography exerts control on patterns of ice flow through both physically resisting flow, and through modulating basal conditions of subglacial hydrology or the strength of the bed. Adverse bedslopes force ice flowing through overdeepenings to flow uphill at the downstream end of the overdeepening causing backstress which retards ice flow (Van der Veen, 1997; Motyka et al., 2003). The ability of an overdeepening to exert backstress and act as a pinning point for glaciers flowing over them was discussed in detail sections 2.3.2.2 and 2.3.2.3 and so will not be covered again in this section. For a full review of the role of overdeepenings in ice sheet dynamics, readers are referred to the comprehensive paper by Cook and Swift (2012). Here, a brief review of the key areas specifically relevant to this thesis will be given.

2.4.1 Hydrological controls on ice sheet dynamics

Adverse bedslopes are anticipated to modulate basal sliding rates and mechanisms through their control on subglacial drainage system morphology and efficiency (Hooke et al., 1989; Jansson, 1995). The action of these processes suggests that ice flow through

overdeepenings may vary, and be more complex, than flow through non-overdeepened areas. As overdeepenings are erosional forms, their location will typically be concentrated in the ablation zone where there is sufficient runoff to enable their formation (see section 2.2.1.1). As a result, overdeepenings may be frequent landscape features in dynamic and sensitive areas of glaciers and ice sheets (Cook and Swift, 2012).

A variety of mechanisms have been proposed by which overdeepenings may exert an influence on the subglacial drainage systems of glaciers. Overdeepenings of the glacial bed may be associated with crevasse formation at the surface resulting in focused delivery of melt to overdeepenings and increased density of links between the surface and the bed (Hooke et al., 1989; Hooke, 1991). The requirement for water to leave an overdeepening by flowing up an adverse slope potentially modulates the subglacial hydrological configuration in a number of ways. It is important to note that the processes discussed below are not discrete: they form part of a continuum of increasing influence on how water flows through an overdeepening and the consequent impact this may have on ice dynamics (Cook and Swift, 2012). Most simply, the need for water to flow uphill reduces the hydraulic gradient, making the system more sluggish and therefore suppresses hydraulically efficient drainage. In addition, higher basal water pressure is maintained on adverse slopes than would be the case on a normal slope due to energy that would ordinarily be available for melt being used to sustain water temperature (Hooke 1991). Further, where the bed-slope to surface-slope ratio exceeds -1.2 to -1.7, the supercooling threshold is exceeded. This is the physical threshold beyond which the pressure melting point rises faster than water can be warmed by viscous dissipation, which may cause some of the water to freeze and water will be unable to cause channel-wall melt (Röthlisberger, 1972; Röthlisberger and Lang, 1987; Hooke, 1991). Below the threshold, this effect would predict smaller, less efficient subglacial channels than would be expected on 'normal' slopes, and at and above the threshold channels may close (or be prevented from forming) completely. As a result, subglacial water pressure would be elevated in comparison to that on normal slopes (Creyts and Clark 2010). Importantly, absence of channel-wall melt predicts that pressure within channels will equalise with ice-overburden pressure, and flow will distribute to flow as a sheet (Rothlisberger 1972; Creyts and Clark 2010). It is therefore expected that water pressures within overdeepenings will be persistently higher than that on normal slopes, and, where

the supercooling threshold is exceeded, the seasonal evolution of channelised drainage (covered in detail in sections 2.3.1.2 and 2.3.1.3) will be delayed or prevented entirely. As such, it would be possible for ice velocity to be faster in overdeepened areas than non-overdeepened areas of a glacier (Cook and Swift, 2012), as a result of greater basal sliding (see Figure 2.25).

There are some caveats that need to be applied to the theory presented in the paragraph above. The stated bed to surface slope supercooling threshold ratios are based on the assumption that water pressure is always at ice overburden pressure (or a constant fraction thereof) (Röthlisberger and Lang, 1987). However, observations have demonstrated that this assumption is often not valid and water pressure downstream of an overdeepening is often well below overburden ((Jansson, 1995; Cook and Swift, 2012; Werder, 2016). The pressure downstream of an overdeepening exerts a control on the pressure within the overdeepening. As such, the bed to surface slope supercooling threshold defined by classic theory sets the threshold beyond which supercooling *may* occur, not when it *will* occur (Werder, 2016). Other factors are also now understood to control supercooling in a more nuanced way than was suggested by classical theory. Classic theory has tacitly ignored the importance of distance, meaning supercooling might be expected to occur at any point along the adverse slope where the threshold is exceeded. More recent work shows that the threshold is itself variable according to the length of the adverse slope, with lower thresholds required for longer stretches of adverse slope because of the longer distance over which energy can be dissipated (Werder, 2016).

In terms of seasonal ice velocity typology, due to the suppression of hydraulically efficient drainage on adverse slopes, lower prevalence of Type 3 seasonal variation, and higher prevalence of Type 2 (see section 2.3.3.3) might be expected in overdeepenings compared to non-overdeepened areas.

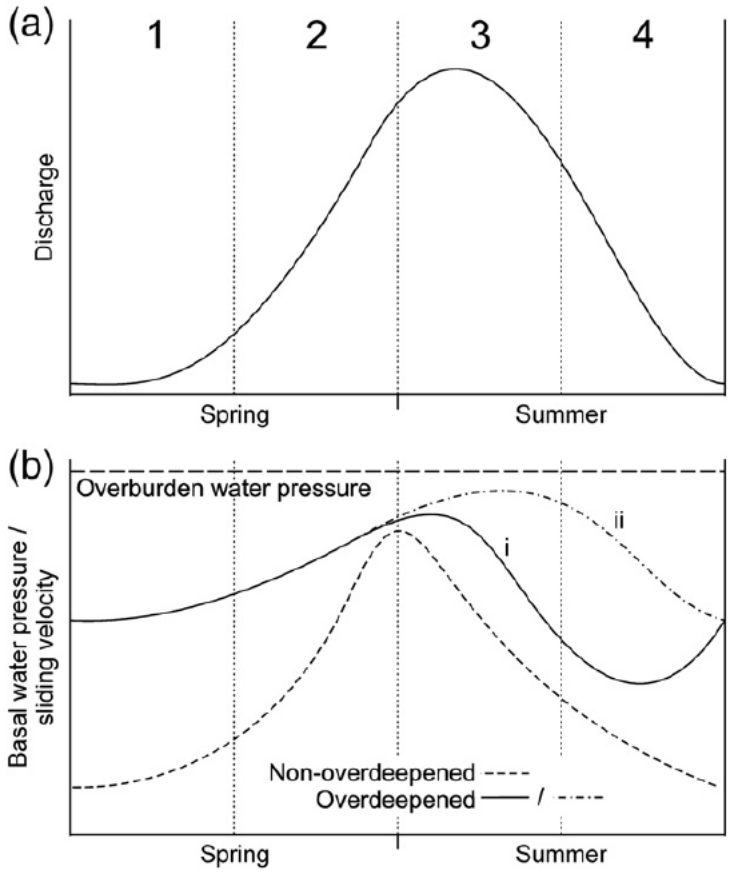

Figure 2.25 Schematic diagram showing basal water pressure and sliding velocity over a melt season for a valley or outlet glacier with an overdeepened or non-overdeepened bed. Water supply from surface runoff and basal melting is shown in A) and hypothesised water pressure and sliding rate in B). For the non-overdeepened bed, water pressure and sliding initially increases with water supply and then declines rapidly as subglacial flow switches from hydraulically inefficient flowpaths to hydraulically efficient subglacial channels. For the overdeepened bed, water pressure and sliding are persistently higher as a result of the lower transmissivity of subglacial flowpaths that must ascend the adverse slope. Higher pressures and sliding rates may also be sustained for longer because drainage system evolution, including switching of flow to alternative englacial flowpaths, is likely to be slow (curve i) or severely limited (curve ii). Figure and caption reproduced from Cook and Swift (2012).

Alternative suggestions have been made as to how melt water flow might traverse an overdeepening. It has been suggested that englacial and lateral conduits could form instead or in addition to subglacial routes in response to the higher water pressures associated with flow at an overdeepened bed (Figure 2.26) (Lliboutry, 1983; Hooke, 1984; Fountain and Walder, 1998). As elevated water pressures at the bed are a pre-condition for this to occur, high basal water pressure would still be expected to be maintained under conditions of lateral and englacial flow, but dynamic response to further water input (e.g. through either enhanced melt conditions or rainfall events) may be muted due to a proportion of the melt avoiding the bed (Cook and Swift, 2012).

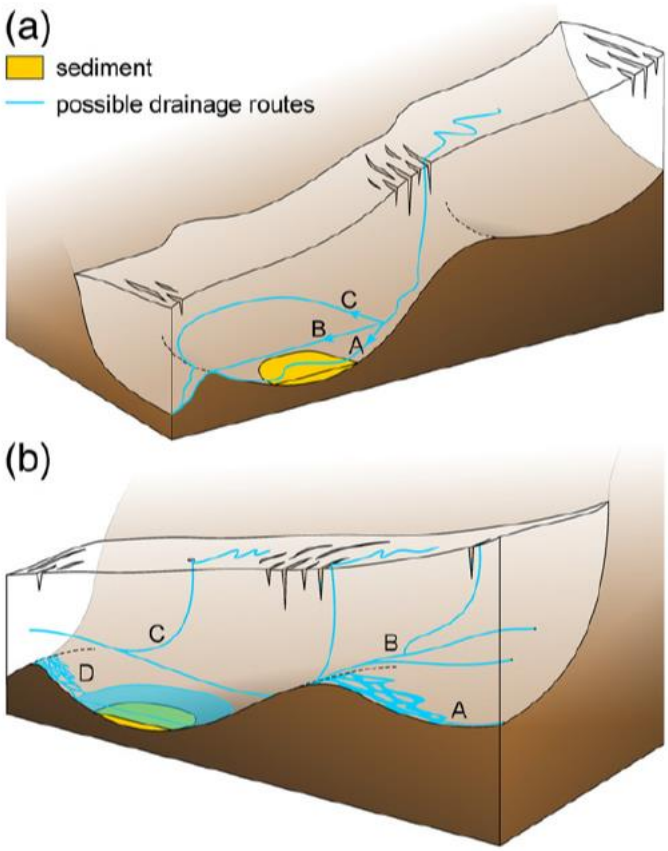

Figure 2.26 Schematic diagrams showing possible glacial drainage system pathways and morphologies of overdeepenings. (a) Surface and/or subglacial runoff that reaches a basin or overdeepening may follow subglacial (A), englacial (B) or lateral (C) pathways. (b) The morphology and efficiency of subglacial flowpaths that ascend an adverse slope (A) Distributed drainage ascending the adverse slope (D). Englacial conduits that traverse an overdeepening may intercept surface runoff before it can reach the bed (B) and may divert subglacial and surface across basins and overdeepenings (C). Figure and caption reproduced from Cook and Swift (2012)

Given that overdeepenings appear to be so ubiquitous near the margin of the GrIS (Patton et al., 2016), and given that theory discussed above suggests that overdeepenings have a profound effect on the dynamics of the ice sheet where they are present (and therefore potentially influence the response to future climate change), it is perhaps surprising that they have been studied so little (Cook and Swift, 2012; Patton et al., 2016). The most substantive contribution to the understanding of the importance of overdeepenings for subglacial hydrology and ice dynamics has arguably come from field studies conducted at Storglaciären, a mountain glacier in northern Sweden. Borehole studies at Storglaciären provide empirical data to support the hypotheses developed from theory, discussed above. Basal water pressures within the overdeepening have been found to be consistently around 90% of overburden pressure, and little variation in ice velocity has been observed (which would normally be expected in response to increased melt). Directly downstream of the

overdeepening, both basal water pressure and dynamic ice response were much more variable through the melt season and in response to short term melt influx (Hooke et al., 1989; Jansson, 1995). This consistently observed high basal water pressure indicates that perpetual inefficient distributed subglacial drainage may be associated with overdeepenings. In addition, both tracer experiments and borehole studies have found extensive englacial conduit systems at Storglaciären, suggesting that at least some (and possibly the majority of) flow does 'bypass' the overdeepened bed (Hooke et al., 1988; Hooke and Pohjola, 1994; Fountain and Walder, 1998; Cook and Swift, 2012). Field studies in other areas have also provided data to support the notion of persistently high subglacial water pressure in overdeepenings, and the prevalence of englacial flow across overdeepenings. Both Iken et al. (1996) and Hock et al. (1999) have found evidence of simultaneously inefficient subglacial flow and efficient englacial flow at glaciers in Switzerland by borehole and tracer studies respectively.

In an ice sheet context, there is a significant and growing body of literature on channelised and distributed subglacial flow in Greenland (see sections 2.3.1.4 and 2.3.1.5) but to date, there has been almost no specific consideration of the influence that overdeepenings may have on drainage routes and their efficiency (Cook and Swift, 2012; Patton et al., 2016). Following the discovery of a much larger number of subglacial lakes under the GrIS than was previously thought (Bowling et al., 2019), there has been intensified interest in subglacial hydrology (Livingstone et al., 2022), though lake formation concepts have rarely been directly discussed in the context of ice-eroded overdeepenings. A subglacial lake is simply an overdeepening where the bed to surface slope ratio exceeds the so-called 'ponding' threshold (where the bed slope exceeds ~10x the ice surface slope) (Cook and Swift, 2012), and it is clear that drainage changes that would similarly increase basal water pressure and reduce ice-bed friction appear likely at much lower thresholds (Röthlisberger and Lang, 1987; Alley et al., 1997; Alley et al., 2003), have perhaps been ignored. For example, in a recent review of the topographic modulation of outlet glacier flow in Greenland by Catania and Felikson (2022), there was only very brief consideration of the impact of overdeepenings on flow, notably the modelling work of Creyts and Clarke (2010) and the field study on Storglaciären by Hooke (1991) in the 1980s.

2.4.2 Bed controls on ice sheet dynamics

The resistance to flow of ice over the bed is not solely controlled by hydrological processes as discussed above. The strength of the bed to support the shear stress exerted by the overlying ice will be a key control on the speed if ice flow. It is established that ice flowing over soft beds (such as saturated, weak till) can deform at low stress and therefore be associated with higher ice velocities in comparison to flow over hard beds (Boulton and Jones, 1979; Alley et al., 1987; Christianson et al., 2014). As the adverse slope restricts the flow of water through the subglacial system (discussed above) and subdues the development of efficient drainage, it follows that the ability for sediment (potentially eroded from the headwall of the overdeepening) to be evacuated from the overdeepening will be restricted once the supercooling threshold is exceeded. This has been hypothesised as a controlling mechanism on the geomorphological evolution of overdeepenings whereby once the supercooling threshold is exceeded, sediment will start to be deposited which will prevent further erosion of the bed and result in the adverse slope gradient stabilising close to the supercooling threshold. The accumulation of soft deformable basal till on the adverse slope may also reduce the strength of the bed and cause ice velocity to increase (Hooke et al., 1989; Hooke, 1991; Alley et al., 2003; Alley et al., 2003). However, it is uncertain how prominent bed deformation within overdeepenings may be as a control on ice velocity, and it has been suggested that basal sliding is the dominant mechanism (Iverson et al., 1995).

2.5 Summary

This chapter has provided a synthesis and review of the key background relating to the aims and objective of the thesis, and has provided further context to the rationale for the study outlined in Chapter 1. The key take aways from the chapter are summarised below.

- Overdeepenings are erosive features and so are therefore likely to occur where erosive potential is greatest. Ice velocity and melt availability are key determining factors of erosive potential. Areas of high erosive potential may lead to deeper overdeepenings, but mechanisms regulating overdeepening erosion controlled by supercooling processes may inhibit overdeepening evolution and restrict the maximum depth they erode to.

- Existing datasets of overdeepening location and morphometry are sparse, and only one previous dataset for overdeepenings in Greenland has been produced. The most recent high resolution bed topography data for Greenland is an order of magnitude higher resolution than the data used in creating the previous dataset of overdeepenings in Greenland, but this has never been used to map overdeepenings.
- The research conducted on mountain glaciers over the last 70 years to develop current theory of subglacial hydrology is now thought to be applicable to the GrIS.
- Melt availability is key to controlling subglacial hydrology and this is directly linked to the concepts of distributed and channelised subglacial hydrology. Switches between distributed and channelised configurations are key to controlling ice velocity and seasonal variation in ice velocity.
- Marine processes controlling calving rates and advance and retreat of the calving front of marine terminating outlet glaciers are also thought to exert a control on seasonal, and interannual velocity variation.
- The balance of importance of marine controls and melt controls on velocity variations are uncertain and contested.
- Only four comprehensive studies of seasonal velocity variation typology in Greenland have been conducted to date. Three of these have only utilised velocity measurements at point locations near the calving fronts of glaciers.
- Overdeepenings can exert control on the subglacial hydrological configuration by suppressing the development of efficient channelised drainage. This is as a result of reduced hydraulic gradient and supercooling restricting the growth of (or even closing) channels in the ice. This has the potential to modulate ice velocity in overdeepenings by elevating basal water pressures and reducing friction at the bed. The potential control of overdeepenings on ice dynamics in Greenland has not been well studied to date.

Chapter 3 Overdeepening location and character under the Greenland Ice Sheet

The primary purpose of this chapter is to develop a semi-automated method to comprehensively identify and map overdeepenings in Greenland. The creation of a comprehensive overdeepening dataset is essential in order to be able to progress to answering RQs 2 and 3 and achieving their associated objectives (see section 1.2). Within this chapter, the overdeepening dataset will be produced and used to fully answer RQ1 ***How common are overdeepenings under the GrIS and how variable is their geometry?*** In order to answer this question, a detailed analysis of the patterns in overdeepening morphometry will be conducted. A wide body of theory exists around overdeepening formation and evolution, but testing of these theories has historically been limited by the availability of data for testing process relationships, especially in ice sheet contexts. Consideration of this theory will be given in light of the new dataset created.

A secondary purpose of this chapter is to utilise the overdeepening dataset to start to answer RQ2 ***Does bed topography modulate ice velocity in overdeepenings?*** This will form a less substantial part of the chapter than the work motivated by RQ1, but analysis will be conducted to explore at an ice sheet scale whether annual mean ice velocity is modulated when flowing through an overdeepening. RQ2 and RQ3 will be comprehensively answered (and their associated objectives met) in the work that follows in Chapters 4, 5 and 6.

3.1 Introduction

Bed topography is known to influence the way in which ice flows over it through a variety of mechanisms. A detailed review of the processes underlying these influences and the expected responses is given in section 2.4. The geometry of an overdeepened basin can exert direct topographic control on ice flow. Flow has been observed to be extensional into the overdeepening, and compressional at the down glacier end of the overdeepening due to the back pressure from the riegel or adverse slope combined with converging bed contours funnelling ice (Hooke et al., 1989; Hooke et al., 1992; Van der Veen, 1997; Cook and Swift, 2012). Bed topography also plays an important role in the hydrology of glacial systems. The majority of glacier motion is due to sliding over the bed where the glacial thermal regime is

warm based (Maier et al., 2022), as is the case for over a third of the GrIS including most areas of fast flowing ice near the margin (MacGregor et al., 2022). Sliding is strongly controlled by the availability of water at the ice bed interface to provide lubrication (Iken and Bindschadler, 1986). Bed topography influences the location of surface features such as crevasses and moulins which are necessary to allow water at the surface to access the bed (Hooke, 1991; Stenborg, 1969; Benn et al., 2009; Sundal et al., 2011). Bed topography also controls how water at the bed flows. Water at the bed of an overdeepening will be forced to flow up the adverse slope to exit the overdeepening resulting in elevated basal water pressure. Where the supercooling threshold is exceeded the evolution of the subglacial hydrological system to an efficient channelised configuration under high melt conditions may be prevented or slowed resulting in hydraulically inefficient conditions persisting with higher prevalence than on non-overdeepened slopes (Hooke, 1991). Hydraulically inefficient subglacial drainage configurations are associated with high basal water pressures (Iken et al., 1983). High basal water pressure reduces sheer stress at the ice bed interface and therefore increases sliding velocity. Indeed, there are numerous studies which report elevated basal water pressure within overdeepenings (e.g. Hooke et al., 1989; Jansson, 1995). The link between meltwater supply variability and ice velocity has been well established (e.g. Zwally et al. 2002), but is complex and non-linear with suggested threshold values of melt which if exceeded actually result in a reduction in ice velocity following the seasonal establishment of efficient channelised sub glacial hydrological systems (Sundal et al., 2011; Sole et al., 2013). Despite the links between ice velocity and subglacial hydrological configuration (e.g. channelised vs distributed), and the links between overdeepenings / adverse slopes and subglacial hydrological configuration, the influence that overdeepenings exert on ice velocity has not received attention within the existing literature.

Comprehensive mapping of overdeepenings at a national or continental scale has only been conducted in a very small number of studies. Haeberli et al. (2016) map overdeepenings and analyse the metrics of their morphology for the Swiss Alps and the Karakoram using a variety of measured and modelled bed geometries, and for the Peruvian Andes using lake bathymetry data, to generate a large dataset of some 17,000 individual overdeepenings across the three study areas. Magrani et al. (2020) use a bedrock elevation model to map

and evaluate the morphometrics of the overdeepenings of the Swiss alps and foreland, but less than 100 overdeepenings are mapped. The only comprehensive mapping and morphometric analysis of overdeepenings at a continental scale has been conducted by Patton et al. (2016) who developed an automated method to map all overdeepenings in Greenland and Antarctica.

In addition to the control that overdeepenings may exert on ice dynamics, ice dynamics control where overdeepenings are located and the size they may evolve to. Overdeepenings are hypothesised to be more likely to occur and to evolve to greater depth where erosive potential is higher (Lloyd et al, 2023). Areas of convergent flow on a glacier will cause ice to thicken and / or accelerate, increasing the erosive potential (Alley et al., 2003; Amundson and Iverson, 2006; MacGregor et al., 2009), and overdeepenings are commonly observed at glacier confluences for the same reasons (Iken et al., 1996; Hock et al., 1999). The resistance of bedrock to glacial erosion has also been shown to influence where overdeepenings form (Preusser et al., 2010), and the shape an overdeepening evolves to, with more resistant bedrock tending towards narrower deeper valleys (Hirano and Aniya, 1988; Augustinus, 1992; Brook et al., 2004; Swift et al., 2008).

Higher quality bed data for Antarctica and Greenland are now available in products like BedMachine (Morlighem et al., 2017) which uses mass conservation approaches to generate bed data at a 150 m resolution. This is a spatial resolution almost 50 times higher than the 1 km Bamber et al. (2013) bed data, and over 1,000 times higher than the 5 km Bedmap2 data (Fretwell, 2013). This new dataset opens up the opportunity to map subglacial features like overdeepenings at an unprecedented level of detail, and at near complete continental coverage. However, these new opportunities are not without challenge. When applying automated processes of mapping and analysis, an order of magnitude increase in spatial resolution will have a knock-on effect order of magnitude increase in processing time. All other things being equal, automated routines that took days to run on 1 km data will take weeks or months to run on 150 m data. As such, it may not be possible to simply apply techniques previously developed to automatically map overdeepenings (such as Patton et al, 2015) to this new, much higher resolution bed data. To date, the high resolution BedMachine data has not been utilised to map overdeepenings for Antarctica or Greenland.

3.1.1 Rationale for this chapter

In summary of the introduction above, the principal rationale for this chapter is as follows:

1. Bed topography controls ice flow, but the understanding of these processes is limited to localised (e.g. single catchment) studies. The wider scale impact of bed topography on ice flow has not been explicitly investigated, and knowledge regarding the number and morphology of overdeepenings remains weak despite the ubiquity of these features.
2. Newer bed elevation model datasets such as BedMachine offer orders of magnitude higher spatial resolution than the data used in overdeepening mapping and analysis studies in Greenland to date. There is value in utilising this higher resolution data to more comprehensively map overdeepenings, and to do so with higher precision and accuracy than in previous studies.
3. A new higher resolution dataset of overdeepening location and morphometry will allow consideration and testing of hypothesised theories of overdeepening formation and evolution that were not previously possible.
4. Previous research on ice dynamics in Greenland has been heavily focused on the role that subglacial topography may play to the stabilising (and destabilising) influence of adverse and normal slopes as calving fronts advance and retreat, and such analysis has often been limited to individual glaciers or small selections of glacier (see section 2.3.2.3). A complete and accurate dataset of overdeepening location will enable the analysis of ice dynamics to be made at the ice sheet scale in the context of adverse and normal bedslopes as well as other potentially important factors relating to overdeepening morphometry .

3.2 Methods

3.2.1 Mapping overdeepenings

For the purposes of this study, the overdeepenings of interest are those located under Greenland outlet glaciers and ice streams. The workflow adopted involved:

1. Identifying and mapping the fronts of all Greenland outlet glaciers and ice streams.
2. Generating flowline fields for each outlet glacier and ice stream from ice velocity

vector data.

3. Selecting the flowline for each glacier that best represents the central flowline.
4. Adding bed data to the central flowline to give a longitudinal bed elevation transect for the flowline.
5. Identifying topographic lows and highs along the central flowline transect. These points are broadly representative of overdeepening elevational minima and the saddles or lip points between overdeepenings.
6. Using the low and high points as a guide, manually select the boundaries of all closed topographic basins (e.g. overdeepenings) from a contour dataset of the Greenland bed and copy them into a new shapefile. This is the output dataset of mapped overdeepenings.

Each step is described in more detail below.

3.2.1.1 Identifying outlet glacier fronts

The fronts of each Greenland outlet glacier and ice stream were digitised in ArcGIS using Landsat 8 optical imagery and MEaSUREs annual ice velocity data for 2016 (Joughin, 2017). The accuracy and precision of these features was not critical as they were used solely to generate seeding points for the flowlines. In order to provide effective seed locations, it was important that the lines were digitised slightly upstream of the ice front within the extent of the ice velocity coverage, and that the full width of the fast moving section of the ice front was covered (see Figure 3.1). Lines did not need to follow the shape of the actual ice front. Where appropriate, the lines were also digitised across the front of tributary glaciers where they join the main glacier. In total 341 ice fronts were identified and mapped.

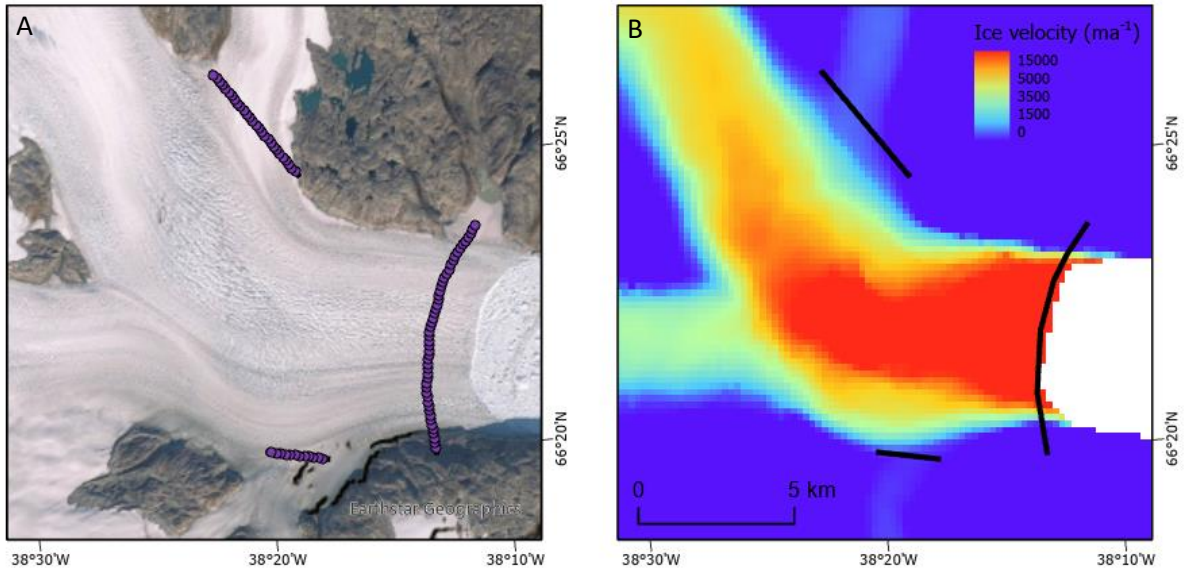

Figure 3.1. Example of ice front mapping for Helheim Glacier, south east Greenland shown over A) Landsat 8 imagery, B) MEaSUREs annual ice velocity data for 2016.

3.2.1.2 Generating flowlines

Accurate visualisation of the patterns of ice flow through each catchment were required in order to aid with the mapping of overdeepenings, analyse ice flow characteristics (e.g. converging / diverging flow) and overdeepening location, and to analyse the relationship between bed topography and flow. Flowlines were created by locating ice-flow seed points at 150 m intervals along each ice front mapped. These were then used to seed flowlines using the 'flowline' function in Matlab R2016a. As this function generates flow downstream from an upstream seed point, the vx and vy vectors of the MEaSUREs 2016 annual velocity data were reversed to calculate flow through the catchment from the seed points on the ice front (see Figure 3.2).

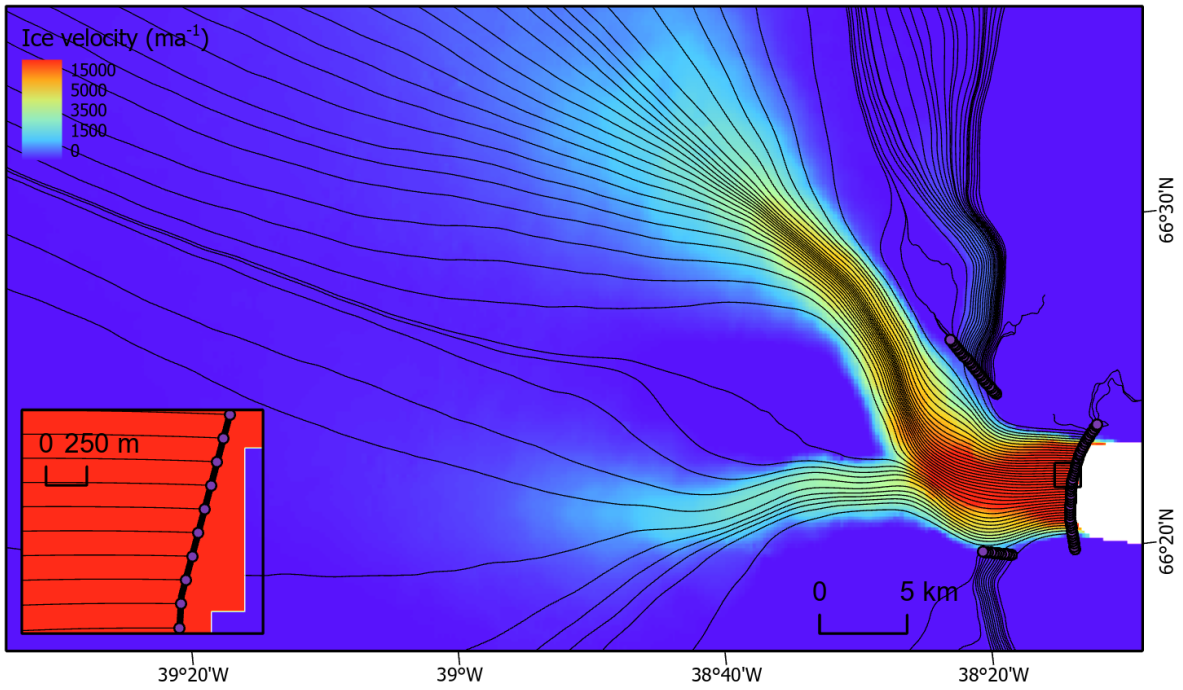

Figure 3.2. Example of ice flowline mapping for Helheim Glacier, south east Greenland showing flowlines over MEaSUREs annual ice velocity data for 2016. Inset shows detail of flow seed points at 150m intervals along the mapped ice front.

3.2.1.3 Identifying central flowlines

Through a process of manual interpretation comparing the flowlines generated with the BedMachine v3 bed topography data (Morlighem et al. 2017), the flowlines best representing the central flowline for each glacier were identified and saved into a separate layer. For more complex glaciers with multiple tributaries more than one central flowline is mapped. An example of this is shown in Figure 3.3 for Helheim glacier where six separate flowlines have been selected to represent central flowlines for the principal sections of the glacier. Figure 3.4 shows the total central flowline dataset that was generated.

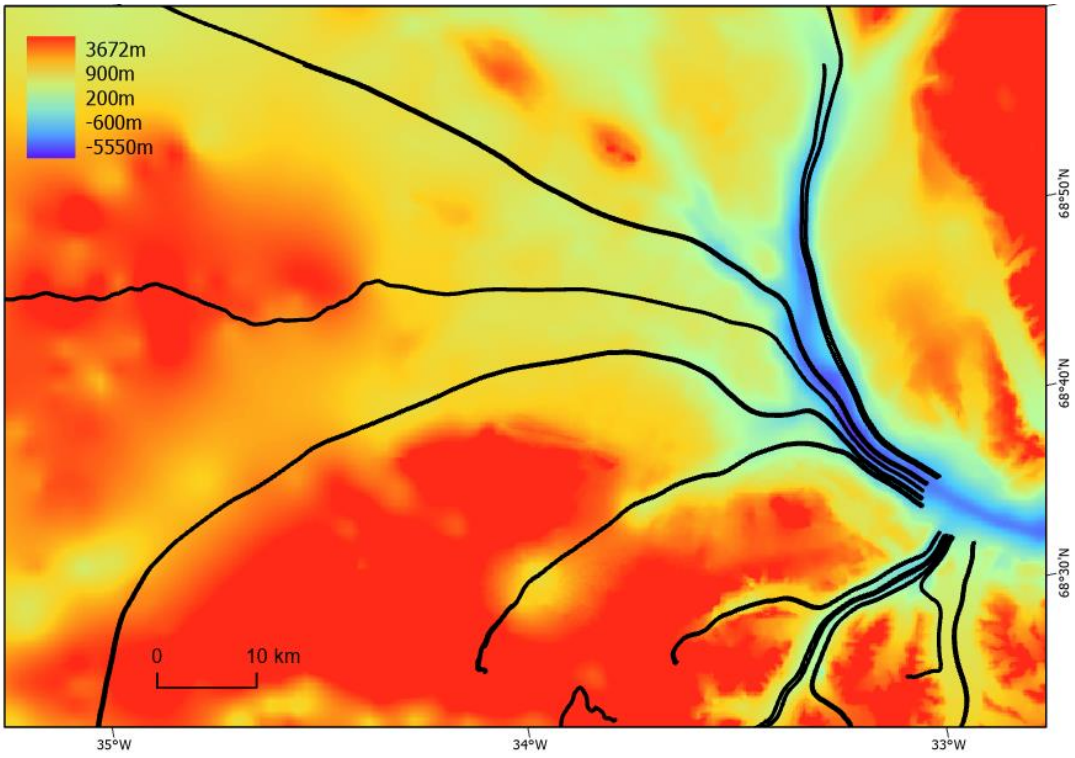

Figure 3.3. Example of central flowline mapping for Helheim Glacier, south east Greenland. Central flowlines are shown as black lines over the BedMachine3 DTM.

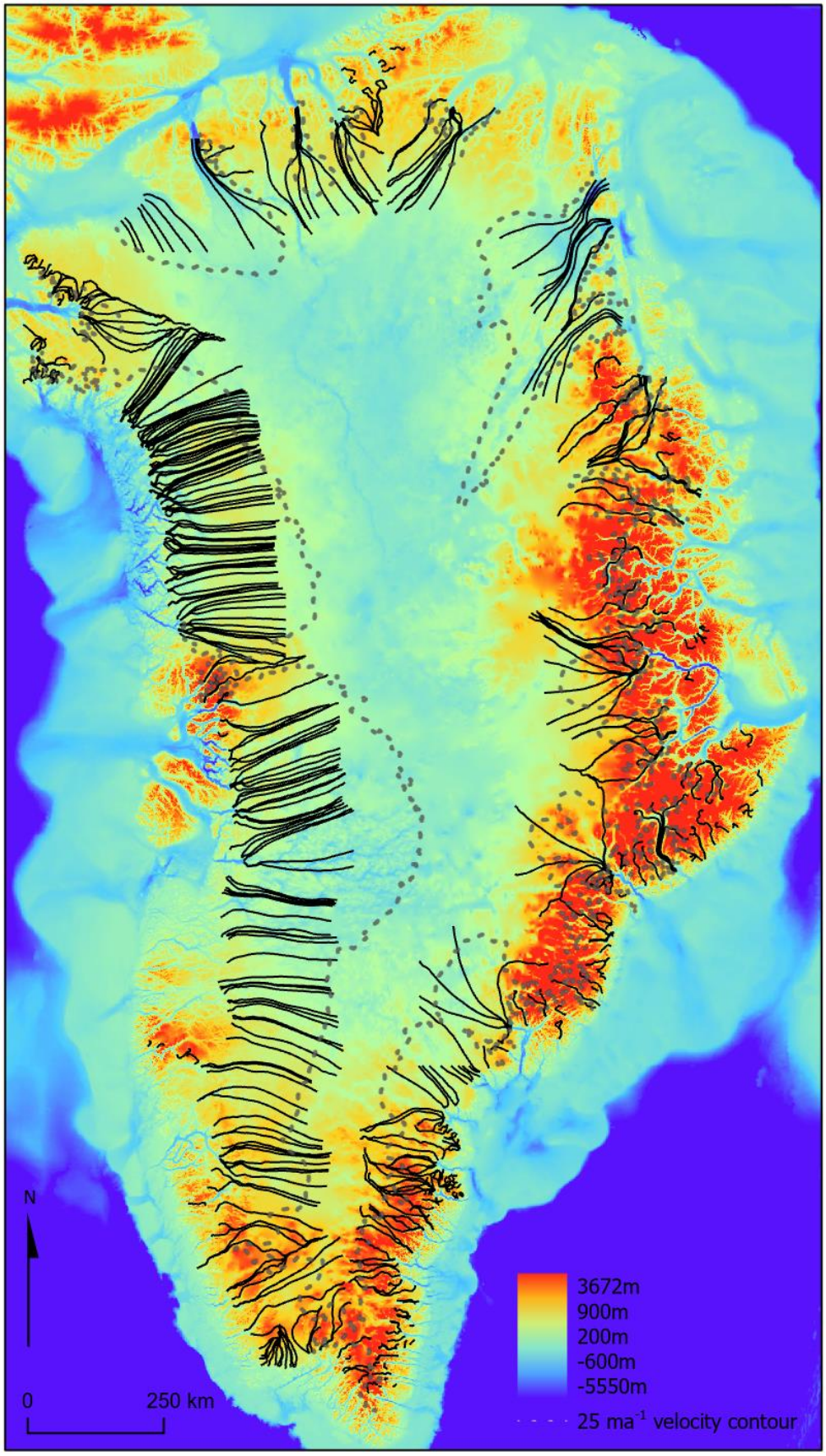

Figure 3.4. The central flowline dataset generated for Greenland. Central flowlines are shown as black lines over the BedMachine3 DTM. Grey dashed line shows the 25 m a^{-1} ice velocity contour

3.2.1.4 Adding data to central flowlines

The central flowlines were used as a visual reference guide for the manual identification and mapping of overdeepenings. To further aid their use as a visual reference, points were added along each central flowline at 150 m intervals. The bed elevation from the BedMachine dataset was then added to these points, essentially converting the 2D central flowlines to 3D longitudinal transects. This facilitated the plotting and further analysis of these transects using custom written Python code. In particular, the 'find_peaks' tool from the scipy.signal library was used to identify peaks in the longitudinal profiles (see Figure 3.5). These peaks were then exported as points and visualised along with the central flowlines in GIS.

3.2.1.5 Manual identification of closed topographic basins

The basis of mapping the overdeepenings was a contour layer generated from the BedMachine bed elevation data in ArcGIS 10.7.1. The Contour tool was used with a contour interval of 50 m, a base interval of 0, and contours generated as polylines. These contours were then overlain with the central flowlines peak points, and underlain by a hillshade of the BedMachine bed elevation layer for reference. The area under and surrounding each central flowline was systematically inspected starting at the glacier front and moving upstream. Peak points were used as a visual aid to identify saddles between overdeepenings, but mapping was not limited to where these points indicated potential overdeepening boundaries. Where closed topographic basins were identified in the contour layer, these were mapped as overdeepenings by selecting, copying, and pasting them into a new GIS layer. All parent and sibling (e.g. nested overdeepenings within overdeepenings) were mapped. Due to computational efficiency in the way very large vector files are handled, and the functionality to custom assign keyboard shortcuts, this mapping was conducted in QGIS 2.14. The contours used for the mapping were polylines so the final mapping step involved running a custom Python script to convert the polylines to polygons, and order them such that the smallest polygons were at the top of the layer with sequentially larger polygons lower in the stack. An example of this workflow is illustrated in Figure 3.5

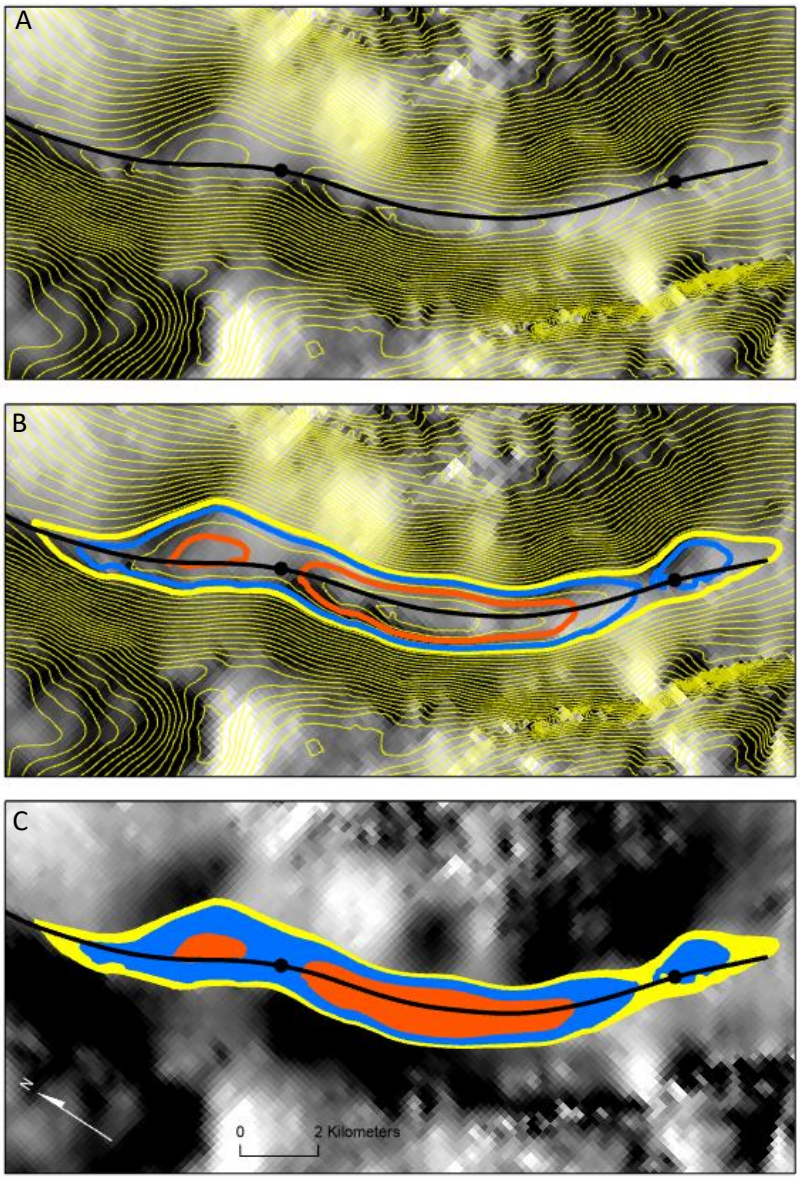

Figure 3.5. Example illustrating the process for mapping overdeepenings, the principal overdeepening for Kangerdlugssuaq glacier, east Greenland, is shown. A) 50m contours generated from the BedMachine3 shown over a hillshade of the same DTM. The black line shows the central flowline, black points mark the automatically generated peaks in the longitudinal transect which are used as a guide for manually identifying closed basins. B) closed basins have been selected and highlighted (yellow = parent basin, blue = child basins, red = grandchild basins). C) Closed basins saved as polygons, colours as in b.

3.2.2 Morphometric Analysis of overdeepenings

Once mapped, a full analysis of the morphology of Greenland overdeepenings was conducted. The approach adopted was based on that implemented by Patton et al. (2016) to enable comparison, and can be summarised as follows:

1. Generate true thalweg line through each parent overdeepening using a least cost path approach.

2. Add points at 150 m intervals to each thalweg and add bed elevation, surface elevation, and mean annual ice velocity data to these points.
3. Create transects normal to the thalweg at 150 m intervals and clip to the overdeepening to measure width. These values were used to create an average width for each parent overdeepening.
4. Apply quality control parameters to remove mapped overdeepenings which are unlikely to be of glacial origin, or where the data resolution is not sufficient to be confident that the closed topographic depression mapped is a genuine overdeepening rather than a Digital Terrain Model (DTM) artefact (e.g. very small depressions).
5. Use code written in Python to generate longitudinal transects through each parent overdeepening using the data added at 150 m intervals along the true thalweg, visualise the transects, and derive, aggregate, and analyse key morphometric parameters.

Each step is described in more detail below.

3.2.2.1 Generating true thalwegs using a least cost path approach

Central flowlines generated for the purposes of the overdeepening mapping exercise (as in Figure 3.3) do not always follow the true thalweg of an overdeepening. It is common for ice to flow at a slight angle to the true thalweg for sections of an overdeepening, especially in longer overdeepenings. This is because the ice is not completely controlled by the local topography and therefore can diverge from the line of continuous maximum descent as it flows through an overdeepening. Also, as flowline seedpoints were arbitrarily generated at the ice front, the flowline selected as the central flowline may not be precisely on the line of continuous maximum descent to start with as it enters the overdeepening. An example of this can be seen in Figure 3.6a; at the downstream end of the overdeepening (to the south east of the map), the central flowline is in the centre of the overdeepening. As the flowline moves up through the overdeepening it diverges off to the north and by the time it reaches the upper end of the overdeepening it is at the lateral margin of the overdeepening, quite a way away from the true thalweg. This inaccuracy is fine when the lines are being used as a visual guide for identifying and mapping overdeepenings, but for the purposes of

morphometric analysis, a more precise determination of the thalweg is required.

To generate true topographic thalwegs, entry and exit lip points for each parent overdeepening were created. Entry points were taken as the node with the highest ice surface elevation in the polygon delineating the overdeepening, exit points as the node with the lowest ice surface elevation. For each overdeepening the Cost Distance tool in ArcGIS Desktop 10.7 was run to generate Cost Distance and Backlink layers with bed slope as the cost surface, and lip entry point as the source. The Least Cost Path Polyline tool was then run using the Best Single setting with the lip exit point as the destination. This generated the true thalweg following the line of continuous maximum descent from the overdeepening entry point to the exit point. Figure 3.6b shows an example of an overdeepening with the thalweg plotted between the entry and exit points of an overdeepening using the least cost path approach. The thalweg is located in the centre of the overdeepening following the line of maximum descent throughout its length, representing the true topographic thalweg, and eliminating the inaccuracy seen using the central flowline method. These true topographic thalwegs were used for all morphometric and velocity analysis in this chapter.

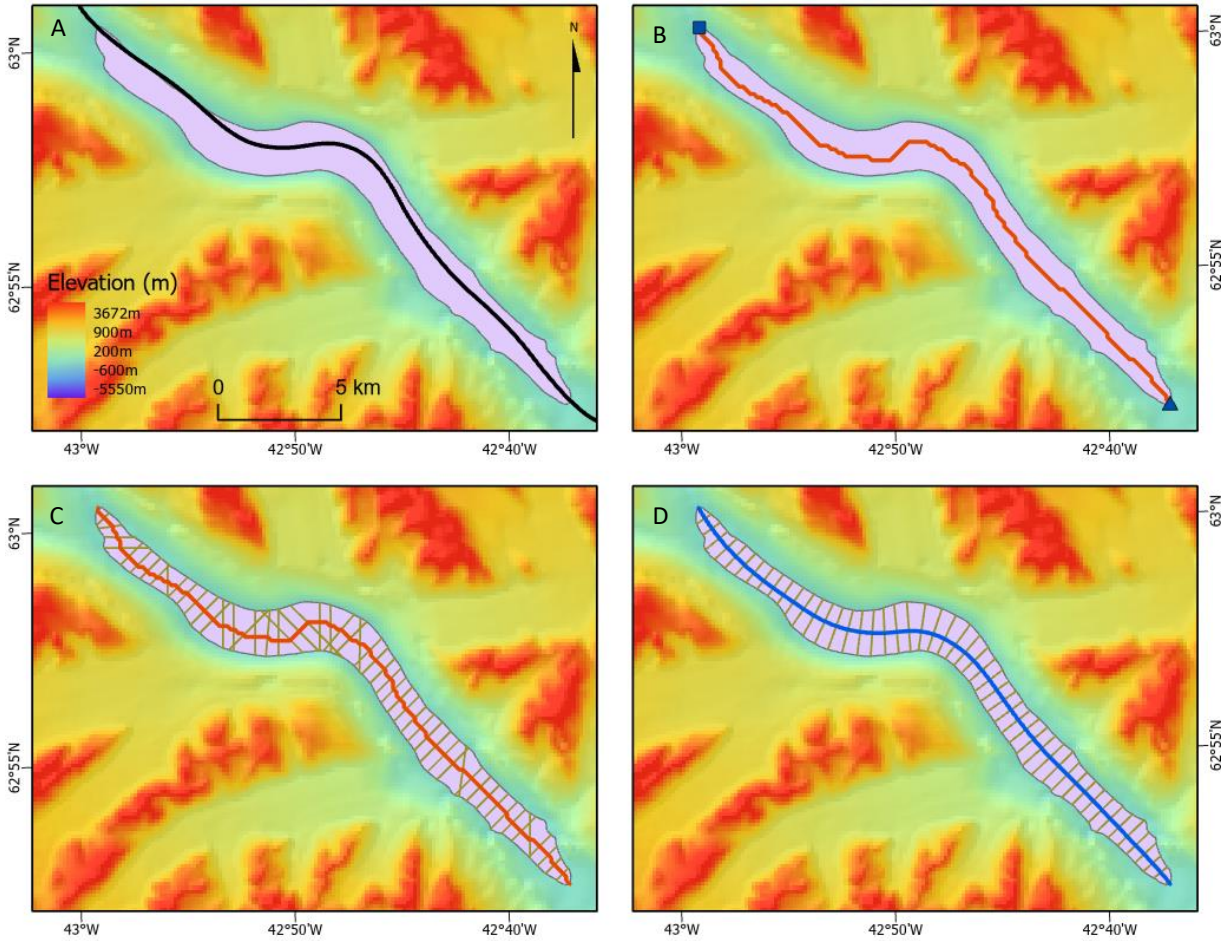

Figure 3.6. Method for mapping true topographic thalwegs shown for a single example overdeepening. Ice flow is from the north west to the south east. The overdeepening is shown over BedMachine3 bed elevation data visualised with a hillshade. A) the purple polygon shows the mapped overdeepening, the black line is the central flowline (as shown in Figure 3.3 and Figure 3.4). B) The red line shows the true topographic thalweg for the overdeepening generated using the least cost path approach. The blue square is the overdeepening entry point, the blue triangle is the overdeepening exit point. C) Green lines show transects plotted at 150 m intervals normal to the thalweg. Note the error induced which over estimates overdeepening width where transects are plotted on a 90 degree bend in the thalweg resulting from the raster origin of the line. D) The smoothed true topographic thalweg is shown in blue with associated accurate transects measuring overdeepening width.

3.2.2.2 Adding data to the thalwegs

In order to conduct morphometric analysis and investigate potential relationships between morphometry and velocity, ice surface elevation, bed elevation, and ice velocity data needed to be associated with each thalweg. Points were generated at 150 m intervals along each thalweg to match the spatial resolution of the BedMachine data. Bed elevation and surface elevation were added from BedMachine v3 (Morlighem et al., 2017), and mean annual ice velocity for 2016 was added from the MEaSUREs dataset (Joughin, 2017).

3.2.2.3 Calculating average overdeepening width

As the least cost path polyline is generated from a raster at the resolution of the slope layer (150 m) the resulting output is quite angular, with curves made up of sequences of individual 90 degree bends (Figure 3.6b). This causes errors when plotting transects to measure average overdeepening width as some of the resulting transects are not truly normal to the overdeepening long axis resulting in an over estimate of width (Figure 3.6c). To resolve this issue the output least cost path polylines were smoothed using the Smooth Line tool in ArcGIS Pro 2.8 applying the PAEK algorithm at a 5000 m smoothing tolerance. An example of the resulting smoothed thalweg line is shown in Figure 3.6d. The transects generated using these smoothed thalweg lines are normal to the overdeepening long axis and give an accurate measurement of the overdeepening width. Mean transect width was calculated using the 150 m spaced transects to give an estimation of mean width for each mapped parent overdeepening.

3.2.2.4 Applying quality control parameters

Quality control parameters were implemented which followed the approach of Patton et al. (2016), to ensure that the features included in the dataset did not include; non-glacial features, features formed under previous ice sheet configurations that are no longer in equilibrium with the present ice sheet, and features that may be artefacts in the DTM rather than genuine morphological features. Some adjustment to the quality control thresholds are made to take account of the higher resolution of the data used in this study, the details of these deviations are highlighted in the workflow below as appropriate. Parameters applied were as follows:

- Mapped overdeepenings with an elongation ratio of less than 2:1 length:width were excluded from the dataset. In total, 103 (8.0%) of the mapped parent overdeepenings were removed from the metric dataset based on this criteria.
- Mapped overdeepenings where long axis orientation is not aligned with ice flow are excluded from the dataset. This was determined by manual visual inspection of each mapped overdeepening with respect to calculated flowlines. Mapped overdeepenings were excluded where the majority of the true thalweg was at an

angle greater than 45° from average ice flow over the overdeepening. Figure 3.7 shows an example of an overdeepening excluded on this basis; 14 (1.1%) of the mapped overdeepenings were removed from the metric dataset based on this criteria.

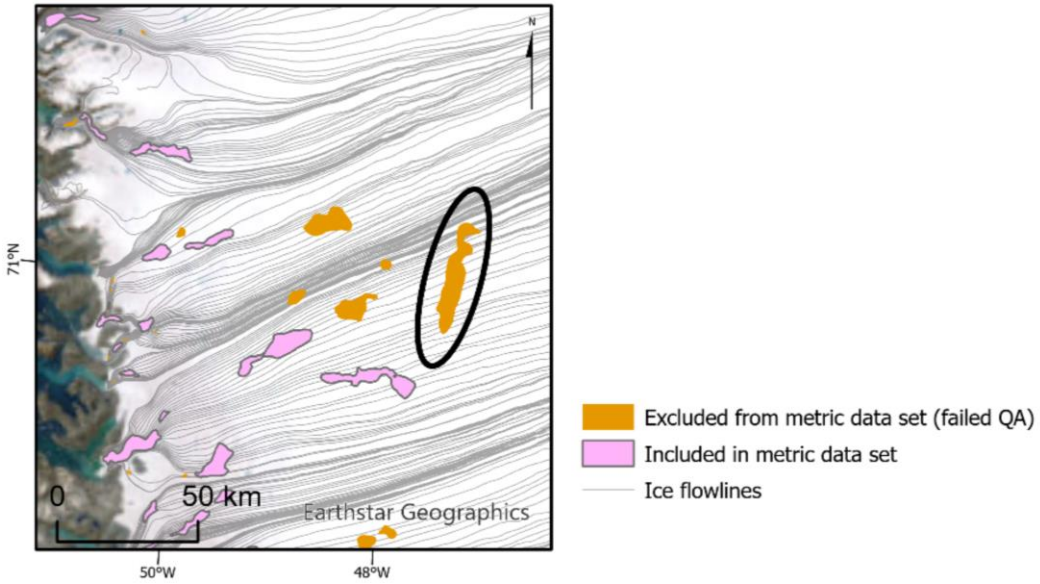

Figure 3.7 The overdeepening circled in black is an example where the mapped overdeepening has been excluded from the metric dataset due to it being misaligned by more than 45° from ice flow. Note: all other overdeepenings in the figure marked as excluded have been so as a result of failing to meet other QA criteria, not misalignment.

- Patton et al. (2016) applied a quality control parameter to exclude overdeepenings with adverse slope length less than 5 km, the resolution of the bed DEM used. In this study, no overdeepenings mapped had an adverse slope length less than the BedMachine v3 resolution of 150 m. As such, none of the mapped overdeepenings were excluded on this basis.
- Mean bed elevation error (using published error estimates from BedMachine v3) was calculated for each mapped overdeepening. Where the mean bed error was greater than the overdeepening depth, overdeepenings were removed from the metric dataset. In total, 546 (42.5%) of the mapped parent overdeepenings were removed from the metric dataset on this basis. Figure 3.8 shows the BedMachine v3 bed elevation error layer in relation to mapped overdeepenings. Overdeepenings mapped as red, orange, and yellow in Figure 3.9c are the overdeepenings excluded from the metric dataset.

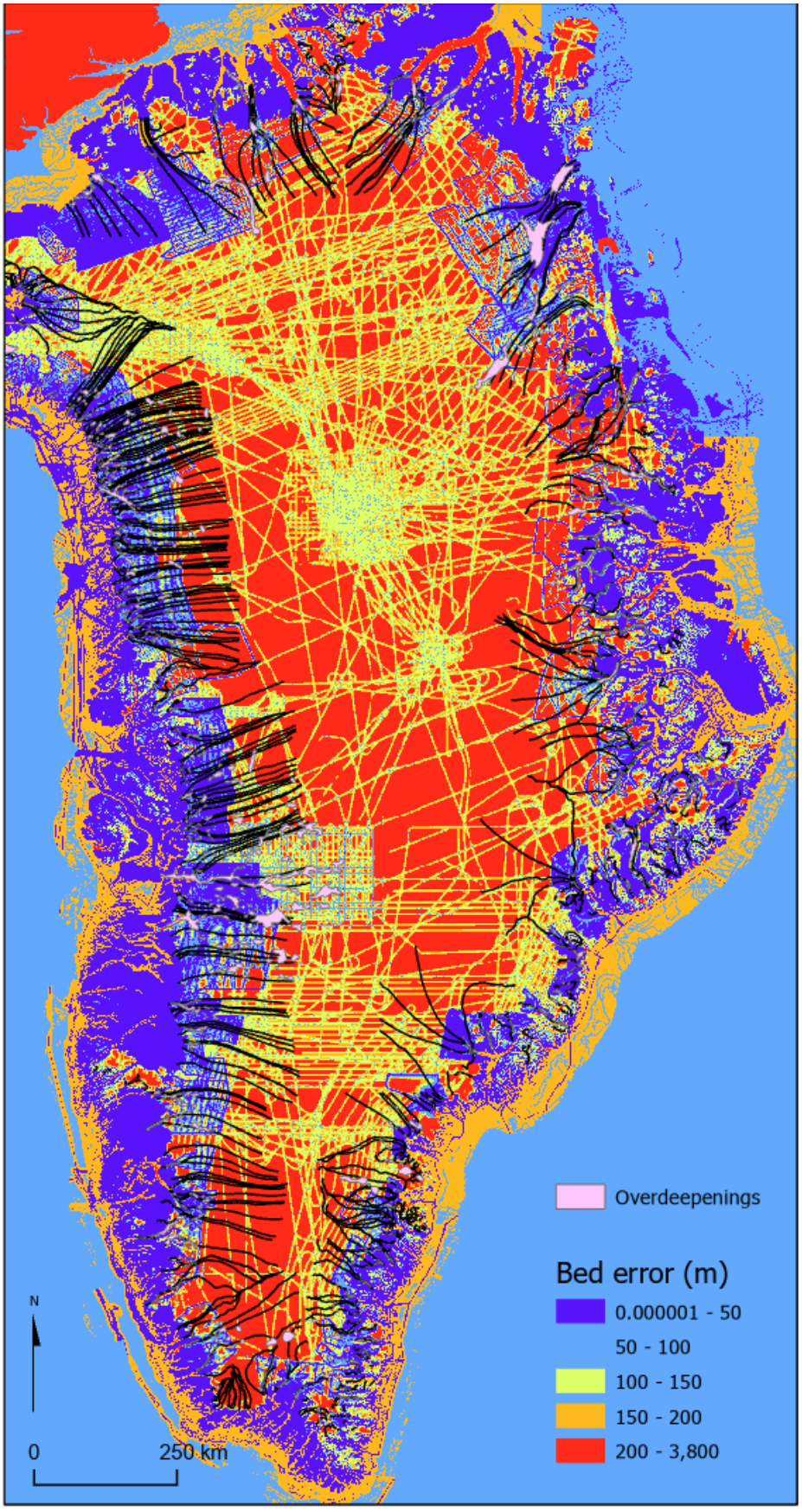

Figure 3.8 Bed elevation error for BedMachine v3 (Morlighem et al. 2016). Mapped overdeepenings are shown in blue, central flowlines as black lines.

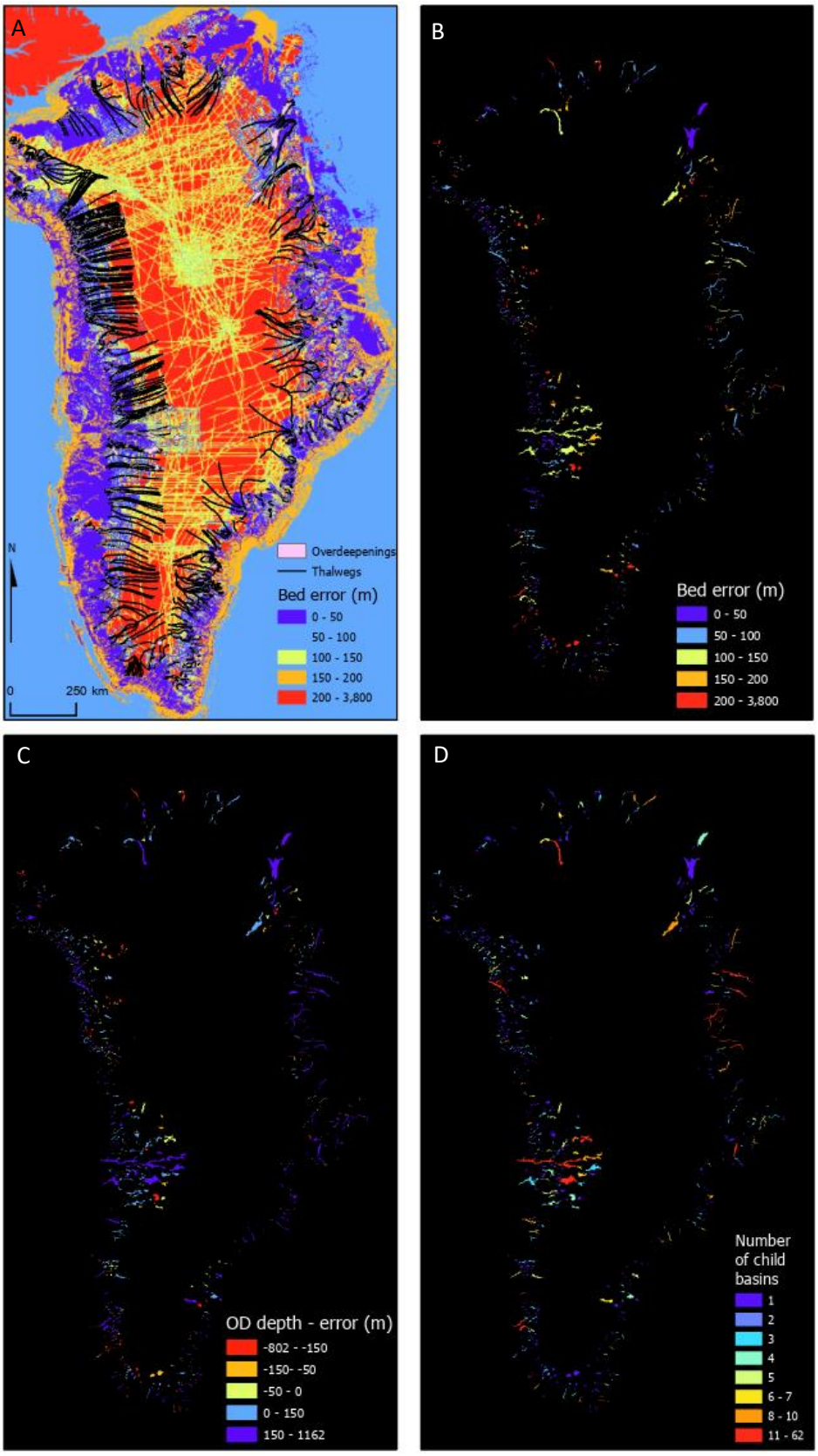

Figure 3.9. Bed elevation error for BedMachine v3 (Morlighem et al. 2016), error relative to overdeepening depth, and overdeepening complexity. A) Published estimated error of BedMachine v3 bed elevation. Mapped overdeepenings are shown in blue, central flowlines are shown as black lines. B) Mean bed error for each mapped parent overdeepening, cold colours represent lower error, hot colours represent higher error. C) The difference between overdeepening depth and mean

overdeepening bed error. Negative values indicate overdeepenings where the mean bed error is greater than the overdeepening depth. D) The number of sub-basins (e.g. child basins) contained within each parent basin.

3.2.2.5 Morphometric analysis using Python

Code was written in Python to plot points at 150 m intervals along the true topographic thalwegs mapped (see 3.2.2.2) and extract bed and surface elevation from BedMachine 3 (Morlighem et al., 2017).The code then iteratively loops through consecutive nodes on each thalweg to calculate the bed gradient, surface gradient, and bed to ice surface slope ratio (BSSR) between each pair of consecutive points. These individual values were then aggregated, and averages calculated for each overdeepening in the metric dataset. Other metrics such as total overdeepening length, adverse slope length, average adverse slope gradient, overdeepening depth, and overdeepening asymmetry were also calculated. The code then created a series of scatter plots of the metrics against one another for comparison (Figure 3.21), and generates a pairwise correlation matrix (Figure 3.22). The code also calculates overall average values of these metrics for the entire metric dataset which can be tabulated for comparison to other studies (Table 3.2). Finally, the code visualises a cross sectional profile of the bed and surface elevation along the true thalweg for each overdeepening in the metric dataset (Figure 3.19).

3.2.2.6 Classification of topographical control

The method adopted by Patton et al. (2016) for determining whether ice flow through an overdeepening is topographically controlled is also implemented in this study. Overdeepenings were classified as being topographically confined where the mean elevation in a 20 km wide buffer area surrounding the overdeepening was more than 500 m higher than the basin perimeter elevation.

3.2.3 Classifying ice flow regime and confluence location

Flow regime refers to the nature of ice flow over the overdeepening. Visual interpretation of the flowlines over each overdeepening was made, and flow regime was classified as either converging, parallel, or diverging. Where there was insufficient flowline coverage over an overdeepening it was marked as unclassified. Figure 3.10 illustrates exemplars of each flow regime. If the flow regime above an overdeepening was complex or a composite of regimes it was also marked as unclassified.

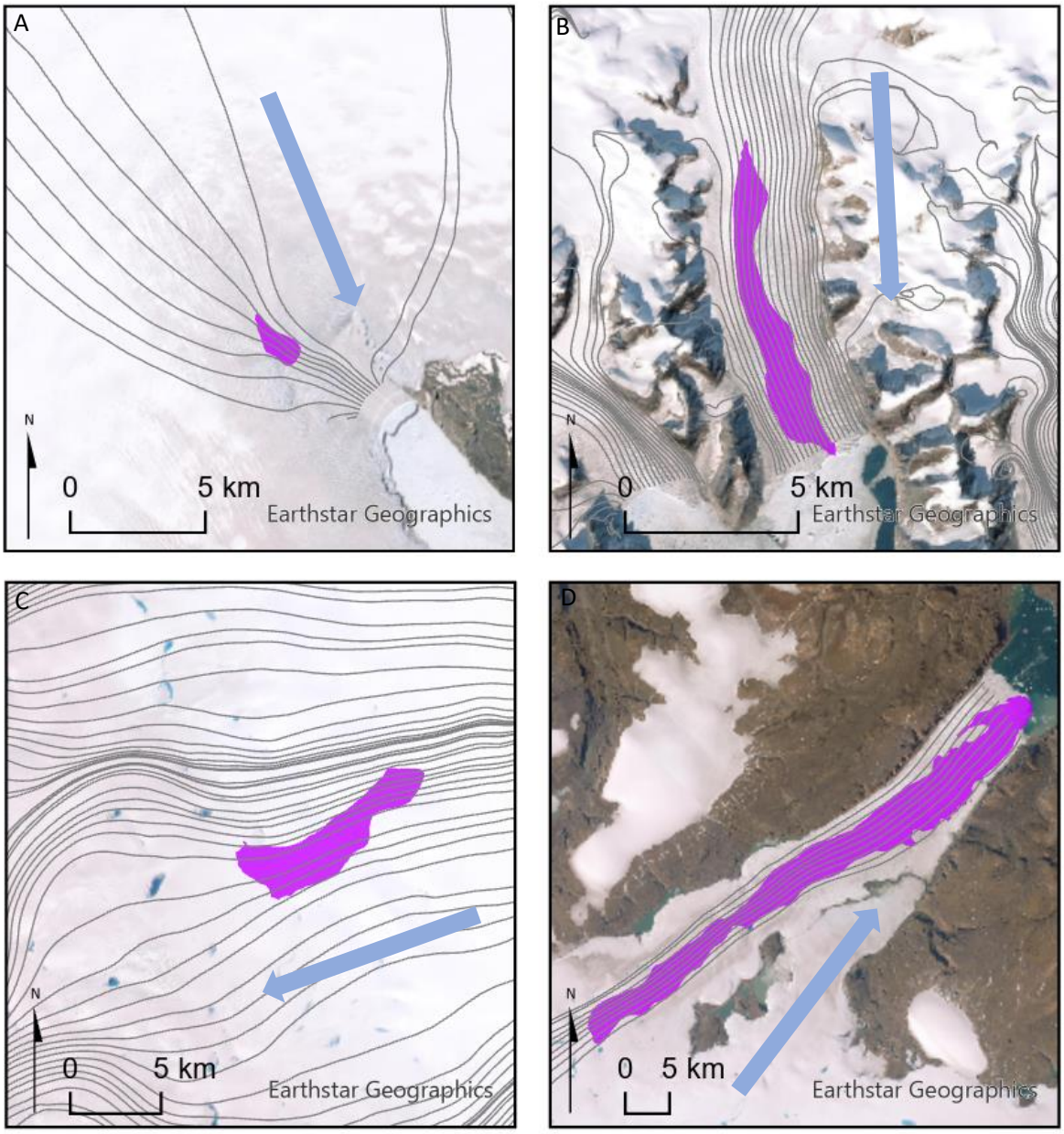

Figure 3.10 Exemplars for each ice flow regime category. Direction of ice flow is indicated by the arrow in each pane. A) An overdeepening situated in "convergent" flow ice flow. B) An overdeepening situated in "parallel" flow ice flow. C) An overdeepening situated in "divergent" flow ice flow. D) An overdeepening where the flow regime was complex and composite. As such, it has not been classified. Due to the large size of the overdeepening, it has elements of convergent, parallel, and divergent flow along different sections of its length.

Each overdeepening was also visually assessed with respect to confluence location using the flowlines dataset. Glacier confluences were manually identified from the flowlines and overdeepenings were classified as being either: at a confluence, straddling a confluence, directly downstream of a confluence, or not at a confluence. Where there was insufficient flowline coverage over an overdeepening it was marked as unclassified. Exemplars of each

classification are illustrated in Figure 3.11 along with details on the decision making process for classification.

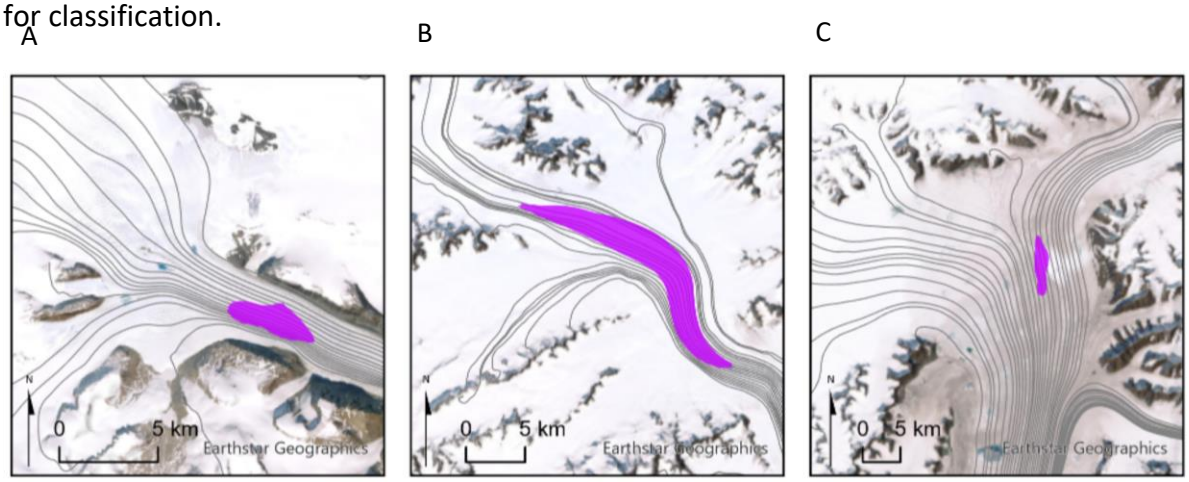

Figure 3.11 Exemplars for each confluence location category. A) An overdeepening located "directly downstream" of a confluence. This is where an overdeepening is within approximately one glacier width of the downstream margin of a glacier confluence, but the overdeepening does not intersect with the zone of confluence. B) An overdeepening "straddling" a confluence. This is where an overdeepening extent extends substantively both upstream and downstream of the zone of confluence, with the centre of the overdeepening approximately located coincident with the centre of the zone of confluence. C) An overdeepening located "at" a confluence. The overdeepening extent intersects with the zone of confluence but does not substantively extend both up and downstream of it.

3.2.4 Lithological composition of underlying bedrock

The dominant lithology underlying each mapped overdeepening was determined by calculating the surface area of each lithology type within the overdeepening, and then categorising the overdeepening as the lithology with the maximum surface area. This analysis was conducted using the Zonal Statistics tool in ArcMap 10.7. Data on lithology was from Gowan et al. (2019).

3.2.5 Velocity analysis

The following steps were taken to create these data to enable the analysis of the variation in ice velocity across normal and adverse slopes that is the focus of RQ2:

1. MEaSUREs 2016 annual mean velocity data (Joughin, 2017) was added to points at 150 m intervals along each parent overdeepening true thalweg.
2. Python code was written to iterate sequentially through the 150 m spaced points along each parent overdeepening true thalweg to calculate the acceleration or deceleration in ice velocity over each 150 m section. Code also then calculated

average values of ice velocity and acceleration for the normal slope and adverse slope of each parent overdeepening.

3. Python code was written to create scatter plots of average ice velocity and acceleration against each of the morphometric parameters measured for parent overdeepenings (Figure 3.26).
4. Python code was written to aggregate ice velocity and acceleration data for 150 m sections into two classes (normal and adverse bed gradients) for each overdeepening, based on the bed gradients calculated for each 150 m section as described in point 3.2.2.5 (above). Python code then calculated average velocity and acceleration values for normal and adverse bed slopes for each parent overdeepening.
5. Python code was written which produced histograms visualising the frequency distributions of average velocity and acceleration across the parent overdeepenings in the metric dataset, and how this varied between normal and adverse bed slopes (Figure 3.27).

3.3 Results

3.3.1 Number and distribution of overdeepenings: how common are overdeepenings under the GrIS?

In total 2,393 overdeepenings were mapped (Figure 3.12). Of these, 1,284 were parent overdeepenings. A total of 621 parent overdeepenings (48.4% of those mapped) met the quality control criteria and are included within the dataset for the morphometric analysis.

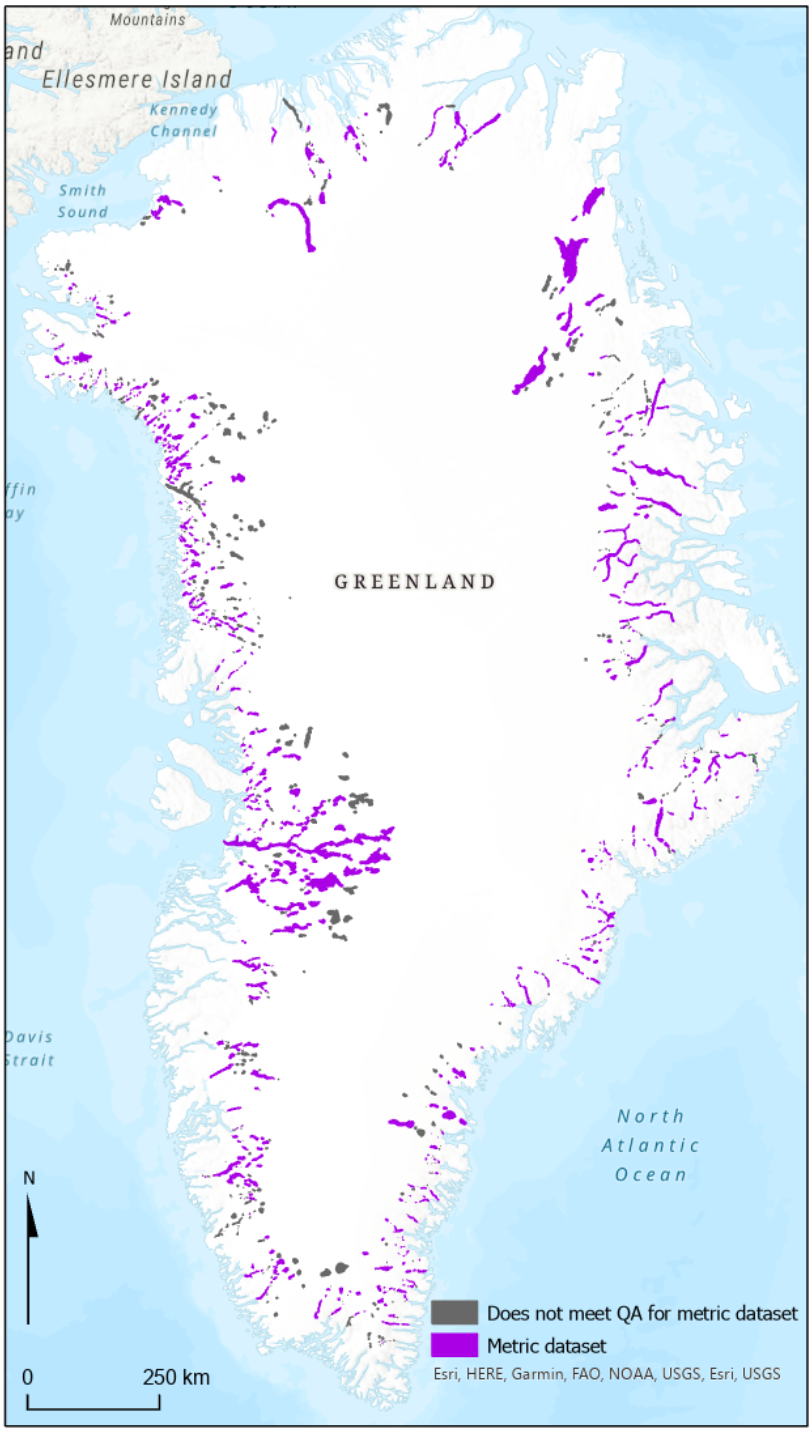

Figure 3.12. Mapped overdeepenings in Greenland, with only parent overdeepenings shown. Overdeepenings in blue meet the quality assurance standard for inclusion in the metric dataset, those in grey do not.

The overall distribution of overdeepenings around the margin of the Greenland Ice Sheet is relatively even. The main areas where overdeepenings are absent strongly coincide with areas where there is a lack of fast streaming ice (e.g. areas along the north coast where there are neither central flowlines or overdeepenings mapped in Figure 3.12 and Figure

3.13). In general, overdeepenings appear more elongated on the east coast where there is a higher proportion of topographically constrained overdeepenings. Overdeepening complexity (e.g. number of child basins contained within a parent basin) is fairly evenly dispersed in terms of spatial distribution.

Overdeepenings are near ubiquitous features under Greenland outlet glaciers. Of the 553 central flowlines mapped (see Figure 3.4), 396 (71.6%) intersect with at least one overdeepening from the metric dataset (Figure 3.13). Many of the central flowlines with no overdeepenings are small peripheral glaciers. Very few large, fast flowing outlet glaciers do not intersect an overdeepening. Average ice velocity values at the terminus of central flowlines not intercepting an overdeepening are substantially lower (mean 825 m a^{-1}, median 367 m a^{-1}) than for central flowlines that do intercept at least one overdeepening (mean 1839 m a^{-1}, median 1102 m a^{-1}) (Figure 3.14).

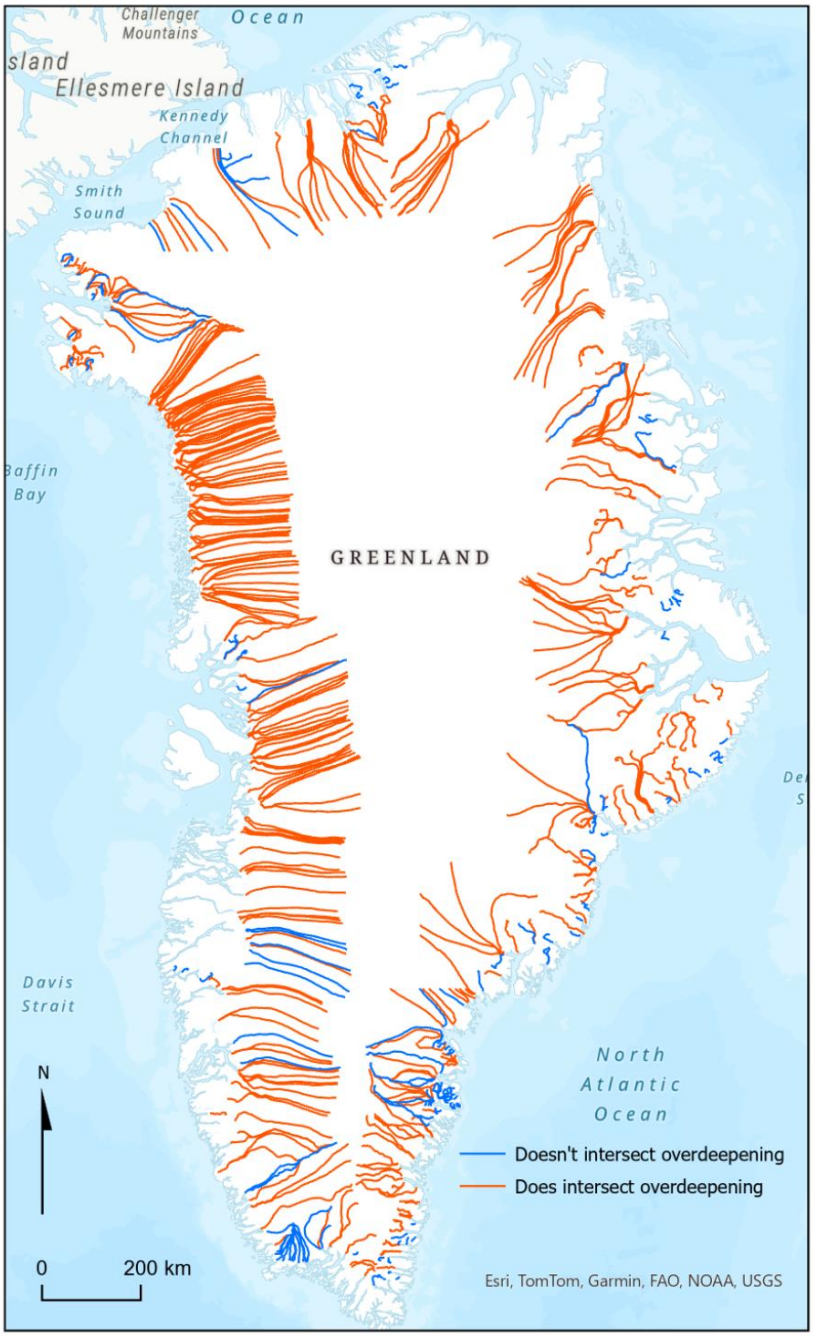

Figure 3.13. Maps show central flowlines generated as in Figure 3.4. Here red shows central flowlines that intersect at least one of the mapped overdeepenings. Central flowlines that do not intersect and overdeepening are shown in blue.

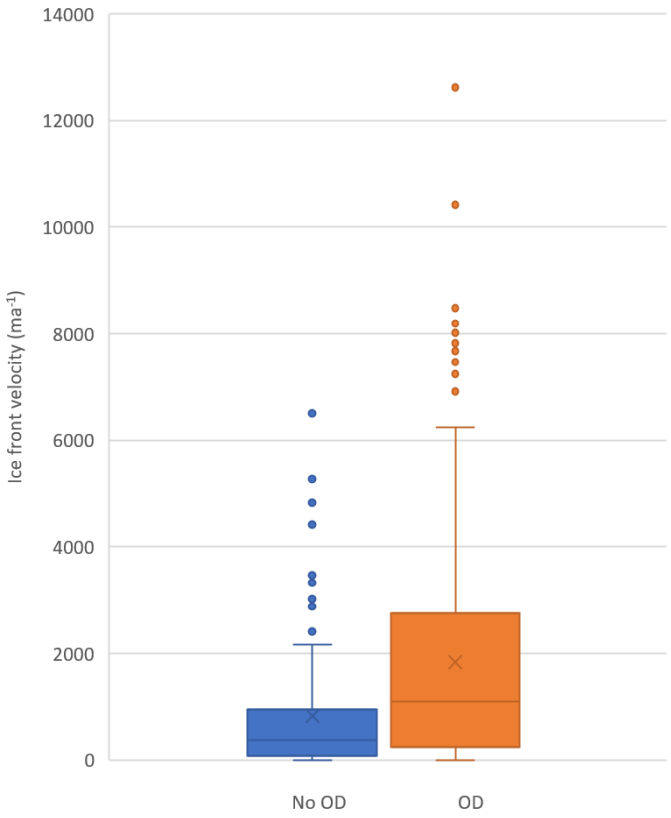

Figure 3.14. Box and whisker plot showing the ice velocity values at the ice front / terminus for central flowlines that do not intersect at least one overdeepening (blue), and central flowlines that do intercept at least one overdeepening (red). The values plotted here are for the central flowlines mapped in Figure 3.13. Velocity data is average annual velocity from 2016 (Joughin, 2017). Crosses show the mean, lines show the median, boxes show the interquartile range (IQR), whiskers show the minimum and maximum values (excluding outliers), outliers (upper > Q3 + 1.5 x IQR, lower < Q1- 1.5 x IQR) are plotted as dots.

3.3.1.1 Controls on overdeepening location

Three of the key factors that have been hypothesised to influence the location and morphology of overdeepenings are ice flow regime, confluence location, and the underlying lithology (see sections 2.2.2.1 and 3.1). The results are presented in turn below.

Ice flow regime

In total, it was possible to determine the flow regime for 456 of the 621 overdeepenings in the metric dataset. The 165 overdeepenings where flow regime was not determined were in locations not covered by the flowlines generated (see section 3.2.1.2). Converging ice flow was the dominant regime within which overdeepenings were located (62%), followed by parallel flow (37%), with only 9% of overdeepenings located under diverging ice (Figure 3.15**Error! Reference source not found.**).

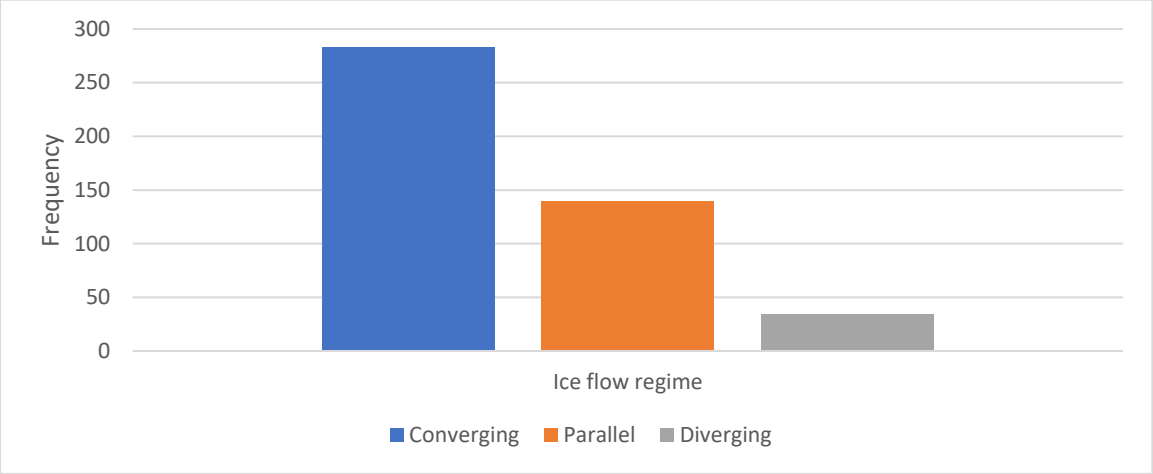

Figure 3.15. Frequency of overdeepenings in each ice flow regime category.

Confluence location

In total, it was possible to determine whether there was co-location with a confluence in ice flow for 493 of the 621 overdeepenings in the metric dataset. As with ice flow regime, the overdeepenings where confluence location was unable to be determined were those that lay outside the flowline data. The vast majority of overdeepenings were not located at a confluence (82%). 9% of overdeepenings were at a confluence, 5% straddled a confluence, and 4% were directly downstream from a confluence (Figure 3.16).

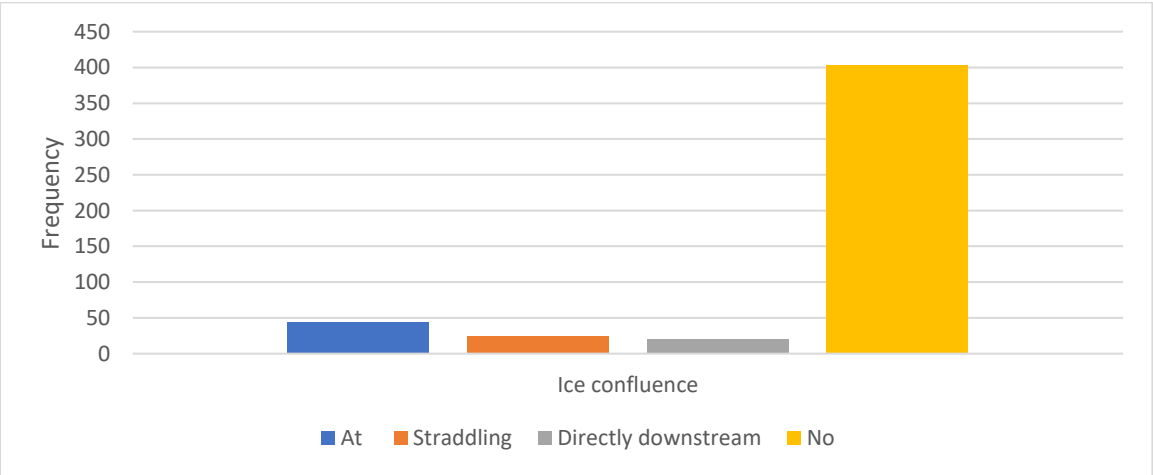

Figure 3.16. Frequency of overdeepenings in each ice confluence location category.

Underlying lithological composition

The underlying lithology was determined for all 621 overdeepenings in the metric dataset (Figure 3.17)

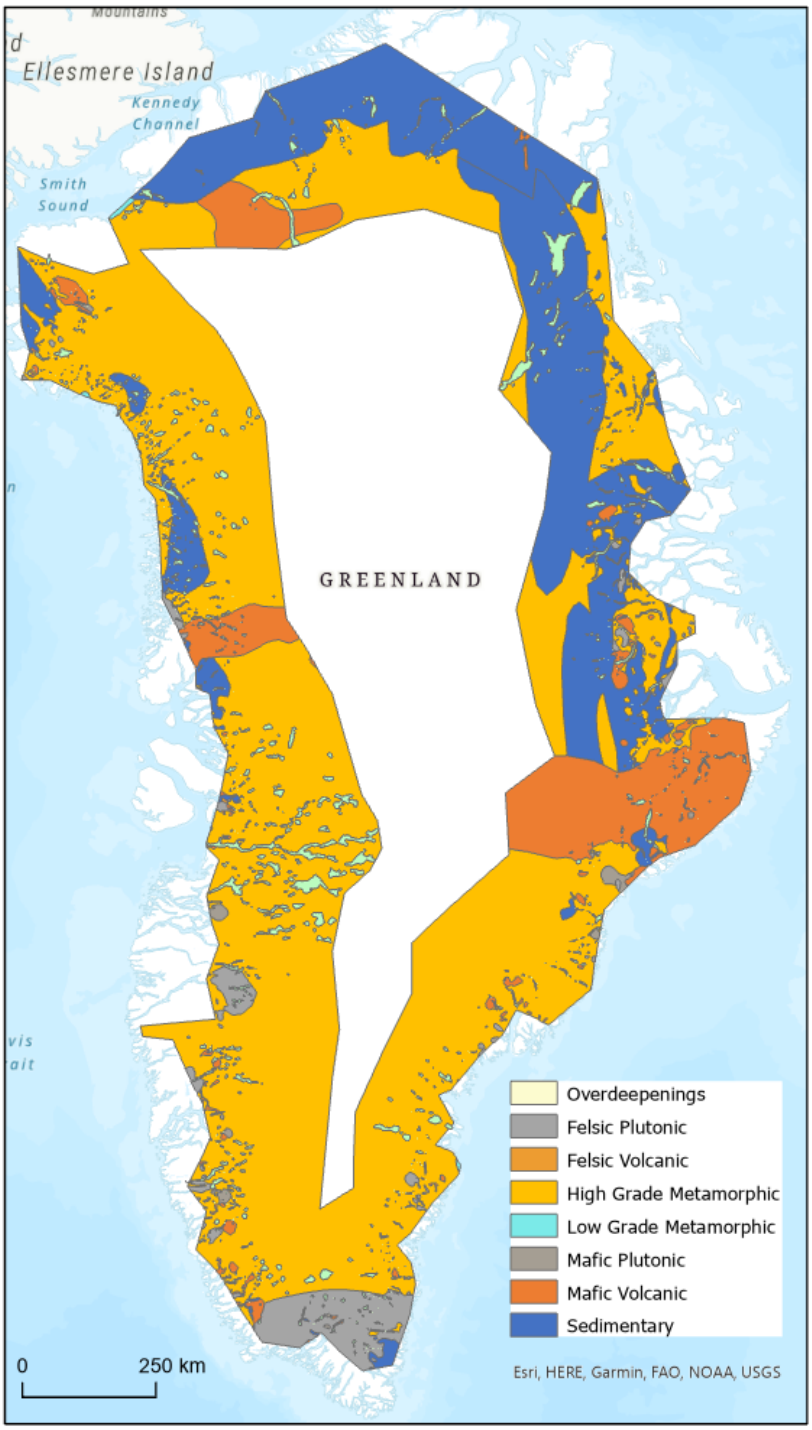

Figure 3.17 location of mapped overdeepenings with respect to bedrock lithology (lithology source: Gowan et al, 2019). Note, only the lithology within the mapping study area is shown.

High grade metamorphic rock is the dominant lithology representing 64% of

overdeepenings. Sedimentary rock represents 18% of overdeepenings, volcanic 10%, and plutonic 8% (Figure 3.18).

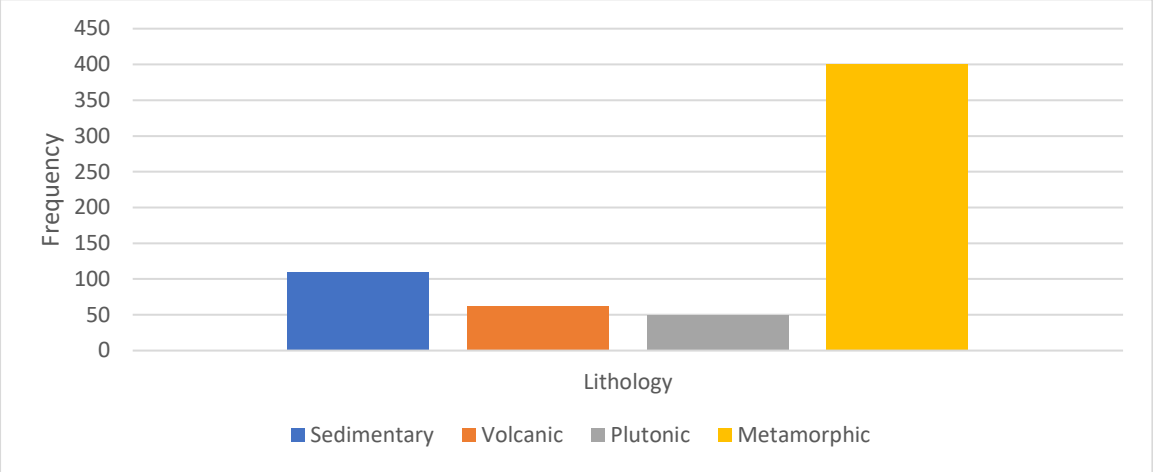

Figure 3.18. Frequency of overdeepenings of each lithology type.

Table 3.1 shows the expected frequency of overdeepenings based on the proportion of the study area covered by each lithology type, the observed number of overdeepenings of each lithology, and observed overdeepening frequency adjusted to give a count of the total number of overdeepenings in the metric dataset weighted by the relative overdeepening surface area percentage of each lithological class in the metric dataset. For example, 25.5% of the total mapped overdeepening surface area in the metric dataset was made up of overdeepenings of sedimentary lithology, therefore the adjusted 'observed' overdeepening frequency is 159 (25.5% of the 621 total overdeepening count). When the data are adjusted in this way to take account of surface area rather than just a simple frequency count, there are slightly more overdeepenings in sedimentary lithologies, and fewer overdeepenings in volcanic lithologies than would be expected based on the relative prevalence of these lithologies as a whole within the study area. The area adjusted observed frequency of overdeepenings for plutonic and metamorphic lithologies is very close the expected frequency (Table 3.1). A Chi -squared test for this data demonstrates there is a statistically significant difference (p value = 0.0082) between the expected and observed overdeepening frequencies.

Table 3.1 Expected, observed, and observed adjusted by area counts of overdeepenings in each lithological category. Expected number of overdeepenings in each lithological category assuming overdeepening frequency in each category is proportional to the area of each lithological category within the total study area. The observed number of overdeepenings in the column on the right has been adjusted to give a frequency count based on the total number of overdeepenings in the metric dataset weighted by the percentage area of the total mapped overdeepening surface area in each lithological category. For example, 25.5% of the total mapped overdeepening surface area is made up of overdeepenings in the sedimentary category, as such, the frequency of 'observed' overdeepenings in this category is 159 (621 x 0.255). A Chi-squared test comparing the adjusted observed to the expected counts returns a p value of 0.0082.

	Expected	**Observed (actual number)**	**Observed (adjusted by area)**
Sedimentary	143 (23.0%)	110	159 (25.5%)
Volcanic	62 (10.0%)	62	38 (6.1%)
Plutonic	23 (3.6%)	49	21 (3.4%)
Metamorphic	393 (63.3%)	400	403 (65.0%)

3.3.2 Overdeepening morphology: how variable is their geometry?

A total of 621 parent overdeepenings (48.4% of those mapped) met the quality control criteria and were included within the dataset for the morphometric analysis. Of these 241 were classed as topographically constrained and 380 as non-topographically constrained. Longitudinal transects along the true thalweg through each overdeepening were generated for all overdeepenings. A sample of transects showing eight of the deepest overdeepenings is shown in Figure 3.19. As all analysis was conducted on parent overdeepenings, there is substantial variation evident in the profiles. Some 'parent' overdeepenings do not contain any child basins and are simple single closed topographic depressions (see Figure 3.19d), whereas others are highly nested and contain many child basins (see Figure 3.19g where the parent overdeepening contains approximately 10 child basins).

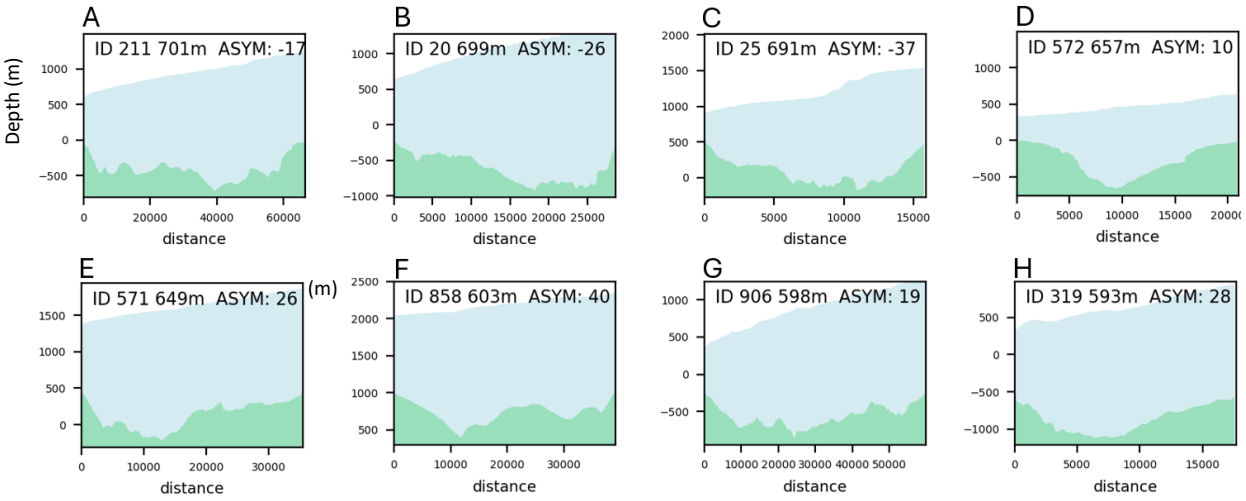

Figure 3.19. Example plots of the longitudinal overdeepening profiles. In all cases ice is flowing right to left. Each transect contains the ID code for the overdeepening, the maximum depth of the overdeepening, and the asymmetry of the overdeepening profile. An asymmetry of 0 represents an elevation minima half way along the profile, -100 is a minima located at the furthest upstream point, and +100 is a minima at the furthest downstream point of the profile. Distance units are in meters.

Summary statistics of the key morphometric parameters for the metric dataset are shown in Table 3.2, and histograms visualising the morphometric data are shown in Figure 3.20. All size-based parameters (width, depth, area etc) are positively skewed with a greater frequency of smaller features than larger features. For overdeepening length and depth, mean values are substantially larger than median values. The distribution of overdeepening width seems to have a less pronounced positive skew and the median value is only very slightly greater than the mean. With the exception of asymmetry and lip elevation (Figure 3.20e and Figure 3.20f) all morphometric parameters in Figure 3.20 display a strong unimodality. This unimodality provides some evidence of a preferred overdeepening morphology. However, there is a wide range of values within all metrics and standard deviation values are generally high.

Table 3.2. Average measured values for key overdeepening parameters from the 621 overdeepenings that passed the quality assurance thresholds.

	Mean	Median	Standard deviation	Min	Max
Length	15.0 km	9.2 km	19.6 km	0.8 km	217.8 km
Width	2.1 km	1.8 km	1.6 km	0.1 km	12.4 km
Elongation Ratio	7.1	5.1	6.1	2.0	51.6
Long profile asymmetry	1.22	0.00	40.78	-96.87	98.88
Depth	196 m	155 m	151 m	2 m	1014 m
Adverse slope gradient	0.069	0.058	0.046	0.012	0.408
BSSR	-2.22	-1.91	2.49	6.43	-19.96

The histograms in Figure 3.20 differentiate between overdeepenings that are topographically constrained and those that are non-topographically constrained. For some of the measured parameters there is very little difference between the two. In terms of length, for topographically constrained overdeepenings there is a very slightly lower frequency at the smallest end of the range, and a slightly higher frequency at the top end of the range than for the non-topographically constrained. The distributions of adverse slope length show very similar patterns with the topographically constrained overdeepenings slightly less frequent at the very low end, but with slightly higher frequency in and around the 10 km adverse slope length region. For other parameters, the difference between topographically constrained and non-topographically constrained overdeepenings is much more pronounced. Figure 3.20b and Figure 3.20c show a much stronger unimodality for the topographically constrained overdeepenings suggesting a preference for a narrower form with smaller surface area. Given that lengths were very similar, it follows that as the topographically constrained overdeepenings are narrower with lower surface area, their elongation ratio is larger than for non-topographically constrained basins. This can be seen

in Figure 3.20g where the non-topographically constrained overdeepening histogram appears much less positively skewed, with lower kurtosis, and a smaller right-hand tail, all indicating a much higher prevalence for high elongation ratios for these basins. The pattern is similar with respect to depth, with topographically constrained overdeepenings showing a tendency to greater depths.

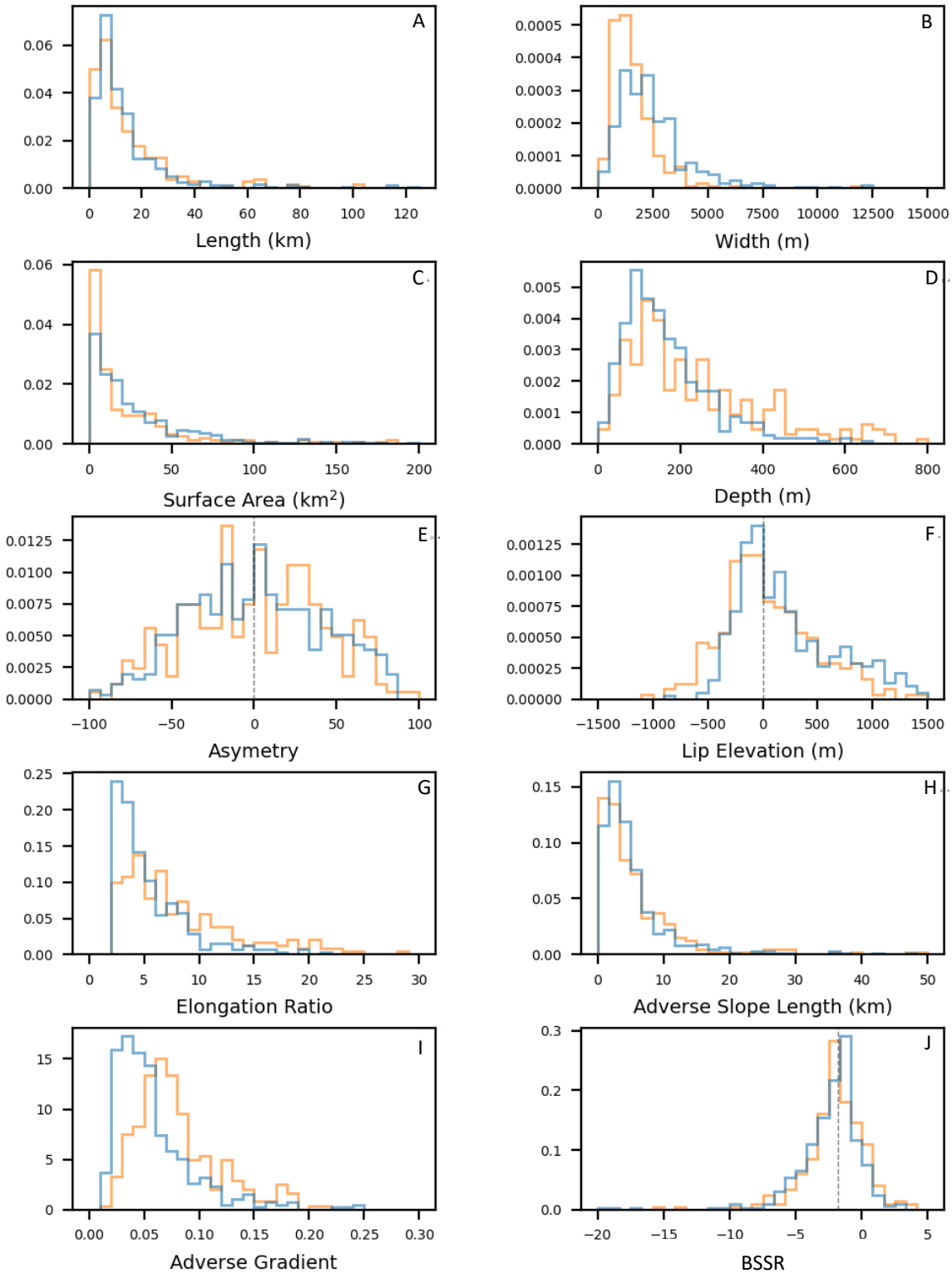

Figure 3.20. Histograms showing the distribution of overdeepening morphological parameters. Orange lines represent topographically constrained overdeepenings, blue lines represent non-topographically constrained overdeepenings. For parameters that are ratios or have negative values a vertical dashed line has been added for reference. E), F), and L) reference lines are at zero. J) reference line is at the BSSR supercooling threshold of -1.8. K) reference line is at one, where average ice velocity on the normal and adverse slopes of the overdeepening is equal.

Whilst the values for asymmetry show a broad peak in frequency around zero, and a relatively symmetrical distribution above and below this, there is a lot more variance in this graph compared to those for other metrics. This is perhaps reflective of the fact that many of the overdeepenings are highly nested (e.g. a parent overdeepening containing many smaller basins), and that as a result of having only calculated the asymmetry of the parent overdeepening (rather than for all child overdeepenings individually), some of the variance shown in Figure 3.20e may be noise rather than a true preference for highly bimodal overdeepening asymmetry. The shape of the frequency distributions for adverse slope gradient (Figure 3.20i) are similar, but with the topographically constrained overdeepenings offset around 0.04 higher with a peak at approximately 0.08 as opposed to approximately 0.04 for the non-topographically constrained overdeepenings. One of the most striking patterns in the morphometric analysis is the clear preference for a BSSR very close to the supercooling threshold of approximately -1.8 (see Figure 3.20j). The non-topographically controlled overdeepenings have a peak frequency just above this threshold, and the topographically controlled just below the threshold.

3.3.3 Relationships between morphometric parameters

A number of scaling relationships are evident in the measured overdeepening parameters (Figure 3.21). The correlations between all pairs of variables in Figure 3.21 are statistically significant at the $p<0.05$ level with the exception of depth vs lip elevation and depth vs asymmetry (Figure 3.21k and Figure 3.21l). A full pairwise correlation matrix giving the Pearson's correlation coefficient (PCC) for all measured variables can be seen in Figure 3.22. Overdeepening depth shows a strong positive correlation with overdeepening length (PCC = 0.55), adverse slope length (PCC = 0.58), elongation ratio (PCC = 0.53),and area (PCC = 0.51). Depth has a moderate positive correlation with adverse gradient (PCC = 0.33). Width and depth have a moderate (PCC = 0.37) positive correlation. Adverse slope gradient has a moderate negative correlation with both width (PCC = -0.45) and length (PCC = -0.43). Adverse slope gradient has a negative correlation with all other parameters where the correlation is both statistically significant and moderate or higher.

The scatter plots in Figure 3.21 also differentiate between those overdeepenings that are

topographically constrained, and those that are not. The patterns in variation that have already been demonstrated and discussed in Figure 3.20 are also apparent here; topographically constrained overdeepenings are generally deeper, more elongated, and have a steeper adverse slope gradient than non-topographically constrained overdeepenings.

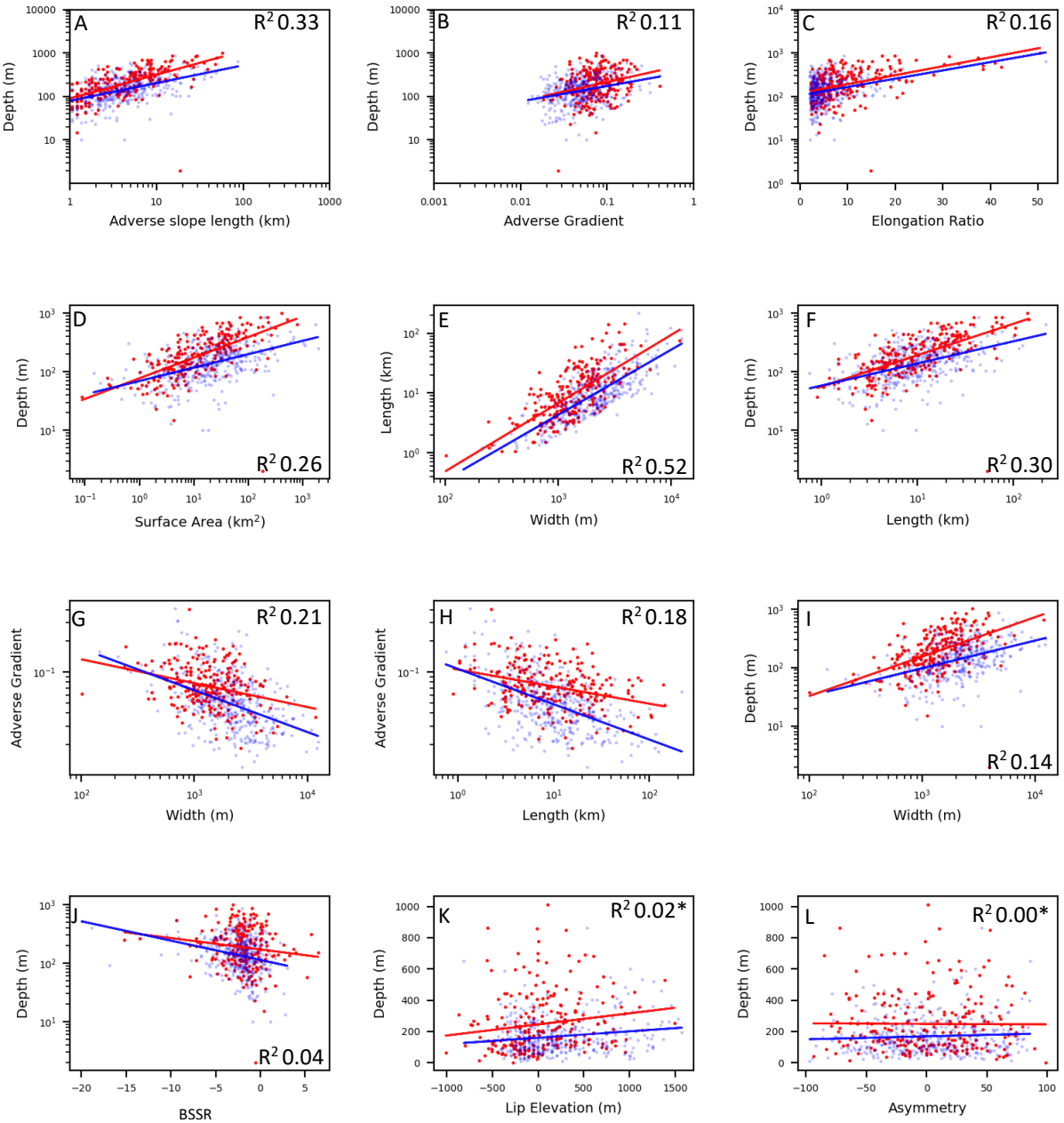

*Figure 3.21. Relationships between a variety of measured overdeepening parameters. Points are plotted for all 621 overdeepenings in the metric dataset. Red points and lines of best fit represent the topographically constrained overdeepenings. Blue points and lines represent the non-topographically constrained points and lines of best fit. All relationships are statistically significant at p <0.05 except those where the R2 is marked with *. Stated R2 values are for the combined dataset.*

Figure 3.22. Pairwise correlation matrix using Pearson's correlation coefficient. Values presented are the Pearson's correlation coefficient. Cells which have been shaded grey where relationships are not statistically significant ($p > 0.05$). A) Correlations coefficients are for non-log values of each parameter. B) Correlation coefficients are for the log values of parameters used in Figure 3.21. *Parameters which have negative values have not been logged.*

3.3.4 Variation of overdeepening morphology within different locational contexts

Here, the variation in overdeepening morphology in differing locational contexts (e.g. ice flow regime, confluence, and lithology, as discussed in section 3.3.1.1) are presented.

3.3.4.1 Ice flow regime

Analysis of the aggregate overdeepening morphometrics within each of the three classifications of flow regime are presented in Table 3.3. Overdeepening depth is substantially greater where ice flow is converging (nearly 40% deeper), than where flow is parallel or diverging. Average adverse slope gradient was also higher (0.07) in areas of converging flow when compared to areas of parallel flow (0.06) and diverging flow (0.06). Figure 3.23 visualises this data as notched box and whisker plots. The notches (which represent the 95% confidence interval) for the converging flow boxes in Figure 3.23a and Figure 3.23c do not overlap with the notches for the parallel and diverging boxes, providing strong evidence that their medians significantly differ. There is some indication that width may be greater and BSSR lower (e.g. more negative and therefore further beyond the supercooling threshold) for areas of diverging flow than the other flow regimes, but the confidence intervals are relatively high for diverging flow due to the low number of overdeepenings in this category. As such, these relationships are inconclusive.

Table 3.3. Morphometric summary statistics aggregated by flow regime. Values in bold are the averages for the total metric dataset. Figures in brackets give the number of overdeepenings in each flow regime.

	Mean	Median	Standard deviation
Length (km)	**15.0**	**9.2**	**19.6**
Converging (283)	11.9	8.9	10.9
Parallel (169)	11.3	7.6	11.8
Diverging (41)	10.7	6.5	13.5
Width (km)	**2.1**	**1.8**	**1.6**
Converging	1.9	1.6	1.3
Parallel	1.9	1.6	1.2
Diverging	2.4	1.9	2.1

Long profile asymmetry	**1.22**	**0.00**	**40.78**
Converging	0.78	0.00	40.49
Parallel	0.26	-2.33	38.07
Diverging	10.07	5.06	38.51
Depth (m)	**196**	**155**	**151**
Converging	197	153	144
Parallel	142	125	97
Diverging	147	102	116
Adverse slope gradient	**0.069**	**0.058**	**0.046**
Converging	0.0705	0.0612	0.0419
Parallel	0.0589	0.0512	0.0342
Diverging	0.0593	0.0514	0.0347
BSSR	**-2.22**	**-1.91**	**2.49**
Converging	-2.07	-1.92	2.49
Parallel	-1.93	-1.59	2.47
Diverging	-2.67	-1.84	2.61

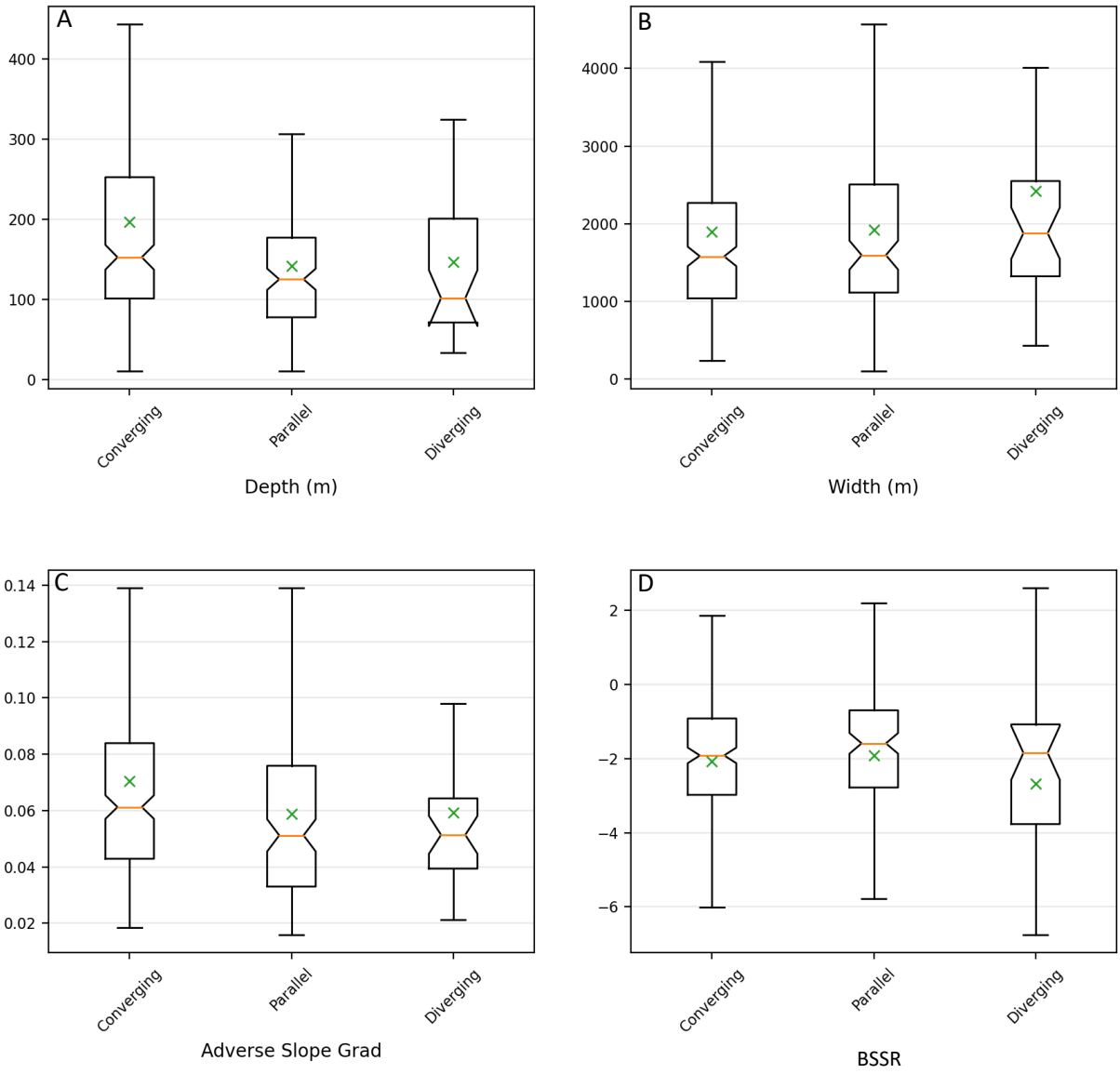

Figure 3.23. Notched boxplots showing morphometric statistics aggregated by flow regime. The line inside the box shows the median, notches show the 95% confidence interval of the median, the box height shows the interquartile range (IQR), whiskers mark the last datums inside 1.5 x IQR beyond the first and third quartiles, and the crosses show the mean.

3.3.4.2 Confluence location

The statistics presented in Table 3.4 show that overdeepenings that straddle a confluence were deeper than overdeepenings not at a confluence (median 274 m vs 140 m). However, this is perhaps a simple scaling relationship as length is also considerably longer for these overdeepenings (median 15.0 km) than for both the overdeepenings not at a confluence (median 9.2 km), and the overall overdeepening average length from the metric dataset (median 9.2 km). There is the potential for some innate bias in the length of overdeepenings that straddle a confluence as overdeepenings that span both upstream and downstream of

a confluence require a certain length to do so on glaciers of this scale (see section 3.2.3).

The depth of overdeepenings directly downstream of a confluence is also much greater than for overdeepenings not at a confluence (mean 290 m vs 169 m, median 170 m vs 140 m). In this case, these overdeepenings have an almost identical median length as overdeepenings not at a confluence. This suggests a process link between the conditions found directly downstream of a confluence and overdeepening depth, rather than just a simple scaling relationship. However, the 95% confidence interval (visualised by the notch in the box plot in Figure 3.24b) is relatively wide due to the low number of overdeepenings in this category, and does overlap with the confidence interval for the depth of overdeepenings not at a confluence. As such, some caution should be exercised when drawing inference from these averages.

Table 3.4. Morphometric summary statistics aggregated by confluence location. Values in bold are the averages for the total metric dataset. Figures in brackets give the number of overdeepenings in each category.

	Mean	Median	Standard deviation
Length (km)	**15.0**	**9.2**	**19.6**
At confluence (44)	9.2	6.8	7.0
Straddling confluence (25)	19.7	15.0	12.9
Downstream of confluence (20)	15.8	9.0	16.0
Not at confluence (404)	13.6	9.2	14.5
Width (km)	**2.1**	**1.8**	**1.6**
At confluence	1.7	1.4	1.3
Straddling confluence	2.0	1.8	1.2
Downstream of confluence	1.8	1.4	1.0
Not at confluence	2.2	1.9	1.5
Long profile asymmetry	**1.22**	**0.00**	**40.78**
At confluence	-10.4	-15.3	36.4
Straddling confluence	22.7	29.2	44.6
Downstream of confluence	-4.2	-10.0	40.0
Not at confluence	3.2	3.2	39.3
Depth (m)	**196**	**155**	**151**

At confluence	193	155	110
Straddling confluence	274	274	274
Downstream of confluence	290	170	253
Not at confluence	169	140	123
Adverse slope gradient	**0.069**	**0.058**	**0.046**
At confluence	0.074	0.069	0.032
Straddling confluence	0.076	0.063	0.038
Downstream of confluence	0.077	0.065	0.044
Not at confluence	0.061	0.052	0.042
BSSR	**-2.22**	**-1.91**	**2.49**
At confluence	-1.01	-1.32	2.36
Straddling confluence	-1.56	-1.55	1.22
Downstream of confluence	-1.16	-1.29	2.01
Not at confluence	-2.22	-1.87	2.37

Average adverse slope gradient is steeper for all three categories of overdeepenings in proximity to a confluence compared to both the average for overdeepenings not at a confluence, and the overall metric dataset average (medians: 0.069 at a confluence, 0.63 straddling a confluence 0.065 directly downstream of a confluence, vs 0.052 not at a confluence, and 0.058 for the whole metric dataset average). The 95% confidence intervals of the median adverse slope gradients for overdeepenings at or straddling a confluence do not overlap those for overdeepenings not at a confluence (Figure 3.24c) providing strong evidence that their medians significantly differ.

Interestingly, whilst the adverse slope gradient is steeper in all three confluence proximity categories than for overdeepenings not at a confluence, the BSSR is lower than for overdeepenings not at a confluence for all three confluence proximity categories (Figure 3.24d). If ice surface gradient remains constant whilst adverse bed gradient increases, this results in a *increase* in BSSR. Given that data presented here show that the adverse slope is steeper for overdeepenings at, straddling, and directly downstream of confluences, and yet the BSSR *decreases* in these scenarios, this must be reflective of substantial increases in ice surface gradients in these areas. However, caution must be exercised when interpreting the data as the box plots for BSSR (Figure 3.24d) show the upper bound of the notch for the 'not

at a confluence box' intersects the notches of all other boxes indicating the medians do not have a statistically significant difference.

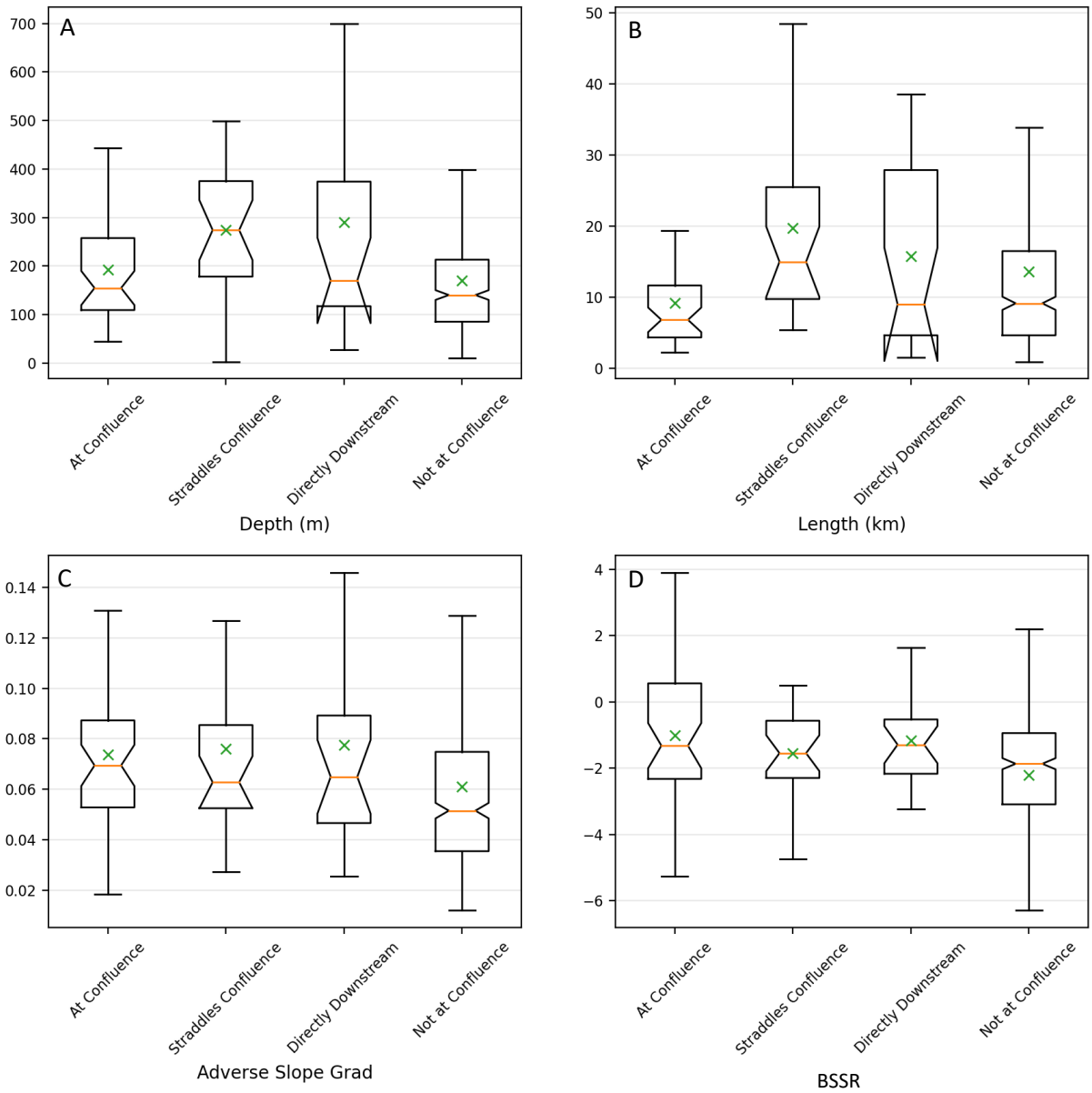

Figure 3.24. Notched boxplots showing morphometric statistics aggregated by confluence location. The line inside the box shows the median, notches show the 95% confidence interval of the median, the box height shows the interquartile range (IQR), whiskers mark the last datums inside 1.5 x IQR beyond the first and third quartiles, and the crosses show the mean.

3.3.4.3 Underlying lithological composition

A full break down of key morphometric overdeepening parameters aggregated by lithology type is given in Table 3.5. For length, width, adverse slope gradient, and BSSR the average values for the dominant metamorphic class are close to the overall metric dataset averages

(as would be expected given that this makes up the majority of the dataset). Values for overdeepenings in the sedimentary category of the dataset suggest longer overdeepenings, of slightly above average depth, but with markedly lower than average adverse slope gradient and BSSR. Overdeepenings of volcanic and plutonic lithology are shorter and narrower than the average overdeepening, but with much steeper adverse slope gradients and BSSRs.

Table 3.5. Average measured values for key overdeepening parameters aggregated by overdeepening lithology. Values in bold refer to the overall averages of the whole metric dataset. Values in bold are the averages for the total metric dataset.

	Mean	**Median**	**Standard deviation**
Length (km)	**15.0**	**9.2**	**19.6**
Sedimentary (110)	19.6	13.2	24.9
Volcanic (62)	13.4	9.4	12.6
Plutonic (49)	10.3	6.3	11.6
Metamorphic (400)	15.5	8.9	19.4
Width (km)	**2.1**	**1.8**	**1.6**
Sedimentary	2.4	2.0	1.8
Volcanic	1.8	1.2	1.0
Plutonic	1.5	1.2	0.9
Metamorphic	2.2	1.9	1.6
Long profile asymmetry	**1.22**	**0.0**	**40.78**
Sedimentary	1.86	2.10	39.13
Volcanic	-1.11	6.77	43.09
Plutonic	-2.29	-7.14	36.60
Metamorphic	1.86	0.0	41.30
Depth (m)	196	155	151
Sedimentary	214	152	171
Volcanic	251	210	182
Plutonic	213	173	153
Metamorphic	186	152	137
Adverse slope gradient	**0.069**	**0.058**	**0.046**
Sedimentary	0.055	0.048	0.028

Volcanic	0.081	0.074	0.042
Plutonic	0.094	0.083	0.057
Metamorphic	0.068	0.057	0.048
BSSR	**-2.22**	**-1.91**	**2.49**
Sedimentary	-2.05	-1.58	2.44
Volcanic	-2.75	-2.72	2.52
Plutonic	-1.98	-2.52	2.48
Metamorphic	-2.21	-1.88	2.49

Figure 3.25 visualises the data aggregated by lithological class in a series on notched box plots. The amount of overlap in the 95% confidence intervals across these plots is in general, less than for the plots of confluence location (Figure 3.24) and flow regime (Figure 3.23). This suggests that lithology exerts a stronger control on overdeepening morphology than flow regime or confluence location. However, it is important to note that confidence intervals are narrower for the lithological analysis than the other factors due to the greater number of overdeepenings in each class, and therefore could simply be reflective of a clearer signal due to more statistically robust data.

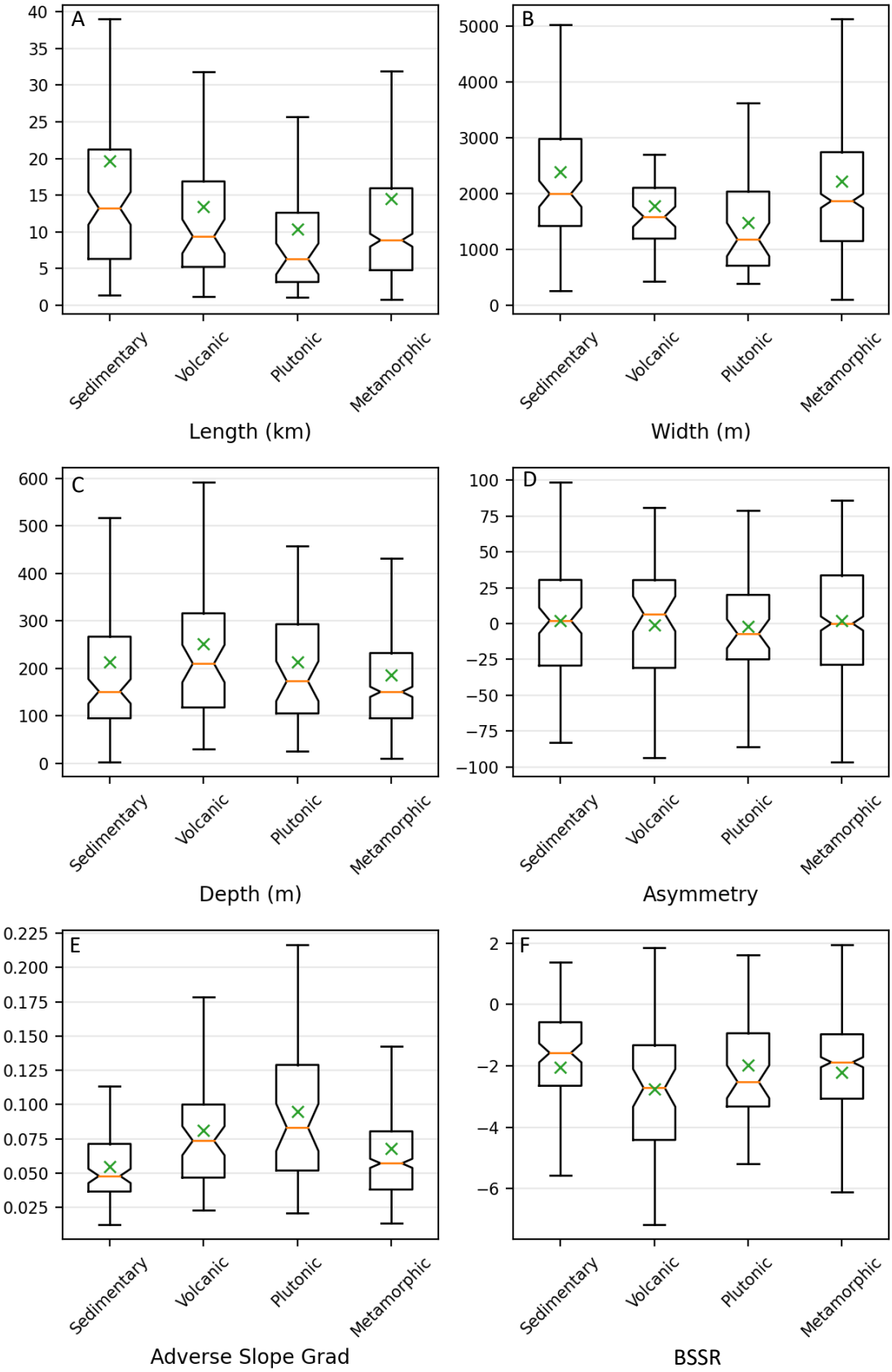

Figure 3.25. Notched boxplots showing morphometric statistics aggregated by overdeepening lithology. The line inside the box shows the median, notches show the 95% confidence interval of the median, the box height shows the interquartile range (IQR), whiskers mark the last datums inside 1.5 x IQR beyond the first and third quartiles, and the crosses show the mean.

3.3.5 Modulation of ice velocity by bed topography

RQ2 is to determine whether *bed topography modulates ice velocity in overdeepenings.* The first stage of this analysis is presented here and considers the simple case of a comparative analysis of mean annual velocities for the normal and adverse slopes of overdeepenings within the metric dataset. Consideration is also given to the relationship between a variety of the measured overdeepening morphometric parameters (presented in section 3.3.2) and ice velocity and acceleration.

3.3.5.1 Relationship between morphometric overdeepening parameters and ice velocity and acceleration.

Figure 3.26 shows the relationship between the measured overdeepening morphometric parameters, and average annual velocity and acceleration through the overdeepening. The relationships between all pairs of variables is statistically significant at $p < 0.05$ with the exception of velocity and depth (Figure 3.26a). However, most of the correlations between pairs of variables are very weak as demonstrated by the low R^2 values. There is a moderate negative correlation (R^2 0.19) between acceleration and width (Figure 3.26d) and between acceleration and length (R^2 0.19) (Figure 3.26f). There is also a weaker (R^2 0.08) but significant negative correlation between velocity and width (Figure 3.26c).

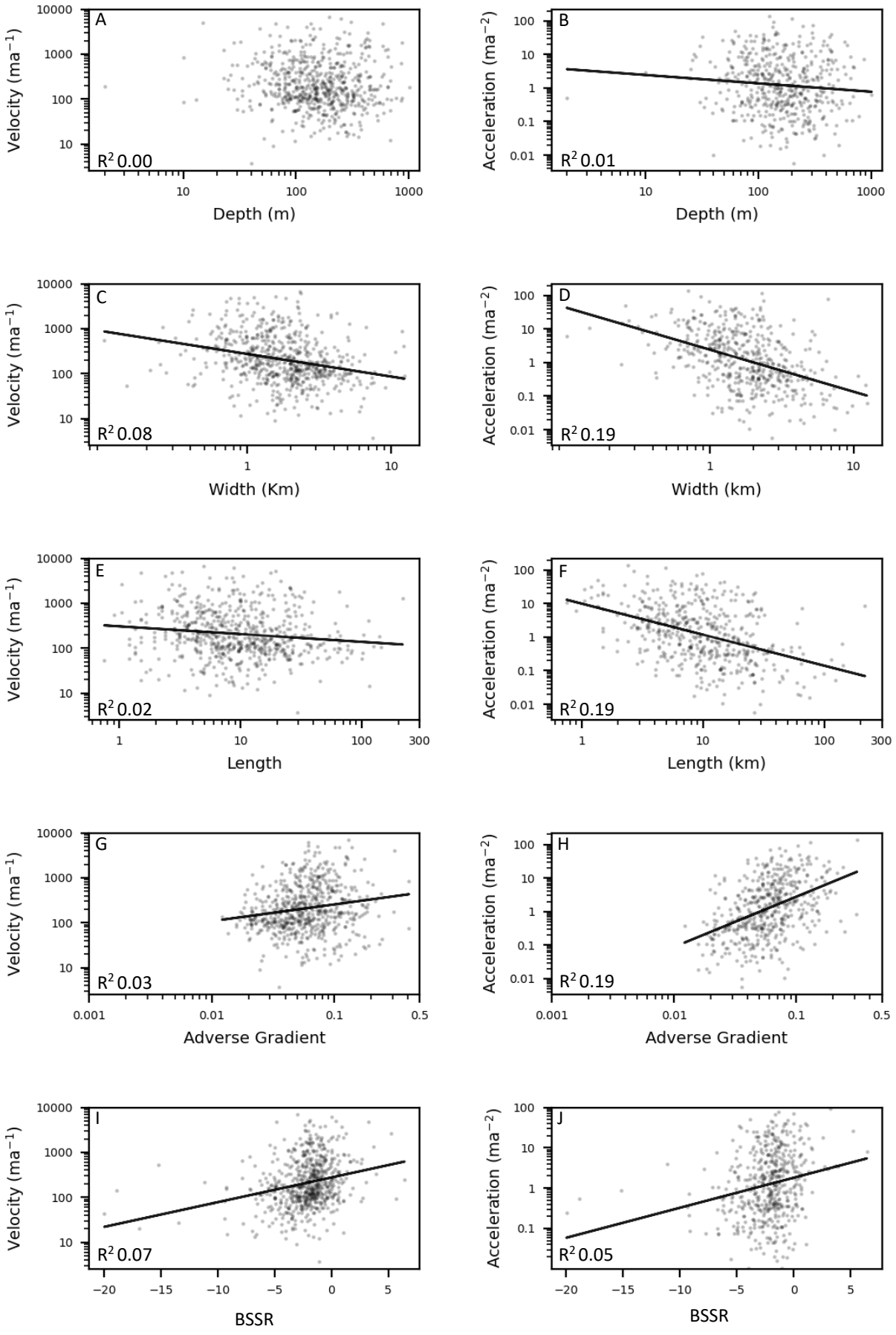
A
Velocity (ma^{-1})
Depth (m)
R^2 0.00
B
Acceleration (ma^{-2})
Depth (m)
R^2 0.01
C
Velocity (ma^{-1})
Width (Km)
R^2 0.08
D
Acceleration (ma^{-2})
Width (km)
R^2 0.19
E
Velocity (ma^{-1})
Length
R^2 0.02
F
Acceleration (ma^{-2})
Length (km)
R^2 0.19
G
Velocity (ma^{-1})
Adverse Gradient
R^2 0.03
H
Acceleration (ma^{-2})
Adverse Gradient
R^2 0.19
I
Velocity (ma^{-1})
BSSR
R^2 0.07
J
Acceleration (ma^{-2})
BSSR
R^2 0.05

Figure 3.26. Scatter plots showing the relationships between overdeepening depth, width, length, adverse slope gradient, and BSSR vs velocity and acceleration. Points are plotted for all 621 overdeepenings in the metric dataset for velocity plots. For the acceleration plots, points are plotted for the 486 overdeepenings in the metric dataset with positive acceleration values. Values of ice velocity and acceleration are overdeepening means. Lines of best fit are plotted for subplots where the p value is < 0.05.

The only morphometric parameter with a moderately strong positive correlation is between acceleration and adverse slope gradient (Figure 3.26h), which has an R^2 value of 0.19. There is no evidence to suggest that the slowdown of ice due to form drag of adverse slopes is a dominant process.

3.3.5.2 Variations in ice velocity and acceleration between normal and adverse slopes. Developing pseudo-overdeepenings to quantify background downstream ice velocity speedup

The generalised pattern of ice velocity in Greenland is increasing velocity as ice flows downstream towards the ice margin, with highest velocities at or near the margin, and lower velocities further inland (Rosenau et al., 2015). This confuses the analysis of the impact of adverse slope on ice velocity. In any individual overdeepening (e.g. a non-nested closed topographic basin), the adverse slope will be downstream of the normal slope. As such, even if the adverse slope has no impact on ice velocity over its length, ice velocity would still be expected to increase as it flows over the adverse slope and moves further downstream. Thus, a potential reduction in ice velocity over an adverse slope due to form drag, or an increase in ice velocity over an adverse slope due to a reduction in skin friction (resulting from elevated basal water pressure), can only be meaningfully assessed if this background downstream ice velocity can be estimated and removed from the signal.

To enable this background to be removed, a dataset of “pseudo overdeepenings” was developed. This is a set of 100,000 individual subsections of the central flowlines (see 3.2.1.3). Python code was written to automatically randomly seed starting points for these sections along lines in the central flowline dataset (irrespective of overdeepening location) and then extract a section of the flowline out downstream from the seed point. The length of these subsections was varied to give an overall length frequency distribution to match the length frequency distribution of the actual overdeepening dataset. For example, 1.3% of overdeepenings were between 0.5 – 1.5 km in length, so 1.3% of the pseudo overdeepening flowline subsections were created to be between 0.5 – 1.5 km in length, 10.0% of overdeepenings were between 1.5 – 2.5 km in length, so 10.0% of the pseudo

overdeepening flowline subsections were created to be between 1.5 – 2.5 km in length, and so on. For each individual pseudo overdeepening section, the line section was split in half, and velocity data from points at 150 m intervals along the line averaged for the upstream half and the downstream half. This facilitated the calculation of the average background down-stream ice velocity speedup to be calculated; e.g. on average, how much faster ice flows on the downstream half of a central flowline section than the upstream half. The data was used to compare how the difference in patterns of ice velocity speedup and slowdown on normal and adverse slopes through overdeepenings varied compared to what would be expected if no overdeepening was present.

Variations in velocity between normal and adverse slopes of overdeepenings

Figure 3.27 demonstrates that the flow of ice over an adverse slope does appear to have a modulating effect on ice velocity. Figure 3.27a shows that in 78.3% of overdeepenings, average ice velocity is faster on the adverse slope than on the normal slope. Figure 3.27b attempts to account for the background downstream speedup signal, and isolate the process impact of ice flow over adverse slopes from it. It shows that in 74.5% of the pseudo overdeepenings the average velocity for the downstream half of the section was faster than the average velocity for the upstream half of the section – this is the general background downstream speedup signal. As such, it can be seen that there is a 5.1% (3.8 percentage point) increase in frequency of occurrence of faster flow on adverse slope than normal slope than would be expected simply from the background downstream velocity speedup signal. Results from a two sample Kolmogorov-Smirnov test (statistic = 0.144, p = $8.122e^{-12}$) indicate that the difference between the distribution of the actual overdeepening adverse / normal velocity ratios from the pseudo overdeepening dataset 'adverse' / 'normal' velocity ratios is statistically significant.

Figure 3.27c shows that acceleration of ice velocity is also higher on adverse slopes (median 0.76 m a^{-2}) than normal slopes (median 0.36 m a^{-2}), and that fewer adverse slopes (19.6%) than normal slopes (25.8%) show deceleration. Results from a two sample Kolmogorov-Smirnov test (statistic = 0.124, p = 0.00014) indicate that the difference between the distributions of acceleration on adverse slopes compared to the distribution on normal slopes is statistically significant.

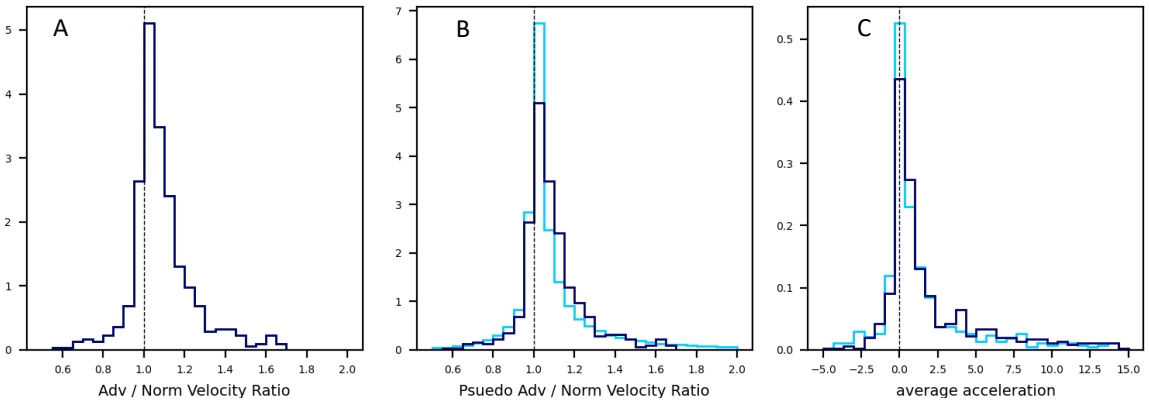

Figure 3.27. Histograms showing variation in ice flow through overdeepenings for the metric dataset. A) Shows the variance in ice velocity between normal slopes and adverse slope within overdeepenings as a ratio of the average velocity on the adverse slope / average velocity on the normal slope. A value of 1 indicates equal velocity on both slopes within an overdeepening, less than 1 indicates higher average velocity on the normal slope, greater than 1 indicates higher average velocity on the adverse slope. B) The light blue line represents the probability density of the ratio in velocity between the upstream and downstream halves of 100,000 randomly located sections along the central flowlines dataset, irrespective of overdeepening location (the "pseudo overdeepenings"). C) Shows average acceleration of ice through an overdeepening. A value of 0 represents no net speedup or slowdown of ice velocity over the reference distance. Values greater than 0 indicate a net acceleration of ice velocity over the reference section, values less than 0 indicate a net deceleration. The light blue line shows the distribution of average acceleration frequency for normal slopes, the dark blue line shows the distribution for adverse slopes.

3.4 Discussion

3.4.1 Where are Greenland overdeepenings located?

The results presented in section 3.3 indicate that overdeepenings are ubiquitous features in glacial systems, certainly in the areas within ~200 km of the margin under ice moving at greater than 25 m a^{-1} that form the study area of the mapping conducted within this study (Figure 3.12). 74% of the 553 mapped central flowlines intersect with at least one overdeepening (Figure 3.13, Figure 3.14). As discussed in the introduction to this chapter (section 3.1) and in more detail in Chapter 2 (section 2.2.2), the only other study to produce a comprehensive dataset of overdeepenings for Greenland is that of Patton et al. (2016). As such, heavy comparison will be drawn with this work throughout the discussion section.

3.4.1.1 Number of overdeepenings mapped and data quality

Patton et al. (2016) mapped a larger total number of overdeepenings (2,393 in this study vs 3,948 in Patton et al., 2016). In part this is due to the different motivations between the two studies. The primary focus of this thesis is the impact of adverse bed slopes on ice dynamics. As such, the study area was limited to ice flowing at a velocity of c. > 25 m a^{-1}. Therefore, the mapping presented in this chapter covers approximately 70% of the area under the

Greenland ice sheet, with mapped overdeepenings heavily concentrated within 200 km of the ice margin (Figure 3.28a). Conversely, Patton et al. (2016) mapped the entire contemporary ice sheet bed in addition to the area beyond the current ice margin out to the continental shelf (Figure 3.28b); 62 of the overdeepenings in the Patton et al. (2016) metric dataset are located in the interior of Greenland outside of the mapping study area used here. As such, whilst the absolute number of overdeepenings mapped here is lower, the density for the area covered is equal or higher to Patton et al. (2016) (Figure 3.28). In addition, the percentage of overdeepenings mapped that passed the data quality threshold in this study is 48.4% (621 of 1,284 parent overdeepenings) compared with only 12.6% in Patton et al. (2016) (335 of 2,663 parent overdeepenings).

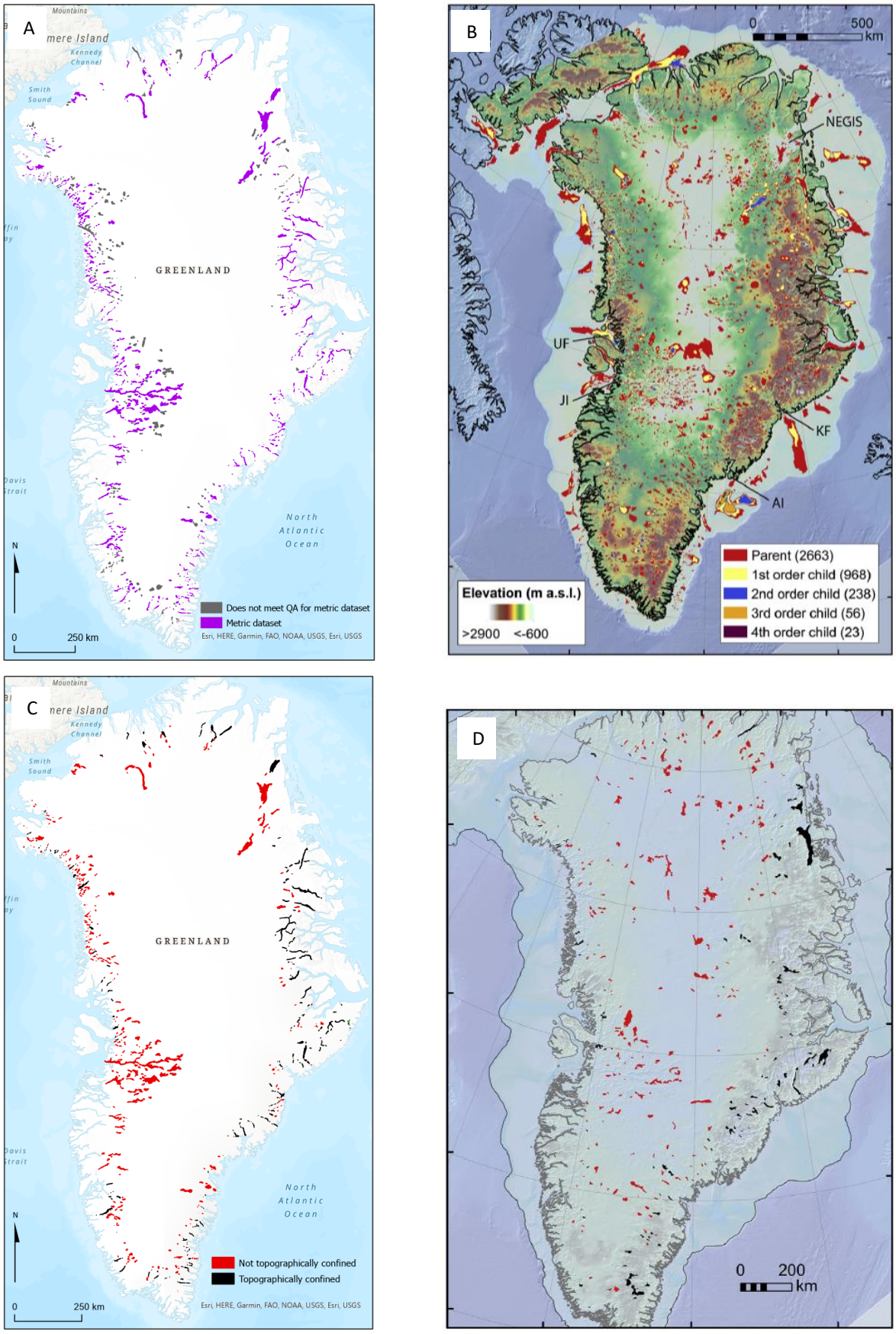

Figure 3.28 Mapped overdeepenings in Greenland. A) The full mapping dataset from this study, overdeepenings that meet the quality assurance threshold and are included in the metric dataset are shown in blue. B) The full mapping dataset from

Patton et al. (2016). C) The metric dataset from this study, overdeepenings that are topographically confined are shown in black, those that are not are in red. D) The metric dataset from Patton et al. (2016), overdeepenings that are topographically confined are shown in black, those that are not are in red.

Whilst the dataset presented here is in part larger than that of Patton et al. (2016) due to the less restrictive length threshold (see section 3.2.2.4) enabled by the higher resolution of the bed data used (163 ODs have been mapped that would have been excluded by the Patton et al. (2016) length threshold of 5 km), this is not the sole reason for the larger dataset. There are also at least 123 (19.8% of the total metric dataset) additional overdeepenings above the 5 km threshold which have been mapped that were not mapped by Patton et al. (2016). Thus, it is not simply that the dataset is bigger due to the inclusion of more smaller overdeepenings; a larger number of bigger overdeepenings also met the quality threshold due to the higher resolution bed data. Many of the overdeepenings included in the dataset that are smaller than those in the Patton et al. (2016) dataset are substantially smaller in terms of width and length, but less so in terms of depth. Width and length averages of the data presented here are approximately 50% less compared to Patton et al. (2016), but the depth averages are only 10% smaller (median 155 m in this study vs 173 m in Patton et al. (2016)) (Table 3.1). This suggests that the higher resolution bed data used and the methods implemented here (such as adopting a semi-automated rather than fully automated mapping methodology) have enabled the mapping of substantive features that were missed by earlier studies. Detailed comparison of individual overdeepenings that have been mapped in both datasets shows that often there is variation. The Patton et al. (2016) mapping is commonly represented by wider overdeepenings with less coherent shapes (Figure 3.29c), very large overdeepenings made up of multiple smaller overdeepenings (sometimes with their long axis transverse to the direction of ice flow (Figure 3.29b)), and a general trend for overdeepenings to be located further upstream and be less elongated, with the overdeepenings proximal to the margin often not mapped (Figure 3.29a). It seems likely that the kind of discrepancies and differences in the mapping output such as those illustrated in Figure 3.29 is likely due to the higher fidelity of contours that were able to be generated from the BedMachine data used in this study. Detailed comparison of the morphometric findings of Patton et al. (2016), and the process implications of these, is given in section 3.4.2, below.

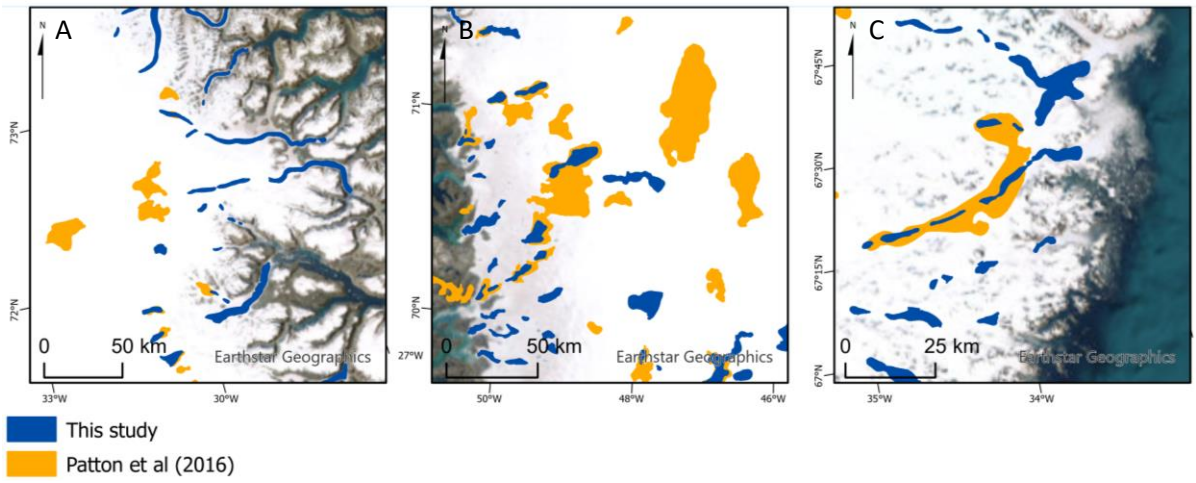

Figure 3.29 A comparison of the differences in mapping output for areas that are mapped in both this study and by Patton et al. (2016). A) Highly elongate topographically constrained overdeepenings proximal to the margin that are mapped in this study, but missed by Patton et al. (2016). B) Overdeepenings mapped by Patton et al. (2016) where the long axis appears perpendicular to ice flow. C) An example of overdeepenings mapped by Patton et al. (2016) where multiple individual discrete parent basins have been mapped as a single larger overdeepening of less coherent shape.

3.4.1.2 Distribution

It is clear from visual interpretation of the two datasets that there is a higher density of overdeepenings mapped close to the margin in the results presented in this chapter compared to Patton et al. (2016) (Figure 3.28, Figure 3.31). The improved mapping of overdeepenings in this zone is important for two reasons. Firstly, it confirms the location of overdeepenings where they would theoretically be expected to be located, i.e. in the ablation zone close to the margin where ice velocity is higher (and therefore has more erosive potential (Sugden and John, 1976; Oerlermans, 1984; Herman et al., 2011), and water availability at the bed is greater (which allows for transport of eroded material out of the catchment (Hooke, 1991; Spedding and Evans, 2002; Cook and Swift, 2012). Secondly, it means that there is now more accurate and complete data on which to base the work which follows in Chapters 4-6 regarding the impact of bed topography on ice dynamics. Data were missing from the mapping in the Patton et al, (2016) study in areas of key glaciological significance. For example, the mapping presented in this chapter shows that large overdeepenings are present close to the margin under each of the three largest Greenland outlet glaciers, whilst the Patton et al, (2016) data only records an overdeepening under Kangerlussuaq, but not under Jakobshavn or Helheim Glaciers (Figure 3.30). Adverse bedslopes near the margin of marine terminating glaciers are thought to exert important controls on the advance and retreat of the calving front. Retreat down an adverse slope into

deeper water may lead to increased floatation and the potential for retreat to accelerate rapidly until a stable grounding position on the normal slope is reached (e.g. (Jamieson et al., 2012; Carr et al., 2015; Clason et al., 2016; Åkesson et al., 2018; O'Regan et al., 2021), see section 2.3.2.3). As such, well constrained models of the bed in these areas are essential for investigating these processes.

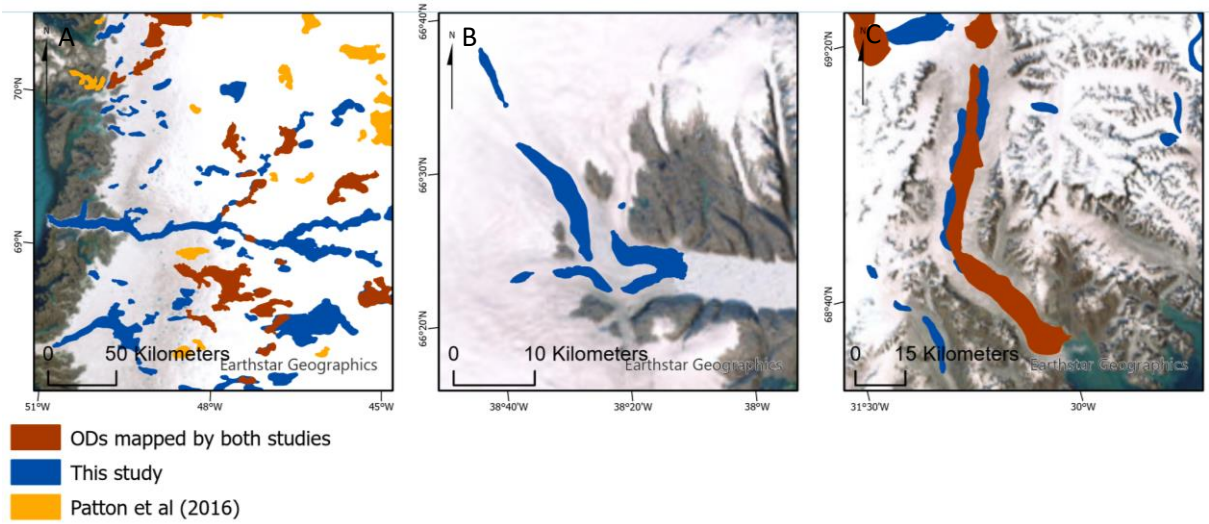

Figure 3.30 Comparison of overdeepenings mapped in the metric dataset with that of Patton et al, (2016) for key outlet glaciers. A) Jakobshavn, B) Helheim, C) Kangerlussuaq. Background imagery is Landsat.

When considering the level of mapping agreement and overlap in the two datasets, 106 of the overdeepenings in the Patton et al. (2016) metric dataset intersect with overdeepenings mapped in the metric dataset of this study (Figure 3.31). 57 of the overdeepenings in the Patton et al. (2016) metric dataset intersect with overdeepenings which were mapped here, but which were removed from the dataset due to not passing quality assurance thresholds. Thus, in total 515 new parent overdeepenings were mapped that meet the quality standard for acceptance in the metric dataset. This represents a substantial advance in the understanding of the location and character of overdeepenings under the Greenland ice sheet.


Ellesmere Island
Kennedy Channel
Smith Sound
GREENLAND
North Atlantic Ocean
ODs mapped by both studies
This study
Patton et al (2016)
0
250 km
Esri, HERE, Garmin, FAO, NOAA, USGS, Esri, USGS

Figure 3.31 Comparison of overdeepenings mapped in the metric dataset with that of Patton et al. (2016). Red shows the overdeepenings mapped by both studies, blue and orange the overdeepenings that were mapped independently by only one of the studies. Note, overdeepenings mapped by Patton et al. (2016) that are located outside the mapping study area have been removed to allow a direct comparison between the two datasets.

3.4.1.3 Factors influencing overdeepening location

3.4.1.3.1 Velocity

Central flowlines are more likely to intersect an overdeepening in faster flowing areas of the ice sheet. The 26% of central flowlines that don't intersect an overdeepening are predominantly smaller, slower glaciers, with average ice velocity at the terminus of less than half that of central flowlines which did intersect an overdeepening (mean 825 m a^{-1} vs mean 1839 m a^{-1}, Figure 3.14). The higher prevalence of overdeepenings in faster flowing areas of the ice sheet is aligned with many models of glacial erosion that suggests that erosive power is proportional to the speed at which ice flows over the bed (Hallet, 1979; Oerlemans, 1984; Anderson et al., 2006; Egholm et al., 2011). Interestingly, when ice velocity is measured at overdeepening location, there does not appear to be a positive relationship between velocity and of the metrics of overdeepening size. Depth vs velocity is not statistically significant and width and length have very weak negative correlations with velocity (Figure 3.26). Process significance of these relationships in terms of overdeepening evolution is discussed in section 3.4.3.1.

As such, it seems there is some evidence to suggest that overdeepenings are more likely to occur in areas of faster flow, but that higher velocity does not result in perpetually higher rates of erosion leading to ever deeper and larger overdeepenings. This supports the notion of self-regulation of overdeepening evolution leading to a transport limited equilibrium profile over time (Alley et al., 2003; Cook and Swift, 2012; Patton et al., 2016)

3.4.1.3.2 Confluences and flow regime

There is a wide body of literature theorising that overdeepenings preferentially form at confluences in ice flow because these represent areas of localised speedup (as a result of a need to conserve mass through the reduced cross sectional area through the confluence) and therefore maximum erosional potential (Glasser 1995, Kessler, et al., 2008, Alley 2003, MacGreggor et al. 2000 and Swift 2008). The methodology adopted here does not allow specific judgement to be made as to the probability of an overdeepening being located at a

confluence vs not at a confluence as not all confluences have been mapped. However, it is clear from the results that the vast majority of overdeepenings (82%) are not located at, or in the vicinity of, a confluence in the ice (Figure 3.16). As such, irrespective of any potential process relationship of confluences on overdeepening formation, it can be concluded that they are not a prerequisite condition for overdeepening location, and as such, they are unlikely to be a dominant factor in overdeepening evolution. This aligns with the findings of Bruckl et al. (2010) whose work on overdeepenings in the Austrian Alps demonstrated that overdeepenings do not always occur at confluences, suggesting instead that high water pressure and weakened bedrock may be more important factors controlling their location. The study by Lloyd et al. (2023) is perhaps the most comprehensive investigation of the influence of confluences on overdeepening location, developing a comprehensive overdeepening dataset for Labrador, Canada. The number of overdeepenings in the dataset is not clear from the results presented, but an overdeepening area of over 64,000 km^2 is mapped. Whilst Lloyd et al. (2023) demonstrate that overdeepenings are 1.7x more likely to be co-located with a confluence than not (based on expected frequency derived from total overdeepening area and total confluence area), there are still only 2.79% of overdeepenings that are co-located with confluences in their study. This is aligned with the findings of this chapter that in absolute terms, the great majority of overdeepenings are not co-located with confluences.

Whilst overdeepenings did not preferentially occur at confluences, most were located in areas of converging flow (62%), with only 9% of overdeepenings located in areas of diverging flow (Figure 3.15**Error! Reference source not found.**). The same hypothesis of ice acceleration to conserve mass in converging flow could be made as was discussed for flow at a confluence (above), and this could be interpreted as an explanation for the high prevalence of overdeepenings in converging flow. One important factor with regard to the analysis of flow regime is that ice in an outlet glacier will generally be converging as it flows towards the margin. As overdeepenings are preferentially located towards the margin (Figure 3.12) the spatial association may be one of chance rather than cause and effect. Further investigation beyond the scope of the work in this chapter would be required to determine this. As direct measurement of velocity within overdeepenings has been made, it is more robust to test the actual relationship between overdeepenings and velocity rather

than infer likely velocity changes based on convergent ice flow and confluence location (see section 3.4.3.1, below). This is a substantial benefit of studying overdeepenings under contemporary ice as opposed to working in palaeo contexts where such proxies for ice velocity must be used (e.g. (Preusser et al., 2010; Lloyd, 2015; Lloyd et al., 2023))

3.4.1.3.3 Lithology

The results suggest some evidence of preferential formation of overdeepenings in certain lithologies. When adjusted for area (rather than relying on simple overdeepening count), overdeepenings are present with underlying sedimentary lithologies 11.2% more frequently than would be expected based on the relative prevalence of sedimentary lithology in the study area as a whole, but less frequently for underlying volcanic lithologies at only 61.3% the expected rate (Table 3.1). The observed frequency of overdeepenings for plutonic and metamorphic lithologies are very close to the expected frequency (Table 3.1). A Chi - squared test for this data demonstrates there is a statistically significant difference between the expected and observed overdeepening frequency ($p < 0.05$). The competency of bedrock has been observed to exert a strong control on overdeepening formation, with preference for weaker lithologies (Pomper et al., 2017; Gegg et al., 2021). As such, overdeepening occurrence might be expected to favour weaker lithologies (Lloyd et al., 2023). The relative strengths of the four classes of lithology used for analysis (in ascending order), are: sedimentary, volcanic, plutonic, and metamorphic (Gowan et al., 2019). As such, process based conclusions that might be drawn with regard to the control of underlying lithology on overdeepening location are inconclusive; the weakest lithology is the most relatively over represented, but the second weakest the most under represented, and the two strongest lithologies very close to the expected prevalence rates.

There are a number of factors that give material context to these results. Firstly, due to the location and orientation of the units of volcanic lithology, a major unit on the north coast, and c. 50% of a major unit on the east coast (which combined make up ~ 40-50% of the total volcanic area) are located further than 100 km from the margin in areas of relatively slow ice flow where overdeepening frequency would be expected to be lower (Figure 3.17). Secondly, the overall competency of bedrock and its resistance to erosion is not solely determined by lithology; faulting of bedrock is also important and erosion will be more effective in heavily faulted and jointed areas (Haynes, 1968; Hooke, 1991; Hallet, 1996;

Seguinot, 2008). Neither of these factors have been considered within the analysis presented here. As the formation and evolution of overdeepenings is very much a secondary aim of this work, further analysis is beyond the scope of this thesis but would be an important and interesting area of future investigation.

3.4.2 Overdeepening morphology

The principal comparison to be made is with the overdeepening mapping and metric dataset created by Patton et al. (2016) as this is the only other study to conduct a comprehensive mapping and analysis of overdeepenings in Greenland. A comparison of the key metrics is given in Table 3.6 below. Detailed discussion is given where relevant in the context of the key process interpretations that follow.

Table 3.6 Comparison of key metric averages from this study, and Patton et al. (2016)

	Mean	**Median**	**Standard deviation**
Length			
This study [n = 621]	15.0 km	9.2 km	19.6 km
Patton et al. [n = 335]	22.2 km	17.1 km	16.5 km
Width			
This study	2.1 km	1.8 km	1.6 km
Patton et al.	5.6 km	4.9 km	3.2 km
Elongation Ratio			
This study	7.1	5.1	6.1
Patton et al.	4.1	3.4	2.2
Long profile asymmetry			
This study	1.22	0.00	40.78
Patton et al.	-20.3	-22.0	36.0

Depth			
This study	196 m	155 m	151 m
Patton et al.	227 m	173 m	195 m
Adverse slope gradient			
This study	0.069	0.058	0.046
Patton et al.	0.023	0.017	0.023
BSSR			
This study	-2.22	-1.91	2.49
Patton et al.	-3.64	-2.51	3.43

3.4.2.1 General size and form

The data presented in this chapter gives detailed coverage of the finer, more elongate overdeepenings close to the margin. These are largely absent in the mapping conducted by Patton et al. (2016) (Figure 3.29 and Figure 3.31). As a result of being able to include these overdeepenings in the metric dataset, reported average values of width (2.2 km in this study vs 5.6 km in Patton et al. (2016)) and length (15.0 km in this study vs 22.2 km in Patton et al. (2016)) are substantially lower than in Patton et al. (2016), and average elongation ratio is much higher (mean 7.1 vs 4.1) (Table 3.6). As was discussed in section 3.4.1.1, whilst width and length averages of the data presented in this chapter are approximately 50% lower compared to Patton et al. (2016), depth averages are only 10% smaller (median 155 m in this study vs 173 m in Patton et al. (2016)) (Table 3.6). This gives confidence in the results and suggests that the additional overdeepenings mapped here, but not by Patton et al. (2016) are genuine features (rather than artifacts in the bed data) which are substantive and important. It also demonstrates that overdeepenings of substantive depth exist that are smaller in width and length than have previously been observed.

The pairwise relationships between individual morphometric parameters that were presented in Figure 3.21 and Figure 3.22 are also well aligned with those presented by Patton et al. (2016) with the direction and strength of the correlations between pairs of parameters similar in most cases. Two notable exceptions are the correlation between

elongation ratio and depth, and between lip elevation and depth. In Patton et al. (2016) the correlation between elongation ratio and depth is not significant, where as in the results presented here there is a moderately strong positive correlation (PCC = 0.58, Figure 3.22). This is likely due to the ability to better resolve highly elongate, narrow overdeepenings that were omitted from the Patton et al. (2016) dataset due to bed resolution constraints. The lack of a significant correlation between lip elevation and depth in the results presented here may be due to the higher number of (often substantive) overdeepenings mapped much closer to the margin (and therefore at lower lip elevation) than was the case in Patton et al. (2016). Patton et al. (2016) attribute the substantial scatter in the data in their study to limitations in data quality and sample size. It is noteworthy that despite a much larger metric dataset derived from higher resolution bed data, the level of scatter in the data and the strength of correlations between parameters is not markedly improved in most cases than in Patton et al. (2016). As such, it may be inferred that these morphometry statistics are actually reflective of the natural variation in overdeepenings, rather than noise induced by error.

3.4.2.1.1 Bed asymmetry

Overdeepening asymmetry varies significantly between the results presented here and those of Patton et al. (2016). Patton et al. (2016) found an average long profile asymmetry of -20.3. This means that on average, the elevational minima of an overdeepening was closer to the upstream entry lip of the basin than the downstream exit lip. This was interpreted as potential evidence of the dominance or importance of quarrying style erosion at the headwall of the overdeepening (Hooke, 1991; Cook and Swift, 2012; Patton et al., 2016). The results presented here do not corroborate these findings. Mean overdeepening long profile asymmetry is 1.2, with a median of 0.0 (Table 3.6). This shows that there is no evidence of a systematic asymmetry in the position of elevational minima along the long profile of overdeepenings. Despite differing from the findings of Patton et al. (2016) for Greenland, other studies have made observations consistent with the results presented here in other geographical areas. In their study of the Swiss Alps Magrani et al. (2020) also found no evidence for a headward asymmetry in the location of elevation minima in their data. The process interpretation of this finding is that there is no evidence to support the hypothesis proposed by Patton et al. (2016) that as the adverse slope erodes to a gradient

that exceeds the supercooling threshold further erosion of the adverse slope is protected by sediment deposition, whilst erosion towards the head of the overdeepening may continue via quarrying of the headwall (Hooke, 1991) leading to further deepening and upstream migration the location of the elevation minima.

One possible explanation for the differences observed is that the mapping dataset contains a higher proportion of child basins than the Patton et al. (2016) mapping. 46% of the total number of overdeepenings mapped in this study were child basins (e.g. overdeepenings nested within larger overdeepenings) compared with only 33% in the Patton et al. (2016) data. The complexity of the nesting of child basins is also much more complex in the data presented in this chapter. In Patton et al. (2016) the maximum "nestedness" of an overdeepening is 4th order (e.g. four levels of nesting). In the data presented here the maximum complexity is much higher. The nestedness has not been measured in a comparable way for all overdeepenings, but parent overdeepenings contain up to 62 child overdeepenings (Figure 3.9d) and there are individual examples where 4th order nesting is far exceeded (e.g. Figure 3.19g). This increased complexity is due to the higher resolution of the bed data. As such, if there is a systematic asymmetry in erosion along the long profile of overdeepenings, but which only operates at the individual child basin scale, not on the parent / composite basin scale, this signal may be more pronounced in the Patton et al. (2016) data where there is a lower level of basin nesting. It would be a valuable area of future study to calculate the asymmetry for each child basin in the metric dataset individually, but the computational difficulty of doing so is substantial, and beyond the scope of the aims of this thesis.

3.4.2.1.2 Limits on overdeepening depth

The role of overdeepenings in ice sheet dynamics, and the feedbacks of these dynamics on the evolution of overdeepening form was discussed in detail in sections 2.2 and 2.4. A key hypothesis proposed by Alley et al. (2003) is the suggestion that overdeepenings are equilibrium forms that all glacier beds should tend towards. A key facet of the equilibrium hypothesis is that as overdeepenings evolve they will tend toward a geometry whereby the energy available for sediment transport becomes limited and erosion halts, thus preventing further deepening. It is hypothesised that the self regulating limit on overdeepening depth will be as the adverse slope gradient reaches the supercooling threshold, as once exceeded

sediment evacuation from the overdeepening will be limited or prevented (Alley et al., 2003; Cook and Swift, 2012). The supercooling threshold has classically been taken to be a BSSR of ~-1.6 (Röthlisberger and Lang, 1987; Alley et al., 2003). As such, support for the equilibrium theory would see a tendency for BSSR at the supercooling threshold when analysing overdeepening morphometry. Figure 3.20J shows very pronounced clustering of the BSSR around this value (this is the most strongly unimodal of any of the morphometric parameters analysed), and the mean BSSR of -2.22 and median of -1.91 are also very close to the supercooling threshold. This provides very strong support of the equilibrium hypothesis. The results of Patton et al. (2016) also observed clustering of values close to the supercooling threshold, but average values were further from the threshold than presented here (mean -3.64, median-2.51).

However, whilst the data shows a tendency to stabilise around a BSSR of ~-2.0, this does not represent an upper limit of this metric. There are a large number of overdeepenings where the BSSR exceeds -1.6, sometimes substantially. There are a number of possible explanations for the supercooling threshold being frequently exceeded. Sediment may continue to be transported through the overdeepening allowing subsequent erosion to occur even once the supercooling threshold has been exceeded, resulting in further steepening of the adverse slope gradient. At the supercooling threshold subglacial conduits can no longer be enlarged by viscous dissipation, but flow may continue (and therefore transport sediment), albeit restricted, under such conditions (Röthlisberger, 1972; Röthlisberger and Lang, 1987; Hooke, 1991). It is only once the BSSR approaches -2.0 that channel water pressure equalises with ice-overburden pressure and flow is likely to distribute across the bed and flow as a sheet (Rothlisberger 1972; Creyts and Clark 2010). It may be at this point that sediment flux from the overdeepening becomes heavily restricted or stopped. This limit accords even more closely with the observed averages of BSSR ratio presented here (mean = -2.22, median = -1.91).

However, such discussion of the nuanced variations in BSSR between -1.6 and -2.0 do not explain the substantial number of observations where the BSSR is far in excess of -2.0. More recent investigation has challenged the classically accepted supercooling threshold and suggested that supercooling may not have a universally applicable BSSR, but may vary between overdeepenings depending on the specific morphological and hydrological

configuration (Werder, 2016). This approach accounts for the fact that water pressure downstream of an overdeepening may be below over burden pressure, and modifies the formula used for calculation of the supercooling threshold to adjust for this in each individual overdeepening. Data from a study in the Swiss Alps suggests that once these adjustments are incorporated to generate a specific supercooling threshold value for each overdeepening, the majority (77%) of overdeepenings which exceed the classic supercooling threshold fall within the new adjusted threshold (Werder, 2016). When this approach is adopted for a dataset in the Swiss Alps, there is evidence to suggest that overdeepenings where the BSSR is as low as -18 may actually still not have exceeded the supercooling threshold (Werder, 2016) (Figure 3.32). It follows then, that within the dataset for Greenland presented in this chapter, many of the overdeepenings that exceed the classic supercooling threshold may actually be under (or at) the true supercooling threshold, and have stabilized their development at this geometry as a result of the feedback mechanisms discussed above. It would be an interesting focus of further study to adopt the approach of (Werder, 2016) to calculate adjusted supercooling threshold values. However, this approach is involved and requires parameterisation not currently generated for the dataset within this study.

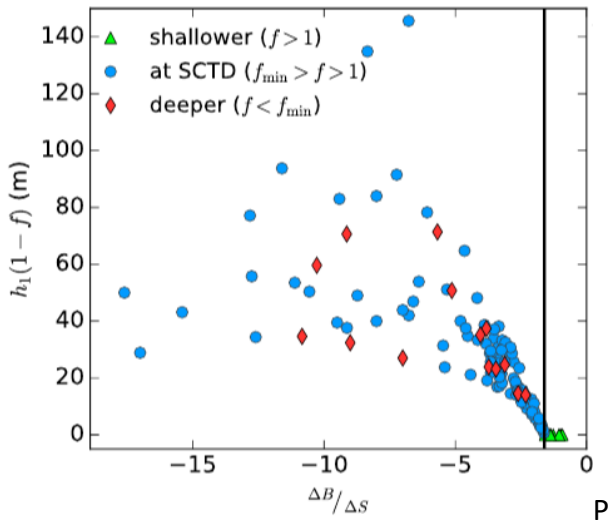

Figure 3.32 Plot of ΔB/ΔS versus correction factor $h_1(1-f)$ at supercooling threshold depth (SCTD) estimated from observations in the Swiss Alps. Symbols encode flotation fraction f at SCTD: ΔB shallower than the classic SCTD (f >1, triangles), ΔB possibly at SCTD ($f_{min} \geq f \geq 1$, circles), and ΔB deeper than the new SCTD ($f < f_{min}$, diamonds). The vertical line indicates the classic supercooling threshold. Figure and caption reproduced from Werder, (2016).

A further characteristic of overdeepening morphometry in support of the equilibrium hypothesis is the distribution of overdeepening depth (Figure 3.20d). The data illustrates a strong preference for lower depths with a pronounced positive skew of the histogram (Figure 3.20d). The fact that relatively few overdeepenings evolve to the maximum possible depths observed (in excess of 1,000 m) but are instead heavily clustered around the median of 155 m, with the majority of overdeepening less than 200 m in depth, suggest that negative feedbacks are limiting the growth of overdeepenings. Other studies both in Greenland (Patton et al., 2016), and in non-ice sheet contexts of the Swiss Alps (Magrani et al., 2020), Peru, and the Himalaya (Haeberli et al., 2016) have reported very similar results for maximum overdeepening depth, and the distribution of overdeepening depth in their data. The fact that these similarities in overdeepening morphometrics are observed in very different settings implies that there are fundamental processes controlling the growth of overdeepenings, rather than situationally dependant relationships. The strong clustering of BSSR around the supercooling threshold indicates that this is likely a key mechanism in limiting the growth of overdeepening depth.

3.4.3 Controlling factors on bed morphology

3.4.3.1 Ice velocity

The relationship between ice velocity and acceleration, and overdeepening size has been tested for all overdeepenings in the metric dataset. The results (Figure 3.26) suggest the relationships between ice velocity and overdeepening depth, width, and length are very weak, and the trends between ice velocity and width and length are inverse, with overdeepenings generally tending to be slightly shorter and narrower as velocity increases. There is no relationship between ice velocity and depth (R^2 0.00). The relationships between ice acceleration and width and length are stronger (R^2 0.19), but again, are inverse with width and length decreasing with increasing acceleration. One possible explanation for the inverse relationship is that many of the highly elongate topographically constrained overdeepenings are located along the east coast, close to the margin where ice velocity is generally high (Figure 3.12). However, these elongate overdeepenings are also generally quite long so the inverse relationship between velocity and length is more difficult to explain in this regard. In summary, considering the metric dataset as a whole, there is simply

no evidence for a pattern of larger or deeper overdeepenings where ice is moving faster or accelerating more rapidly. This is counter to inferences in the literature that overdeepenings may be deeper in areas of increased ice velocity due to increased erosive power (Glasser, 1995; Kessler et al., 2008).

3.4.3.2 Ice flow regime and confluence location

It is commonly suggested that convergent flow and locations of ice confluence are likely to be conducive to erosion and transport and therefore that overdeepening depth may be exacerbated under such flow regimes (Holtedahl, 1967; Alley et al., 2003; Kessler et al., 2008). Mean overdeepening width and length were very similar for areas where ice flow was converging, parallel, and diverging, but overdeepenings were over 30% deeper where ice was converging than when flow was parallel or diverging (Table 3.3). As converging flow was the dominant flow regime observed (62% of overdeepenings), the average depths in these situations was almost exactly the same as the averages for the overdeepening dataset as a whole, with average depths for parallel and diverging flow substantially below the overall average (Table 3.3). Similarly, mean overdeepening width does not meaningfully vary between overdeepenings located at or near a confluence compared to the mean width for overdeepenings not at or near a confluence.

The analysis of the morphology of overdeepenings in relation to confluence location is complicated slightly by the way in which overdeepenings were classified. Those overdeepenings classified as straddling a confluence are inherently longer due to the fact that they need to be long enough to extend upstream and downstream of the confluence. Due to the general form relationship of depth increasing with length (Figure 3.21f) one would expect the longer overdeepenings straddling a confluence to be deeper than average, and this is the case (mean 274m compared to overall metric dataset mean of 196 m). The most compelling results are for overdeepenings either directly downstream of a confluence, or at a confluence. There is no inherent bias in the length of an overdeepening directly downstream of a confluence, overdeepenings of any length could be situated in the locations required to be included in this class, and the mean overdeepening length is almost exactly the same as the metric dataset mean length. However, the mean depth for overdeepenings directly downstream of an overdeepening is substantially greater, at 290 m. Further to this, the overdeepenings located at confluences have the opposite bias to those

straddling a confluence; in order for their location to be at, but not extend up or downstream of a confluence, they are likely to have a shorter than average length (9.2 km vs metric dataset average of 15.0, see Table 3.4). Despite their much shorter length, these overdeepenings have a mean depth almost identical to the metric dataset mean (193 m vs 196 m), and a higher mean depth than those overdeepenings not at a confluence (193 m vs 169 m) (Table 3.4).

As such, the analysis of overdeepening morphology in relation to ice flow regime and confluence location presented here strongly suggest that in areas of converging ice flow and areas near to ice confluences, erosive power is increased (or was in the past at the time of active overdeepening formation), leading to deeper (but not necessarily longer or wider) overdeepenings. An interesting question, which is not definitively answerable from the data presented in this thesis, is what is causing the increased depth of overdeepenings at confluences and where ice flow is converging? The most common reason why erosion is hypothesised to be higher in these regions is due to increased ice velocity as a consequence of conservation of mass as the same amount of ice flows through a smaller cross sectional area (Holtedahl, 1967; Alley et al., 2003; Kessler et al., 2008). However, the results presented in this chapter do not show any evidence of a relationship between ice velocity and overdeepening depth in the dataset as a whole (3.4.3.1). This suggests that either a) current patterns of ice velocity are not representative of those when the overdeepenings formed, or b) there are other processes controlling overdeepening depth where ice is converging / at confluences. The former is difficult to ascertain, but some suggestions relating to the later follow below.

One possibility already discussed in section 3.4.1.3 is that there might be some spatial bias in the location of converging flow, with greater prevalence towards the margin. The same bias may be true of confluence location; by their nature confluences occur downstream, and therefore may be more prevalent closer to the margin. Closer to the margin surface elevation is lower, and therefore melt would be expected to be higher (Moon et al., 2014; Solgaard et al., 2022), and it may be this increased melt which is providing the erosional potential leading to greater overdeepening depth (Cook and Swift, 2012). Relatively few studies have investigated the mechanics of ice deformation at glacier confluences, possibly because of the complexity of the processes operating as ice masses merge (Gudmundsson

et al., 1997). However, some observations made of the specifics of ice dynamics at glacier confluences may explain why the results presented here show increased depth at confluences, but not a general velocity / depth relationship. Firstly, the type of velocity data used within this chapter (annual averages in the horizontal plane) may be inherently limiting. Theoretical work on ice deformation has suggested that at a Y-shaped junction of glaciers there will be some circulating flow induced with a downward flow component in the central area of the confluence, which could increase erosive potential (Collins, 1970). Changes in vertical velocities or internal flow would not be identified within the horizontal velocity data used in this chapter. Field observations at a confluence on Unteraargletscher in the Swiss Alps have also suggested that seasonal velocity speedup in the summer may be greater at a confluence than further upstream, and that use of annual velocity data for investigating physical processes operating at the confluence is therefore questionable (Gudmundsson et al., 1997). As such, the coarse temporal resolution of the velocity data used in this chapter may not adequately resolve the period at which erosive potential is increased at confluence locations.

3.4.3.3 Bed lithology

The analysis of overdeepening morphology when overdeepenings are categorised by underlying bed lithology shows significant variation between lithologies for all morphological parameters measured, with the exception of overdeepening asymmetry. This suggests that bed lithology is exerting a control on overdeepening morphology (see section 3.3.4.3). There are interesting parallels that can be drawn between the results for lithological control of overdeepening morphology within this study, and lithological control of other erosional geomorphological features within the wider literature. It is established that lithological strength exerts control on fjord morphology (Swift et al., 2005; Stroevan and Swift, 2008; Paxman, 2021). More resistant bedrock lithology is likely to constrain the initial width of valleys formed prior to glaciation via fluvial action. When these regions then become glacierised, the erosion is focused down (Swift et al., 2008; Cook and Swift, 2012).

There is some evidence in the results to suggest a level of similarity between the patterns of lithological control on fjord morphology observed in other studies, and the patterns of potential lithological control on overdeepening morphology in Greenland. The least resistant category of lithology in the results is sedimentary, followed by volcanic, plutonic,

and with metamorphic as the most resistant (Dawes, 2009; Gowan et al., 2019). The results for average overdeepening width and length are inversely proportional to lithology strength for overdeepenings in the sedimentary, volcanic, and plutonic categories (i.e. highest average length and width for overdeepenings in sedimentary rock, then volcanic, with lowest width and length in the plutonic class). The opposite is partially true for overdeepening depth over these three categories of lithology; the weakest lithology (sedimentary) has the lowest average depth, plutonic has a higher average depth than sedimentary, with the volcanic class displaying the deepest average overdeepenings (Figure 3.25). Adverse slope gradient shows a positive relationship with lithological strength, with the lowest average gradient for overdeepenings of sedimentary lithology, and highest for overdeepenings of plutonic lithology.

The overdeepenings of metamorphic lithology, the strongest of the four categories, do not follow these trends between lithological strength and length, width, depth, and adverse slope gradient. For all the metrics, the metamorphic class is neither the highest nor the lowest of the four lithology categories. This is perhaps due to the fact that metamorphic lithology is the dominant overdeepening lithology (accounting for 64% of all overdeepenings in the metric dataset) having over four times as many overdeepenings as the next biggest category, and therefore broadly represents the average metric values of the whole metric dataset. As the metamorphic category is the largest in terms of area within the study area, it may also be that this category has more internal variation than the other smaller classes, although this is speculative and has not been tested.

In summary, there is some evidence to support the hypothesis that stronger lithology exerts greater topographic control by laterally confining ice flow (therefore imposing relative limits to lateral and longitudinal expansion of overdeepenings as they grow) (e.g. Swift et al., 2008), whilst focusing further erosion downward leading to greater average depths. As such, stronger lithologies can be characterised by shorter, narrower, deeper overdeepenings that can sustain higher adverse slope gradients, whilst weaker lithologies are characterised by longer, wider, shallower overdeepenings with less steep adverse slope gradients. However, the variation within the strongest (metamorphic) class of lithology, which makes up the majority of the dataset, limits the confidence with which these conclusions can be drawn.

3.4.4 Is ice velocity modulated when flowing through an overdeepening?

Fundamentally, there are two key ways in which flow through an overdeepening may modulate ice velocity. In order to exit an overdeepening, ice has to flow up hill, which may exert a back pressure on the ice due to form drag (Hooke et al., 1989; Hooke et al., 1992; Van der Veen, 1997; Cook and Swift, 2012). If all other forces remained equal, this would reduce the velocity of the ice. Water flowing subglacially will also have to flow uphill in order to exit the overdeepening. This is observed to result in perpetually high basal water pressure in overdeepenings (Hooke et al., 1989; Jansson, 1995). High basal water pressure reduces the effective pressure of ice at the bed reducing skin friction and causing ice velocity to accelerate (Lliboutry, 1968; Iken et al., 1983). These processes are covered in detail in sections 2.3.1.2 and 2.4.

The results presented in this chapter demonstrate that ice flows faster on the adverse slope of an overdeepening than on the normal slope of an overdeepening in 78.3% of cases, and that this represents a genuine speedup even when the expected background signal of downstream speedup is accounted for (Figure 3.27a). As such, it seems likely that when considering annual mean velocity, backstress exerted due to form drag by flow over the adverse slope of an overdeepening is less than the reduction in skin friction at the bed caused by elevated basal water pressure.

The analysis of modulation of ice velocity by overdeepenings presented in this chapter is highly simplified, but still of significance. This is the first time that observations of this type have been made, and conclusions drawn as to the effect on ice velocity of flow through overdeepenings at an ice sheet scale. Here, average annual velocities for a single year have been used. As such, this is generating a static picture of what is known to be a highly dynamic system. Basal water pressure, skin friction, and form drag are all interrelated, and will vary substantially based on both temperature and melt availability (Iken et al., 1983; Hooke et al., 1989; Van Der Veen and Whillans, 1989; Willis, 1995; Zwally et al., 2002). These more complex variabilities in ice velocity, and the role that overdeepenings play in modulating them on seasonal time scales, will be the focus of Chapters 4, 5 and 6.

3.4.5 Conclusion

The dataset produced within this chapter has identified the location of overdeepenings

under the fast flowing regions of the GrIS more precisely and accurately than has previously been possible. This dataset will enable the investigation of the potential control overdeepenings may exert on ice dynamics in the chapters that follow, and will be of potential use in a wide range of studies beyond this thesis. Mapping using bed data of a higher resolution than was previously available and utilised by existing studies was found to be beneficial and gives greater coverage of mapping, identifying more overdeepenings, and at higher fidelity than was previously possible. In particular, identification of highly elongate overdeepenings proximal to the ice margin that were missing in previous datasets is substantially increased. This is important as these areas of the ice sheet are of primary importance when investigating the impact of bed topography on ice dynamics.

There is broad agreement between the data presented in this chapter and previous studies (Patton et al., 2016) in terms of the morphometry of overdeepenings and the relationships between morphometric parameters. In particular, the tendency for overdeepenings to favour shallower depths (rather than evolve to the maximum possible depth) and to tend towards BSSRs around the classically held supercooling threshold (-1.2 to -1.8) suggests that the suppression of channelised subglacial drainage on adverse slopes of overdeepenings may exert a limiting feedback on the evolution of overdeepenings.

There is a difference between how ice flows on the normal and adverse slopes of overdeepenings with evidence that ice flows faster and accelerates more on adverse slopes than normal slopes. However, whilst statistically significant, this effect was found to be small once the background downstream velocity speedup signal was accounted for. There is no evidence that form drag as ice flows up the adverse slope of overdeepenings causes velocity to decrease.

Chapter 4 Seasonal velocity patterns along Greenland Ice Sheet marine-terminating glacier centre lines

The primary purpose of this chapter is to fully answer RQ2 ***does bed topography modulate ice velocity in overdeepenings?*** Chapter 3 achieved Objective A associated with RQ2 by demonstrating that at an ice sheet scale, mean annual velocity does appear to be modulated when flowing through an overdeepening, with systematic increases in velocity on the adverse slope compared to the normal slope. This chapter will be focused on Objective B, ***to determine whether seasonal ice velocity (e.g. timing and magnitude of speedup and slowdown) varies along glacier length, and the extent to which these variations may be linked to bed topography***.

The approach taken within this chapter is to shift from the ice sheet scale study of Chapter 3 and conduct two detailed case studies on selected individual glaciers. These will act as pilot studies to establish whether there is seasonal variation along glacier centre lines, before moving back to explore these patterns at the ice sheet scale in Chapters 5 and 6.

4.1 Introduction

Ice dynamics of Greenland outlet glaciers are complex and the impact of a warming climate on ice dynamics are not fully understood (Vaughan and Arthern, 2007; Nick et al., 2009). Approximately 85% of GrIS outlet glaciers are marine terminating (Mouginot et al., 2019) and are therefore potentially impacted by changes in both atmospheric and ocean temperatures. Warming ocean temperatures will increase submarine melting potentially destabilising or causing the breakup of ice tongues or mélange. This breakup reduces buttressing forces, resulting in increased inland ice velocity and therefore flux from the ice sheet (Howatt et al., 2008; Podrasky et al., 2014; Bondzio et al., 2016; Morlighem et al., 2016). Submarine melt due to warming oceans can also undercut the ice front and increase calving rates, which similarly enhances flux (O'Leary and Christoffersen, 2013; Benn, Åström, et al., 2017; Wood et al., 2024). Historically, these processes, primarily driven by ocean warming operating at the ice margin, have been seen to be the dominant mode by which climate change has increased ice flux to the ocean; essentially a model of destabilisation and speedup initiated at the margin, with consequent ice velocity speedup further inland. This has been referred to as dynamic draw down of ice sheets (Pritchard et al., 2009; Newton

and Huuse, 2017; Walker and Gardner, 2017) and could be conceptualised as speedup initiation at the margin which then *pulls* ice out from the interior. These processes have been inferred by some work to be dominant across the ice sheet (King et al., 2020), and in controlling ice velocity variation at Helheim specifically (Nick et al., 2009; Cheng et al., 2022). A range of recent work has presented support for a counter model where ice velocity increase is initiated inland (upstream) from the margin due to sliding caused by seasonal melt increase, and then *pushes* ice out towards the margin (Bevan et al., 2015; Davison et al., 2020; Ultee et al., 2022). Here, increased calving and retreat observed at the ice front is considered to be a *result* of the acceleration upstream, not the cause of it.

Intuitively, it seems likely that both push and pull mechanisms will be impacting the ice dynamics of an outlet glacier system, but with varying magnitudes at different points within the system, and at different times in the seasonal melt cycle. In certain scenarios ice acceleration at the margin and inland will be interlinked, in other scenarios they may be independent. In their recent paper, Larsen et al. (2023) demonstrate evidence in support of this notion, observing that in 2014 when there was a substantial retreat of the terminus of Upernavik Isstrøm II, this dominated the velocity patterns up to 6 km inland. In other years where there was less pronounced retreat, velocity patterns were dependant on the availability of surface meltwater. Further investigation into these nuances are recommended as important areas for future study by Larsen et al. (2023). Notably, the impact of adverse bed slopes on subglacial hydrology and the role it may play in determining the complexities of the drivers of ice dynamics has largely been ignored to date, and there have been no studies specifically focused on this in Greenland.

Previous work in this area has broadly fallen into one of two camps. A number of studies have considered velocity along the length of Greenland glaciers, but these have normally focused on singular (or small number of) glaciers, and have primarily considered interannual patterns and retreat rates, with the impact of bed geometry on glacier stabilisation limited to the basal and lateral pinning points and the control this may exert on retreat and thinning (Felikson et al., 2017, 2021; Catania et al., 2018; Catania and Felikson, 2022). Previous work which does relate specifically to seasonal velocity variation at the ice sheet scale is limited, and a full review was given in Section 2.3.3, but a brief recap is given here. Three studies have specifically investigated intra-seasonal velocity patterns (Moon et al., 2014; Vijay et al.,

2019, 2021), but only considering single points very close to the margin for each glacier. As such, there are questions over how representative of the ice sheet as a whole these findings are, given the questions on push and pull processes raised above. Only one study (Solgaard et al., 2022) has conducted a spatially comprehensive analysis of seasonal velocity modes, but the classifications of the entire velocity rasters that are implemented do not make it straight forward to relate findings back to individual glaciers, or to analyse the impact of wider parameters (such as bed geometry) to explain what is causing different seasonal velocity patterns.

In this chapter, proof-of-concept pilot studies are conducted to investigate the variability of seasonal velocity patterns at points along glacier centre lines to a) ascertain whether there are variations along the centre line, and b) determine the extent to which any variations may be linked to bed topography.

4.2 Methods and data

The approach taken in this chapter is to investigate two case study glaciers. The first is Helheim glacier on the east coast. The second case study glacier is Upernavik Isstrøm II on the west coast. Details on these glaciers and why they were selected as case studies is given in the case study introductions in sections 4.2.1 and 4.2.2. The overarching rationale was to first investigate how seasonal velocity patterns vary along the centre line on a very prominent and well studied glacier on the central east coast (Helheim), and then observe whether similar patterns are found on a glacier in a different setting, further north and on the west coast (Upernavik Isstrøm II). The second case study also examines in more detail the potential process relationships driving seasonal velocity patterns and how these may link to bed topography in more by utilising much higher temporal resolution velocity data.

4.2.1 Case study 1: Helheim glacier

4.2.1.1 Site location and context

Helheim is a large, fast flowing marine terminating outlet glacier in central east Greenland (63.35°N, 38.20°W) (Figure 4.1). Average ice velocity at the terminus is approximately 7 km/yr during the study year of 2014 (Figure 4.3b). The study area extends from the terminus

upstream approximately 35 km. The subglacial topography consists of a normal slope in the main trunk of the glacier extending from the calving front 10 km inland. At this point there is a very prominent riegel at the down glacier lip of a ~700 m deep overdeepening which extends inland for approximately 20 km (Figure 4.3). Helheim has the second largest solid ice discharge of any GrIS outlet glacier and accounted for approximately 7% of total GrIS solid ice discharge in 2019 (Mankoff et al., 2020). As such, it is of significance to the mass balance of the GrIS, and is well studied in the existing literature e.g. (Howat et al., 2005; Bevan et al., 2012, 2015; Williams, Gourmelen, Nienow, et al., 2021; Cheng et al., 2022; Ultee et al., 2022).

4.2.1.2 Data and methods

Helheim Glacier was selected as a case study area to test the seasonal variation in ice velocity at different points along the glacier centre line. The velocity dataset used was that generated by Rosenau et al. (2015) which provides ice velocities for over 300 Greenland outlet glaciers at a spatial resolution of 150 m. The velocities are generated using feature tracking algorithms on sequential pairs of over 16,000 Landsat images. A benefit of this dataset is that all coherent pairs of imagery are matched, not just the temporally contiguous image-pairs. This offers the possibility of high temporal resolution, with over 400 individual annual time slices (some of which overlap) for some years within the 1972-2014 range of the dataset. A downside of this approach is that many of the velocity time slices contain gaps, and these can be highly variable both spatially and temporally. These data gaps are managed by aggregating the data, as discussed further below. Data presented here are for 2014. The error for the velocity data used is estimated to have a median error of 0.11 m/day with a 3rd quartile error estimate of 0.57 m/day (Rosenau et al., 2015). BedMachine v3 (Morlighem et al., 2017) is used for glacier bed and ice surface elevation. Helheim has a good coverage of radar flight lines resulting in low bed error in the BedMachine v3 dataset (Morlighem et al., 2017), which was a key reason for selecting it. Mean error in the bed data along the glacier centreline is 50.3 m, with a maximum error of 101.7 m (Morlighem et al., 2017). This represents a mean bed error of less than 10% the depth of the overdeepening.

Melt data estimates are from MAR (Fettweis, 2007) and are daily total runoff averages for Greenland for 2014, which are then aggregated into seasonal periods (discussed below).

Ice flow streamlines were generated using the approach as described in Chapter 2 (Figure

4.1a). Code was written in Python to automate the following processes:

- Nodes were added at 150 m spacing along each streamline and velocity values for each time slice in 2014 were added to each node.
- Glacier bed and ice surface elevation values were added for each node, which allows longitudinal transects against ice velocity to be plotted for selected flowlines (Figure 4.1b). This is the same approach as adopted in Chapter 3 (see section 3.2.1).
- The central streamline that best represented the glacier centreline (number 8 in Figure 4.1b) was manually identified and used for the detailed analysis of seasonal velocity variation patterns.
- To reduce noise in the velocity data and fill gaps in individual time slices due to poor coherence between individual Landsat image pairs velocity values were aggregated into defined seasonal periods (DOY 0-139 (winter – pre-melt onset), DOY 140- 163 (spring – first melt), DOY 164-237 (summer – peak melt), and DOY 238-365 (autumn – post melt)). The graph of melt used to define these seasonal break points is shown in Figure 4.3a.
- Absolute ice velocities at each node along the centreline were aggregated to produce a mean velocity for each of the defined seasonal periods (winter, spring, summer, and autumn, as above).
- The sum of the variance of the four seasonal mean velocities from the annual mean is calculated at each node.
- Graphs of seasonal velocity variation at six points along the centreline (three downstream and three upstream of the riegel) are plotted using velocities normalised by local annual mean velocity at each node to facilitate comparison between regions of differing absolute velocity, similar to the approach taken by Moon et al. (2014) (Figure 4.3c).

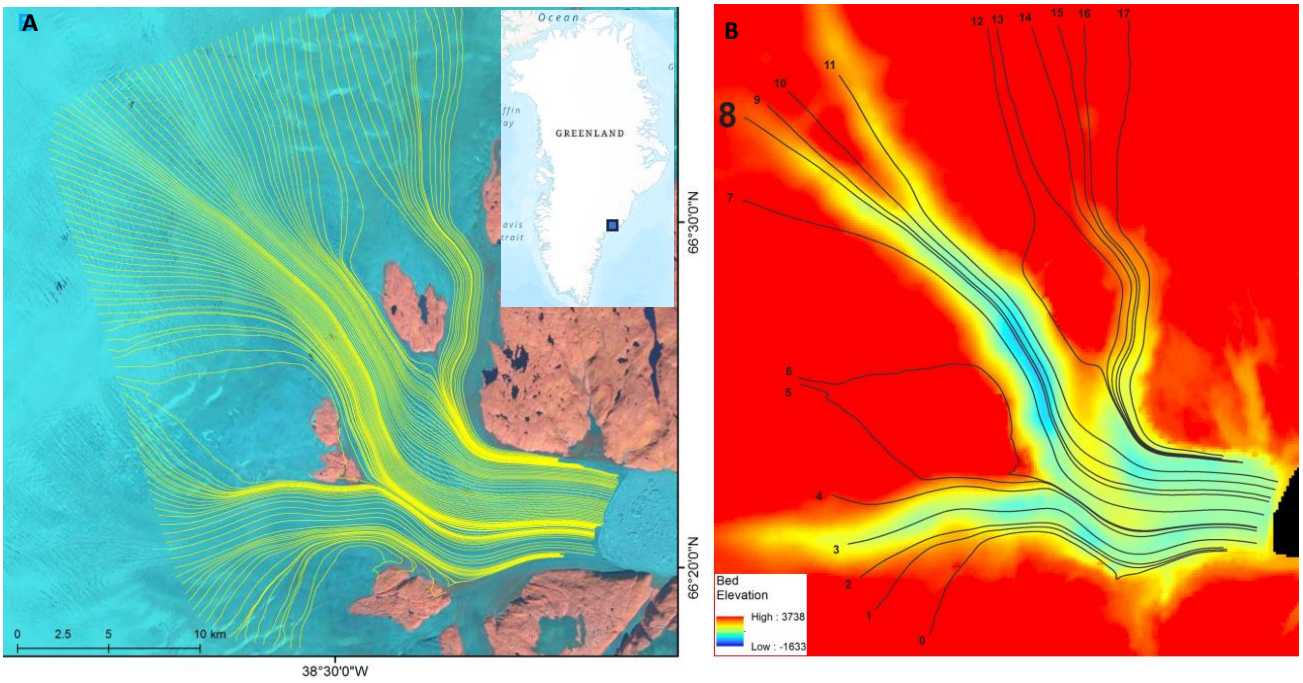

Figure 4.1 A) Ice flowlines generated for Helheim glacier (shown over Landsat 8 imagery, bands 5, 4, 3). Inset map shows the location of Helheim (bounding box is not to scale). B) A selected subset of streamlines, with the streamline best representing the main Helheim centreline highlighted (streamline 8). Bed elevation is from BedMachine v3 (Morlighem et al., 2014).

4.2.2 Case study 2: Upernavik Isstrøm II

4.2.2.1 Site location and context

Upernavik Isstrøm II is a large, fast flowing marine terminating outlet glacier in north west Greenland (72.95°N, 53.95°W) (Figure 4.2a). Average ice velocity at the terminus is between 3-4 km/yr during the study period of 2015-2017 (Figure 4.2b). The study area extends from the terminus upstream approximately 30 km.

The subglacial topography consists of a steeply incised trough running along the central flowline with a prominent overdeepening approximately 450 m deep (Figure 4.2c). For reference on figures, and for the purpose of some data aggregation in the analysis, the study area is segmented into three zones; the terminal zone (from the terminus to the riegel, 6km upstream), the adverse slope (from the riegel to the midpoint of the overdeepening, 13km upstream from the terminus), and the normal slope (from the

midpoint of the overdeepening to a position 21km upstream from the terminus) (see Figure 4.5).

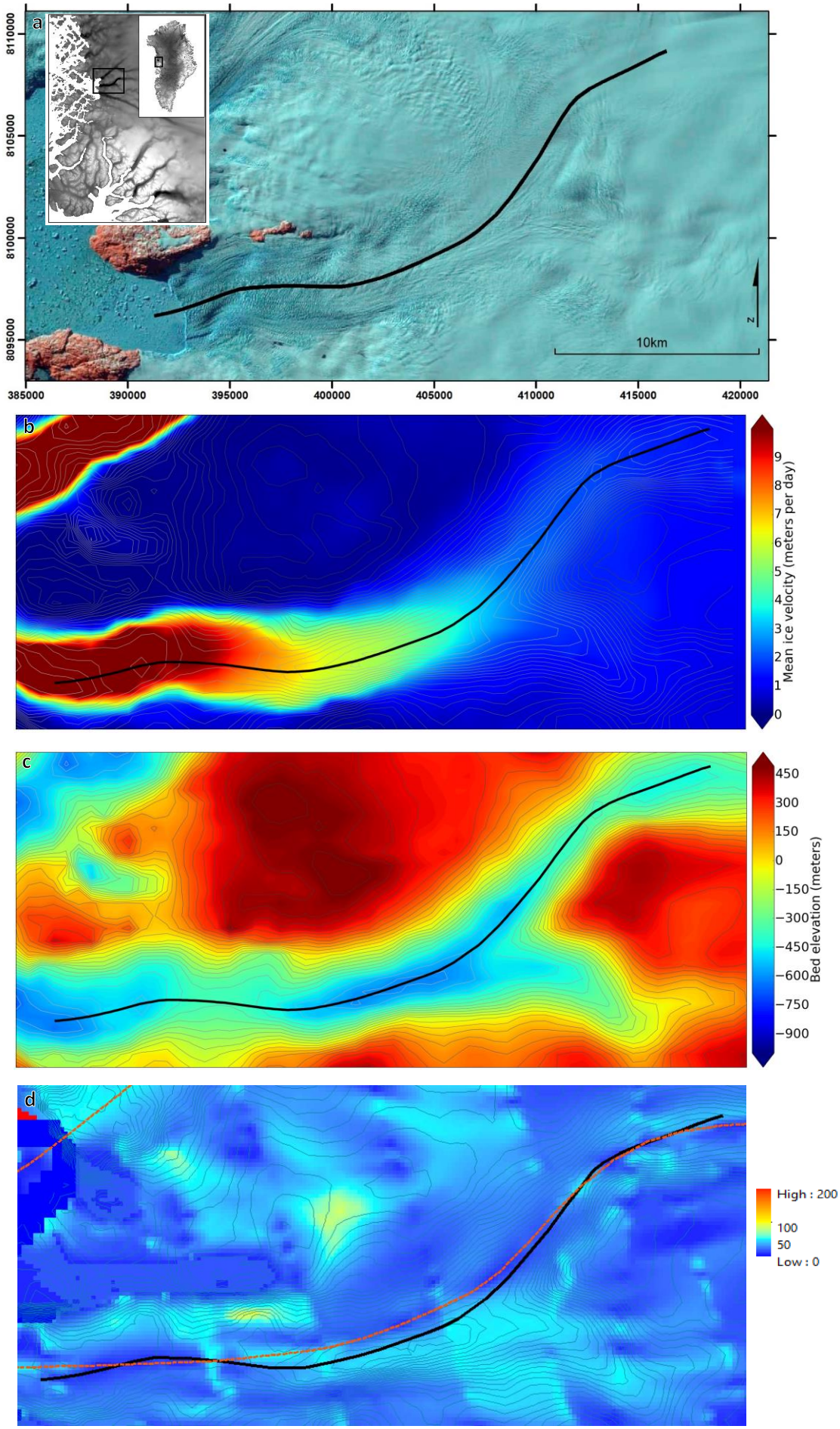
a
8110000
8105000
8100000
8095000
385000
390000
395000
400000
405000
410000
415000
420000
10km
N
b
Mean ice velocity (meters per day)
9
8
7
6
5
4
3
2
1
0
c
Bed elevation (meters)
450
300
150
0
−150
−300
−450
−600
−750
−900
d
High : 200
100
50
Low : 0

Figure 4.2 Upernavik Isstrøm II. A) Glacier centreline displayed over a Landsat 8 satellite image from June 2016 showing the location of Upernavik Isstrøm II Coordinates are in WGS1984 UTM 22N. B) Mean surface ice velocity 2015-2017 derived from Vijay et al. (2019). C) Subglacial topography of the glacier with 50m contours (Morlighem et al, 2017). D) Estimated error (in metres) of subglacial topography depicted at C) (Morlighem et al, 2017), the red dashed line indicates the flight line of the 2013 CReSIS radar depth sounding acquisition (CReSIS, 2016).

4.2.2.2 Data and methods

For this case study glacier, surface velocity data derived by Vijay et al. (2019) was utilised. I conducted the analysis for this case study after the analysis for case study 1 had been completed. The Vijay et al. (2019) dataset represents a technical improvement over the Rosenau et al. (2015) dataset. The velocity data is generated using SAR intensity offset tracking on Sentinel 1 IW single-look complex images. As such, issues of data gaps due to cloud cover which are common when using optical imagery (as in Rosenau et al. (2015)) are almost eliminated. The image pairs used for generating velocities in the Vijay et al. (2019) dataset are 24 day averages. As such, specific dates quoted in the results actually represent the middle day of the 24 period.

Ice surface elevation and bed elevation are from BedMachine v3 (Morlighem et al., 2017). A key consideration in selecting Upernavik Isstrøm II was the quality of the bed data. There is a CReSIS radar line almost exactly coincident with the central flowline used to extract data, as such the BedMachine error is very low and is under 50 m for the majority of the flowline (Figure 4.2d). Melt data is from the MAR 3.9.5 regional climate model (ftp://ftp.climato.be/fettweis/MARv3.9/Greenland/), and 10 km daily runoff values are used.

Ice front retreat was measured from 57 Landsat 8 scenes between 22nd February 2015 and 16th October 2017. Retreat or advance along the central streamline of the glacier was measured from a datum of the 22nd February 2015 position. For 2016 (the primary year of interest), a more detailed analysis of ice front position area change was conducted using the box method (Moon and Joughin, 2008).

To visualise velocity changes in relation to bed geometry, the central flowline for Upernavik Isstrøm II generated (as discussed in section 3.2.1) was taken as the starting point. 1k m wide transects normal to the central flowline were then generated at 150 m intervals and 8 nodes were then plotted at equal intervals along the transect. Velocity data for each time

slice, bed data, and ice surface data were then extracted to each node, and a mean taken from these values and joined back to the transect. This allowed the data used to be a swath along the central flowline which removes some noise and is more representative of the system than values along a single flowline. In addition to the values at 150 m intervals along the flowline, data were also aggregated into points on the normal slope, points on the adverse slope, and points downstream of the exit lip / riegel of the overdeepening. The transects and regions of aggregation are shown in Figure 4.4b. Means were calculated for velocity within each of region for each timeslice, shown in Figure 4.4c. Mean velocity for the whole study period was also calculated for each cell in the raw velocity rasters, and these averages were used to calculate a normalised percentage velocity variance from mean value for each cell in the raster for each time slice in the dataset. These values can be seen for all time slices in 2016 in Figure 4.5a-l. This was done to allow direct comparison of velocity variation (e.g. seasonal speedup and slowdown) between areas of differing absolute velocity. These normalised velocity variation values were also added to transect nodes as described above (Figure 4.4d), and aggregated into normal and adverse slope averages (Figure 4.4e).

4.3 Results and discussion

4.3.1 Case Study 1

Results

It is clear that ice velocity at Helheim varies along the centreline of the glacier, and that variability is non-linear (both in in terms of distance from the ice margin and with regard to depth / ice thickness) and complex (Figure 4.3). The nature of this variability indicates there may be some process relationship between ice velocity and bed topography. Ice accelerates from ~ 5 m d^{-1} to ~12 m d^{-1} as it enters the overdeepening before velocity plateaus part way down the normal slope (Point F on Figure 4.3b), slows slightly as it reaches the low point of the overdeepening (Point E on Figure 4.3b), and then accelerates on the adverse slope to ~17.5 m d^{-1}. Immediately downstream of the riegel (Point C on Figure 4.3b), there is a sudden and marked deceleration over the space of 2-3 km with velocity decreasing by ~2 m d^{-1} (greater than 10% slowdown) before a return to continued acceleration to the margin (Figure 4.3b).

The seasonal velocity mode (e.g. pattern of speedup and slowdown) also varies at different points along the centreline (Figure 4.3c). The seasonal velocity mode is a hybrid of Moon Type 2 and Type 3 (see section 2.3.3.3) within the overdeepening (e.g. a peak in velocity from winter baseline which then returns back to baseline, but with the maximum velocity in spring rather than summer); this is clear and consistent. Immediately downstream of the riegel the mode switches to Moon Type 1 (e.g. no pronounced peak coincident with melt onset or peak melt, rather a gradual acceleration from spring onward culminating in maximum velocity in autumn). The point closest to the margin has an indeterminate mode with a small peak in spring, a summer minimum, followed by a substantial acceleration into an autumn maximum.

Whilst variability in seasonal velocity mode is most clearly evident in the normalised velocity graphs for selected locations shown in Figure 4.3c, these patterns can also be identified in the line graphs plotting the absolute velocity averaged for each season continuously every 150 m along the central flowline shown in Figure 4.3b. The switch to a clear maximum velocity recorded in autumn (indicating Type 1) can be observed approximately half way up the adverse slope of the overdeepening approximately 2 km down glacier from point D (Figure 4.3b).

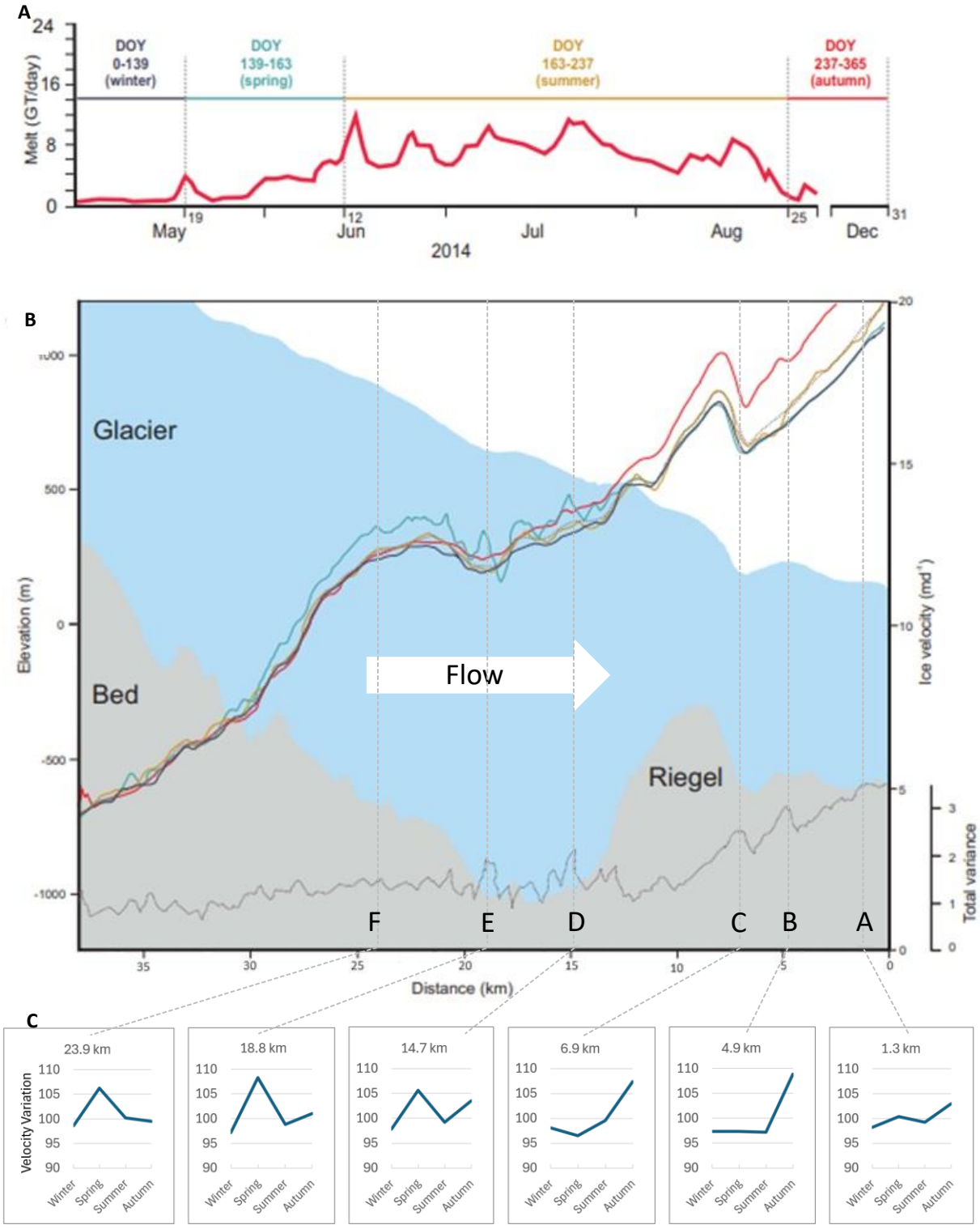

Figure 4.3 Seasonal ice velocity variation along the centreline of Helheim glacier (flowline 8 in Figure 4.1) in 2014. A) Melt rates for Greenland used to determine season break points. B) mean ice velocities for each season shown along the flowline (seasons as defined in A, colours correspond, dashed line shows the annual mean velocity). Total variance shows the sum of the variation of each of the four seasonal lines from the annual mean (in md^{-1}). 0 km on the right of the x axis is at the grounding line. Note, the estimated error in the velocity data of 0.57 m/day is lower than the seasonal ice velocity variation observed which is between 0.85 – 2.0 m/day depending on the distance from the ice front. Figure 4.3 .C) Graphs show seasonal speedup and slowdown patterns at three points upstream of the riegel and three points downstream.

4.3.1.1 Distinct seasonal velocity modes up and downstream of the riegel

Ice close to the margin at Helheim is very likely to be at or near floatation. Williams et al. (2021) estimate that in 2016 (the closest year to the study year) ice within ~ 2 km of the grounding line was at floatation. This may explain the lack of correlation between ice velocity and seasonal melt observed in this region of the glacier (e.g. reference points A, B and C on Figure 4.3b), where data show peak ice velocity occurring coincident with cessation of melt in autumn. Sea ice stability, calving processes, and terminus position / retreat likely dominate ice dynamics here as is established on other glaciers where a Type 1 seasonal velocity mode is common (Howat et al., 2008; Joughin, Das, et al., 2008; Sole et al., 2013; Tedesco et al., 2013; Moon et al., 2014; Rathmann et al., 2017; Cheng et al., 2022). The seasonal velocity patterns observed in the area down glacier from the riegel are indicative of the *pull* mechanisms outlined in section 4.1.

Upstream of the riegel a clear and distinct switch of seasonal velocity mode is evident with the Moon Type 2/3 hybrid consistently observed. Upstream from the riegel, ice substantially thickens and the surface slope steepens over a short distance (doubling from approximately 800 m thick at the riegel, to approximately 1600 m thick only 8 km further upstream at the deepest point of the overdeepening). As such, ice is solidly grounded and not near floatation. In this position, ice dynamics are much more likely to be controlled by changes in basal hydrological conditions and configuration, and the seasonal ice velocity patterns appear isolated from marine processes at the calving front. The seasonal velocity mode here is similar to that observed in mountain glacier contexts (Bindschadler et al., 1977; Iken and Truffe, 1997; Gudmundsson et al., 2000; Nanni et al., 2023), and terrestrially terminating glaciers in Greenland (Zwally et al., 2002; Sundal et al., 2011; Van De Wal et al., 2015). The seasonal velocity patterns observed inland of the riegel within the overdeepening are indicative of the *push* mechanisms outlined in section 4.1.

4.3.1.2 Comparison with seasonal velocity mode of Helheim identified by other studies

Three previous studies have analysed the seasonal velocity mode of Helheim Glacier. Initial work by Moon et al. (2014) suggests the velocity mode at Helheim varies over time and is sometimes indistinct, being classified as a different mode (or hybrid of modes) in each of the years covered by the study (2009-2013). However, in three of the five years, Helheim is

classified as partially Type 1 (e.g. broadly increasing velocity through the year). Vijay et al. (2019) adopted the methods and approach initially developed by Moon et al. (2014) and applied them to a higher temporal resolution velocity dataset spanning 2015-2017. They conclude that for these years Helheim's seasonal velocity mode is classified as Type 1. Unfortunately, neither of these two studies overlap with the study year of 2014, so a direct comparison is not possible. However, the overall picture of Helheim is of a glacier where velocity mode can sometimes be indistinct or variable from year to year, but that there are often elements of Type 1 present in the seasonal velocity signature. This aligns with the patterns seen in Figure 4.3c in the section of the study area beyond the riegel where the analysis also suggests a Type 1 mode (e.g. forced by marine processes).

A clear and unequivocal difference between the findings made here and those of Moon et al. (2014) and Vijay et al. (2019) is the dominance of Type 2 / 3 seasonal variation upstream of the riegel (e.g. reference points D, E and F on Figure 4.3b). There is no indication of Type 1 modality upstream of the riegel in the data presented in this chapter. The methodology adopted by both Moon et al. (2014) and Vijay et al. (2019) in their studies involved taking a single velocity measurement for each glacier for each available time slice at a position very close to the terminus (approximately one half width from the terminus in Moon et al. (2014) and within 1 km of the terminus in Vijay et al. (2019)). At Helheim, this locates the measurements between the terminus and the riegel.

The only other study to have attempted to determine seasonal velocity modality for Helheim is Solgaard et al. (2022). Their approach was to assess individual modality for each cell in a 500 m spatial resolution raster grid covering the entire Greenland Ice Sheet. This approach considers the velocity at many 1000s of points for Helheim and offers the possibility to investigate spatial variation in patterns of seasonal velocity mode not offered by a single point approach. Their results show a classification of Helheim as a mix of Type 2 and Type 3 seasonal velocity modes. This varies from year to year, with some years dominated by a single mode, and other years show different modes in different areas of the glacier. Interestingly, Solgaard et al. (2022) use a machine learning based method to automate the classification of seasonal velocity modes of pixels (rather than the manual visual interpretation of patterns adopted by Moon et al. (2014) and Vijay et al. (2019)), and there is no class identified by the K means algorithm that represents a Type 1 mode within

their ice sheet wide dataset. Recent work by Larsen et al. (2023) shows that the impact of dynamic response to retreat at the front may be limited to a zone close to the margin, with the impact of basal hydological driven processes relating to surface melt increasingly prominent further upglacier. If this is the case more widely there will obviously be a skew to the location of Type 1 modes in areas close to the terminus of marine terminating glaciers. It follows that methodological approaches that only take measurements close to the margin will overestimate the prevalence of Type 1 modes if findings are extrapolated to the ice sheet as a whole. The absence of a cluster representing Type 1 modes in Solgaard et al. (2022) study can potentially be explained by the fact that the vast majority of their study area is beyond the zone close to the terminus where marine effects can be identified in velocity dynamics. As the proportion of data points in their dataset within this zone is very low it may not be significant enough to generate a distinct cluster in the K means analysis. Thus, it is clear that approaches where measurements are limited solely to areas very close to the terminus may overestimate the prevalence of Type 1 modes, whilst the approach taken by Solgaard et al. (2022) which indiscriminately considers the entire ice sheet excludes the identification of important factors (due to being located at the ice flux gate to the ocean) in the of overall picture of seasonal ice sheet dynamics.

In a recent study of Helheim, Ultee et al. (2022) conducted normalised cross correlation analysis between runoff, terminus position, and ice velocity variability using a variety of lag periods to try and determine whether marine processes or melt processes were the dominant control in velocity variation. They found that in all years of their study, Helheim's ice velocity is at least as well correlated with runoff as with terminus position, and that the strongest correlations between ice velocity and terminus position were actually for negative lag periods indicating that terminus position may be *responding* to velocity variation rather than *causing* the variation. They conclude that runoff is likely the dominant control on velocity variation at Helheim for seasonal and inter-annual timescales, but that terminus position is the dominant control over multi-annual timescales (2009-2017 in this case) (Ultee et al., 2022).

The approach taken within this chapter gives due consideration to processes operating in all areas of the ice sheet (not simply the margin), but without taking in so much data as to obfuscate important but less prevalent processes. The observational study by Larsen et al.

(2023) at Upernavik Isstrøm II suggests inland limit of marine influence is c. 8 x ice thickness, which for ice thickness between 700-1,800 m at Helheim would give a limit of between 5.6–14.4 km. Empirical modelling results have suggested a likely stress-coupling length (SCL) of between 1–3 km for the main trunk of Helheim, and up to ~6 km for the tributaries (Enderlin et al., 2016).The analysis for Helheim presented here suggests a zone of marine influence of c. 7-12 km, but it appears that this limit may be predominantly due to the riegel isolating the marine influence downstream of its position. All process relationships identified are also directly tied to individual glaciers allowing nuanced investigation of potential process relationships (such as the effect of bed topography in relation to the direction of flow) rather than simply relying on interpretation of broad trends aggregated at a regional scale.

4.3.2 Case Study 2

Results

Inter and intra-annual (seasonal) velocity variations across a swath along the longitudinal transect of Upernavik Isstrøm II from 2015 to 2017 are shown in Figure 4.4d and Figure 4.4e. The general pattern of speedup and slowdown in each year is similar on the normal and adverse slopes, but with important differences in the magnitude of velocity variations. Patterns of seasonal velocity variation are set against an overall trend of increasing velocity over the study period. The timing and magnitude of melt varies across all three years.

4.3.2.1 General relationships between velocity and melt

In 2015 speedup occurred at melt onset followed by slowdown to below 2015 initial spring velocity after peak melt, then subsequent speed up to above the spring 2015 velocity by December which is then maintained throughout the winter. Melt started on 10th May 2015 and remained low (below 10 mm WE d^{-1} (water equivalent per day)) until the 15th June when there is a rapid increase in melt. A sustained peak of melt around 40-60 mm WE d^{-1} is maintained until the 20th July. There is small secondary melt spike lasting 14 days and peaking at 19 mm WE d^{-1} on 14th August. It is not possible to identify the exact timing of peak velocity in 2015 due to a lack of data between 2nd June and 1st August, but the window in which peak velocity occurs is coincident with peak melt. The cumulative melt in 2015 is relatively high: 88.4% of the 2016 cumulative melt (the highest melt year in the study period).

In 2016 there is speedup at melt onset followed by slowdown after peak melt. From mid-September velocity re-accelerates to a speed approaching the 2016 maxima which is then maintained over winter. Initial melt onset is early in 2016 starting on the 9th April with a series of short lived (4-6 days), low magnitude (<10 mm WE d^{-1}) daily melt events interspersed by gaps of 8-10 days. From 1st June melt steadily increases and then decreases symmetrically around peak melt of 70 mm WE d^{-1} on 18th July. Peak melt coincides with peak velocity. There is a further prominent melt event lasting 12 days and peaking at 42 mm WE d^{-1} on 24th August. The cumulative melt in 2016 is the highest of the three years in the study period.

In 2017 there is initial slowdown at melt onset followed by subsequent speedup coincident with peak melt, then slowdown back to (but not falling below) a velocity approximately that of the initial 2017 spring velocity. From a high initial velocity, variations in velocity during 2017 were of a lower magnitude than in 2015 and 2016. Melt in the early part of the season is relatively high with sustained melt rates of between 10-20 mm WE d^{-1} in the first two weeks of June. Beyond this point, melt is low compared to 2015 and 2016 with melt generally in the 20-30 mm WE d^{-1} range. There is a short melt spike with individual daily melt level reaching above 40 mm WE d^{-1} and up to 67 mm WE d^{-1} for a period of eight days between the 23rd July and the 30th July. Peak melt coincides with peak velocity. Cumulative melt in 2017 is relatively low (74.4% of the 2016 cumulative melt).

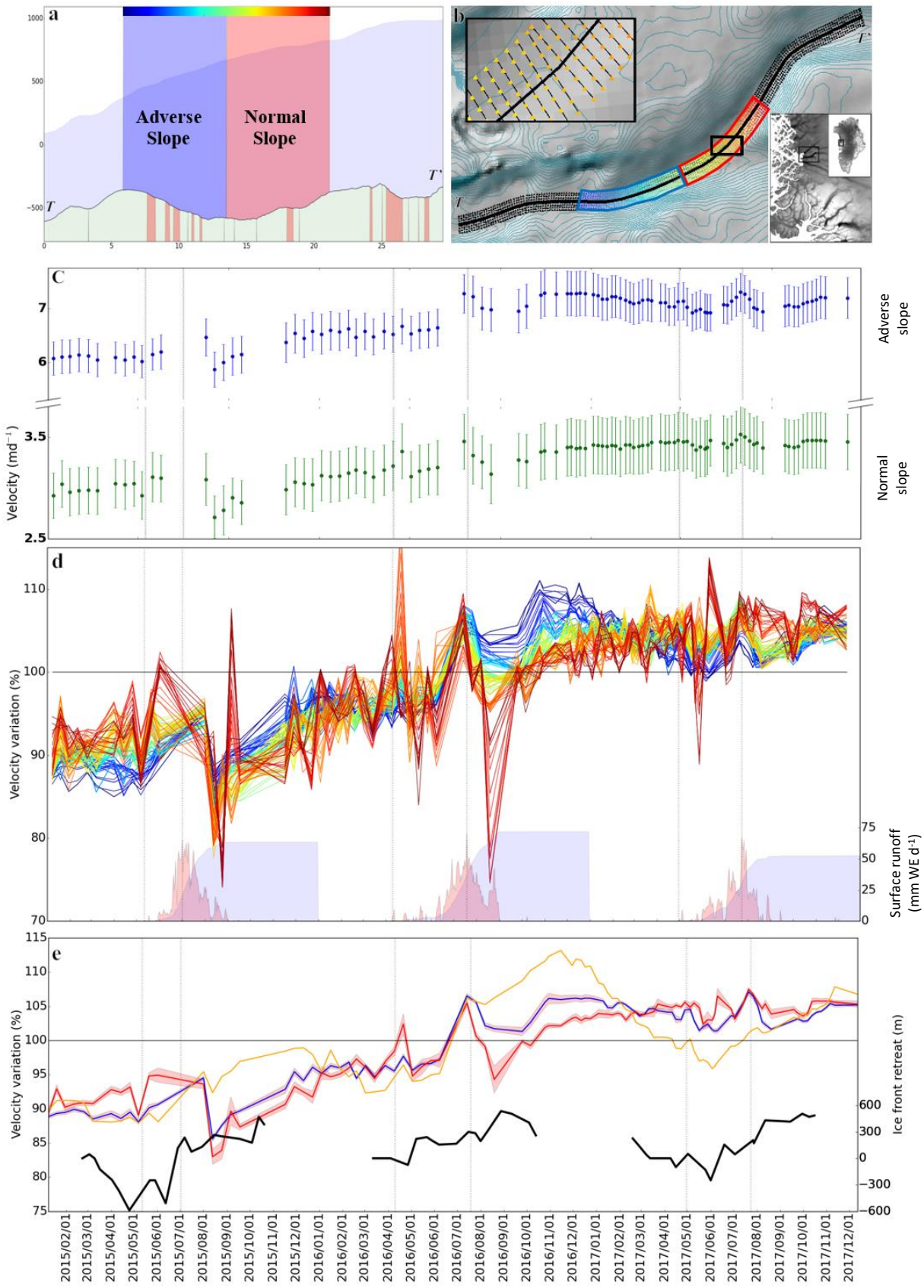
a
Adverse Slope
Normal Slope
T
T'
b
C
Velocity (md⁻¹)
Adverse slope
Normal slope
d
Velocity variation (%)
Surface runoff (mm WE d⁻¹)
e
Velocity variation (%)
Ice front retreat (m)
2015/02/01
2015/03/01
2015/04/01
2015/05/01
2015/06/01
2015/07/01
2015/08/01
2015/09/01
2015/10/01
2015/11/01
2015/12/01
2016/01/01
2016/02/01
2016/03/01
2016/04/01
2016/05/01
2016/06/01
2016/07/01
2016/08/01
2016/09/01
2016/10/01
2016/11/01
2016/12/01
2017/01/01
2017/02/01
2017/03/01
2017/04/01
2017/05/01
2017/06/01
2017/07/01
2017/08/01
2017/09/01
2017/10/01
2017/11/01
2017/12/01

Figure 4.4 Percentage variation in ice velocity (from the local 2015-2017 mean at each point) along the central streamline of Upernavik Isstrøm II between 2015 and 2017. A) Cross section of bed topography along the central streamline. The colour ramp along the top of the figure locates the transects plotted in B and D. B) Location of transects plotted for the purpose of data aggregation and analysis. C) Average velocity for points in the normal slope regions (green) and adverse slope region (blue). With 1 standard deviation of the mean shown by bars. D) Velocity variation for 1km wide transects normal to the centreline spaced at 150m intervals. Variation is shown as a percentage of the local mean velocity (calculated over the entire time period) for each transect. Colours indicate the location of each transect (see A and B). Modelled daily melt is shown on the bottom graphs in pink, cumulative annual melt is shown in blue. Dashed vertical lines indicate onset of melt and peak melt for each year. E) Average surface ice velocity for points in the normal slope region (red), and adverse slope region (blue) for each time slice between 01-01-2015 and 31-12-2017, lines show a 95% confidence interval. Orange line shows the average velocity variation in the terminus region. Black lines show ice front retreat.

4.3.2.2 Spatial variations in velocity response

Whilst the general pattern of variation in ice velocity are similar on the adverse and normal slopes, there are important, significant, and systematic differences.

A distinct pulse of acceleration initiated upon melt onset appears to be characteristic of the normal slope. In 2016 and 2017 this then drops back to the pre-melt onset velocity before reaccelerating to a seasonal maxima coincident with the timing of peak melt. It is unclear whether this pattern of variation occurs in 2015 due to a lack of velocity data between 2nd June and 1st August. Figure 4.5 shows maps of velocity variation for 12 time slices between late spring and early autumn 2016. The distinct melt onset acceleration pulse on the normal slope in 2016 can also be seen in the map in Figure 4.5b. There is no evidence of a melt onset acceleration pulse on the adverse slope at all during the study period. In all three years speedup on the adverse slope commences when melt becomes sustained and then accelerates more rapidly as melt increases.

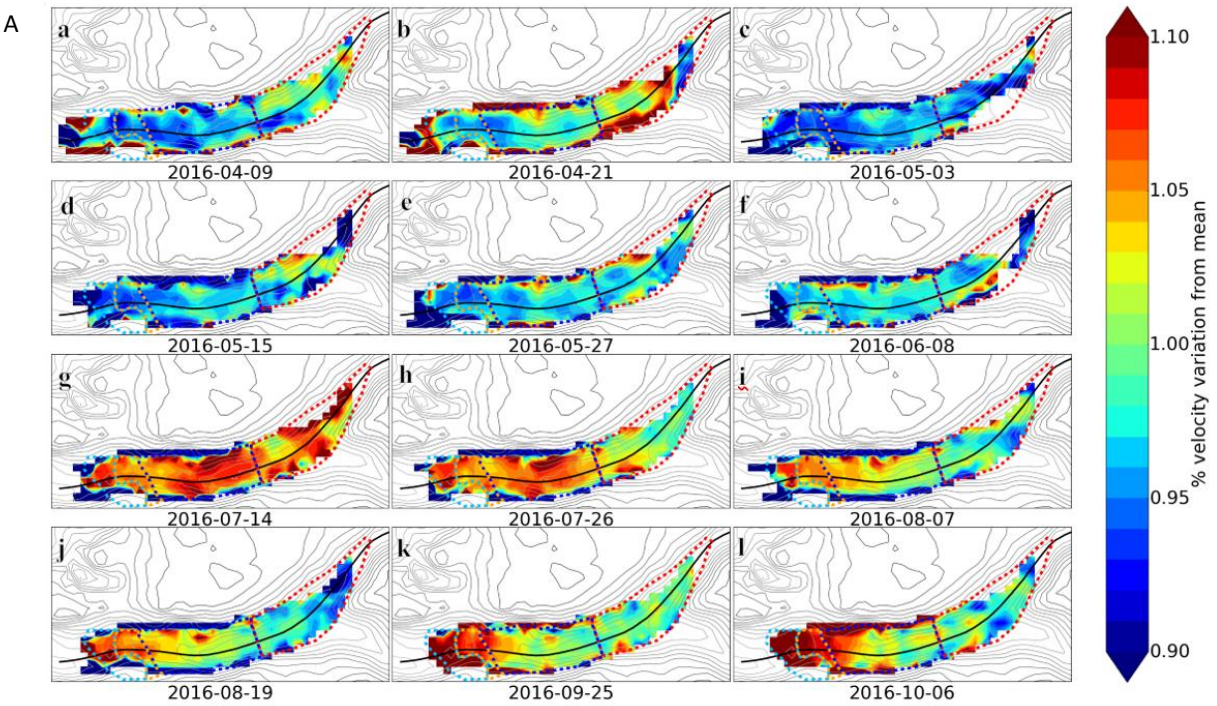
A
a
b
c
d
e
f
g
h
i
j
k
l
2016-04-09
2016-04-21
2016-05-03
2016-05-15
2016-05-27
2016-06-08
2016-07-14
2016-07-26
2016-08-07
2016-08-19
2016-09-25
2016-10-06
1.10
1.05
1.00
0.95
0.90
% velocity variation from mean

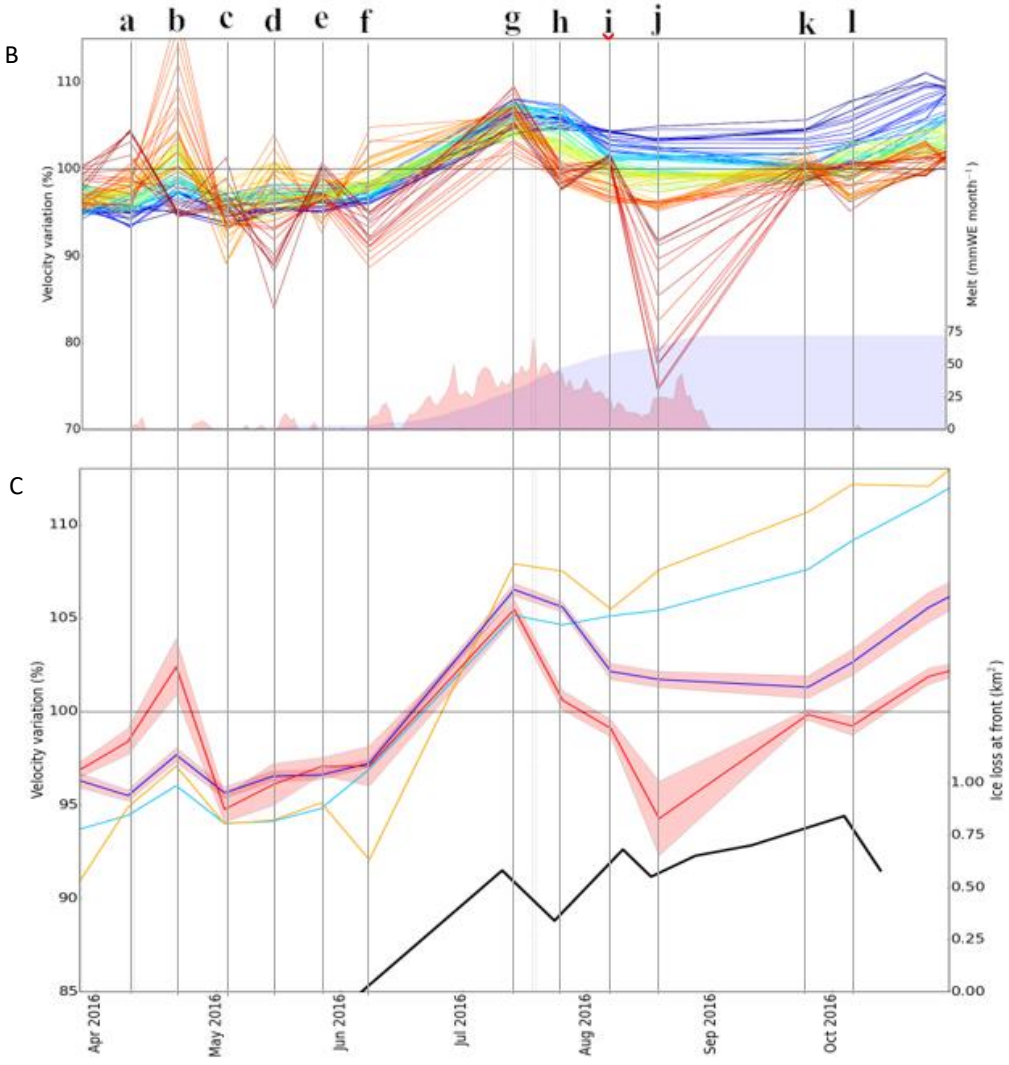
B
a b c d e f g h i j k l
Velocity variation (%)
Melt (mmWE month⁻¹)
C
Velocity variation (%)
Ice loss at front (km²)
Apr 2016
May 2016
Jun 2016
Jul 2016
Aug 2016
Sep 2016
Oct 2016

Figure 4.5 A) Ice velocity variation for Upernavik Isstrøm II at 12 time slices between 09-04-16 and 06-10-16. Variations are normalized to show the percentage of the mean for each cell in the velocity raster over the period 01-01-2015 to 31-12-17. Dashed coloured lines show the zones of adverse and normal slope from Figure 4.4 and the terminus region downstream of the overdeepening (split into two subsections, light blue and orange). B) and C) The data from Figure 4.4d and Figure 4.4e is reproduced for 2016 with lines marking the timing of panes a-l. Mean velocity variation has been added to C) for the two terminal zones downstream of the overdeepening. These relate to the light blue and orange areas marked on A).

In the higher melt years of 2015 and 2016 late summer slowdowns coincide with secondary spikes in melt (around the 15th August in 2015 and the 19th August in 2016). In both years slowdown occurs on the normal and adverse slopes, but is more pronounced on the normal slope. In 2015 peak velocity around the time of peak melt is 92% of mean on both the normal and adverse slopes. During the secondary melt spike, velocity slows down to 81% on the normal slope, and 83% on the adverse slope. In 2016 peak velocity (coincident with peak melt) is 105% of mean on the normal slope and 106% on the adverse slope. During the secondary melt spike, velocity slows down to 93% of mean on the normal slope and102% on the adverse slope.

The transition into this exaggerated slowdown on the normal slope for 2016 is highlighted in Figure 4.5. At the point of peak melt on the 14th July (Figure 4.5g), all areas of the glacier speedup fairly uniformly by approximately 10%. As melt starts to decrease on the 26th July (Figure 4.5h) and the 8th August (Figure 4.5i), velocities decrease below 100% for most areas within the main normal slope zone. There is some very modest slowdown in the adverse slope zone (mostly concentrated around the adverse / normal zone boundary) demonstrated in Figure 4.5h. Areas of slowdown widen in the adverse slope zone in Figure 4.5i but almost all velocities remain above 100%. There is a late summer spike in melt around the end of August coincident with the 19th August velocity timeslice (Figure 4.5j). At this point the velocity in the main normal slope zone drops markedly with all velocities below 100% and velocities in the upglacier half of the zone dropping below 90% of mean velocity and below 80% in areas furthest upglacier. During the strong slowdown on the normal slope zone demonstrated in Figure 4.5j, no significant further slowdown is seen in the adverse slope zone.

The spatial patterns of velocity response in 2017 are distinctly different from 2015 and 2016. Baseline velocities on both the normal and adverse slopes at the start of 2017 are

very high at 102% of mean on the normal slope, and 103% on the adverse slope. Velocity trends continue from the end of 2016 with gradual acceleration on the normal slope and gradual deceleration on the adverse slope. When melt becomes sustained around the 1st June the initial velocity response mirrors that of 2016 with a distinct acceleration pulse followed by reacceleration to a peak velocity coincident with melt on the normal slope, and a single consistent acceleration to a velocity peak coincident with peak melt on the adverse slope. Maximum velocity is identical (105% of mean) on both slopes. Following peak melt, velocity slows down in line with decreasing melt on both slopes. The slowdown is very marginally more pronounced on the adverse slope with velocity dropping to 99% of mean whilst slowdown on the normal slope only reaches 101%. This is the opposite of the patterns in 2015 and 2016 where slowdown was more pronounced on the normal slope. However, the variations between normal and adverse slopes in 2017 are very small and so caution must be taken making any inference from these.

4.3.2.3 Terminus velocity patterns

Upernavik Isstrøm II has a prominent riegel at the down glacier end of the main overdeepening approximately 6 km from the terminus. Velocity variation in the zone between the riegel and the ice front demonstrates a much stronger correlation with frontal position (Figure 4.4e). Seasonal velocity maxima shows a stronger association with retreating front positions than with peak melt. There are minor spikes in velocity coincident with peak melt in the terminus zone in all three years, but in each case, there is subsequent continued speedup of greater magnitude continuing into late autumn and early winter as frontal retreat persists.

Discussion

4.3.2.4 Marine effect

Processes specific to glaciers terminating in a marine environment can affect ice dynamics (Howat et al., 2008; Bevan et al., 2012; Moon et al., 2014; Kehrl et al., 2017; Vijay et al., 2019). These were introduced in detail in section 2.3.2, and discussed in relation to Helheim in section 4.3.1, but are presented here in the specific context of the interpretation of the observed patterns of ice velocity at Upernavik Isstrøm II. At Upernavik Isstrøm II, the current

topographic context is not conducive to rapid retreat. Ice is retreating up a normal slope and into a narrowing pinning point at the riegel.

Upernavik Isstrøm II has previously been identified as exhibiting a correlation between ice velocity and frontal change, with increased velocity at the terminus associated with retreat of the front (Vijay et al., 2019). This is the seasonal velocity pattern known as Type 1, also observed downstream of the riegel at Helheim (see section 4.3.1.2). The results in the terminal zone downstream of the riegel show agreement with this pattern. Ice dynamics are most closely linked to ice front position, with velocity increasing steadily from mid-summer through to mid-winter in response to frontal retreat, although with a subtle signal relating to melt patterns superimposed (Figure 4.4). However, this marine effect appears to be largely isolated downglacier of the riegel. Upglacier of the riegel speedup and slowdown is dominated by melt inputs and often opposite to that seen at the terminus. Late summer slowdowns occur on both the normal and adverse slopes in all three years despite frontal retreat driving ice acceleration at the terminus during these periods, providing further support that the riegel is having an isolating effect subduing the marine influence from fully propagating upglacier of the riegel (Figure 4.4). However, it is impossible to rule out that there may be some influence of the late season marine driven speedup downstream of the riegel having an impact on the down glacier end of the adverse slope. A recent study by Larsen et al. (2023) also concluded that the limit of marine influence on seasonal ice dynamics at Upernavik Isstrøm II is 6 km from the terminus (almost the exact position of the riegel). They conclude that seasonal velocity variation is Type 1 near the margin. In their paper there is no discussion of the bed topography and the limit of marine influence is attributed to stress coupling lengths. They specifically recommend that analysis of seasonal velocity patterns is not restricted to areas close to the margin (to avoid bias of marine influence) and recommend that theoretical stress coupling lengths (e.g. (Kamb and Echelmeyer, 1986)) are taken into account when selecting locations for analysis (Larsen et al., 2023).

4.3.2.5 Seasonal velocity variation typology upglacier of riegel

In the region inland of the riegel the seasonal velocity variation is broadly characteristic of Moon Type 2 / Type 3 in all years on both the adverse and normal slopes of the overdeepening (Figure 4.4e). Peak velocity is coincident with peak melt and then decreases

as melt decreases. The pattern in 2015 is less clear due to poor temporal resolution of velocity data between mid-May and the beginning of August. However, in 2015 on both the adverse and normal slope, and in 2016 on the normal slope, there is a late summer slowdown to below the initial spring velocity. As such, these velocity profiles have some of the characteristics of Moon Type 3. There is no evidence of Type 1 velocity variation inland from the riegel. These observations are in agreement with the findings of Larsen et al. (2023) who also concluded that seasonal variation was Type 3 in this region of the glacier, with late summer slowdown events dominant. Larsen et al. (2023) also observed that intensity of maximum seasonal speedup increased with distance from the calving front. There is no evidence of that in the results presented here; the magnitude of speedup at seasonal maximum velocity is almost identical on the normal and adverse slopes. 2017 was a lower melt year and there is no evidence of late summer slowdown in this year. The observations of late summer slowdown in higher melt years, but not in lower melt years are similar to the patterns of self-regulation of net ice flux by lowered autumn and winter velocities under high melt conditions identified by Sole et al. (2013) (see section 2.3.1.5).

4.3.2.6 Modulation of subglacial hydrology by bed topography

Late summer slowdown

The variations in ice velocity for 2015 and 2016 bear the hallmarks of late summer slowdown which have been hypothesized to be indicative of an evolution in basal hydrological mode from an inefficient distributed configuration to an efficient channelized regime (Fig. 4.5) (Bingham et al., 2003; Truffer et al., 2005; Sundal et al., 2011). These processes were discussed in detail in sections 2.3.1.3, 2.3.1.4, and 2.3.3.2. That these late summer slowdowns are evident in the two higher melt years, but not in 2017 when melt was lower, further support this notion that seasonal velocity patterns are being driven by melt accessing the bed and modulating the subglacial hydrological configuration (e.g., Sole et al., 2013).

In both late summer slowdowns (2015 and 2016) the slowdown is more pronounced on the normal slope. In particular, Figure 4.5f shows that following peak melt and coincident with a secondary melt spike on the 13th August 2016 velocity at the up-glacier end of the normal slope drops from approximately 105% of the average, to under 75% of the average. The

velocity during the same period at the down glacier end of the adverse slope demonstrates a much more modest slowdown from approximately 105% to 102% of the average. That ice velocity remains higher on the adverse slope, despite potentially being subject to additional backstress from flowing uphill (Van der Veen, 1997; Motyka et al., 2003), can be explained by the way in which ice flowing through an overdeepening modulates subglacial hydrological conditions. The requirement for water to leave an overdeepening by flowing up an adverse slope results in higher basal water pressure than on the normal slope (Hooke et al., 1989; Jansson, 1995). Where the BSSR exceeds 1.2-1.7 the supercooling threshold is exceeded causing subglacial channels to constrict rather than expand, thus maintaining or increasing subglacial water pressure (Creyts and Clark, 2010). The supercooling threshold is exceeded for approximately a third of the length of the longitudinal transect over the adverse slope for Upernavik Isstrøm II (Figure 4.4a), and the seasonal response on the adverse slope compared to that on the normal slope is aligned with the theorised impact of supercooling on subglacial hydrology of adverse slopes discussed in section 2.4. Even where the supercooling is not occurring, the reduced hydraulic gradient as water flows up the adverse slope of the overdeepening will suppress the development of channelised drainage.

4.3.2.7 Conceptual model

The conceptual model presented below (Figure 4.6) has been conceived to explain the variations in seasonal velocity patterns between the normal and adverse slopes of the Upernavik Isstrøm II overdeepening in 2015, 2016 and 2017. It is proposed that the variations observed can be explained by four distinct configurations of subglacial hydrology which are dependent on the level of melt and the influence of supercooling processes on the adverse slope.

In all years the initial subglacial hydrological configuration is hypothesised to be as shown in A (Figure 4.6). Subglacial hydrology is distributed on both the normal and adverse slopes, but on the adverse slope there is persistent over winter melt at the bed which was unable to exit the overdeepening at the end of the previous summer due to supercooling restricting flow along the adverse slope. As such, elevated water pressures are maintained on the adverse slope. The configuration on the adverse and normal slopes are essentially analogous to the graphs of seasonal velocity variations in overdeepened and non-overdeepened beds respectively, as illustrated by Cook and Swift (2012) in Figure 2.25

(section 2.4). As a result of these initial conditions, it is the more pronounced repressurisation of the subglacial hydrological system on the normal slope upon melt onset that causes the distinct pulse of acceleration observed in all years. This hypothesis is also aligned with the findings of Iken et al. (1983) that the initial pressurisation of the subglacial system is a key driver of velocity increase, and may be more important than subsequent further increase in melt delivered to the bed (see Figure 2.2, section 2.3.1.2).

In all years, as peak velocity (which is coincident with peak melt) occurs, the subglacial hydrological configuration is hypothesised to be as shown in B (Figure 4.6). Drainage is distributed on both the normal and adverse slopes as the normal slope has transitioned from configuration A to configuration B following the initial early season melt pulse and sustained melt throughout the first half of the melt season

In 2015 the sustained period of high melt (in excess of 50 mm WE d^{-1}) for 35 days from 15th June is hypothesised to have induced a switch from configuration B to configuration D (where drainage is channelised on both the normal and adverse slope, Figure 4.6) resulting in the slowdown to below the initial 2015 spring velocity across all areas of the bed.

In 2016, whilst the cumulative melt over the season is high, the more gradual increase in melt (which is not sustained at a very high level for an extended period, as is the case in 2015) is hypothesised to be sufficient to induce a switch to subglacial hydrology from configuration B to configuration C (where there is channelised drainage on the normal slope, but on the adverse slope distributed drainage is maintained, Figure 4.6). This results in a slowdown to below spring 2016 velocity on the normal slope, whereas velocity on the adverse slope slows down as melt reduces, but remains above the initial spring velocity. These responses are analogous to the patterns observed by Sundal et al. (2011) for higher (channelised) and lower (distributed) melt years, but expressed here on the normal and adverse slopes of the overdeepening in the same year.

In 2017 melt is generally low with a single, short lived melt peak. Melt is hypothesised to be insufficient to force evolution to a channelised system on either the adverse or the normal bedslope, and configuration B (Figure 4.6) is maintained throughout the melt season. The resulting velocity speedup and slowdown is symmetrical and synchronous with increasing and decreasing melt, returning to (but not below) the initial spring velocity on both the adverse and normal slopes.

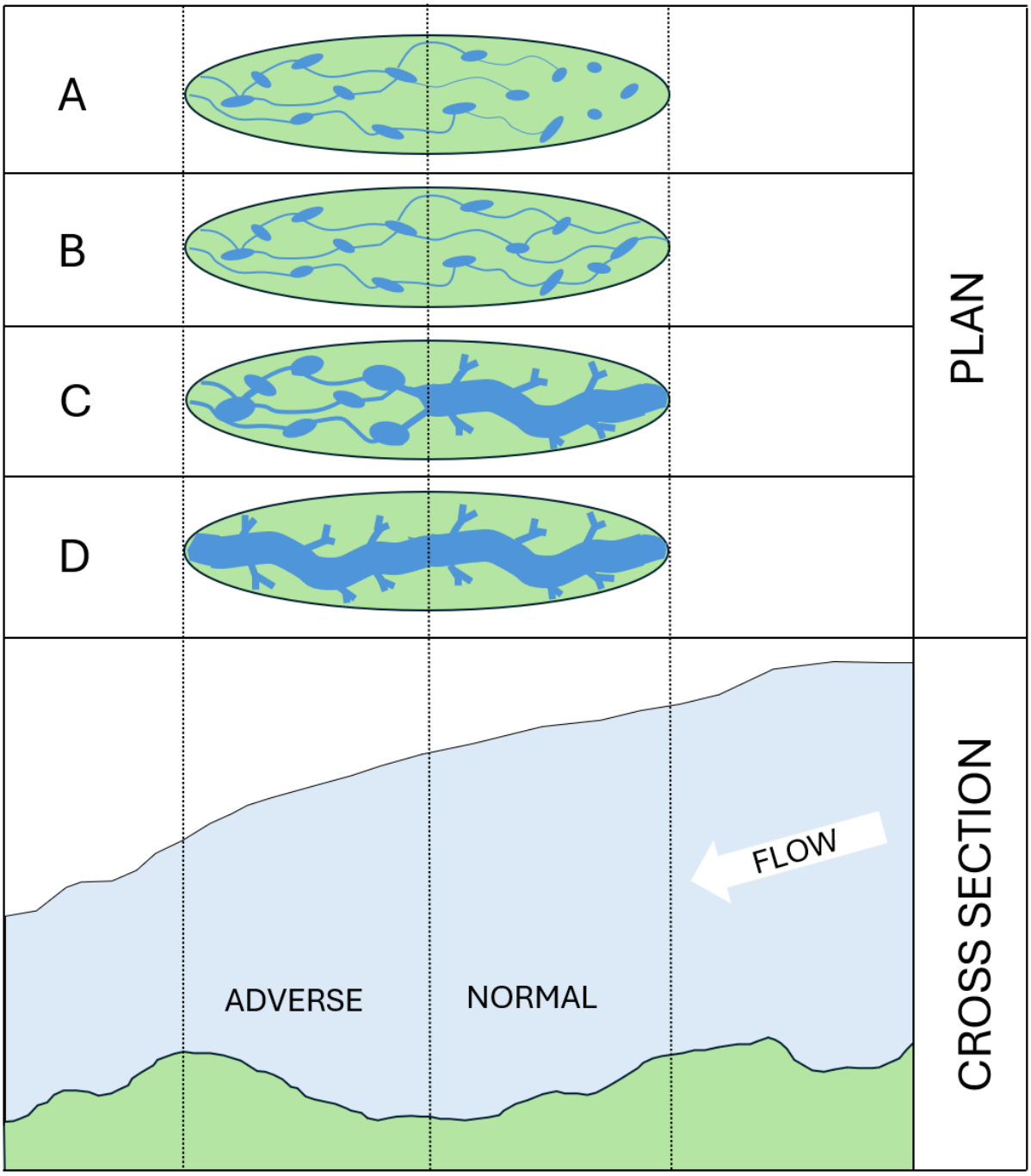

Figure 4.6 Conceptual model presenting the four hypothesised subglacial drainage configurations for the overdeepening at Upernavik Isstrøm II. The bottom pane shows a longitudinal cross section along the central flowline transect T-T' in Figure 4.4, the top pane shows a cartoon of the subglacial drainage of the overdeepening in plan view for each configuration. A) Represents the configuration at the end of each winter period. Drainage is distributed on both the adverse and normal slope but drainage is less well connected on the normal slope. On the adverse slope higher melt has been retained over winter and the system has remained at a higher pressure than on the normal slope. B) Represents the configuration at peak melt in all years of the study. The drainage system is distributed and pressurised evenly across both he normal and adverse slopes. C) The level of subglacial discharge has been sufficient to switch the drainage on the normal slope to a channelised configuration, but the supercooling on the adverse slope has been sufficient to maintain a distributed configuration. D) A sustained high level of subglacial discharge has been sufficient to induce a switch to channelised drainage on both the adverse and normal slopes of the overdeepening.

4.3.3 Comparison of the two case studies

The two case studies were conducted in series during the course of the research, largely for two specific and distinct reasons; to determine whether seasonal velocity patterns vary along glacier centre lines (case study 1), and to determine whether there is variation in seasonal velocity patterns between the adverse and normal slope of an overdeepening (case study 2). However, the case study locations were also selected to cover a variety of settings within Greenland (east and west coasts) and so some comparison of the findings of the two case studies is warranted.

Both case studies identified clear variation in seasonal velocity patterns along the centre lines of glaciers. As such, together they provide strong evidence that methodologies that implement analysis of ice velocity at a single point on a glacier (e.g. Moon et al., 2014; Vijay et al., 2019, 2021) cannot be assumed to be representative of seasonal ice velocity patterns elsewhere on the glacier. Both case studies also have a prominent riegel within 6-8 km of the calving front, and at both glaciers there are distinctly different seasonal velocity patterns up and downstream of the riegel. At both Upernavik Isstrøm II and Helheim seasonal speed up downstream of the riegel appears linked to seasonal retreat of the calving front indicating that in these zones proximal to the calving front, marine processes are the dominant control on seasonal ice velocity patterns (e.g. Moon type 1). In the areas upstream of the riegel, both glaciers show very limited correlation between seasonal retreat of the calving front and seasonal ice velocity patterns. In these zones further inland, seasonal velocity patterns appear to be more similar to those traditionally associated with land terminating glaciers or mountain glaciers, and are highly correlated with patterns in surface melt and runoff (e.g. Moon types 2 and 3). As such, both case studies indicate that riegels associated with prominent overdeepenings close to the margin of marine terminating outlet glaciers may isolate the influence of marine processes on ice dynamics to the region downglacier of the riegel.

Whilst the overarching patterns in seasonal ice velocity observed at both case study glaciers accord well with one another, there are noteworthy differences in the results. At Helheim, upglacier of the riegel peak velocity was observed in spring (in the period between surface melt onset and peak surface melt). Upglacier of the riegel at Upernavik Isstrøm II, peak

velocity was in the summer, coincident with peak melt. There are a range of potential explanations for this difference. The earlier peak velocity at Helheim is as would be observed for a Moon Type 3 seasonal velocity pattern. This could be interpreted to be representative of a more channelised subglacial hydrology within the overdeepening at Helheim than at Upernavik Isstrøm II (Moon et al., 2014). However, the velocity in summer and autumn does not drop below the initial winter baseline velocity (as would be expected for Type 3) so such interpretations should be considered with caution. An important consideration when making comparisons between the two case studies is the differing methodology applied in each. The winter, spring, summer and autumn periods for which average velocities were calculated for Helheim were based on break points in the seasonal melt graph (Figure 4.3a). The melt data used was mean annual Greenland surface melt, not melt specific to Helheim. As such, the precise timing and magnitude of melt may not have been fully representative of Helheim and this may have influenced the apparent observation of a spring velocity maximum. There is also variation in the context and setting of the overdeepenings studied in the two case studies. The complexity of both the glacier configuration and the subglacial topography is greater at Helheim than at Upernavik Isstrøm II. The overdeepening at Helheim is located at the confluence of two large tributaries with the main trunk of the glacier, and the riegel is oblique to the direction of ice flow. The setting at Upernavik Isstrøm II is much more straight forward with no confluence coincident with the overdeepening, ice flow parallel to the long axis of the overdeepening, and the riegel perpendicular to ice flow. As such, it is reasonable to expect that there may be a different range of confounding variables and process feedbacks operating in each of the case study systems.

Different ice velocity datasets were used in each of the case studies. In the time between conducting the research for case study 1 and case study 2 a much higher temporal resolution velocity dataset had become available. This facilitated detailed comparison between seasonal velocity patterns on the normal and adverse slopes of the overdeepening at Upernavik Isstrøm II, and it was from this analysis that the conceptual model in section 4.3.2.7 was developed. As such, it is not possible (based on the analysis conducted within this chapter) to test the extent to which the conceptual model applies to Helheim. Analysis of the wider applicability of the conceptual model at an ice sheet scale will be considered in

detail in Chapter 6.

4.4 Conclusions and implications of findings

It has been clearly demonstrated that seasonal velocity modes can vary along the centreline of glaciers. Processes dominant near the margin of marine terminating glaciers may be important, but not necessarily representative of the glacier as a whole. At Helheim glacier distinct seasonal velocity modes are identified up and downstream of the riegel, with Type 1 modes dominant downstream and Type 2 and 3 dominant upstream. This suggests an isolating effect from the marine influence on ice dynamics upstream of the riegel.

Findings of Chapter 2 show that overdeepenings are ubiquitous features in Greenlandic outlet glaciers. As such, many outlet glaciers will potentially have riegels isolating the ocean forced dynamic processes at the margin from the majority of the glacier located upstream of the riegel where subglacial hydrological processes driven by seasonal melt may be dominant. As a result, measurements and analysis conducted on limited point data at the margin (or even using flux gate type approaches at the margin) may not be representative of other parts of the glacier, and may not be a good approximation of the dominant processes controlling net ice flux and the sea level rise associated with this. There is currently significant uncertainty in our understanding of whether ice flux to the ocean from the GrIS (and the resulting sea level rise) is controlled by forces resisting flow at the margin (e.g. back pressure from ice shelfs, grounded ice, and lateral sheer stresses) and the impact these have on calving processes, or conversely, whether calving rates are actually responding to processes further inland which control ice velocities. To further understand the dynamics of glacial systems, and investigate the processes controlling ice dynamics, analysis exploiting a fuller range of the spatial resolution of velocity archives should be implemented than studies that have historically relied on single point measurements near glacier termini.

The patterns of seasonal ice velocity observed at Upernavik Isstrøm II demonstrate that in some years there is a different velocity response on the normal and adverse slopes of the overdeepening. In the highest melt year (2016) there is a late summer slowdown to below the initial spring velocity on the normal slope, but not on the adverse slope. In 2015 there is a late summer slowdown observed on both the normal and adverse slope, but this is more

pronounced on the normal slope. This is potentially due to shallower hydraulic gradient and supercooling processes suppressing channelised drainage developing on the adverse slope. A conceptual model (Figure 4.6) was proposed to explain the different subglacial hydrological configurations required in the overdeepening to explain the differing seasonal velocity patterns observed.

Chapter 5 Identification and classification of seasonal ice velocity typologies using machine learning.

5.1 Introduction

5.1.1 Aims and structure of this chapter

Chapter 4 demonstrated that at some individual Greenland outlet glaciers, seasonal velocity patterns vary at different locations along the central flowline. There was also evidence that in the case studies presented, bed topography may be modulating or controlling these patterns. Here, focus shifts back to the ice sheet scale to investigate how widespread the findings from the two case studies may be.

The purpose of this chapter is to begin to address RQ3 ***Are there any broad scale patterns that link seasonal velocity signature to bed topography or other GrIS-wide factors?*** The chapter will be relatively technical and methods focused. Specifically, it will achieve Objective A associated with RQ3. The first element of this objective is ***to develop an automated workflow for identifying distinct seasonal velocity variation typologies***. The second element of this objective is to ***classify velocity time series data points into these typologies at an ice sheet scale.*** A brief initial overview of the resulting dataset will be presented within the chapter, but the primary result of this chapter is the development of the method to automatically classify seasonal velocity typologies. The detailed spatial and temporal analysis of the dataset, and investigation of potential process relationships, will form the final results chapter (Chapter 6) that follows.

5.1.2 Background

This chapter builds directly on Chapter 4 and develops a methodology to enable the implementation of the recommendations made in that chapter. Chapter 4 establishes that, to fully understand the behaviour of glacier dynamics and patterns and potential drivers, there is a need to analyse velocity at multiple locations for each glacier, rather than simply a single point near the calving front. Doing so will enable the identification and analysis of the full range of seasonal velocity typologies, allowing us to start to build a more comprehensive understanding of the processes that drive seasonal velocity typology. For understanding to be representative of the ice sheet as a whole, the analysis needs to be at a commensurate

scale, requiring coverage of hundreds of glaciers. These ambitious aims are not without technical difficulty. Very large velocity datasets have been openly available for over 10 years (Nagler et al., 2015; Rosenau et al., 2015; Joughin et al., 2018) but relatively little research has made full use of these, no doubt in part due to the technical challenges posed. This chapter will present the development of an automated method of classifying seasonal velocity typology, leveraging a machine learning approach which enables the inclusion of hundreds of thousands of data points in the analysis, rather than hundreds of data points used historically in manual methods.

There is a reasonable body of literature investigating seasonal glacier velocity variations, both in ice sheet (Voss et al.; Joughin, Howat, et al., 2008; Howat et al., 2010; Hoffman et al., 2011; Moon et al., 2015; Kehrl et al., 2017) and mountain glacier (Iken and Bindschadler, 1986; Hooke et al., 1989; Mair et al., 2002; Vincent and Moreau, 2016; Sanders et al., 2018) contexts. However, it is only due to recent advances in large velocity datasets derived from satellite imagery (as well as the computational ability to analyse these large datasets), that has enabled the study of large numbers of glaciers. The vast majority of studies only consider a small number (e.g. 1-10) of glaciers (e.g. Rathmann et al., 2017; Davison et al., 2020; Sakakibara and Sugiyama, 2020). Often when studies do include a larger number of glaciers, they simplify analysis either by considering limited data spatially (e.g. single points near the margin (Moon et al., 2014; Vijay et al., 2019, 2021; Williams, Gourmelen, Nienow, et al., 2021), or temporally (e.g. aggregating velocity into simply summer and winter (Armstrong et al., 2017)). As such, the full potential of the velocity archives available to science has yet to be fully realised, these datasets having been utilised by very few studies.

Much of the previous work involving some consideration of seasonal velocity variation has been conducted in quite broad terms. The primary focus has often been limited to coarse investigation of apparent correlations between velocities and terminus positions, with consideration of the role of the bed topography largely limited to scenarios of retreat down an adverse bedslope, and the impact this may have on ice stability (Nick et al., 2009; Carr et al., 2015; Åkesson et al., 2018; Lemos et al., 2018). Analysis is often constrained to a relatively limited number of positions along the glacier centreline, and data is often presented (and analysed) using absolute velocity measurements (Joughin et al., 2018). As velocity generally decreases with distance from the terminus of tidewater glaciers, the use

of absolute velocity values has the result of diminishing the appearance of any seasonal patterns in ice speedup or slowdown at points along the glacier length (e.g. see Figure 5.1).

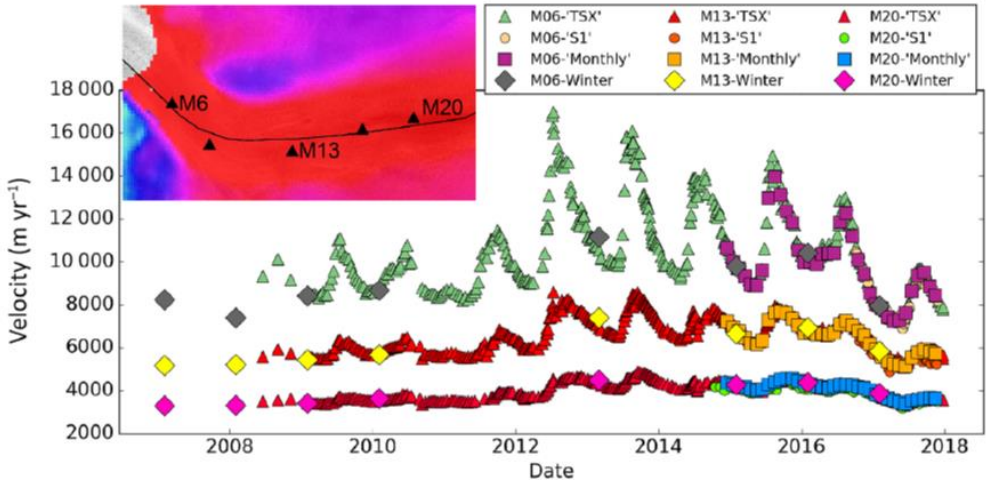

Figure 5.1 An example of seasonal velocity analysis conducted on Jakobshavn Isbræ using absolute velocity data. Note the apparent effect this has of making the relative speedup and slowdown less obvious at locations further from the terminus where ice velocity is lower (Joughin et al., 2018).

There has been relatively little research conducted using velocity data for relatively large numbers of Greenland glaciers (n < 40) that has focused on variations in seasonal ice dynamics, in particular the identification of common typologies of seasonal ice dynamics and the investigation of its possible controls. The four existing studies that have conducted this kind of work are discussed in detail in section 2.3.3.2 (Moon et al., 2014; Vijay et al., 2019; Solgaard et al., 2022), but key benefits and limitations of each study will be discussed briefly below in the context of the aims of this chapter.

Both Moon et al. (2014) and Vijay et al. (2019) focused on individual glaciers but only by analysing velocity at a single point near the terminus for each glacier. The number of glaciers covered (approximately 50) was much greater than in previous studies, but by no means offering complete coverage of the GrIS. Solgaard et al. (2022) used much more detailed spatial data which extend inland beyond the margin, but individual typologies of seasonal velocity variation were not linked back to specific glaciers and as such could only make very general comment on process relationships which may be driving typology type. In terms of the analytical approach taken, both Moon et al. (2014) and Vijay et al. (2019) relied on manual visual interpretation of each individual seasonal velocity variation graph to assign

to typology classes which severely limited the amount of data that could be processed.

Vijay et al. (2021) progressed the study of seasonal velocity typologies by implementing a semi-automated method for classifying typology for the first time. The classification was performed by adopting a statistical approach, selecting exemplar glaciers for each typology and then measuring the cumulative residuals of each individual glacier's seasonal velocity response graph to the exemplars and classifying them if they are within a prescribed residual limit. The study only classifies glaciers as Type 2 or Type 3. Type 1 is excluded from the study, the reasons for this are not made completely clear. The semi-automated approach did allow the inclusion of a much larger number of glaciers (221) than in previous studies, and gave a complete coverage around the margin of the ice sheet for the first time (Figure 2.22). Solgaard et al. (2022) used a machine learning based K means clustering approach to automate classification which allowed much more data to be processed. However, this approach was limited to generating only four clusters in the K means analysis (identifying only Type 2 and Type 3 seasonal velocity typologies) for reasons that are not fully justified. The paper makes clear that there is potential value in having a greater number of clusters (and recommends this as an area for future work) to draw more nuance out of the data; this is one of the key aims of this chapter. It is possible that iterative examination of their data was challenging due to the very large number of points considered as a result of the extensive spatial coverage and very high temporal resolution of the velocity data.

In this chapter a methodological approach is designed which attempts to create a hybrid of the two approaches discussed above, benefiting from the pros, whilst mitigating some of the limitations. Data analysed and classified into distinct seasonal velocity typologies will be linked back to individual glaciers (to allow consideration of potential process relationships using data already gathered for those glaciers (e.g. Chapter 3)). However, a K means machine learning approach will be implemented to automate classification of typologies allowing hundreds of thousands of points to be classified giving a comprehensive coverage of the GrIS which is not limited to areas close to the margin. Lower temporal resolution velocity data will be used which will facilitate the possibility of deriving larger numbers of clusters to generate more nuanced seasonal velocity typologies.

5.2 Methods

5.2.1 Velocity data coverage and temporal resolution

The velocity data used for the analyses presented in this chapter is from the MEaSUREs Greenland Quarterly Ice Sheet Velocity Mosaics dataset (Joughin, 2018a, Joughin et al., 2010, 2018). The spatial resolution of the velocity data (200 m) facilitates detailed spatial coverage of Greenland and inclusion of the largest possible number of areas of overdeepening mapped in Chapter 3. The MEaSUREs dataset is also robust and does not have too many gaps, whilst the temporal resolution (three months) is sufficient for analysis of seasonal ice dynamics. Higher temporal resolution velocity datasets are available, providing velocity averages for monthly (Joughin et al., 2010, 2018) and even down to near weekly averages (Rosenau et al., 2015; Vijay et al., 2021), which offer potential to analyse process on very short (e.g. diurnal melt-driven) timescales (Iken and Bindschadler, 1986 ; Nienow et al., 2005; Shepherd et al., 2009). However, the increased temporal resolution means these datasets have more gaps. When conducting analysis at an individual glacier scale this is not necessarily a significant issue as there is the potential to select the case study glacier based on data quality and coverage, or to manually manipulate and aggregate individual time slices of data to maintain data coverage. However, when attempting to conduct automated analysis at the whole ice sheet scale, this type of ad hoc data wrangling becomes unmanageable. Further, the computationally demanding machine learning methods implemented in this chapter make analyses of such temporally detailed datasets for large areas of Greenland impractical. Finally, the existence of important behaviours could be masked where datasets are too detailed in time as a result of data errors or statistical changes that are not significant in terms of ice flux and sea level. Nonetheless, such detailed analyses at individual glaciers (e.g. Chapter 4) could be instructive of potential drivers, and these issues will be revisited in the Discussion (Chapter 7).

5.2.2 Data processing workflow

Data on seasonal velocity typology was generated for both central flowlines and overdeepenings for separate but related purposes. As such, the output of the analysis is two separate datasets, the central flowline dataset and the overdeepening dataset. A graphic illustration of the processing workflow for deriving these datasets can be seen in Figure A.1

(Appendix A). The analysis of seasonal velocity typology for mapped overdeepenings is of value as it can be related back to the morphometric parameters defined for each individual overdeepening in Chapter 3. This allows analysis of the impact that overdeepenings may have on seasonal velocity typology, especially in relation to adverse slope gradient and supercooling threshold. Analysis is extended to the longer, overall central flowlines (extending far beyond overdeepenings) in order to consider more comprehensively the spatial patterns in seasonal velocity typology across the GrIS, and explore the process that are not specific to overdeepenings that may be controlling seasonal typologies.

For each dataset, there is a set of points of interest. The term 'points of interest' is used to define the individual point locations within each dataset that velocity data were extracted and joined to, and which seasonal velocity typology was classified for. Each point of interest has a discrete seasonal velocity typology classification for each of the four years in the study period for which there are data that passes the quality assurance checks (details below). For central flowlines, the points of interest are points spaced at 500 m intervals along the central flowlines (as generated and used in Chapter 3 (see section 3.2.1.2, Figure 3.13). For overdeepenings, the points of interest are points at 150 m intervals along the true thalweg of the overdeepening as generated and used in Chapter 3 (see section 3.2.2.1). Overdeepenings used were the subset of 621 overdeepenings mapped that met the quality control criteria (referred to as the metric dataset). For overdeepenings, the points along the true thalweg of each overdeepening were then aggregated to mean values of velocity (individual means for spring, summer, autumn and winter) for points on normal slopes and adverse slopes within the overdeepening. It is these seasonal velocity graphs (seasonal means for adverse slope and seasonal means for normal slope) that were classified using the K means analysis (details below). As such, in the overdeepening seasonal velocity typology dataset there are a maximum of two seasonal velocity typologies classified for each year of the study period (for adverse and normal slopes).

Quality assurance for the velocity data involved removal of any velocities where the published error was greater than 20% of the stated velocity. This was conducted at the first stage in the data processing; points in the dataset were only included for a year where spring, summer, autumn, and winter velocity values were all available and within the prescribed error range for that year. This is the same approach taken by Solgaard et al.

(2022). As such, there was some variation in the number of points / overdeepenings considered for each year depending on the variations in data accuracy between years, and some points / overdeepenings are included in the datasets for some years but not others.

Average yearly spring, summer, autumn and winter velocity data that meets the quality threshold (directly from the MEaSUREs velocity data) is extracted to points of interest for 2016, 2017, 2018, and 2019. Once quarterly velocity values have been added for each point in each year, they are then normalised by dividing each velocity value by the maximum velocity value in that year at that point. This gives each velocity a value between 0 and 1. This is the approach taken by Solgaard et al. (2022). Data for each year starts from spring to avoid inheritance of background over-winter velocity from the preceding year impacting on the typology of the year in question. The study years are 2016, 2017, 2018, and 2019. These years are selected as this is the earliest date the archive goes back to and contains two relatively high melt years (2016 and 2019) and two relatively low melt years (2017 and 2018). Further details specific to the melt regime in each year are given in Chapter 6 (section 6.2.4).

5.2.3 K means cluster analysis

K means cluster analysis was conducted feeding in data for all points for all years in each set (e.g. overdeepening dataset points is one set, central flowline dataset points is the other, with two separate K means cluster analyses conducted). The Scikit SKlearn Python library was used to conduct the K means cluster analysis. The "greedy K means ++" algorithm was implemented. This optimises the randomisation of the initial cluster centre starting points using the approach developed by Arthur and Vassilvitskii (2007) before then running the Lloyd algorithm (Lloyd, 1982). The "n_init" parameter was set to 10 to run the algorithm 10 times each with different centroid seeds with the output with lowest inertia selected for final use. The conceptual basis upon which a K means algorithm works is illustrated in Figure 5.2.

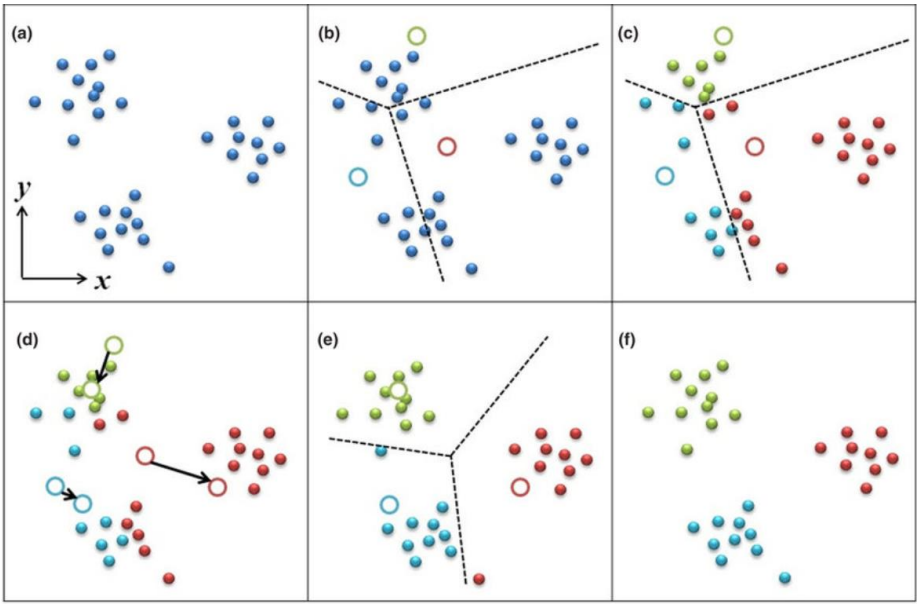

Figure 5.2 An illustration of the conceptual basis K Means clustering algorithm for one iteration of the algorithm. A) The initial data points in 2D Euclidean space. B) Generation of three pseudo random initial cluster centres (hollow coloured points). C) Each data point allocated to the closest cluster based on distance to centre points (solid coloured points). D) Cluster centre points recalculated as mean coordinates of all points now allocated to the cluster. E) Points reallocated to nearest cluster based on new cluster centre location following d. F) the allocation of points to clusters after one iteration of the algorithm. The algorithm will continue to run until a specified maximum number of iterations has been completed, or a percentage change threshold is reached following an iteration. Adapted from Chen and Lai (2018).

The K means clustering analysis was run independently for the central flowline and overdeepening velocity datasets. In both cases, all data points for all years were included in the same K means analysis; for example, if an overdeepening (or central flowline point) had complete velocity data for all four of the study years, the four years of velocity data would

be fed to the algorithm as four separate data points. An alternative approach would be to run a cluster analysis for each of the four years in the datasets independently. The latter approach was tested, but rejected as it was deemed less robust, especially for the overdeepening dataset which contains a more limited number of data points. In particular, when individual K means analysis were run for each year, some seasonal velocity topologies were omitted for some years where there were fewer examples of that typology (e.g. in insufficient number to generate a distinct cluster representing that typology in the analysis). In such instances, data points which truly represent the missing typology in a given year were allocated to a cluster representing a different typology (by the algorithm, in error). Aggregating all years of data to run a single K means cluster analysis for each of the two datasets maximised the chances of individual data points having their seasonal velocity typology correctly classified and ensured that the output data were fairly comparable across years.

5.2.4 Optimising the number of clusters

The key factor in producing an effective classification using K Means clustering algorithms is determining the most appropriate number of clusters to use (Sinaga and Yang, 2020). Too few clusters will over aggregate the data resulting in higher residual errors and risk genuine patterns or processes being occluded by the merging of multiple genuine end members into hybrid classes (Sinaga and Yang, 2020). In some cases this may involve the merging of a less dominant end member into a more dominant end member, effectively diluting the signal of the dominant end member slightly and removing the non-dominant end member from the classification outputs (Figure 5.3b). In other cases the merging of two equally dominant end members may be forced resulting in the dilution of the signal of both classes (Figure 5.3a). In contrast, specifying too many clusters will result in multiple classes representing single end members. This is not a problem in and of itself and is an valid approach often taken to optimise unsupervised clustering outputs (Alvarez et al., 2003), but does require manual post processing to identify clusters that are similar (and therefore potentially representing the same end member), and amalgamate them. This takes time and effort and risks inducing error. On balance, the risks of over-aggregation due to too few clusters being specified are more problematic (due them being fundamental and unfixable) than the extra processing

required to amalgamate clusters that may be required if too many clusters are specified. As such, it is logical to err on the side of more clusters than less if in any doubt. The limitations of specifying too few clusters is highlighted by Solgaard et al. (2022) in their study and one of their recommendations for further study is exploring the possibility offered by running a greater numbers of clusters.

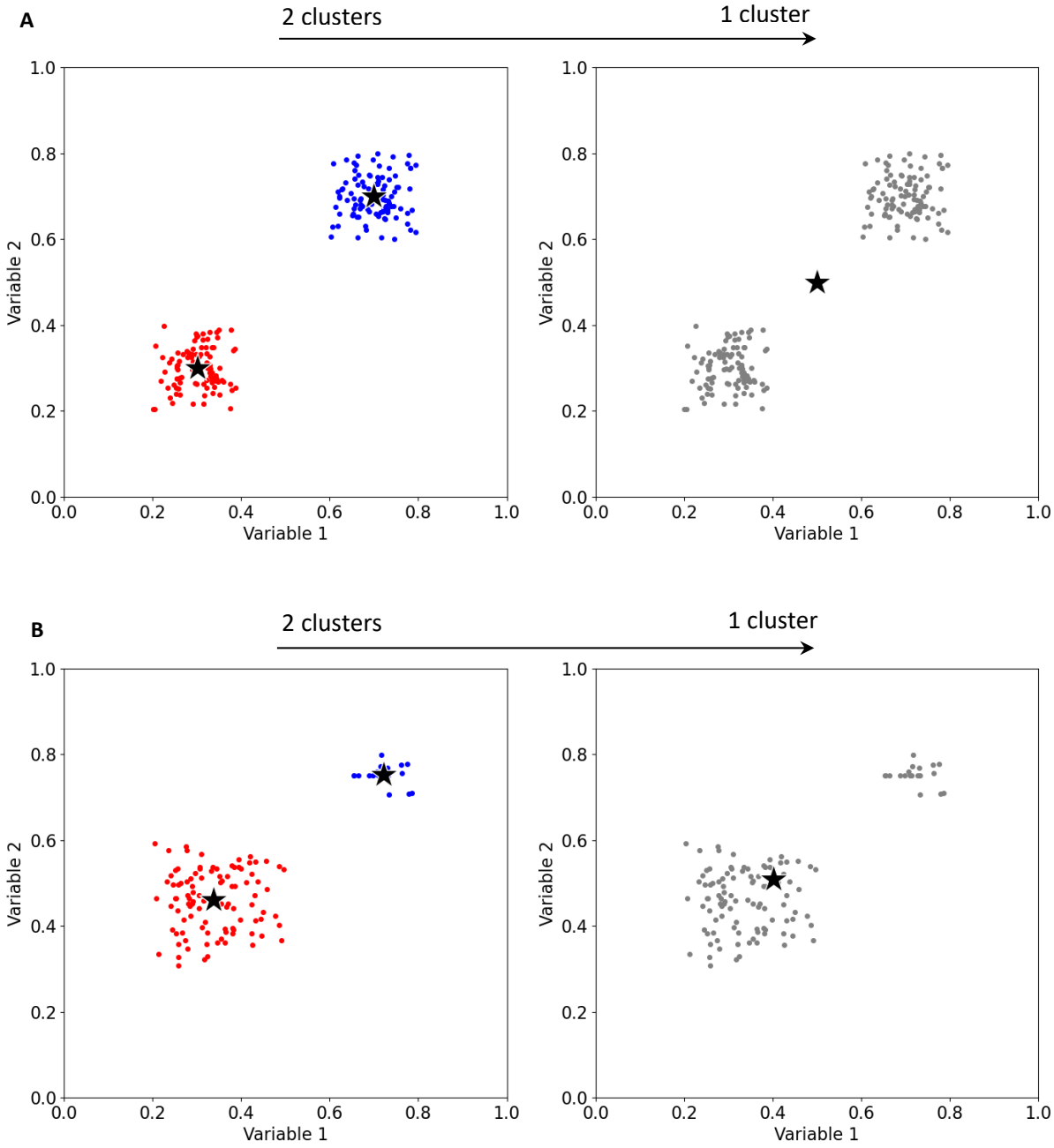

Figure 5.3 Cartoon showing possible effects of over-agglomerating data by running too few clusters in a K Means analysis. The left hand panes represent a situation where the number of clusters allows for two classes in the subset of data visualised on the figure, the right hand panes represent a situation where all data visualised is aggregated into a single cluster. Red and blue points show individual data points when the data is in two classes, grey points show the same individual data points when the Black stars show the class mean centre points. The data visualised is in arbitrary 2D vector space and is purely illustrative. A) Merging two equally prominent end members resulting in a class mean centre point not

truly representative of either discrete end member. B) Merging a small but discrete end member into a more dominant end member class. In this case the smaller end member is no longer represented in the classification output.

The classic approach adopted in machine learning for the identification of an appropriate number of clusters is the analysis of elbow plots of the sum of squared errors (SSE) (Makwana et al., 2013; Umargono et al., 2020). Elbow plots were generated for both the central flowline and overdeepening datasets (Figure 5.4). An indicator for the optimal number of clusters for a dataset is marked at the point where the decrease in error with addition of further clusters becomes linear e.g. the 'elbow' of the plot (Sammouda et al., 2021; Solgaard et al., 2022). However, in some cases there is no clear breakpoint which can be unambiguously identified, rather, a gradual decrease in the gradient, or even multiple elbows. As can be seen from Figure 5.4b, there is a dramatic decrease in gradient between two clusters and four clusters, but the gradient of the line continues to decrease until somewhere between 10 and 13 clusters. The pattern is similar for the elbow plot of the central flowline dataset, but with a slightly less pronounced initial drop in SSE as the number of clusters increases. The trend becomes linear at a point somewhere between 12 and 14 clusters (Figure 5.4a).

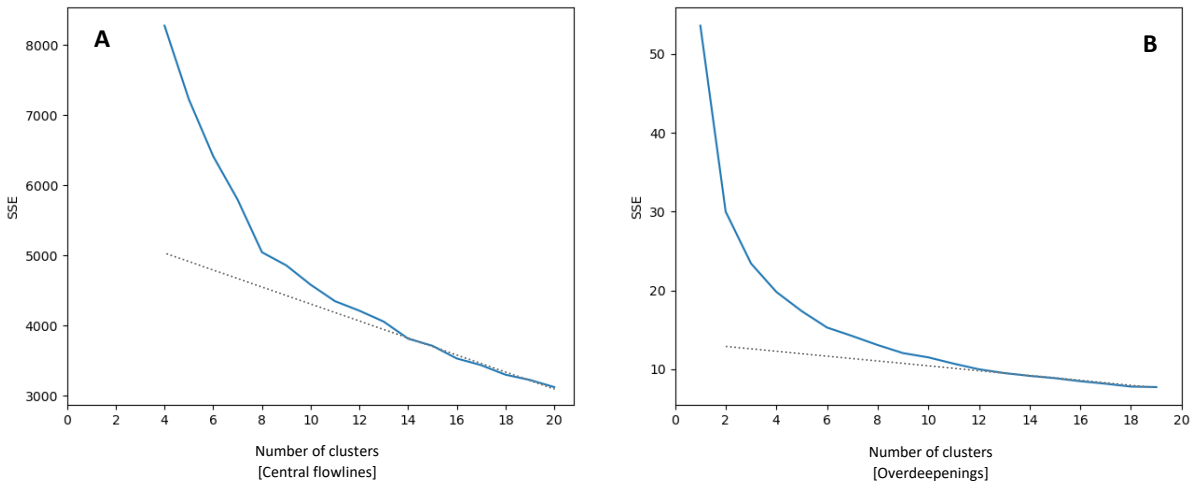

Figure 5.4 Elbow plots showing rate of reduction of Sum of Squared Errors (SSE) with increasing cluster numbers for the K Means analysis. Straight dashed lines are included for visual reference as to where the trend becomes linear. A) Data for the central flowline dataset. Note – SSE values for 1-3 clusters are omitted as the SSE was so high their inclusion would skew the scaling of the Y axis such that the true elbow is very difficult to discern. B) Data for the overdeepening dataset.

5.2.4.1 The impact of different numbers of clusters

Figure 5.5 and Figure 5.6 show the impact on the outputs of running the K means cluster analysis with lower and higher numbers of clusters respectively. Table 5.1 gives the groupings of the clusters, indicated by the colours on Figure 5.5 and Figure 5.6. With a lower number of clusters (8 in Figure 5.5), some of the typologies identified when using 12 clusters are not represented. In the example given, typologies T1 (representative of one of the original Moon typologies) and T23 are not represented. The number of objects in the 'other' cluster (where no pattern is obvious) also increases by over 50%. With a higher number of clusters (16 in Figure 5.6) there are more duplicate clusters for individual typologies in the output; four individual clusters are T3, three clusters are T2. The number of objects in the 'other' cluster (where no pattern is obvious) decrease by just over 10%, but this results in some of the clusters representing quite flat lines where there is relatively little seasonal velocity variation apparent (e.g. cluster 0 and cluster 10, Figure 5.6). As such, some of the lines that are in typology clusters in the 16 cluster analysis may have been more accurately classified in the 'other' cluster, as they were in the 12 cluster analysis. Based on the analysis of the elbow plots (Figure 5.4) and experimenting with different numbers of clusters in the K means analysis, 12 clusters were used in the final analysis.

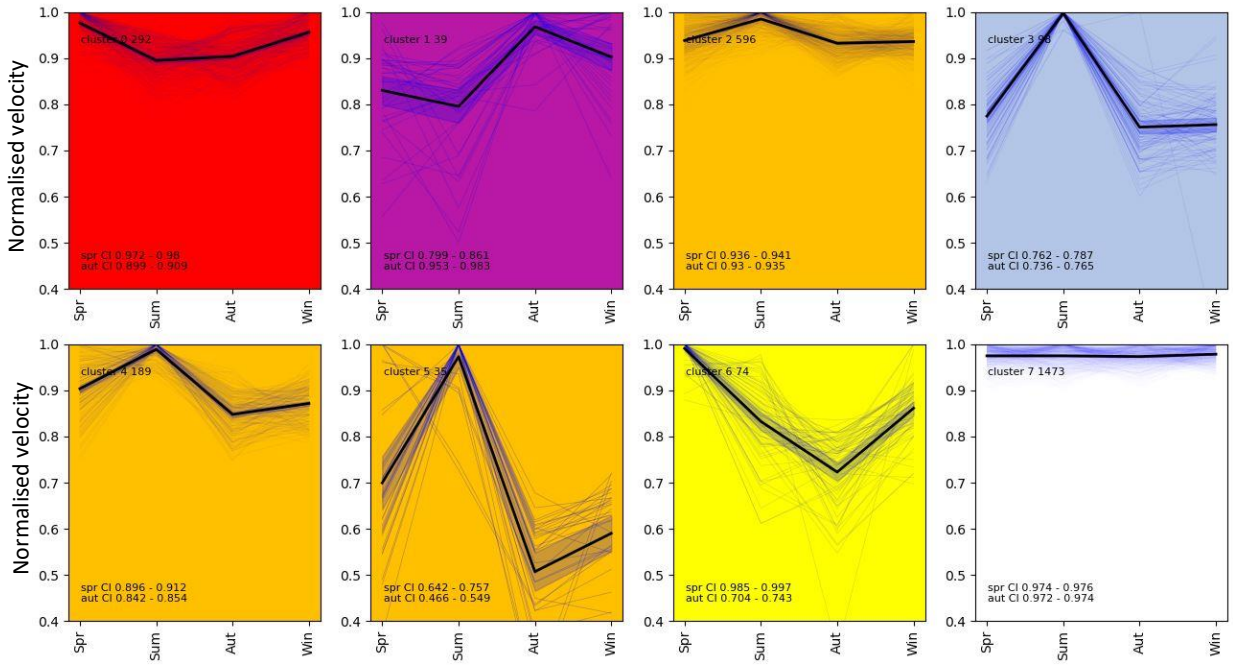

Figure 5.5 Comparison of K means cluster outputs for the overdeepening dataset for different numbers of clusters, here the number of clusters specified is 8. With the lower numbers of cluster, typologies T1 and T23 are not represented.

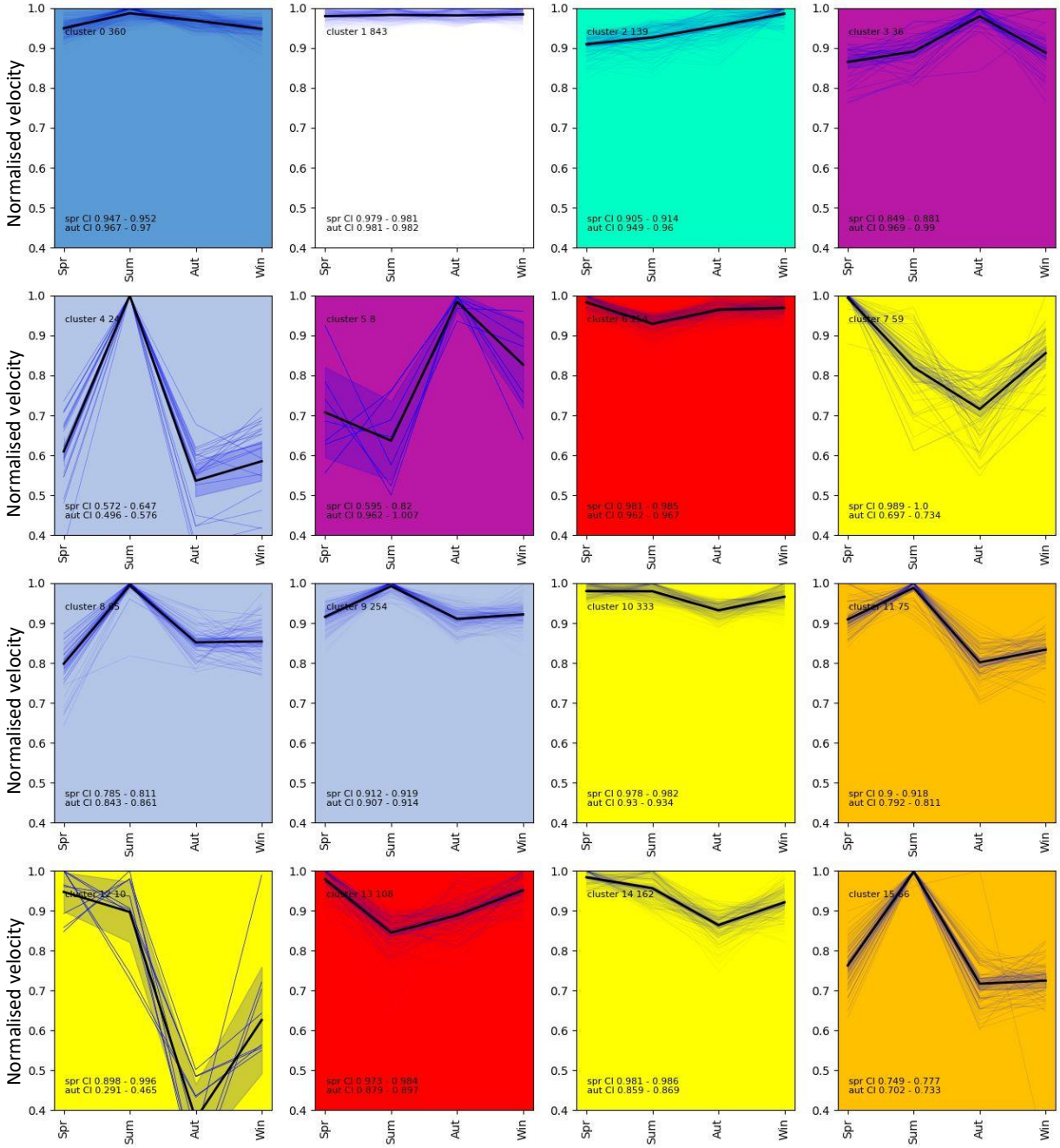

Figure 5.6 Comparison of K means cluster outputs for the overdeepening dataset for different numbers of clusters, here the number of clusters specified is 16. With the higher number of clusters there are large numbers of duplicate clusters representing the same typology.

5.2.4.2 Rationale for 12 clusters

For both the overdeepening and the central flowline datasets there are multiple clusters that have been merged into single seasonal velocity typologies. Taking the overdeepening dataset as an example (Figure 5.7), there was one cluster representative of T1 (cluster 7),

five clusters representative of T2 (clusters 2, 6, 8, 10 and 11), and three representative of T3 (clusters 0, 1, and 4). The fact that there are large numbers of clusters apparently representing the same seasonal velocity typology may at first appear to indicate that too many clusters have been parameterised within the K means model, but there are two important reasons why this is not the case.

Firstly, some of the clusters representing the same typology have the same shape, but with differing magnitudes of velocity variation. For example, Clusters 0, 1, and 4 all have the same shape (maximum velocity in spring, continued deceleration through summer and autumn reaching minimum velocity in autumn, with an acceleration into winter reaching a velocity approximately equal to spring), but with markedly different rates of slowdown and speedup (Figure 5.7). The slowdown is most pronounced in cluster 1 where the summer minimum is approximately 70% of the spring maximum. For cluster 0 the summer velocity drops to approximately 85%, and for cluster 4 it only drops to approximately 92% of the spring velocity (Figure 5.7). Simply removing two clusters when parameterising the K means analysis would not necessarily result in the objects from these three clusters being agglomerated into one singular replacement cluster. Some objects may be reclassified (in error) into classes where objects have more similar *magnitudes* of variation (but with different shape), rather than into classes where objects have the same *shape* of variation, but at a different magnitude. For the purposes of this chapter the shape of the seasonal variation is more important than the magnitude and so it is vital to maximise chances of correctly classifying on this basis.

Secondly, whilst running a higher number of clusters may risk generating unwanted duplicate clusters, it also allows the possibility of identifying nuanced subtypes of flow typologies. Within the five clusters broadly representative of a speedup in summer followed by a slowdown in autumn (clusters 2, 6, 8, 10 and 11), it is possible to identify individual subtypes (Figure 5.7). Cluster 8 has a peak velocity in summer which then slows to a velocity very similar to spring in autumn and winter, this is termed T2. Clusters 2, 6, and 10 all demonstrate a maximum velocity in summer which then slows down to a velocity in autumn which is lower than the initial spring velocity. This typology is termed T21. To avoid any subjectivity in determining whether autumn velocity was lower than spring velocity, clusters were allocated to T21 when the lower bounds of the 95% confidence interval for the spring

average was above the upper bounds of the 95% confidence interval for the autumn average. Spring and autumn confidence intervals for each cluster are shown on Figure 5.7 and Figure 5.8 both graphically on the graphs, and as annotations stating the values.

5.3 Results

Analysis of elbow plots (as per Figure 5.4, section 5.2.4) indicated 12 clusters were appropriate. The resulting clusters for the overdeepenings and the central flowline nodes can be seen in Figure 5.7 and Figure 5.8 respectively.

5.3.1 Allocating clusters to seasonal velocity typologies

Clusters were identified as representing distinct seasonal velocity typologies primarily by visual assessment of the shapes of the mean velocity lines in the output figures (Figure 5.7, Figure 5.8). This is the approach taken by Solgaard et al. (2022). Clusters are generated by the K means algorithm independent of any a priori ideas of what seasonal velocity response may look like, they are simply representing a semi-consistent typology of ice velocity behaviour exhibited by a sufficient number of data points to generate a distinct cluster. The visual interpretation of the output clusters then involves identifying any which are indicative of established seasonal velocity typologies represented in the literature, and identifying and acknowledging any typologies which do not conform to previous studies.

Table 5.1 outlines the individual typologies and gives a descriptor of each typology. The shape of the graphs are quite distinct and in general the individual seasonal typologies were obvious. For both the overdeepening and central flowline datasets all three of the typologies identified by Moon et al. (2014) were identifiable in the cluster outputs and these are highlighted in Table 5.1.

Table 5.1 Seasonal velocity typologies identified from the K means cluster analysis. Typologies relate to both the overdeepening dataset (Figure 5.7) and the central flowline dataset (Figure 5.8).

0	'Other' class [e.g. very little seasonal variation]
1	Gradual continual rise from spring through winter [Moon Type 1]
2	Rise in summer matching falling back to spring level in autumn [Moon Type 2]
21	Rise in summer but falling back in autumn to level below spring starting point.
23	Rise in summer but maintained into autumn giving less pronounced slowdown with flatter peak.
3	Spring peak with substantial slowdown through to autumn [Moon Type 3]
4	Decreasing velocity from spring with a low in summer which then rises through autumn and winter.
5	Pronounced peak in autumn.

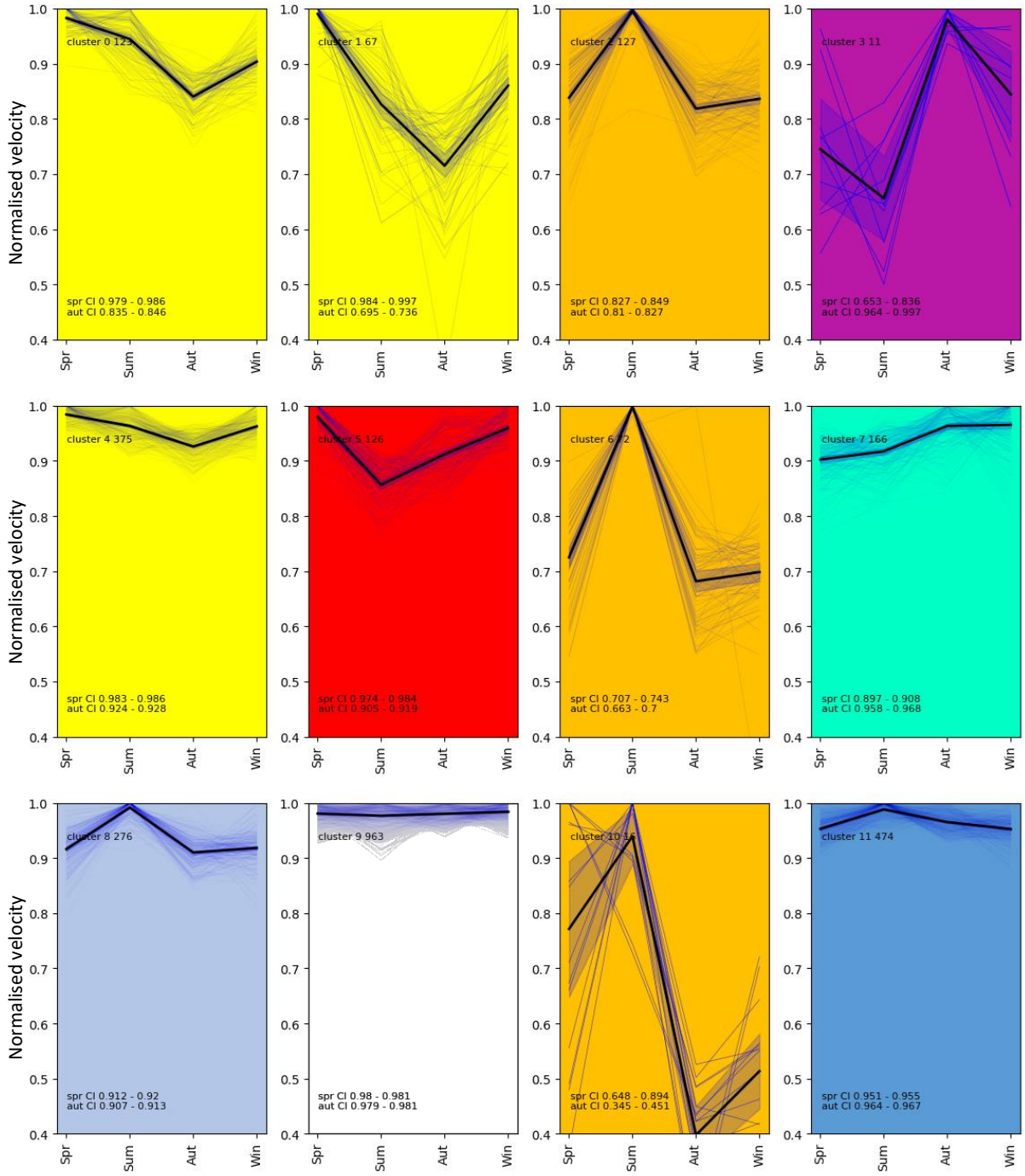

Figure 5.7 Seasonal velocity typologies clusters for the overdeepening dataset. Colours show the classification of typology as presented in Table 5.1. Fine lines show the individual time series data points allocated to each cluster. The thicker black line on each plots shows the mean of the individual time series for the cluster, blue shading around the mean is the 95% confidence interval.

For the overdeepening dataset (Figure 5.7) there was one cluster representative of T1 (cluster 7), five clusters representative of T2 (clusters 2, 6, 8, 10 and 11), three representative of T3 (clusters 0, 1, and 4), one representative of T4 (cluster 5) and one

representative of T5 (cluster 3).

In addition to the Moon typologies (and sub-typologies), two new typologies are identified by the cluster analysis. T4 is representative of velocity slowing from spring to a minimum in summer, with velocity then gradually rising through autumn back to a winter velocity near the spring starting velocity. T5 is representative of a pronounced peak autumn velocity.

The break down of the number of clusters representing each typology for the central flowline dataset is very similar to the overdeepening dataset. T21 and T3 have three clusters each (of varying magnitudes of seasonal response, as per the overdeepening dataset). T2 has one cluster (as in the overdeepening dataset), but T23 is not represented. It is worthy of note that for the central flowline dataset the T2 cluster has a much less distinct autumn slowdown and is approximately half way between the T2 and T23 clusters from the overdeepening dataset. The T2 and T23 typologies are the most similar within the overall typology schema and will therefore be the most difficult for the K means analysis to differentiate and separate. Due to their similarity, it is also the two clusters where errors of commission and omission between the clusters is of least concern in terms of the impact it will have on the resulting analysis conducted using the classification output. T4 has two cluster for the central flowline dataset (compared to one in the overdeepening dataset) representing more and less pronounced variations of the typology. T5 has one cluster, as in the overdeepening dataset. T0, T1 and T5 all have one cluster, as in the overdeepening dataset.

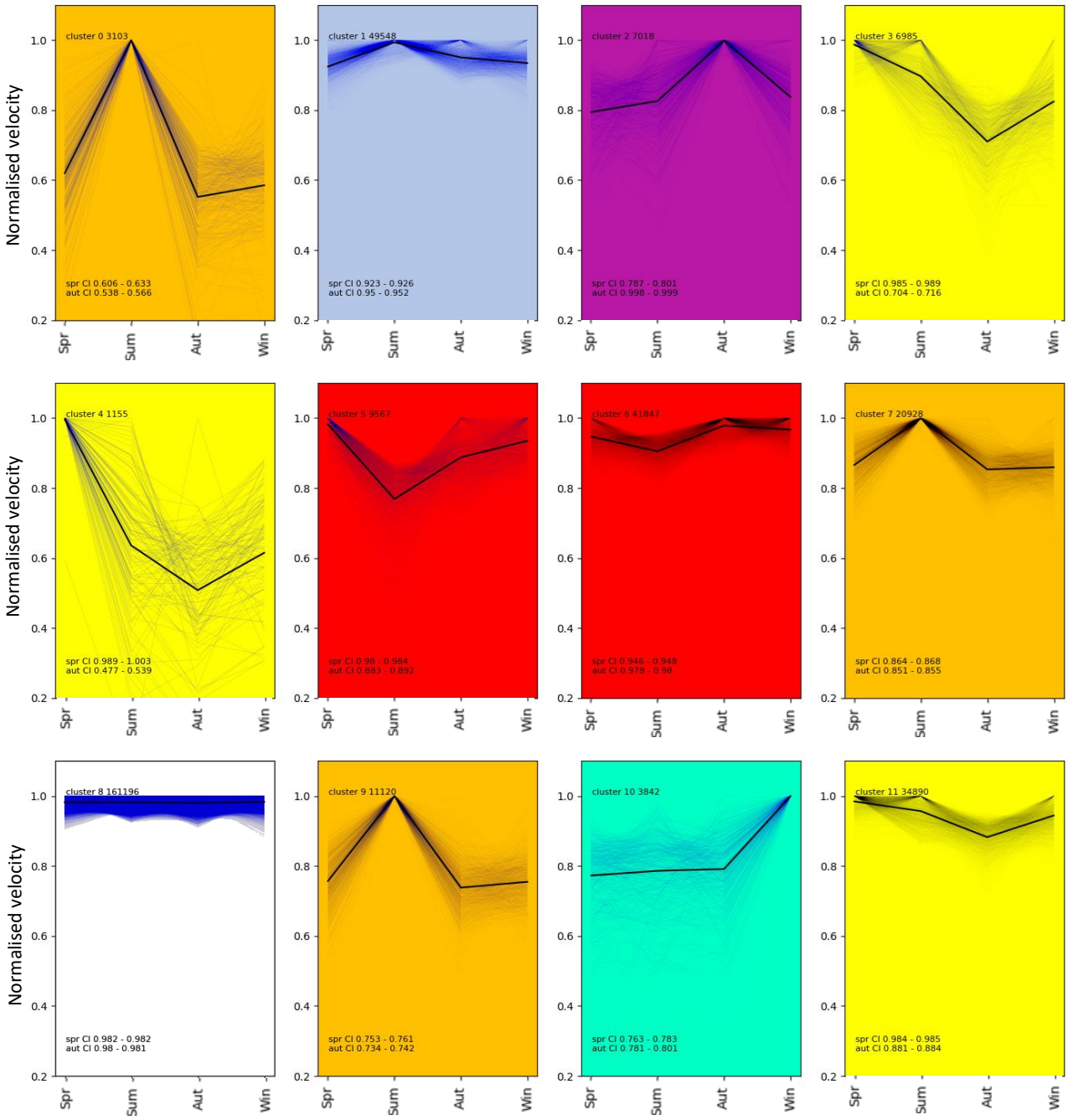

Figure 5.8 Seasonal velocity typologies clusters for the central flowline dataset. Colours show the classification of typology as presented in Table 5.1. Fine lines show the individual time series data points allocated to each cluster. The thicker black line on each plots shows the mean of the individual time series for the cluster, blue shading around the mean is the 95% confidence interval.

5.4 Discussion

5.4.1 Seasonal velocity typology prevalence

As was set out in the introduction, this chapter is primarily focused on the development of the automated classification method and the identification of discrete seasonal velocity

typologies using this method. As such, the discussion will be similarly focused on the nature of the individual typologies, and specifically, possible process drivers for them. A full spatial and temporal analysis of the prevalence and distribution of the seasonal velocity typologies will be given in Chapter 6. A brief overarching breakdown of seasonal velocity typology is given here which will facilitate a comparison with the findings of other studies in section 5.4.4.

Figure 5.9 shows a summary of the relative prevalence of each seasonal velocity typology for the overdeepening and the central flowline datasets. There are some interesting differences between the composition of typologies for the central flowline dataset (which is more representative of the ice sheet as a whole) and the overdeepening dataset (which is representative of a much more limited and specific subset of the ice sheet). The central flowline dataset has a slightly smaller (22.6% vs 30.8%) proportion of T3 typology than the overdeepening dataset, but a slightly higher proportion of T21 (18.5% vs 11.7%). The sum proportion of T3 and T21 typologies (the two typologies characterised by autumn velocity minima) is therefore very similar between the two datasets (41.1% and 42.5%). The overdeepening dataset has a much greater proportion of T1 than the central flowline dataset (9.1% vs 2.0%). The central flowlines dataset has a far greater proportion of T4 than the overdeepening dataset (27.1% vs 6.9%). T2 is more prevalent in the central flowlines dataset (26.1% vs 15.1%). However, as discussed above, the T2 and T23 typologies are the most similar in shape, and when the two typologies are combined the overdeepening dataset actually has a greater prevalence of this type of seasonal velocity variation (40.9% vs 26.1%).

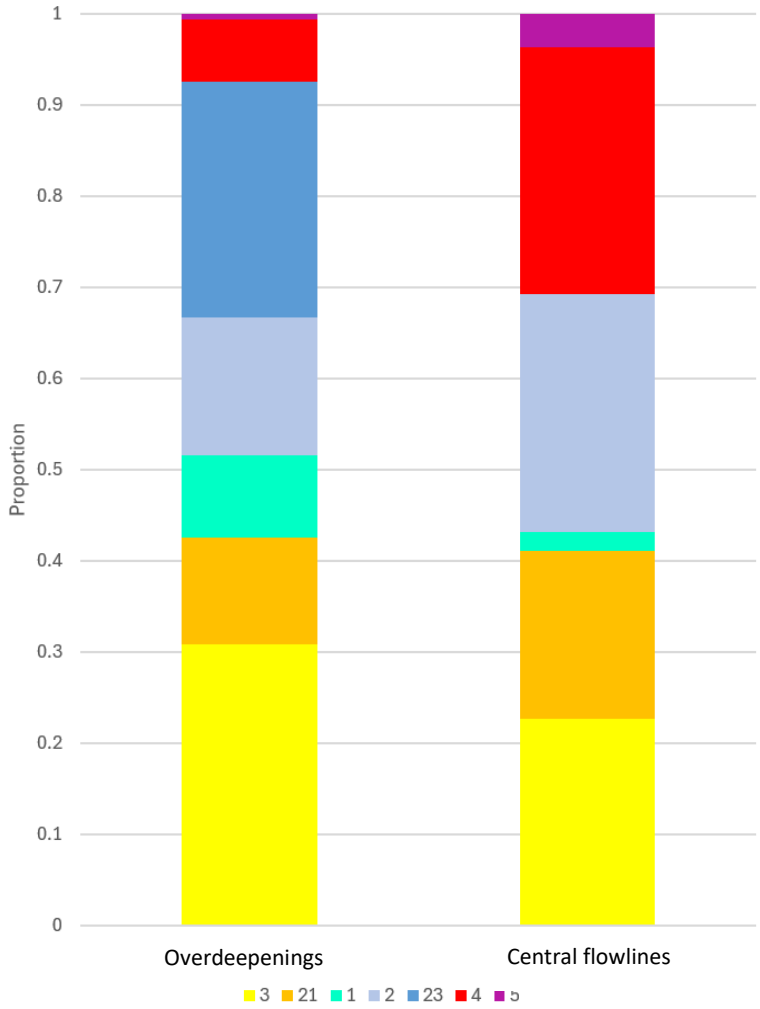

Figure 5.9 Proportion of overdeepening and central flowline data points classified as each seasonal velocity typology

5.4.2 Process significance of typologies

The two key sets of processes which may influence the seasonal velocity typology of a glacier are changes in the resistive stress a glacier experiences due to contact with fjord walls and the bed as a result of marine driven advance and retreat of the terminus (see section 2.3.2), and increase and decrease of basal water pressure due to seasonal melt and the control this exerts on the configuration of subglacial hydrological drainage regime (e.g. distributed or channelised) (see sections 2.3.1 and 2.3.3). In this section, each of the seven distinct seasonal velocity typologies identified in section 5.3.1 (Table 5.1) will be discussed in turn with interpretation of the likely process drivers for each typology hypothesised. Three of the typologies generated from the K means clustering analysis are interpreted to be representative of the three seasonal velocity typologies identified by Moon et al. (2014). For

reference, the original Moon typologies can be seen in Figure 2.20. It is important to note that where relationships between seasonal velocity typology and melt are discussed below, these are hypothesised based on comparison of the observed velocity responses with those of Moon et al. (2014). Melt has not been measured in association with seasonal velocity typology in this chapter, but will be specifically analysed in Chapter 6.

A note on terminology. For the remainder of the thesis a distinction will be attempted to be made when talking about the conceptual typologies identified by Moon et al. (2014) which are now in popular usage within the relevant wider literature, and the specific data generated in this chapter. For reference to the wider concepts presented by Moon et al. (2014) the terms “Type 1”, “Type 2” and “Type 3” will be used. When specifically referring to the data and patterns generated in this thesis, the terms “T1”, “T2” and “T3” will be used.

5.4.2.1 T1

The shape and timing of change in the T1 typology is very close to the Moon Type 1 typology and is therefore interpreted to be representative of the same process drivers hypothesised by Moon et al. (2014) for Type 1. Melt may play a role in initiating some early speedup in spring (Figure 5.10a) but Type 1 patterns are dominated by strong correspondence between variations in speed and terminus position throughout the season, with retreat of the calving front coincident with speedup (Figure 5.10b) and advance of the calving front coincident with slowdown (Joughin, Howat, et al., 2008; Kehrl et al., 2017; Lemos et al., 2018). Sustained speedup occurs after cessation of melt and runoff (Figure 5.10c).

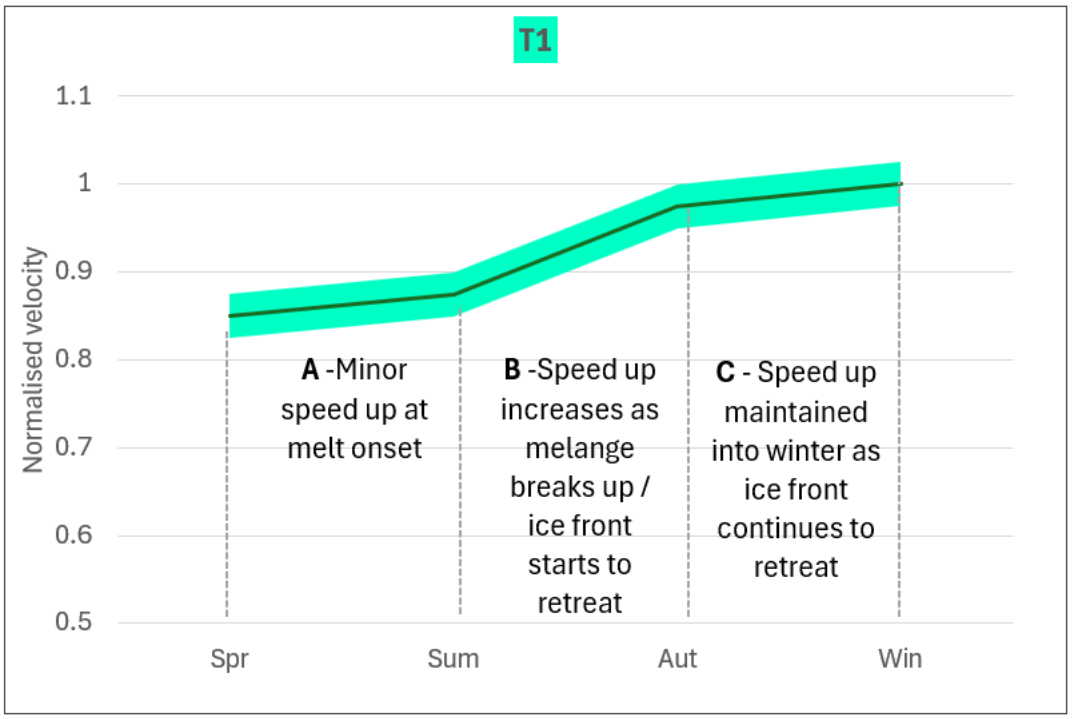

Figure 5.10 Cartoon showing the pattern of seasonal velocity variation for the T1 typology and the hypothesised process drivers.

5.4.2.2 T2

The shape and timing of change in the T2 typology is very close to the Moon Type 2 typology and is therefore interpreted to be representative of the same process drivers hypothesised by Moon et al. (2014) for Type 2. Type 2 shows a strong correspondence between velocity and runoff with summer speedup initiating with melt onset. As air temperatures start to rise in spring and surface ice begins to melt, runoff will be routed through supraglacial streams into crevasses and moulins enabling it to reach the bed. The meltwater pressurises the subglacial hydrological system, reducing the effective pressure causing sliding to increase and ice velocity to speedup (Zwally et al., 2002; Palmer et al., 2011) (Figure 5.11a). As melt decreases in late summer, the subglacial hydrological system depressurises and there is a subsequent deceleration (Figure 5.11b). Velocity returns to the pre-melt onset spring speed after melt ceases and remains stable through the winter (Figure 5.11c). As no mid or late season velocity low is observed, this suggests that channelised subglacial drainage is not developed (or is limited), for Type 2 glaciers. There is no obvious relationship between seasonal speed and the expected timing of changes in ice front position.

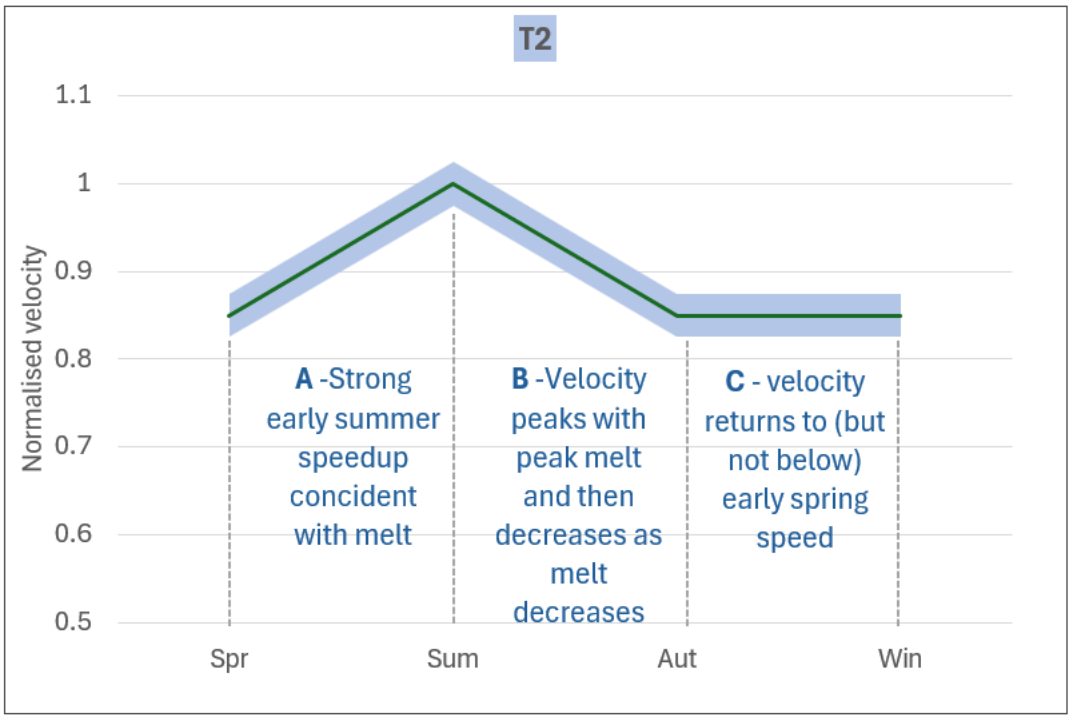

Figure 5.11 Cartoon showing the pattern of seasonal velocity variation for the T2 typology and the hypothesised process drivers. Blue text represents periods where the subglacial hydrology is hypothesised to be distributed, red text indicated periods where subglacial hydrology is hypothesised to be channelised.

5.4.2.3 T3

The shape and timing of change in the T3 typology is very close to the Moon Type 3 typology and is therefore interpreted to be representative of the same process drivers hypothesised by Moon et al. (2014) for Type 3. Type 3 is associated with a substantial ice velocity slowdown either as soon as melt starts, or very shortly after (Figure 5.12a). Velocity decreases from spring to summer and the slowdown continues to autumn (Figure 5.12b). This is interpreted as being representative of a subglacial hydrological configuration which is either already channelised before the melt season starts, or is very sensitive to melt and switches from distributed to channelised drainage very quickly at a low melt threshold early in the melt season (Figure 5.12a). This type of response is commonly seen in mountain glacier contexts where maximum velocity is observed to occur almost immediately upon melt onset in late spring or early summer as the subglacial system becomes pressurised, with velocity quickly falling as the subglacial system rapidly becomes channelised (Iken et al., 1983) (see section 2.3.1). Acceleration through autumn and winter is also characteristic of Type 3 (Figure 5.12c). This is hypothesised by Vijay et al. (2019) to be potentially due to water availability retained in the system that did not evacuate through channels during the

melt season repressurising the system as creep closure of channels starts to occur after melt cessation (Vieli et al., 2004). Similar winter responses have been observed in mountain glacier contexts in the Yukon (Abe et al., 2015) and the Karakoram (Quincey et al., 2009).

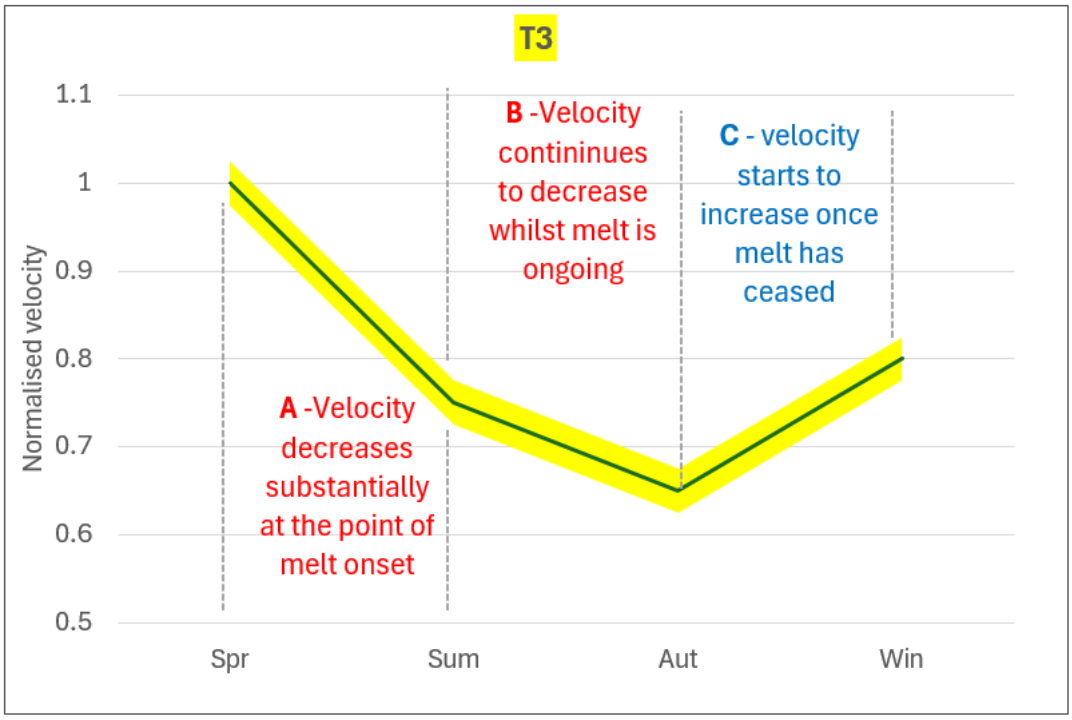

Figure 5.12 Cartoon showing the pattern of seasonal velocity variation for the T3 typology and the hypothesised process drivers. Blue text represents periods where the subglacial hydrology is hypothesised to be distributed, red text indicated periods where subglacial hydrology is hypothesised to be channelised.

5.4.2.4 T21

Two variations of Moon Type 2 were identified as typologies from the K means clustering (T21 and T23). It has been hypothesised by Moon et al. (2014) and also by studies that followed (Solgaard et al., 2022) that Type 2 and Type 3 are not discrete and separate from one another, but that they are dynamic responses that lie at either end of a continuum as end members, dependant on melt availability and subglacial hydrological configuration. This will be discussed further in section 5.4.3, below.

T21 is interpreted to be between Type 2 and Type 3 on the continuum. Initial response in the early melt season is as for Type 2 with velocity observed to increase with melt. Peak velocity may often be more pronounced than for Type 2 (Figure 5.14a), potentially due to higher melt availability. Peak velocity is reached with peak melt, but then decreases much more substantially than for Type 2, reaching an autumn minimum below the spring starting

velocity (Figure 5.14b). This is hypothesised to be due to a threshold melt level having been exceeded leading to channelisation of the subglacial system. The shape of the seasonal velocity response for T21 is very close to that observed in south west Greenland by Sundal et al. (2011) where a threshold surface runoff of ~14 mm WE d^{-1} is exceeded (see Figure 2.8b). It has been observed that increases in peak summer velocity under higher melt years can be offset by subsequent slowdown over the following winter and it is this style of seasonal velocity typology that has been hypothesised to drive the negative feedback between increased surface melt and net ice flux observed in south west Greenland in the 2000s (Sole et al., 2013; Tedstone et al., 2013, 2015) (see section 2.3.1.7).

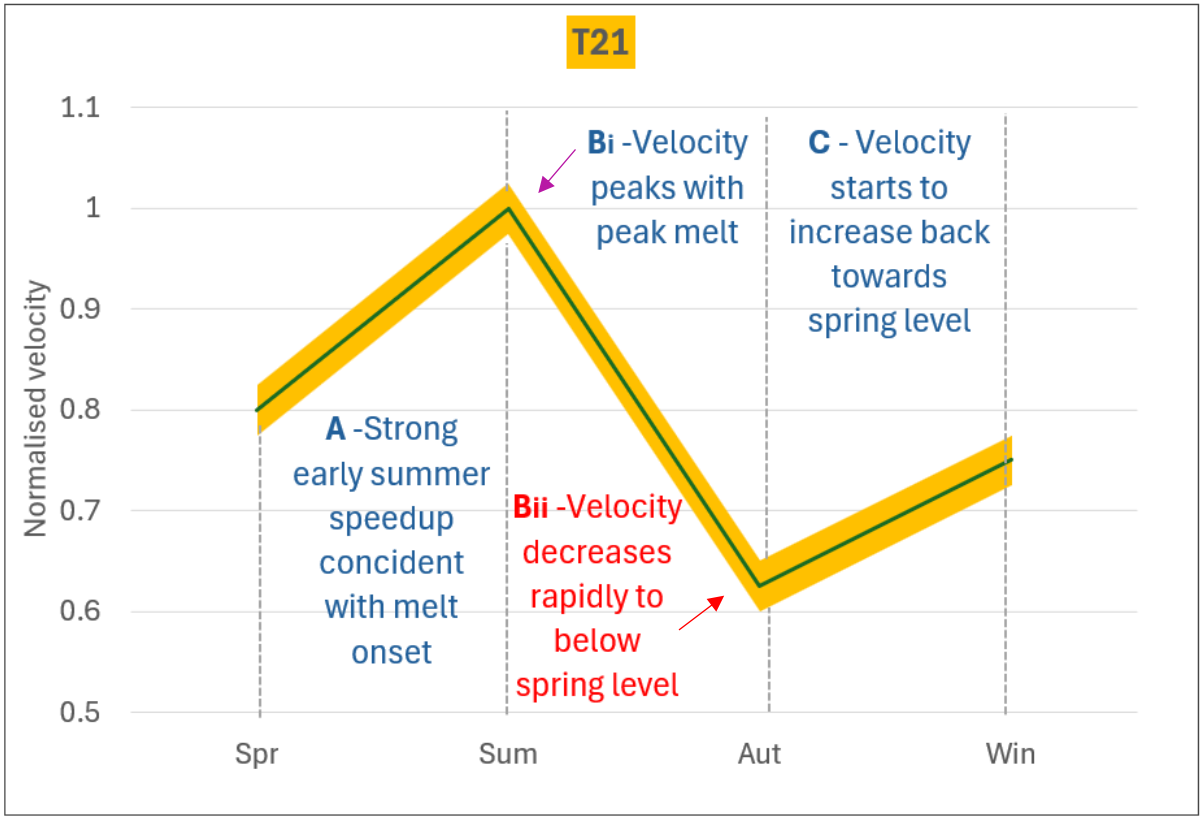

Figure 5.13 Cartoon showing the pattern of seasonal velocity variation for the T21 typology and the hypothesised process drivers. Blue text represents periods where the subglacial hydrology is hypothesised to be distributed, red text indicated periods where subglacial hydrology is hypothesised to be channelised.

5.4.2.5 T23

T23 is a subtle variation of Moon Type 2, only observed for the overdeepening dataset. The pattern and interpretation is as for T2 but seasonal variation in velocity is smaller in magnitude and the autumn velocity remains slightly elevated with velocity not returning to the original spring speed until winter (Figure 5.14b). The more muted response may be

indicative of a system where even less melt is present than for T2. As such, it may lie on the far end of the hypothesised Type 2 – Type 3 continuum, potentially beyond the Type 2 end member. However, the fact that velocity does not return to the spring starting value after melt has ceased in autumn is not well explained by the hypothesis that T23 may be related to lower melt availability and so this interpretation should be treated with caution until further analysis of the melt relationship has been directly measured in Chapter 6.

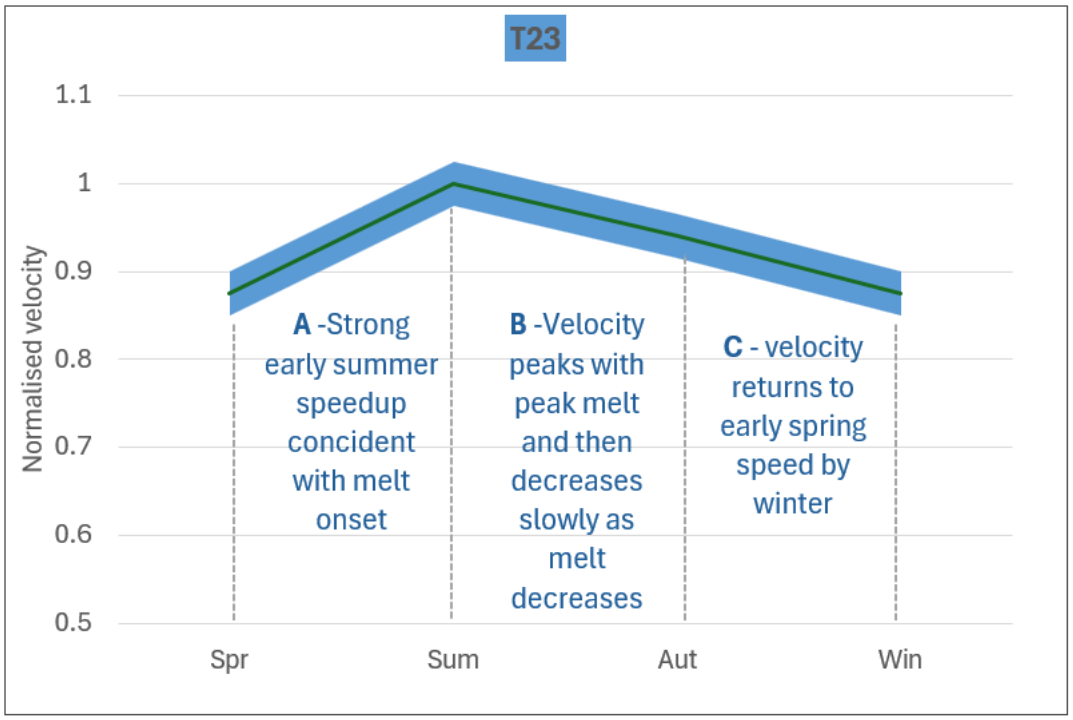

Figure 5.14 Cartoon showing the pattern of seasonal velocity variation for the T23 typology and the hypothesised process drivers. Blue text represents periods where the subglacial hydrology is hypothesised to be distributed, red text indicated periods where subglacial hydrology is hypothesised to be channelised.

5.4.2.6 T4

T4 is similar in shape to T3, but with the minimum velocity in summer rather than autumn Figure 5.15a-b). This suggests potential pre-conditioning of the subglacial hydrological system such that channels have not completely closed over winter and melt may be withheld with the system. As such a small amount of melt input at the beginning of the melt season is sufficient to rapidly reopen the 'primed' channels again to the extent that subglacial drainage becomes efficient, water pressure drops, and velocity decreases (Hodge, 1974; Holmlund and Hooke, 1983; Iken and Bindschadler, 1986; Kamb and Engelhardt, 1987; Krimmel and Vaughn, 1987) (see section 2.3.1.2). A possible process driver for the earlier

reacceleration (Figure 5.15b-c) compared to T3 would be if the T4 pattern of seasonal velocity were occurring at higher elevations, thus experiencing earlier channel closure and therefore earlier potential for repressurisation due to late season melt events or melt released from subglacial stores or firn aquifers (Hodge, 1974; Sugiyama and Gudmundsson, 2003; Harper et al., 2005; Hart et al., 2019; Nanni et al., 2023) (see section 2.3.1.2).

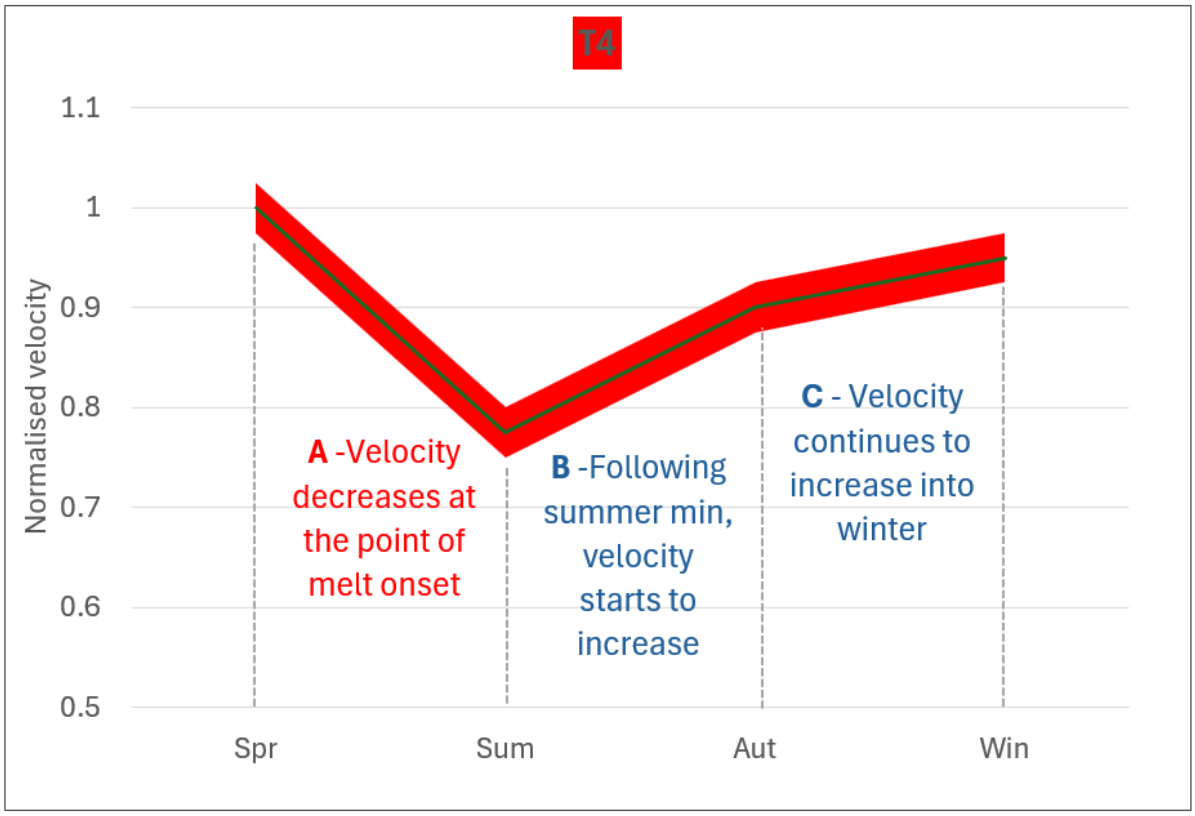

Figure 5.15 Cartoon showing the pattern of seasonal velocity variation for the T4 typology and the hypothesised process drivers. Blue text represents periods where the subglacial hydrology is hypothesised to be distributed, red text indicated periods where subglacial hydrology is hypothesised to be channelised.

5.4.2.7 T5

T5 has the same shape of velocity response to T2, but shifted back one season with peak velocity in autumn rather than summer (Figure 5.16b). As such, the process interpretation is the same as for T2, but needs to account for the delayed onset of speedup in the locations where this typology is observed. This could be potentially be explained by later onset of melt due to higher surface elevation, or a longer time period for threshold melt required for speedup to initiate in lower melt contexts at higher latitude.

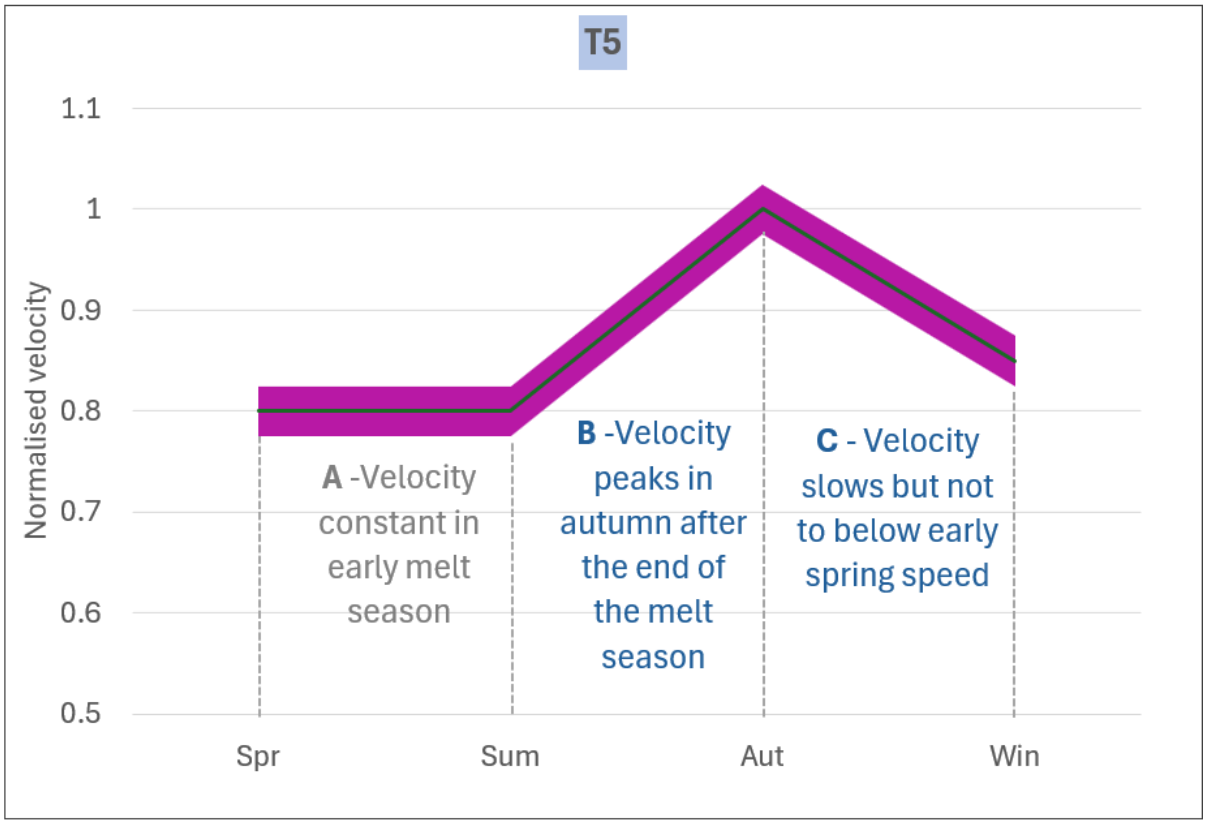

Figure 5.16 Cartoon showing the pattern of seasonal velocity variation for the T5 typology and the hypothesised process drivers. Blue text represents periods where the subglacial hydrology is hypothesised to be distributed, red text indicated periods where subglacial hydrology is hypothesised to be channelised, grey text indicates periods when the subglacial drainage configuration is uncertain.

5.4.3 Type 2 – Type 3 continuum

Type 2 and Type 3 seasonal velocity typologies have been hypothesised to sit at either end of a continuum, or be end members on a spectrum, since they were first conceptualised by Moon et al. (2014). Associated follow up studies of ice sheet wide seasonal velocity typology have also reaffirmed this hypothesis (Solgaard et al., 2022). However, this conceptual model of a continuum has been largely extrapolated from the process interpretations made of Type 2 and Type 3 in previous studies. Essentially, Type 2 and Type 3 are hypothesised to be representative of distributed and channelised drainage respectively, it is understood that there is a continuum from distributed to channelised drainage (see section 2.3.1.2), therefore it has been assumed in previous studies that Type 2 and Type 3 must similarly be on a continuum. Existing empirical support for the concept of a continuum are limited to the fact that some locations change typology from year to year (inferred (but not observed) to be driven by differing melt conditions), and that a small number of observations on

individual case study glaciers show a transition from Type 3 to Type 2 further inland at higher elevations (therefore with lower melt regimes) (Moon et al., 2014; Solgaard et al., 2022). This evidence is limited to one glacier in Moon et al. (2014), and five individual glaciers in Solgaard et al. (2022). Observations of plume activity at the calving front of Kangiata Nunaata Sermia (in combination with analysis of seasonal velocity patterns) have also been used to infer channelised subglacial hydrology despite Type 2 velocity patterns, and this has been hypothesised to be representative of a glacial system close to transitioning from Type 2 to Type 3, and likely to do so were higher melt conditions to be experienced (Davison et al., 2020).

However, no previous studies have *observed* seasonal velocity patterns representative of points between the Type 2 and Type 3 end members on the continuum. The results presented here offer some evidence of this for the first time. The differing magnitudes of T21 response in the K means clusters generated (Figure 5.7 and Figure 5.8) show good evidence of progression along a continuum as illustrated in Figure 5.17. The graphs plotted in the cartoon are conceptual (for clarity), but there are clusters in the data presented in this chapter that align with each. For example, clusters 8, 2, 6, 10 and 1 in Figure 5.7 are very close in shape to Figure 5.17a-e respectively.

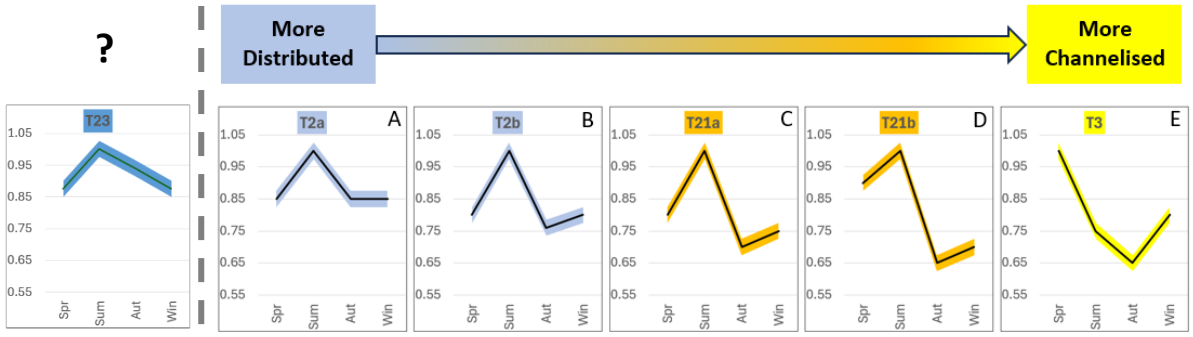

Figure 5.17 Cartoon illustrating the conceptual model of progression along a continuum of seasonal velocity typology with T2 and T3 as end members. The subscripts a and b for typologies T2 and T21 in A), B), C), and D) do not represent discrete typologies, rather are used to differentiate observed variation within the T2 and T1 typologies.

5.4.4 Comparison to previous studies

This section will give brief consideration to how the results from this study compare with

the 4 key existing studies closely aligned with this work, those of Moon et al. (2014), Vijay et al. (2019), Vijay et al. (2021) and Solgaard et al. (2022).

The studies are all comparable as the broad aims are similar and the typologies are presented in a similar way following the approach initially adopted by Moon et al. (2014) of normalising the velocities at a given point to allow direct inter comparison of the shape of seasonal relationships between points of differing absolute velocities. The four studies are all based in Greenland, and go beyond a small number of glaciers in a limited single location study area.

5.4.4.1 Spatial coverage

Moon et al. (2014) and Vijay et al. (2019) both select a subset of outlet glaciers for their studies (n = 55 and n = 45 respectively). The spatial distribution of the glaciers included varies slightly between the two studies (Figure 5.18). Both include the sector in the north west from Kong Oscar down to Upernavik Isstrøm II, which also extends down to Jakobshavn in Moon et al. (2014). The second substantive sector in the Moon et al. (2014) is the south east, from Kangerdlugssuaq all the way down to the far south of the east coast around Heimdal. The second substantive sector in the Vijay et al. (2019) is different and covers from Helheim north to Fredriksborg. In addition, Moon et al. (2014) cover two further glaciers in the south west, and Vijay et al. (2019) cover three further glaciers in the north east. As such, whilst the spatial coverage of these two studies is much higher than any previous similar work, they do not represent a complete audit, and are not fully representative of Greenland outlet glaciers due to the lack of data for the south west, north east, and north coasts.

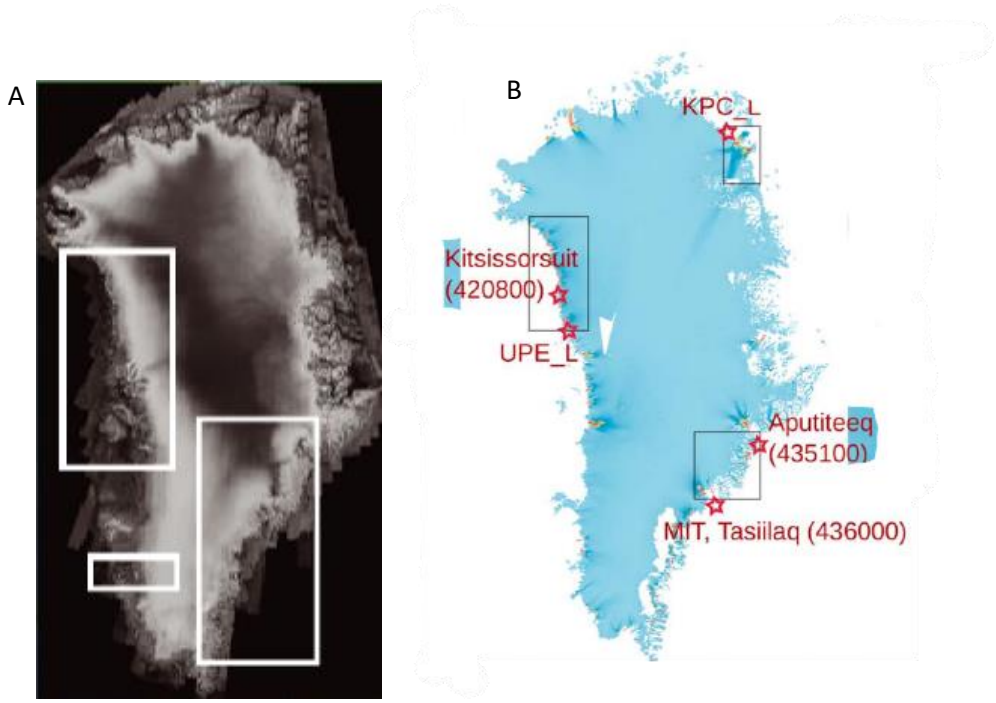

Figure 5.18 Coverage of the studies by A) Moon et al. (2014), and B) Vijay et al. (2019). Figures reproduced from Moon et al. (2014), and Vijay et al. (2019).

In contrast, Solgaard et al. (2022) take the same approach as for the data presented within this chapter and provide complete coverage for all Greenland outlet glaciers. Vijay et al. (2021) also present extremely comprehensive spatial coverage of Greenland presenting data for 221 glaciers, but this analysis is limited to single point velocity measurement very close to the calving front as in Moon et al. (2014) and Vijay et al. (2019).

5.4.4.2 Temporal resolution of velocity time series

The temporal resolution of the velocity time series that are used for the determination of seasonal velocity typology is possibly the area where there is most variation between studies. The apparent temporal resolution of velocity data in the Moon et al. (2014) study is the most similar to that used in this chapter, but still has material differences. Both datasets have single velocity values representative of each season (for each point of interest), but the way in which these are generated is different. Moon et al. (2014) took 3-6 velocity measurements for each glacier each year, approximately timed to coincide with winter, spring, summer and autumn. Each of these measurements was derived from a single 11 day (or occasionally a 22 day) repeat pair of satellite images. As such, these represent velocity averaged over a short interval timed to be within a season, not an average representative of

velocity over the whole season. This means that some velocity values used may be atypical of the seasonal average and this is acknowledged in their paper. The MEaSUREs Quarterly Greenland velocity data used in this chapter averages all available velocity values derived from 6 day repeat Sentinel-1A and 1B image pairs for a given 3 month period. This results in up to 30 individual velocity values being averaged to give the seasonal mean. As such, there are always four seasonal velocity values per year, and they are a representative average of the velocity over that season.

Vijay et al. (2019), Vijay et al. (2021) and Solgaard et al. (2022) use much higher temporal resolution velocity datasets in their analysis. Vijay et al. (2019) implement offset tracking on 6 day and 12 day repeat Sentinel-1A and 1B image pairs to generate a dense time-series of approximately 30-45 velocity measurements for each glacier for year of their study. The data used by Vijay et al. (2021) is extremely similar to the data used by Vijay et al. (2019) both in terms of derivation and resolution.

5.4.4.3 Typologies identified

Table 5.1 summarises the findings of the four comparator studies in terms of the typologies that each study identifies, and the overall proportion of observations that each typology represents. To allow a more direct comparison with these previous studies, the three subtypes of Type 2 identified within this chapter have been aggregated and included as an additional value in the Type 2 line of the table, as the previous studies do not make this differentiation.

Table 5.2 Comparison of results from this study with those from the three other key studies on Greenland seasonal velocity typology (Moon et al., 2014; Vijay et al., 2019; Solgaard et al., 2022).

Typology	Moon et al. (2014) [n = 205, 2009 - 2013]	Vijay et al. (2019) [n~105, 2015 - 2017]	Vijay et al. (2021) [n = 358, 2017 - 2019]	Solgard et al. 2022) [n = 632,835, 2017 - 2021]	This study (ODs) [n = 1833, 2016 - 2019]	This study (Central flowlines) [n = 190,003, 2016 - 2019]
1	21.0%	28.6%	excluded	-	9.1%	2.2%
2	46.8%	17.1%	36.0%	54.4%	15.1% (*52.7%)	26.1% (*44.6%)
23	-	-	-	-	25.9%	-
21	-	-	-	-	11.7%	18.5%
3	32.2%	54.3%	64.0%	45.6%	30.8%	22.6%
4	-	-	-	-	6.9%	27.1%
5	-	-	-	-	0.6%	3.7%

In four of the datasets summarised in Table 5.2 (Moon et al., 2014; Solgaard et al., 2022) and both datasets from this study) the order by which each of the three original Moon typologies (typologies 1, 2, and 3) are ranked by prevalence is the same, with Type 2 most common (with a value between 45% and 55% in all studies), then Type 3, and with Type 1 least common. Solgaard et al. (2022) do not report any evidence of Type 1 in their results, and Vijay et al. (2021) made a methodological decision to not include Type 1 in their analysis from the outset. The agreement between the findings of these previous studies and the results presented here is reassuring and gives confidence to new findings and conclusions that may be drawn in this chapter beyond what has previously been established. In Vijay et al. (2019) Type 2 is actually the least common typology with Type 3 the most common and Type 1 in the middle. Vijay et al. (2021) report much higher prevalence of Type 3 than any other studies, but these values are perhaps exaggerated due to the exclusion of Type 1 from their analysis. One key methodological difference between Vijay et al. (2019) and the other

studies is that they only classify a glacier where there is a consistent typology evident in all three years of their study. In all other studies, each location for each year is considered as a distinct data point and classified even if the typology varies from year to year. As such, if Type 2 was a typology more prevalent in glaciers where typology varies from year to year, this would explain the anomalous results of Vijay et al. (2019) when compared to the other three studies which show similar prevalence rankings of typologies. If the interpretation is of Type 2 as being representative of distributed subglacial drainage throughout the season, and Type 3 as being representative of a switch from distributed to channelised drainage part way through the season, then it is not unreasonable to expect that some glaciers may be Type 2 in lower melt years, but Type 3 in higher melt years. Such behaviour would also be consistent with the concept of a Type 2 – Type 3 continuum (section 5.4.3). Indeed, this has been shown to be the case for a number of glaciers in south west Greenland (Sundal et al., 2011)). The anomalous results of Vijay et al. (2019) therefore, are perhaps not completely unexpected.

Another key pattern evident in the data is that Type 1 is the least prevalent of the three original Moon typologies in three of the four studies where Type 1 was considered (again, Vijay et al. (2019) is the exception in this regard). Both Moon et al. (2014) and Vijay et al. (2019) suggest that there is good evidence to support the hypothesis that the Type 1 seasonal typology is a result of reduction of resistive stresses due to seasonal retreat of the calving front. Another key methodological difference between the studies being compared here is that Moon et al. (2014), Vijay et al. (2019) and Vijay et al. (2021) only record ice velocity measurements for each glacier at a single point, very close (1-5 km) to the calving front. In the approach taken in this chapter and that of Solgaard et al. (2022) velocity measurements are taken at hundred or thousands of locations for each glacier, distributed all across the glacier. It follows then, that if Type 1 is a typology driven by marine processes, so long as the effect of these process are isolated to areas in close proximity to the calving front, the relative prevalence of Type 1 reported by a study should be proportional to the ratio of velocity readings taken in close proximity to the calving front. This is what is seen in Table 5.2. Moon et al. (2014) and Vijay et al. (2019) (where all measurements are taken very close to the calving front) have the highest rates of Type 1 observed (21.0% and 28.6% respectively). For methodologies that take measurements across the glacier, the proportion

of measurements near the calving margin will broadly scale inversely with the number of observation points. Solgaard et al. (2022) has the highest number of observations (632,835) and do not identify a Type 1 typology. This is likely due to the very small proportion of their points which are near calving fronts being insufficient in number to generate a cluster in their K means analysis, especially given they only ran four clusters. This is potentially a significant limitation of the approach they adopt as it essentially ignores a typology that whilst perhaps less prevalent than others, is still very important owing to the fact that it is representative of a process operating a) at the flux gate of ice discharge to the ocean, and b) consequently, at the sea-ice interface and therefore subject to potential substantive future change as a result of warming sea temperatures. Type 1 is identified in the analysis both for the overdeepening dataset and the central flowline dataset, but at a much lower prevalence (9.1% and 2.2% respectively) than found by Moon et al. (2014) and Vijay et al. (2019). As hypothesised above, there is far less prevalence of T1 in the central flowline dataset where the number of observation points is much higher, and therefore a lower proportion of points are at or near the calving front.

5.4.5 Effectiveness of method

Overall, the method developed for the analysis of seasonal velocity typology appears to be robust, and a step forward from what has been established in previous studies.

The method is truly automated and requires very little user input or decision making. User input is limited to determining the optimum number of clusters and then categorising and aggregating (if required) the outputs of the cluster analysis. Unlike the methods developed by Moon et al. (2014) and Vijay et al. (2019) there is no manual visual inspection of individual time series for individual glaciers to allocate typologies. This means that datasets can be scaled up to cover many more points of interest and truly represent the ice sheet as a whole. It also means that the analysis can be run relatively easily on new datasets in the future. The approach of Vijay et al. (2021) semi-automates the classification of seasonal velocity typology by developing a cumulative absolute residual thresholding criteria for fitting the velocity time series for each glacier to model Type 2 and Type 3 glacier velocity time series graphs. This facilitates the analysis of much larger datasets, but requires that a model or ideal velocity time series graph can be identified to classify to, and does not enable

the patterns inherent in the data to be drawn out using an inductive approach.

The method presented in this chapter adopts a similar machine learning based approach to determining seasonal velocity typology as Solgaard et al. (2022) by implementing a K means clustering algorithm. However, there are substantial differences in the implementation of the approach which appear to have yielded some benefits. Rather than attempt complete coverage of all areas of all outlet glaciers by calculating a time series for every cell in the input velocity rasters (the approach taken by Solgaard et al. (2022)), points at 500 m intervals along the centreline of each glacier are selected. Each glacier is still included in the analysis, but the amount of data to process is reduced substantially. Accounting for the fact that Solgaard et al. (2022) have five years in their study compared to four years here, the approach used in this chapter requires approximately 38% the number of spatial points to still give full coverage of all outlet glaciers. The approach of using quarterly velocity averages rather than non-aggregated velocity time series with ~30 values per year further reduces the number of data points fed into the K means algorithm by a factor of ~7.5 giving a total data processing reduction of ~95% compared to Solgaard et al. (2022). The obvious potential downside to using much lower temporal resolution data is that subtle patterns in seasonal variation may be missed leading to a lower number of identifiable typologies. However, this does not seem to be the case as Solgaard et al. (2022) determine that the optimum number of clusters from their analysis is four, allowing them to identify two seasonal velocity typologies compared to 12 clusters and seven typologies presented here. A further benefit of the approach adopted here is that typologies are identified for known points on known glaciers, rather than undefined cells in a large raster. This means that typology can be easily cross referenced against other metrics (such as those developed in Chapter 3) established for individual glaciers and overdeepenings to provide a focused and detailed analysis of potential links between related processes and seasonal velocity typology rather than the more general regional summary analysis given by Solgaard et al. (2022).

5.5 Conclusion

The approach developed for automated classification of seasonal velocity typology appears to function well and generate outputs that align well with previous studies. The approach represents a good balance between Moon et al. (2014) and Solgaard et al. (2022). Entire

glaciers are taken account of, not just single points near the terminus, so the outputs are more widely representative of processes in all parts of the ice sheet. The approach means that seasonal velocity typology data is also all linked directly back to individual glaciers which facilitates further analysis of process drivers offering the potential for increased understanding.

The seasonal velocity typologies identified by previous studies are represented within the results, and in similar orders of prevalence to what previous studies have found. However, Type 1 is much less prevalent than studies which only analyse velocity very close to the terminus. Two new subtypes of Moon Type 2 are also identified; T21 which shows a summer peak followed by a slowdown to below spring velocity (potentially representative of a threshold melt level being reached causing a switch from inefficient to efficient subglacial hydrological configuration, similar to that identified by Sundal et al. (2011)), and T23 which has a less pronounced / flatter slowdown in autumn. Two new seasonal velocity typologies are identified (T4 and T5) where minimum velocity is in summer, followed by autumn acceleration.

The identification of the T21 typology, and the fact that it is represented in differing magnitudes of response in different clusters in the K means outputs, indicates further support for the hypothesis that Type 2 and Type 3 are end members on a continuum, with T21 sitting between Type 2 and Type 3 on the continuum.

Chapter 6 Seasonal ice velocity typologies in Greenland: an ice sheet wide analysis of patterns and control

6.1 Introduction

6.1.1 Aims

The aim of this chapter is to answer **RQ3** - are there any broad scale patterns that link seasonal velocity signature to bed topography or other GrIS-wide factors? This research question has two associated objectives:

- **RQ3 objective B -** Explore the extent to which there is evidence at the ice sheet scale for patterns in ice dynamics modulated by overdeepenings identified for individual glaciers in **RQ2 B** (Chapter 4).
- **RQ3 objective C –** Quantify the spatial and temporal patterns (and potential process relationships) between seasonal ice velocity typology and other relevant factors.

A fundamental motivation for this chapter is to explore whether the specific findings used to build the conceptual model developed in Chapter 4 are widespread at the ice sheet scale. This is the basis of **RQ3 objective B**. The amount of data created and analysed to ascertain this is substantial, and as such Chapter 6 is quite long. Within this objective, the following sub questions (SQs) and issues are of prime concern, and these will be addressed as required:

- **SQ1** Is there a relationship between overdeepening morphometry (specifically BSSR) and seasonal velocity typology?
- **SQ2** Is there a variation between the seasonal velocity typology of the normal and adverse slopes of overdeepenings, or between the seasonal velocity typology of ice flowing across an overdeepening compared to ice immediately up and downstream of an overdeepening?
- **SQ3** Is there a variation in the magnitude of ice velocity speedup or slowdown *within* the seasonal velocity typology of an overdeepening when comparing the normal and adverse slopes?

The conceptual model presented in Chapter 4, which links predicted ice velocity patterns on adverse and normal slopes of overdeepenings to drainage system changes hypothesised to

be associated with such slopes, is used to assess the support for RQ3B as follows:

SQ1 It is hypothesised that channelised subglacial drainage may be suppressed on the adverse slopes of overdeepenings due to supercooling preventing the enlargement of (or even closing) channels in the ice (section 4.3.2.7). Therefore, if this hypothesis is supported, distributed subglacial drainage should be more common on the adverse slopes of overdeepenings where the BSSR exceeds the supercooling threshold of ~-1.8, than in overdeepenings where the supercooling threshold is not exceeded. It follows that seasonal velocity typologies interpreted to be representative of distributed subglacial drainage configurations (e.g. T2, T23 (see section 5.4.2)) should have higher relative prevalence in overdeepenings where the supercooling threshold is exceeded.

SQ2 It is hypothesised that channelised subglacial drainage may be suppressed on the adverse slopes of overdeepenings both due to reduced hydraulic gradient and supercooling preventing the enlargement of (or even closing) channels where the supercooling threshold is exceeded. Therefore, if this hypothesis is supported, distributed subglacial drainage should be more common on the adverse slopes of overdeepenings than both on the normal slopes of overdeepenings and than on areas directly up or downstream of the overdeepening boundary. It follows that seasonal velocity typologies interpreted to be representative of distributed subglacial drainage configurations (e.g. T2, T23 (see section 5.4.2)) should have higher relative prevalence on adverse slopes compared to normal slopes. Changes in seasonal velocity typology would also be expected to be observed as ice flows through overdeepenings (e.g. typologies representative of channelised drainage up and / or downstream of the overdeepening (e.g.T3, T21 (see section 5.4.2)), with typologies representative of distributed drainage (e.g. T2 / T23) within the overdeepening).

SQ3 It is hypothesised that channelised subglacial drainage may be suppressed on the adverse slopes of overdeepenings both due to reduced hydraulic gradient and supercooling preventing the enlargement of (or even closing) channels where the supercooling threshold is exceeded. Therefore, if this hypothesis is supported, the *magnitude* of late summer slowdown would be expected to be lower on the adverse slope than the normal slope of an overdeepening, even if the seasonal velocity *typology* is the same on both slopes. An example of this would be both normal and adverse slopes classified as T21, but with more significant late summer slowdown on the normal slope (e.g. cluster 10, Figure 5.7) than on

the adverse slope (e.g. cluster 2, Figure 5.7).

Whilst the principal aim of this thesis is to explore the control that overdeepenings may exert on the ice dynamics of the GrIS, it is acknowledged that these potential controls are only one factor in a wide range of processes that influence the dynamics of the ice sheet. The compilation of the data and methods which enable the analysis of overdeepenings also affords investigation of these other factors and this is the motivation for **RQ3 objective C.** A set of sub questions have therefore also been created relating to this objective, these are:

- **SQ4** How dominant a control are marine processes on seasonal velocity typology at the calving front of marine terminating outlet glaciers and is the typology at the margin representative of typologies further inland?
- **SQ5** What role does surface runoff play in seasonal velocity typology?
- **SQ6** What are the spatial variations in seasonal velocity typology across the GrIS?
- **SQ7** What are the temporal variations in seasonal velocity typology across the GrIS?

6.2 Methods and data

6.2.1 Study area and datasets

The study area for this chapter is the whole GrIS. The analyses have been conducted on two separate datasets, overdeepenings and central flowlines. The details of these two datasets are as follows:

The **overdeepening** points of interest are based on the overdeepening metric dataset created in Chapter 3. For each of the 621 overdeepenings all data used within this chapter are added to points spaced at 150 m intervals along the true thalweg of the overdeepening (as described in section 3.2.2.2). Means are then taken for points on the adverse slope and for points on the normal slope. For parameters that vary by year (runoff and ice velocity) normal and adverse slope means are calculated for each overdeepening for each year. As such, each overdeepening is represented by a maximum of eight data points, normal and adverse slope means for each of the four study years (2016-2019) giving a total maximum number of 4,968 data points within the overdeepening dataset. The rationale for using this

dataset is that it allows the seasonal velocity typology to be compared for adverse and normal slopes (**SQ1 and SQ2**) and the relationship between overdeepening morphometry and seasonal velocity typology to be explored (**SQ3**). The coverage of the central flowline dataset can be seen in Figure 3.12.

The **central flowline** points of interest are points at 500 m spacing along the 553 central flowlines generated in Chapter 3 (see section 3.2.1.2). This dataset includes all datapoints along all available flowlines, rather than being restricted to points within designated overdeepenings, and therefore comprises 183,003 spatial points and a total dataset of 732,012 data points (spatial points x four years in the study). The rationale for using this dataset is that it has a much higher number of data points than the overdeepening dataset (and so therefore may be more statistically robust), covers a much wider area, and allows the investigation of changes in seasonal velocity typology before and after ice flows over an overdeepening (e.g. SQ2). The coverage of the central flowline dataset can be seen in Figure 6.3.

It is important to note that the number of data points generated for analysis is substantially lower for both the overdeepening dataset and the central flowline dataset than the maximums stated above due to the quality assurance checks for velocity data (see section 5.2.2).

6.2.2 Overview

Full technical methodological detail on the generation of velocity typology clusters is explained in detail in Chapter 5. An overview of the workflow adopted in this chapter is summarised below, with additional data and methods presented where necessary.

1. Clusters representing seasonal velocity typologies were generated using the K means clustering approach presented in Chapter 5.
2. Modèle Atmosphéric Régional (MAR) (MAR v3.12 (Fettweis, 2007; Fettweis et al., 2017)) modelled runoff data was aquired at daily, monthly, and quarterly temporal resolutions for the whole of Greenland for all 4 study years (2016-2019).
3. Overdeepening metrics (from Chapter 3) were added to the overdeepening points of interest.

4. Latitude, elevation and quarterly MAR runoff data (agregated to match the quarterly periods of the MEaSUREs quarterly velocity data) are added to all points in both the overdeepening and central flowline dataset.
5. Python code written to analyse the data from points 3 and 4 (above).
6. Variation in seasonal velocity response between normal and adverse slopes of each overdeepening for each year were calculated. The same K means clustering approach developed for automatically classifying seasonal velocity typology in Chapter 5 is adopted to generate clusters representing normal / adverse slope variation typology.
7. A kernel density analysis was conducted for the central flowline dataset for 2017 and 2019.

6.2.3 Seasonal velocity typologies

Clusters representing seasonal velocity typologies were generated using the K means clustering approach presented in Chapter 5. This was done for both the overdeepening dataset and the central flowline dataset. The output is a classification of typology for each point of interest (either an individual point in central flowline dataset or agregated values for the normal and adverse slope of each overdeepening) for each year where there is a full velocity time series for that point. Full details on the method adopted and the resulting typologies is given in Chapter 5.

6.2.4 MAR runoff data

MAR is a regional climate model which simulates the coupled surface-atmosphere system over Greenland (MAR v3.12 (De Ridder and Schayes, 1997; Gallée, 1997; Fettweis, 2007; Fettweis et al., 2017; Antwerpen et al., 2022)), and has been widely used across a range of studies in Greenland (Alexander et al., 2014; Colgan et al., 2015; Koenig et al., 2016; Schlegel et al., 2016). Modelled runoff data is provided at daily and monthly temporal resolutions for the whole of Greenland for all 4 study years (2016-2019). The spatial resolution of the data is 20 km for the daily data, and 1 km for the monthly data. The MAR data was used for two

purposes within this chapter. Runoff data were spatailly aggregated for the whole of Greenland to asses the overall level of melt for Greenland to identify high and low melt years within the study period. The runoff data were also added to each point of interest for each quaterly period within the study to enable the analysis of relationships between melt and seasonal velocity typology. Extraction of MAR data to points (and the subsequent temporal aggregation of monthly totals to quaterly totals) was achieved by utilising the netCDF4 Python library and the numpy .argmin() function to return the index of minimim distance along each axis of the array to locate the closets cell to each of the data points in the MAR netCDF.

Runoff data were used for two purposes, to add as a parameter to points for which seasonal velocity typology has been established to allow these relationships to be explored (SQ5), and to determine which years in the study period are relatively high and low melt years to allow comparison in ice sheet behaviour under overall high and low melt regimes (SQ5). The patterns of runoff show that the study period contains two relatively high melt years (2016 and 2019) where runoff is in excess of the 2000-2021 mean, and two relatively low melt years with runoff below the 2000-2021 mean (2018 and 2019) (Figure 6.1a). It is also clear that, in all years, the vast majority of total annual melt occurs within the summer period (June, July, and August); 90% of total in 2016, 87% in 2017, 93% in 2018, and 88% in 2019 (Figure 6.1b). As such, in the results and analysis that follows in this chapter, 2016 and 2019 will be considered high melt years and referred to as such, and 2017 and 2018 considered low melt years. All reference to ‘summer runoff’ refers to the total June, July, August runoff modelled by MAR.

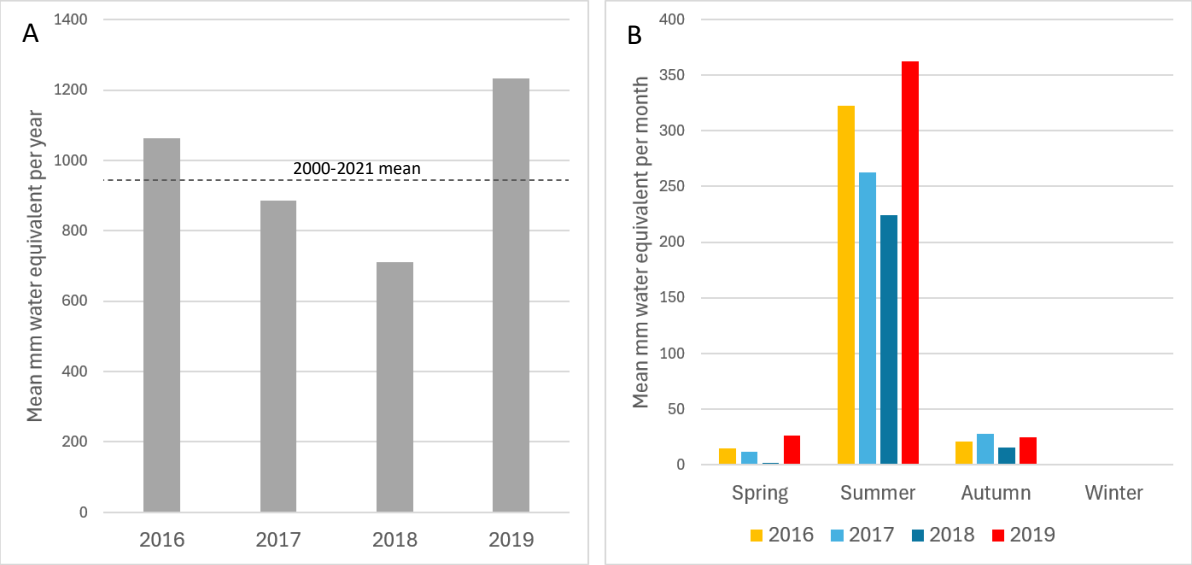

Figure 6.1 MAR modelled runoff data for Greenland 2016-2019. Data shown is aggregate mean values of water equivalent runoff for Greenland. A) MAR v3.12 ERAS annual mean runoff for Greenland. Grey dashed line shows the 2000-2021 mean annual runoff. B) MAR v3.12 ERAS monthly runoff aggregated into seasons; spring (mean of March, April, May), summer (mean of June, July, August), autumn (mean of September, October, November), and winter (mean of December, January, February).

6.2.5 Additional attribute data and analyses

In order to facilitate the analysis of possible causal process relationships which may be driving seasonal velocity typology (SQ6, SQ7), a range of additional parameters needed to be added to the points for which typology had been identified in Chapter 5. In addition to the MAR runoff data (described above) this included; surface elevation and latitude for both datasets, and in addition, overdeepening depth, adverse slope length, and BSSR for the overdeepening dataset. Surface elevation was taken from BedMachine v3 (Morlighem et al., 2017; Morlighem, 2022), which is originally derived from the Greenland Mapping Project (GIMP) DEM (Howat et al., 2014). The native projected coordinate system of our points is WGS84 / NSIDC Sea Ice Polar Stereographic North, latitude values were added to all points in ArcGIS Pro v3.2.0. All overdeepening morphometrics are those presented in Chapter 3.

Code was written in Python 3.11 to allow the control of the aggregation of data into individual years and normal and adverse slopes as required, and also to present graphs and boxplot figures of the analysis.

6.2.6 Variation in seasonal velocity response between normal and adverse slopes

A key area of interest to focus on in this chapter is the possibility of systematic variation in seasonal velocity typology (or the magnitude of the signal in the typology) between normal and adverse slopes of an overdeepening (SQ3). This has been approached by adopting the same K means cluster analysis methodology used to define and classify seasonal velocity typology in Chapter 5, but applied to classify typologies of variation (Figure 6.2) between normal and adverse slopes. This is best explained by considering a graphically illustrated example. Figure 6.2 shows the seasonal velocity pattern for a hypothetical overdeepening of T21 seasonal velocity typology. In this example, it can be seen that the response on the normal and adverse slope is very similar between spring and summer, but the late season slowdown between summer and autumn is much more pronounced on the normal slope than the adverse slope. The velocity recovery between autumn and winter is then stronger on the normal slope than on the adverse slope. The relationship between the two lines (one for the adverse slope, one for the normal slope) shown in Figure 6.2a can be simplified and represented as a single line by subtracting one line from the other. The normal slope line has been subtracted from the adverse slope line, so anywhere on the variation graph (Figure 6.2b) above zero represents higher normalised velocity on the adverse slope, anywhere below the line represents higher normalised velocity on the normal slope. In the case of the adverse and normal slopes having an identical seasonal velocity pattern, the velocity variation graph would be a straight line at y = 0.

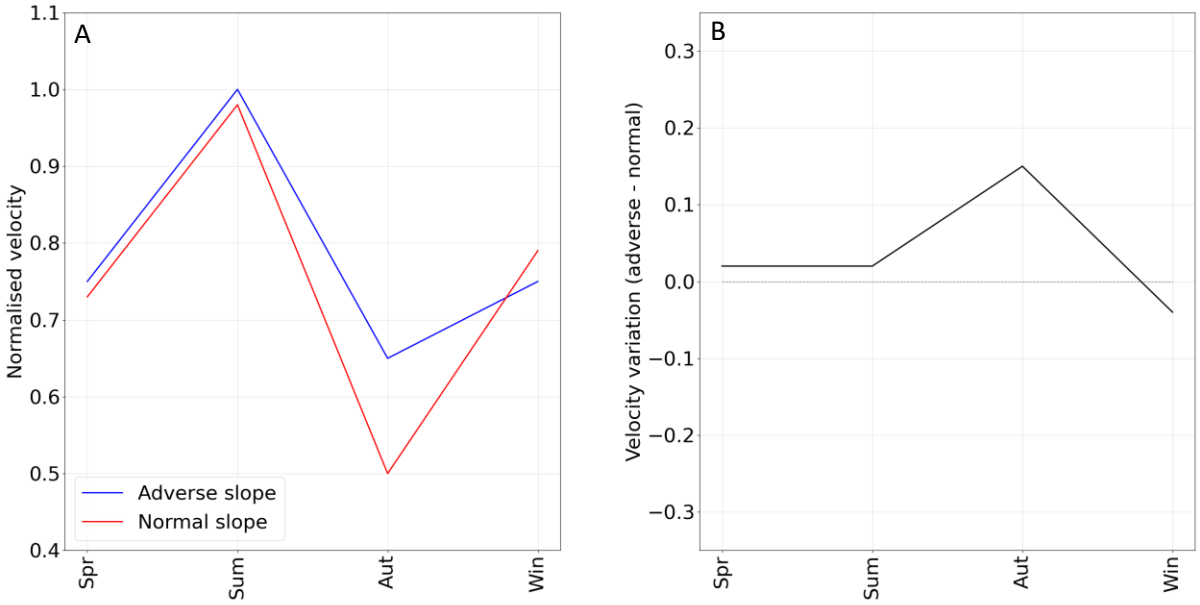

Figure 6.2 Cartoon illustrating the seasonal velocity pattern for a hypothetical overdeepening of T21 typology. A) The seasonal speedup and slowdown for adverse slope (blue) and normal slope (red) in the overdeepening. B) Variation in velocity between the adverse and normal slope calculated by subtracting the normal slope velocity from the adverse slope velocity. The dashed line marks zero variation where adverse and normal slope variations are equal. Where the line is above zero adverse slope velocity is faster, below zero the normal slope velocity is faster.

The differencing operation of subtracting the normal slope seasonal velocity pattern from the adverse slope seasonal pattern was performed for all overdeepenings in the dataset for each year where there was a full velocity time series for the overdeepening, generating a line graph as in Figure 6.2b. The resulting dataset was used as the input for a K means analysis conducted identically as for the identification of seasonal velocity typologies in Chapter 5. Following analysis of the elbow plot and visual interpretation of the output clusters for a range of cluster numbers, eight clusters were chosen as most appropriate for the analysis. These clusters are presented in the results section (6.3.1.3).

6.2.7 Kernel density analysis

In addition to the challenges posed in the data handling, processing, and analysis of large datasets, it can also be difficult to effectively visualise results when working with such datasets. This is particularly difficult when trying to map a dense array of vector points on a small scale map. Figure 6.3a illustrates this issue. When visualising the whole of Greenland, the scale of the map is almost 1:20,000,000; trying to map over 180,000 points in such a small area on the page inevitably results in a large number of points overlapping. As a result,

only the small number of points plotted last by the GIS software are visible, and may not be representative of the dataset as a whole inducing error or bias into the interpretation of the data. In contrast, when viewed at a larger scale (Figure 6.3b) colour coding points is extremely effective if due care is taken when choosing the style and size of the symbology.

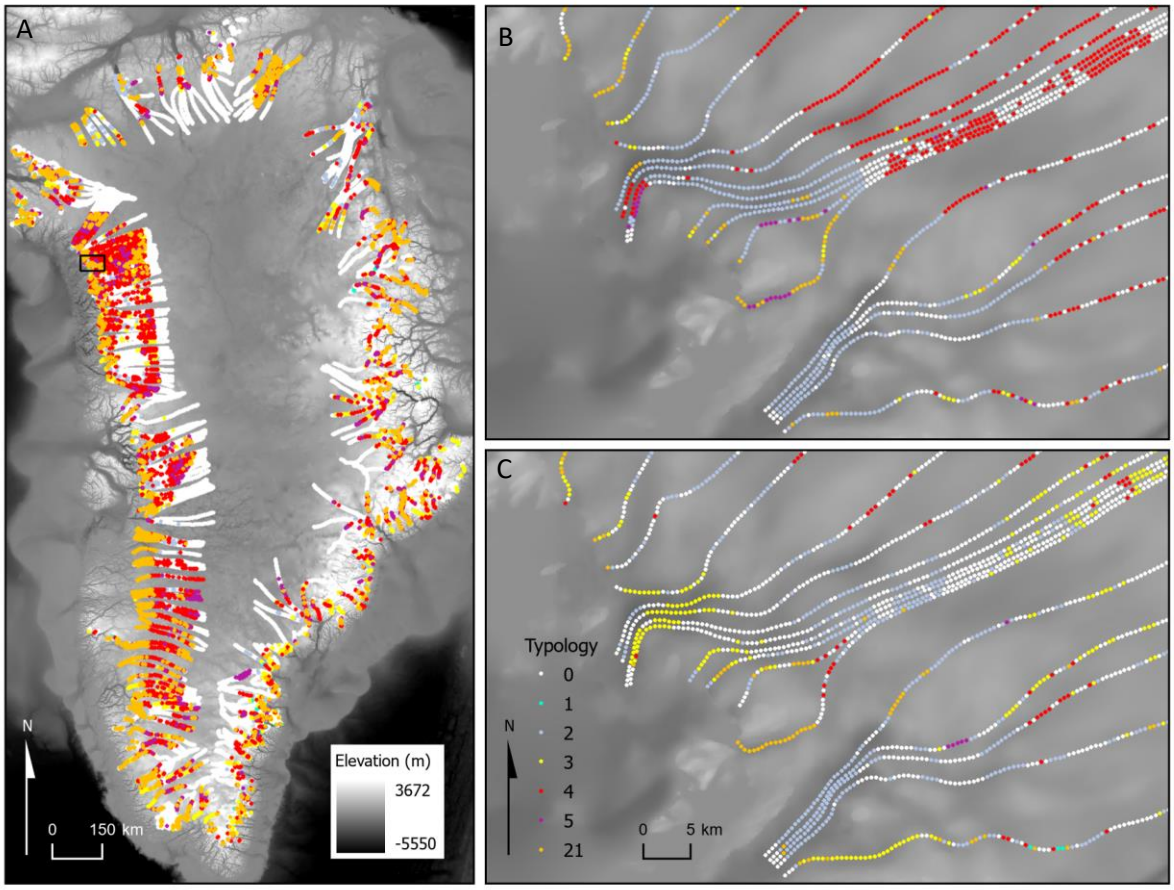

Figure 6.3 2017 seasonal velocity typology for the central flowline dataset. Legends for colour of points and the background DEM (Bed Machine bed elevation (Morlighem, 2022)) apply to all panes. (A) When viewed for the whole of Greenland points overlap and occlude one another. B) A smaller subsection of NW Greenland, marked by the black rectangle in pane A. At a much large scale (approximately 1:400,000) points do not overlap and the data is clearly presented. Data is for 2017 (a low melt year). C) The same area as pane B, but data is for 2019 (a high melt year).

It is important that data can be visualised at the ice sheet scale, and so to overcome the issues discussed above, central flowline dataset were converted from vector points into a raster of point density using the Kernel Density tool in ArcGIS Pro v3.2.0. The Kernel Density tool works by fitting a smoothly curved three dimensional surface over each point in the vector dataset (each central flowline dataset point in our case), the value of which is at its maximum directly over the point and decreases with increasing distance form the point, to a

value of zero at the edge of the search radius (specified as 100 km here). The total value under this surface is 1 for each point. The algorithm produces one such surface for each point in the vector dataset, and then sums the value of all kernel surfaces where they overlay a cell centre of the output raster. The function is based on the quartic kernel function (Silverman, 1986, 2018). Figure 6.4 shows an indicative kernel density output, which in this case simply represents the overall density of central flowline dataset points. Figure 6.4 covers exactly the same area as Figure 6.3a.

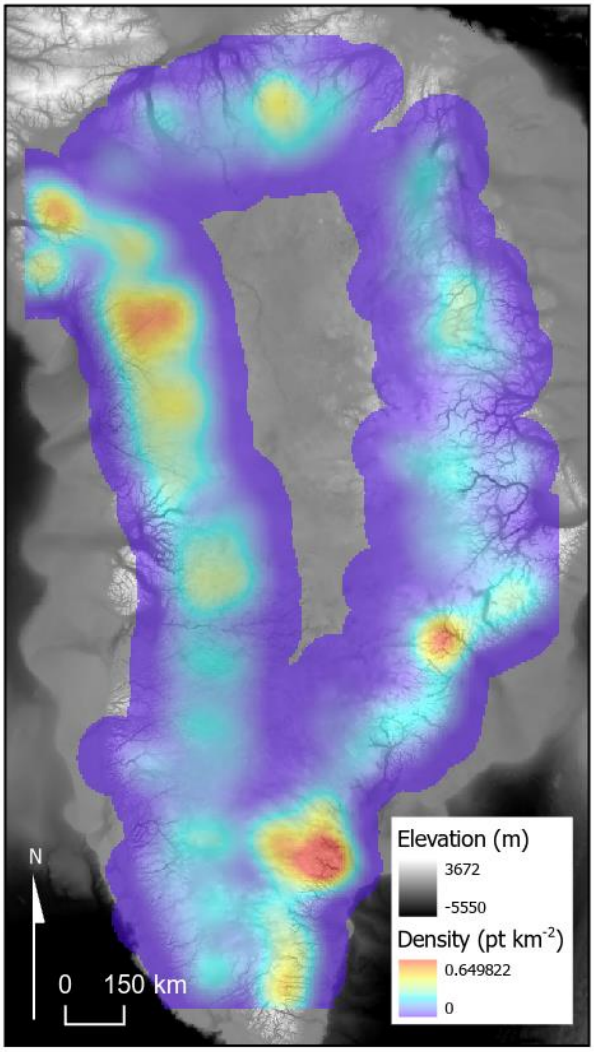

Figure 6.4 Kernel density output for the central flowline dataset. The colour gradient shows the density of central flowline dataset points (in points per km²), the background DEM is Bed Machine bed elevation (Morlighem, 2022).

It is clear that whilst some fidelity is lost, at the ice sheet scale this visualisation of the data makes it much easier to make accurate assessment of spatial patterns. As the colour scale is being used to represent the point density in a kernel density map, it does mean that to

represent the different seasonal velocity typologies requires that that dataset is split into subsets and one kernel density output is produced for each seasonal velocity typology for each year of interest. Having the data represented as raster kernel density outputs also enables other modes of analysis. The kernel density layers calculated for each seasonal velocity typology were normalised by dividing them by the total central flowline dataset point kernel density layer to give a value of the percentage of each typology in each cell in the raster. This then also allows analysis of the spatial change in prevalence of different typologies in different years (for example between low and high melt years), by differencing rasters of typology prevalence.

6.3 Results

The structure of the results will be split into two sub-sections. Firstly, the spatial patterns in seasonal velocity typology will be presented, both for the overdeepening dataset and the central flowline dataset. Following this, patterns in the temporal distribution will be presented for both datasets.

6.3.1 Spatial patterns in seasonal velocity typology

6.3.1.1 Overdeepening dataset

The data presented in this section is aligned with SQ6 *What are the spatial variations in seasonal velocity typology across the GrIS?* and specifically concerns the velocity typology within overdeepenings (i.e. adverse and normal slopes of the overdeepenings in the mapped overdeepening dataset; Chapter 3).

There is substantial variation in the spatial distribution of different seasonal velocity typologies in the overdeepening dataset. Along the south and south west coasts there is almost complete dominance of T3 and T21 up to approximately 67°N. The highest combined T3 and T21 levels are seen in the south west (66.9% of region total) and central west (48.4% of region total) regions (Figure 6.6). On the west coast north of 68°N T2 and T23 become the dominant typologies. T3 remains frequent north of 68°N but with the distribution skewing west, closer towards the ice margin. Along the north coast most overdeepenings show a dominance of T2 and T23 typology, with some overdeepenings classified as either T21, T3 or

T4 in a minority of years. Only one overdeepening (at approximately 33°W) along the north coast has a T21 or T3 typology in a majority of years. If T2 and T23 percentages are combined (as these typologies are similar variations of one another, as discussed in Chapter 5) these values represent a majority of the total in the north west (50.7%), the north (65.1%), and the north east (54.4%) regions (Figure 6.6).

In general, very few overdeepenings exhibit T4 as their dominant typology, but there is an even and consistent distribution across the study area of overdeepenings that display T4 in some years. The exception to this pattern is in the region between 67°N and 73°N on the east coast where 10 overdeepenings (approximately 15% of all overdeepenings in this region) are classified as T4 for half of years or more (Figure 6.5). In total, 13.3% of all overdeepening typologies identified in the south east region and 12.3% in the central east region are T4 (Figure 6.6), the highest two of the seven regions.

T21 is much less prevalent on the east than on the west with very few overdeepenings of this typology in this area. In regional percentage terms, T21 is focused in the centre and south of the west coast (24.2% and 21.9% of regional totals respectively) with fewer T21 overdeepenings in the north west (7.8%). In contrast, the opposite pattern is seen on the east coast. Set against an overall low level of T21 on the east coast as a whole, the north east shows a higher level of T21 (14.8%) than the centre east (7.2%) or the south east (2.0%).

T1 is evenly and consistently distributed along the west coast north of 70°N, but at much lower density than seen on the east coast. There is very little prevalence of T1 south of 70°N on the west coast, or on the north coast (Figure 6.5). T1 prevalence is much higher on the east coast representing 14.1% of the total in the centre west and 18.9% in the south east (Figure 6.6).

There is an extremely low number of overdeepenings classified as T5. With the exception of the north east region, (2.2% T5), regional T5 prevalence is below 1%.

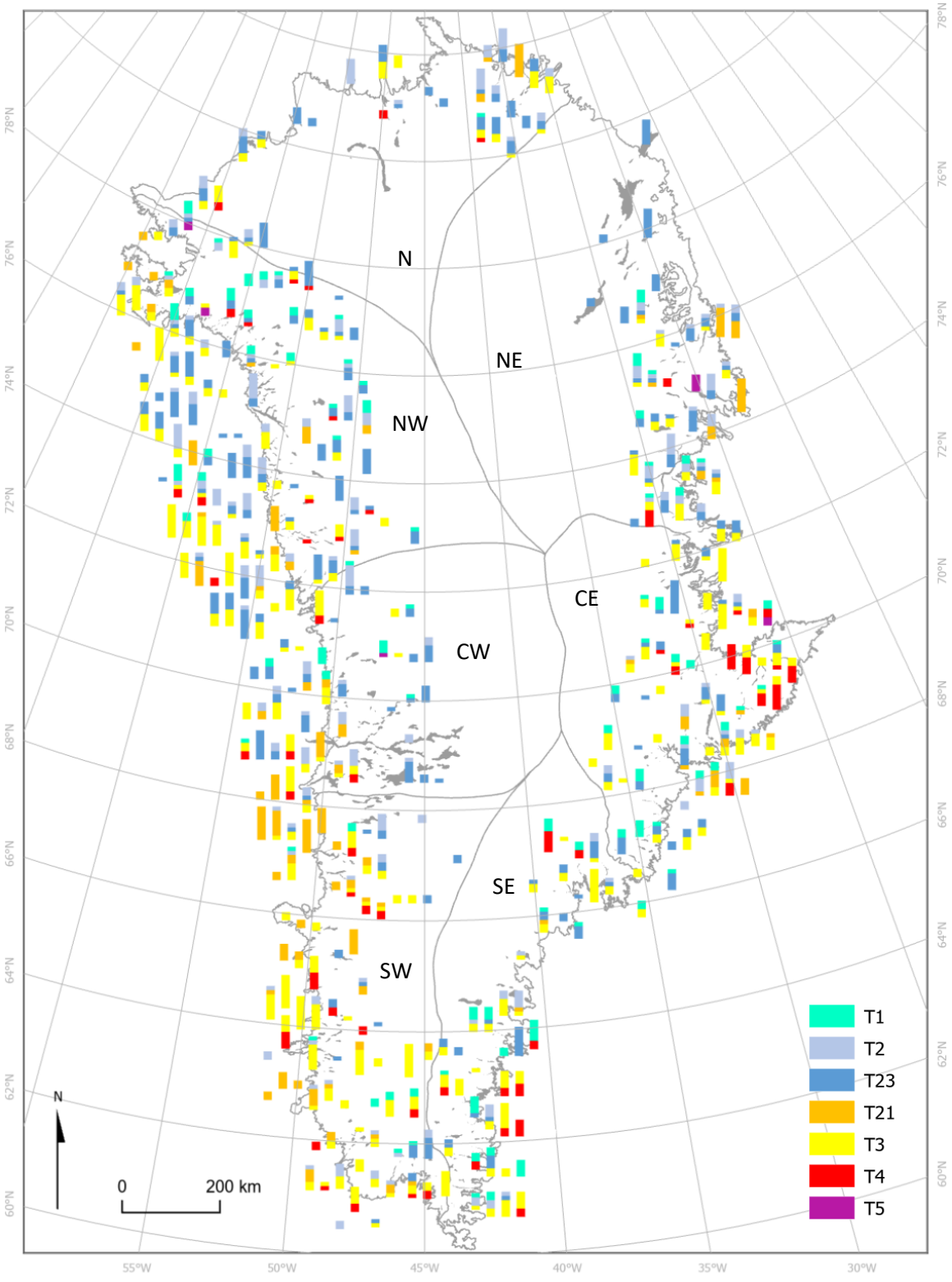

Figure 6.5 Seasonal velocity typology for each overdeepening for the period 2016 – 2019. Each overdeepening is represented by a stacked bar graph. Bar graphs have up to eight values, four for the normal slope (one for each year) and four for the adverse slope of each overdeepening. Overdeepenings that have incomplete velocity data for some years will have bar graphs of reduced height. The grey boundaries mark the regions referred to in the text (regions boundaries reworked from Mouginot et al. (2019)). Overdeepenings mapped in Chapter 3 are shown in light grey. The location of the bars on the map are illustrative only and do not precisely represent the location of the overdeepenings. The 'prevent chart overlap' function was used in ArcGIS Pro v3.2.0 to automatically reposition bars to optimise their position. This means that the relative position of the bars to one another should be accurate and allow broad spatial patterns to be inferred, but not

the absolute distance to the margin or other points. This distortion will be more pronounced in areas where overdeepenings are more densely located.

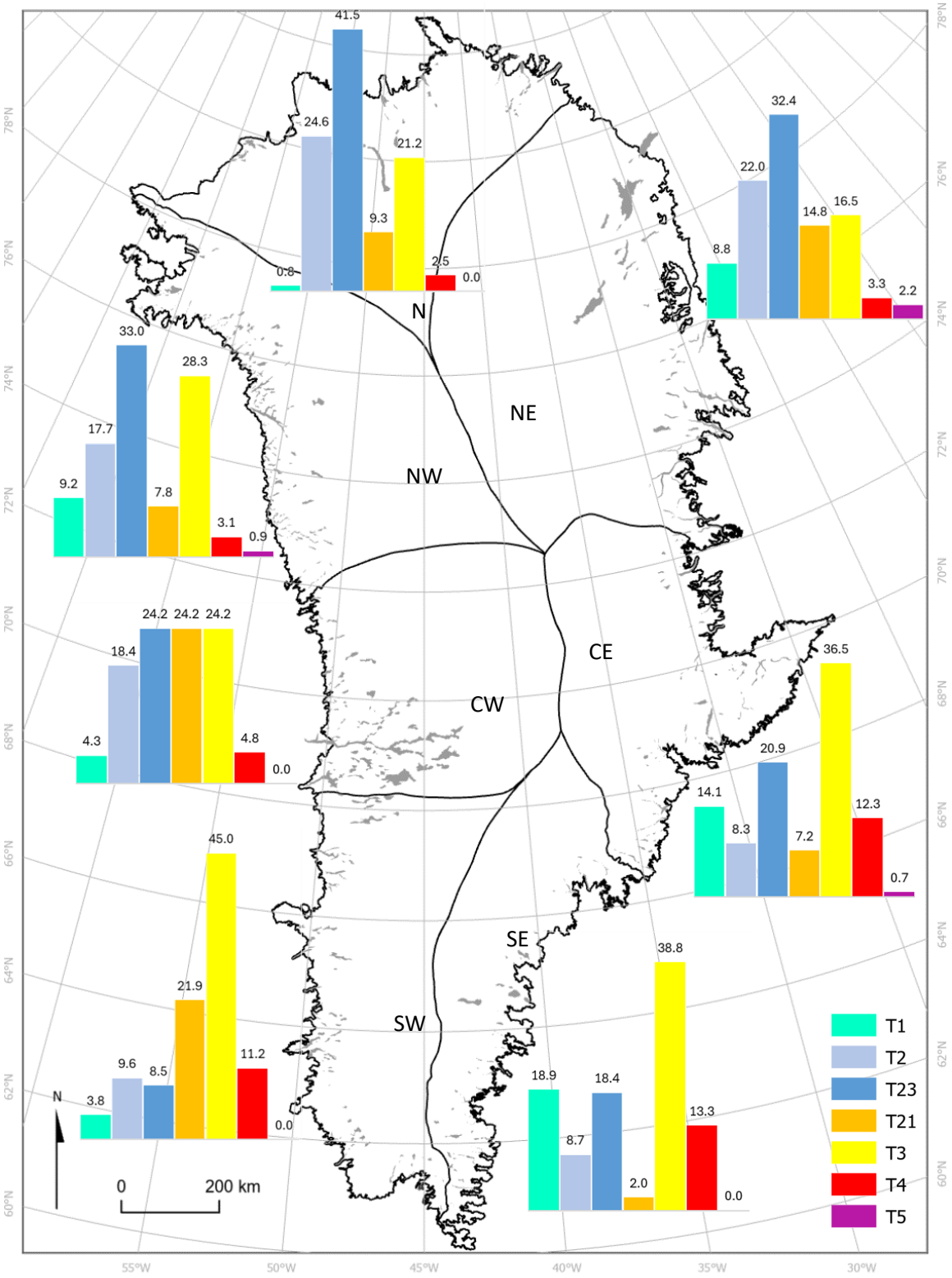

Figure 6.6 Seasonal velocity typology prevalence for the overdeepening dataset for the period 2016 – 2019. The data for individual overdeepenings in each year has been aggregated by region. Values shown on the bar graphs are the percentage of data points of each typology in each region (regions boundaries reworked from Mouginot et al. (2019)). Overdeepenings mapped in Chapter 3 are shown in light grey.

6.3.1.2 Central flowline dataset

The data presented in this section is aligned with SQ6 *What are the spatial variations in seasonal velocity typology across the GrIS?* but in this case the data covers the full study area across all central flowlines, where data met the quality threshold, and is therefore not restricted to points inside mapped overdeepenings.

The results presented in Chapter 5 showed that there was a substantial variation in the prevalence of different seasonal velocity typologies for the central flowline dataset (T1 = 2.0%, T2 = 26.1%, T21 = 18.5%, T3 = 22.6%, T4 = 27.1%, T5 = 3.7%). There is also substantial spatial variation in the distribution of these typologies across the study area.

T1 has the highest level of spatial variation of all typlogies in terms of distribution across the study area. Considered in isolation from other typologies (Figure 6.7a) there are higher densities in the north east, small patches of higher density in the north west and south east, but very little occurrence for most of the study area. This pattern is exacerbated when the data is normalised to percentage of total central flowline dataset points (Figure 6.7b).

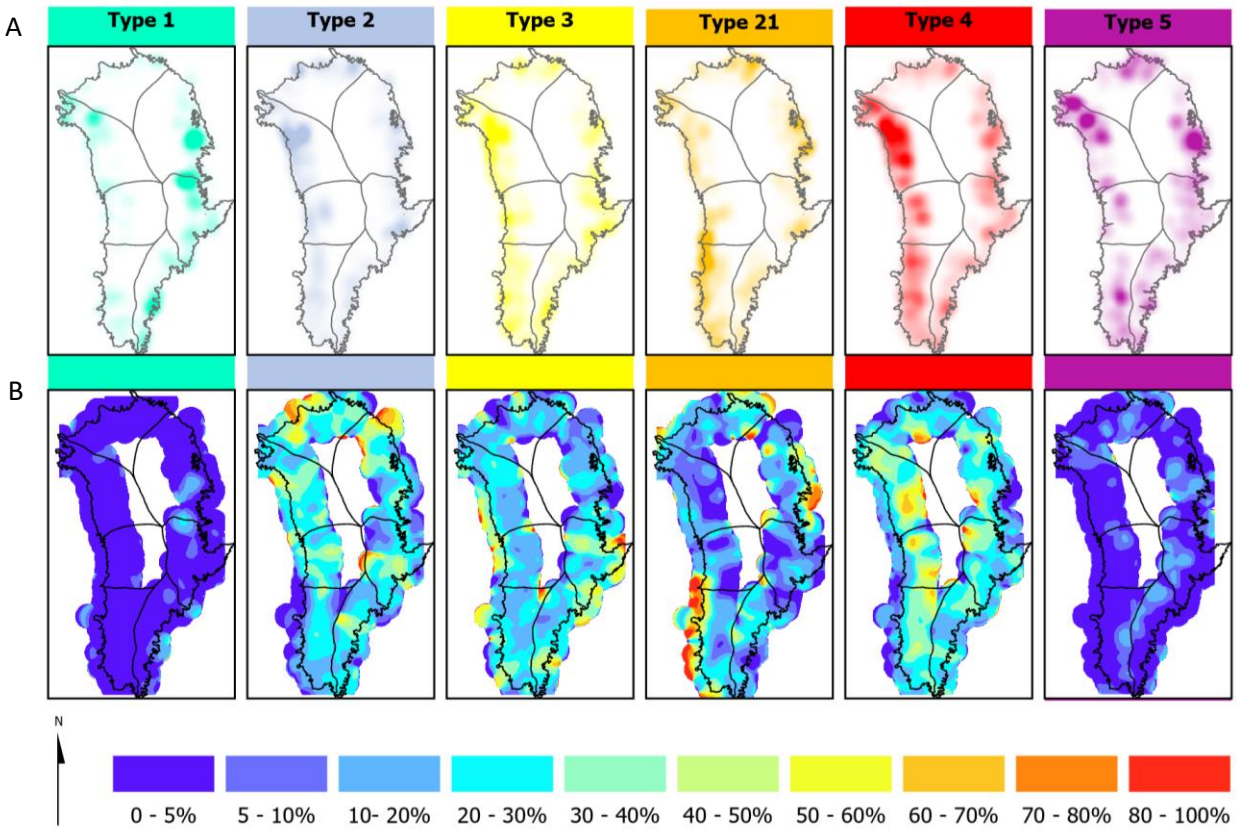

Figure 6.7 Seasonal velocity typologies for all central flowline points (2016-2019) visualised by kernel density analysis for each type. Outline of GrIS adapted from Mouginot et al. (2019)Mouginot et al. (2019) A) Panels on the top row illustrate the overall density and spread of points in each typology. Colours match those used to represent each typology in Chapter 5. Note – this data is not normalised and so the relative density of different typologies is not comparable between panels. B) The data in the bottom row of panels has been normalised to show the percentage of total central flowline point density made up by the individual typology at a given location.

All other typologies are present to some extent across the study area, but with substantial spatial variation in the density of occurrence.

T2 is relatively prevalent (approx. 20-50% of total central flowline dataset points) across most of the centre west and north west regions. There are also more isolated hotspots of up to 50-60% prevalence in the centre east and south east regions. T2 is the dominant typology across most of the north region consistantly making up 50-70% of total central flowline data points (Figure 6.7b). .

T3 is present across most regions, but with lower overall prevalence in the north and north east. The distribution within regions is skewed heavily towards the margin within only relatively isolated hotspots of higher prevalence located further inland (Figure 6.7b). .

T21 has the most uneven spatial distribution of all the typologies. There is intense clustering of T21 in the south west and north east areas with T21 prevalence of up to 70-100%. As with the pattern of T3 distribution, areas of high T21 prevalence are heavily skewed towards the margin, with only more isloated hotspots observed further inland (Figure 6.7b). .

T4 is perhaps the most evenly distributed typology over the study area as a whole. Overall prevalence is higher all along the west, and slightly lower in the south east and north. Converse to the patterns seen for T3 and T21, the distribution of T4 within regions is skewed inland, with lower realtive prevalence closer to the margin of the ice sheet (Figure 6.7b). .

T5 is a much less dominant typology but with consistant occurrence in the east and north. As was seen for T4, the distribution of T5 within regions is skewed inland, with lower realtive prevalence closer to the margin (Figure 6.7b).

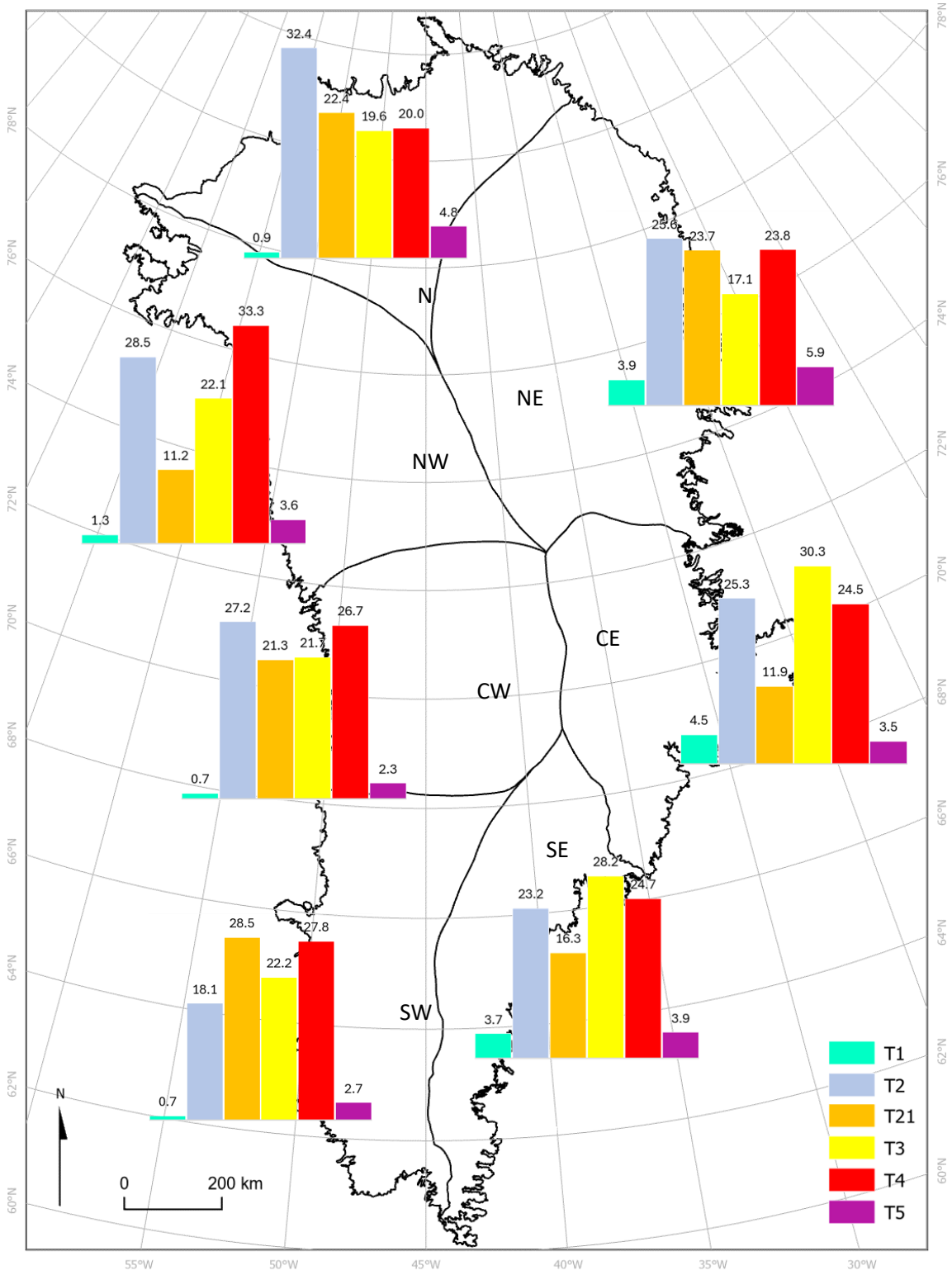

Figure 6.8 Seasonal velocity typology prevalence for the central flowline dataset for the period 2016 – 2019. The data for individual points in each year has been aggregated by region. Values shown on the bar graphs are the percentage of data points of each typology in each region (regions boundaries reworked from Mouginot et al. (2019)).

6.3.1.3 Typologies of variation in seasonal velocity response between normal and adverse slopes of overdeepenings

This section (and 6.3.1.4) presents the results of the cluster analysis (see section 6.2.6) and is aligned with SQ3 *Is there a variation in the magnitude of ice velocity speedup or slowdown within the seasonal velocity typology of an overdeepening when comparing the normal and adverse slopes?* In short, in this section, typologies were anticipated to cluster such that they indicated consistent behaviour on adverse and normal slopes that indicated support for the conceptual model. Here the typologies of variation are presented and interpretations of what these represent given. Analysis of the spatial patterns of these clusters follows in section 6.3.1.4.

Figure 6.9 permits observation of the variation in seasonal velocity response between the adverse and normal slopes of each overdeepening in each year, and identified five distinct typologies from the eight clusters run in the K means analysis. These are summarised in Table 6.1. In the majority (61.3%) of cases, there was no difference between the seasonal velocity response on the normal and adverse slopes of an overdeepening in a given year (cluster 1, Figure 6.9).

Typologies T-A and T-B (clusters 2, 4, and 7 in Figure 6.9) are representative of situations where the normalised velocity is lower on the adverse slope than the normal slope for the majority of the year. In typology T-B the normalised velocity starts lower on the adverse slope, regains parity with the normal slope by summer, but then drops below the normal slope again in autumn and winter. There are two clusters in typology T-B, both show the same pattern of variation but in cluster 2 this is more pronounced and in cluster 7 it is more subtle. In typology T-A (cluster 4) normalised velocity is equal on the adverse and normal slope in spring. The adverse slope velocity then drops below the normal slope in summer and autumn before returning to parity in winter.

Table 6.1 Seasonal adverse / normal slope velocity variation types identified from the K means cluster analysis.

0	'Other' class [e.g. very little variation between normal and adverse slopes]
T-A	Velocities similar in spring and winter but substantially lower on adverse slope of the overdeepening in summer and autumn.
T-B	Winter velocity starts slower on adverse slope, velocities are equal by spring, but then substantially lower velocity on adverse slope in autumn and winter.
T-C	Spring velocity starts slower on adverse slope, variation narrows through summer with autumn and winter velocities similar on both adverse and normal slopes.
T-D	Velocities similar in summer, but higher on adverse slope in spring, autumn, and winter.
T-E	Velocity similar on both adverse and normal slopes for most of the year, with the exception of summer where velocity is higher on the adverse slope.

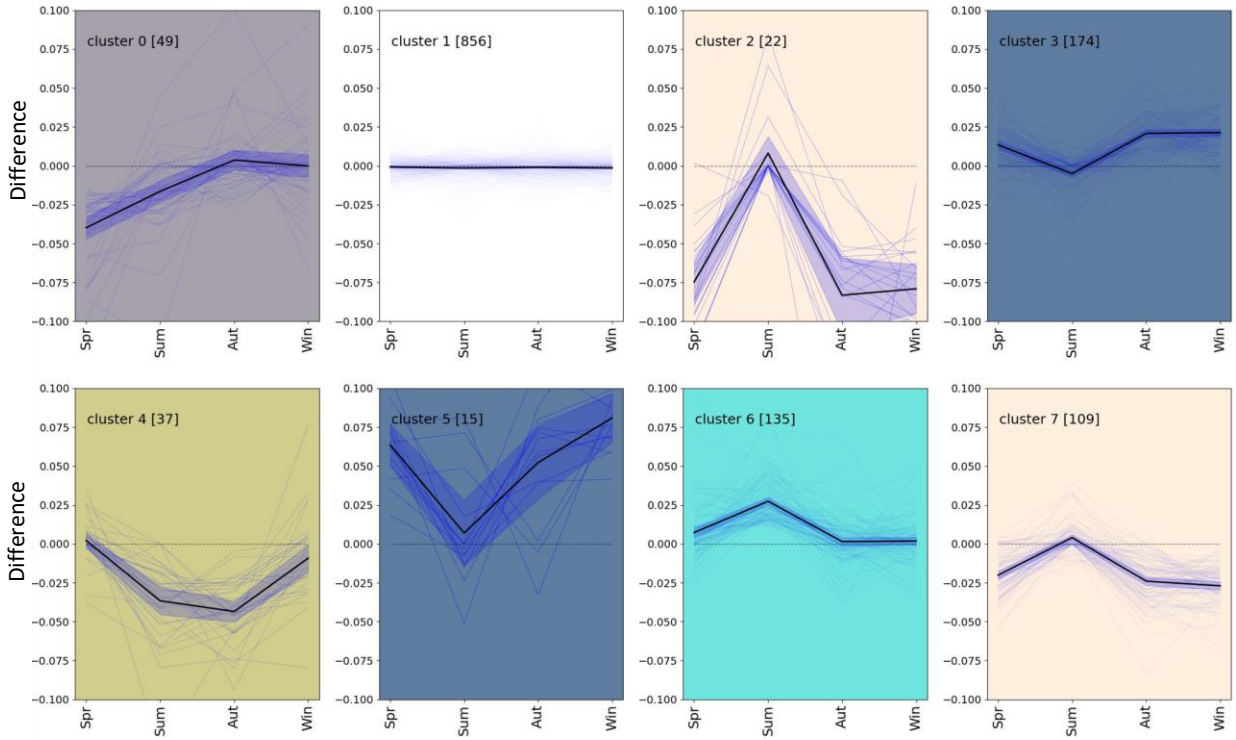

Figure 6.9 Clusters grouping typologies of seasonal velocity variation between adverse and normal slopes for the overdeepening dataset (all years combined). The values are calculated by subtracting the normalised adverse slope velocity from the normalised normal slope velocity (as used in Figure 5.7 and Figure 5.8) for each overdeepening. Negative values represent higher normalised velocity on the normal slope, positive values represent higher normalised velocity values on the adverse slope. Colours indicate the typology that each clusters has been allocated to and match the key in Table 6.1.

In overdeepenings classified as Typology T-C (cluster 0 in Figure 6.9), normalised veolocity is lower on the adverse slope in winter, but the difference then narrows through summer reaching parity (or slightly above) the normal slope velocity in autumn and winter.

Typologies T-D and T-E (clusters 3, 5 and 6 in Figure 6.9) are representative of situations where the normalised velocity is higher on the adverse slope than the normal slope for the majority of the year. In typology T-D the normalised velocity on the adverse slope is higher than on the normal slope in spring, in the summer the velocities are equal, but adverse slope velocity then exceeds the normal slope velocity in autumn and winter. There are two clusters in typology T-D, both show the same pattern of variation but in cluster 5 this is more pronounced and in cluster 3 it is more subtle (Figure 6.9). In typology T-E (cluster 6 in Figure 6.9) normalised velocity is slightly higher on the adverse slope in spring, this difference increase through to summer and then closes in autumn and winter when the normalised volocities are similar on both the normal and adverse slopes of the overdeepening.

The representation within the five typologies identified is uneven (Table 6.2). Typology T-D is dominant with nearly 35% of overdeepening data points being included in this class. A substantial proportion of overdeepening data points are also classified as typology T-B and typology T-E (24.2% and 25.1%, respectively). Typology T-A and typology T-C are much less common (6.9% and 9.1%, respectively).

Table 6.2 Prevalence of each typology of adverse / normal slope seasonal velocity response variation. Values show the percentage of overdeepening data points across the four study years classified as each typology (as shown in Figure 6.9 and Table 6.1)

Typology	T-A	T-B	T-C	T-D	T-E
Prevalence	**6.9%**	**24.2%**	**9.1%**	**34.8%**	**25.1%**

6.3.1.4 Spatial patterns in adverse / normal slope typologies of variation in seasonal velocity response.

The distribution of typologies of adverse / normal slope variation in seasonal velocity response (section 6.3.1.3) is not even across the study area, and there are some spatial patterns evident in the data when visualised (Figure 6.10).

There is a north / south pattern in the prevalence of T-D. The NW, N, and NE regions all have higher than average (34.8%) occurrence (38.6%, 70.4%, and 38.3%, respectively). CW and CE regions have slightly below average T-D prevalence (31.5% and 30.9%, respectively), and the SW and SE regions have the lowest prevalence (28.2% and 22.0%, respectively) (Figure

6.11).

T-E shows above average (24.2%) prevalence in the CE, SE, and SW regions (39.4%, 30.5%, and 26.9%, respectively), and below average prevalence in the CW, NW, N, and NE regions (18.5%, 22.3%, 11.1%, and 15.0%, respectively) (Figure 6.11). This pattern is the same for T-A; above average (6.9%) prevalence in the CE, SE, and SW regions (7.4%, 15.3%, and 14.1% respectively), and below average prevalence in the CW, NW, N, and NE regions (0.0%, 3.6%, 3.7%, and 5.0%, respectively) (Figure 6.11).

There is substantial differences in prevalence between regions for T-B, but the spatially patterns appear to have a less obvious or consistant north / south, east / west skews. In the centre and south the typology B rates are much higher on the west than the east (CW = 46.3%, SW = 29.5%, CE = 11.7%, SE = 11.9%), but in the NW and NE this pattern is reversed (24.7% and 33.3%, respectively). The N region has the lowest prevalece of T-B (11.1%) (Figure 6.11). T-C shows a similar pattern, but flipped along the east / west axis; above average (9.1%) prevalence in the SE and CE (20.3% and 10.6%, repsectively) and below average prevalence in the SW and CW (1.3% and 3.7%, respectively). This then switches with above average in the NW (10.8%) and below average in the NE (8.3%). Prevalence in the N region is 3.7%) (Figure 6.11).

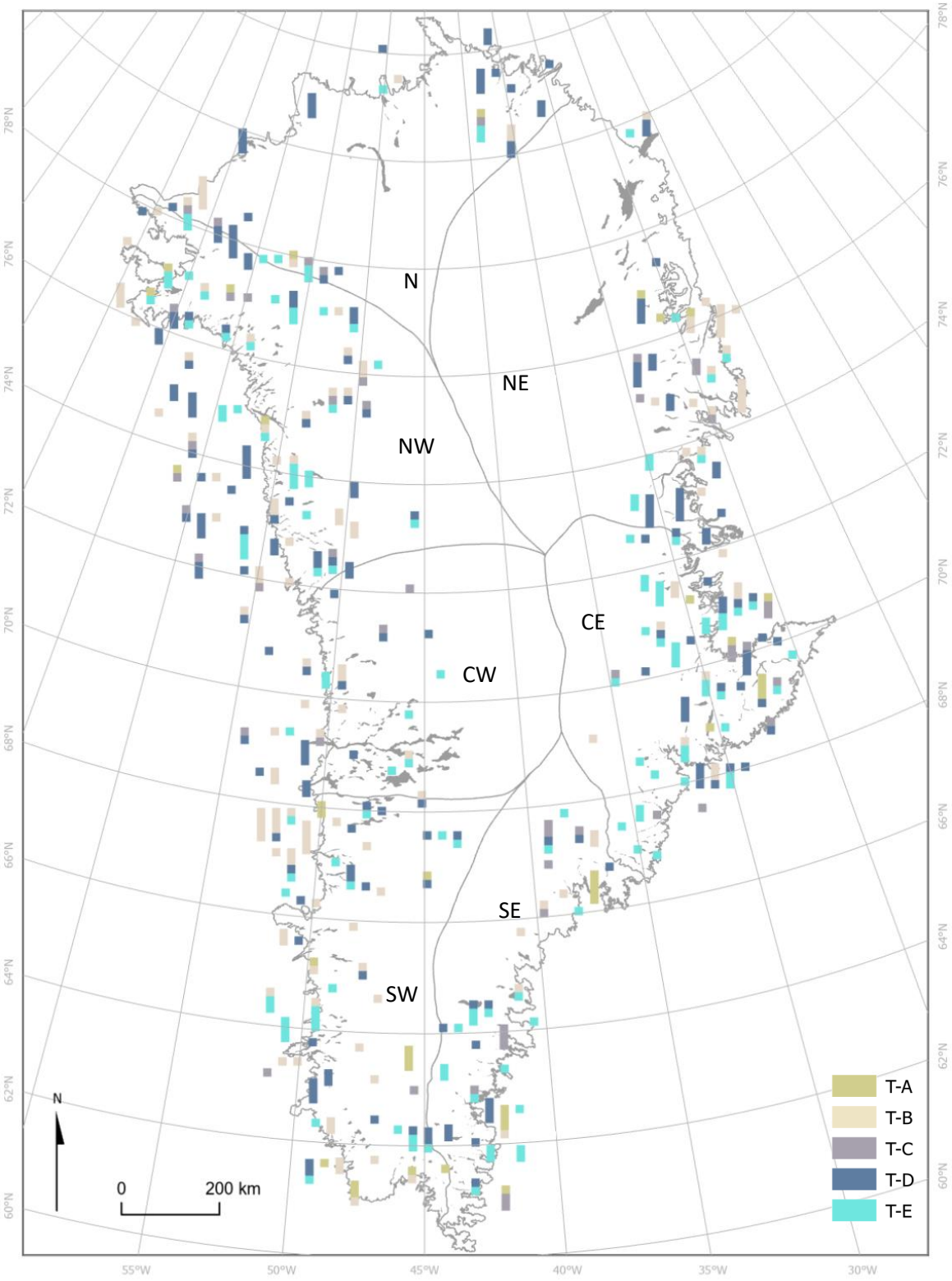

Figure 6.10 Seasonal velocity variation type for each overdeepening for the period 2016 – 2019. Each overdeepening is represented by a stacked bar graph. Bar graphs have up to four values, one for each year. Overdeepenings that have incomplete velocity data for some years, or where there is no variation between normal and adverse slopes will have bar graphs of reduced height.

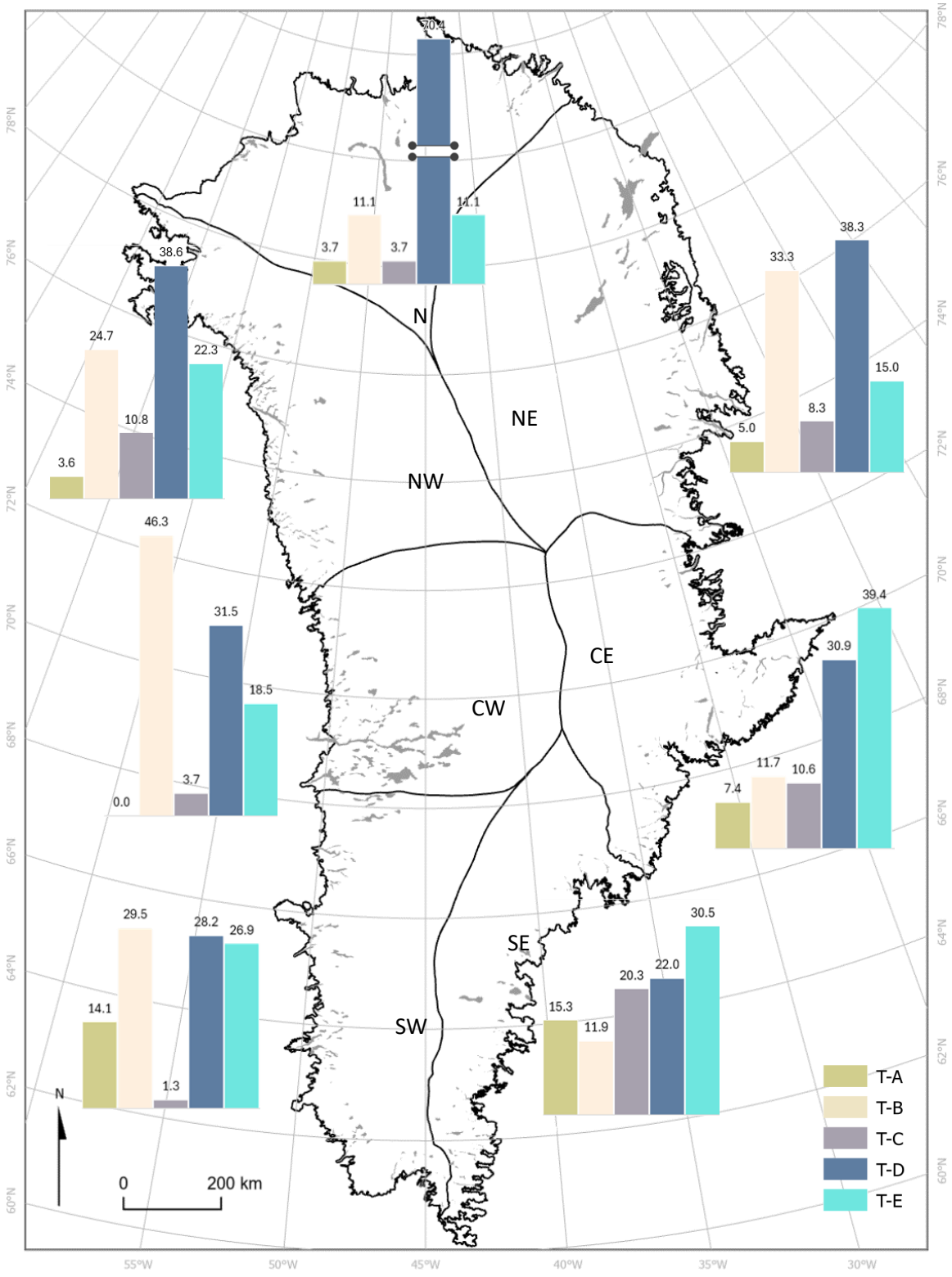

Figure 6.11 Seasonal velocity normal / adverse slope variation typology prevalence for the central flowline dataset for the period 2016 – 2019. The data for individual overdeepenings in each year has been aggregated by region. Values shown on the bar graphs are the percentage of data points of each typology in each region (regions boundaries reworked from Mouginot et al. (2019)).

6.3.1.5 Relationships between seasonal velocity typology and runoff, elevation, and latitude.

The data presented in this section are aligned with SQ5 *What role does surface runoff play in seasonal velocity typology?* For this section, data have been analysed in order to permit observations regarding the relationship between velocity typology and runoff, elevation, and latitude, for both the overdeepening dataset and the central flowline dataset. In this section the central flowline dataset and the overdeepening dataset will be presented together rather than split into separate sections.

There is a clear relationship evident between the prevalence of some seasonal velocity typologies and summer runoff. As runoff increases, the proportion of T21 and T3 also increases. This is seen for both the central flowline and overdeepening datasets (Figure 6.12a-d). The logistic regression analysis shows that these relationships are statistically significant at a 99% confidence interval (Table 6.3 and Table 6.4). A logistical regression analysis allows the quantification of the increase (or decrease) in the odds of a data point being classified as a given typology per increase in unit runoff. This is given by the equation:

$$e^{\beta} - 1 \qquad \text{(EQ 1)}$$

where β is equal to the logistic regression coefficient (Roncek, 1991; Cameron and Trivedi, 2013).

It follows therefore, that for the coefficient of 0.0004 for T21 for the central flowline dataset, every 1,000 mm increase in summer runoff is associated with a 40% increase in the likelihood of a data point being classified as T21. The coefficient of 0.0003 for T3 for the central flowline dataset indicates that every 1,000 mm increase in summer runoff is associated with a 30% increase in the likelihood of a data point being classified as T3. The prevalence of T21 and T3 for the overdeepening dataset are also positively correlated with runoff. The slightly higher coefficients of 0.0005 for T21 and 0.0004 for T3 are associated with 50% and 40% increases per 1,000 mm increase in summer runoff in the likelihood of being classified as being of those typologies. In addition to the overarching positive

correlation between runoff and T21 / T3 prevalence, when visualised using deciles to bin runoff values on the graphs (Figure 6.12b and Figure 6.12c) both datasets appear to show stable prevalence of T21 /T3 typologies which do not increase with increasing runoff values until a threshold of approximately 300 – 500 mm water equivalent is exceeded. It is once this threshold is exceeded (forth stacked bar form the left on both Figure 6.12b and Figure 6.12c) that T21 / T3 prevalence starts to increase with runoff.

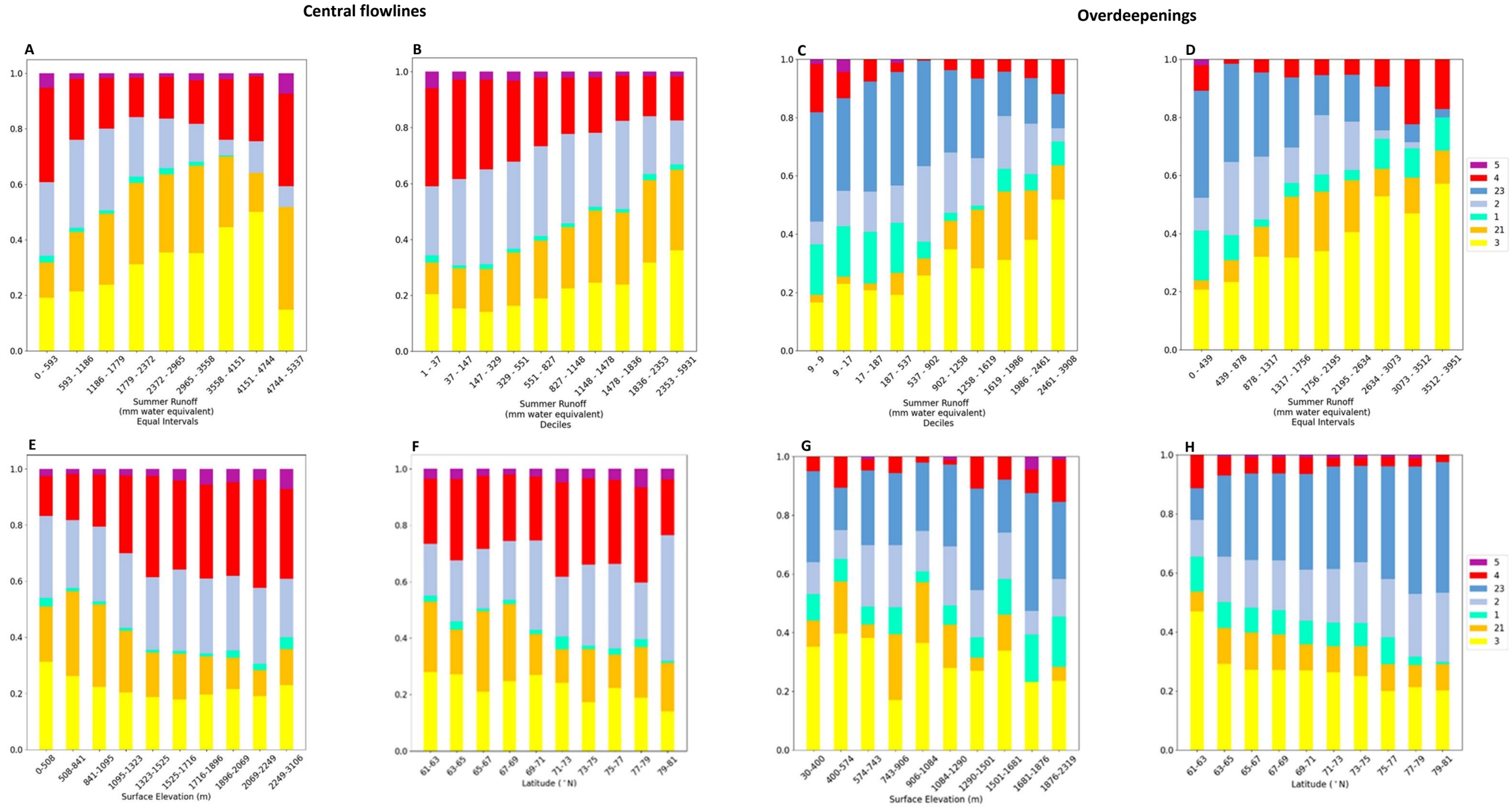

Figure 6.12 Stacked bar charts showing the proportion of seasonal velocity typologies for different levels of melt (A, B, C, D), surface elevation (E & G), and latitude (F & H). A, B, E & F show data for the central flowline dataset, C, D, G & H show data for the overdeepening dataset.

Table 6.3 Logistic regression analysis of summer runoff against typology for the central flowline dataset

Typology	**1**	**2**	**21**	**3**	**4**	**5**
Coefficient	**-0.0001**	**-0.0001**	**0.0004**	**0.0003**	**-0.0005**	**-0.0006**
P value	0.000	0.000	0.000	0.000	0.000	0.000

Table 6.4 Logistic regression analysis of summer runoff against typology for the overdeepening dataset

Typology	**1**	**2**	**23**	**21**	**3**	**4**	**5**
Coefficient	**-0.0004**	-0.0001	**-0.0005**	**0.0005**	**0.0004**	0.0001	**-0.0042**
P value	0.000	0.054	0.000	0.000	0.000	0.144	0.021

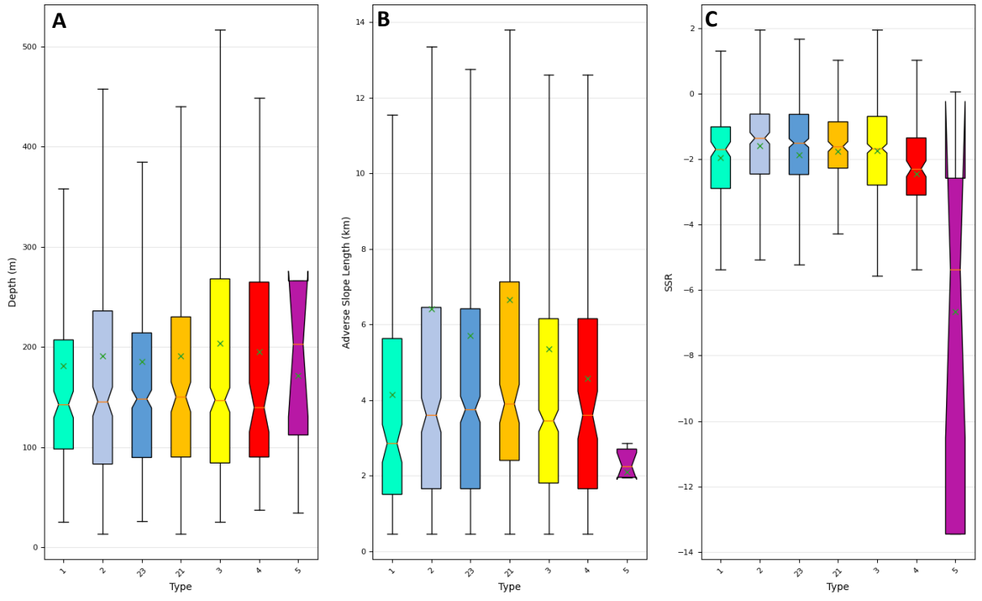

Figure 6.13 Morphometric analysis of all overdeepenings. Line = median, x = mean, notches = 95% CI, box = IQR

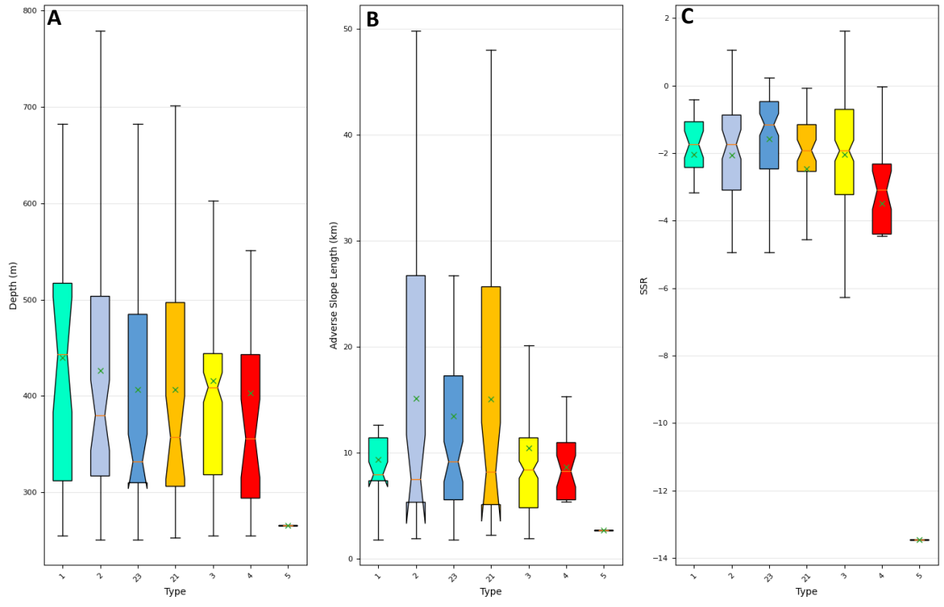

Figure 6.14 Morphometric analysis of the subset of overdeepenings that are over 250 m in depth.

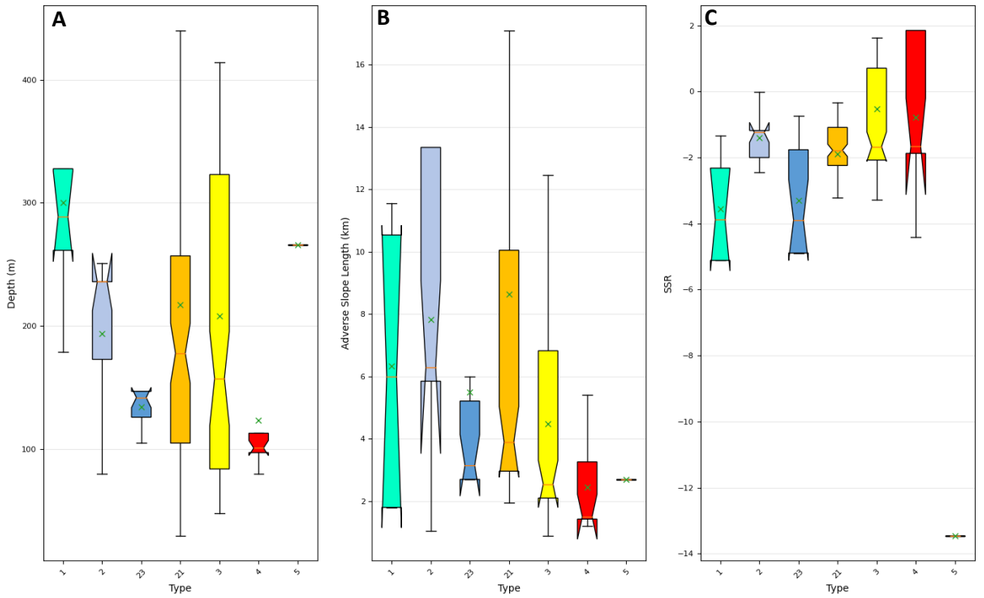

Figure 6.15 Morphometric analysis of the subset of overdeepenings which have a consistent seasonal velocity typology type across all years for which there is data. Number of ODs in each class is as follows: T1 = 3, T2 = 6, T23 = 5, T21 = 23, T3 = 21, T4 = 5, T5 = 1.

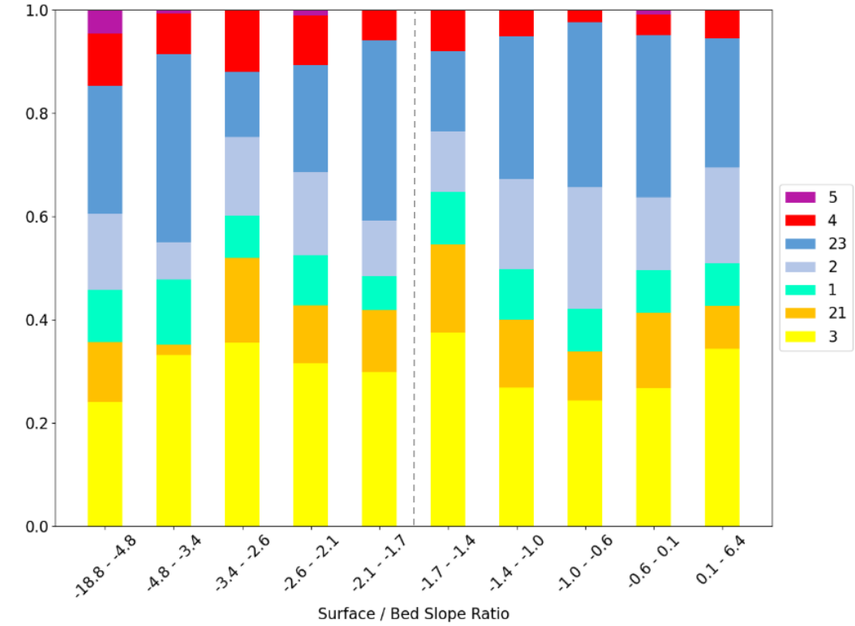

Figure 6.16 Stacked bar chart showing the proportion of seasonal velocity typologies for different ranges of surface / bed slope ratio. Dashed grey line marks the approximate value of the supercooling threshold.

The strongest correlation between summer runoff and any of the seasonal velocity typologies is for T5 with coefficients of -0.0006 for the central flowline dataset and -0.0042 for the overdeepening dataset (Table 6.3 and Table 6.4). T5 shows a negative correlation with increasing summer runoff with each 1,000 mm increase in runoff associated with a 60% decrease in the likelihood of a data point in the central flowline dataset being classified as T5, and a decrease of 421% in the likelihood of a data point in the overdeepening dataset being classified as T5. The correlation for the central flowline dataset is significant at a 99% confidence interval, the correlation for the overdeepening dataset is significant at a 95% confidence interval.

T1 has a statistically significant (99% confidence interval) negative correlation with runoff for both datasets. The coefficient is relatively low for the central flowline dataset (-0.0001) giving a decrease of only 10% in the likelihood of a data point being classified as T1 per 1,000 mm of increase in runoff (Table 6.3). For the overdeepening dataset the coefficient is -0.0004 giving a decrease of 40% in the likelihood of a data point being classified as T1 per 1,000 mm of increase in runoff (Table 6.4).

T4 has a statistically significant (99% confidence interval) negative correlation with runoff for the central flowline dataset, but the relationship is not statistically significant for the overdeepening dataset. The shape of the data for T4 for the overdeepening dataset (Figure 6.12c and Figure 6.12d) suggests that there could be a more complex, non-linear relationship with runoff. T4 prevalence appears higher for extreme lows and highs of runoff, decreasing to a minimum near median runoff around the central bars of the graphs. The coefficient for the central flowline dataset is -0.0005 giving a decrease of 50% in the likelihood of a data point being classified as T4 per 1,000 mm of increase in runoff (Table 6.3).

T2 has a statistically significant (99% confidence interval) negative correlation with runoff for the central flowline dataset, but the relationship is not statistically significant for the overdeepening dataset. However, the relationship between T23 and summer runoff is significant (99% confidence interval) for the overdeepening dataset. T23 is not represented within the central flowline dataset. The coefficient for the central flowline dataset is relatively low (-0.0001) giving a decrease of 10% in the likelihood of a data point being classified as T2 per 1,000 mm of increase in runoff (Table 6.3). The coefficient for the overdeepening dataset is relatively high (-0.0005) giving a decrease of 50% in the likelihood of a data point being

classified as T23 per 1,000 mm of increase in runoff (Table 6.4).

Patterns in typology prevalence broken down by latitude broadly follow the inverse of the patterns observed for runoff (Figure 6.12f, Figure 6.12h), but the relationships appear less distinct and more noisy, especially for the overdeepening dataset. T21 and T3 show a clear decrease in prevalence with increasing latitude. For the overdeepening dataset T2 and T23 show a clear increase with latitude, but the relationship for T2 for the central flowline dataset is less pronounced. T4 prevalence seems to show a consistent decrease with latitude for the overdeepening dataset with no evidence of the bimodal type distribution associated with runoff. T4 and T5 for the central flowline dataset show no clear patterns with respect to latitude.

Patterns in typology prevalence broken down by surface elevation follow the inverse of the patterns observed for runoff almost exactly for the central flowline dataset (Figure 6.12e). For the overdeepening dataset the break down by surface elevation (Figure 6.12g) is very noisy with no clear patterns evident.

6.3.1.6 Relationships between seasonal velocity typology and overdeepening morphometrics

The data presented in this section is aligned with SQ1 *Is there a relationship between overdeepening morphometry (specifically* BSSR*) and seasonal velocity typology?* As it relates specifically to the overdeepening morphometry data, only data from the overdeepening dataset is presented.

Analysis of the complete overdeepening dataset reveals relatively little variation in the depth, adverse slope length, and BSSR between different seasonal velocity typologies (Figure 6.13). In terms of overdeepening depth, there is some variation in mean depth of each typology, but the medians are very similar and the 95% confidence intervals (illustrated by the notches on the boxplots) overlap for all typologies (Figure 6.13a). Variations in adverse slope length are greater than for depth (Figure 6.13b). The 95% confidence intervals for the typologies with the two longest adverse slope lengths (T21 and T23) do not overlap with the two typologies with the shortest adverse slope lengths (T1 and T5) indicating a statistically significant difference between the adverse slope lengths of these typologies. T5 has the shortest adverse slope length of all typologies and the 95% confidence interval does not overlap with that of any of the other typologies. However, it is challenging to draw meaningful inference about T5 due to

the very low number of overdeepenings of this typology and as such, no further commentary will be given to it here.

Mean and median BSSRs for typologies T1, T2, T23, T21 and T3 are all between -1.2 to -2, around the supercooling threshold. The 95% confidence intervals of all these classes overlap. The average BSSR for T4 is lower at approximately -2.5 and the confidence interval does not overlap any of the other typologies suggesting a statistically significant difference. T4 is also the only typology where the entire range of the 95% confidence interval is below the supercooling threshold. Figure 6.16 shows the breakdown of typology prevalence for a range of BSSRs. T4 shows a general trend of increasing prevalence as BSSR increases, but no other typologies show any clear trend, and there is no marked difference in typology prevalence breakdown above or below the supercooling threshold.

To explore the possibility of stronger relationships between overdeepening morphology and seasonal velocity typology in more prominent overdeepenings, the dataset was filtered to only include overdeepenings when thresholds for each morphometric parameter were exceeded. A range of permutations and combinations of thresholds were tested, but no clear patterns were identified as a result. One such example is shown in Figure 6.14 where a threshold overdeepening depth of 250 m has been specified. Overdeepenings which show a consistent seasonal velocity typology in all years were also isolated for analysis (Figure 6.15). This subset of data was challenging to analyse due to the low numbers of overdeepenings showing a consistent typology across years for some typologies. Perhaps of most interest here was not actually in the pattens in the morphometry of overdeepeinings of consistent typology across years, but the variation in how common it was for different typologies to be the sole typology of an overdeepening. T1, T2, T23, T4, and T5 all had low numbers of overdeepenings (3, 6, 5, 5 and 1 respectively) consistently of that typology. T21 and T3 had high numbers of overdeepenings consistently of those typologies (23 and 21 respectively). A such, in terms of overdeepenings that always have a consistent seasonal velocity typology, T21 and T3 combined make up 68.8% of overdeepenings with a consistent typology, despite only making up 42.5% of total data points in the complete overdeepening dataset.

6.3.1.7 Relationships between typologies of adverse / normal slope variation in seasonal velocity response and overdeepening morphometrics.

The data presented in this section is aligned with SQ3 *Is there a variation in the magnitude of ice velocity speedup or slowdown within the seasonal velocity typology of an overdeepening when comparing the normal and adverse slopes?* Specifically, the results presented investigate whether there is a relationship between the typology of variation between the adverse and normal slope of an overdeepening (as presented in section 6.2.6) and any of the morphometric parameters measured.

Analysis of the patterns in overdeepening morphometry between the typologies of adverse / normal slope variation in velocity response showed limited systematic variation (Figure 6.17). T-A is made up of larger overdeepenings with higher average depth and adverse slope length than other typologies. However, T-A has a wide spread of data for these parameters resulting in a high level of overlap in the confidence intervals of all other typologies suggesting that these differences are not statistically significant.

T-C has the lowest average BSSR, but again, there is considerable overlap in the confidence intervals of all typologies for this metric suggesting that there are no statistically significant differences between typologies. T-C, T-D, and T-E all have their entire 95% confidence interval range below the supercooling threshold. The 95% confidence interval notches for T-A and T-B on the boxplots in Figure 6.17c are intersected by the supercooling threshold.

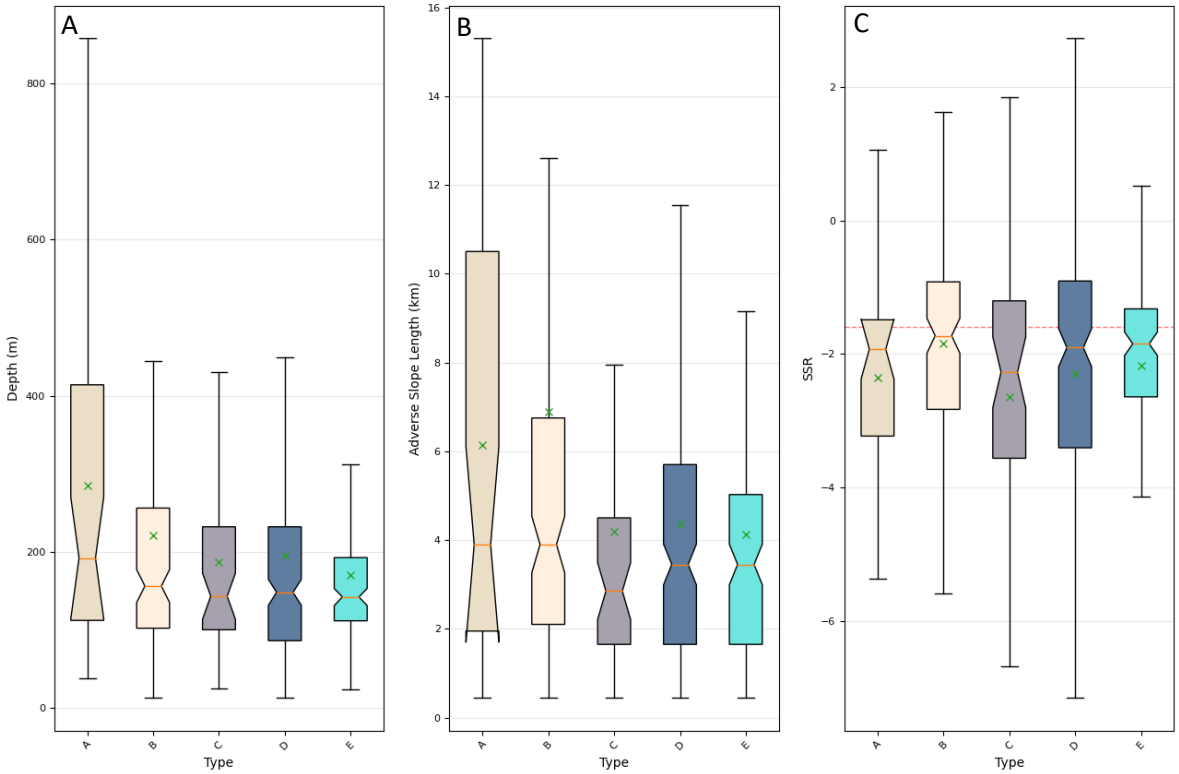

Figure 6.17 Morphometric analysis of overdeepenings grouped by normal / adverse slope variation type clusters. The dashed line in C marks -1.6, the classic theory suggested supercooling threshold value. Line = median, x = mean, notches = 95% CI, box = IQR.

6.3.2 Temporal patterns

As was established in section 6.2.4 the study period contains two relatively high melt years (2016 & 2019), and two relatively low melt years (2017 & 2018). Results from both the overdeepening and centre flowline datasets are reported simultaneously. Temporal patterns will be presented first, followed by spatiotemporal patterns.

6.3.2.1 Variations in seasonal velocity typology prevalence between years

The data presented in this section is aligned with SQ7 *What are the temporal variations in seasonal velocity typology across the GrIS?* Observations are made for both the overdeepening dataset and the central flowline dataset. The data presented in Figure 6.19 specifically relates to SQ2 *Is there a variation between the seasonal velocity typology of the normal and adverse slopes of overdeepenings?*

Figure 6.18 shows that some typologies show distinct temporal patterns linked to high and low melt years for both the central flowline and overdeepening datasets. T3 prevalence is higher in both the high melt years than the low melt years for both datasets. For the central flowline

dataset T3 is 24.0% in 2016 before dropping to 21% and then 18% in 2017 and 2018, rising back to 27% in 2019 (Table 6.5). For the overdeepening dataset T3 is 30.0% in 2016 drops to 22% in 2017, rises to 29% in 2018 and then further to 40% in 2019 (Table 6.6).

T21 shows minimal variation between years for both central flowline and overdeepening datasets and there is no consistency in the direction of changes between high and low melt years. Minimum T21 prevalence does occur in 2018 for both datasets (Table 6.5, Table 6.6).

T1 prevalence shows almost no variation between years for the central flowline dataset with values of either 2% or 3% in each year (Table 6.5). There is greater variation for the overdeepening dataset with values ranging between 5% and 14% but this does not appear linked to melt. The lowest value (5%, 2019) is in a high melt year and the highest value in a low melt year (14%, 2017), with the other high and low melt years both having a T1 prevalence of 9% (Table 6.6).

T2 is higher in both low melt years than the high melt years for the central flowline dataset rising from 23% to 30% in 2017, higher still to 32% in 2018, and then dropping back to 21% in 2019 (Table 6.5). T2 shows minimal variation between years for the overdeepening dataset, but the patterns for T23 mirror those for T2 in the central flowline dataset. T23 starts at 23% in 2016, raises to 31% and then 33% in 2017 and 2018 before falling back to 18% in 2019 (Table 6.6). As discussed in section 5.4.2.5, it is appropriate to consider T2 and T23 together as they are minor variations of very similar typologies, and the K means analysis did not identify a T23 cluster in the central flowline dataset.

T4 prevalence is higher in both the high melt years than the low melt years for both datasets. For the central flowline dataset T4 is 29% in 2016 before dropping to 24% in 2017 and then increasing to 27% in 2018, and then to 28% in 2019 (Table 6.5). For the overdeepening dataset T4 is 7% in 2016 drops to 4% in 2017, rises to 6% in 2018 and then further to 10% in 2019 (Table 6.6).

T5 shows very little variation between years for either dataset (Table 6.5, Table 6.6).

Table 6.5 Yearly seasonal velocity typology prevalence for the central flowline dataset.

Year	T3	T21	T1	T2	T23	T4	T5
2016	0.24	0.19	0.02	0.23	-	0.29	0.03
2017	0.21	0.2	0.02	0.3	-	0.24	0.04
2018	0.18	0.17	0.02	0.32	-	0.27	0.05
2019	0.27	0.18	0.03	0.21	-	0.28	0.04

Table 6.6 Yearly seasonal velocity typology prevalence for the overdeepening dataset.

Year	T3	T21	T1	T2	T23	T4	T5
2016	0.30	0.13	0.09	0.17	0.23	0.07	0.0
2017	0.22	0.13	0.14	0.16	0.31	0.04	0.0
2018	0.29	0.08	0.09	0.14	0.33	0.06	0.02
2019	0.40	0.13	0.05	0.14	0.18	0.1	0.01

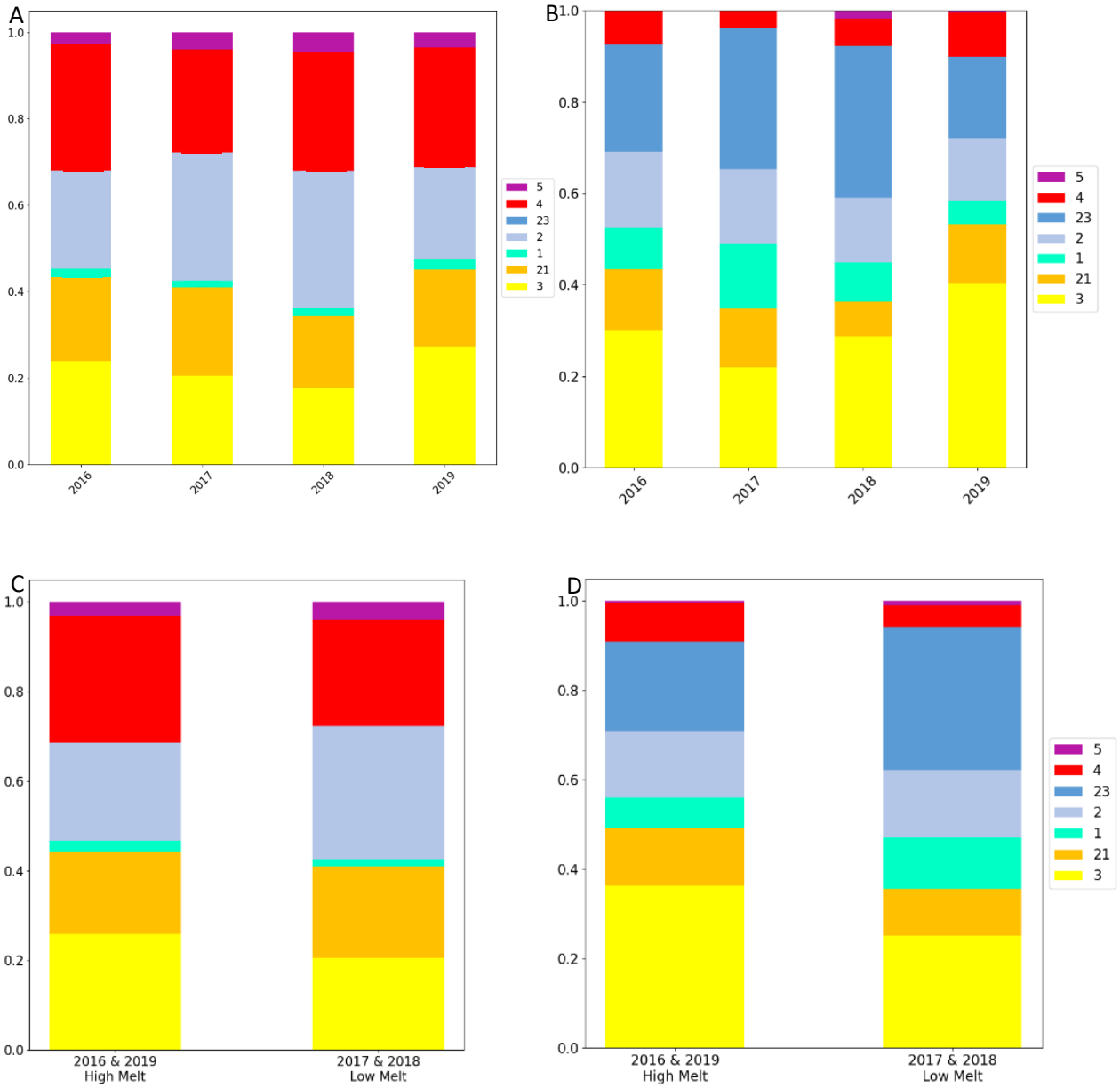

Figure 6.18 Proportion of data points classified as each seasonal velocity typology. A) Data for the central flowline dataset shown grouped by year B) Data for the central flowline dataset shown grouped by year. C) Data for the central flowline dataset shown grouped by high and low melt years (2016 & 2019 are high melt years, 2017 & 2018 are low melt years). D) Data for the overdeepening dataset shown grouped by high and low melt years.

Figure 6.19 disaggregates the data presented for the overdeepening dataset in Figure 6.18b to give separate values of typology prevalence for each year for the adverse and normal slopes of overdeepenings. The variation between normal and adverse slopes within individual years appears to be very minimal, and is certainly much lower than the overall variation in typology prevalence between years. The within year variation also shows no systematic relationship with high and low melt years. For example, T3 prevalence is very slightly higher on normal slopes than adverse slopes in one high melt year (2016), and very slightly higher on adverse slopes than normal slopes in the other high melt year (2019). The same is true in the low melt years; very slightly higher T3 prevalence on adverse slopes in

2017, but very slightly higher T3 prevalence on normal slopes in 2018.

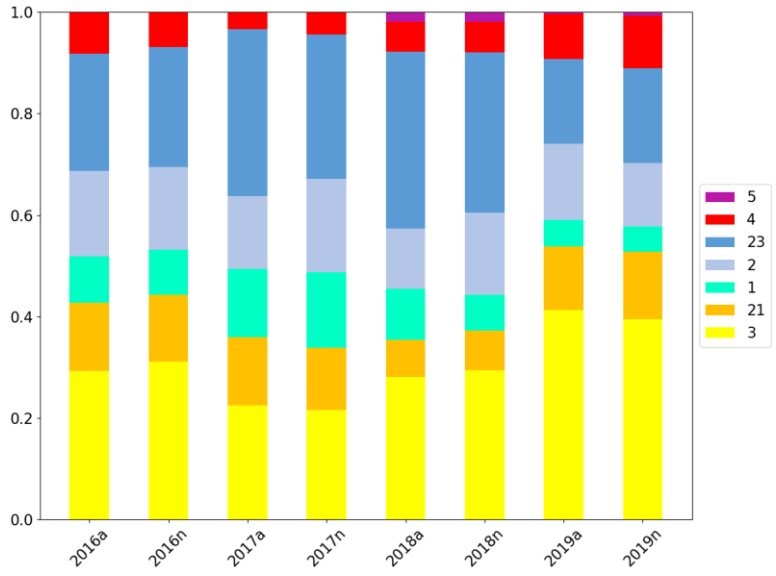

Figure 6.19 Overdeepenings are shown grouped by year, but split into subgroups of adverse and normal slopes for each year.

6.3.2.2 Spatio-temporal patterns in seasonal ice velocity typologies.

Ice sheet scale

The data presented in this section is aligned with SQ6 *What are the spatial variations in seasonal velocity typology across the GrIS?*

Figure 6.20 expands on the spatial patterns already presented for the complete central flowline dataset in aggregate (2016-2019, Figure 6.7) by subsetting out two individual years, one representative of low melt (2017) and one representative of high melt (2019). The variance between these two years is also calculated and visualised to explore where typology prevalence increases and decreases under high and low melt scenarios.

T2 is much more evenly distributed in the low melt year with some areas of 40-50% prevalence or higher across most regions of the study area, and with particularly high prevalence (>70%) in areas across the north. Substantial changes in the spatial patterns of prevalence are evident in the high melt year. Reductions in T2 prevalence of over 25% are observed in areas closest to the margin along most of the CW and NW regions, and the western half of the N region. Similar levels of reduction in T2 prevalence is observed across most of the NE and CE regions. Increases in T2 prevalence in the higher melt year of above

25% are seen in the areas closer to the interior in the CE, and NE regions, and across much of the SE region (Figure 6.20).

T3 displays concentrated areas of high prevalence interspersed between areas of very low prevalence in the low melt year. T3 prevalence is relatively high in the SE region, the southern sections of the SW and CE regions, and the interior reaches of the NW region. In the high melt year there is a substantial increase in T3 prevalence across most of the study area. Exceptions are decreases in the interior reaches of the NW and CE regions, and the SE region (Figure 6.20).

T21 prevalence shows similar spatial patterns in both the high and low melt year. There are coherent bands of high T21 prevalence running along areas closer to the margin in the SW and NE regions, and less coherent hotspots of high prevalence along the north coast. In the high melt year however, the relative T21 prevalence in the coherent band in the SW decreases significantly by over 25%. Relative prevalence also decreases in more isolated patches across much of the study area, predominantly in areas closer to the margin. Increase in relative T21 prevalence in the high melt year is observed in the upper reaches of the SE regions, and in other more isolated patches across the study area, generally closer to the interior (Figure 6.20).

Patterns of T4 distribution are broadly similar in both the high and low melt year, with T4 present in all regions with a skew to higher prevalence in areas further inland towards the interior. Prevalence increases and extends further downstream towards the margin in all regions in the higher melt year (Figure 6.20).

Prevalence of T1 and T5 show minimal variation between the high and low melt years in most areas due to their low overall prevalence. Some isolated T1 hotspots of prevalence appear on the SE coast and further inland in the CE region in the high melt year (Figure 6.20).

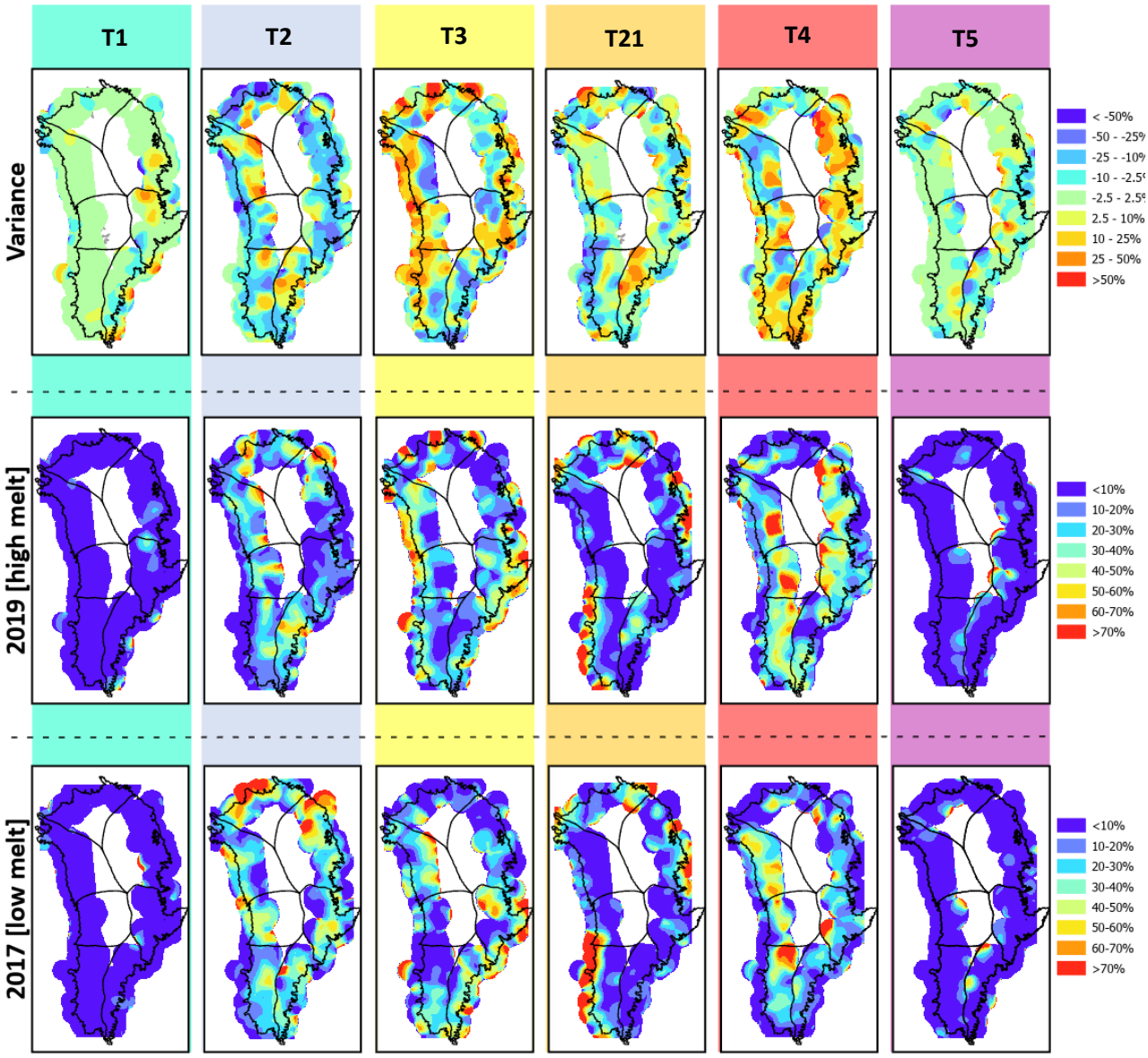

Figure 6.20 Kernal density analysis of central flowline dataset seasonal velocity types. Data shows the proportion of central flowline dataset points classified in each seasonal velocity typology at each cell in the kernel density raster for a high melt year (2019) and a low melt year (2017). The maps of variance show the 2017 values subtracted from the 2019 values – as such, hot colours show where a typology is more prevalent in 2019, cool colours where a typology is more prevalent in 2017.

6.3.2.2.1 Subregional scale examples

Implementation of the kernel density approach (as used in Figure 6.20 and Figure 6.7) is very effective for visualising and analysing the entire ice sheet as a whole, but by its very nature, this heavily reduces the original fidelity of the data and makes identification of more nuanced signals in the data very challenging. Likewise, aggregating the data and attempting

to identify broad relationships between overdeepening morphometric parameters and seasonal velocity typology using statistical approaches (such as implemented in sections 6.3.1.6 and 6.3.1.7) dilutes the signal of individual glaciers and removes some of the nuance and subtlety in the underlying data. Both approaches also fail to facilitate the possibility of more qualitatively 'reading' the ice as it flows into, through, and out of individual overdeepenings. Despite lacking the ability to identify universal process controls acting across the ice sheet, qualitative examination of individual case study areas reveals some interesting spatial and temporal patterns at a range of scales.

6.3.2.2.2 Subregional scale

The data presented in this section (and the sections on individual glaciers and individual overdeepenings that follow below) is aligned with SQ2 *Is there a variation between the seasonal velocity typology of the normal and adverse slopes of overdeepenings, or between the seasonal velocity typology of ice flowing across an overdeepening compared to ice immediately up and downstream of an overdeepening?* The seasonal velocity typology data visualised in figures is the individual points from the central flowline dataset. This is shown in relation to the overdeepenings mapped in the metric dataset in Chapter 3 to explore potential modulation of ice dynamics by overdeepenings as ice flows over them.

When the data is considered at a subregional scale (c. 2-5 glaciers) there are examples evident where there is substantial variation in the seasonal velocity typology of neighbouring glaciers. There are also examples where neighbouring glaciers demonstrate differences in how seasonal velocity typology varies between high and low melt years. Figure 6.21 illustrates three glaciers in the centre of the north coast, Steensby Gletsjer (SG), Ryder Gletsjer (RG), and C.H. Ostenfeld Gletsjer (CHG). All glaciers are at the same latitude of approximately 81.5°N and are within 150 km of one another.

In 2017 (a low melt year) all three glaciers showed different patterns of seasonal velocity typology. RG is dominated by T2 in a coherent band from the margin to approximately 45 km inland (marked area 2 on Figure 6.21a), with some patches of T3 and T21 on the east and west most streamlines respectively. Further inland beyond this band of T2 there are more concentrated areas of T4 and T3, and much less T2. In 2017 SG is dominated by T2 in the region from the margin to approximately 35 km inland (marked area 1 on Figure 6.21a),

interspersed with three small but coherent 3 bands of T21, There are isolated patches of T4 which become more dominant further inland beyond this area as well as some sporadic points of T3. CHO is formed of a larger trunk glacier flanked by two smaller / tributary glaciers. In 2017 the central trunk is completely dominated by T2 in a region from the margin to approximately 40 km inland (marked area 3 on Figure 6.21a). Further inland beyond this region one streamline is T21 and one is T4. The western CHO tributary glacier is almost entirely dominated by T21. The eastern CHO tributary glacier is dominated by T2, but with some T21, T3 and T4.

In 2019 (a high melt year) the way in which the typologies of seasonal velocity change from their low melt year configuration is inconsistent across the three glaciers. RG shows the most marked shift changing from dominant T2 in the low melt year to very dominant T3 across most of the glacier in the high melt year (marked area 2 on Figure 6.21b). CHO shows shifts from T2 to T21 on both the main trunk (marked area 3 on Figure 6.21b) and the tributary to the east, but only in the 5-10 km of the glacier closest to the margin in both cases. Further inland there is some limited and patchy change from T2 to T3 in these areas, but this is in contrast to the almost complete switch to T3 at RG. Some limited change from T21 to T3 is also seen in the western tributary. SG shows little variation between the two years in terms of the overall pattern of typologies along the glacier, but whilst the general locations of T21, T3, and T4 remain the same, the patches of these typologies become larger and more consolidated in 2019.

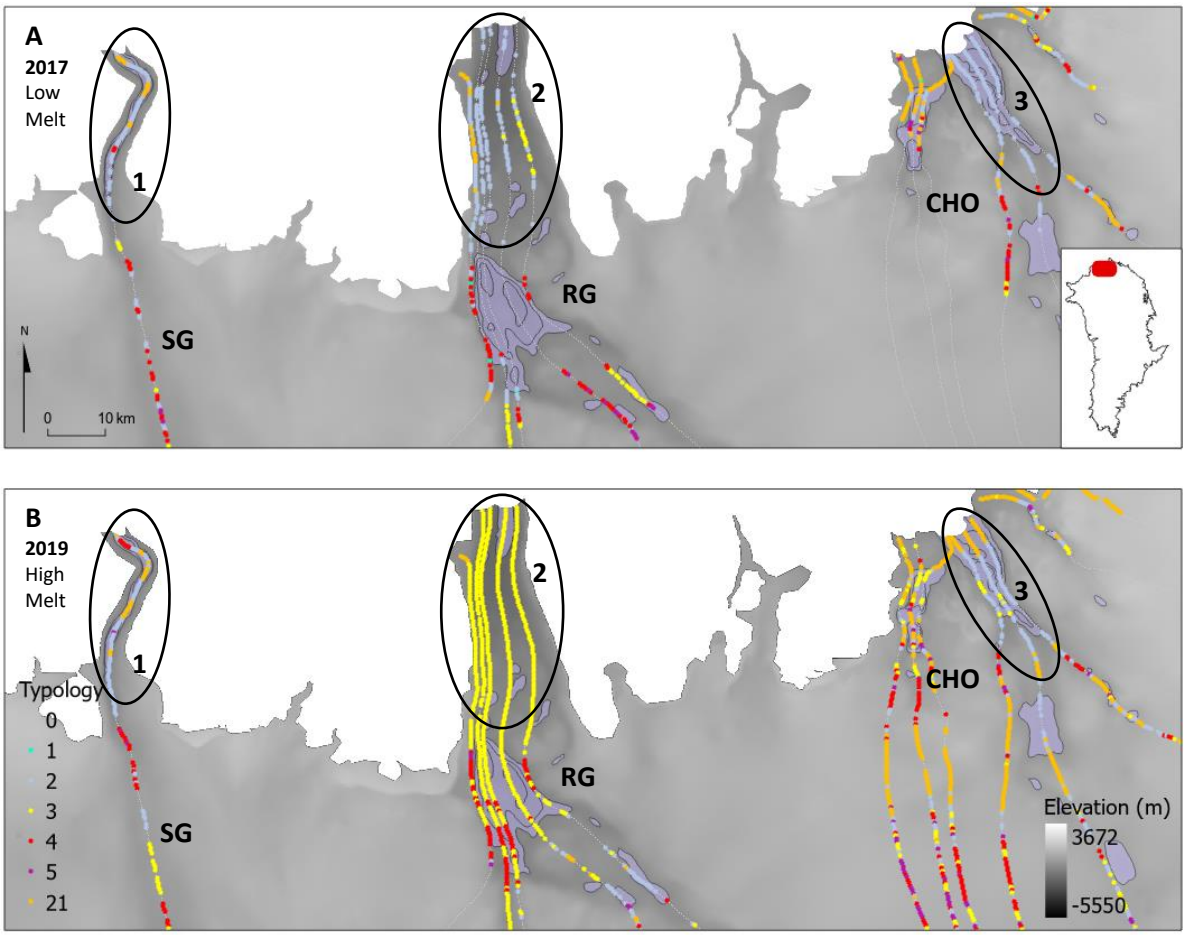

Figure 6.21 An example of local variation in seasonal velocity typology both within and between years on neighbouring glaciers. L – R: *Steensby Gletsjer (SG, 81.38N, 54.03W), Ryder Gletsjer (RG, 81.55N, 50.25W), C.H. Ostenfeld Gletsjer (CHO, 81.54N, 45.37W). A) data for a low melt year (2017). B) Data for a high melt year (2019).*

6.3.2.2.3 Individual glacier scale

There are numerous examples across the GrIS where seasonal velocity typology varies in large continuous coherent blocks, which are sometimes coincident with overdeepening location. Figure 6.22 demonstrates one such example of this at Academy Gletsjer. At the furthest inland area of data coverage (area marked 1 in Figure 6.22) the seasonal velocity typology is dominated by T21. As the ice flows over the cluster of overdeepenings (area marked 2 in Figure 6.22) there is a transition to dominant T2 which persists for approximately 70 km. As the ice leaves area 2 and enters area 3 it converges and the overdeepenings become much more elongated towards the margin. In the low melt year (2017) T2 remains the dominant typology in area 3 until ice enters the last large nested overdeepening approximately 30-30 km form the margin, at which point it reverts to T21. In the high melt year (2019) T3 becomes the dominant typology as soon as ice enters area 3.

There are also some noteworthy smaller scale patterns in seasonal velocity typology at Academy Gletsjer. Area 4 on Figure 6.22c highlights a saddle between two more prominent overdeepenings within the overall nested collection of overdeepening. Area 5 on Figure 6.22c highlights a small gap between two overdeepenings. In both cases for the low melt year (2017) seasonal velocity typology before and after these areas is T2, but whilst the ice is flowing over these areas the typology changes to T4.

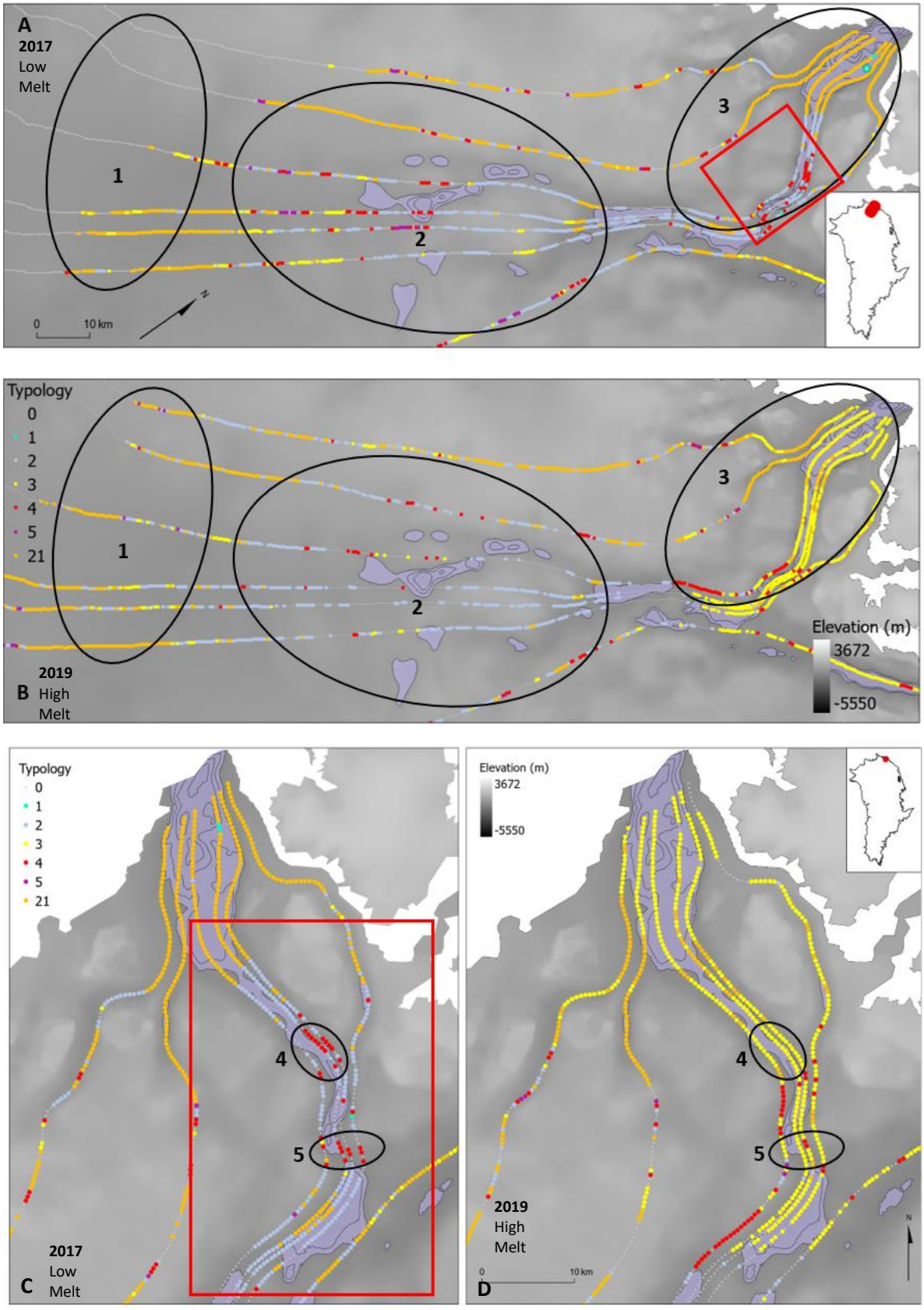

Figure 6.22 Large scale variation in seasonal velocity typology at a single glacier scale. Academy Gletsjer (81.57N, 32.25W). A) data for a low melt year (2017). B) Data for a high melt year (2019).C) Zoomed in view around the red square in A, data is for 2017. D) Area covered is the same as in C, but data is for 2019

6.3.2.2.4 Individual overdeepening scale

There are many examples across Greenland where seasonal velocity typology along a streamline is in coherent blocks where the transition points between typologies are precisely located as ice enters or exits overdeepenings.

Figure 6.23 shows seasonal velocity typology along flowlines over the two overdeepenings closest to the margin of Inngia Insbræ. In the low melt year (2017, Figure 6.23a), T2 is dominant across all areas with the exception of a small patch of T21 on flowline 1 just before entering the area marked 1 on Figure 6.23a, and a small patch of T5 right at the terminus. In the high melt year (2019, Figure 6.23b) typology through OD1 is T2 until just before ice leaves the overdeepening at which point it switches to T3. T3 is maintained until the precise location where ice enters OD2. Typology is not classified on the normal slope for OD2 due to the ice velocity error threshold not being met, but on the adverse slope of OD2 typology switches back to T2. Also of note is that for flowline 1 (which does not flow through OD1), transition from T2 to T3 occurs approximately 5 km further upglacier than for flowline 2 (which does flow through OD1) (Figure 6.23b).

A similar pattern (switch from T2 to T3 as ice exits an overdeepening with typology then reverting to T2 as ice enters another overdeepening further down glacier) is illustrated on K.J.V Steenstrup Nordre Bræ in Figure 6.24b. Seasonal velocity typology is T3 on the normal slope of OD1, switches to T2 on the adverse slope of OD1, then switches back to T3 just before ice exits the overdeepening (the area marked 1 on Figure 6.24b). Just before ice enters OD2, typology reverts to T2. As ice exits OD2 typology changes to T4, and then to T1 shortly after entering OD3.

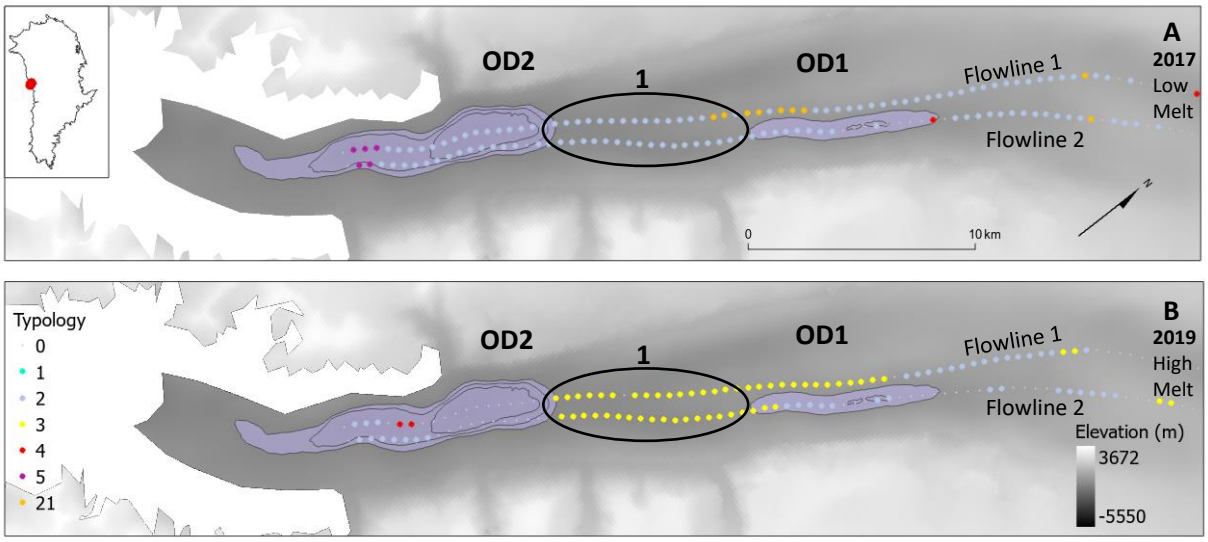

Figure 6.23 Extremely coherent maintenance of switch to T3 from T2 in high melt year ONLY between overdeepenings. central flowline points along flowline that skirts W of OD1 also switches whilst flowline inside OD1 does not. Inngia Isbræ, 72.04N, 52.61W. A) data for a low melt year (2017). B) Data for a high melt year (2019).

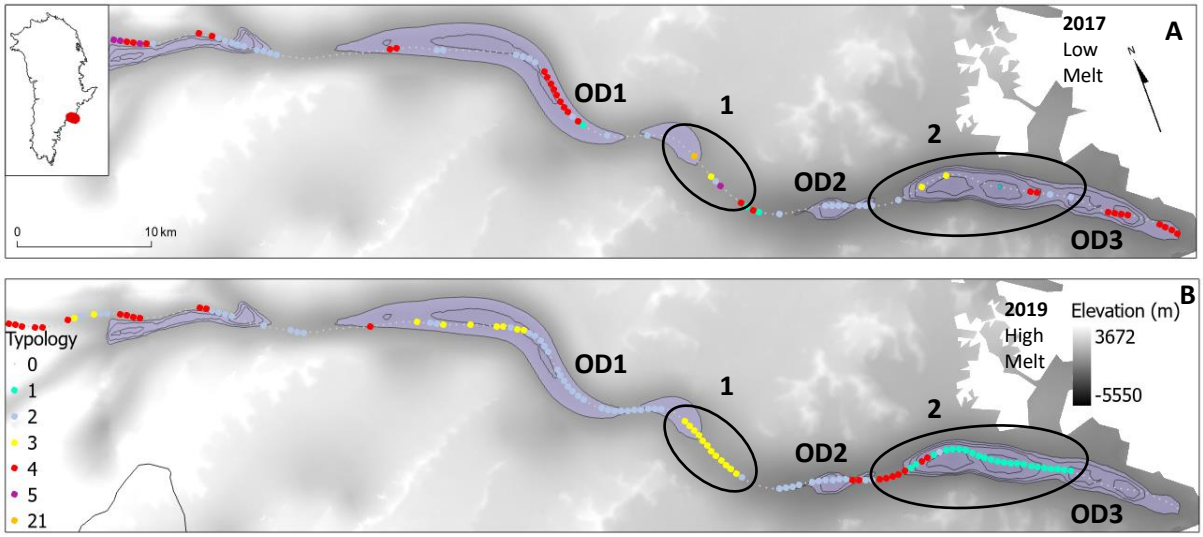

Figure 6.24 Transition from T2 to T3 at exit of overdeepening 1 (marked OD1 on figure) followed by transition back to T2 on entering overdeepening 2 (marked OD2 on figure). This is also one of relatively few examples of T1 at the margin, potentially reflecting marine processes / calving driven ice flux. K.J.V Steenstrup Nordre Bræ, 66.60N, 34.73W. A) data for a low melt year (2017). B) Data for a high melt year (2019).

6.4 Discussion

6.4.1 Introduction

The aim of this discussion is to address the RQs, objectives and SQs outlined in the introduction to this chapter, these being:

RQ3 Are there any broad scale patterns that link seasonal velocity signature to bed topography or other GrIS-wide factors?

- **RQ3 objective B** Explore the extent to which there is evidence at the ice sheet scale for patterns in ice dynamics modulated by overdeepenings identified for individual glaciers in **RQ2 B** (Chapter 4).
    - **SQ1** Is there a relationship between overdeepening morphometry (specifically BSSR) and seasonal velocity typology?
    - **SQ2** Is there a variation between the seasonal velocity typology of the normal and adverse slopes of overdeepenings, or between the seasonal velocity typology of ice flowing across an overdeepening compared to ice immediately up and downstream of an overdeepening?
    - **SQ3** Is there a variation in the magnitude of ice velocity speedup or slowdown *within* the seasonal velocity typology of an overdeepening when comparing the normal and adverse slopes?

- **RQ3 objective C** Quantify the spatial and temporal patterns (and potential process relationships) between seasonal ice velocity typology and other relevant factors.
    - **SQ4** How dominant a control are marine processes on seasonal velocity typology at the calving front of marine terminating outlet glaciers and is the typology at the margin representative of typologies further inland?
    - **SQ5** What role does surface runoff play in seasonal velocity typology?
    - **SQ6** What are the spatial variations in seasonal velocity typology across the GrIS?
    - **SQ7** What are the temporal variations in seasonal velocity typology across

the GrIS?

6.4.2 Evidence for broad scale patterns in ice dynamics modulated by overdeepenings [RQ3 B]

This section will aim to analyse whether there is evidence to suggest that the key driving factors hypothesised in the conceptual model of the modulation of ice dynamics by overdeepenings in Chapter 4 are widespread and significant at the ice sheet scale. Specifically, it addresses the expected patterns outlined for SQs 1-3 in section 6.1.1 and 6.4.1.

6.4.2.1 SQ1 Is there a relationship between overdeepening morphometry (specifically BSSR) and seasonal velocity typology?

The conceptual model developed for Upernavik Isstrøm II (section 4.3.2.7) proposed supercooling on the adverse slope slowing or preventing a transition from distributed to channelised subglacial drainage compared to the normal slope. This was hypothesised to lead to more pronounced slowdown following peak summer velocities on the normal slope than the adverse slope of an overdeepening. For Upernavik Isstrøm II in 2016 this was observed to result in different seasonal velocity typologies on the normal (T3) and adverse (T2) slopes. The rationale for adopting the hypothesis as described was that Moon Type 2 has frequently been interpreted to be representative of distributed drainage, and Moon Type 3 interpreted as representative of channelised drainage (Moon et al., 2014; Vijay et al., 2019, 2021; Solgaard et al., 2022), and supercooling processes on adverse slopes have been observed to maintain relatively higher basal water pressures suggesting that the seasonal evolution to channelised drainage configurations has been limited in these contexts (Holmlund and Hooke, 1983; Hooke et al., 1987, 1989; Cook and Swift, 2012). A key aim of this chapter is to establish whether there is widespread evidence of this pattern at the ice sheet scale, which may indicate that processes modulating the flow of ice through overdeepenings are a significant control on GrIS dynamics.

If modulational of seasonal velocity patterns driven by supercooling processes on the adverse slopes of overdeepenings were widespread in space and substantial in magnitude, a difference in the breakdown of seasonal velocity typology prevalence in overdeepenings

would be expected where the adverse slope exceeds the supercooling threshold compared to overdeepenings where the supercooling threshold is not exceeded. Specifically, it would be expected for there to be higher prevalence of typologies suggestive of persistent distributed subglacial drainage (T2 and T23) where the supercooling threshold is exceeded, and higher prevalence of typologies suggestive of an evolution to channelised subglacial drainage (T21 and T3) where the supercooling threshold is not exceeded.

Overall, there does not appear to be any systematic trend in the seasonal velocity typology breakdown with relation to overdeepening morphometry (Figure 6.13). This includes the BSSR, where there was no coherent and consistent difference in the ratio of T2 & T23 to T21 & T3 above and below the supercooling threshold (Figure 6.16). This suggests that when the data is evaluated aggregated at the ice sheet scale, there is limited evidence for universal process relationships between overdeepening morphometry and seasonal ice velocity typology, or at least that their magnitude is not evident with the fidelity of data utilised in this study.

6.4.2.2 SQ2 Is there a variation between the seasonal velocity typology of the normal and adverse slopes of overdeepenings, or between the seasonal velocity typology of ice flowing across an overdeepening compared to ice immediately up and downstream of an overdeepening?

This question is considered at two different scales in the analysis presented within the results. Firstly in the aggregated statistical data for the whole overdeepening dataset across the GrIS, and secondly in the observations of the central flowline dataset as ice flows over individual overdeepenings. These will be considered in turn.

6.4.2.2.1 Ice Sheet Scale

If a widespread systematic variation in seasonal velocity typology between the normal and adverse slopes of overdeepenings were present, this would be expected to lead to a variation in the prevalence of each typology when the data is aggregated for normal and adverse slopes for the whole of the GrIS. Given the conceptual model developed in Chapter 4 (section 4.3.2.7) and the process interpretations of typologies in Chapter 5 (section 5.4.2), evidence of support for the modulation of ice dynamics due to suppression of channelised drainage on the adverse slopes of overdeepenings would be expected to present as relatively higher prevalence of T2/T23 on the adverse slope, and relatively higher

prevalence of T21/T3 on the normal slope.

When the difference in seasonal velocity typology prevalence between normal and adverse bedslopes for each year were analysed (Figure 6.19) the variation in a given year were minimal. In addition to the fact that the variations in prevalence between the normal and adverse slopes are very small, there is no systematic pattern obvious in the variations. In 2016 and 2018 the proportion of T21/T3 on the adverse slopes is slightly lower than on the normal slopes. However, in 2017 and 2019 the reverse is true with a higher proportion of T21/T3 on the adverse slopes. As such, statistical analysis of the variation between typology prevalence on normal and adverse slopes in the dataset aggregated as a whole does not provide evidence in support of a systematic difference. There are various possible explanations for these observations.

Firstly, there could simply be no widescale variation in typology between normal and adverse slopes. Secondly, the results for Upernavik Isstrøm II in Chapter 4 only show a differential seasonal velocity typology on the normal and adverse slopes for one of the three years in the study period, and the conclusion reached was that it was the specific pattern and magnitude of surface runoff in that year that led to the differential typologies. The approach taken in this chapter (section 6.3.2.1) where years are simply classified as relatively high or low melt based on ice sheet averages may lack the nuance to aggregate the data in a way where the adverse / normal slope typology differential is identifiable. An interesting area for future study would be to extract the annual runoff graphs for each overdeepening for each year and classify the shape of these using a K means clustering approach in an attempt to identify where melt patterns are similar to that of Upernavik Isstrøm II in 2016. Analysis could then be conducted of all overdeepenings with this archetypal melt pattern to investigate if a systematic typology differential between normal and adverse slopes exists within this more specific subset. Finally, the much coarser temporal resolution of the velocity data used in this chapter (four velocity values per year each averaged over a three month period compared to ~10-15 individual velocity values per year each average over a 24 day period for the analysis of Upernavik Isstrøm II in section 4.2.2.2) may be insufficient to identify what appear to be processes possibly operating under quite short timescales. The differential seasonal velocity typology between normal and adverse slopes at Upernavik Isstrøm II in 2016 are evident for somewhere between 3-6

weeks (Figure 4.5) so it is possible that the magnitude of the differential velocity response between the normal and adverse slope is not great enough to be resolved in the quarterly average velocity data.

6.4.2.2.2 Glacier scale

In addition to ice sheet scale statistical analysis facilitated by the overdeepening dataset (section 6.4.2.2.1), there are also valuable insights to be gained by visually interrogating the relationship between the patterns of seasonal velocity typology in the central flowline dataset in spatial relation to the overdeepenings mapped in Chapter 3.

Figure 6.22, Figure 6.23b, and Figure 6.24b all show very clear examples where there is a an area of T21 or T3 upglacier of an overdeepening (or cluster of overdeepenings). This is reflective of pronounced late season slowdown interpreted to be caused by a switch to channelised drainage. As ice encounters the overdeepenings there are then extremely coherent switches to T2. This is reflective of a lack of pronounced late season slowdown interpreted to reflect distributed subglacial drainage being maintained through the melt season. As ice leaves the overdeepening, or in close proximity to the glacier terminus, seasonal velocity typology then either reverts to T21 / T3 or switches to T1/T4. In previous studies investigating seasonal ice velocity typology in Greenland, melt has been suggested as the dominant control determining variations in typology (Sundal et al., 2011; Moon et al., 2014; Vijay et al., 2019, 2021; Solgaard et al., 2022). The spatially isolated switches to T2 sandwiched between areas of T21/T3 up and down glacier (Figure 6.22, Figure 6.23b, and Figure 6.24b) cannot be explained solely by melt thresholds being exceeded and forcing a switch to channelised subglacial drainage. The areas of T21/T3 up glacier of the areas of T2 are at higher elevation and therefore will have lower melt rates than the areas of T2. As such, it holds that if a melt threshold has been exceeded in the area upglacier of the area of T2, it will also have been exceeded in the area of T2, and therefore if melt is the control of switch to T2 there should be no T2 observed down glacier of areas of T21/T3.

One alternative interpretation of the T2 anomalies coincident with overdeepenings is that there is some mechanism by which ice flow through the overdeepenings is restricting the transit of surface melt water to the bed, and therefore impeding the evolution of the subglacial hydrology to a channelised system in these areas. It seems unlikely that surface melt would be prevented from entering the glacial system given that extensional flow into

overdeepenings is more normally associated with increased crevassing at the head of the overdeepening (Hooke, 1991) which will in turn enhance moulin development through hydrofracture and aid transit of water from the surface to the bed (Stenborg, 1969; Benn et al., 2009). However, it could be that melt water is traversing the overdeepening englacially. Extensive englacial drainage bypassing overdeepenings has been observed at Storglaciären (Hooke et al., 1988; Hooke and Pohjola, 1994), and at Gornergletscher (Iken et al., 1996) and Aletschgletscher (Hock et al., 1999) in the Swiss Alps.

These examples of spatially isolated switches to T2 coincident with the ice encountering an overdeepening provide evidence to support the notion of modulation of ice dynamics by overdeepenings. The signal observed is aligned with what would be expected were supercooling processes, to be restricting subglacial channel development and preventing or slowing a seasonal evolution from distributed to channelised subglacial drainage. However, as discussed above, it is not possible to definitively attribute the observed patterns to such supercooling processes as other processes including the diversion of melt away from the bed by englacial networks, could result in similar ice velocity patterns over the adverse slope by other mechanisms (e.g. a restriction of melt accessing the bed (englacial flow) as opposed to a restriction of melt flowing along the bed (via supercooling limiting subglacial channel development)). However, despite the specifics of the process control operating, the results do provide further evidence of apparent modulation of ice dynamics by overdeepenings supporting the notion that these are potentially important features in relation to ice dynamics.

In addition to the spatial patterns considered above, there are also some interesting temporal patterns clearly evident when the data are visually interpreted at the individual glacier scale. These primarily relate to variations in the way that typology changes across an overdeepening in high melt years compared to low melt years. Two examples will be given here.

Figure 6.23 shows the ice flow over the two overdeepenings at Inngia Isbræ. In the low melt year (2017) seasonal velocity typology is consistently T2 across almost all of the glacier (Figure 6.23a). This suggests that melt did not exceed the threshold required to cause a transition to channelised subglacial drainage at any point on the glacier in the low melt year. In the high melt year (2019) there is a coherent band of T3 between the overdeepenings

suggesting development of channelised subglacial drainage in this area (marked 1 on Figure 6.23b). However, the fact that T3 is limited almost exclusively to areas outside overdeepenings, and reverts to T2 in overdeepening 2 (further downglacier from the band of T3 between the overdeepenings) provides strong evidence that overdeepenings may be modulating the ice dynamics at Inngia Isbræ and preventing a whole scale switch to T3 in high melt years.

Figure 6.21 shows the ice flow through the terminal overdeepening in the main trunk of C.H. Ostenfeld Gletsjer (the area marked 3 on the figure). In the low melt year (2017, Figure 6.21a) all areas within the overdeepening are T2, but there is T21 in the areas outside the overdeepening up glacier to the south. In the high melt year (2019, Figure 6.21b), there is a switch to T21 inside the overdeepening in the 5 km zone closest to the margin, some switching to T3 on the normal slope of the overdeepening, but the central section of the adverse slope is maintained as T2. In the overdeepening up glacier to the south of area 3 there is also a coherent switch from T21 to T2 as ice enters the overdeepening, whilst either side of the overdeepening (at the same elevation and latitude) the typology is consistently T21. Again, this demonstrates the possible modulation of ice dynamics through overdeepenings interpreted to be driven by supercooling on the adverse slope controlling seasonal evolution of subglacial drainage regime and restricting the development of channelised systems.

6.4.2.3 SQ3 Is there a variation in the magnitude of ice velocity speedup or slowdown within the seasonal velocity typology of an overdeepening when comparing the normal and adverse slopes?

When Moon et al. (2014) first proposed the concept of typologies of seasonal velocity variation, they were clear that they considered these typologies to be representative of end members of a continuum rather than distinct labels for isolated and unrelated processes, and subsequent studies have reaffirmed this notion (Solgaard et al., 2022). As such, the absence of a relationship between overdeepening morphometry and discrete seasonal velocity *typology* (as indicated in sections 6.4.2.1 and 6.4.2.2) does not preclude the possibility that overdeepening morphometry may be exerting some control on seasonal velocity *variation*, as this variation may be occurring within the discrete boundaries of individual seasonal velocity typologies. This is illustrated in the data for Upernavik Isstrøm II presented in Chapter 4 where different seasonal velocity typologies on the normal and

adverse slopes of the overdeepening were only observed in one of the three study years, but within typology variation was observed in all three years (Figure 4.4). Conceptualising seasonal velocity typology as a continuum also aligns with the fact that the subglacial processes being investigated as potential drivers of seasonal velocity patterns (e.g. the effect that bed gradient may have on hydraulic gradient and supercooling and how this in turn controls the configuration of subglacial hydrology) are also considered to act as a continuum (section 2.4.1).

It was the desire to explore these potential variations within seasonal velocity typology that provided the impetus to develop the additional classification schema for variation between seasonal velocity response on the normal and adverse slope of each overdeepening presented in section 6.3.1.3. Figure 6.25 further contextualises how the concept of seasonal velocity typology as a continuum and the typologies of variation between normal and adverse slopes relate to one another.

Figure 6.25a-e illustrates the seasonal velocity typologies on a continuum from T2 to T21 to T3. Figure 6.25f-j shows cartoons of a series of hypothetical situations where the seasonal velocity response on the adverse slope is one step further towards 'more distributed' on the continuum than the response on the normal slope. Figure 6.25k-o shows the difference between the normalised velocity on the adverse and normal slopes, where a positive value represents higher normalised velocity on the adverse slope. It is these types of graphs of the difference in velocity between the adverse and normal slopes that were classified using the K means approach in section 6.2.6 to generate the typology of variation between adverse and normal slopes of overdeepenings.

In the typologies generated from the K means clustering analysis (Figure 6.9, Table 6.1) typologies T-A and T-B are representative of overdeepenings where the difference between normalised velocities on the adverse and normal slopes is negative for the majority of the year. This means that normalised velocity on the adverse slope is lower than on the normal slope. As such, T-A and T-B are interpreted as being *counter* to the signal expected (e.g. late season slowdown on the adverse slope is greater than on the normal slope, rather than less) were an adverse slope to restricting subglacial channel development and thus maintain a more distributed or less efficient form of channel system. Typologies T-D and T-E are representative of overdeepenings where the difference between normalised velocities on

the adverse and normal slopes is positive for the majority of the year. This means that normalised velocity on the adverse slope is higher than on the normal slope. As such, T-D and T-E are interpreted as being *aligned* with the signal expected were an adverse slope to restricting subglacial channel development and thus maintain a more distributed or less efficient form of channel system. Typology T-C is more difficult to interpret with regard to expected modulation from adverse slope processes as it represents higher normalised velocities on the normal slope in the spring and summer, but slightly higher velocities on the adverse slope in autumn and summer.

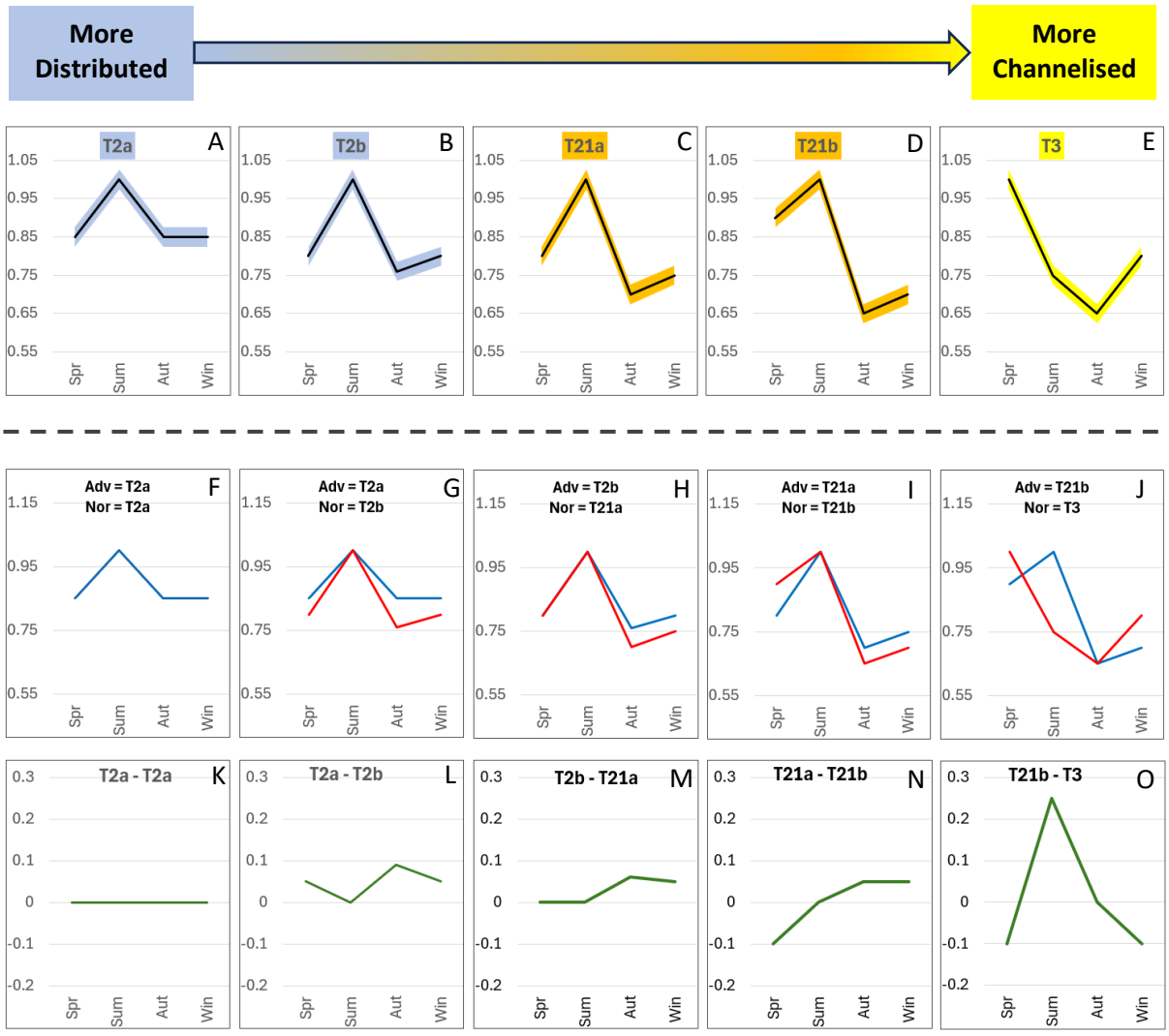

Figure 6.25 Schematic illustrating the concept of seasonal velocity typology as a continuum. A-D) Shows cartoons of idealised seasonal velocity typologies that go from more distributed subglacial drainage on the left, to more distributed on the right. F-J) Cartoons showing hypothetical seasonal velocity responses on an adverse slope (blue line) and a normal slope (red line). In panes G-J the adverse slope line is always one step closer towards 'distributed' on the continuum than the normal slope. K-L) Cartoons plotting the variation between the adverse and normal slope seasonal velocity patterns shown in F-J.

Figure 6.9 shows that in 39% of cases there is an identifiable variation between the seasonal velocity response on the adverse and normal slopes of an individual overdeepening. Where there is a variation in seasonal velocity response between the normal and adverse slopes of an overdeepening, 59.9% of cases are typologies T-D or T-E, whilst only 31.1% are typologies T-A or T-B (Table 6.2). As such, we can conclude that variation typologies aligned with the signal expected from adverse slopes restricting subglacial channel development (and thus maintaining a more distributed or less efficient form of channel system) occur almost twice as frequently as variation typologies that conflict with the expected signal. This offers some support for the hypothesis proposed in the conceptual model in Chapter 4 (Figure 4.6) that ice flow through overdeepenings is modulated by subdued transition to channelised drainage on the adverse slope in Greenland outlet glaciers.

The relationship between typologies of adverse / normal slope variation and overdeepening morphometry do not appear to be strong (Figure 6.17). Typologies T-A and T-B both show greater ranges of values and higher averages for overdeepening depth and adverse slope length then T-C, T-D, and T-E, but these differences are not statistically significant (Figure 6.17). Similarly, BSSRs do not demonstrate a statistically significant difference between variation typologies. It is also important to note when interpreting the results on typologies of variation between normal and adverse slopes that in three of the clusters in the K means analysis (clusters 3, 6, and 7, Figure 6.9) the variation between the adverse and normal slope is small (~ 2-3%). As such, the measured signal may lie within the error of the velocity data, and caution must be applied when drawing inference from this data.

6.4.3 Wider factors

The second section of the discussion will be focused on RQ3 objective C and answering the aligned SQs 4-7. These focus on the wider patterns in ice dynamics and the processes that may be driving them, beyond any specific influence of overdeepenings. An assessment of how dominant a control marine processes are on the seasonal dynamics at the margin of marine terminating outlet glaciers will also be made. Substantial consideration will be given to the role of surface melt availability in driving ice sheet dynamics. The potential

application of the seasonal velocity typology dataset for mapping the inland subglacial channelisation limit will be considered. The section will then go on to give a more general discussion of the spatial and temporal patterns in seasonal velocity typology across the GrIS including comparison with the findings of other studies.

6.4.3.1 SQ4 How dominant a control are marine processes on seasonal velocity typology at the calving front of marine terminating outlet glaciers and is the typology at the margin representative of typologies further inland?

In Chapter 4 the case study example of Helheim illustrated that distinct patterns in seasonal ice velocity change varied up and down glacier of a prominent riegel of a large overdeepening close to the terminus, with T1 seasonal variation identified down glacier of the riegel, but an immediate switch to T2 style typology upglacier of the riegel. Type 1 style seasonal variation is commonly identified as being representative of situations where seasonal velocity dynamics are controlled by marine processes with speedup through summer and autumn being linked to break up of ice mélange and retreat and thinning of the calving front causing a reduction in backstress, and subsequent slowdown over winter as mélange reforms and ice thickens and advances (Joughin, Das, et al., 2008; Joughin, Howat, et al., 2008; Nick et al., 2009; Andersen et al., 2010; Moon et al., 2014; Kehrl et al., 2017; Vijay et al., 2019). However, Type 1 typologies are relatively uncommon (Moon et al., 2014; Vijay et al., 2019)) and even when pronounced seasonal variation in ice front position are observed, many glaciers behave like land terminating glaciers with speedup and slowdown correlated with melt rather than retreat (Howat et al., 2010; Davison et al., 2020). Such patterns (where frontal retreat and ice speedup are not correlated) were observed in the Upernavik Isstrøm II case study example in Chapter 4. The uncertainty over which processes control seasonal velocity typology (e.g. marine influenced frontal retreat vs subglacial hydrological regime driven by melt accessing the bed) may be exacerbated by the heavy focus in the literature on a relatively limited number of glaciers (such as Jakobshavn Isbræ) which have exhibited marine influenced Type 1 typologies in some studies, but which may be atypical and not representative of the majority of outlet glaciers (Howat et al., 2010).

This chapter contributes to the discussions around the prevalence and importance of marine influence on Greenland outlet glacier dynamics by focusing on i) how common are Type 1 seasonal velocity typologies, ii) are they spatially located close to the margin (as would be expected if they are reflected of a marine signal)? iii) are there other seasonal velocity

typologies that show an association with the margin?

Figure 6.12e and Figure 6.12g show the relationship between seasonal velocity typology prevalence and ice surface elevation for both the overdeepening and central flowline dataset. If we take surface elevation as a proxy for proximity to the margin (as the lowest elevations will be at the margin of the ice sheet), we would expect to see higher prevalence of T1 at lower elevations if the typology was representative of marine processes. There is mixed evidence to support this in the data. For the central flowline dataset there is some evidence in support of the hypothesis; the distribution of T1 appears bimodal with the highest prevalences at the lowest and highest elevations, and the minimum prevalence in the mid elevation ranges (Figure 6.12e). For the overdeepening dataset there is no clear overall pattern in the data and the three highest prevalences of T1 are actually in the three highest elevation ranges, the opposite of what we would expect to see if T1 was being driven by marine processes. However, it is established that any marine influence in ice dynamics is likely to be restricted to a zone proximal to the margin and the extent of this will be controlled by the stress coupling length (Enderlin et al., 2016; Larsen et al., 2023). The stress coupling length has historically been taken to be in the range of 4-11 x ice thickness (H) (Kamb and Echelmeyer, 1986), and more recent empirical work on large outlet glaciers in Greenland has suggested the lower end of the range, close to 4 x H is most likely (Enderlin et al., 2016; Felikson et al., 2022). With ice thickness near the margin of large Greenlandic outlet glaciers such as Helheim (see Chapter 4) in the range of 750-1500 m, it is likely that the zone of any marine influence on ice dynamics will potentially only extend inland between 3,000-15,000 m. As such, when evaluating patterns of T1 prevalence we may not expect to see a linear inverse trend of T1 decreasing as distance from the margin increases. Rather, a high prevalence at the margin and within the zone determined by the stress coupling length might be expected, which then drops very sharply once the stress coupling length is exceeded. The location of prominent riegels in proximity to the margin may also exert a control on isolating the influence of marine processes by acting as breakpoints from where the ice is suddenly not near buoyancy (Ultee et al., 2022).

Table 6.7 shows dominant seasonal velocity typology in a subset of the central flowline dataset limited to points within 4 km of outlet glacier termini, and gives a much clearer picture of exactly what is happening at the margin. Even in this zone directly proximal to the

margin, overall T1 prevalence is still very low (4.8%). However, this does represent an increase in prevalence of 120.1% compared to the total dataset T1 prevalence (2.2%), indicating that typology is much more likely to be T1 at the terminus than in areas further inland. When considering the typology prevalence for marine terminating glaciers in isolation the prevalence increases further to 5.5% (151.1% of the total dataset prevalence). Also noteworthy is that there are no land terminating outlet glaciers in the dataset that have a dominant T1 typology at the terminus. The substantial increase in T1 prevalence (compared to the whole data average) at the terminus of marine terminating glaciers, combined with the complete absence land of terminating glaciers with a dominant T1 typology at the terminus, demonstrates support for the hypothesis that the T1 typology is (at least in part) representative of dynamics driven by marine processes at the margin of the ice sheet.

Table 6.7 The prevalence of seasonal velocity typology at the terminus of outlet glaciers in the central flowline dataset for 2019. Values are given for the whole dataset and also subdivided into land terminating and marine terminating outlet glaciers. Variance is shown for each category against the overall typology prevalence in the full central flowline dataset.

	T3	**T21**	**T1**	**T2**	**T4**	**T5**
Total dataset	22.6%	18.5%	2.2%	26.1%	27.1%	3.7%
All termini	37.0%	24.7%	4.8%	18.2%	14.5%	0.7%
Variance	**+63.9%**	**+33.5%**	**+120.1%**	**-30.4%**	**-46.4%**	**-80.4%**
Land Terminus	27.5%	70.6%	0.0%	0.0%	2.0%	0.0%
Variance	**+21.5%**	**+281.6%**	**-100.0%**	**-100.0%**	**-92.8%**	**-100.0%**
Marine Terminus	38.4%	19.1%	5.5%	19.9%	16.3%	0.8%
Variance	**+69.9%**	**+3.0%**	**+151.1%**	**-23.8%**	**-39.9%**	**-77.6%**

Whilst there appears to be evidence linking the T1 typology to marine processes, the fact that it is limited in absolute prevalence, even in at the margin of marine terminating outlet glaciers, does call in to question assertions made in previous studies of the importance of the processes associated with marine influence in terms of overall ice sheet dynamics. For example, in their study of Helheim, Jakobshavn, and Kangerdlugssuaq glaciers, Shapero et

al. (2016) model basal resistance under fast flowing areas using inverse methods constrained by satellite observations. They conclude that basal resistance is very low and that resistance due to forces at the shear margin and terminus are more likely to control ice dynamics in these systems. As such, they conclude that modulation of basal resistance due to effective pressure changes in subglacial hydrology should be limited in the main trunks of outlet glaciers. They infer that basal resistance will be low even at low effective pressure due to weak dilatant till and so the potential for further modulation of flow by effective pressure changes is limited. Indeed, they use the lack of late summer slowdown in their Jakobshavn results as evidence in support of their hypothesis. They concluded that their findings on the three glaciers in their study "*may be broadly representative of the ~200 others that drain the ice sheet, many of which flow rapidly through deep troughs*" (Shapero et al., 2016, pg. 178).

The results presented in this chapter suggest caution should be taken when making such extrapolations, for multiple reasons. Having studied all outlet glaciers (rather than a sample of three), it is clear that typologies representative of late summer slowdown (T21 and T3) *are dominant* at the terminus of the majority (57.5% of total) of marine terminating outlet glaciers in 2019. Indeed, the data shows that in 2019 Jakobshavn experienced late summer slowdown in the zone near the terminus with 60% of points within 5 km of the margin having a T21 seasonal velocity typology (See Annex 1, Figure A2b). The results presented in this chapter results suggest that the observations of melt induced speedups driven by modulation of subglacial water pressure at a limited number of outlet glaciers in other studies (e.g. Helheim (Andersen et al., 2010; Bevan et al., 2015), North Lake and South Lake (Joughin et al., 2008), Kangerlussuaq (Kehrl et al., 2017), Kangiata Nunata Sermia (Sole et al., 2011), and Bowdoin (Sugiyama et al., 2015)) are actually very widespread. The results presented in this chapter strongly support the conclusions of Davison et al. (2020) who suggested (based on three neighbouring marine terminating glaciers in southwest Greenland) that marine terminating glaciers may behave more similarly to land terminating glaciers (e.g. with ice dynamics dominated by melt driven changes in subglacial water pressure) than has previously been accepted.

Recent studies investigating larger numbers of glaciers (e.g. Solgaard et al. (2022)), also indicate T1 is much less prominent than previously thought (Moon et al., 2014; Vijay et al.,

2019). Other studies have also dismissed correlation between seasonal speedup and terminus position, instead attributing surface melt as the dominant driver of speedup (Sakakibara and Sugiyama, 2020). As the temporal resolution of available velocity data increases, so we see concomitant shifts in the resolution of investigation. This enables analysis of the variations in the dominance of processes at different temporal scales. Recent work by Ultee et al. (2022) at Helheim finds that patterns of ice dynamics correlate most strongly with runoff at seasonal to interannual time scales, but that dynamics at multi-annual time scales correlate more strongly with multi-annual patterns of terminus variability. Their results also suggest that behaviour at the terminus may be a *response to*, rather than a *cause of* changes further upglacier driven by melt, providing further support for the hypothesis of melt driven speedup 'priming' the system for calving events (Andersen et al., 2010). The results of seasonal ice velocity typology prevalence at the termini of Greenland outlet glaciers presented in this chapter strongly support the findings of Solgaard et al. (2022), Sakakibara and Sugiyama (2020), and Ultee et al. (2022) in questioning the traditionally assumed dominance of the marine influence on the ice dynamics at the front of marine terminating outlet glaciers in Greenland.

When analysing the data on seasonal velocity typology and the prevalence of typology in relation to other parameters with the aim of making process associations to explain the typologies, there is of course the possibility of equifinality in the typologies identified. T4 has been interpreted as being representative of processes relating to low melt, at higher elevations, further inland (section 5.4.2.6). The significant inverse correlation with melt for the central flowline dataset supports this (Table 6.3). However, there is some evidence to suggest that T4 could also be representative of the marine processes attributed to T1. The shape of T4 (Figure 5.7) shows acceleration from summer through to winter which aligns with the possibility of speedup due to seasonal break up of mélange and frontal retreat, although the slowdown from spring to summer is difficult to explain. Despite the inverse correlation between melt and T4 prevalence in the central flowline dataset, the distribution appears to be slightly bimodal for both the central flowline dataset and the overdeepening dataset, with relatively high levels of T4 prevalence at very high melt as well as very low melt (Figure 6.12a, Figure 6.12c, Figure 6.12d), and there was no statistically significant relationship between T4 prevalence and melt for the overdeepening dataset (Table 6.4). T4

prevalence at glacier termini was also much higher (16.3%) at marine terminating glaciers compared to land terminating glaciers (2.9%) (Table 6.3). Further investigation of this possible equifinality in the T4 typology is an important area for future work. However, even if T4 prevalence is in part representative of marine influence at the terminus, the combined prevalence of T1 and T4 at the terminus of marine terminating outlet glaciers is still a small minority of the total, and less than a third that of combined T21 / T3 prevalence. As such, the questions over the importance of marine processes in driving ice dynamics remains irrespective of the interpretation taken on T4.

6.4.3.2 SQ5 What role does surface runoff play in seasonal velocity typology?

There is a strong relationship between seasonal velocity typology and runoff (Figure 6.12a-d, Table 6.3, Table 6.4). Considered non-spatially as independent observations in time, the proportion of typologies interpreted as representing a seasonal switch from distributed to channelised subglacial hydrological regime (T21 & T3) increase with runoff. This is seen in both the central flowline (Figure 6.12a, Figure 6.12b) and the overdeepening (Figure 6.12c, Figure 6.12d) datasets. The logistical regression conducted suggests that for the central flowline dataset every 1,000 mm increase in summer runoff is associated with a 40% increase in the likelihood of a data point being classified as T21 and a 30% increase in the likelihood of a data point being classified as T3 (Table 6.3). For the overdeepening dataset the strength of the relationship is greater, with every 1,000 mm increase in summer runoff associated with a 50% increase in the likelihood of a data point being classified as T21 and a 40% increase in the likelihood of a data point being classified as T3 (Table 6.4). The correlation of the inverse relationship between runoff and prevalence of T2 (interpreted as being representative of distributed drainage being maintained throughout the season) was much weaker. For the central flowline dataset every 1,000 mm increase in summer runoff is associated with only a 10% decrease in T2 prevalence and for the overdeepening dataset the relationship between runoff and T2 prevalence was not statistically significant (Table 6.3, Table 6.4). Interestingly, the correlation of the inverse relationship between runoff and prevalence of T23 (interpreted as being a variant of T2 and therefore also representative of distributed drainage being maintained throughout the season (section 5.4.2.5) for the overdeepening dataset was significant and substantive with every 1,000 mm increase in summer runoff associated with a 50% decrease in T23 prevalence. This demonstrates the

value in not over-aggregating classes in the K means clustering analysis, and that clusters that are variants of other typologies (such as T2 and T23) offer the possibility of identifying process relationships that may be obscured if wider, more general clusters are developed to classify seasonal velocity typology.

The link between runoff and late season slowdown has been observed previously in studies considering both small numbers of glaciers (Sole et al., 2011; Sundal et al., 2011) and large numbers of glaciers (Moon et al., 2014; Vijay et al., 2019; Solgaard et al., 2022). However, the results presented in this chapter are the first time a statistically significant relationship between runoff and late season slowdown occurrence has been established.

Analysis of the runoff data indicates a possible minimum threshold summer runoff value of ~300-500 mm water equivalent (~ 3.2 – 5.4 mm water equivalent per day) below which T21/T3 prevalence does not increase in line with runoff (Figure 6.12b and Figure 6.12c). This threshold was similar for both the central flowline and overdeepening datasets. This threshold for onset of *increase* in prevalence of T21/T3 with runoff is substantially lower than the threshold of 14 mm per day water equivalent monthly runoff established by Sundal et al. (2011) as a threshold for late summer slowdown *onset.* However, this data (Sundal et al., 2011) was derived from only six proximal glaciers in southwest Greenland and so may not be more widely representative. Other modelling work has suggested that late summer slowdown onset can occur in the range of 10-20 mm daily water equivalent runoff (Schoof, 2010). It is also important to note that as the runoff data presented in this chapter are a three month summer total, peak monthly and daily runoff values will be much higher than a value given by simply extrapolating a daily melt average from the seasonal total, and therefore peak runoff rates may well be in the region suggested by Sundal et al. (2011) and Schoof (2010). Given the variation in the way in which runoff data has been used between the results presented here and the work of Sundal et al. (2011) direct comparison is challenging. There are also a range of other factors which are material to the level of melt required for channelisation to occur, and these will be discussed in more detail in section 6.4.3.2.3, below.

6.4.3.2.3 Inland channelisation limit

A comprehensive review of the self-regulating effect comprising the negative feedback on ice velocity caused by long term increases in melt leading to increasingly channelised

subglacial drainage was given in section 2.3.1.5. A number of studies have suggested that dynamic ice loss from the SW of the GrIS decreased during the period of record levels of surface melt between 2000 – 2012 (Sole et al., 2013; Tedstone et al., 2015; Williams et al., 2020). The implications of these findings have been interpreted to infer that channelisation will become more widespread under even higher levels of future surface melt, stabilising the ice sheet with respect to dynamic losses (Fox-Kemper et al., 2021). However, the findings of studies on the hydro-dynamic coupling of the SW GrIS have not been entirely consistent (Joughin 2018), and there is some uncertainty as to how channelisation of subglacial hydrology will respond as the channelisation limit expands further inland under thicker ice as surface melting increases and the ELA rises (Doyle et al., 2014; De Fleurian et al., 2016; Koziol and Arnold, 2018). It is also important to note that the studies that identified the velocity decreases in SW Greenland in the 2000s only inferred that the decrease was as a result of changes in seasonal patterns of channelisation; no seasonal velocity observations were made and the hypotheses were put forward based on the likely drivers of the observed changes in annual velocity.

Current estimates of the inland channelisation limit are restricted to a relatively small number of point measurements and the outputs of modelling studies (see Table 2.1). The results presented in this chapter are only the second time (after Solgaard et al. (2022)) that a dense array of measurements of seasonal velocity variation have been taken across the GrIS. This represents an opportunity to explore whether these measurements may be utilised to determine the location of the inland channelisation limit. It has been hypothesised throughout this thesis that T2 and T23 are representative of distributed subglacial drainage configurations, whilst T21 and T3 are representative of channelised subglacial drainage. If these hypotheses are correct then a coherent transition between T21/T3 and T2 may be expected in the central flowline dataset that reflects the inland channelisation limit. To explore this possibility, a manual visual analysis of the raw points from the central flowline dataset was undertaken for 2019. A coherent block of T21 / T3 was identified extending inland from the margin along the entire western margin of the ice sheet (Figure 6.26b-d). The inland limit of this coherent block was mapped with a line joining the T21 / T3 limit along each of the central flowlines Figure 6.26a. At the point interpreted as marking the inland limit of the coherent T21/T3 block on each central flowline, values for Ice

surface and bed elevation from BedMachine V3 (Morlighem et al., 2017), total summer surface runoff from MAR (as in section 6.2.4), summer ice velocity from the MEaSUREs Greenland Quarterly Ice Sheet Velocity Mosaic for 2019 (as in section 5.2.1), and Euclidean distance to the ice sheet margin were extracted. This data is plotted along with latitude in Figure 6.28.

Figure 6.26 shows that the estimated inland channelisation limit plotted aligns very closely with the existing data points on subglacial hydrological configuration and channelisation limit from other studies. The observations and modelling outputs of distributed subglacial hydrology from the literature (points 1, 7, and 10 in Figure 6.26 from Doyle et al. (2018), Chandler et al. (2013) and Dow et al. (2014), respectively) are all further inland of the proposed channelisation limit plotted within this chapter. The two studies that propose an actual inland limit for channelisation (as opposed to simply observing either distributed of channelised subglacial drainage) are within 5 km of the estimated channelisation limit presented in this chapter (points 6 and 9 (Koziol and Arnold (2018) and De Fleurian et al. (2016), respectively, on Figure 6.26d). The five observations and modelling outputs of channelised drainage from the literature (points 3, 4, 5, 7 and 8 (Banwell et al. (2016), Van De Wal et al. (2015), Meierbachtol et al. (2013), Chandler et al. (2013), and Chandler et al. (2021), respectively, on Figure 6.26c-d).) are all located closer to the margin than the channelisation limit estimated here (Figure 6.26).

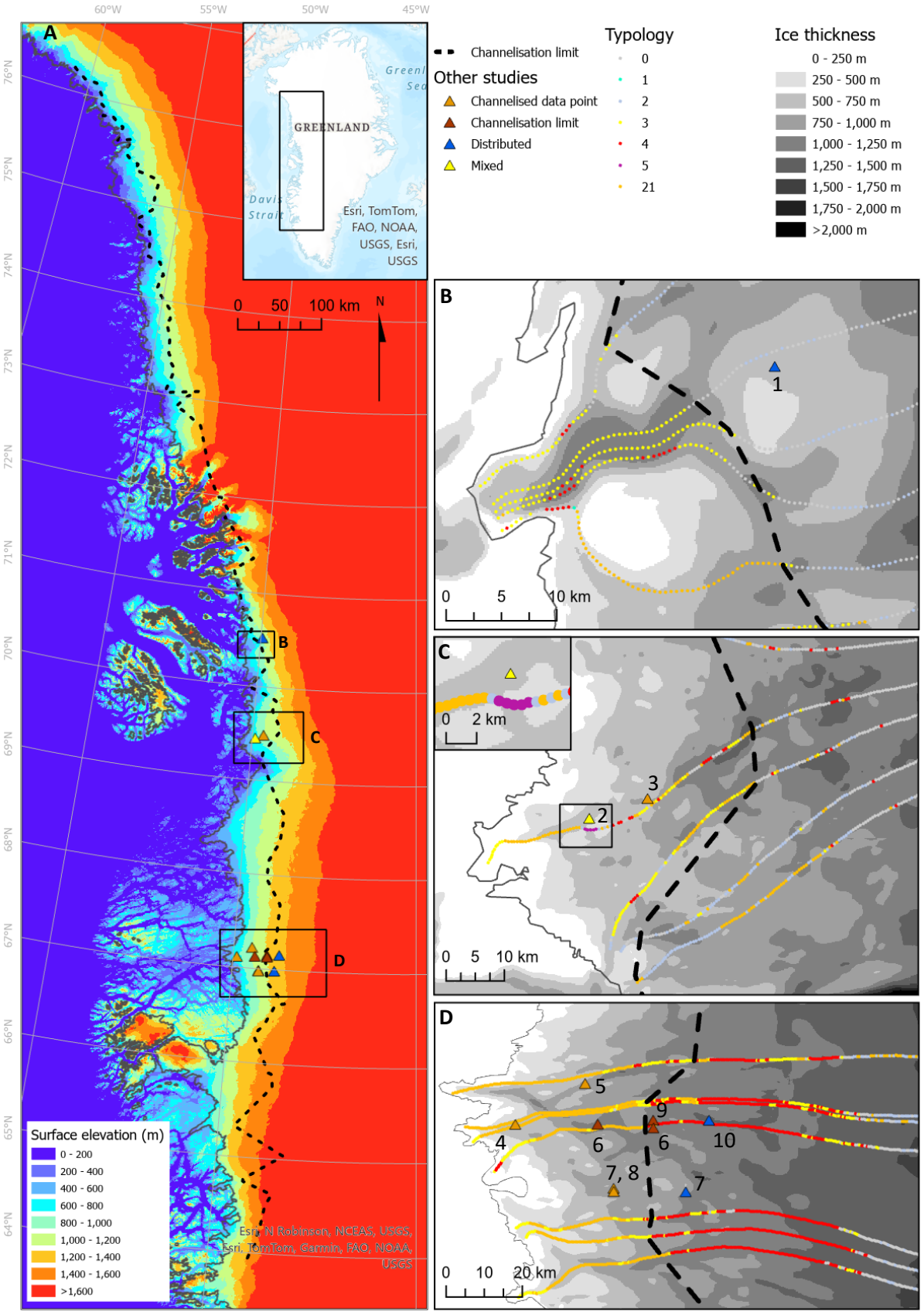

Figure 6.26 Estimation of the inland channelisation limit for 2019 derived by mapping the inland margin of the coherent band of T21/T3 seasonal velocity typology in the central flowline dataset. A) the estimated channelisation limit shown over the BedMachine V3 surface elevation layer. Location of inset panes B, C, and D are shown which contain the locations of

data points indicating channelised and distributed subglacial drainage configurations from other studies (as summarised in Table 2.1). B) 1. (Doyle et al., 2018). C) 2. (Andrews et al., 2014), 3. (Banwell et al., 2016). D) 4. (Van De Wal et al., 2015), 5. (Meierbachtol et al., 2013), 6. (Koziol and Arnold, 2018), 7. (Chandler et al., 2013), 8. (Chandler et al., 2021), 9. (De Fleurian et al., 2016), 10. (Dow et al., 2014).

Figure 6.27 demonstrates that the estimated inland channelisation limit ascertained from flow typology aligns extremely closely with the limit modelled by Maier et al. (2022). Given how close the plotted channelisation limit agrees with the Maier et al. (2022) output, it is important to note that the digitisation of the inferred limit was plotted completely independently from the Maier et al. (2022) output and only overlaid after it was completed. Combined with the results presented on Figure 6.26, overall there is a high level of agreement between the inland channelisation limit inferred from seasonal velocity typology presented here and all existing estimates from field observations and modelling work presented in the literature. As such, a high level of confidence can be held in the results presented, and this suggests that there is future potential for the method adopted in terms of estimating the inland channelisation limit more widely across Greenland, and across different years.

Plotting the channelisation limit as a line allows for the extraction of the values of key parameters at nodes along the proposed limit to facilitate further analysis of potential process relationships. Figure 6.28 illustrates how surface runoff, ice thickness, and ice velocity, which are hypothesised to exert a control on channelisation limit (Nye, 1953, 1953; Hooke et al., 1990, 1990; Schoof, 2010, 2010; Sundal et al., 2011, 2011; Chandler et al., 2013, 2013; Doyle et al., 2014, 2014; Meyer et al., 2016) vary along the channelisation limit plotted in Figure 6.26. If one parameter were to exert an absolute control on the inland limit of channelisation then it would be represented as a flat line (e.g. a constant value) on the graph in Figure 6.28a. Hypothetically for example, if there were an absolute limit of 1,000 mm WE runoff for channelisation to occur (and no other parameters were exerting a control) then channelisation would extend inland until available runoff dropped below 1,000 mm WE and thus the inland limit would always be at 1,000 mm WE on the graph. It is clear that this is not the case for any of the parameters displayed, with all showing variation along the mapped inland channelisation limit (Figure 6.28). This indicates that the controls on channelisation limit are likely multifaceted and complex.

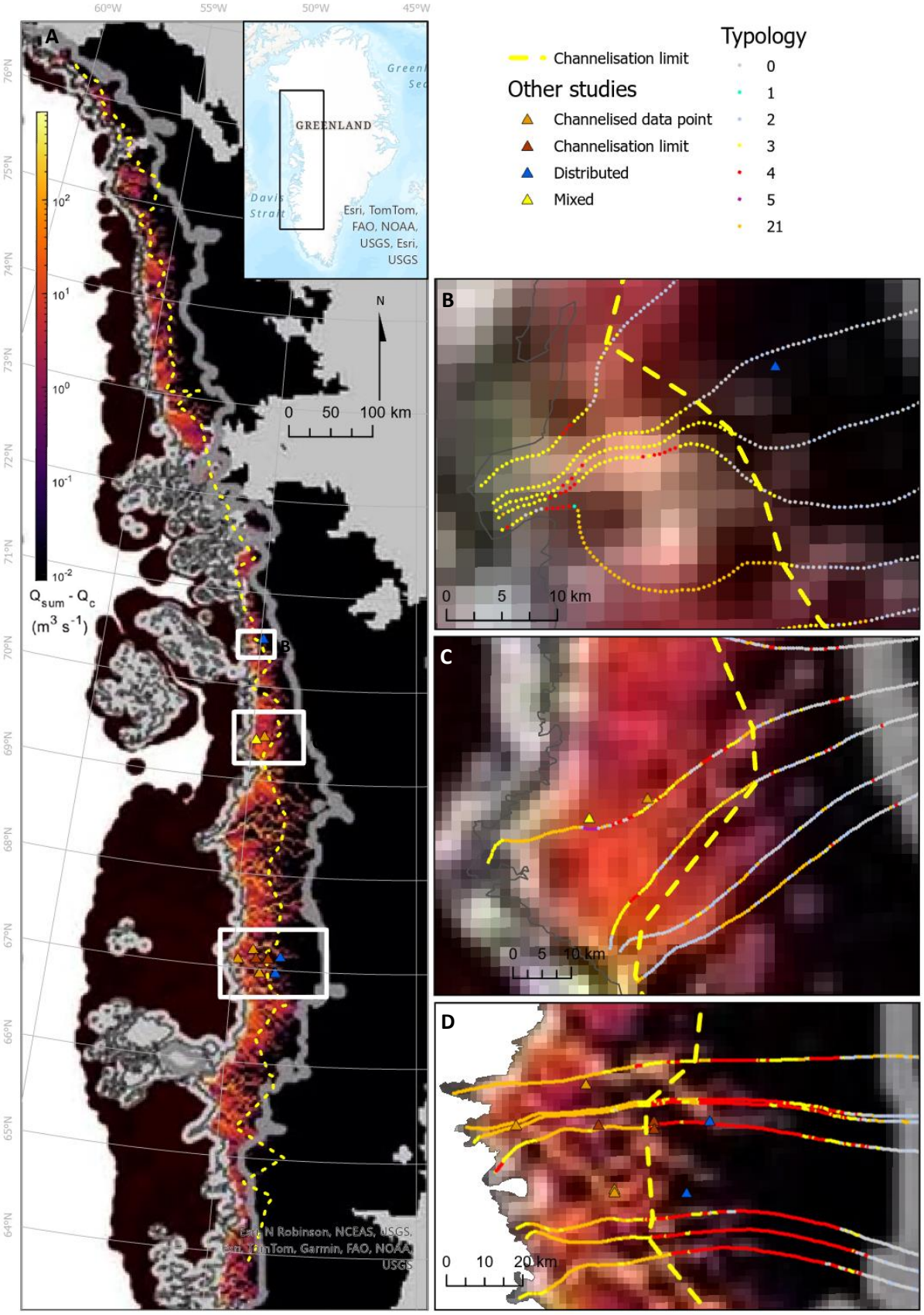

Figure 6.27 Estimation of the inland channelisation limit for 2019 derived by mapping the inland margin of the coherent

band of T21/T3 seasonal velocity typology in the central flowline dataset. The data plotted is as in Figure 6.26 but displayed over the modelled channelisation limit reproduced from Maier et al. (2022). Q_{sum} is the modelled accumulated discharge, Q_C is the modelled critical discharge beyond which channelisation is modelled to occur. As such, channelisation is modelled to occur where $Q_{sum} - Q_C > 0$.

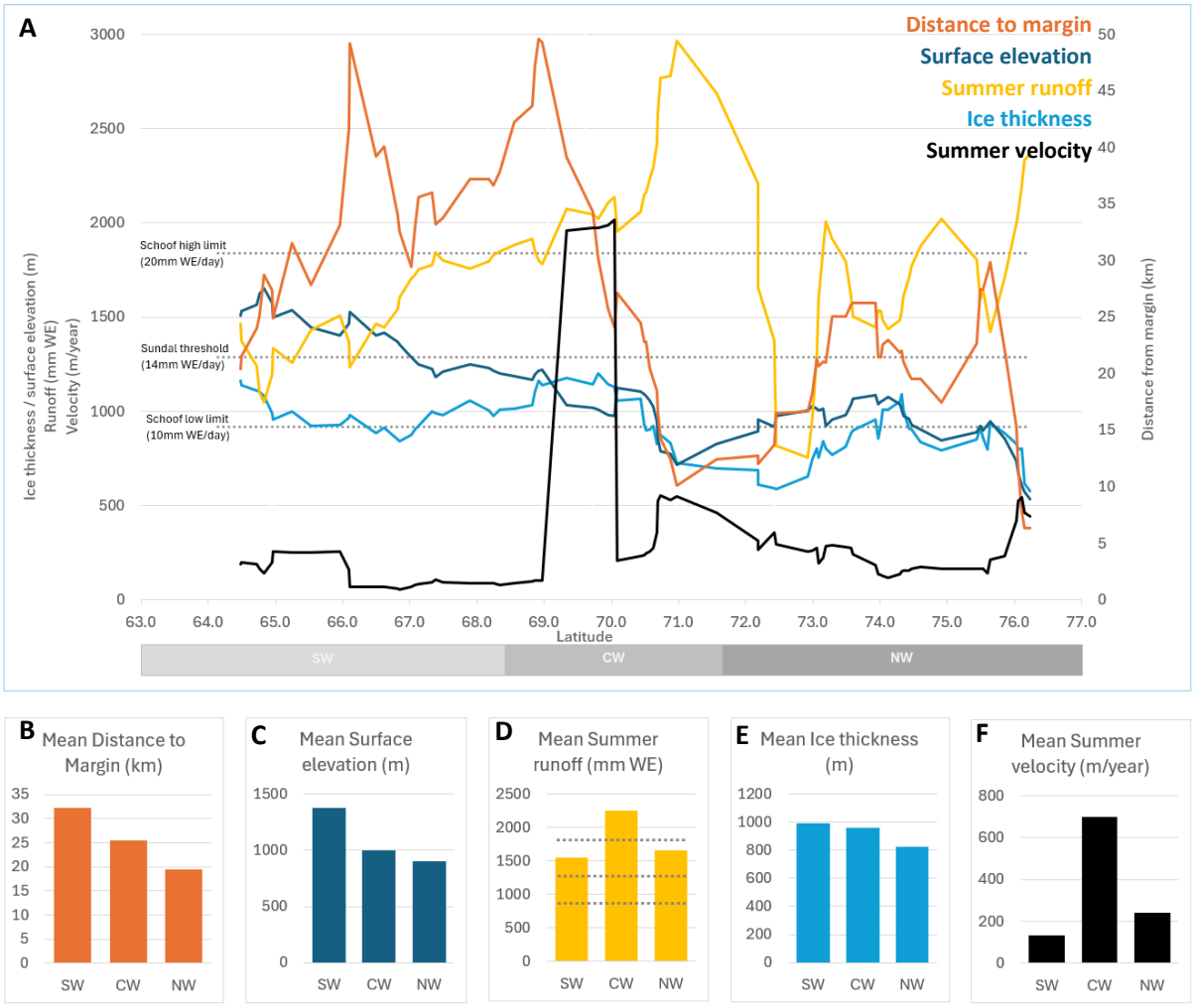

Figure 6.28 Distance to margin, ice surface elevation, summer runoff, ice thickness, and 2019 summer velocity plotted for the transect marked by the estimated inland channelisation limit plotted in Figure 6.26. A) The lines plotted are a 4 point moving average to smooth the noise in the data and enable comparison of the broader trends between the parameters. The bars underneath the x axis show the limits of the SW, CW, and NW regions (reworked from Mouginot et al. (2019)) which have been used to generate the regional means for each parameter in panes B-F. B) Mean distance to margin by region. B) Mean surface elevation by region. C) B) Mean summer surface runoff by region. The dashed lines show (from lowest to highest) the low limit for channelisation suggested by Schoof equivalent to 10 mm WE/day, the runoff threshold for channelisation suggested by Sundal et al. equivalent to 14 mm WE/day, and the high limit for channelisation suggested by Schoof equivalent to 10 mm WE/day. E) Mean ice thickness by region. F) Mean 2019 summer ice velocity by region.

A minimum level of melt availability is required for channelisation to occur (as discussed in section 6.4.3.2). The lower limit of melt availability of 10 mm WE/day proposed by Schoof (2010) is exceeded at the inland channelisation limit for all except two data points providing support for the hypothesis that widespread channelisation is unlikely below this limit on the western margin of the GrIS (Figure 6.28a). For the majority of the extent of the inland channelisation limit, the level of summer runoff is below the upper limit for channelisation viability of 20 mm WE/day suggested by Schoof (2010). However, runoff is above this level at a number of locations north of approximately 68°N, which marks the boundary between predominantly terrestrially terminating glaciers to the south, and predominantly marine terminating glaciers to the north. Ice velocity jumps markedly at approximately 69°N (Jakobshavn Isbræ) and maintains an elevated level (compared to the SW region) north of this location. Further, as ice velocity increases at 69°N, the distance of the channelisation limit inland from the margin decreases substantially from 50 km at ~68.5°N to only ~11 km at ~71°N. As the distance to the margin is decreasing over this sector, the runoff *increases* by 50% (Figure 6.28a). As such, the decreased distance inland of the channelisation limit cannot be due to melt availability.

One explanation for the decreased channelisation limit whilst melt availability increases may be the substantial increase in velocity in the CW and NW regions. Higher ice velocities are associated with greater longitudinal velocity gradients which increase creep closure rates of channels (Nye, 1953). Greater longitudinal velocity gradients also increases the antiplane shear strain rate. This decreases effective viscosity, softening the ice, and increases creep closure rates resulting in distributed drainage being maintained at flow rates that would otherwise force evolution to channelised drainage (Meyer et al., 2016). As such, the higher velocity in the CW and NW (~240 m/year and ~700 m/year respectively vs ~130 m/year in the SW, Figure 6.28f) may explain why the average distance of the channelisation limit from the margin is lower in the CW and NW compared to the SW (~19 km and ~26 km respectively vs ~32 km, Figure 6.28b) despite the higher melt availability (SW ~ 1,550 mm WE, CW ~2,250 mm WE, NW ~1,650 mm WE).

In addition to the ice rheology based controls due to velocity gradients, ice thickness may also be a significant control on channelisation limits with higher overburden pressures associated with thicker ice either precluding channel formation or forcing rapid creep

closure (Nye, 1953; Hooke et al., 1990; Chandler et al., 2013; Doyle et al., 2014). Ice thickness demonstrates the least variation along the inland channelisation limit of any of the measured parameters (Figure 6.28a, Figure 6.28e) supporting the notion that it may be a significant control on the inland limit of channelisation

6.4.3.3 SQ6 What are the spatial variations in seasonal velocity typology across the GrIS?

This section will discuss the spatial patterns in seasonal velocity typology, and in particular set the results of this chapter in the context of other comparable studies. Substantial discussion which is of a spatial nature has already been given in sections 6.4.3.1 and 6.4.3.2 where directly relevant to marine influence and surface melt driven processes. The purpose of this section is to pick on spatial patterns more widely, beyond the specifics already covered. Unless specifically stated otherwise, all reference is to the central flowline dataset.

6.4.3.3.1 Ice sheet scale

Only two previous studies have conducted research allowing meaningful analysis of spatial patterns in seasonal velocity typology at the ice sheet scale (Vijay et al., 2021; Solgaard et al., 2022). Direct comparison of these studies with the findings of this chapter are slightly challenging as both papers only consider a binary T2 or T3 classification. In Table 6.8 data presented in this chapter has been manipulated to align as closely as possible by presenting T2 prevalence as a percentage for the T2 + T3 total, excluding all other typologies. A rank ordering of regions (from 1 for highest T2 prevalence, to 6 for lowest prevalence) is also shown. All three studies show highest T2 prevalence in the NO region and have the NE ranked in the top 3. The results presented in this chapter and those of Vijay et al. (2021) also have the NW ranked in the top 3 regions for T2 prevalence. Solgaard et al. (2022) have the NW ranked lower (5^{th}), but their absolute prevalence value for the NW is very similar to Vijay et al. (2021) (43.8% and 45.3% respectively). All three studies show that the SE and SW regions have low T2 prevalence and are ranked 4 or lower, with the absolute prevalence similar for the SW (all studies within 5 percentage point of each other), but the Vijay et al. (2021) prevalence for the SE is much lower (at 12.1%) than the other two studies which both have values of 45%. The CW region has the greatest variation in results of the three studies. The Vijay et al. (2021) prevalence for the CW region is less than 50% of that of the other two studies. Solgaard et al. (2022) have CW T2 prevalence ranked much higher than the other 2 studies, but the absolute value is only 10% points higher that the results in this chapter.

Table 6.8 Regional T2 seasonal velocity prevalence. Numbers in brackets indicate the regional ranking of T2 prevalence (1 is high, 6 is low). Regions relate to those defined in Mouginot et al. (2019), but with the SE and CE regions merged to match the outputs of Solgaard et al. (2022). Data from this study has been reconfigured to show T2 prevalence in respect of the T2/T3 total. As such, the T3 values can be calculated as 100-T2% from the table for all studies.

Region	Solgaard et al. (2022) 2017-21	Vijay et al. (2021) 2017-19	This study 2016-19
NW	43.8% (5)	45.3% (3)	56.3% (3)
NO	76.2% (1)	93.0% (1)	62.3% (1)
NE	55.2% (3)	60.7% (2)	59.6% (2)
CW	65.8% (2)	27.6% (5)	55.6% (4)
SE	45.2% (4)	12.1% (6)	45.3% (5)
SW	41.0% (6)	45.2%% (4)	44.9% (6)

The broad spatial patterns show good overall agreement between the three studies, and reaffirm the conclusions of Vijay et al. (2021) that the prevalence of T2 is higher in the colder northern regions where melt seasons are shorter and less intense, whilst T3 prevalence is higher in the central and southern regions where the melt season starts earlier and is longer and more intense. The absolute T2 prevalence values of the results in this chapter are closer to those of Solgaard et al. (2022) (RMSE = 9.04) than those of Vijay et al. (2021) (RMSE = 22.19), but the rank ordering of T2 prevalence by region is closer to that of Vijay et al. (2021) (Spearman's Rank = +0.99) than Solgaard et al. (2022) (Spearman's Rank = +0.5) (Table 6.9).

Table 6.9 Spearman's Rank Correlation Coefficient and RMSE values for the T2 prevalence data presented in Table 6.8.

Datasets	Spearman's Rank	RMSE
Solgaard et al. (2022) vs this study	+0.5	9.04
Vijay et al. (2021)	+0.99	22.19

vs this study		
Solgaard et al. (2022)	+0.38	21.94
vs Vijay et al. (2021)		

6.4.3.3.2 Individual glaciers

Analysis was conducted for one sample year (2019) to comprehensively compare all seasonal velocity typology classifications from Vijay et al. (2021) with the results presented in this chapter (see Annex 1, Table A.1) Similar comparison with the Solgaard et al. (2022) study was not conducted as the structure of the reporting of the data in their paper does not make this possible. Of the 200 glaciers in the Vijay et al. (2021) dataset, 38.6% were also classified in this work. Of the glaciers that were classified in both studies, the level of agreement in classification is good. 55.3% of glaciers had an identical classification and 23.7% had distinctly different classifications. 21.1% were classified as T2 or T3 by Vijay et al. (2021) and were classified as T21 in the results presented here. As the T21 typology is interpreted to sit between T2 and T3 (e.g. as a hybrid class, similar to T2 in that it has a peak velocity close to peak melt, but then similar to T3 in that there is a late summer slowdown in velocity), these results are not a complete mismatch. If the T21 class were removed, all these observations would be allocated to either T2 or T3 class. As such, they are consider a partial match. Of the glaciers classified as T21 in this chapter, 15.8% were classified as T2 by Vijay et al. (2021), and 5.3% were classified as T3. Combining the identical and partial matches gives an agreement between the two studies of 79% in 2019.

Vijay et al. (2021) comment specifically on the seasonal velocity typology of a number of glaciers in their paper; in general there is good agreement between their findings and the results presented in this chapter. For example, Vijay et al. (2021) find that Upernavik Isstrøm I is consistently T3. T3 is also dominant at the calving front in the results presented here in both 2017 and 2019 (see Annex 1, Figure A.6), but beyond ~5 km from the front there is a switch to T21 and some T4 is apparent at the calving front in 2019 (a higher melt year). This demonstrates that whilst taken at face value the results from the two studies agree, the higher spatial resolution of the data presented here data enable the illustration of nuance and detail in the ice dynamics that are not possible from a single measurement

taken at the calving front.

Vijay et al. (2021) also give some commentary on specific glaciers where they were unable to classify typology, or where their classification varies from other studies. Vijay et al. (2021) were unable to classify Kangerlussuaq as it demonstrates high autumn and winter velocity values and therefore does not fit with either the T2 or T3 models that their study is limited to. In the results presented here, Kangerlussuaq is classified as T4 in both 2017 and 2019 (see Annex 1, Figure A.4). This demonstrates the ability of a classification schema with more classes to include a wider range of glacier typologies and therefore maximise the number of glaciers classified and reduce gaps in the data. It also illustrates the power of analysing the entire dataset to derive classification types (as in the K means approach adopted in chapter 5) as opposed to selecting exemplars of known end members and building a model to match the wider dataset to (as adopted by Vijay et al. (2021) in their methodology). The situation is similar for Jakobshavn which is also unclassified by Vijay et al. (2021), due to patterns of summer speedup and winter slowdown which are not recognised by their model. In the results presented here Jakobshavn is classified as a mix of T21 / T5 which represent these patterns of summer speedup and winter slowdown (see Annex 1, Figure A.3). Hagen Bræ is an interesting case study as this glacier was transitioning back to a quiescent phase during the study period following the end of a period of surging between ~2002-2012 (Solgaard et al., 2020). Vijay et al. (2021) classified Hagen Bræ as T2 in all years 2017-2019, but note in their discussion that Solgaard et al. (2020) found the glacier to be switching between T2 and T3 in recent years following the end of the surge. The results presented here classify the calving front as T21 in 2017 and 2019, with a transition to T3 approximately 10 km upglacier from the calving front in 2019 (a high melt year). If T21 is interpreted as a hybrid class on the continuum between T2 and T3, then the results presented here more closely align with the observations of Solgaard et al. (2020) than the classification presented by Vijay et al. (2021).

6.4.3.4 SQ7 What are the temporal variations in seasonal velocity typology across the GrIS?

6.4.3.4.1 Ice sheet scale

T3 prevalence is higher in high melt years than low melt years. The data presented in this chapter shows T3 prevalence is 28.6% higher in 2019 than in 2017 (Table 6.5). A very similar level of increase in T3 prevalence in high melt years has also been reported by both other studies that have conducted an ice sheet scale spatio-temporal analysis (Vijay et al., 2021; Solgaard et al., 2022)). Vijay et al. (2021) reported a 23.1% increase in T3 prevalence in 2019 compared to 2017. Solgaard et al. (2022) do not report overall yearly mean prevalence values, but calculation of a mean of their regional yearly typology prevalence values gives an ice sheet wide increase in T3 prevalence of 28.1% in 2019 compared to 2017.

As both Vijay et al. (2021) and Vijay et al. (2019) adopt binary classifications of seasonal velocity typology, any increase in T3 they observe must be offset by an equal decrease in T2. This is not the case in the results presented here where there are a total of seven distinct typologies. However, a reduction in overall T2 prevalence of 30.0% in 2019 compared to 2017 is observed (Table 6.5). A more modest decrease is seen in T21 prevalence of 10.0% in 2019 compared to 2017. This is interesting, and perhaps somewhat unexpected given that T21 is hypothesised to be representative of late summer slowdown caused by melt driven transition to channelised subglacial drainage (section 5.4.2.4). This is the same mechanism hypothesised to explain the increase in T3 prevalence in high melt years discussed above. As such, we might expect to see *increased* T21 prevalence in high melt years if the hypothesis is to be supported. This will be discussed further in section 6.4.3.4.2, below.

6.4.3.4.2 Regional scale

North Greenland

The changes in seasonal velocity typology prevalence between high and low melt years are spatially variable over the ice sheet. In 2017 the highest T2 prevalence is focused in the NO. In 2019 the T2 prevalence decreases substantially in the NO region, the most intense decrease of any typology prevalence between the high and low melt years (Figure 6.20). This broad regional pattern is also observed for the NO by Solgaard et al. (2022). This is

hypothesised to be representative of runoff being below the threshold required to generate a switch to channelised subglacial drainage in low melt years, but above the threshold in high melt years (Solgaard et al., 2022). Solgaard et al. (2022) attribute T2 decreases in the NO in high melt years to T3 increases. The results presented here show that the resultant seasonal velocity typologies in the high melt year are not uniformly T3, but that actually the five major catchments along the north coast alternate between T3 and T21, with Sermersuaq, Ryder and Academy all switching from T2 in 2017 to T3 in 2019, but with Petermann and Jungersen switching from T2 to T21 (Figure 6.29). There is also one anomaly present with Hobbs demonstrating an increase in T2 prevalence in the higher melt year. The variability in typology change between high and low melt years over relatively short distances between neighbouring glacial catchments in the NO region suggests that the processes controlling seasonal velocity typology are not solely limited to changes in atmospheric and ocean temperatures. Other processes operating at more localised spatial scales must also be a significant control on seasonal ice dynamics in order to explain this local variation.

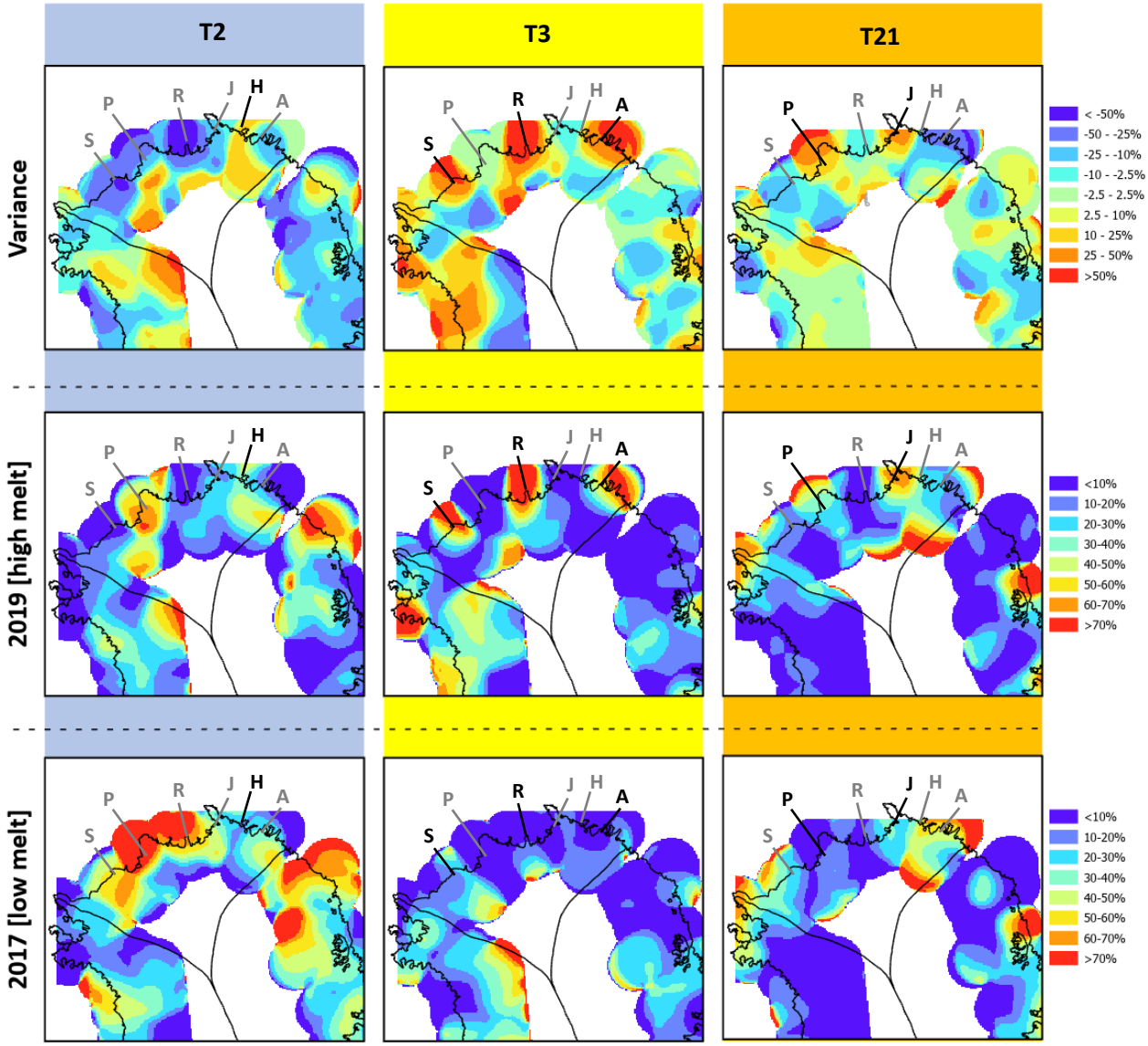

Figure 6.29 Kernal density analysis of the central flowline dataset seasonal velocity types in the NO region. This is a zoomed in view on the north coast, data is as presented for the whole of Greenland in Figure 6.20. Six principal glaciers are marked for reference; L-R Sermersuaq [Humbolt] (S), Petermann (P), Ryder (R), Jungersen (J), Hobbs (H), Academy (A). Data shows the proportion of central flowline dataset points classified in each seasonal velocity typology at each cell in the kernel density raster for a high melt year (2019) and a low melt year (2017). The maps of variance show the 2017 values subtracted from the 2019 values – as such, hot colours show where a typology is more prevalent in 2019, cool colours where a typology is more prevalent in 2017.

South West Greenland

Comparison with other studies in this chapter has generally shown broad agreement, with any difference relatively limited and nuanced, rather than contradictory. However, the findings in the SW region show a greater difference from previous work. One of Solgaard et al.'s (2022) key conclusions was that the SW region is insensitive to available runoff and that as a result the correlations between runoff and typology prevalence seen in other regions

are not observed in the SW. They infer that this is due to the background average runoff rate in the SW region possibly already being beyond the threshold for development of efficient channelised subglacial drainage. Whilst there appears to be some logic to this hypothesis, more detailed analysis of the data raises questions that need to be considered. Solgaard et al. (2022) do find the SW to have the lowest Type 2 rates of any region over their study period, but the average SW Type 2 prevalence is still reported as 41.0%. As Solgaard et al. (2022) interpret Type 2 as being representative of a distributed drainage configuration, so long as Type 2 prevalence is above zero, then it follows that there are some areas within the region where the threshold runoff level required to force channelised subglacial drainage formation is *not* exceeded. For example, it has been demonstrated that as melt increases due to atmospheric warming, the area experiencing seasonal velocity variation above the current ELA increases (Doyle et al., 2014; De Fleurian et al., 2016). As such, there is scope for increased Type 3 prevalence in higher melt years. If increases are not observed in higher melt years, this must either be due to other (as yet unidentified) processes preventing transition from Type 2 to Type 3, runoff increases being restricted to areas of the ice sheet already beyond the runoff threshold (possibly due to the local hypsometry of the ice sheet), or inaccuracies in the seasonal velocity typology data generated.

The data presented in this chapter demonstrates that T2 prevalence in the SW region *does decrease* in high melt years, with an average prevalence in 2016 & 2019 (high melt years) of 14.3% compared to the 2017 & 2018 (low melt years) average of 21.1% (Table 6.10). The results also show that T3 prevalence in the SW region *does increase* in high melt years, with an average prevalence in 2016 & 2019 (high melt years) of 25.6% compared to the 2017 & 2018 (low melt years) average of 20.2% (Table 6.10). This contradicts the findings of Solgaard et al. (2022) that Type 2 / Type 3 prevalence in the SW is insensitive to available runoff. One additional interesting finding from the results presented here in this regard is that the T21 prevalence in the SW region shows a *decrease* in high melt years (2016 & 2019 average of 25.8% vs 2017 & 2018 average of 32.7% (Table 6.10). This may seem counterintuitive given that T21 has been interpreted to be representative of channelised subglacial drainage (see section 5.4.2.4) which would be expected to increase with increasing runoff. However, if the typology of individual points is switching from T21 in a

lower melt year to T3 in in higher melt year, this provides further support for the notion of typologies being end members of a spectrum, and of T3 being a more pronounced expression of T21 requiring higher available runoff (see section 5.4.3). As Solgaard et al. (2022) do not have the T21 class (relying on only Type 2 and Type 3 as classification options), then many of the T21 points which switch to T3 in higher melt years in the results presented here may have already been initially classified as Type 3 by Solgaard et al. (2022) in the lower melt years, resulting in no change between high and low melt years, and the appearance of insensitivity to runoff availability. The actual situation may be that higher melt is driving a shift from more moderate late summer slowdown (T21), to more pronounced late summer slowdown (T3).

Table 6.10 Seasonal velocity typology prevalence values for points from the central flowline dataset in the SW region for each year in the study period, and average into high melt years (2016 & 2019), and low melt years (2017 & 2018).

Typology	2017	2019	2016	2018	High (2016 & 2019)	Low (2017 & 2018)
1	2.7%	0.5%	2.2%	0.3%	1.3%	0.3%
2	21.5%	16.9%	11.8%	20.8%	14.3%	21.1%
21	30.9%	23.0%	28.5%	34.4%	25.8%	32.7%
3	17.8%	22.3%	28.8%	22.6%	25.6%	20.2%
4	26.3%	33.6%	26.2%	21.2%	29.9%	23.8%
5	3.2%	3.7%	2.5%	0.7%	3.1%	1.9%

Further support for the notion of typologies forming a continuum (as opposed to discrete classes representing discrete processes) can be seen in the spatial patterns of change in the SW region. Whilst overall T2 prevalence decreases in high melt years, this is not caused by a uniform decrease in all areas. Decrease is greatest in areas of lower elevation closer to the margin of the ice sheet. In some areas of higher elevation further into the interior there are actually increases in T2 prevalence in the SW in higher melt years (Figure 6.30). The

situation is similar for T21 with the decrease focused at lower elevations close to the margin, and some increases further inland despite the overall decrease in prevalence of this typology in higher melt years (Figure 6.30). Increased prevalence of T3 in higher melt years is much more widespread (reflecting the net increase of this typology in the region), but the increases are most prominent in areas closer to the margin at lower elevations (Figure 6.30). This suggests therefore that it is possible that in some areas that are located where melt received is insufficient for channelisation to occur in low melt years (and are therefore T2) may be pushed over the melt threshold for channelisation in high melt years (and become T21). This is the process that is observed by Sundal et al. (2011), but rather than the six observations in one very geographically limited area of SW Greenland made in their study, here the observation is reproduced for many hundreds of points across large areas of the ice sheet. Similarly, the spatio-temporal patterns of decrease in T21 close to the margin in high melt years (coincident with areas of T3 increase) suggests that increased melt in these areas has pushed the seasonal velocity typology one step further along the continuum into a state representative of earlier onset and more sustained channelisation.

It has been suggested that inland migration of the channelisation limit under higher melt scenarios may be constrained due to enhanced creep closure under the thicker ice (Dow et al. 2014; Meierbachtol et al. 2013). However, whilst the specific mapping of the inland channelisation limit presented in section 6.4.3.2 was only conducted for a single year (2019), the patterns presented for 2017 (low melt) and 2019 (high melt) for the SW (Figure 6.30) are indicative of potential inland migration of the channelisation limit based on the level of melt available in a given year. It should be made clear that a full analysis of the inland channelisation limit has not been conducted for multiple years, so this inference is speculative. Further expansion in this area is a recommended focus for future work.

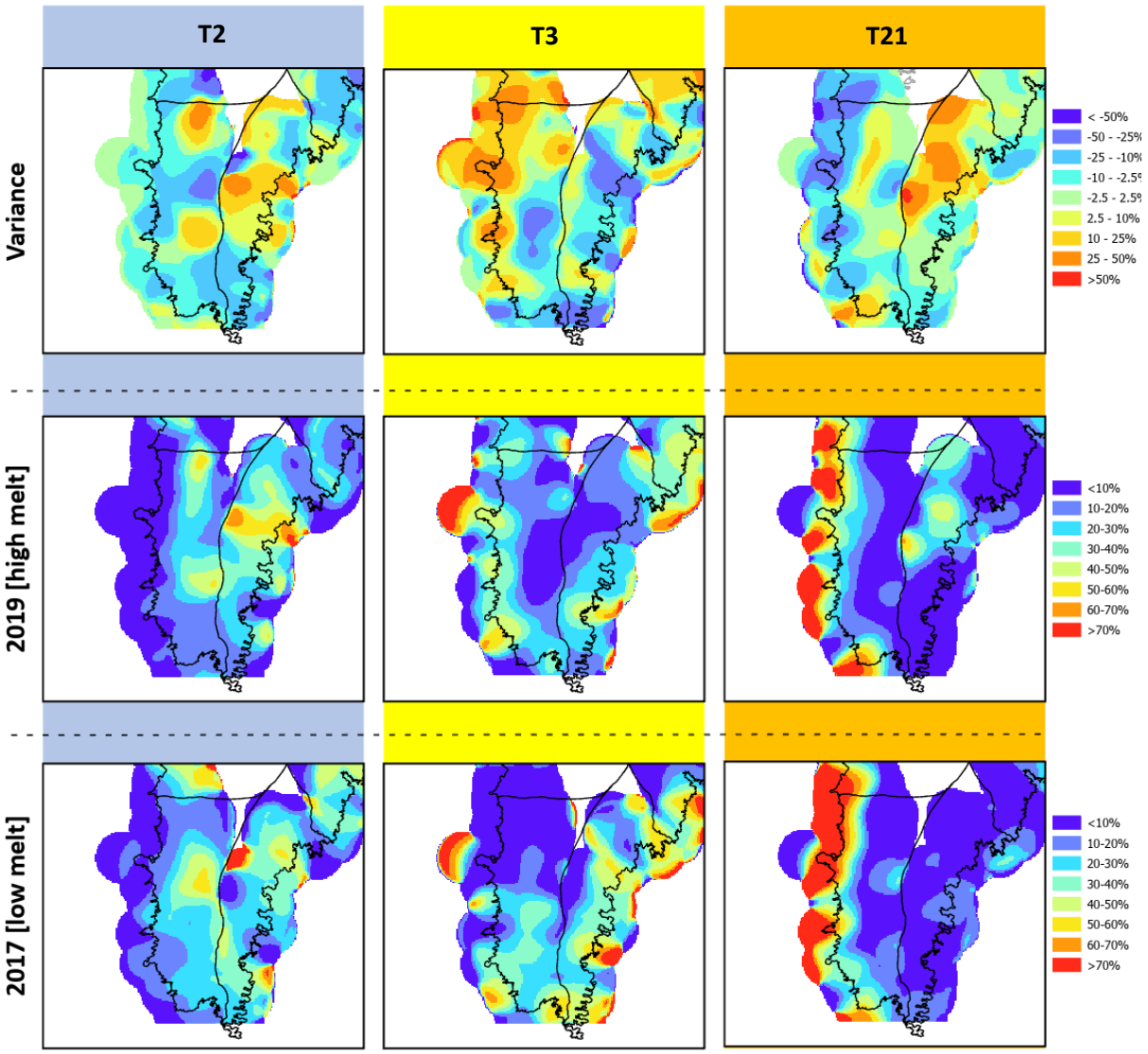

Figure 6.30 Kernal density analysis of central flowline dataset seasonal velocity types in the SW region. This is a zoomed in view of the SW, data is as presented for the whole of Greenland in Figure 6.20*. Data shows the proportion of central flowline dataset points classified in each seasonal velocity typology at each cell in the kernel density raster for a high melt year (2019) and a low melt year (2017). The maps of variance show the 2017 values subtracted from the 2019 values – as such, hot colours show where a typology is more prevalent in 2019, cool colours where a typology is more prevalent in 2017.*

Work on individual glaciers in the SW has also identified patterns that are representative of seasonal velocity typologies on a continuum (see Figure 6.25) rather than discrete, isolated classes. In their study of three neighbouring marine terminating glaciers in SW Greenland (Kangiata Nunaata Sermia (KNS), Narsap Sermia (NS), and Akullersuup Sermia (AS)), Davison et al. (2019) classified NS and AS as T3 in all years of their study period (2014-2018). KNS they classified as T2 in all years of the study. However, they also present evidence (by

mapping pro-glacial plumes) that suggests a switch to channelised drainage at KNS in high melt years, despite their T2 classification. Their analysis of high temporal resolution velocity data indicates that deceleration occurred as the subglacial system evolved to a channelised configuration, but this was late enough in the season that velocity did not drop below the baseline velocity. They conclude that their data illustrates a shift towards T3, and that if runoff were to increase further in future years, KNS could move to a position of being classified as T3 (Davison et al., 2020). The results in the central flowline dataset for NS and AS are in agreement with Davison et al. (2020) and they are classified as T3 at the calving front (see Annex 1, Figure A.7). The results presented in this chapter for KNS are also aligned with the findings of Davison et al. (2020) that typology is T2 but could shift to T3 in very high melt years. The results in the central flowline dataset classify KNS as a mixture of T2 and T21 in 2017 (low melt), and in 2019 (a high melt year) classification is a mixture of T2 and T21 within ~5 km of the calving front, but then transitions to T3 further upglacier from this position (see Annex 1, Figure A.7). This further consolidates the notion that T21 is representative of a hybrid typology that sits between T2 and T3 on a continuum of seasonal velocity typologies.

6.5 Conclusion

Ice sheet wide statistical analysis did not reveal a link between overdeepening morphometrics and patterns in seasonal ice velocity typology. There was not a statistically significant relationship between adverse slopes that exceed the supercooling threshold and the prevalence of seasonal velocity typologies interpreted to be reflective of distributed subglacial drainage being maintained throughout the melt season (T2 and T23). T2 and T23 were not found to be more prevalent on the adverse slopes of overdeepenings compared to the normal slopes, as might be expected if supercooling processes were having a significant, substantive and widespread impact on ice dynamics, or if channelised drainage was being suppressed on adverse slopes due to reduced hydraulic gradient.

However, visual interpretation of the central flowline dataset highlighted numerous examples of a very strong spatial relationship between overdeepenings and seasonal velocity typology, with coherent switching of typology as ice flows into and out of an

overdeepening. In these examples the typology switches were reflective of a switch from channelised subglacial hydrological system upglacier of the overdeepening, to a distributed system within the overdeepening, then reverting back to a channelised system down glacier of the overdeepening. This pattern is what would be expected if channelised drainage was being suppressed on adverse slopes and aligns with the conceptual model developed in Chapter 4.

When considering the typology of variation between the adverse and normal slopes of individual overdeepenings, variation typologies potentially reflective of adverse slopes modulating late summer slowdown via suppression of channelised drainage (T-D and T-E) were almost twice as prevalent as typologies reflective of the opposite (T-A and T-B). This is aligned with the conceptual model developed in Chapter 4, but it is important to note that the variations between normal and adverse slopes in the typologies were small, and may lie within error limits.

Typologies reflective of marine influence were found to be low in absolute prevalence, even in the spatial subset of the data limited to within 4 km of the ice front. This suggests that marine influence on the seasonal velocity dynamics of Greenland outlet glaciers may not be as significant as has been historically assumed.

The link between runoff availability and the prevalence of T2 and T3 typologies has been suggested in a number of previous studies (Moon et al., 2014; Vijay et al., 2019, 2021; Solgaard et al., 2022), but here a statistically significant relationship between runoff and typology prevalence is demonstrated for the first time. Typologies demonstrating late summer velocity slowdown (T21 and T3), interpreted as being representative of a seasonal evolution to channelised subglacial hydrological regime, were found to be positively correlated with total summer runoff. Typologies which do not demonstrate late summer velocity slowdown (T2 and T23), interpreted as being representative of distributed subglacial hydrological regime being maintained throughout the melt season, were found to be inversely correlated with total summer runoff.

Plotting the position of the inland limit of coherent blocks of T21 / T3 in the west coast to estimate the inland channelisation limit aligned very closely with existing field and modelling data indicating this limit. This suggests that the T21 / T3 boundary may be a suitable proxy for the inland channelisation limit.

There is close agreement between the results presented in this chapter and the specific findings of previous related studies (Vijay et al., 2019; Davison et al., 2020; Sakakibara and Sugiyama, 2020; Solgaard et al., 2020, 2022). This agreement suggests a good level of confidence in the accuracy of the approach taken within this study. In particular, the overall ice sheet wide and regional patterns and trends in seasonal velocity typology are well aligned to studies which had used much higher temporal resolution data (Vijay et al., 2021). Comparison of results for individual glaciers from these studies (where this was possible) also showed good agreement with the results. This demonstrates the efficacy of using low temporal resolution, but high spatial resolution velocity data for furthering understanding of the dynamics of the Greenland ice sheet.

Using a higher numbers of clusters in the K means analysis enabled the identification of a higher number of different seasonal velocity typologies than has been possible in previous studies. This was valuable when investigating nuanced spatio-temporal patterns of change and enabled further process understanding (such as sensitivity to runoff in SW Greenland) to be developed further than has been possible in previous studies. The higher number of typologies also allowed the notion of typologies being part of a continuum to be developed further and there is good support for this. There were numerous examples (both at the regional and individual glacier scale) of uncertainty over whether a typology is T2 or T3 in other studies, whereas the results presented here gave a T21 typology. This provides evidence to support the notion that T21 is a hybrid typology between T2 and T3 end members on a continuum.

Chapter 7 Discussion

In this chapter the research aim, research questions and objectives (section 1.2) will be revisited with a brief review of which chapters were associated with each. A summary of key findings will follow. The implications of the key findings for future change in Greenland will be presented, and the chapter will conclude by discussing limitations of this study, and potential directions for future research.

7.1 Review of research aim, questions and objectives

The principal aim of this thesis was to determine the location and morphology of overdeepenings under the Greenland Ice Sheet, and to examine their impact on hydrology and ice dynamics. To achieve the aim a number of research questions (RQs) were developed, each with associated objectives (section 1.2). These were:

RQ1: How common are overdeepenings under Greenland outlet glaciers and how variable is their geometry?

> **a)** Develop a semi-automated workflow for mapping all overdeepenings under fast flowing ice on the Greenland Ice Sheet and extracting morphometric parameters, and implement this to derive a high-resolution dataset of all overdeepenings (Chapter 3).
>
> **b)** Investigate patterns and potential process relationships in overdeepening morphometry (Chapter 3).

RQ2: Does bed topography modulate ice velocity in overdeepenings?

> **a)** Explore at an ice sheet scale whether annual mean ice velocity is modulated when flowing through an overdeepening (Chapter 3).
>
> **b)** Determine whether seasonal ice velocity (e.g. timing and magnitude of speedup and slowdown) varies along glacier length, and the extent to which these variations may be linked to bed topography (Chapters 4 and 6).

RQ3: Are there any broad scale patterns that link the seasonal ice velocity signature to bed topography or other GrIS-wide factors?

> **a)** Develop an automated workflow for identifying distinct seasonal velocity variation

typologies and classify velocity time series data points into these typologies at an ice sheet scale (Chapters 5, 6).

b) Explore the extent to which there is evidence at the ice sheet scale for patterns in ice dynamics modulated by overdeepenings identified for individual glaciers in **RQ2** (Chapter 6).

c) Quantify the spatial and temporal patterns (and potential process relationships) between seasonal ice velocity typology and other relevant factors. (Chapter 6).

7.2 Summary of key findings

This section revisits each research question and summarises the principal findings of the thesis.

7.2.1 RQ1: How common are overdeepenings under Greenland outlet glaciers and how variable is their geometry?

Chapter 3 demonstrated that overdeepenings are extremely common features under outlet glaciers of the GrIS. In total, 2,393 individual overdeepenings were identified, of which 1,284 were parent overdeepenings. Of these, 621 passed the quality assurance process and were included in the metric dataset utilised for all further analysis in Chapters 3-6. All further reference to the overdeepening dataset in this chapter is to this metric dataset. Overdeepenings were present across the entire study area with no substantive sectors of fast flowing ice not having overdeepenings present (Figure 3.12).

The semi-automated method developed for mapping overdeepenings in Chapter 3 was efficient and effective in generating a high-quality dataset. The resulting dataset represents a substantial improvement on the only other previous Greenland-wide overdeepening dataset, which mapped 335 overdeepenings to the quality standard of the metric dataset (Patton et al., 2016). The semi-automated approach enabled the BedMachine bed topography dataset (Morlighem et al., 2017) to be used for mapping overdeepenings in Greenland for the first time. The spatial resolution of the BedMachine data (150 m) is over 40 times higher than the Bamber et al. (2013) (1000 m) bed data used by Patton et al. (2016). As a result of this increased resolution, not only are more overdeepenings mapped, but they are mapped at a higher fidelity. The ability to resolve finer features using the

BedMachine dataset facilitates the identification of features close to the margin which are often narrow and highly elongate, which were therefore not identified by Patton et al. (2016). In total, 515 new overdeepenings that were not mapped by Patton et al. (2016) are included in the dataset, and many of these are located close to the margin (Figure 3.31). These overdeepenings near the margin are under the fastest flowing ice in the region of the ice sheet most sensitive to future change (Catania et al., 2020). As such, knowing their location and geometry is key to our understanding of how the dynamics of the GrIS may respond to a changing climate, and to model the nature, timing and impact of these changes more accurately (Catania et al., 2018; Fox-Kemper et al., 2021).

Many models of glacial erosion suggest that erosive power is proportional to the speed at which ice flows over the bed (Hallet, 1979; Oerlemans, 1984; Anderson et al., 2006; Egholm et al., 2011)**.** It can therefore be extrapolated that overdeepenings (as erosive features) are preferentially located in areas of higher ice velocity, and that overdeepening depth scales with velocity (Cook and Swift, 2012). There does seem to be some evidence in Chapter 3 to partially support this hypothesis. Of the 553 central glacier flowlines mapped, 396 (71.6%) intersected at least one overdeepening in the metric dataset (Figure 3.13). Central glacier flowlines that did not intersect an overdeepening were located in areas of slower ice (mean velocity at terminus 825 m a^{-1}) than those that did intersect overdeepenings (mean velocity at terminus 1839 m a^{-1}) (Figure 3.14). However, there was no correlation found between overdeepening depth and mean ice velocity (Figure 3.26). Thus, when the overdeepening dataset is analysed as a whole, there is some evidence for the preferential location of overdeepenings in faster flowing ice, but no evidence that in areas where contemporary ice velocity is higher this has systematically led to greater overdeepening depth.

Ice flow confluences are typically areas of localised speedup (as a result of a need to conserve mass as ice flows through a reduced cross sectional area), and for the reasons related to erosive potential discussed above, have been widely suggested as preferential locations for overdeepenings formation (Glasser, 1995; Kessler et al., 2008; Alley, 2003; MacGreggor et al., 2000; Swift, 2008). Chapter 3 demonstrates that 82% of overdeepenings in the dataset do not occur at a confluence. Thus, irrespective of any potential process relationship of confluences on overdeepening formation, it can be concluded that they are not a prerequisite condition for overdeepening location, and as such, they are unlikely to be

a dominant factor in overdeepening evolution.

Convergent ice flow is thought to facilitate the erosion of deeper overdeepenings (Holtedahl, 1967; Alley et al., 2003; Kessler et al., 2008). The findings of Chapter 3 support this hypothesis. Overdeepenings are over 30% deeper where ice is converging compared to when ice flow is parallel or diverging (Table 3.3), and overdeepenings are also observed to be deeper when located in the proximity of a confluence (Table 3.4). However, there is the potential for spatial bias in these results because both convergent ice flow is likely more prevalent towards the ice margin (section 3.4.2.4) where ice velocity and melt availability are higher. Given the lack of correlation between ice velocity and overdeepening depth it seems unlikely that velocity is a confounding variable. Melt availability has not been specifically analysed in relation to overdeepening morphology, but this would be an interesting area for further study.

The results presented in Chapter 3 demonstrate that there is substantial variation in the range of values for each morphometric parameter measured for overdeepenings in the dataset (Table 3.2). Such variation was also noted by Patton et al. (2016), but it was suggested that this may be due to limitations in the resolution of the data, or the limited number of overdeepenings in the metric dataset of that study. The findings in Chapter 3 show that despite almost doubling the number of overdeepenings in the metric dataset and utilising bed data of more than an order of magnitude higher resolution when compared to Patton et al. (2016), the variation in the morphometric data is not dramatically reduced (Table 3.7) and the strength of correlations between pairs of morphometric parameters are not substantially increased (Figure 3.21 and Figure 3.22). This suggests that rather than noise being due to methodological and data limitations, the variation apparent in the morphometric data may simply be reflective of the true variation of overdeepening geometry. Substantial variation in overdeepening geometry is also observed in studies in high mountain contexts (Haeberli et al., 2016).

Despite the variation recorded in overdeepening geometry, there are certain parameters that show a clear trend towards preferred values. Overdeepening depth shows a strong preference for shallower depths and very few overdeepenings evolve to the depths of greater than 1000 m (Figure 3.14d). This supports the hypothesis that overdeepenings reach an equilibrium state and stabilise once they reach a certain geometry rather than continuing

to erode until they reach the maximum depth possible. The morphometric parameter that shows the strongest preference for a particular value is the BSSR which is strongly unimodal with distribution heavily focused around the median of -1.91 (Figure 3.20j). This is very close to the value of ~-1.6 classically taken as the supercooling threshold (Röthlisberger and Lang, 1987; Alley et al., 2003). Strong preference for a BSSR close to the supercooling threshold suggests that this may be a key control limiting overdeepening depth (section 3.4.2.1). Other studies have also observed that overdeepenings exhibit a strong preference for a bed geometry near the supercooling threshold (Table 7.1), but none as close to the supercooling threshold as the results in Chapter 3.

Table 7.1 Comparison of median BSSR reported by a range of studies. N shows the number of overdeepenings analysed in each study.

Study	**Median BSSR**
This study [n = 621]	-1.91
Patton et al. (2016) [n = 335]	-2.51
Werder (2016) [n = 147]	-3.22

7.2.2 RQ2: Does bed topography modulate ice velocity in overdeepenings?

Chapter 3 demonstrated that mean annual ice velocity is higher on the adverse slope of an overdeepening than the normal slope when the dataset is analysed in aggregate for all overdeepenings of the GrIS (see Figure 3.27, section 3.4.4). However, this is not universal and in 21.7% of overdeepenings velocity is faster on the normal slope. Attempting to identify complex process relationships using such highly aggregated data at the ice sheet

scale is inherently challenging. In particular, the fact that ice velocity generally trends to higher speeds closer to the margin confounds the interpretation of the observations within individual overdeepenings. Adverse slopes are downstream of normal slopes, and we might therefore expect velocity on them to be faster than the normal slope even if the adverse slope is not having a modulating effect. This was attempted to be controlled for by measuring the background ice speedup signal using the pseudo overdeepening analysis (section 3.3.5.2). This showed that there was still an average speedup pattern on adverse slopes once the background effect was accounted for. This was much smaller (5.1% increase in prevalence of higher velocity on adverse slope than normal slope in an overdeepening), but still significantly significant (section 3.3.5.2). Perhaps the most valuable finding of this analysis was that there was no evidence for a systematic slowdown on adverse slopes. This is interpreted as indicating that any backstress induced by form drag over the adverse slope of an overdeepening is offset by reduction in skin drag due to elevated basal water pressures on the adverse slope. This interpretation of the modulating impact of ice velocity on adverse slopes is aligned with empirical field measurements on individual mountain glaciers such as Storglaciären, which suggest elevated basal water pressures and therefore higher ice velocity on adverse slopes of overdeepenings (Hooke et al., 1989; Hooke and Pohjola, 1994) (see section 2.4). However, the impact of overdeepenings on ice dynamics has not been well studied and there are limited examples beyond Storglaciären to draw from in the existing literature (Cook and Swift, 2012). To the best of my knowledge the results presented in Chapter 3 are the first time that the modulating effect of overdeepenings on ice dynamics in Greenland has been investigated.

Observations from the two individual outlet glacier case studies (Helheim and Upernavik Isstrøm II) in Chapter 4 demonstrate that seasonal velocity patterns vary along the centre line of some glaciers. In both cases there were distinct changes in the seasonal velocity patterns either side of the riegel at the downstream lip of the overdeepenings. On the downstream side of the riegel the pattern of seasonal velocity was aligned with the Moon Type 1 typology (gradual increase in ice velocity from summer on which continues after melt ceases in autumn (Moon et al., 2014)) in both case studies. This is widely interpreted in the literature to be indicative of seasonal velocity variation controlled by marine processes linked to the seasonal retreat of the calving front (Moon et al., 2014; Vijay et al., 2019, 2021;

Solgaard et al., 2022). Ice velocity increases with retreat of the calving front due to reduced back stress, velocity increase is not directly linked to melt, and continues to increase after melt ceases in late summer (Howat et al., 2008; Joughin, Das, et al., 2008; Sole et al., 2013; Tedesco et al., 2013; Moon et al., 2014; Rathmann et al., 2017; Cheng et al., 2022). On the upstream / inland side of the riegel (e.g. within the overdeepening) there was no evidence of Type 1 seasonal variation at either Helheim or Upernavik Isstrøm II. At both glaciers variation inland of the riegel was strongly linked to melt and the associated subglacial hydrological regimes (e.g. Moon Type 2 and Type 3 seasonal variation), as is often observed on mountain glaciers (Bindschadler et al., 1977; Iken and Truffe, 1997; Gudmundsson et al., 2000; Nanni et al., 2023) and land terminating sectors of the GrIS (Nienow et al., 2017; Davison et al., 2019). The results presented in Chapter 4 demonstrating differing typologies of seasonal velocity variation either side of the riegel have been independently corroborated for Upernavik Isstrøm II in a paper published by Larsen et al. (2023) after the analysis for Chapter 4 was completed. No directly comparable studies for Helheim have been conducted to date.

Intriguingly, both at Helheim and Upernavik Isstrøm II, the riegel is positioned almost exactly at the theoretical stress-coupling length (SCL) limit (Enderlin et al., 2016; Larsen et al., 2023). As such, it may be expected that direct strain influences from reduced backstress at the margin associated with frontal retreat (i.e. the 'pulling' forces introduced conceptually in (section 4.1) might be dissipating at these locations irrespective of the presence of the riegel. However, influence of forces at the margin may be expected beyond the SLC limit due to dynamic thinning (Pritchard et al., 2009; Newton and Huuse, 2017; Walker and Gardner, 2017). This is not seen in the seasonal signal inland of the riegels at Helheim or Upernavik Isstrøm II suggesting that the riegel may be isolating ice further inland from dynamics at the calving margin. Irrespective of the uncertainty in terms of the processes controlling the observed seasonal velocity variations either side of the riegel, it is clear from Chapter 4 that seasonal velocity patterns can vary along glacier centre lines. Therefore, approaches to investigating seasonal velocity variations that constrain analysis to locations at or very close to the terminus (e.g. Moon et al., 2014; Vijay et al., 2019, 2021) cannot be taken to be representative of the patterns within the wider system.

Case study 2 in Chapter 4 considered the seasonal velocity dynamics of an outlet glacier

using the highest possible spatial and temporal resolution data available at the time the research was conducted. The results show perhaps the most compelling evidence within the thesis to support the hypothesis that supercooling processes on the adverse slope result in relatively higher basal water pressures being maintained, reducing the likelihood of an evolution from distributed to channelised subglacial drainage configuration as melt increases through the summer. This was most clearly demonstrated for 2016 at Upernavik Isstrøm II where markedly different velocity responses were observed on the adverse and normal slope of the overdeepening, indicative of evolution to channelised drainage on the normal slope whilst distributed drainage on the adverse slope appeared to be maintained (Figure 4.5). These observations were used to develop a conceptual model of four configurations of subglacial drainage in overdeepenings which explain all observed patterns of seasonal evolution of ice velocity in the overdeepening of Upernavik Isstrøm II between 2015-2017 (Figure 4.6,). Chapter 6 also presented results for a wider range of glaciers (but in less detail) beyond Upernavik Isstrøm II which were aligned with the expected seasonal velocity response of configuration C of the conceptual model (Figure 4.6), where subglacial hydrology has evolved to be channelised upstream or downstream of an adverse slope but remains distributed on the adverse slope (e.g. Academy Gletsjer (Figure 6.22), Inngia Isbræ (Figure 6.23), and K.J.V Steenstrup Nordre Bræ (Figure 6.24), Section 6.3.2.2).

7.2.3 RQ3: Are there any broad scale patterns that link seasonal velocity signature to bed topography or other GrIS-wide factors?

Chapter 5 was closely focused around RQ3 Objective A and presented the development of an automated method for classifying velocity time series data points into seasonal velocity variation typologies. The method adopted a machine learning approach utilising a K means clustering algorithm. The final implementation of the method classified the data into 12 clusters which were then manually aggregated into seven typologies each interpreted to be representative of a distinct pattern of seasonal ice velocity variation. Compared with previous studies that have established either two (Vijay et al., 2021; Solgaard et al., 2022) or three (Moon et al., 2014; Vijay et al., 2019) typologies, this provided a more nuanced analysis of seasonal velocity variation and the processes that may be controlling them. All three of the previously established typologies (Moon et al., 2014) were represented in the

clusters along with two additional variants of Moon Type 2, and two further typologies not previously identified in classifications of other studies (T4 and T5). The identification of the T21 typology represented the first time that direct observation of a seasonal velocity typology sitting between Type 2 and Type 3 as end members on a continuum had been made providing further support for this hypothesis (Figure 5.17).

Comparison with previous studies (when they aligned spatially and temporally) gave confidence that the method could reproduce the findings of these studies. The most comprehensive analysis possible was with the dataset of Vijay et al. (2021) for 2019. Despite the fact that Vijay et al. (2021) only identify two typologies in their study, of the 77 glaciers classified by both studies, the level of agreement was approximately 79% (section 6.4.3.3). Agreements in seasonal velocity variation typology were also identified with a range of other studies considering individual, or small numbers of glaciers (Davison et al., 2020; Sakakibara and Sugiyama, 2020). Of particular importance was the high-level of agreement with other studies, despite the method used within this thesis utilising lower temporal resolution velocity data (quarterly means). In comparison to the four individual velocity averages per year used in the analysis in Chapters 5 and 6, Vijay et al. (2021) used ~6 day velocity averages giving ~45-60 individual velocity averages per year. The high level of agreement between the results of this thesis and Vijay et al. (2021) demonstrates that meaningful and accurate classification of seasonal velocity typologies can be made with low temporal resolution data. This allows the computational resources available for processing and analysis to be utilised to give greater spatial coverage. Specifically, this allowed analysis of over 190,000 spatial locations compared to only 358 by Vijay et al. (2021) (Table 5.3).

A primary motivation for RQ3 was to establish whether the evidence of potential modulation of seasonal ice dynamics by hydrological processes on adverse slopes where the supercooling threshold is exceeded (as observed for Upernavik Isstrøm II, Section 4.3.2) is widespread, and objective B of RQ3 focussed on this. Ice sheet wide statistical analysis in Chapter 6 did not reveal a clear link between overdeepening morphometrics and seasonal ice velocity typology. There was not a statistically significant relationship between adverse slopes which exceed the supercooling threshold, and the prevalence of seasonal velocity typologies interpreted to be reflective of distributed subglacial drainage maintained throughout the melt season. This potentially reflects the fact that differential speedup and

slowdown on the normal and adverse slopes of overdeepenings due to supercooling processes operate at short timescales of days to weeks (section 4.3.2.6) which are not resolvable in the quarterly averaged velocity data used in Chapter 6. The use of the classic supercooling threshold may also not accurately reflect when supercooling is and is not actually occurring (Werder, 2016). These methodological limitations and constraints are discussed in more detail in section 7.4, below.

Despite the fact that there was no association found between seasonal velocity typology *prevalence* and overdeepening morphometry there was some support for seasonal dynamics being modulated by adverse slope processes in the typology of variation between the adverse and normal slopes of individual overdeepenings. The generation of this distinct variation typology (Section 6.3.1.3) was designed to pick up more nuanced difference in the behaviour between adverse and normal slopes of an individual overdeepening. For example, an individual overdeepening may be classified as T21 on both the adverse and normal slope. As such, any analysis investigating typology *prevalence* will identify no variation between the adverse and normal slopes. However, it is established that there is potentially variation in the magnitude of seasonal patterns *within* a typology (Section 5.2.4.2). For example, whilst both the adverse and normal slopes might be classified as T21, the autumn slowdown may be more pronounced on the normal slope. This is what the variation typologies measure. Analysis in Chapter 6 demonstrated that the variation typologies suggestive of more muted autumn slowdown on the adverse slopes of overdeepenings (T-D and T-E) were twice as prevalent as those typologies that suggest the opposite (T-A and T-B) (Section 6.4.2.3).

RQ3 objective C considered other factors not directly related to overdeepening morphology and how these may be controlling seasonal velocity typology at an ice sheet scale. It has been consistently hypothesised that seasonal velocity typology (especially Type 2 and Type 3) is controlled by melt, with Type 2 thought to be representative of scenarios where melt is insufficient to induce a switch to channelised drainage, and Type 3 representative of where melt is sufficient to cause a seasonal evolution from distributed to channelised drainage (Sundal et al., 2011; Moon et al., 2014; Vijay et al., 2019, 2021; Davison et al., 2020; Solgaard et al., 2022). However, despite drawing associations, no previous studies have demonstrated a statistically significant relationship between melt and seasonal velocity

typology. In Chapter 6, a statistically significant relationship between runoff and seasonal velocity typology was demonstrated for the first time (Table 6.3 and Table 6.4). Logistic regression analysis established the percentage probability increase or decrease in a point of interest being classified as a given typology based on a set level of runoff increase. For every 1,000 $mmWEa^{-1}$ increase in runoff, the likelihood of seasonal velocity typology being T21 or T3 (e.g. a typology hypothesised to be reflective of a channelised subglacial drainage configuration) increased by between 30-50% (Table 6.2 and Table 6.3). This relationship was demonstrated both for the central flowline dataset covering the entire study area, and also for the dataset limited to areas within overdeepenings.

Previous studies have also hypothesised that Type 2 and Type 3 typologies are not discrete, but end members on a spectrum of seasonal velocity response driven primarily by melt availability (Moon et al., 2014; Vijay et al., 2019, 2021; Davison et al., 2020; Solgaard et al., 2022). Evidence presented in Chapter 6 provides further support for this hypothesis. The identification of T21 which is interpreted to be a hybrid typology between Type 2 and Type 3 (Figure 5.17, section 5.4.3) is strongly conceptually aligned with the continuum hypothesis. Examples of specific glaciers classified as T21 in Chapter 6 coincided with locations where previous studies had been unable to classify seasonal velocity typology. This was the case for Kangiata Nunaata Sermia in 2017 and 2019 (Davison et al., 2020). Support for the Type 2 / Type 3 continuum hypothesis was also evident in the spatiotemporal analysis of changes in seasonal typology patterns at the ice sheet scale where apparent migration of typologies was observed between low and high melt years. In higher melt years T3 becomes more prominent at lower elevations closer to the margin, T21 shifts to higher prevalence in mid-elevation positions, and T2 becomes viable at higher elevations and redistributes further inland accordingly (Figure 6.20). These patterns are well aligned with the observations of differential seasonal velocity patterns dependent on melt availability made by Sundal et al. (2011).

The influence of marine processes on calving rates of marine terminating outlet glaciers has historically been well studied and often hypothesised to be a dominant control on the dynamics of such glaciers (Howat et al., 2008; Joughin et al., 2010; Murray et al., 2010; Bevan et al., 2012) (see section 2.3.2.1). Type 1 has been hypothesised to be the typology associated with such processes (Moon et al., 2014; Vijay et al., 2019, 2021; Solgaard et al.,

2022).The analysis in Chapter 6 investigating these connections presents two interesting findings. Support for the hypothesis that Type 1 is representative of the influence of marine process presented in previous studies is further strengthened. T1 prevalence in the zone at the terminus of marine terminating outlet glaciers was found to be 151.1% that of the prevalence in the dataset as a whole, and no land terminating glaciers were classified as T1 at their terminus (Table 6.8). As such, there appears to be support in the data that T1 is associated with marine processes. However, only 5.5% of marine terminating outlet glaciers were classified as T1 close to the terminus (Table 6.8). This suggests that whilst T1 might be controlled by marine processes, for the vast majority of outlet glaciers in Greenland, marine processes are not the dominant control on seasonal velocity variations. A potential explanation for the seeming disparity between the established links between ice dynamics at the calving fronts of marine terminating glaciers (Howat et al., 2008; Joughin et al., 2010; Murray et al., 2010; Bevan et al., 2012) and the very low observed prevalence of T1 in the terminal zone of outlet glaciers presented in Chapter 6 may be a result of the temporal resolution of the study. Recent observations and analysis of the dynamics of Helheim glacier find that melt driven processes are the dominant control of ice dynamics at seasonal and interannual timescales, but that frontal retreat becomes dominant over multiannual timescales (Ultee et al., 2022).

Finally, perhaps one of the findings that may have the greatest relevance to the future stability of the GrIS was the observation in Chapter 6 (section 6.4.3.2) that the boundary where seasonal velocity changes from a coherent zone of T21/T3 to a coherent zone of T2 may represent a proxy for the inland channelisation limit (Figure 6.26). When mapped the position of this switch in typology was in very strong agreement with the limit of channelisation inferred from previous field observations (Chandler et al., 2013, 2021; Meierbachtol et al., 2013; Andrews et al., 2014; Van De Wal et al., 2015; Doyle et al., 2018), and modelling studies (Dow et al., 2014; Banwell et al., 2016; De Fleurian et al., 2016; Koziol and Arnold, 2018; Maier et al., 2022). The details of these findings and their implications are discussed further in Section 7.3.2.

7.3 Implications for future GrIS change

The principal relevance of the findings of this thesis with regard to implications of future change of the GrIS cover two key areas:

1. Overdeepenings are known to modulate the rate at which the ice sheets retreat particularly in marine contexts due to marine ice sheet instability (Weertman, 1974; Schoof, 2007).
2. Inland limits of channelisation of the subglacial hydrological system are fundamental to ice velocity feedbacks under future increased melt.

The findings of this thesis have advanced the understanding of these areas, and these will be discussed in turn below.

7.3.1 Modulation of ice retreat by overdeepenings

It is well established that bed topography can have a substantial stabilising or destabilising effect as ice retreats over it (Catania et al., 2020). If ice is *advancing* up the adverse slope of an overdeepening it will generate back stress, which needs to be overcome for advance to continue, and therefore exert a stabilising control on advance (Brinkerhoff et al., 2017; Motyka et al., 2006; Nick et al., 2009). When the ice front is *retreating* back up a normal slope, this will have a similar stabilising effect. However, if retreat of a marine terminating glacier causes the ice front to enter an overdeepening, and therefore start to retreat down an adverse bedslope, the back stress is removed, and retreat into deeper water may accelerate retreat dramatically (Meier and Post, 1987; McNabb and Hock, 2014). Such rapid retreat may continue until a stabilising position on the normal slope of the overdeepening is reached (Catania et al., 2020) (see section 2.3.2.3). It has been demonstrated that the total amount of retreat of a glacier is strongly linked to the length of the overdeepening behind the calving front at the onset of sustained retreat. Observations of 15 marine terminating outlet glaciers in west Greenland by Catania et al. (2018) found that approximately 80% of retreat over their study period could be explained by the length of the overdeepening ice was retreating into. The lengths of overdeepenings in their study were found to be heterogenous, and this was suggested as a potential explanation for the variable retreat of neighbouring glaciers found in numerous other studies (Walsh et al., 2012; Moon et al.,

2015; Murray et al., 2015; Carr et al., 2017). Catania et al. (2018) go on to use the relationships they establish to predict the likely future retreat of the 15 glaciers in their study based on the current topographic setting of each glacier.

The comprehensive mapping of overdeepenings achieved in Chapter 3 has resulted in a detailed high quality dataset of overdeepenings near the margin for the entire GrIS for the first time. It was therefore possible to extend the analytical approach taken by Catania et al. (2018) to the whole ice sheet. Using the central flowline and overdeepening datasets generated in Chapter 3, the straight-line distance from the front of each flowline (which is at the terminus of the glacier it represents) to the point where it first intersects an overdeepening was measured. The straight line distance from where the flowline enters the overdeepening to where it exits the overdeepening was also measured. Straight line distances were used for ease of computation.

Figure 7.1 illustrates how close the terminus of each outlet glacier in Greenland is to the nearest overdeepening (e.g. how far it would have to retreat until the terminus entered an overdeepening), and how far each glacier would likely retreat once the calving front entering the overdeepening before reaching the other side of the overdeepening. Figure 7.2 shows these data in histograms aggregated by region. The data is presented here to demonstrate the additional value and application of the datasets generated in Chapter 3 beyond the specific aims and objectives of this thesis. It is for this reason that they were not included in the main results chapters of the thesis. As such, detailed interpretation and analysis is beyond the scope of the thesis, but some brief discussion follows.

The 15 glaciers studies by Catania et al. (2018) are all in the CW region, and it is clear that the heterogeneity of the patterns they observe within their dataset apply more widely within the CW, and are even more pronounced in other regions (Figure 7.1). This further supports the suggestions of Catania et al. (2018) that substantive variations amongst the beds of neighbouring glaciers may explain variations in patterns of retreat observed in other studies (Walsh et al., 2012; Moon et al., 2015; Murray et al., 2015; Carr et al., 2017). However, there are also regional patterns and trends that help to explain retreat and advance observed in the past, and for predicting change in the future. Numerous studies of patterns of advance and retreat in the 2000s have found significant variation between glaciers in the SE compared to those further north on the east coast. Glaciers in the SE were

observed to show more pronounced patterns of retreat in the early 2000s followed by readvance in the late 2000s (Murray et al., 2015). Conversely, other studies have reported a different pattern of behaviour over the same time period north of 69°N, with glaciers north of this latitude showing stable front positions (Seale et al., 2011; Walsh et al., 2012). The authors hypothesise that the variations in dynamics north and south of 69°N are controlled by the presence of warmer waters in the southern fjords (transported by ocean currents) that are not present in the north.

It is clear from Figure 7.1 that in addition to any control exerted by ocean currents there is also a distinct and substantial increase in the distance from the calving front to overdeepenings north of 69°N. As such, most outlet glaciers north of 69°N will be grounded on stable normal bed slopes, often needing to retreat more than 15 km before entering an overdeepening and becoming grounded in a less stable position on an adverse slope. Only 8% of overdeepenings in the NE currently terminate in an overdeepening, with a further 6% terminating within 2 km (Figure 7.2). In contrast, south of 69°N on the east coast glaciers terminate much closer to overdeepenings and are therefore much more likely to be grounded in unstable positions characterised by sustained retreat on adverse slopes. In the SE region 38% of glaciers currently terminate in an overdeepening, with a further 21% terminating within 2 km (Figure 7.2). Overdeepenings closest to the terminus in the SE are also generally much smaller than those in the NE (Figure 7.1), with overdeepenings within 2 km of the terminus having a mean length of only 8.2 km compared to 28.1 km for the NE region. This combination of factors means that retreat in the SE region is more likely to occur due to the relative instability of the positions the grounding lines are in, but is also more likely to stabilise on the normal slope within a few kilometres (due to the shorter overdeepening lengths) therefore having the potential to readvance to the initial grounding line (or beyond) when conditions become favourable for this. As such, the analysis of bed data based on the overdeepenings and flowlines generated in Chapter 3 provide an additional hypothesis (not entirely contingent on ocean currents) to explain the patterns of retreat and advance observed on the east coast of Greenland in the 2000s.

The data presented in Figure 7.1 and Figure 7.2 also offers the possibility of identifying potential future patterns of retreat of outlet glaciers of the GrIS. Glaciers that are situated with their terminus close to overdeepenings are more likely to experience sustained retreat

in the near future due to the probability of retreating into an unstable position on an adverse slope. The longer the overdeepening a glacier becomes grounded in, the greater the sustained retreat it is likely to experience (Catania et al., 2018). As such, the areas most at risk of retreat in the coming decades are those with glaciers with large overdeepenings very close to the terminus. The areas that appear to be at greatest risk of retreat are the southern halves of the SE and SW regions, the southern and northern margins of the CE region, and the eastern side of the N region Figure 7.1).

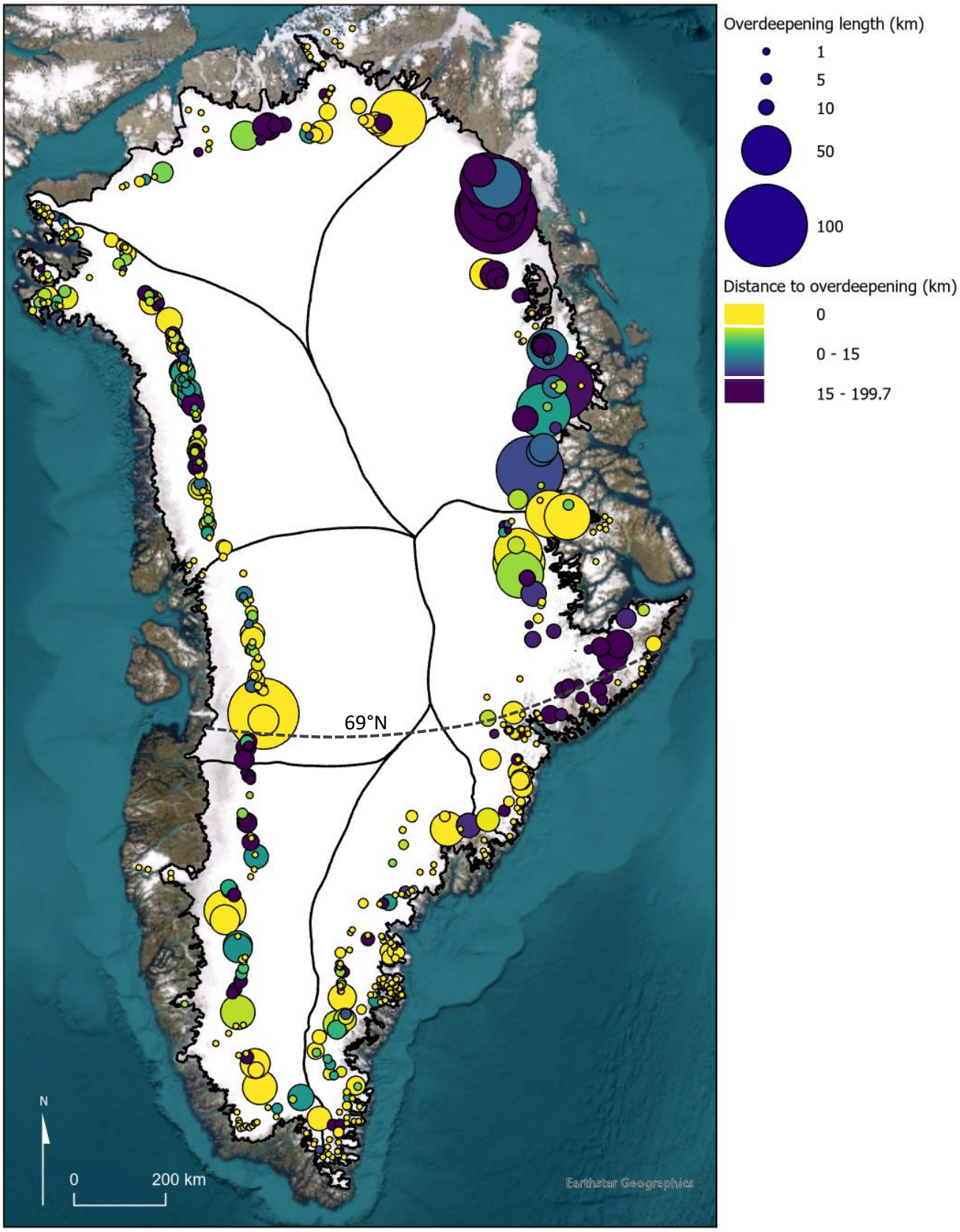

Figure 7.1 Distance from the terminus of each glacier to when an overdeepening is first encountered. Point colour shows distance to overdeepening, point size shows the length the glacier will retreat through the overdeepening before a stabilising point is reached on the normal slope. Dashed grey line indicates 69°N. Note, point location is at the geometric centre of each flowline for clarity of visualisation, not the location of the overdeepening.

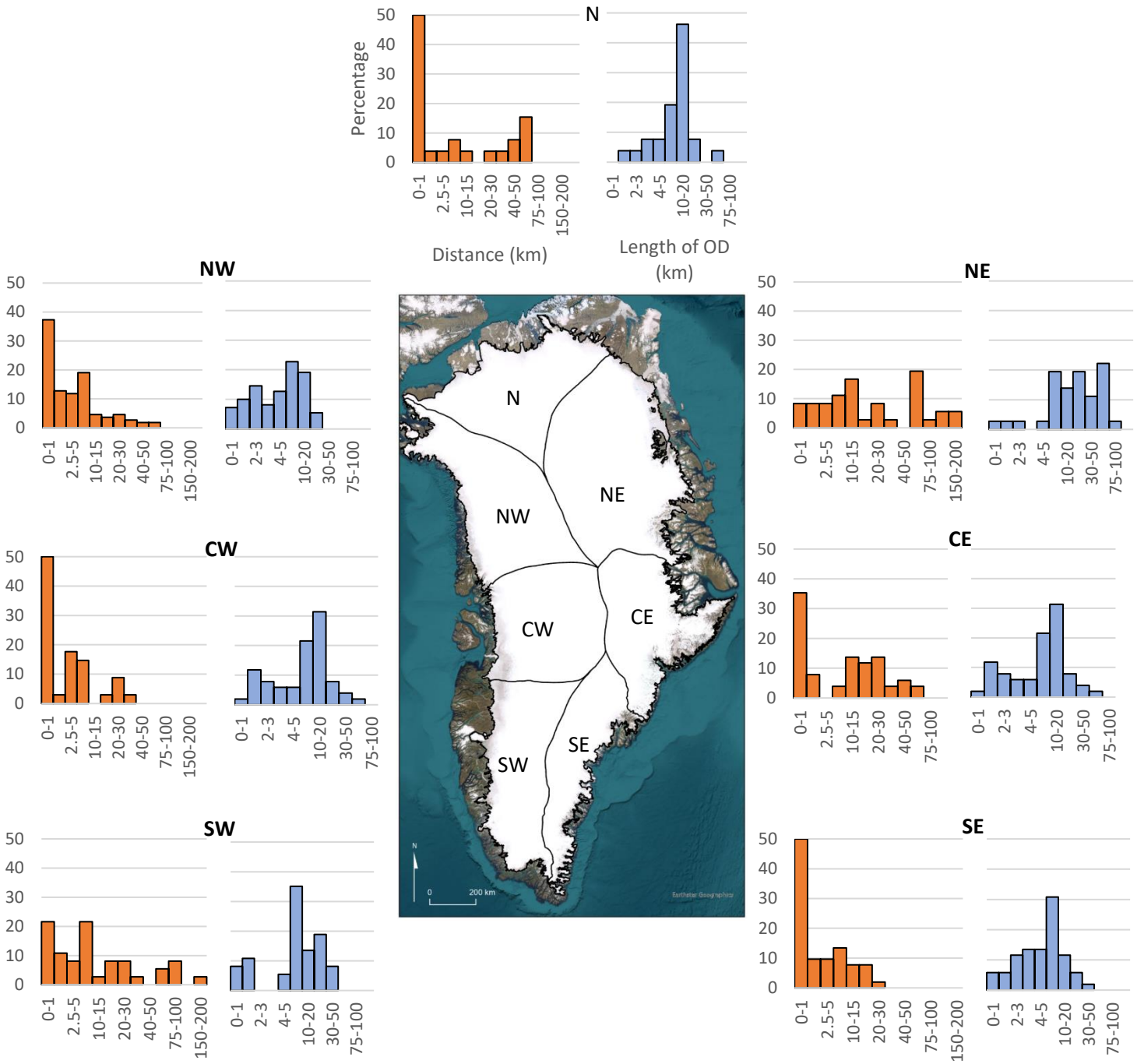

Figure 7.2 Histograms showing the 'distance to overdeepening' (red) and 'length of overdeepening' (blue) metrics visualised in Figure 7.1 aggregated by region.

7.3.2 Inland limit of channelisation

How ice sheet dynamics respond to a warming climate and the impact this will have on the future stability of the GrIS have been much debated over the last 20 years (Zwally et al., 2002; Sundal et al., 2011; Sole et al., 2013; Tedstone et al., 2013; Joughin et al., 2018; Williams, Gourmelen, and Nienow, 2021). The results in Chapter 6 demonstrate that the position on the ice sheet where seasonal ice velocity typology transitions from T21/T3 to T2 or T4 may indicate the inland channelisation limit (Figure 6.26 and Figure 6.27). It therefore offers a potential substantial development in the ability to monitor and predict subglacial drainage processes influencing the dynamics of the ice sheet.

Following the observation by Zwally et al. (2002) of seasonal speedup over 30 km inland from the margin of the ice sheet driven by surface melt, there has been significant research into whether future increased surface melting in summer would cause net ice flux to increase (see section 2.3.1.4). The current consensus is that terrestrially terminating glaciers in the ablation zone self-regulate, with increased melt causing greater ice flow speeds during the summer, but that this is offset by a subsequent slowdown in late-summer due to increased channelisation and drainage of water out of cavities (e.g. Sole et al., 2013; Tedstone et al., 2013; Tedstone et al., 2015; Stevens et al., 2016; van de Wal et al., 2008; Van De Wal et al., 2015). Indeed, decadal studies indicate that elevated melt observed between 2000-2010 in the land terminating sector in the SW of the GrIS resulted in a net velocity slowdown (Tedstone et al., 2013; 2015).

This new consensus is reflected in the IPCC Special Report on the Ocean and Cryosphere in Changing Climate which states "*there is now high confidence that for most of the GrIS, increased surface melt has not led to sustained increases in glacier flux on annual timescales because subglacial drainage networks have evolved to drain away the additional water inputs"* (Pörtner et al., 2019). However, this seems surprisingly definitive given the scientific data supporting the assertion. Of the five citations given in the report to support the statement, two are studies of individual glaciers within 200 km of each other in the land terminating region in the SW of the GrIS (Sole et al., 2013; Stevens et al., 2016), one is a regional remote sensing based study also in the SW that only covers ~15% of the west coast (Tedstone et al., 2015) and has some methodological quirks that result in its findings contradicting with results from other studies (e.g. Joughin et al. (2018), see section 2.3.1.3

for detailed discussion), and one is a review paper broadly drawing on the papers already mentioned here (Nienow et al., 2017). Other studies have been conducted that are not cited in the report which also offer some support for the position (Williams et al., 2021), but these are still spatially limited to the SW of the GrIS. The only study that has been conducted at the ice sheet scale covering all of Greenland is that of King et al. (2018) which measures ice flux from the largest 230 outlet glaciers in Greenland between 2000-2016 and correlates flux changes with front position and surface runoff. King et al. (2018) conclude that ice flux is more strongly correlated with changes in front position than changes in runoff at seasonal, annual, and decadal temporal scales. However, the approach taken to the analysis is quite coarse (due to the scale of the study) and the findings contradict those of more nuanced studies that suggest that at seasonal and interannual timescales, changes in front position are likely a *reaction* to melt driven velocity change further inland (Ultee et al., 2022). The findings of King et al. (2018) are also not well aligned with the observations of very low T1 prevalence at the margin of marine terminating outlet glaciers presented in Chapter 6.

To summarise the previous two paragraphs, it could be argued that the evidence for the hypothesis that increased surface melt does not lead to increased ice flux is based on limited data that may not be representative of the ice sheet as a whole. As such, there is a case for further study, in particular to attempt to specifically measure channelisation limits rather than simply measure ice flux and apply blunt statistical regressions with parameters such as runoff rates and front position to try and infer where channelisation might be occurring. The approach adopted to mapping the inland channelisation limit from the inland boundary of T21/T3 introduced in Chapter 6 is one way in which detailed process understanding could be improved in this area. There are multiple benefits to this approach. The method is automated and could therefore be applied across the ice sheet giving comprehensive spatial coverage. Currently there is very limited data on channelisation limits beyond the SW region, and there appears to be no literature discussing channelisation limits on the north or east coasts so generating data in these areas will be extremely valuable. Again, due to the relative ease of generating the data, it would be possible to reproduce the data generated for 2019 in Chapter 6 for a range of different years to investigate how the channelisation limit may vary under differing past melt scenarios. This would then offer the

possibility of parameterising models to predict the inland channelisation limit under projected future melt scenarios. The analysis of the inland channelisation limit in Chapter 6 also further supports the hypothesis that channelisation is not simply a function of melt availability, but that other factors such as ice thickness and velocity exert a strong control (Meierbachtol et al., 2013; Dow et al., 2014; Doyle et al., 2014). As such, as the ELA increases due to a warming climate and becomes situated above thicker ice than at present, the response of the ice sheet to melt input in terms of channelisation and the associated impact this has on ice dynamics may vary from patterns currently observed (Koziol and Arnold, 2018). The control of ice thickness on channelisation can be observed in the results presented in Chapter 6 (Figure 6.28) as the channelisation limit does not scale precisely with melt and the inland limit is reduced where ice is thicker. Velocity also appears to exert some control on the inland channelisation limit, with the limit closer to the margin where velocity is higher. This is potentially due to enhanced creep closure rates as ice velocity increases (Nye, 1953; Meyer et al., 2016). Given that ice velocity is considerably slower in the land terminating sector of the GrIS than for marine terminating glaciers which make up the vast majority of GrIS outlet glaciers, caution should be exercised when extrapolating out findings from this region as they may not be representative of the wider ice sheet.

7.4 Limitations and constraints

A number of the limitations of the research conducted are related to the quality and resolution of the data that has been utilised in the analysis. In part, this is an inherent constraint on trying to conduct analysis at the ice sheet scale using the data that is currently available (or was available at the time this research was undertaken). There is always a balance between the consistency of low error data coverage, and the level of temporal aggregation of the data. Put simply, the more individual time slices of velocity data that are compiled into an aggregated product, the less gaps there will be in it. Issues of the data quality available are slightly more complex than may sometimes be the case as this thesis has been completed part time over a period of 10 years. As such, there have been substantial advances made in the velocity data archives that are available for Greenland over this period. For example, the Rosenau (2015) velocity data used for the Helheim case study in Chapter 4 was the best velocity data available when that analysis was conducted in 2015-2016, and it offered the potential for very high temporal resolution. However, the

individual velocity time slices had considerable gaps due to cloud cover in the Landsat imagery being used for feature tracking and required aggregating to much courser resolution to mediate this. The velocity data used for the Upernavik Isstrøm II case study in Chapter 4 (Vijay et al, 2019) was more consistent in coverage due to utilising Sentinel 1 SAR data for feature tracking, but the coverage of the dataset was only available for select glaciers when the analysis for the case study was conducted in 2019-20. As such, it was not suitable for the ice sheet scale analysis conducted in Chapters 5 and 6. The MEaSUREs Greenland Quarterly Ice Sheet Velocity Mosaics dataset (Joughin, 2018a; Joughin et al., 2010, 2018) was one of the only datasets available at the time of analysis (c. 2020) that offered complete coverage of the GrIS, for multiple years, with relatively few gaps in coverage. As such, despite its course temporal resolution it was the most suitable product to use at the time. The course temporal resolution also makes file sizes much more manageable for processing on a desktop computer.

Using quarterly velocity data in Chapters 5 and 6 is perhaps why the patterns of differing seasonal velocity typologies on the adverse and normal slopes of the overdeepening observed for Upernavik Isstrøm II in Chapter 4 were not apparent in the ice sheet scale analysis in Chapter 6. The processes operating at Upernavik Isstrøm II appeared to be operating over a period of days to weeks so may just not be observable in the quarterly data. The fact that these signals are not observable over such timescales is a negative finding of some value none the less, as it indicates that if differential seasonal velocity patterns *are* occurring on adverse and normal slopes of overdeepenings, they are seemingly not of sufficient magnitude to alter the net annual dynamics of the GrIS. Higher temporal resolution velocity data is now available for the whole of the GrIS, and its application in future research will be discussed in section 7.5, below.

Other key datasets used in the thesis were superseded by improved products during the 10 year period over which the thesis was conducted. BedMachine v3 (Morlighem et al., 2017) was used throughout the project for bed topography. Two further versions have subsequently been released, but the improvements in these newer versions are focused on inclusion of multi beam bathymetry to better constrain the beds of fjords in open water, increased radar data to better constrain the interior of the ice sheet, and better data for marginal ice caps surrounding the GrIS (Morlighem, 2022), none of which are of relevance to

the fast moving ice close to the margin which was the focus of this thesis. As such, the consistent use of BedMachine v3 throughout the thesis is appropriate. Improved datasets on the geology under the GrIS have also been recently released which offer a marked advances compared to the data used from Gowan et al. (2019) for the analysis in Chapter 3. The difficulties of determining the geology underlying 1000s of metres of ice is obvious, and has historically relied on interpolation of observations made in ice free areas at the margin. The most recent datasets incorporate geophysical constraints from seismic, gravity, magnetic, and topographic data (MacGregor et al., 2024).

A fundamental aim of this thesis was to investigate whether bed topography modulates the dynamics of the ice flowing over it. In particular, the control that the adverse slopes of overdeepenings may exert. There are a variety of ways in which such modulation may occur, including form drag, and reduction of hydraulic gradient on the adverse slope suppressing channelised drainage (see section 2.4). However, the potential control exerted by supercooling processes was of significant interest and has been much discussed throughout the thesis. The approach taken has been to analyse the relationship between BSSR with regard to ice velocity and seasonal velocity typologies, and especially to look for differences where the supercooling threshold according to classic theory (e.g. Röthlisberger and Lang (1987)) is exceeded. As was summarised in section 7.2.3, evidence of differences above and below the supercooling threshold were limited. Recent work by Werder (2016) has suggested that some of the assumptions made in the classic theory of supercooling may not be valid, and proposes a new supercooling threshold which takes into account the floatation fraction at the lip of the overdeepening to apply a correction factor to the threshold adverse slope gradient required for supercooling to occur, which is specific to each individual overdeepening. Reanalysis of the datasets presented in this thesis using Werder's (2016) supercooling threshold formula should be a priority for future research, but the additional parameterisation required is challenging at the ice sheet scale and was beyond the scope of the work presented here.

7.5 Future research

7.5.1 Integrating other data sources and approaches as proxies for subglacial hydrological regime

The approach taken in this thesis has been to analyse 2D patterns in ice velocity speedup and slowdown, and to use this as a proxy to infer the subglacial hydrological conditions at the ice bed interface using hypotheses derived from established theory. There is also an important vertical component to the dynamics of the GrIS that have not been considered. Differential seasonal acceleration and deceleration in different areas of a glacier may lead to thickening where ice is slowing and thinning where ice is speeding up (Bevan et al., 2015). As such, high temporal resolution analysis of changes in ice surface elevation data to assess the relative timing of thickening and thinning of ice may offer insights into where forces driving ice velocity are tension or compression. This would enable further investigation into the question of whether pull or push mechanisms are controlling ice dynamics at glaciers like Helheim (Ultee et al., 2022). Differential Interferometric Synthetic Aperture Radar (DInSAR) derived maps of ice surface deformation can be generated from satellite products like RADARSAT-2 can be constructed to map deformation occurring over periods of days to weeks (Samsonov, 2019) and there is significant potential in the use of these techniques to better resolve the balance of forces within Greenland outlet glaciers. Assessing where on the glacier thickness changes are occurring first will give an indication of whether changes at the calving front are driving changes further inland, or changes due to subglacial hydrology inland from the margin are driving changes at the calving front. Similarly, analysis of crevasse patterns and how these change can be used as a proxy for strain within the glacier (Harper et al., 1998; Jennings and Hambrey, 2021). Analysis of the timing and nature of changes in crevasse patterns at very high temporal resolution may assist in determining the key controls on the seasonal ice dynamics of Greenland outlet glaciers and this would be an interesting area for future study in collaboration with the assessment of seasonal velocity patterns.

7.5.2 Advances in data and methods

Velocity data derived from SAR feature tracking of similar quality to that used for the Upernavik Isstrøm II case study in Chapter 4 (500 m posting, 30 time slices per year) is now available with multi-year coverage for the whole GrIS (Solgaard et al., 2021). Extension of

the analysis conducted in Chapters 5 and 6 using this data is an important priority for future work. Inevitably, technological progress will lead to ever increasing resolution (temporal and spatial) satellite imagery becoming available. The shift in importance away from large satellite platforms focused on individual satellites programmes (such as Landsat and Sentinel) towards constellations of large numbers (~2-300) of nanosatellites seems set to continue, and this imagery is likely to become a more significant component of the imagery used in scientific work. Figure 7.3 shows the rapid growth in the use PlanetScope imagery since the end of the 2010s.

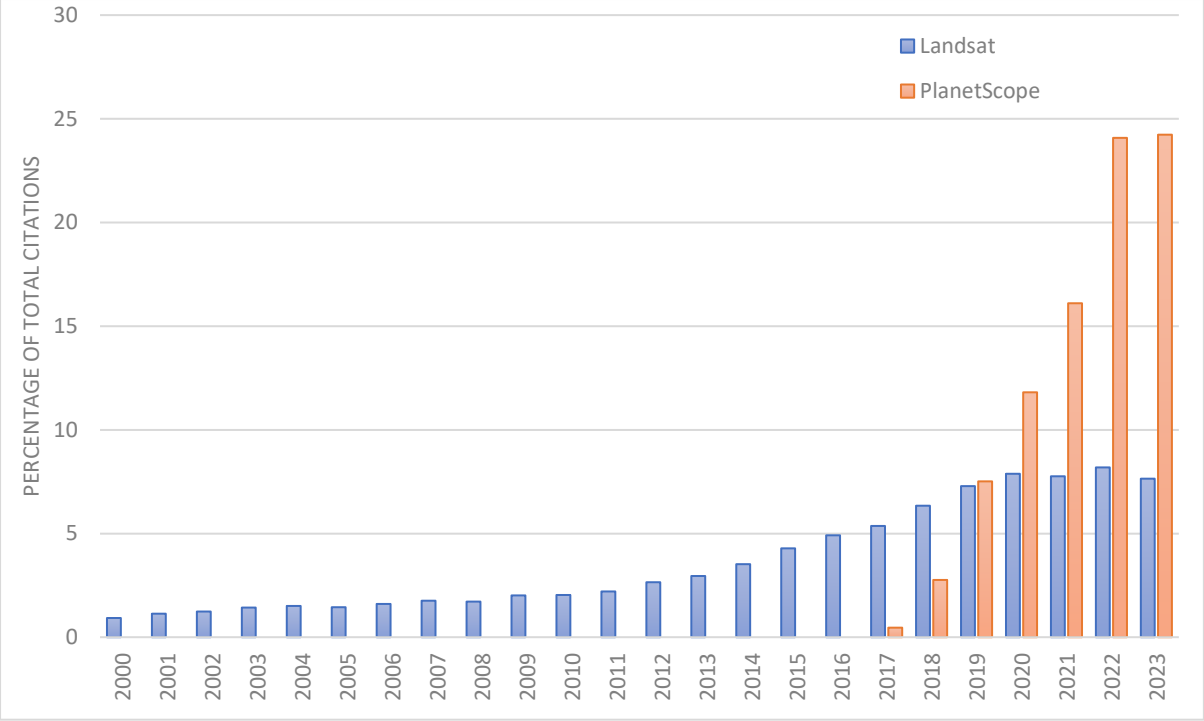

Figure 7.3 Web of Science search results for the terms "Landsat" and "PlanetScope". Total number of citations for Landsat over this period is 38,477, total number of citations for PlanetScope is 652.

PlanetScope is an imagery product of 3 m spatial resolution that is taskable to provide daily repeat imagery made possible by a constellation of nearly 250 nanosatellites (Frazier and Hemingway, 2021). The potential that these types of technologies offer for the advancement of earth observation science are as profound as the initial launch of Landsat in the early 1970s. The absolute number of studies using PlanetScope imagery is still small (approximately 5% of the number of papers published using Landsat imagery (Figure 7.3)), but the use of this type of data in cryosphere science seems set only to increase (Bhushan et al., 2022; Liu et al., 2024).

7.5.3 Field study

There is substantial scope to use some of the work presented within this thesis (or further implementation of the methods adopted) to identify individual candidate study sites (such as Upernavik Isstrøm II) to repeat the work conducted here which used satellite remote sensing approaches, but in the field at ultra high spatial and temporal resolution. This would likely utilise Small Uncrewed Aerial Vehicle (sUAV) surveys to build repeated high precision 3D models of the ice surface from structure from motion techniques (Macelloni et al., 2023) to measure when surface uplift is occurring as the subglacial system becomes pressurised (Mair et al., 2008). High spatial and temporal resolution aerial imagery from an sUAV can also be used to generate sub-daily velocity data to investigate diurnal adverse slope processes controls on ice dynamics (Chudley et al., 2019). Field based studies would also enable the empirical measurements of subglacial water pressure (via boreholes (Andrews et al., 2014) or remote sensors such as Cryoeggs (Prior-Jones et al., 2021)) to confirm the interpretation of subglacial hydrological configuration made from velocity and uplift pattens.

7.5.4 Expand work to Antarctica

Finally, a key area of future study aligned with the work presented in this thesis is to reproduce it in Antarctica. Patton et al. (2016) mapped overdeepenings in both Greenland and Antarctica in their study. There is substantial similarity in the overall pattern of distribution and the morphometry of the overdeepenings mapped in the two areas (Patton et al., 2016) (Figure 7.4). As such, it is a logical assumption that the improvements made on the Patton et al. (2016) overdeepening data for Greenland in this thesis may be replicated if the methodology was applied in Antarctica.

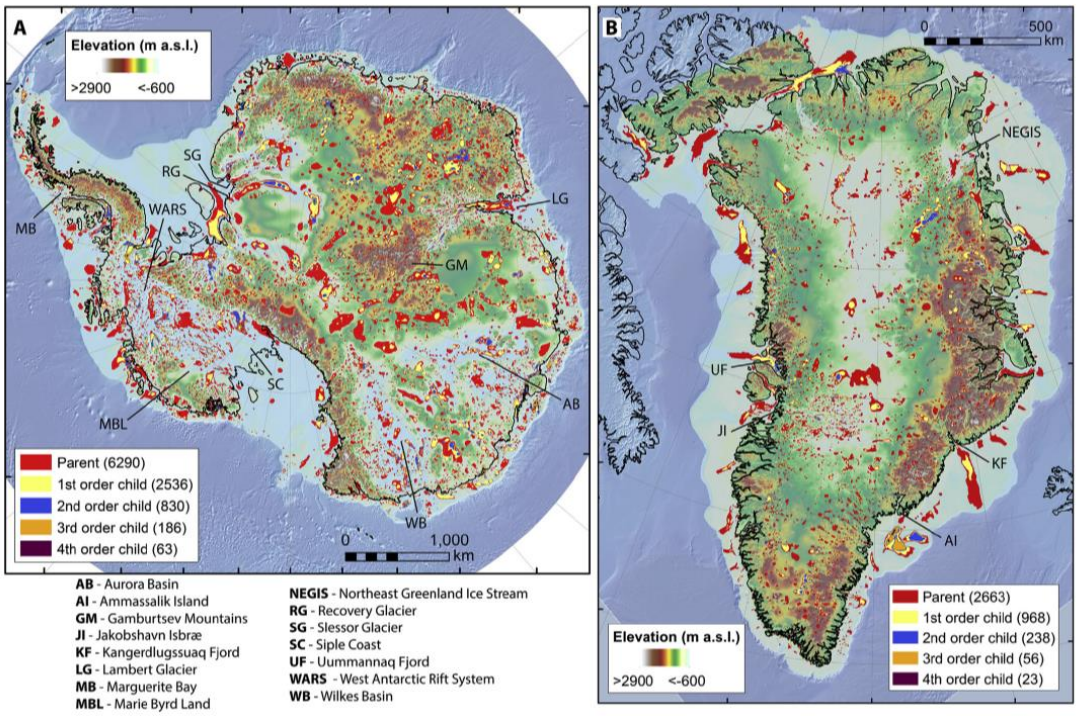

Figure 7.4 Maps of overdeepenings. A) Antarctica. B) Greenland. Reproduced from Patton et al. (2016).

It is only relatively recently that observations have been made of surface meltwater in the Antarctic Peninsula draining to the bed and causing rapid accelerations in ice velocity due to the pressurisation of the subglacial drainage system (Tuckett et al., 2019). As such, it is now established that mechanisms of ice dynamics first identified over 20 years ago for Greenland (Zwally et al., 2003) are now also relevant in Antarctic contexts. As surface melt in Antarctica increases under future warming climate scenarios (Gilbert and Kittel, 2021), Greenland becomes a more and more relevant proxy for future Antarctic ice dynamics, and the understanding developed in this thesis becomes ever more relevant.

7.5.5 Future modelling work

Due to the challenges in determining the impact of complex feedbacks in ice dynamics, they have often been omitted from models and estimates of future change (Goelzer et al., 2020). For example, models accounting for seasonal subglacial hydrological processes were not included at all in IPCC ARs 1-5, and are only included in some of the predictions of future sea level rise in the most recent AR6 (Fox-Kemper et al., 2021). The current understanding of the role of bedrock topography on ice dynamics is well summarised by the statement from AR6 that "…*although there is* ***high confidence*** *that the dynamic response of Greenland outlet*

*glaciers is controlled by bedrock topography, there is **low confidence** in quantification of future mass loss from Greenland triggered by warming ocean conditions, due to limitations in the current understanding of ice–ocean interactions, its implementation in ice-sheet models, and knowledge of bedrock topography*." (Fox-Kemper et al., 2021, pg. 1258).

A key area of future work is to engage with the modelling community to start to incorporate bedrock topography as a process control into models of ice dynamics. The dataset of overdeepenings created in Chapter 3 represents a significant improvement on what was previously available. In particular, the number of overdeepenings identified proximal to the ice margin has been substantially increased which will allow more accurate parameterisation of short and medium term ice retreat rates (see section 7.3.1). Subglacial topographic feature (such as overdeepenings) have often been omitted from models of ice dynamics not due to their importance, not due to the fact that features are often at or below the resolution of bed DEMs used in models. Developing a better understanding of where overdeepenings are (Chapter 3) and how they may modulate ice dynamics (Chapter 4) offers the possibility to parameterise for these processes in models where the resolution of the model cannot physically resolve such features. Similar approaches to incorporating trough systems into models of glacial dynamics has been shown to increase model performance and increase the predicted level of ice flux to the ocean (Herzfeld et al., 2012).

The ability to potentially identify the location of the inland channelisation limit from spatial patterns in seasonal velocity typology (see section 6.4.3.2.3) is of substantial benefit in advancing understanding of the controls on the extent of channelisation of the subglacial hydrological system. Understanding where subglacial hydrology is channelised and how the inland limit of channelisation will change under a warming climate and retreating ice front is fundamental to accurately modelling the rate of dynamic ice flux into the ocean, which currently accounts for approximately 40% **of sea level rise caused by Greenland ice sheet loss** (IMBIE Team, 2020).

Chapter 8 Conclusions

The main aim of this thesis was to determine the location and morphology of overdeepenings under the GrIS, and to examine their potential impact on hydrology and therefore ice dynamics. The findings have led to an improved understanding of where overdeepenings are located and contributed to a better understanding of controls that overdeepenings exert on subglacial hydrology and the seasonal ice dynamic patterns that are associated with seasonal melt. In the process of generating data to achieve this primary aim, advances have also been made in understanding ice flow processes and controls in a much wider context that is independent of overdeepenings.

Overdeepenings were mapped using high spatial resolution (sub-kilometre) bed topography (BedMachine v3) for the first time. In total 621 parent overdeepenings were mapped, almost double the number of the only other existing dataset (Patton et al., 2016). 515 of the overdeepenings had not previously been mapped before, and many of these were highly elongate features close to the margin that would not have been apparent in lower resolution bed data. Analysis of the morphometry of overdeepenings showed strong tendency for shallower overdeepening depths, and high clustering around a bed to surface slope ratio close to the classically held supercooling threshold. This suggested support for the hypothesis that as adverse slopes grade towards the supercooling threshold, channelised drainage is suppressed, limiting evacuation of sediment from the overdeepening and preventing further erosion (and therefore deepening) of the bed.

Overdeepenings were shown to exert some control on ice velocity with annual mean ice velocity higher on the adverse slopes than the normal slopes of overdeepening. It has been common in past research on seasonal glacial dynamics of the GrIS for ice velocity to only be considered at a limited number of points along the length of a glacier, or often only at a single point near the terminus. Analysis of seasonal velocity typology along the centre lines of glaciers showed that there was often substantial variation in seasonal velocity patterns at different locations on the glacier. Some variations were inferred to be linked to differing configurations of subglacial hydrology on the adverse and normal slopes of overdeepenings due to the suppression of channelised drainage on adverse slopes. However, others were related to the presence of prominent riegels at the downglacier lip of overdeepenings,

notably at Helheim and Upernavik Isstrøm II, where these riegels were observed to have an isolating effect on the influence of marine processes, preventing them from propagating fully into the overdeepening and thereby affecting the flow of inland ice. Within the overdeepenings at these two case study glaciers there was a transition to seasonal velocity typologies commonly associated with land terminating glaciers. A key recommendation of this work is that studies should carefully consider where velocity measurements are taken, and that for a full process understanding of the dynamics of Greenland outlet glaciers, velocity should be analysed at regular intervals along the centre line.

The detailed mapping of overdeepenings facilitated an analysis of the distance from the ice sheet margin to each overdeepening, and how far through each overdeepening a glacier would have to retreat before being grounded in a stable position again on the normal slope of the overdeepening. Substantial regional variations were identified for both metrics. The southern halves of the SE and SW regions, the southern and northern margins of the CE region, and the eastern side of the N region displayed the greatest prevalence of large overdeepenings close to the margin. Glaciers in these areas are therefore at the highest risk of significant retreat in the near future.

A machine learning based approach utilising K-means clustering was developed to automatically classify seasonal velocity responses for a dataset of nearly 200,000 time series points into distinct seasonal velocity typologies. Seven different typologies were identified. The three typologies previously identified by existing studies; Type 1, Type 2, and Type 3 (Moon et al., 2014) were represented. Two further variations of Type 2 were identified (T21 and T23) in addition to two new typologies found that were representative of minimum velocity in summer followed by acceleration into autumn (T4 and T5). The T21 typology was of particular interest as it suggests a typology situated between Type 2 and Type 3 as end members on a continuum, a concept that had previously been hypothesised but never directly observed (Moon et al., 2014; Solgaard et al., 2022). Statistical analysis at the ice sheet scale did not reveal a widespread variation between seasonal velocity typology on the normal and adverse slopes of overdeepenings. However, further examples of individual glaciers exhibiting velocity patterns were observed that indicate that overdeepenings likely do modulate the efficiency of subglacial drainage. As part of this, analysis of the seasonal velocity typology of all marine terminating Greenland outlet glaciers was made for the first

time. The higher relative prevalence of the T1 typology close to the calving front of marine terminating outlet glaciers provides further support for the established hypothesis that this typology is associated with marine processes controlling advance and retreat of the calving front. However, the relatively low overall prevalence of the T1 typology in areas close to the calving front of glaciers suggested that marine processes were not a dominant control on seasonal ice dynamics for outlet glacier flow for the GrIS as a whole. Notably, T21 and T3 were found to be the dominant typologies even in areas close to the calving front of marine terminating glaciers. Further, surface runoff was found to be linked with the prevalence of certain seasonal velocity typologies, notably shown by a statistically significant correlation between the amount of surface runoff and the presence of the Type 3 typology, observed for the first time. This supports the hypothesis that Type 3 is linked to hydrological processes and is likely representative of channelised subglacial drainage.

A key control on the future stability of the GrIS is the extent to which channelised subglacial drainage will migrate further inland under warming climates and higher surface runoff. Channelised drainage has been inferred by previous studies to have increase under elevated melt conditions in the 2000s leading to autumn and winter velocity slowdowns that offset increased summer velocities. Current data on inland channelisation extent is sparse. The inland boundary of T21/T3 typologies (reflective of channelised drainage) was mapped for the west coast in 2019. The estimated limit derived from this approach appeared to align very closely with field data and modelling estimates of the channelisation limit, and may therefore offer a straightforward approach to estimate changing channelisation limits in the future.

Through the work undertaken for this thesis, understanding of the detail of GrIS outlet glacier dynamics and the role that overdeepenings potentially play has been greatly advanced. However, much remains to be studied, and the current understanding of these vital systems and how they influence the stability of the ice sheet is insufficient to enable accurate prediction of future changes under a warming climate. Key areas for the focus of further study include: the continued updating of the work conducted within this thesis using new remote sensing data products of higher resolution and quality, consideration of ice sheet dynamics in three spatial dimensions to build a more detailed and nuanced picture of the processes operating, combining satellite remote sensing based research with empirical

field study to validate hypotheses generated from proxies used to infer subglacial conditions, and to expand the research conducted here to an Antarctic setting.

References

Abe, T, Furuya, M and Sakakibara, D (2015), Brief Communication: Twelve-Year Cyclic Surging Episode at Donjek Glacier in Yukon, Canada. *Cryosphere Discussions*, 9(6).

Åkesson, Henning, Nisancioglu, Kerim H and Nick, Faezeh M (2018), Impact of Fjord Geometry on Grounding Line Stability. *Frontiers in Earth Science*, 6: 303989.

Alexander, PM, Tedesco, M, Fettweis, Xavier, Van De Wal, RSW, Smeets, CJPP and Van Den Broeke, MR (2014), Assessing Spatio-Temporal Variability and Trends in Modelled and Measured Greenland Ice Sheet Albedo (2000-2013). *The Cryosphere*, 8(6): 2293–2312.

Alley, R B, Lawson, D E, Larson, G J, Evenson, E B and Baker, G S (2003), Stabilizing Feedbacks in Glacier-Bed Erosion. *Nature*, 424(6950): 758–60.

Alley, RB, Cuffey, KM, Evenson, EB, Strasser, JC, Lawson, DE and Larson, GJ (1997), How Glaciers Entrain and Transport Basal Sediment: Physical Constraints. *Quaternary Science Reviews*, 16(9): 1017–1038.

Alley, Richard B, Blankenship, DD, Rooney, ST and Bentley, CR (1989), Sedimentation beneath Ice Shelves—the View from Ice Stream B. *Marine Geology*, 85(2-4): 101–120.

Alley, Richard B, Blankenship, Donald D, Bentley, Charles R and Rooney, ST (1987), Till beneath Ice Stream B: 3. Till Deformation: Evidence and Implications. *Journal of Geophysical Research: Solid Earth*, 92(B9): 8921–8929.

Alley, Richard B, Lawson, Daniel E, Evenson, Edward B and Larson, Grahame J (2003), Sediment, Glaciohydraulic Supercooling, and Fast Glacier Flow. *Annals of Glaciology*, 36: 135–141.

Alley, Richard B and Whillans, Ian M (1984), Response of the East Antarctica Ice Sheet to Sea-Level Rise. *Journal of Geophysical Research: Oceans*, 89(C4): 6487–6493.

Alvarez, R, Bonifaz, R, Lunetta, RS, Garc'\ia, C, Gómez, G, Castro, R, Bernal, A and Cabrera, AL (2003), Multitemporal Land-Cover Classification of Mexico Using Landsat MSS Imagery. *International Journal of Remote Sensing*, 24(12): 2501–2514.

Amundson, Jason M, Fahnestock, Mark, Truffer, Martin, Brown, Jed, Lüthi, Martin P and Motyka, Roman J (2010), Ice Mélange Dynamics and Implications for Terminus Stability, Jakobshavn Isbræ, Greenland. *Journal of Geophysical Research: Earth Surface*, 115(F1).

Amundson, JM and Iverson, NR (2006), Testing a Glacial Erosion Rule Using Hang Heights of Hanging Valleys, Jasper National Park, Alberta, Canada. *Journal of Geophysical Research: Earth Surface*, 111(F1).

Andersen, Morten L, Larsen, Tine B, Nettles, Meredith, Elosegui, Pedro, Van As, D, Hamilton, Gordon S, Stearns, Leigh A, Davis, James L, Ahlstrøm, Andreas P, de Juan, Julia and others

(2010), Spatial and Temporal Melt Variability at Helheim Glacier, East Greenland, and Its Effect on Ice Dynamics. *Journal of Geophysical Research: Earth Surface*, 115(F4).

Anderson, Robert S, Molnar, Peter and Kessler, Mark A (2006), Features of Glacial Valley Profiles Simply Explained. *Journal of Geophysical Research: Earth Surface*, 111(F1).

Andrews, Lauren C, Catania, Ginny A, Hoffman, Matthew J, Gulley, Jason D, Lüthi, Martin P, Ryser, Claudia, Hawley, Robert L and Neumann, Thomas A (2014), Direct Observations of Evolving Subglacial Drainage beneath the Greenland Ice Sheet. *Nature*, 514(7520): 80–3.

Antwerpen, Raf M, Tedesco, Marco, Fettweis, Xavier, Alexander, Patrick and van de Berg, Willem Jan (2022), Assessing Bare-Ice Albedo Simulated by MAR over the Greenland Ice Sheet (2000-2021) and Implications for Meltwater Production Estimates. *The Cryosphere*, 16(10): 4185–4199.

Armstrong, William H, Anderson, Robert S and Fahnestock, Mark A (2017), Spatial Patterns of Summer Speedup on South Central Alaska Glaciers. *Geophysical Research Letters*, 44(18): 9379–9388.

Arthur, David and Vassilvitskii, Sergei (2007), K-Means++ the Advantages of Careful Seeding, 1027–1035, in: *Proceedings of the eighteenth annual ACM-SIAM symposium on Discrete algorithms*.

Augustinus, Paul C (1992), The Influence of Rock Mass Strength on Glacial Valley Cross-Profile Morphometry: A Case Study from the Southern Alps, New Zealand. *Earth Surface Processes and Landforms*, 17(1): 39–51.

Bamber, Jonathan L, Griggs, JA, Hurkmans, RTW, Dowdeswell, JA, Gogineni, SP, Howat, Ian, Mouginot, Jeremie, Paden, John, Palmer, Steven, Rignot, Eric and others (2013), A New Bed Elevation Dataset for Greenland. *The Cryosphere*, 7(2): 499–510.

Banwell, Alison, Hewitt, Ian, Willis, Ian and Arnold, Neil (2016), Moulin Density Controls Drainage Development beneath the Greenland Ice Sheet. *Journal of Geophysical Research: Earth Surface*, 121(12): 2248–2269.

Bartholomew, ID, Nienow, P, Sole, A, Mair, D, Cowton, T, King, MA and Palmer, S (2011), Seasonal Variations in Greenland Ice Sheet Motion: Inland Extent and Behaviour at Higher Elevations. *Earth and Planetary Science Letters*, 307(3-4): 271–278.

Benn, Douglas, Gulley, Jason, Luckman, Adrian, Adamek, Artur and Glowacki, Piotr S (2009), Englacial Drainage Systems Formed by Hydrologically Driven Crevasse Propagation. *Journal of Glaciology*, 55(191): 513–523.

Benn, Douglas I, Åström, JAN, Zwinger, Thomas, Todd, JOE, Nick, Faezeh M, Cook, Susan, Hulton, Nicholas RJ and Luckman, Adrian (2017), Melt-under-Cutting and Buoyancy-Driven Calving from Tidewater Glaciers: New Insights from Discrete Element and

Continuum Model Simulations. *Journal of Glaciology*, 63(240): 691–702.

Benn, Douglas I, Cowton, Tom, Todd, Joe and Luckman, Adrian (2017), Glacier Calving in Greenland. *Current Climate Change Reports*, 3: 282–290.

Bevan, SL, Luckman, AJ and Murray, T (2012), Glacier Dynamics over the Last Quarter of a Century at Helheim, Kangerdlugssuaq and 14 Other Major Greenland Outlet Glaciers. *The Cryosphere*, 6(5): 923–937.

Bevan, Suzanne L, Luckman, Adrian, Khan, Shfaqat A and Murray, Tavi (2015), Seasonal Dynamic Thinning at Helheim Glacier. *Earth and Planetary Science Letters*, 415: 47–53.

Bhushan, Shashank, Shean, David, Alexandrov, Oleg and Henderson, Scott (2022), Automated Tools to Derive Short-Term Glacier Velocity from High-Resolution Commercial Satellite Imagery. *Authorea Preprints*.

Bindschadler, R, Harrison, WD, Raymond, CF and Crosson, R (1977), Geometry and Dynamics of a Surge-Type Glacier. *Journal of Glaciology*, 18(79): 181–194.

Bingham, Robert G, Nienow, Peter W, Sharp, Martin J and Copland, Luke (2006), Hydrology and Dynamics of a Polythermal (mostly Cold) High Arctic Glacier. *Earth Surface Processes and Landforms: The Journal of the British Geomorphological Research Group*, 31(12): 1463–1479.

Bondzio, Johannes H, Seroussi, Hélène, Morlighem, Mathieu, Kleiner, Thomas, Rückamp, Martin, Humbert, Angelika and Larour, Eric Y (2016), Modelling Calving Front Dynamics Using a Level-Set Method: Application to Jakobshavn Isbræ, West Greenland. *The Cryosphere*, 10(2): 497–510.

Bougamont, M, Christoffersen, Poul, Hubbard, AL, Fitzpatrick, AA, Doyle, Samuel Huckerby and Carter, Sasha P (2014), Sensitive Response of the Greenland Ice Sheet to Surface Melt Drainage over a Soft Bed. *Nature communications*, 5(1): 1–9.

Boulton, GS (1996), Theory of Glacial Erosion, Transport and Deposition as a Consequence of Subglacial Sediment Deformation. *Journal of Glaciology*, 42(140): 43–62.

Boulton, GS, Dobbie, KE and Zatsepin, S (2001), Sediment Deformation beneath Glaciers and Its Coupling to the Subglacial Hydraulic System. *Quaternary International*, 86(1): 3–28.

Boulton, GS and Jones, AS (1979), Stability of Temperate Ice Caps and Ice Sheets Resting on Beds of Deformable Sediment. *Journal of Glaciology*, 24(90): 29–43.

Bowling, JS, Livingstone, SJ, Sole, AJ and Chu, W (2019), Distribution and Dynamics of Greenland Subglacial Lakes. *Nature communications*, 10(1): 2810.

Van den Broeke, Michiel R, Enderlin, Ellyn M, Howat, Ian M, Kuipers Munneke, Peter, Noël, Brice PY, Van De Berg, Willem Jan, Van Meijgaard, Erik and Wouters, Bert (2016), On the

Recent Contribution of the Greenland Ice Sheet to Sea Level Change. *The Cryosphere*, 10(5): 1933–1946.

Brook, Martin S, Kirkbride, Martin P and Brock, Ben W (2004), Rock Strength and Development of Glacial Valley Morphology in the Scottish Highlands and Northwest Iceland. *Geografiska Annaler: Series A, Physical Geography*, 86(3): 225–234.

Brough, Stephen, Carr, J Rachel, Ross, Neil and Lea, James M (2019), Exceptional Retreat of Kangerlussuaq Glacier, East Greenland, between 2016 and 2018. *Frontiers in Earth Science*, 7: 123.

Calov, Reinhard, Beyer, Sebastian, Greve, Ralf, Beckmann, Johanna, Willeit, Matteo, Kleiner, Thomas, Rückamp, Martin, Humbert, Angelika and Ganopolski, Andrey (2018), Simulation of the Future Sea Level Contribution of Greenland with a New Glacial System Model. *The Cryosphere*, 12(10): 3097–3121.

Cameron, A Colin and Trivedi, Pravin K (2013), *Regression Analysis of Count Data*. Cambridge university press.

Carlson, Anders E, Kilmer, Zoe, Ziegler, Leah B, Stoner, Joseph S, Wiles, Greg C, Starr, Kaitlin, Walczak, Maureen H, Colgan, William, Reyes, Alberto V, Leydet, David J and others (2017), Recent Retreat of Columbia Glacier, Alaska: Millennial Context. *Geology*, 45(6): 547–550.

Carr, J Rachel, Bell, Heather, Killick, Rebecca and Holt, Tom (2017), Exceptional Retreat of Novaya Zemlya's Marine-Terminating Outlet Glaciers between 2000 and 2013. *The Cryosphere*, 11(5): 2149–2174.

Carr, J Rachel, Vieli, Andreas, Stokes, CR, Jamieson, SSR, Palmer, SJ, Christoffersen, P, Dowdeswell, JA, Nick, FM, Blankenship, DD and Young, DA (2015), Basal Topographic Controls on Rapid Retreat of Humboldt Glacier, Northern Greenland. *Journal of Glaciology*, 61(225): 137–150.

Catania, GA, Stearns, LA, Moon, TA, Enderlin, EM and Jackson, RH (2020), Future Evolution of Greenland's Marine-Terminating Outlet Glaciers. *Journal of Geophysical Research: Earth Surface*, 125(2): e2018JF004873.

Catania, GA, Stearns, LA, Sutherland, DA, Fried, MJ, Bartholomaus, TC, Morlighem, M, Shroyer, E and Nash, J (2018), Geometric Controls on Tidewater Glacier Retreat in Central Western Greenland. *Journal of Geophysical Research: Earth Surface*, 123(8): 2024–2038.

Catania, Ginny and Felikson, Denis (2022), Topographic Modulation of Outlet Glaciers in Greenland: A Review. *Annals of Glaciology*: 1–7.

Chandler, David M, Wadham, Jemma L, Nienow, Peter W, Doyle, Samuel H, Tedstone, Andrew J, Telling, Jon, Hawkings, Jonathan, Alcock, Jonathan D, Linhoff, Benjamin and Hubbard, Alun (2021), Rapid Development and Persistence of Efficient Subglacial

Drainage under 900 M-Thick Ice in Greenland. *Earth and Planetary Science Letters*, 566: 116982.

Chandler, DM, Wadham, JL, Lis, GP, Cowton, Tom, Sole, A, Bartholomew, I, Telling, J, Nienow, P, Bagshaw, EB, Mair, D and others (2013), Evolution of the Subglacial Drainage System beneath the Greenland Ice Sheet Revealed by Tracers. *Nature Geoscience*, 6(3): 195–198.

Chen, Yu-Zhong and Lai, Ying-Cheng (2018), Sparse Dynamical Boltzmann Machine for Reconstructing Complex Networks with Binary Dynamics. *Physical Review E*, 97(3): 032317.

Cheng, Gong, Morlighem, Mathieu, Mouginot, Jérémie and Cheng, Daniel (2022), Helheim Glacier's Terminus Position Controls Its Seasonal and Inter-Annual Ice Flow Variability. *Geophysical Research Letters*, 49(5): e2021GL097085.

Christianson, Knut, Peters, Leo E, Alley, Richard B, Anandakrishnan, Sridhar, Jacobel, Robert W, Riverman, Kiya L, Muto, Atsuhiro and Keisling, Benjamin A (2014), Dilatant till Facilitates Ice-Stream Flow in Northeast Greenland. *Earth and Planetary Science Letters*, 401: 57–69.

Chu, Vena W (2014), Greenland Ice Sheet Hydrology: A Review. *Progress in Physical Geography*, 38(1): 19–54.

Chudley, Thomas R, Christoffersen, Poul, Doyle, Samuel H, Abellan, Antonio and Snooke, Neal (2019), High-Accuracy UAV Photogrammetry of Ice Sheet Dynamics with No Ground Control. *The Cryosphere*, 13(3): 955–968.

Clarke, Garry KC (1987), A Short History of Scientific Investigations on Glaciers. *Journal of Glaciology*, 33(S1): 4–24.

Clason, Caroline C, Greenwood, Sarah L, Selmes, Nick, Lea, James M, Jamieson, Stewart SR, Nick, Faezeh M and Holmlund, Per (2016), Controls on the Early Holocene Collapse of the Bothnian Sea Ice Stream. *Journal of Geophysical Research: Earth Surface*, 121(12): 2494–2513.

Colgan, William, Box, Jason E, Andersen, Morten L, Fettweis, Xavier, Csatho, Beata, Fausto, Robert S, Van As, Dirk and Wahr, John (2015), Greenland High-Elevation Mass Balance: Inference and Implication of Reference Period (1961-90) Imbalance. *Annals of Glaciology*, 56(70): 105–117.

Collins, IF (1970), A Slip-Line Field Analysis of the Deformation at the Confluence of Two Glacier Streams. *Journal of Glaciology*, 9(56): 169–193.

Colonia, Daniel, Torres, Judith, Haeberli, Wilfried, Schauwecker, Simone, Braendle, Eliane, Giraldez, Claudia and Cochachin, Alejo (2017), Compiling an Inventory of Glacier-Bed Overdeepenings and Potential New Lakes in de-Glaciating Areas of the Peruvian Andes:

Approach, First Results, and Perspectives for Adaptation to Climate Change. *Water*, 9(5): 336.

Cook, Simon J and Swift, Darrel A (2012), Subglacial Basins: Their Origin and Importance in Glacial Systems and Landscapes. *Earth-Science Reviews*, 115(4): 332–372.

Copland, Luke, Sharp, Martin J and Nienow, Peter W (2003), Links between Short-Term Velocity Variations and the Subglacial Hydrology of a Predominantly Cold Polythermal Glacier. *Journal of Glaciology*, 49(166): 337–348.

Creyts, Timothy T and Clarke, Garry KC (2010), Hydraulics of Subglacial Supercooling: Theory and Simulations for Clear Water Flows. *Journal of Geophysical Research: Earth Surface*, 115(F3).

Das, Sarah B, Joughin, Ian, Behn, Mark D, Howat, Ian M, King, Matt A, Lizarralde, Dan and Bhatia, Maya P (2008), Fracture Propagation to the Base of the Greenland Ice Sheet during Supraglacial Lake Drainage. *Science*, 320(5877): 778–781.

Davison, Benjamin Joseph, Sole, Andrew John, Livingstone, Stephen John, Cowton, Tom R and Nienow, Peter William (2019), The Influence of Hydrology on the Dynamics of Land-Terminating Sectors of the Greenland Ice Sheet. *Frontiers in Earth Science*, 7: 10.

Davison, BJ, Sole, Andrew John, Cowton, TR, Lea, JM, Slater, Donald A, Fahrner, Dominik and Nienow, PW (2020), Subglacial Drainage Evolution Modulates Seasonal Ice Flow Variability of Three Tidewater Glaciers in Southwest Greenland. *Journal of Geophysical Research: Earth Surface*, 125(9): e2019JF005492.

Dawes, Peter R (2009), The Bedrock Geology under the Inland Ice: The next Major Challenge for Greenland Mapping. *GEUS Bulletin*, 17: 57–60.

Van De Wal, RSW, Smeets, CJPP, Boot, W, Stoffelen, M, Van Kampen, R, Doyle, SH, Wilhelms, F, Van den Broeke, MR, Reijmer, CH, Oerlemans, J and others (2015), Self-Regulation of Ice Flow Varies across the Ablation Area in South-West Greenland. *The Cryosphere*, 9(2): 603–611.

Van Der Veen, Cornelis J and Whillans, IM (1989), Force Budget: I. Theory and Numerical Methods. *Journal of Glaciology*, 35(119): 53–60.

Dow, CF, Kulessa, B, Rutt, IC, Doyle, Samuel Huckerby and Hubbard, Alun (2014), Upper Bounds on Subglacial Channel Development for Interior Regions of the Greenland Ice Sheet. *Journal of Glaciology*, 60(224): 1044–1052.

Doyle, Samuel H, Hubbard, Alun, Fitzpatrick, Andrew AW, As, Dirk, Mikkelsen, Andreas B, Pettersson, Rickard and Hubbard, Bryn (2014), Persistent Flow Acceleration within the Interior of the Greenland Ice Sheet. *Geophysical Research Letters*.

Doyle, Samuel H, Hubbard, Bryn, Christoffersen, Poul, Young, Tun J, Hofstede, Coen, Bougamont, Marion, Box, JE and Hubbard, Alun (2018), Physical Conditions of Fast Glacier Flow: 1. Measurements from Boreholes Drilled to the Bed of Store Glacier, West Greenland. *Journal of Geophysical Research: Earth Surface*, 123(2): 324–348.

Echelmeyer, Keith and Harrison, William D (1990), Jakobshavns Isbræ, West Greenland: Seasonal Variations in Velocity-or Lack Thereof. *Journal of Glaciology*, 36(122): 82–88.

Egholm, David L, Knudsen, Mads F, Clark, Chris D and Lesemann, Jerome E (2011), Modeling the Flow of Glaciers in Steep Terrains: The Integrated Second-Order Shallow Ice Approximation (iSOSIA). *Journal of Geophysical Research: Earth Surface*, 116(F2).

Egholm, David L, Nielsen, SB, Pedersen, Vivi K and Lesemann, J-E (2009), Glacial Effects Limiting Mountain Height. *Nature*, 460(7257): 884–887.

Egholm, DL, Pedersen, Vivi Kathrine, Knudsen, Mads Faurschou and Larsen, Nicolaj Krog (2012), Coupling the Flow of Ice, Water, and Sediment in a Glacial Landscape Evolution Model. *Geomorphology*, 141: 47–66.

Enderlin, Ellyn M, Hamilton, Gordon S, O'Neel, Shad, Bartholomaus, Timothy C, Morlighem, Mathieu and Holt, John W (2016), An Empirical Approach for Estimating Stress-Coupling Lengths for Marine-Terminating Glaciers. *Frontiers in Earth Science*, 4: 104.

Enderlin, Ellyn M, Howat, Ian M, Jeong, Seongsu, Noh, Myoung-Jong, Van Angelen, Jan H and Van Den Broeke, Michiel R (2014), An Improved Mass Budget for the Greenland Ice Sheet. *Geophysical Research Letters*, 41(3): 866–872.

Favier, Lionel, Pattyn, Frank, Berger, Sophie and Drews, Reinhard (2016), Dynamic Influence of Pinning Points on Marine Ice-Sheet Stability: A Numerical Study in Dronning Maud Land, East Antarctica. *The Cryosphere*, 10(6): 2623–2635.

Felikson, Denis, A Catania, Ginny, Bartholomaus, Timothy C, Morlighem, Mathieu and Noël, Brice PY (2021), Steep Glacier Bed Knickpoints Mitigate Inland Thinning in Greenland. *Geophysical Research Letters*, 48(2): e2020GL090112.

Felikson, Denis, Bartholomaus, Timothy C, Catania, Ginny A, Korsgaard, Niels J, Kjær, Kurt H, Morlighem, Mathieu, Noël, Brice, Van Den Broeke, Michiel, Stearns, Leigh A, Shroyer, Emily L and others (2017), Inland Thinning on the Greenland Ice Sheet Controlled by Outlet Glacier Geometry. *Nature Geoscience*, 10(5): 366–369.

Felikson, Denis, Nowicki, Sophie, Nias, I, Morlighem, Mathieu and Seroussi, Helene (2022), Seasonal Tidewater Glacier Terminus Oscillations Bias Multi-Decadal Projections of Ice Mass Change. *Journal of Geophysical Research: Earth Surface*, 127(2): e2021JF006249.

Fettweis, Xavier (2007), Reconstruction of the 1979-2006 Greenland Ice Sheet Surface Mass Balance Using the Regional Climate Model MAR. *The Cryosphere*, 1(1): 21–40.

Fettweis, Xavier, Box, Jason E, Agosta, Cécile, Amory, Charles, Kittel, Christoph, Lang, Charlotte, van As, Dirk, Machguth, Horst and Gallée, Hubert (2017), Reconstructions of the 1900-2015 Greenland Ice Sheet Surface Mass Balance Using the Regional Climate MAR Model. *The Cryosphere*, 11(2): 1015–1033.

Fischer, Urs H, Bebiolka, Anke, Brandefelt, Jenny, Cohen, Denis, Harper, Joel, Hirschorn, Sarah, Jensen, Mark, Kennell, Laura, Liakka, Johan, Näslund, Jens-Ove and others (2021), Radioactive Waste under Conditions of Future Ice Ages, 323–375, in: *Snow and Ice-Related Hazards, Risks, and Disasters*. Elsevier.

De Fleurian, Basile, Morlighem, Mathieu, Seroussi, Helene, Rignot, Eric, van den Broeke, Michiel R, Kuipers Munneke, Peter, Mouginot, Jeremie, Smeets, Paul CJP and Tedstone, Andrew J (2016), A Modeling Study of the Effect of Runoff Variability on the Effective Pressure beneath Russell Glacier, West Greenland. *Journal of Geophysical Research: Earth Surface*, 121(10): 1834–1848.

Forbes, JD (1842), Second Letter on Glaciers. *Chamouni*, 10: 341–344.

Fountain, Andrew G (1994), Borehole Water-Level Variations and Implications for the Subglacial Hydraulics of South Cascade Glacier, Washington State, USA. *Journal of Glaciology*, 40(135): 293–304.

Fountain, Andrew G and Walder, Joseph S (1998), Water Flow through Temperate Glaciers. *Reviews of Geophysics*, 36(3): 299–328.

Fox-Kemper, B, Hewitt, HT, Xiao, C, A\dhalgeirsdóttir, G, Drijfhout, SS, Edwards, TL, Golledge, NR, Hemer, M, Kopp, RE, Krinner, G and others (2021), Ocean, Cryosphere and Sea Level Change. Climate Change 2021: The Physical Science Basis. Contribution of Working Group I to the Sixth Assessment Report of the Intergovernmental Panel on Climate Change. *P. Zhai, editor;, A. Pirani, editor*.

Frazier, Amy E and Hemingway, Benjamin L (2021), A Technical Review of Planet Smallsat Data: Practical Considerations for Processing and Using Planetscope Imagery. *Remote Sensing*, 13(19): 3930.

Frederikse, Thomas, Landerer, Felix, Caron, Lambert, Adhikari, Surendra, Parkes, David, Humphrey, Vincent W, Dangendorf, Sönke, Hogarth, Peter, Zanna, Laure, Cheng, Lijing and others (2020), The Causes of Sea-Level Rise since 1900. *Nature*, 584(7821): 393–397.

Fretwell, P, Pritchard, Hamish D, Vaughan, David G, Bamber, JL, Barrand, NE, Bell, R, Bianchi, C, Bingham, RG, Blankenship, DD, Casassa, G and others (2013), Bedmap2: Improved Ice Bed, Surface and Thickness Datasets for Antarctica. *Cryosphere*, 7(1).

Gallée, Hubert (1997), Air-Sea Interactions over Terra Nova Bay during Winter: Simulation with a Coupled Atmosphere-Polynya Model. *Journal of Geophysical Research: Atmospheres*, 102(D12): 13835–13849.

Gegg, Lukas, Deplazes, Gaudenz, Keller, Lorenz, Madritsch, Herfried, Spillmann, Thomas, Anselmetti, Flavio S and Buechi, Marius W (2021), 3D Morphology of a Glacially Overdeepened Trough Controlled by Underlying Bedrock Geology. *Geomorphology*, 394: 107950.

Gilbert, E. and Kittel, C., (2021). Surface melt and runoff on Antarctic ice shelves at 1.5 C, 2 C, and 4 C of future warming. *Geophysical Research Letters*, *48*(8), p.e2020GL091733.

Glasser, Neil F (1995), Modelling the Effect of Topography on Ice Sheet Erosion, Scotland. *Geografiska Annaler. Series A. Physical Geography*: 67–82.

Glasser, Neil F and Bennett, Matthew R (2004), Glacial Erosional Landforms: Origins and Significance for Palaeoglaciology. *Progress in Physical Geography*, 28(1): 43–75.

Goelzer, Heiko, Nowicki, Sophie, Payne, Anthony, Larour, Eric, Seroussi, Helene, Lipscomb, William H, Gregory, Jonathan, Abe-Ouchi, Ayako, Shepherd, Andy, Simon, Erika and others (2020), The Future Sea-Level Contribution of the Greenland Ice Sheet: A Multi-Model Ensemble Study of ISMIP6. *The Cryosphere Discussions*, 2020: 1–43.

Gogineni, Silvaprasad, Tammana, Dilip, Braaten, David, Leuschen, Carl, Akins, Torry, Legarsky, Justin, Kanagaratnam, Pannir, Stiles, Jim, Allen, C and Jezek, K (2001), Coherent Radar Ice Thickness Measurements over the Greenland Ice Sheet. *Journal of Geophysical Research: Atmospheres*, 106(D24): 33761–33772.

Gowan, Evan J, Niu, Lu, Knorr, Gregor and Lohmann, Gerrit (2019), Geology Datasets in North America, Greenland and Surrounding Areas for Use with Ice Sheet Models. *Earth System Science Data*, 11(1): 375–391.

Grau Galofre, A, Whipple, KX, Christensen, PR and Conway, SJ (2022), Valley Networks and the Record of Glaciation on Ancient Mars. *Geophysical Research Letters*, 49(14): e2022GL097974.

Greene, Chad A, Gardner, Alex S and Andrews, Lauren C (2020), Detecting Seasonal Ice Dynamics in Satellite Images. *The Cryosphere*, 14(12): 4365–4378.

Greenwood, Sarah L, Clason, Caroline C, Helanow, Christian and Margold, Martin (2016), Theoretical, Contemporary Observational and Palaeo-Perspectives on Ice Sheet Hydrology: Processes and Products. *Earth-Science Reviews*, 155: 1–27.

Gudmundsson, G Hilmar, Iken, Almut and Funk, Martin (1997), Measurements of Ice Deformation at the Confluence Area of Unteraargletscher Bernese Alps, Switzerland. *Journal of Glaciology*, 43(145): 548–556.

Gudmundsson, Gudmundur H, Bassi, A, Vonmoos, M, Bauder, Andreas, Fischer, Urs H and Funk, Martin (2000), High-Resolution Measurements of Spatial and Temporal Variations

in Surface Velocities of Unteraargletscher, Bernese Alps, Switzerland. *Annals of Glaciology*, 31: 63–68.

Haeberli, Wilfried, Linsbauer, Andreas, Cochachin, Alejo, Salazar, Cesar and Fischer, Urs H (2016), On the Morphological Characteristics of Overdeepenings in High-Mountain Glacier Beds. *Earth Surface Processes and Landforms*, 41(13): 1980–1990.

Halas, Paul, Mouginot, Jérémie, de Fleurian, Basile and Langebroek, Petra M (2023), Impact of Seasonal Fluctuations of Ice Velocity on Decadal Trends Observed in Southwest Greenland. *Remote Sensing of Environment*, 285: 113419.

Hallet, Bernard (1979), A Theoretical Model of Glacial Abrasion. *Journal of Glaciology*, 23(89): 39–50.

Hallet, Bernard (1996), Glacial Quarrying: A Simple Theoretical Model. *Annals of Glaciology*, 22: 1–8.

Harper, Joel T, Humphrey, Neil F, Pfeffer, W Tad, Fudge, Tyler and O'Neel, Shad (2005), Evolution of Subglacial Water Pressure along a Glacier's Length. *Annals of Glaciology*, 40: 31–36.

Harper, Joel T, Humphrey, Neil F, Pfeffer, W Tad and Lazar, Brian (2007), Two Modes of Accelerated Glacier Sliding Related to Water. *Geophysical research letters*, 34(12).

Harper, Joel T, Humphrey, NF and Pfeffer, W Tad (1998), Crevasse Patterns and the Strain-Rate Tensor: A High-Resolution Comparison. *Journal of Glaciology*, 44(146): 68–76.

Hart, Jane K, Martinez, Kirk, Basford, Philip J, Clayton, Alexander I, Robson, Benjamin A and Young, David S (2019), Surface Melt Driven Summer Diurnal and Winter Multi-Day Stick-Slip Motion and till Sedimentology. *Nature communications*, 10(1): 1599.

Haynes, Valerie M (1968), The Influence of Glacial Erosion and Rock Structure on Corries in Scotland. *Geografiska Annaler: Series A, Physical Geography*, 50(4): 221–234.

Herman, Frédéric, Beaud, Flavien, Champagnac, Jean-Daniel, Lemieux, Jean-Michel and Sternai, Pietro (2011), Glacial Hydrology and Erosion Patterns: A Mechanism for Carving Glacial Valleys. *Earth and Planetary Science Letters*, 310(3): 498–508.

Herzfeld, U. C., Fastook, J., Greve, R., McDonald, B., Wallin, B. F., & Chen, P. A. (2012). On the influence of Greenland outlet glacier bed topography on results from dynamic ice-sheet models. *Annals of Glaciology*, *53*(60), 281–293. doi:10.3189/2012AoG60A061

Hirano, Masasgige and Aniya, Masamu (1988), A Rational Explanation of Cross-Profile Morphology for Glacial Valleys and of Glacial Valley Development. *Earth Surface Processes and Landforms*, 13(8): 707–716.

Hock, Regine, Iken, Almut and Wangler, Alexander (1999), Tracer Experiments and Borehole Observations in the Overdeepening of Aletschgletscher, Switzerland. *Annals of Glaciology*, 28(1): 253–260.

Hodge, Steven M (1974), Variations in the Sliding of a Temperate Glacier. *Journal of Glaciology*, 13(69): 349–369.

Hoffman, MJ, Catania, GA, Neumann, TA, Andrews, LC and Rumrill, JA (2011), Links between Acceleration, Melting, and Supraglacial Lake Drainage of the Western Greenland Ice Sheet. *Journal of Geophysical Research: Earth Surface*, 116(F4).

Holmlund, Per and Hooke, Roger Leb (1983), High Water-Pressure Events in Moulins, Storglaciären, Sweden. *Geografiska Annaler: Series A, Physical Geography*, 65(1-2): 19–25.

Holtedahl, Hans (1967), Notes on the Formation of Fjords and Fjord-Valleys. *Geografiska Annaler. Series A. Physical Geography*: 188–203.

Hooke, R (1984), On the Role of Mechanical Energy in Maintaining Subglacial Water Conduits at Atmospheric Pressure. *Journal of Glaciology*, 30(105): 180–187.

Hooke, Roger Leb (1991), Positive Feedbacks Associated with Erosion of Glacial Cirques and Overdeepenings. *Geological Society of America Bulletin*, 103(8): 1104–1108.

Hooke, Roger LeB, Calla, Peter, Holmlund, Per, Nilsson, Mats and Stroeven, Arjen (1989), A 3 Year Record of Seasonal Variations in Surface Velocity, Storglaciären, Sweden. *Journal of Glaciology*, 35(120): 235–247.

Hooke, Roger Leb, Holmlund, Per and Iverson, Neal R (1987), Extrusion Flow Demonstrated by Bore-Hole Deformation Measurements over a Riegel, Storglaciären, Sweden. *Journal of Glaciology*, 33(113): 72–78.

Hooke, Roger Leb, Laumann, T and Kohler, J (1990), Sub Glacial Water Pressures and the Shape of Subglacial Conduits. *Journal of Glaciology*, 36(122).

Hooke, Roger Leb, Miller, Sarah B and Kohler, Jack (1988), CHARACTER OF THE ENGLACIAL AND SUB GLACIAL DRAINAGE SYSTEM IN THE UPPER PART OF THE ABLATION AREA OF STORGLACIAREN, SWEDEN. *Journal oJ Glaciology*, 34(117).

Hooke, Roger LeB and Pohjola, Veijo A (1994), Hydrology of a Segtnent of a Glacier Situated Overdeepening, Storglaciaren, Sweden. *Journal of Glaciology*, 40(134).

Hopkins, William (1862), XXXI. On the Theory of the Motion of Glaciers. *Philosophical Transactions of the Royal Society of London*, (152): 677–745.

Howat, Ian M, Box, Jason E, Ahn, Yushin, Herrington, Adam and McFADDEN, Ellyn M (2010), Seasonal Variability in the Dynamics of Marine-Terminating Outlet Glaciers in Greenland.

Journal of Glaciology, 56(198): 601–613.

Howat, Ian M and Eddy, Alex (2011), Multi-Decadal Retreat of Greenland's Marine-Terminating Glaciers. *Journal of Glaciology*, 57(203): 389–396.

Howat, Ian M, Joughin, I, Tulaczyk, S and Gogineni, S (2005), Rapid Retreat and Acceleration of Helheim Glacier, East Greenland. *Geophysical Research Letters*, 32(22).

Howat, Ian M, Joughin, Ian, Fahnestock, Mark, Smith, Benjamin E and Scambos, Ted A (2008), Synchronous Retreat and Acceleration of Southeast Greenland Outlet Glaciers 2000-06: Ice Dynamics and Coupling to Climate. *Journal of Glaciology*, 54(187): 646–660.

Howat, Ian M, Negrete, A and Smith, Benjamin E (2014), The Greenland Ice Mapping Project (GIMP) Land Classification and Surface Elevation Datasets. *The Cryosphere*, 8(4): 1509–1518.

Hubbard, Bryn and Nienow, Peter (1997), Alpine Subglacial Hydrology. *Quaternary Science Reviews*, 16(9): 939–955.

Iken, A, Röthlisberger, H, Flotron, A and Haeberli, W (1983), The Uplift of Unteraargletscher at the Beginning of the Melt Season—a Consequence of Water Storage at the Bed? *Journal of Glaciology*, 29(101): 28–47.

Iken, Almut (1981), THE EFFECT OF THE SUBGLACIAL THE SLIDING VELOCITY OF A. *Journal of Glaciolo*, 27(97).

Iken, Almut and Bindschadler, Robert A (1986), Combined Measurements of Subglacial Water Pressure and Surface Velocity of Findelengletscher, Switzerland: Conclusions about Drainage System and Sliding Mechanism. *Journal of Glaciology*, 32(110): 101–119.

Iken, Almut, Fabri, Kristian and Funk, Martin (1996), Water Storage and Subglacial Drainage Conditions Inferred from Borehole Measurements on Gornergletscher, Valais, Switzerland. *Journal of Glaciology*, 42(141): 233–248.

Iken, Almut and Truffe, Martin (1997), The Relationship between Subglacial Water Pressure and Velocity of Findelengletscher, Switzerland, during Its Advance and Retreat. *Journal of Glaciology*, 43(144): 328–338.

Iverson, Neal R (1991), Potential Effects of Subglacial Water-Pressure Fluctuations on Quarrying. *Journal of Glaciology*, 37(125): 27–36.

Iverson, Neal R, Hanson, Brian, Hooke, Roger LeB and Jansson, Peter (1995), Flow Mechanism of Glaciers on Soft Beds. *Science*, 267(5194): 80–81.

Jamieson, Stewart SR, Sugden, David E and Hulton, Nicholas RJ (2010), The Evolution of the Subglacial Landscape of Antarctica. *Earth and Planetary Science Letters*, 293(1): 1–27.

Jamieson, Stewart SR, Vieli, Andreas, Livingstone, Stephen J, Cofaigh, Colm Ó, Stokes, Chris, Hillenbrand, Claus-Dieter and Dowdeswell, Julian A (2012), Ice-Stream Stability on a Reverse Bed Slope. *Nature Geoscience*, 5(11): 799–802.

Jansson, Peter (1995), Water Pressure and Basal Sliding on Storglaciären, Northern Sweden. *Journal of Glaciology*, 41(138): 232–240.

Jennings, Stephen JA and Hambrey, Michael J (2021), Structures and Deformation in Glaciers and Ice Sheets. *Reviews of Geophysics*, 59(3): e2021RG000743.

Jones, A. H., Swift, D. A., & Livingstone, S. J. (2016, April). Influence of ice sheet bed morphology on spatial and seasonal patterns of ice flow in Greenland: preliminary results from an automated method for interpreting high resolution ice velocity data derived from Landsat imagery. In *EGU General Assembly Conference Abstracts* (pp. EPSC2016-17421).

Jones, A. H., Swift, D. A., and Livingstone, S.J. (2018) Subglacial bed morphology as a controlling mechanism for variation in seasonal speed up and slow down of ice velocity across longitudinal profiles of Greenland glaciers.. Geophysical Research Abstracts Vol. 20,

Jordan, Peter (2010), Analysis of Overdeepened Valleys Using the Digital Elevation Model of the Bedrock Surface of Northern Switzerland. *Swiss Journal of Geosciences*, 103(3): 375–384.

Joughin, Ian, Abdalati, Waleed and Fahnestock, Mark (2004), Large Fluctuations in Speed on Greenland's Jakobshavn Isbrae Glacier. *Nature*, 432(7017): 608–610.

Joughin, Ian, Das, Sarah B, Flowers, GE, Behn, Mark D, Alley, Richard B, King, Matt A, Smith, BE, Bamber, Jonathan L, van den Broeke, Michiel R and Van Angelen, JH (2013), Influence of Ice-Sheet Geometry and Supraglacial Lakes on Seasonal Ice-Flow Variability.

Joughin, Ian, Das, Sarah B, King, Matt A, Smith, Ben E, Howat, Ian M and Moon, Twila (2008), Seasonal Speedup along the Western Flank of the Greenland Ice Sheet. *Science*, 320(5877): 781–783.

Joughin, Ian, Howat, Ian M, Fahnestock, Mark, Smith, Ben, Krabill, William, Alley, Richard B, Stern, Harry and Truffer, Martin (2008), Continued Evolution of Jakobshavn Isbrae Following Its Rapid Speedup. *Journal of Geophysical Research: Earth Surface*, 113(F4).

Joughin, Ian, Smith, Ben E and Howat, Ian (2018), Greenland Ice Mapping Project: Ice Flow Velocity Variation at Sub-Monthly to Decadal Timescales. *The Cryosphere*, 12(7): 2211–2227.

Joughin, Ian, Smith, Ben E, Howat, Ian M, Scambos, Ted and Moon, Twila (2010), Greenland Flow Variability from Ice-Sheet-Wide Velocity Mapping. *Journal of Glaciology*, 56(197): 415–430.

Joughin, Ian, Tulaczyk, Slawek, Fahnestock, Mark and Kwok, Ron (1996), A Mini-Surge on the Ryder Glacier, Greenland, Observed by Satellite Radar Interferometry. *Science*, 274(5285): 228–230.

Kamb, Barclay and Echelmeyer, Keith A (1986), Stress-Gradient Coupling in Glacier Flow: I. Longitudinal Averaging of the Influence of Ice Thickness and Surface Slope. *Journal of Glaciology*, 32(111): 267–284.

Kamb, Barclay and Engelhardt, Hermann (1987), Waves of Accelerated Motion in a Glacier Approaching Surge: The Mini-Surges of Variegated Glacier, Alaska, USA. *Journal of Glaciology*, 33(113): 27–46.

Kehrl, LM, Joughin, I, Shean, DE, Floricioiu, D and Krieger, L (2017), Seasonal and Interannual Variabilities in Terminus Position, Glacier Velocity, and Surface Elevation at Helheim and Kangerlussuaq Glaciers from 2008 to 2016. *Journal of Geophysical Research: Earth Surface*, 122(9): 1635–1652.

Kessler, Mark A, Anderson, Robert S and Briner, Jason P (2008), Fjord Insertion into Continental Margins Driven by Topographic Steering of Ice. *Nature Geoscience*, 1(6): 365–369.

Khan, Shfaqat A, Aschwanden, Andy, Bjørk, Anders A, Wahr, John, Kjeldsen, Kristian K and Kjaer, Kurt H (2015), Greenland Ice Sheet Mass Balance: A Review. *Reports on progress in physics*, 78(4): 046801.

King, Michalea D, Howat, Ian M, Candela, Salvatore G, Noh, Myoung J, Jeong, Seongsu, Noël, Brice PY, van den Broeke, Michiel R, Wouters, Bert and Negrete, Adelaide (2020), Dynamic Ice Loss from the Greenland Ice Sheet Driven by Sustained Glacier Retreat. *Communications Earth \& Environment*, 1(1): 1.

King, Michalea D, Howat, Ian M, Jeong, Seongsu, Noh, Myoung J, Wouters, Bert, Noël, Brice and van den Broeke, Michiel R (2018), Seasonal to Decadal Variability in Ice Discharge from the Greenland Ice Sheet. *The cryosphere*, 12(12): 3813–3825.

Kochtitzky, William and Copland, Luke (2022), Retreat of Northern Hemisphere Marine-Terminating Glaciers, 2000-2020. *Geophysical Research Letters*, 49(3): e2021GL096501.

Koenig, Lora S, Ivanoff, Alvaro, Alexander, Patrick M, MacGregor, Joseph A, Fettweis, Xavier, Panzer, Ben, Paden, John D, Forster, Richard R, Das, Indrani, McConnell, Joesph R and others (2016), Annual Greenland Accumulation Rates (2009-2012) from Airborne Snow Radar. *The Cryosphere*, 10(4): 1739–1752.

Koziol, Conrad P and Arnold, Neil (2018), Modelling Seasonal Meltwater Forcing of the Velocity of Land-Terminating Margins of the Greenland Ice Sheet. *The Cryosphere*, 12(3): 971–991.

Krimmel, Robert M and Vaughn, Bruce H (1987), Columbia Glacier, Alaska: Changes in Velocity 1977-1986. *Journal of Geophysical Research: Solid Earth*, 92(B9): 8961–8968.

Larsen, Signe H, Ahlstrøm, Andreas P, Karlsson, Nanna B, Kusk, Anders, Langen, Peter L and Hvidberg, Christine S (2023), Outlet Glacier Flow Response to Surface Melt: Based on Analysis of a High-Resolution Satellite Dataset. *Journal of Glaciology*: 1–9.

Lawson, Daniel E, Strasser, Jeffrey C, Evenson, Edward B, Alley, Richard B, Larson, Grahame J and Arcone, Steven A (1998), Glaciohydraulic Supercooling: A Freeze-on Mechanism to Create Stratified, Debris-Rich Basal Ice: I. Field Evidence. *Journal of Glaciology*, 44(148): 547–562.

Lemos, Adriano, Shepherd, Andrew, McMillan, Malcolm, Hogg, Anna E, Hatton, Emma and Joughin, Ian (2018), Ice Velocity of Jakobshavn Isbræ, Petermann Glacier, Nioghalvfjerdsfjorden, and Zachariæ Isstrøm, 2015-2017, from Sentinel 1-A/b SAR Imagery. *The Cryosphere*, 12(6): 2087–2097.

Linsbauer, Andreas, Frey, Holger, Haeberli, Wilfried, Machguth, Horst, Azam, MF and Allen, Simon (2016), Modelling Glacier-Bed Overdeepenings and Possible Future Lakes for the Glaciers in the Himalaya—Karakoram Region. *Annals of Glaciology*, 57(71): 119–130.

Liu, Jukes, Gendreau, Madeline, Enderlin, Ellyn Mary and Aberle, Rainey (2024), Improved Records of Glacier Flow Instabilities Using Customized NASA autoRIFT Applied to PlanetScope Imagery. *EGUsphere*, 2024: 1–24.

Livingstone, Stephen J, Li, Yan, Rutishauser, Anja, Sanderson, Rebecca J, Winter, Kate, Mikucki, Jill A, Björnsson, Helgi, Bowling, Jade S, Chu, Winnie, Dow, Christine F and others (2022), Subglacial Lakes and Their Changing Role in a Warming Climate. *Nature Reviews Earth \& Environment*, 3(2): 106–124.

Lliboutry, Louis (1968), General Theory of Subglacial Cavitation and Sliding of Temperate Glaciers. *Journal of Glaciology*, 7(49): 21–58.

Lliboutry, Louis (1983), Modifications to the Theory of Intraglacial Waterways for the Case of Subglacial Ones. *Journal of Glaciology*, 29(102): 216–226.

Lloyd, Christopher T (2015), Controls upon the Location and Size of Glacial Overdeepenings.

Lloyd, Christopher T, Clark, Chris D and Swift, Darrel A (2023), The Effect of Valley Confluence and Bedrock Geology upon the Location and Depth of Glacial Overdeepenings. *Geografiska Annaler: Series A, Physical Geography*: 1–26.

Luckman, Adrian and Murray, Tavi (2005), Seasonal Variation in Velocity before Retreat of Jakobshavn Isbræ, Greenland. *Geophysical Research Letters*, 32(8).

Luckman, Adrian, Murray, Tavi, De Lange, Remko and Hanna, Edward (2006), Rapid and Synchronous Ice-Dynamic Changes in East Greenland. *Geophysical Research Letters*,

33(3).

Macelloni, Myrta M, Cina, Alberto, Grasso, Nives and Morra di Cella, U (2023), Multi-Temporal and Multi-Sensor Glacier Monitoring. *The International Archives of the Photogrammetry, Remote Sensing and Spatial Information Sciences*, 48: 165–171.

MacGregor, Joseph A, Chu, Winnie, Colgan, William T, Fahnestock, Mark A, Felikson, Denis, Karlsson, Nanna B, Nowicki, Sophie MJ and Studinger, Michael (2022), GBaTSv2: A Revised Synthesis of the Likely Basal Thermal State of the Greenland Ice Sheet. *The Cryosphere*, 16(8): 3033–3049.

MacGregor, Joseph A, Colgan, William T, Paxman, Guy JG, Tinto, Kirsty J, Csathó, Beáta, Darbyshire, Fiona A, Fahnestock, Mark A, Kokfelt, Thomas F, MacKie, Emma J, Morlighem, Mathieu and others (2024), Geologic Provinces beneath the Greenland Ice Sheet Constrained by Geophysical Data Synthesis. *Geophysical Research Letters*, 51(8): e2023GL107357.

MacGregor, Kelly R, Anderson, Robert S and Waddington, Edwin D (2009), Numerical Modeling of Glacial Erosion and Headwall Processes in Alpine Valleys. *Geomorphology*, 103(2): 189–204.

Magnin, Florence, Haeberli, Wilfried, Linsbauer, Andreas, Deline, Philip and Ravanel, Ludovic (2020), Estimating Glacier-Bed Overdeepenings as Possible Sites of Future Lakes in the de-Glaciating Mont Blanc Massif (Western European Alps). *Geomorphology*, 350: 106913.

Magrani, Fabio, Valla, Pierre G, Gribenski, Natacha and Serra, Elena (2020), Glacial Overdeepenings in the Swiss Alps and Foreland: Spatial Distribution and Morphometrics. *Quaternary Science Reviews*, 243: 106483.

Maier, Nathan, Gimbert, Florent and Gillet-Chaulet, Fabien (2022), Threshold Response to Melt Drives Large-Scale Bed Weakening in Greenland. *Nature*, 607(7920): 714–720.

Mair, Douglas, Hubbard, Bryn, Nienow, Peter, Willis, Ian and Fischer, Urs H (2008), Diurnal Fluctuations in Glacier Ice Deformation: Haut Glacier d'Arolla, Switzerland. *Earth Surface Processes and Landforms: The Journal of the British Geomorphological Research Group*, 33(8): 1272–1284.

Mair, Douglas, Nienow, Peter, Sharp, Martin, Wohlleben, Trudy and Willis, Ian (2002), Influence of Subglacial Drainage System Evolution on Glacier Surface Motion: Haut Glacier d'Arolla, Switzerland. *Journal of Geophysical Research: Solid Earth*, 107(B8): EPM–8.

Mair, Douglas, Willis, Ian, Fischer, Urs H, Hubbard, Bryn, Nienow, Peter and Hubbard, Alun (2003), Hydrological Controls on Patterns of Surface, Internal and Basal Motion during Three "spring Events": Haut Glacier d'Arolla, Switzerland. *Journal of Glaciology*, 49(167): 555–567.

Makwana, P, Kodinariya, TM and Makwana, PR (2013), Review on Determining of Cluster in K-Means Clustering Review on Determining Number of Cluster in K-Means Clustering. *International Journal of Advance Research in Computer Science and Management Studies*, 1(6): 90–95.

Mankoff, Kenneth D, Solgaard, Anne, Colgan, William, Ahlstrøm, Andreas P, Khan, Shfaqat Abbas and Fausto, Robert S (2020), Greenland Ice Sheet Solid Ice Discharge from 1986 through March 2020. *Earth System Science Data*, 12(2): 1367–1383.

Marshall, Shawn J, Clarke, Garry KC, Dyke, Art S and Fisher, David A (1996), Geologic and Topographic Controls on Fast Flow in the Laurentide and Cordilleran Ice Sheets. *Journal of Geophysical Research: Solid Earth*, 101(B8): 17827–17839.

McNabb, RW and Hock, Regine (2014), Alaska Tidewater Glacier Terminus Positions, 1948-2012. *Journal of Geophysical Research: Earth Surface*, 119(2): 153–167.

Meier, MF and Post, Austin (1987), Fast Tidewater Glaciers. *Journal of Geophysical Research: Solid Earth*, 92(B9): 9051–9058.

Meierbachtol, T, Harper, J and Humphrey, N (2013), Basal Drainage System Response to Increasing Surface Melt on the Greenland Ice Sheet. *Science (New York, N.Y.)*, 341(6147): 777–9.

Meyer, Colin R, Fernandes, Matheus C, Creyts, Timothy T and Rice, James R (2016), Effects of Ice Deformation on Röthlisberger Channels and Implications for Transitions in Subglacial Hydrology. *Journal of Glaciology*, 62(234): 750–762.

Mohr, Johan J, Reeh, Niels and Madsen, Søren N (1998), Three-Dimensional Glacial Flow and Surface Elevation Measured with Radar Interferometry. *Nature*, 391(6664): 273–276.

Moon, T, Joughin, I, Smith, B and Howat, I (2012), 21st-Century Evolution of Greenland Outlet Glacier Velocities. *Science*, 336(6081): 576–578.

Moon, Twila and Joughin, Ian (2008), Changes in Ice Front Position on Greenland's Outlet Glaciers from 1992 to 2007. *Journal of Geophysical Research: Earth Surface*, 113(F2).

Moon, Twila, Joughin, Ian and Smith, Ben (2015), Seasonal to Multiyear Variability of Glacier Surface Velocity, Terminus Position, and Sea Ice/ice Mélange in Northwest Greenland. *Journal of Geophysical Research: Earth Surface*, 120(5): 818–833.

Moon, Twila, Joughin, Ian, Smith, Ben, Broeke, Michiel R, Berg, Willem Jan, Noël, Brice and Usher, Mika (2014), Distinct Patterns of Seasonal Greenland Glacier Velocity. *Geophysical research letters*, 41(20): 7209–7216.

Morlighem, M, Rignot, E, Mouginot, J, Seroussi, H and Larour, E (2014), Deeply Incised Submarine Glacial Valleys beneath the Greenland Ice Sheet. *Nature Geoscience*.

Morlighem, M. Williams C. Rignot E. An L. Arndt J. E. Bamber J. Catania G. Chauché N. (2022), *IceBridge BedMachine Greenland, Version 5.* Boulder, Colorado, USA.

Morlighem, Mathieu, Bondzio, Johannes, Seroussi, Hélène, Rignot, E, Larour, E, Humbert, Angelika and Rebuffi, S (2016), Modeling of Store Gletscher's Calving Dynamics, West Greenland, in Response to Ocean Thermal Forcing. *Geophysical Research Letters*, 43(6): 2659–2666.

Morlighem, Mathieu, Williams, Chris N, Rignot, Eric, An, Lu, Arndt, Jan Erik, Bamber, Jonathan L, Catania, Ginny, Chauché, Nolwenn, Dowdeswell, Julian A, Dorschel, Boris and others (2017), BedMachine v3: Complete Bed Topography and Ocean Bathymetry Mapping of Greenland from Multibeam Echo Sounding Combined with Mass Conservation. *Geophysical research letters*, 44(21): 11–051.

Motyka, Roman J, O'Neel, Shad, Connor, Cathy L and Echelmeyer, Keith A (2003), Twentieth Century Thinning of Mendenhall Glacier, Alaska, and Its Relationship to Climate, Lake Calving, and Glacier Run-Off. *Global and Planetary Change*, 35(1): 93–112.

Mouginot, Jérémie, Rignot, Eric, Bjørk, Anders A, Van den Broeke, Michiel, Millan, Romain, Morlighem, Mathieu, Noël, Brice, Scheuchl, Bernd and Wood, Michael (2019), Forty-Six Years of Greenland Ice Sheet Mass Balance from 1972 to 2018. *Proceedings of the national academy of sciences*, 116(19): 9239–9244.

Murray, Tavi, Scharrer, K, James, TD, Dye, SR, Hanna, Edward, Booth, AD, Selmes, N, Luckman, Adrian, Hughes, ALC, Cook, Susan and others (2010), Ocean Regulation Hypothesis for Glacier Dynamics in Southeast Greenland and Implications for Ice Sheet Mass Changes. *Journal of Geophysical Research: Earth Surface*, 115(F3).

Murray, Tavi, Scharrer, Kilian, Selmes, Nick, Booth, Adam D, James, Timothy D, Bevan, Suzanne L, Bradley, J, Cook, Susan, Llana, L Cordero, Drocourt, Yoann and others (2015), Extensive Retreat of Greenland Tidewater Glaciers, 2000-2010. *Arctic, antarctic, and alpine research*, 47(3): 427–447.

Nagler, Thomas, Rott, Helmut, Hetzenecker, Markus, Wuite, Jan and Potin, Pierre (2015), The Sentinel-1 Mission: New Opportunities for Ice Sheet Observations. *Remote Sensing*, 7(7): 9371–9389.

Nanni, Ugo, Scherler, Dirk, Ayoub, Francois, Millan, Romain, Herman, Frederic and Avouac, Jean-Philippe (2023), Climatic Control on Seasonal Variations in Mountain Glacier Surface Velocity. *The Cryosphere*, 17(4): 1567–1583.

Nettles, Meredith, Larsen, Tine B, Elosegui, Pedro, Hamilton, Gordon S, Stearns, Leigh A, Ahlstrøm, Andreas P, Davis, Jim L, Andersen, Morten L, de Juan, Julia, Khan, Shfaqat Abbas and others (2008), Step-Wise Changes in Glacier Flow Speed Coincide with Calving

and Glacial Earthquakes at Helheim Glacier, Greenland. *Geophysical Research Letters*, 35(24).

Newton, Andrew MW and Huuse, Mads (2017), Glacial Geomorphology of the Central Barents Sea: Implications for the Dynamic Deglaciation of the Barents Sea Ice Sheet. *Marine Geology*, 387: 114–131.

Nick, Faezeh M, Vieli, Andreas, Howat, Ian M and Joughin, Ian (2009), Large-Scale Changes in Greenland Outlet Glacier Dynamics Triggered at the Terminus. *Nature Geoscience*, 2(2): 110–114.

Nick, FM, Luckman, Adrian, Vieli, Andreas, Van der Veen, Cornelis J, Van As, Dirk, Van De Wal, RSW, Pattyn, Frank, Hubbard, AL and Floricioiu, Dana (2012), The Response of Petermann Glacier, Greenland, to Large Calving Events, and Its Future Stability in the Context of Atmospheric and Oceanic Warming. *Journal of Glaciology*, 58(208): 229–239.

Nienow, Peter, Sharp, Martin and Willis, Ian (1998), Seasonal Changes in the Morphology of the Subglacial Drainage System, Haut Glacier d'Arolla, Switzerland. *Earth Surface Processes and Landforms: The Journal of the British Geomorphological Group*, 23(9): 825–843.

Nienow, PW, Hubbard, AL, Hubbard, BP, Chandler, DM, Mair, DWF, Sharp, MJ and Willis, IC (2005), Hydrological Controls on Diurnal Ice Flow Variability in Valley Glaciers. *Journal of Geophysical Research: Earth Surface*, 110(F4).

Nienow, PW, Sole, AJ, Slater, Donald Alexander and Cowton, TR (2017), Recent Advances in Our Understanding of the Role of Meltwater in the Greenland Ice Sheet System. *Current Climate Change Reports*, 3: 330–344.

Nye, John Frederick (1953), The Flow Law of Ice from Measurements in Glacier Tunnels, Laboratory Experiments and the Jungfraufirn Borehole Experiment. *Proceedings of the Royal Society of London. Series A. Mathematical and Physical Sciences*, 219(1139): 477–489.

O'Leary, Martin and Christoffersen, Poul (2013), Calving on Tidewater Glaciers Amplified by Submarine Frontal Melting. *The Cryosphere*, 7(1): 119–128.

O'Neel, Shad, Pfeffer, W Tad, Krimmel, Robert and Meier, Mark (2005), Evolving Force Balance at Columbia Glacier, Alaska, during Its Rapid Retreat. *Journal of Geophysical Research: Earth Surface*, 110(F3).

O'Regan, Matt, Cronin, Thomas M, Reilly, Brendan, Alstrup, Aage Kristian Olsen, Gemery, Laura, Golub, Anna, Mayer, Larry A, Morlighem, Mathieu, Moros, Matthias, Munk, Ole L and others (2021), The Holocene Dynamics of Ryder Glacier and Ice Tongue in North Greenland. *The Cryosphere*, 15(8): 4073–4097.

Oerlemans, J (1984), Numerical Experiments on Large-Scale Glacial Erosion: Zeitschrift Für Gletscherkunde Und Glazialgeologie, v. 20.

Parizek, Byron R and Alley, Richard B (2004), Implications of Increased Greenland Surface Melt under Global-Warming Scenarios: Ice-Sheet Simulations. *Quaternary Science Reviews*, 23(9): 1013–1027.

Patton, Henry, Swift, DA, Clark, CD, Livingstone, Stephen J and Cook, Simon J (2016), Distribution and Characteristics of Overdeepenings beneath the Greenland and Antarctic Ice Sheets: Implications for Overdeepening Origin and Evolution. *Quaternary Science Reviews*, 148: 128–145.

Patton, Henry, Swift, Darrel A, Clark, Chris D, Livingstone, Stephen J, Cook, Simon J and Hubbard, Alun (2015), Automated Mapping of Glacial Overdeepenings beneath Contemporary Ice Sheets: Approaches and Potential Applications. *Geomorphology*, 232: 209–223.

Pattyn, Frank, Favier, Lionel, Sun, Sainan and Durand, Gaël (2017), Progress in Numerical Modeling of Antarctic Ice-Sheet Dynamics. *Current climate change reports*, 3: 174–184.

Pfeffer, WT (2007), A Simple Mechanism for Irreversible Tidewater Glacier Retreat. *Journal of Geophysical Research: Earth Surface*, 112(F3).

Podrasky, David, Truffer, Martin, Lüthi, Martin and Fahnestock, Mark (2014), Quantifying Velocity Response to Ocean Tides and Calving near the Terminus of Jakobshavn Isbræ, Greenland. *Journal of Glaciology*, 60(222): 609–621.

Pomper, Johannes, Salcher, Bernhard C, Eichkitz, Christoph, Prasicek, Günther, Lang, Andreas, Lindner, Martin and Götz, Joachim (2017), The Glacially Overdeepened Trough of the Salzach Valley, Austria: Bedrock Geometry and Sedimentary Fill of a Major Alpine Subglacial Basin. *Geomorphology*, 295: 147–158.

Preusser, Frank, Reitner, Jürgen M and Schlüchter, Christian (2010), Distribution, Geometry, Age and Origin of Overdeepened Valleys and Basins in the Alps and Their Foreland. *Swiss Journal of Geosciences*, 103(3): 407–426.

Prior-Jones, Michael R, Bagshaw, Elizabeth A, Lees, Jonathan, Clare, Lindsay, Burrow, Stephen, Werder, Mauro A, Karlsson, Nanna B, Dahl-Jensen, Dorthe, Chudley, Thomas R, Christoffersen, Poul and others (2021), Cryoegg: Development and Field Trials of a Wireless Subglacial Probe for Deep, Fast-Moving Ice. *Journal of Glaciology*, 67(264): 627–640.

Pritchard, Hamish D, Arthern, Robert J, Vaughan, David G and Edwards, Laura A (2009), Extensive Dynamic Thinning on the Margins of the Greenland and Antarctic Ice Sheets. *Nature*, 461(7266): 971–975.

Pörtner, Hans-Otto, Roberts, Debra C, Masson-Delmotte, Valérie, Zhai, Panmao, Tignor, Melinda, Poloczanska, Elvira and Weyer, NM (2019), The Ocean and Cryosphere in a Changing Climate. *IPCC special report on the ocean and cryosphere in a changing climate*, 1155.

Quincey, DJ, Copland, Luke, Mayer, C, Bishop, M, Luckman, A and Belò, M (2009), Ice Velocity and Climate Variations for Baltoro Glacier, Pakistan. *Journal of Glaciology*, 55(194): 1061–1071.

Rathmann, NM, Hvidberg, CS, Solgaard, AM, Grinsted, Anders, Gudmundsson, G Hilmar, Langen, Peter L, Nielsen, KP and Kusk, Anders (2017), Highly Temporally Resolved Response to Seasonal Surface Melt of the Zachariae and 79N Outlet Glaciers in Northeast Greenland. *Geophysical Research Letters*, 44(19): 9805–9814.

Reeh, Niels (1985), Was the Greenland Ice Sheet Thinner in the Late Wisconsinan than Now? *Nature*, 317(6040): 797–799.

Reeh, Niels and Olesen, Ole B (1986), Velocity Measurements on Daugaard-Jensen Gletscher, Scoresby Sund, East Greenland. *Annals of Glaciology*, 8: 146–150.

De Ridder, Koen and Schayes, Guy (1997), The IAGL Land Surface Model. *Journal of Applied Meteorology and Climatology*, 36(2): 167–182.

Rignot, E, Box, JE, Burgess, E and Hanna, E (2008), Mass Balance of the Greenland Ice Sheet from 1958 to 2007. *Geophysical Research Letters*, 35(20).

Rodriguez-Morales, Fernando, Gogineni, Sivaprasad, Leuschen, Carlton J, Paden, John D, Li, Jilu, Lewis, Cameron C, Panzer, Benjamin, Alvestegui, Daniel Gomez-Garcia, Patel, Aqsa, Byers, Kyle and others (2013), Advanced Multifrequency Radar Instrumentation for Polar Research. *IEEE Transactions on Geoscience and Remote Sensing*, 52(5): 2824–2842.

Roncek, Dennis W (1991), Using Logit Coefficients to Obtain the Effects of Independent Variables on Changes in Probabilities. *Social Forces*, 70(2): 509–518.

Rosenau, R, Scheinert, M and Dietrich, R (2015), A Processing System to Monitor Greenland Outlet Glacier Velocity Variations at Decadal and Seasonal Time Scales Utilizing the Landsat Imagery. *Remote Sensing of Environment*, 169: 1–19.

Röthlisberger, H and Lang, H (1987), Glacial Hydrology. InGlacio-Fluvial Sediment Transfer, Ed. AM Gurnell, MJ Clark.

Röthlisberger, Hans (1972), Water Pressure in Intra-and Subglacial Channels. *Journal of Glaciology*, 11(62): 177–203.

Sakakibara, Daiki and Sugiyama, Shin (2020), Seasonal Ice-Speed Variations in 10 Marine-Terminating Outlet Glaciers along the Coast of Prudhoe Land, Northwestern Greenland.

Journal of Glaciology, 66(255): 25–34.

Sammouda, Rachid, El-Zaart, Ali and others (2021), An Optimized Approach for Prostate Image Segmentation Using K-Means Clustering Algorithm with Elbow Method. *Computational Intelligence and Neuroscience*, 2021.

Samsonov, Sergey (2019), Three-Dimensional Deformation Time Series of Glacier Motion from Multiple-Aperture DInSAR Observation. *Journal of Geodesy*, 93(12): 2651–2660.

Sanders, JW, Cuffey, KM, MacGregor, KR, Kavanaugh, JL and Dow, CF (2018), Variations in the Surface Velocity of an Alpine Cirque Glacier. *Journal of Glaciology*, 64(248): 969–976.

Saurabh Vijay, Shfaqat Abbas Khan Anders Kusk Anne M. Solgaard Twila Moon Anders Anker Bjørk (2019),

Schlegel, Nicole-Jeanne, Wiese, David N, Larour, Eric Y, Watkins, Michael M, Box, Jason E, Fettweis, Xavier and Van Den Broeke, Michiel R (2016), Application of GRACE to the Assessment of Model-Based Estimates of Monthly Greenland Ice Sheet Mass Balance (2003-2012). *The Cryosphere*, 10(5): 1965–1989.

Schoof, Christian (2007), Ice Sheet Grounding Line Dynamics: Steady States, Stability, and Hysteresis. *Journal of Geophysical Research: Earth Surface*, 112(F3).

Schoof, Christian (2010), Ice-Sheet Acceleration Driven by Melt Supply Variability. *Nature*, 468(7325): 803–6.

Seale, Anthony, Christoffersen, Poul, Mugford, Ruth I and O'Leary, Martin (2011), Ocean Forcing of the Greenland Ice Sheet: Calving Fronts and Patterns of Retreat Identified by Automatic Satellite Monitoring of Eastern Outlet Glaciers. *Journal of Geophysical Research: Earth Surface*, 116(F3).

Seguinot, Julien (2008), Glacial Quarrying and Development of Overdeepenings in Glacial Valleys; Modelling Experiments and Case Studies at Erdalen, Western Norway. *Unpublished Thesis. Terre-atmosphère-ocean department of the Ecole normale superieure, Paris*.

Shannon, Sarah R, Payne, Antony J, Bartholomew, Ian D, van den Broeke, Michiel R, Edwards, Tamsin L, Fettweis, Xavier, Gagliardini, Olivier, Gillet-Chaulet, Fabien, Goelzer, Heiko, Hoffman, Matthew J and others (2013), Enhanced Basal Lubrication and the Contribution of the Greenland Ice Sheet to Future Sea-Level Rise. *Proceedings of the National Academy of Sciences*, 110(35): 14156–14161.

Shapero, Daniel R, Joughin, Ian R, Poinar, Kristin, Morlighem, Mathieu and Gillet-Chaulet, Fabien (2016), Basal Resistance for Three of the Largest Greenland Outlet Glaciers. *Journal of Geophysical Research: Earth Surface*, 121(1): 168–180.

Shepherd, Andrew, Hubbard, Alun, Nienow, Peter, King, Matt, McMillan, Malcolm and Joughin, Ian (2009), Greenland Ice Sheet Motion Coupled with Daily Melting in Late Summer. *Geophysical Research Letters*, 36(1).

Shepherd, Andrew and Wingham, Duncan J (2008), Antarctic Glacier Thinning, 1992-2003. *Scottish Geographical Journal*, 124(2-3): 154–164.

Shreve, RL (1972), Movement of Water in Glaciers. *Journal of Glaciology*, 11(62): 205–214.

Silverman, B. W. (1986), *Density Estimation for Statistics and Data Analysis*. Chapman and Hall.

Silverman, Bernard W (2018), *Density Estimation for Statistics and Data Analysis*. Routledge.

Sinaga, Kristina P and Yang, Miin-Shen (2020), Unsupervised K-Means Clustering Algorithm. *IEEE access*, 8: 80716–80727.

Sohn, Hong-Gyoo, Jezek, Kenneth C and van der Veen, Cornelis J (1998), Jakobshavn Glacier, West Greenland: 30 Years of Spaceborne Observations. *Geophysical Research Letters*, 25(14): 2699–2702.

Sole, Andrew John, Mair, Douglas Watson Fraser, Nienow, Peter W, Bartholomew, ID, King, MA, Burke, Matt J and Joughin, Ian (2011), Seasonal Speedup of a Greenland Marine-Terminating Outlet Glacier Forced by Surface Melt-Induced Changes in Subglacial Hydrology. *Journal of Geophysical Research: Earth Surface*, 116(F3).

Sole, Andrew, Nienow, Peter, Bartholomew, Ian, Mair, Douglas, Cowton, Thomas, Tedstone, Andrew and King, Matt A (2013), Winter Motion Mediates Dynamic Response of the Greenland Ice Sheet to Warmer Summers. *Geophysical Research Letters*, 40(15): 3940–3944.

Solgaard, AM, Rapp, D, Noël, BPY and Hvidberg, CS (2022), Seasonal Patterns of Greenland Ice Velocity From Sentinel-1 SAR Data Linked to Runoff. *Geophysical Research Letters*, 49(24): e2022GL100343.

Solgaard, AM, Simonsen, SB, Grinsted, A, Mottram, R, Karlsson, NB, Hansen, K, Kusk, A and Sørensen, LS (2020), Hagen Bræ: A Surging Glacier in North Greenland—35 Years of Observations. *Geophysical Research Letters*, 47(6): e2019GL085802.

Solgaard, Anne, Kusk, Anders, Boncori, John Peter Merryman, Dall, Jørgen, Mankoff, Kenneth D, Ahlstrøm, Andreas P, Andersen, Signe B, Citterio, Michele, Karlsson, Nanna B, Kjeldsen, Kristian K and others (2021), Greenland Ice Velocity Maps from the PROMICE Project. *Earth System Science Data Discussions*, 2021: 1–29.

Spedding, Nick and Evans, David JA (2002), Sediments and Landforms at Kv\iárjökull, Southeast Iceland: A Reappraisal of the Glaciated Valley Landsystem. *Sedimentary*

Geology, 149(1-3): 21–42.

Stange, Kurt Martin, van Balen, Ronald, Vandenberghe, Jef, Peña, Jose Luis and Sancho, Carlos (2013), External Controls on Quaternary Fluvial Incision and Terrace Formation at the Segre River, Southern Pyrenees. *Tectonophysics*, 602: 316–331.

Stenborg, Thorsten (1969), Studies of the Internal Drainage of Glaciers. *Geografiska Annaler: Series A, Physical Geography*, 51(1-2): 13–41.

Stevens, Laura A, Behn, Mark D, Das, Sarah B, Joughin, Ian, Noël, Brice PY, van den Broeke, Michiel R and Herring, Thomas (2016), Greenland Ice Sheet Flow Response to Runoff Variability. *Geophysical Research Letters*, 43(21): 11295–11303.

Sugiyama, Shin and Gudmundsson, G Hilmar (2003), Diurnal Variations in Vertical Strain Observed in a Temperate Valley Glacier. *Geophysical Research Letters*, 30(2).

Sugiyama, Shin, Sakakibara, Daiki, Tsutaki, Shun, Maruyama, Mihiro and Sawagaki, Takanobu (2015), Glacier Dynamics near the Calving Front of Bowdoin Glacier, Northwestern Greenland. *Journal of glaciology*, 61(226): 223–232.

Sundal, Aud Venke, Shepherd, Andrew, Nienow, Peter, Hanna, Edward, Palmer, Steven and Huybrechts, Philippe (2011), Melt-Induced Speed-up of Greenland Ice Sheet Offset by Efficient Subglacial Drainage. *Nature*, 469(7331): 521–4.

Swift, Darrel A, Persano, Cristina, Stuart, Finlay M, Gallagher, Kerry and Whitham, Andrew (2008), A Reassessment of the Role of Ice Sheet Glaciation in the Long-Term Evolution of the East Greenland Fjord Region. *Geomorphology*, 97(1): 109–125.

Talbot, CJ (1999), Ice Ages and Nuclear Waste Isolation. *Engineering Geology*, 52(3-4): 177–192.

Taylor, WP and Wilson, CDV (1997), Tectonically Influenced Glacial Erosion, and Ensuing Valley Infill: A Geophysical Survey. *Quarterly Journal of Engineering Geology and Hydrogeology*, 30(2): 97–113.

The IMBIE Team (2020), Mass Balance of the Greenland Ice Sheet from 1992 to 2018. *Nature*, 579(7798): 233–239.

Tedesco, Marco, Willis, Ian C, Hoffman, Matthew J, Banwell, Alison F, Alexander, Patrick and Arnold, Neil S (2013), Ice Dynamic Response to Two Modes of Surface Lake Drainage on the Greenland Ice Sheet. *Environmental Research Letters*, 8(3): 034007.

Tedstone, Andrew J, Nienow, Peter W, Gourmelen, Noel, Dehecq, Amaury, Goldberg, Daniel and Hanna, Edward (2015), Decadal Slowdown of a Land-Terminating Sector of the Greenland Ice Sheet despite Warming. *Nature*, 526(7575): 692–695.

Tedstone, Andrew J, Nienow, Peter W, Sole, Andrew J, Mair, Douglas W F, Cowton, Thomas R, Bartholomew, Ian D and King, Matt A (2013), Greenland Ice Sheet Motion Insensitive to Exceptional Meltwater Forcing. *Proceedings of the National Academy of Sciences of the United States of America*, 110(49): 19719–24.

Thomas, Robert H (1979), The Dynamics of Marine Ice Sheets. *Journal of Glaciology*, 24(90): 167–177.

Tuckett, P.A., Ely, J.C., Sole, A.J., Livingstone, S.J., Davison, B.J., Melchior van Wessem, J. and Howard, J., 2019. Rapid accelerations of Antarctic Peninsula outlet glaciers driven by surface melt. *Nature Communications*, *10*(1), p.4311.

Ultee, Lizz, Felikson, Denis, Minchew, Brent, Stearns, Leigh A and Riel, Bryan (2022), Helheim Glacier Ice Velocity Variability Responds to Runoff and Terminus Position Change at Different Timescales. *Nature Communications*, 13(1): 6022.

Umargono, Edy, Suseno, Jatmiko Endro and Gunawan, SK Vincensius (2020), K-Means Clustering Optimization Using the Elbow Method and Early Centroid Determination Based on Mean and Median Formula, 121–129, in: *The 2nd International Seminar on Science and Technology (ISSTEC 2019)*.

Vaughan, David G and Arthern, Robert (2007), Why Is It Hard to Predict the Future of Ice Sheets? *Science(Washington)*, 315(5818): 1503–1504.

Van der Veen, C.J., 1997. Backstress: what it is and how it affects glacier flow. *Byrd Polar Research Center Report No. 15*, pp.173-180.

Van der Veen, CJ (2002), Calving Glaciers. *Progress in Physical Geography*, 26(1): 96–122.

Vieli, Andreas, Jania, Jacek, Blatter, Heinz and Funk, Martin (2004), Short-Term Velocity Variations on Hansbreen, a Tidewater Glacier in Spitsbergen. *Journal of Glaciology*, 50(170): 389–398.

Vieli, Andreas and Nick, Faezeh M (2011), Understanding and Modelling Rapid Dynamic Changes of Tidewater Outlet Glaciers: Issues and Implications. *Surveys in geophysics*, 32: 437–458.

Vijay, Saurabh, Khan, Shfaqat Abbas, Kusk, Anders, Solgaard, Anne M, Moon, Twila and Bjørk, Anders Anker (2019), Resolving Seasonal Ice Velocity of 45 Greenlandic Glaciers with Very High Temporal Details. *Geophysical Research Letters*, 46(3): 1485–1495.

Vijay, Saurabh, King, Michalea D, Howat, Ian M, Solgaard, Anne M, Khan, Shfaqat Abbas and Noël, Brice (2021), Greenland Ice-Sheet Wide Glacier Classification Based on Two Distinct Seasonal Ice Velocity Behaviors. *Journal of Glaciology*, 67(266): 1241–1248.

Vincent, Christian and Moreau, Luc (2016), Sliding Velocity Fluctuations and Subglacial Hydrology over the Last Two Decades on Argentière Glacier, Mont Blanc Area. *Journal of Glaciology*, 62(235): 805–815.

Voss, Kelsey, Alley, Karen E, Lilien, David A and Dahl-Jensen, Dorthe The Role of Near-Terminus Conditions in the Ice-Flow Speed of Upernavik Isstrøm in Northwest Greenland. *Annals of Glaciology*: 1–51.

Van de Wal, Roderik SW, Boot, W, Van den Broeke, MR, Smeets, CJPP, Reijmer, CH, Donker, JJA and Oerlemans, J (2008), Large and Rapid Melt-Induced Velocity Changes in the Ablation Zone of the Greenland Ice Sheet. *science*, 321(5885): 111–113.

Walker, CC and Gardner, Alex S (2017), Rapid Drawdown of Antarctica's Wordie Ice Shelf Glaciers in Response to ENSO/Southern Annular Mode-Driven Warming in the Southern Ocean. *Earth and Planetary Science Letters*, 476: 100–110.

Walsh, KM, Howat, IM, Ahn, Y and Enderlin, EM (2012), Changes in the Marine-Terminating Glaciers of Central East Greenland, 2000-2010. *The Cryosphere*, 6(1): 211–220.

Weertman, Johannes (1957), On the Sliding of Glaciers. *Journal of glaciology*, 3(21): 33–38.

Weertman, Johannes (1964), The Theory of Glacier Sliding. *Journal of Glaciology*, 5(39): 287–303.

Weertman, Johannes (1974), Stability of the Junction of an Ice Sheet and an Ice Shelf. *Journal of Glaciology*, 13(67): 3–11.

Weertman, Johannes and others (1962), Catastrophic Glacier Advances.

Werder, Mauro A (2016), The Hydrology of Subglacial Overdeepenings: A New Supercooling Threshold Formula. *Geophysical Research Letters*, 43(5): 2045–2052.

Williams, Joshua J, Gourmelen, Noel and Nienow, Peter (2020), Dynamic Response of the Greenland Ice Sheet to Recent Cooling. *Scientific Reports*, 10(1): 1647.

Williams, Joshua J, Gourmelen, Noel and Nienow, Peter (2021), Complex Multi-Decadal Ice Dynamical Change Inland of Marine-Terminating Glaciers on the Greenland Ice Sheet. *Journal of Glaciology*, 67(265): 833–846.

Williams, Joshua J, Gourmelen, Noel, Nienow, Peter, Bunce, Charlie and Slater, Donald (2021), Helheim Glacier Poised for Dramatic Retreat. *Geophysical Research Letters*, 48(23): e2021GL094546.

Willis, Ian C (1995), Intra-Annual Variations in Glacier Motion: A Review. *Progress in Physical Geography*, 19(1): 61–106.

Wood, Michael, Khazendar, Ala, Fenty, I, Mankoff, K, Nguyen, AT, Schulz, Kirstin, Willis, Josh K and Zhang, Hong (2024), Decadal Evolution of Ice-Ocean Interactions at a Large East Greenland Glacier Resolved at Fjord Scale with Downscaled Ocean Models and Observations. *Geophysical Research Letters*, 51(7): e2023GL107983.

Zwally, H Jay, Abdalati, Waleed, Herring, Tom, Larson, Kristine, Saba, Jack and Steffen, Konrad (2002), Surface Melt-Induced Acceleration of Greenland Ice-Sheet Flow. *Science*, 297(5579): 218–222.

How Kernel Density Works. available at https://pro.arcgis.com/en/pro-app/latest/tool-reference/spatial-analyst/how-kernel-density-works.htm [7–2 2024].

Annex 1


Generate Points of Interest (POIs) for each dataset
Central Flowlines:
Points spaced at 500 m intervals along Greenland glacier central flowlines (derived in Chapter 3 (fig 3.4)).
Overdeepenings:
Points spaced at 150 m intervals along true overdeepening thalwegs for the metric dataset overdeepenings (derived in Chapter 3 (fig 3.5)).
Add MEaSUREs quarterly velocity:
Velocity data added for each quarter (2016-2019) to each POI. Velocity is then normalised to percentage of local annual max.
Adverse & Normal slope averages:
Average velocity calculated for points on the normal slope and adverse slope of each overdeepening, for each quarter (2016-2019)
Filter POIs:
Remove any data points which do not meet the specified quality threshold (published error less than 20% of stated velocity). Remove the individual year time series for any POI where there is not a velocity value for all four quarters in that year.
Run K means cluster algorithm:
Each POI year time series of normalised velocity is an independent input to the clustering analysis.
Run K means cluster algorithm:
Each POI year time series of normalised velocity is an independent input to the clustering analysis.
Flowlines dataset output clusters
Overdeepenings dataset output clusters
Identify common clusters:
Aggregate individual clusters into identified seasonal velocity typologies (T1, T2, T21, T23, T3, T4, T5).
Identify common clusters:
Aggregate individual clusters into identified seasonal velocity typologies (T1, T2, T21, T23, T3, T4, T5).

Figure A.1 Process workflow for deriving seasonal velocity typologies via K means cluster analysis

Solgaard 2022 notes the large scale switch from T2 at Ryder glacier in 2017 to T3 in 2019, and the same switch on areas on Academy glacier in 2019. Our results mirror these patterns and show the same results for both glaciers (Figure 6.21, Figure 6.22).

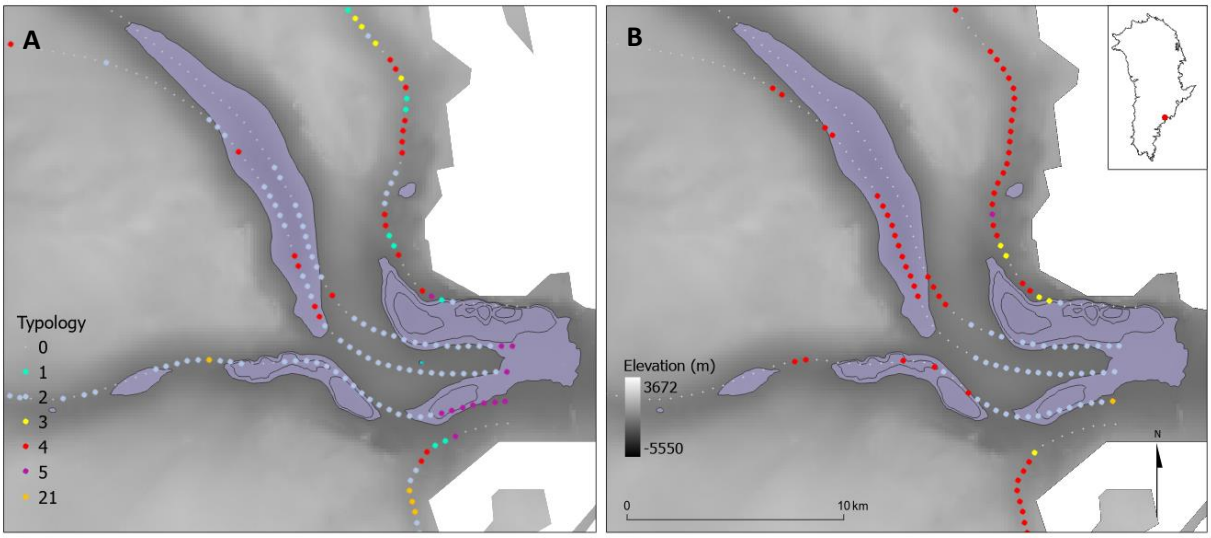

Figure A.2 Helheim, 66.37N, 38.31W. A) 2017 (low melt year). B) 2019 (high melt year)

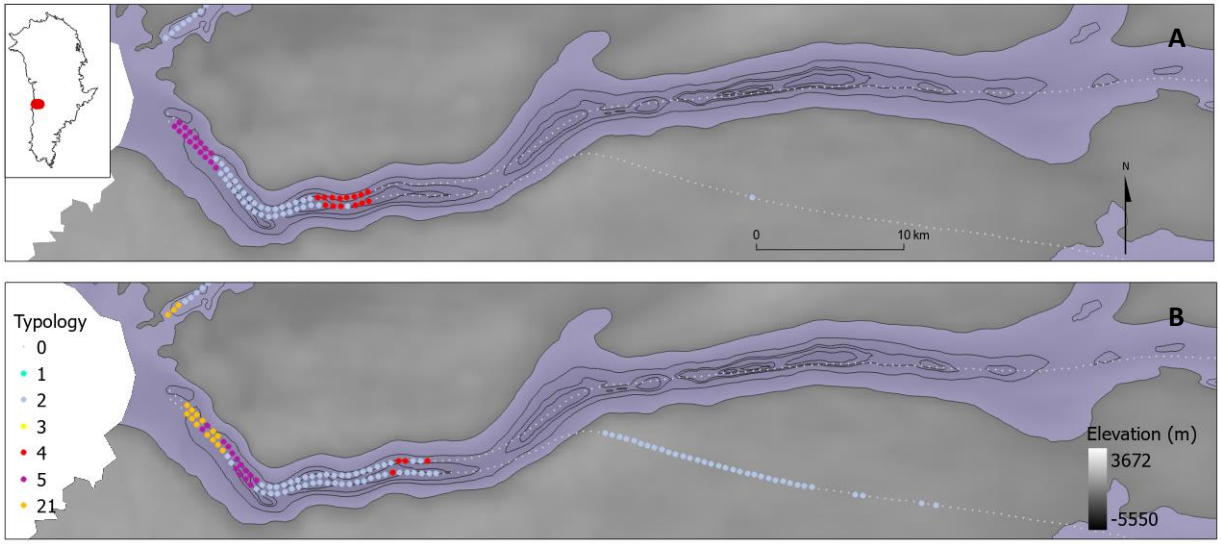

Figure A.3 Jakobshavn Isbræ, 66.37N, 38.31W. A) 2017 (low melt year). B) 2019 (high melt year)

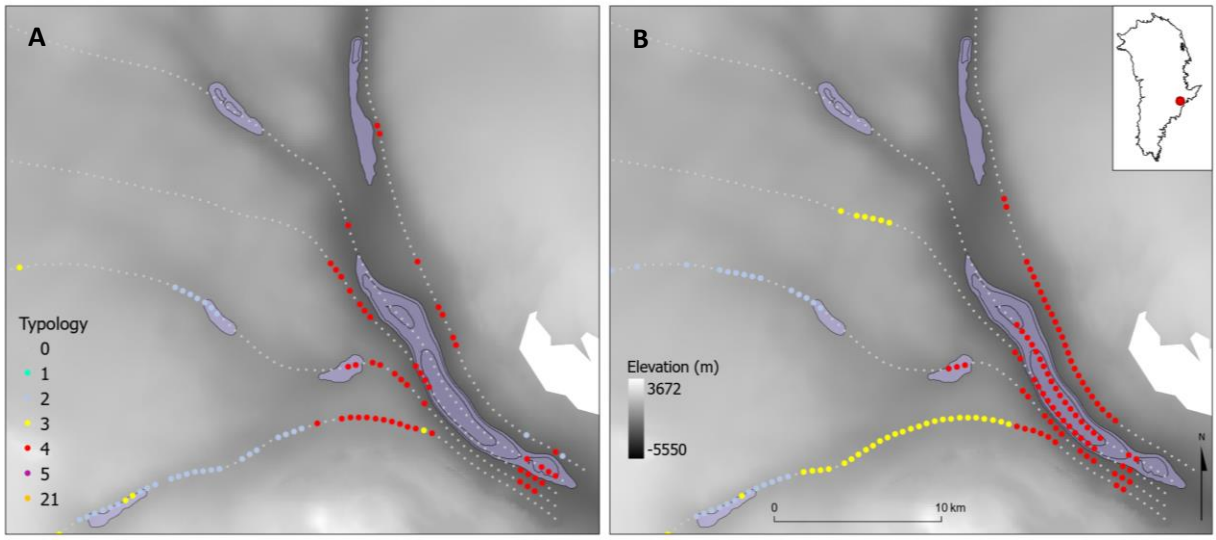

Figure A.4 Kangerlussuaq Gletsjer, 68.67N, 33.08W. A) 2017 (low melt year). B) 2019 (high melt year)

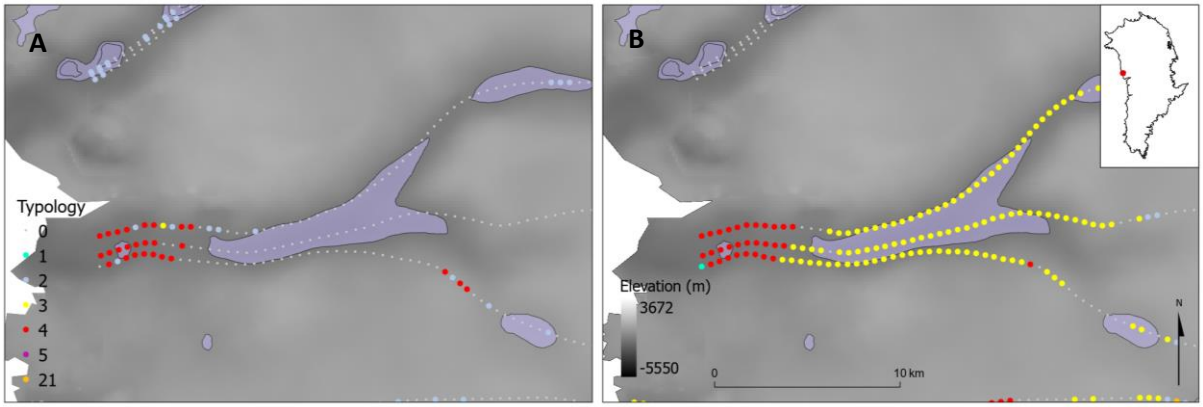

Figure A.5 Upernavik Isstrøm III, 72.84N, 54.28W. A) 2017 (low melt year). B) 2019 (high melt year)

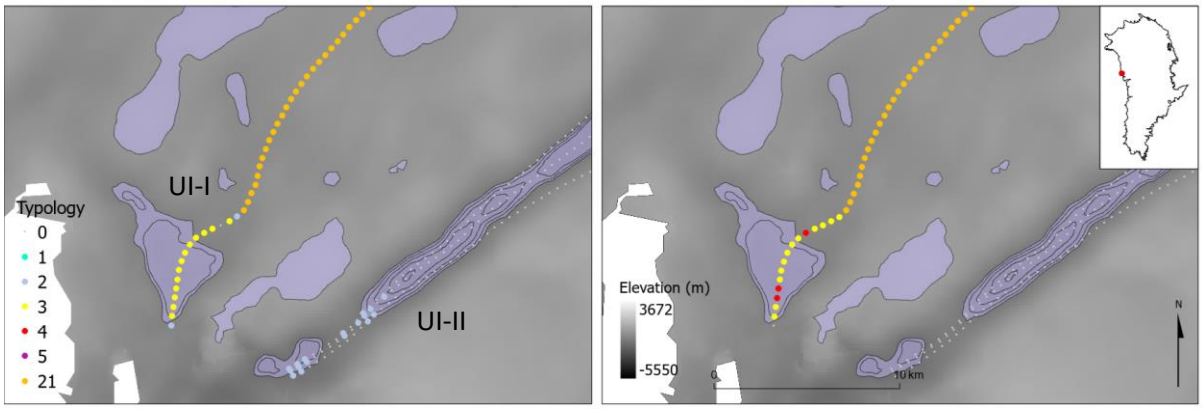

Figure A.6 Upernavik Isstrøm I & II, 73.10N, 54.35W. A) 2017 (low melt year). B) 2019 (high melt year)

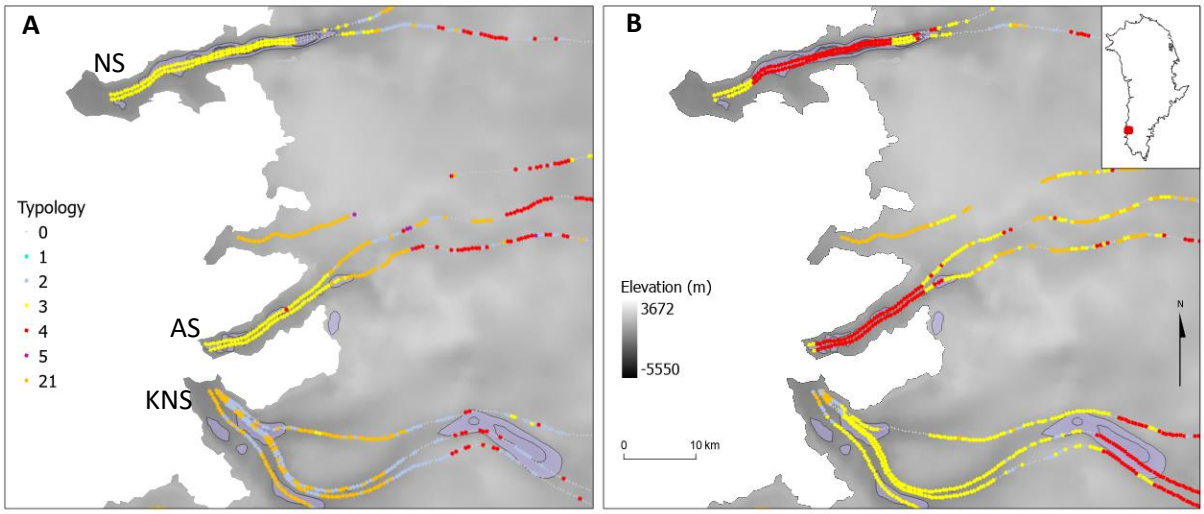

Figure A.7 Kangiata Nunaata Sermia (KNS), Narsap Sermia (NS), and Akullersuup Sermia (AS), 64.39N, 49.51W. A) 2017 (low melt year). B) 2019 (high melt year).

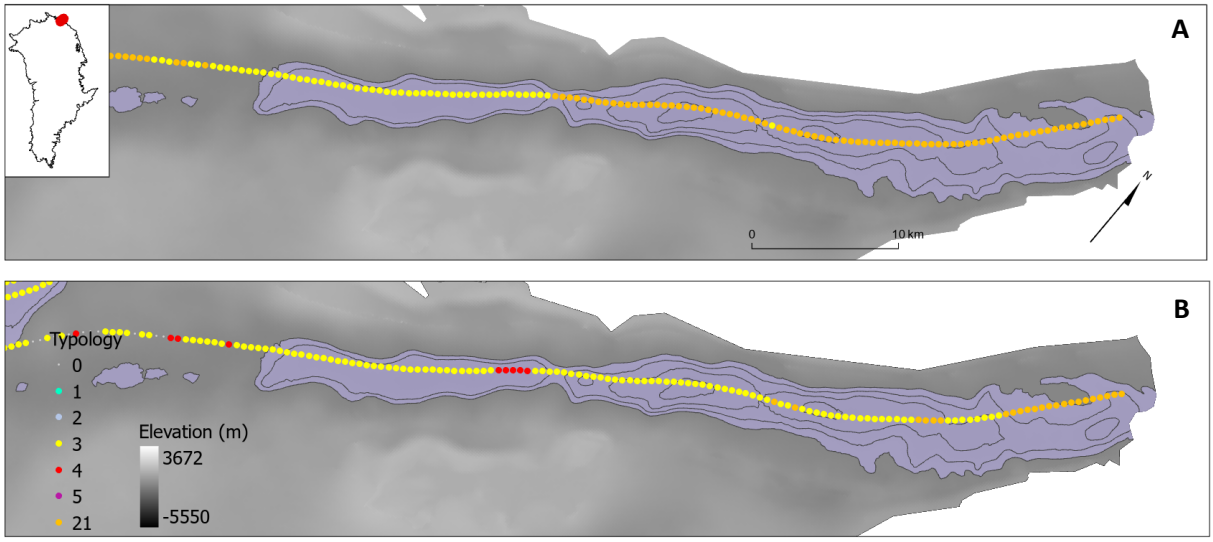

Figure A.8 Hagen Bræ, 81.30N, 29.61W. A) 2017 (low melt year). B) 2019 (high melt year).

Table A.1 Comparison between the classification of the dominant typology at the terminus of outlet glaciers in the thalweg dataset for 2019 and the results from Vijay et al. (2021) for 2019. In the Result column, 0 = classified by both studies, not matched; , 1 = classified by both studies, full match; 111 = classified by this study but not by Vijay et al. (2021), 21 = partial match (2 in Vijay et al. (2021), 21 in this study); 213 = partial match (3 in Vijay et al. (2021), 21 in this study); 1111 = not classified by this study but classified by Vijay et al. (2021), 11 = not classified by both studies.

Name	LAT	LONG	Vijay Class19)	AJclass19	Result
Unnamed	60.93	-43.53	3	1	0
Sermeq	60.96	-44.94	0	21	111
Jespersen	61	-45.01	3	3	1

Qalerallit	61.04	-46.61	0	2	111
Sermilik	61.04	-46.92	0	4	111
Nordre	61.05	-47.67	2	21	21
S ├©ndre	61.06	-47.47	2	21	21
Unnamed	61.08	-47.21	3	21	213
Unnamed	61.1	-44.93	3		1111
Unnamed	61.21	-43.3	0	1	111
Qooqqup	61.22	-45.15	0	4	111
Eqalorutsit	61.27	-46.19	0	2	111
Arsuk	61.3	-47.83	0	21	111
Unnamed	61.33	-43.31	0	1	111
Eqalorutsit	61.35	-45.78	3	3	1
Unnamed	61.5	-43.02	3		1111
Sioralik	61.53	-48.09	0	21	111
Sermiligaarsuk	61.6	-48.23	3	4	0
Unnamed	61.64	-43.13	3	1	0
Unnamed	61.8	-42.87	3		1111
Unnamed	61.84	-42.84	0	2	111
Unnamed	61.91	-42.6	0		11
Sermilik	61.96	-48.69	3		1111
Unnamed	62.06	-42.5	0	5	111
Nigerlikasik	62.07	-48.79	0	4	111
Avannarleq	62.22	-48.99	0	3	111
Unnamed	62.29	-42.55	0	4	111
Unnamed	62.38	-43.04	0	4	111
Unnamed	62.49	-43.14	3	3	1
Frederiksh ├Ñb	62.54	-49.98	2	21	21
Unnamed	62.57	-43.13	3	2	0
Unnamed	62.75	-43.28	0		11
Heimdal	62.89	-42.65	3	3	1
Nakkaasorsuaq	63.07	-49.64	3	3	1
Guldfaxe	63.23	-42.2	3	3	1
Unnamed	63.25	-49.49	3	21	213
Skinfaxe	63.26	-41.88	0	3	111
Thrym	63.56	-41.81	3	3	1
Storebj ├©rn	63.68	-41.66	0	2	111
Gerd	63.7	-40.89	3		1111
A.P.	63.86	-41.73	0	4	111
Gungner	63.88	-40.76	0		11
Sleipner	63.89	-41.4	0	2	111
Unnamed	63.93	-40.91	3		1111
Unnamed	64.24	-41.66	0	2	111
Unnamed	64.36	-41.3	0	2	111
Gr ├Ñulv	64.37	-41.54	0	4	111
Unnamed	64.41	-40.89	3		1111
Unnamed	64.51	-40.68	3	3	1

Unnamed	64.74	-40.87	0		11
Unnamed	64.85	-41.09	0	2	111
Unnamed	65	-41.22	0	2	111
Unnamed	65.18	-40.17	0		11
Unnamed	65.2	-41.21	0	3	111
Unnamed	65.23	-40.74	0	21	111
Unnamed	65.24	-40.1	0		11
Unnamed	65.38	-39.99	0		11
Unnamed	65.53	-40.21	0	2	111
Unnamed	65.6	-40.05	3	2	0
Unnamed	65.64	-39.72	0		11
Unnamed	65.71	-39.68	0		11
Unnamed	65.8	-39.31	0	21	111
Br ├╝ckner	65.93	-38.47	0		11
Heim	66	-38.52	0	2	111
Kattilertarpia	66.07	-38.37	0		11
Apuseerajik	66.18	-38.1	3		1111
Helheim	66.38	-38.32	0	2	111
Fenris	66.39	-37.6	0	2	111
Glacier	66.45	-35.99	0	4	111
K.J.V.	66.49	-34.75	3		1111
Franche	66.51	-36.76	3	3	1
K.J.V.	66.55	-34.61	0		11
Unnamed	66.73	-34.3	0		11
Unnamed	67.03	-34.2	3	3	1
Unnamed	67.22	-33.8	0		11
Unnamed	67.43	-33.62	0	1	111
Unnamed	67.58	-33.46	3	3	1
Unnamed	67.62	-33.4	0	4	111
Nordre	67.72	-32.92	3		1111
Unnamed	67.78	-33.4	3	4	0
Unnamed	67.86	-32.68	3		1111
Polaric	67.9	-32.45	3		1111
Hutchinson	68.14	-32.29	3		1111
Frederiksborg	68.29	-31.5	0		11
Sorgenfri	68.38	-30.15	3	3	1
Rosenborg	68.45	-28.87	0	4	111
Kronborg	68.48	-28.64	3		1111
Unnamed	68.51	-28.52	3		1111
Courtauld	68.53	-32.18	3		1111
Borggraven	68.64	-28.11	0	4	111
Kangerlussuaq	68.64	-33.02	0		11
Unnamed	69.81	-50.19	3	4	0
Unnamed	69.92	-50.29	0	4	111
Kista	69.95	-27.5	3	3	1
Magga	69.95	-27.22	2	2	1

Unnamed	69.99	-50.14	0	2	111
Unnamed	70.08	-50.29	3	3	1
Vestfjord	70.36	-29.22	3	3	1
Unnamed	70.4	-50.5	0	3	111
Unnamed	70.54	-50.48	0	0	111
Rolige	70.58	-28.39	2	21	21
Unnamed	70.64	-50.6	3	4	0
Unnamed	70.73	-50.61	2	21	21
Unnamed	70.84	-50.72	3	4	0
Unnamed	70.99	-50.78	2	0	1111
Eielson	71.16	-27.87	2		1111
Unnamed	71.45	-51.36	0	4	111
Unnamed	71.76	-52.4	3	4	0
Unnamed	71.77	-51.59	0	4	111
Daugaard-Jensen	71.88	-28.69	3	2	0
Unnamed	72.05	-28.98	3	2	0
Unnamed	72.09	-52.51	0	2	111
Jomfru	72.11	-27.53	3		
Unnamed	72.14	-28.74	3	2	0
Unnamed	72.39	-53.43	3	0	
Hisinger	72.84	-27.53	3	3	1
Unnamed	72.85	-54.23	3	3	1
Unnamed	72.94	-54.2	0	4	111
Unnamed	73.04	-54.27	0	0	111
Unnamed	73.05	-54.56	3	3	1
Nordenski ├Âld	73.13	-27.86	3	3	1
Unnamed	73.24	-55.11	3	3	1
J ├ªttegletsjer	73.46	-27.56	2		1111
Unnamed	73.48	-55.24	0	4	111
Gerard	73.55	-27.23	3	3	1
Unnamed	73.6	-55.5	3	3	1
Unnamed	73.83	-55.56	3	3	1
Waltershausen	73.87	-24.28	2	21	21
Unnamed	73.95	-55.64	0	0	111
Nunatakgletsjer	73.96	-25.93	3	3	1
Wordie	74.16	-22.81	2	21	21
Unnamed	74.25	-56.02	3	3	1
Unnamed	74.31	-56.07	2	3	0
Unnamed	74.41	-55.98	3	3	1
Unnamed	74.63	-55.93	0	1	111
Unnamed	74.76	-56.39	0	2	111
Unnamed	74.8	-56.46	0	2	111
Unnamed	74.88	-56.73	3	0	
Unnamed	74.95	-57.08	0	0	111
Unnamed	75.05	-57.54	3	3	1
Unnamed	75.15	-57.58	3	4	0

Heinkel	75.17	-22.61	3	3	1
Unnamed	75.32	-57.84	3	3	1
Unnamed	75.41	-58.03	2	0	1111
Unnamed	75.46	-57.94	0	4	111
Sverdrup	75.63	-58.03	0	2	111
Ejnar	75.67	-22.41	2	21	21
Unnamed	75.77	-58.55	3		1111
Nansen	75.78	-58.87	3	3	1
Nordenski ├Âld	75.85	-58.95	0	3	111
Unnamed	75.9	-59.11	0	3	111
Kong	76.02	-59.71	0	2	111
Issuusarsuit	76.08	-60.63	3	4	0
Nasersorfik	76.09	-67.26	3		1111
Appakkooriaq	76.1	-68.2	0		11
Unnamed	76.1	-60.06	3	3	1
Soranerbr ├ªen	76.16	-21.93	3		1111
Unnamed	76.2	-67.58	0	3	111
Helland	76.22	-64.8	3		1111
Savigssuaq	76.23	-65.23	2		1111
Unnamed	76.23	-60.59	0		11
Rink	76.25	-60.83	0		11
Pituffik	76.26	-68.69	2		1111
Unnamed	76.26	-61.39	3		1111
Unnamed	76.27	-67.38	3	3	1
Unnamed	76.27	-66.45	0		11
D ├Âcker	76.29	-61.7	3		1111
Unnamed	76.3	-64.61	3		1111
Unnamed	76.34	-66.77	3	3	1
Unnamed	76.34	-61.92	3		1111
Unnamed	76.36	-65.44	3		1111
Harald	76.58	-67.59	0		11
Chamberlin	76.71	-68.46	0		11
Salisbury	76.71	-68.69	2		1111
Knud	76.73	-67.84	0		11
Unnamed	76.99	-69.42	2	21	21
Sermiarsupaluk	77.09	-66.27	0		11
Marie	77.21	-65.97	3		1111
Leidy	77.25	-65.99	2	21	21
Heilprin	77.52	-65.84	3	3	1
Hubbard	77.55	-67.79	3	21	213
Tracy	77.66	-65.83	3	1	0
Bowdoin	77.7	-68.58	3	3	1
Hart	77.71	-67.2	3	21	213
Farquhar	77.73	-66.21	3	3	1
Sharp	77.73	-66.93	3	3	1
Melville	77.75	-66.61	3	3	1

Meehan	77.89	-70.25	0		11
Moris	77.91	-71.04	2		1111
Clements	77.94	-71.87	0		11
Diebitsch	77.95	-71.59	2	2	1
Humboldt	79.84	-63.58	0	2	111
Petermann	80.76	-60.89	2	2	1
Hagen	81.35	-28.49	2	21	21
Steensby	81.44	-54.21	2	4	0
Academy	81.61	-32.3	3		1111
Ryder	81.7	-50.47	3	3	1
Marie	81.79	-33.07	2		1111
Hobbs	81.91	-35.6	2		1111
Adams	82.14	-39.68	2	21	21